

SPECTROSCOPIC AND FUNCTIONAL CHARACTERIZATION OF MONOTHIOL  
GLUTAREDOXINS AND THE FUMARATE NITRATE REDUCTION REGULATORY  
PROTEIN

by

BO ZHANG

(Under the Direction of Michael K. Johnson)

ABSTRACT

The objectives of this work were to investigate the properties and functions of iron-sulfur (Fe-S) cluster-bound forms of monothiol glutaredoxins with CGFS active-site (CGFS-Grxs), a ubiquitous family of proteins involved in Fe-S cluster biogenesis and Fe homeostasis, and to elucidate the O<sub>2</sub>-sensing mechanism of the *E. coli* fumarate and nitrate reduction transcriptional regulatory protein (FNR). The approach involved using a combination of biophysical techniques to elucidate the nature and properties of the Fe-S centers under steady-state conditions and/or during *in vitro* cluster transfer. Our results show that the recombinant *S. cerevisiae* mitochondrial Grx5 is a versatile Fe-S protein that is able to accommodate [2Fe-2S]<sup>2+</sup>, linear [3Fe-4S]<sup>+</sup>, and [4Fe-4S]<sup>2+</sup> clusters *in vitro* depending on the reconstitution conditions and that the [4Fe-4S]<sup>2+</sup> cluster-bound *Sc* Grx5 is competent for *in vitro* activation of apo aconitase at physiological relevant rates. These results suggested potential roles of *Sc* Grx5 in scavenging linear [3Fe-4S]<sup>+</sup> clusters released during protein unfolding under oxidative stress conditions and in the maturation of [4Fe-4S]<sup>2+</sup> cluster-containing proteins. Functional studies of [2Fe-2S]<sup>2+</sup> cluster-bound CGFS-Grxs were carried out using *A. vinelandii* Grx5 and Grx-nif by investigating *in vitro* cluster

exchange of these two proteins with physiologically relevant partners from the ISC and NIF cluster assembly pathways, respectively. The results show that CGFS-Grxs can efficiently mediate  $[2\text{Fe-2S}]^{2+}$  cluster trafficking from U-type primary scaffolds to apo acceptor proteins via intact cluster transfer. Moreover, *Av* Grx5 and Grx-nif have the potential to accept  $[2\text{Fe-2S}]^{2+}$  clusters from  $[4\text{Fe-4S}]^{2+}$  cluster-containing scaffolds and/or carrier proteins. These results provide further support for the proposed Fe-S cluster trafficking and storage functions of CGFS-Grxs. Spectroscopic and mass spectrometry investigation of the  $\text{O}_2$ -induced  $[4\text{Fe-4S}]^{2+}$ -to- $[2\text{Fe-2S}]^{2+}$  cluster conversion in FNR revealed formation of atypical  $[2\text{Fe-2S}]^{2+}$  clusters with one or two cysteine persulfide ligands that result from sulfur-based oxidation and retention of bridging sulfides. The cluster transformation can be reversed under anaerobic conditions upon incubation with DTT and  $\text{Fe}^{2+}$  ion. The observation of analogous  $\text{O}_2$ -induced  $[4\text{Fe-4S}]^{2+}$ -to- $[2\text{Fe-2S}]^{2+}$  cluster conversion in enzymes with  $\text{O}_2$ -sensitive  $[4\text{Fe-4S}]$  clusters suggests that this novel type of cluster interconversion may represent a new mechanism for the assembly and repair of biological  $[4\text{Fe-4S}]$  clusters.

**INDEX WORDS:** Iron-sulfur cluster, iron-sulfur cluster biogenesis, monothiol glutaredoxin, FNR, gene regulation, oxygen sensing, cluster conversion.

SPECTROSCOPIC AND FUNCTIONAL CHARACTERIZATION OF MONOTHIOL  
GLUTAREDOXINS AND THE FUMARATE NITRATE REDUCTION REGULATORY  
PROTEIN

by

BO ZHANG

B.S., Peking University, Beijing, China, 2007

A Dissertation Submitted to the Graduate Faculty of The University of Georgia in Partial  
Fulfillment of the Requirements for the Degree

DOCTOR OF PHILOSOPHY

ATHENS, GEORGIA

2013

© 2013

Bo Zhang

All Rights Reserved

SPECTROSCOPIC AND FUNCTIONAL CHARACTERIZATION OF MONOTHIO  
L  
GLUTAREDOXINS AND THE FUMARATE NITRATE REDUCTION REGULATORY  
PROTEIN

by

BO ZHANG

Major Professor: Michael K. Johnson

Committee: Michael W. W. Adams  
Todd C. Harrop

Electronic Version Approved:

Maureen Grasso  
Dean of the Graduate School  
The University of Georgia  
May 2013

DEDICATION

To my loving parents

Mr. Yongsheng Zhang and Ms. Aiping Chen

## ACKNOWLEDGEMENTS

It is difficult to include everyone who has done so much to help me towards finishing this dissertation, but I shall try my best.

First and foremost, I wish to truly thank my major professor and mentor Dr. Michael Johnson for his continuous guidance, support and trust. I will always admire his sharp scientific intuition and attention to detail.

I would like to extend my sincere gratitude towards all the members of the Johnson lab. I have been very fortunate to have shared a laboratory with exceptional colleagues. I wish to thank Daphne, Yao, Angela and Sowmya for teaching me the research techniques and for the helpful discussions. I thank Sajini, Priyanka and Brain for always being so understanding and patient with me. Your companies have made the occasional frustrations and disappointments that come along with research easier to endure.

I would also like to acknowledge my advisory committee, Dr. Todd Harrop and Dr. Michael Adams, for valuable suggestions and kind support throughout the course of my graduate study and beyond.

The research groups in the area of iron-sulfur cluster biogenesis form a tight and collaborative community. I feel so privileged to be part of it and am also to be able to make a small contribution towards the understanding of such an important and amazingly sophisticated biological process. I am indebted to many people whose efforts have been indispensable for the completion of this dissertation. I wish to thank our collaborators: Dr. Nicolas Rouhier at Nancy Universite for generously providing plasmids and proteins; Dr. Vincent Huynh at Emory

University for the meticulous analysis of the Mössbauer data; Dr. Jason Crack, Dr. Nick Le Brun and Dr. Andrew Thomson for the opportunity to work on such a fascinating project and for trusting me with their delicate protein samples. I truly wish to thank Dr. Patricia Dos Santos, Dr. Caryn, Dr. Wayne Outten, and Dr. Dennis Dean for giving me the opportunity to present my research at our annual meeting (the LabFest), for offering unreserved advices and helpful suggestions, and for generously opening their homes to me.

Back to the Chemistry Department at UGA, I have benefited tremendously from the expertise of the professionals as well as fellow graduate students from other research groups. It was midway through my graduate research when I started to realize what it entails to work in a spectroscopy-oriented lab in addition to one's research: the challenge of instruments troubleshooting! I was lucky enough to have Dr. Dennis Phillips and Dr. Greg Wylie generously sharing their knowledge and expertise on scientific equipments. I cannot thank both of them enough for the help they have offered. I would like to additionally thank Dr. Dennis Phillips for the help with the use of the mass spectrometry. While the Johnson lab is located on the second floor, I have never failed to find company and help from the members of the Harrop and the Douberly labs. Many thanks to them for the help in taming the stubborn gas tanks and cylinders on numerous occasions. Furthermore, their enthusiasm for research is contagious and has always been a great motivation to me.

Last but definitely not least, I must express my gratitude to my parents for installing in me the value of hard work and the importance to be responsible. It would not be possible for me to complete this dissertation without their love, understanding and constant support.

## TABLE OF CONTENTS

	Page
ACKNOWLEDGEMENTS .....	v
LIST OF TABLES .....	xi
LIST OF FIGURES .....	xii
CHAPTER	
1 INTRODUCTION AND LITERATURE REVIEW .....	1
Background .....	1
Human disease associated with defects in the Fe-S cluster biogenesis .....	2
Structures and properties of biological Fe-S centers .....	4
Cluster conversions .....	11
Functions of biological Fe-S centers .....	14
Biogenesis of Fe-S clusters .....	23
Roles of monothiol glutaredoxins in Fe-S cluster biogenesis and Fe regulation .....	34
Transcriptional regulator FNR .....	43
Summary of presented work .....	48
Abbreviations .....	51
References .....	53
2 ASSEMBLY OF LINEAR $[3\text{Fe-4S}]^+$ , $[2\text{Fe-2S}]^{2+}$ AND $[4\text{Fe-4S}]^{2+}$ CLUSTERS IN <i>SACCHAROMYCES CEREVISIAE</i> MITOCHONDRIAL GLUTAREDOXIN 5:	

SPECTROSCOPIC CHARACTERIZATION AND IMPLICATIONS FOR	
FUNCTIONS .....	98
Abbreviations .....	99
Abstract .....	100
Introduction .....	102
Experimental procedures .....	105
Results .....	109
Discussion .....	121
References .....	129
3 MONOTHIOLE GLUTAREDOXINS FUNCTION IN STORING AND	
TRANSPORTING [2Fe-2S] CLUSTERS ASSEMBLED ON ISCU SCAFFOLD	
PROTEINS .....	161
Abbreviations .....	162
Abstract .....	163
Introduction .....	164
Experimental procedures .....	165
Results and discussion .....	170
Acknowledgments .....	173
References .....	174
4 POTENTIAL ROLES FOR MONOTHIOLE GLUTAREDOXINS IN [2Fe-2S]	
CLUSTER TRAFFICKING AND STORAGE .....	185
Abbreviations .....	186
Abstract .....	187

Introduction.....	189
Experimental procedures .....	193
Results.....	196
Discussion.....	205
Acknowledgments.....	211
References.....	212
5 REVERSIBLE CYCLING BETWEEN CYSTEINE PERSULFIDE-LIGATED [2Fe-2S] AND CYSTEINE-LIGATED [4Fe-4S] CLUSTERS IN THE FNR REGULATORY PROTEIN .....	229
Abbreviations.....	230
Abstract.....	231
Introduction.....	232
Experimental procedures .....	234
Results.....	236
Discussion.....	243
Acknowledgments.....	248
References.....	249
6 CONCLUSIONS AND FUTURE DIRECTIONS.....	272
References.....	284
APPENDICES	
A SPECTROSCOPIC AND FUNCTIONAL CHARACTERIZATION OF IRON-BOUND FORMS OF <i>AZOTOBACTER VINELANDII</i> <sup>NIF</sup> ISCA .....	292

B	SPECTROSCOPIC AND FUNCTIONAL CHARACTERIZATION OF IRON-SULFUR CLUSTER-BOUND FORMS OF <i>AZOTOBACTER VINELANDII</i> <sup>NIF</sup> ISCA .....	355
C	MONOTHIOGLUTAREDOXINS AND A-TYPE PROTEINS: PARTNERS IN FE-S CLUSTER TRAFFICKING .....	416

## LIST OF TABLES

	Page
Table 2.1: Primers used for <i>S. cerevisiae</i> Grx5 cloning and mutagenesis .....	135
Table 2.2: Mössbauer parameters for the linear [3Fe-4S] <sup>+</sup> cluster in <i>Sc</i> Grx5 .....	136
Table 5.1: Comparison of the resonance Raman Fe-S frequencies, assignments, and <sup>32</sup> S/ <sup>34</sup> S-bridging isotope shifts for [4Fe-4S] <sup>2+</sup> centers in a synthetic analog complex, <i>C. pasteurianum</i> ferredoxin, and <i>Escherichia coli</i> FNR .....	253

## LIST OF FIGURES

	Page
Figure 1.1: Structures of fundamental types of Fe-S centers as determined by X-ray crystallography.....	78
Figure 1.2: Ranges of midpoint potential for the major classes of biological Fe-S centers in their physiologically assessable redox states .....	70
Figure 1.3: Ground state spin and valence localization/delocalization patterns for fundamental types of Fe-S centers.....	82
Figure 1.4: Schematic representation summarizing the types of cluster interconversions observed in Fe-S proteins .....	84
Figure 1.5: Structures of some Fe-S clusters that constitute enzyme active sites.....	86
Figure 1.6: Organization of genes involved in <i>nif</i> , <i>isc</i> and <i>suf</i> Fe-S cluster assembly operons in selected prokaryotic organisms.....	88
Figure 1.7: Schematic representation of classification and domain organization of classes I and II Grxs.....	90
Figure 1.8: Comparison of the crystal structures of <i>E. coli</i> Grx4 and human Grx2. ....	92
Figure 1.9: Superimposition of apo and cluster-bound structures of <i>E. coli</i> Grx4.....	94
Figure 1.10: The predicted structure of a FNR monomer.....	96
Figure 2.1: Reconstructed ESI-quadrupole mass spectra of as-isolated apo-Grx5.....	137
Figure 2.2: Comparison of UV-visible absorption and visible CD spectra of the linear [3Fe-4S] <sup>+</sup> cluster-bound and [4Fe-4S] <sup>2+</sup> cluster-bound forms of <i>S.cerevisiae</i> Grx5 and the [2Fe-2S] <sup>2+</sup> cluster-bound <i>S.cerevisiae</i> Grx3 homodimer .....	139

Figure 2.3: Mössbauer evidence for linear [3Fe-4S] <sup>+</sup> clusters in <i>Sc</i> Grx5 reconstituted with <sup>57</sup> Fe in the presence of GSH .....	141
Figure 2.4: X-band EPR evidence for linear [3Fe-4S] <sup>+</sup> clusters in <i>Sc</i> Grx5.....	143
Figure 2.5: VTMCD spectra of linear [3Fe-4S] <sup>+</sup> clusters in <i>Sc</i> Grx5 .....	145
Figure 2.6: VHVT MCD saturation magnetization data for the linear [3Fe-4S] <sup>+</sup> center of <i>S.cerevisiae</i> Grx5 .....	147
Figure 2.7: Resonance Raman spectra of linear [3Fe-4S] <sup>+</sup> cluster-bound <i>Sc</i> Grx5 with 406.7, 457.9, 487.9 and 514.5 nm laser excitations.....	149
Figure 2.8: Resonance Raman spectra of the <sup>32</sup> S <sub>b</sub> - and <sup>34</sup> S <sub>b</sub> -reconstituted linear [3Fe-4S] <sup>+</sup> cluster in <i>Sc</i> Grx5 showing <sup>34</sup> S/ <sup>32</sup> S isotopic shifts.....	151
Figure 2.9: Mössbauer spectrum of [4Fe-4S] <sup>2+</sup> cluster-bound <i>Sc</i> Grx5.....	153
Figure 2.10: Resonance Raman spectrum of [4Fe-4S] <sup>2+</sup> cluster-bound <i>Sc</i> Grx5 with 487.9 nm laser excitation. ....	155
Figure 2.11: Activation of apo-aconitase using [4Fe-4S] <sup>2+</sup> cluster-bound <i>Sc</i> Grx5 .....	157
Figure 2.12: UV–visible absorption spectrum of the linear [3Fe-4S] <sup>+</sup> cluster-bound <i>Sc</i> Grx5 C90S mutant.....	159
Figure 3.1: Time course of cluster transfer from <i>A. vinelandii</i> [Fe <sub>2</sub> S <sub>2</sub> ]-IscU to apo-Grx5 monitored by UV–visible CD spectroscopy at 23 °C.....	177
Figure 3.2: Time course of cluster transfer from <i>A. vinelandii</i> [Fe <sub>2</sub> S <sub>2</sub> ]-IscU to apo-Grx in the presence of 0.10 mM <i>A. vinelandii</i> HscA and HscB, 40 mM MgCl <sub>2</sub> , 2 mM ATP, and 150 mM KCl monitored by UV–visible CD spectroscopy at room temperature .....	179
Figure 3.3: Comparison of the kinetics of cluster transfer from <i>A. vinelandii</i> [Fe <sub>2</sub> S <sub>2</sub> ]-IscU to apo- Grx5 in the presence and in the absence of HscA/HscB/ATP.....	181

Figure 3.4: Time course of cluster transfer from <i>A. vinelandii</i> [Fe <sub>2</sub> S <sub>2</sub> ]-Grx5 to apo-IscFdx monitored by UV-visible CD spectroscopy at 23 °C.....	183
Figure 4.1: UV-visible absorption and visible CD spectra of [2Fe-2S]-Grx5 and [2Fe-2S]-Grx-nif .....	217
Figure 4.2: Resonance Raman spectra of [2Fe-2S]-Grx5 and [2Fe-2S]-Grx-nif with 457.9, 487.9 and 514.5 nm laser excitations.....	219
Figure 4.3: UV-visible absorption spectra of chromatographically resolved fractions of cluster-bound forms of Grx5.....	221
Figure 4.4: Time course of cluster transfer from <i>A. vinelandii</i> [4Fe-4S]-IscU to apo Grx5 monitored by UV-visible CD spectroscopy .....	223
Figure 4.5: Time course of cluster transfer from <i>A. vinelandii</i> [4Fe-4S]-NfuA to apo Grx5 monitored by UV-visible CD spectroscopy .....	225
Figure 4.6: Time course of cluster transfer from [4Fe-4S]-containing NifU to apo Grx-nif monitored by UV-visible CD spectroscopy .....	227
Figure 5.1: Summary of the in vivo and in vitro cluster and oligomeric state interconversions reported for <i>E. coli</i> FNR .....	254
Figure 5.2: Resonance Raman spectra of the O <sub>2</sub> -induced [4Fe-4S] <sup>2+</sup> to [2Fe-2S] <sup>2+</sup> cluster conversion of FNR with natural abundance and <sup>34</sup> S-labeled bridging sulfides.....	256
Figure 5.3: Comparison of the resonance Raman spectra of air-exposed FNR obtained in the absence and presence of GSH or DTT.....	258
Figure 5.4: Time course of the resonance Raman spectrum of FNR after exposure to air.....	260
Figure 5.5: Resonance Raman studies of the interconversion between [4Fe-4S] <sup>2+</sup> and [2Fe-2S] <sup>2+</sup> clusters in FNR. ....	262

Figure 5.6: UV-visible absorption and CD time course of [2Fe-2S] <sup>2+</sup> to [4Fe-4S] <sup>2+</sup> cluster conversion in FNR without repurification of [2Fe-2S] <sup>2+</sup> -FNR.....	264
Figure 5.7: UV-visible absorption and CD time course of [2Fe-2S] <sup>2+</sup> to [4Fe-4S] <sup>2+</sup> cluster conversion in FNR after repurification of [2Fe-2S] <sup>2+</sup> -FNR .....	266
Figure 5.8: Time course of air-exposure of [4Fe-4S]-FNR monitored by MS.....	268
Figure 5.9: Comparison of the resonance Raman spectra of the air-exposed samples of [4Fe- 4S] <sup>2+</sup> cluster-containing FNR and BioB .....	270
Figure 6.1: Proposed model for the cluster carrier and storage roles of CGFS-Grxs in Fe-S cluster biogenesis.....	288
Figure 6.2: Schematic representation of the proposed mechanisms for the maturation and repair of oxygen sensitive [4Fe-4S] <sup>2+</sup> cluster-requiring proteins.....	290

## CHAPTER 1

### INTRODUCTION AND LITERATURE REVIEW

#### **Background**

Iron-sulfur (Fe-S) clusters are among the most ancient and ubiquitous biological metal-containing cofactors. The cluster cores generally consist of non-heme irons bridged by inorganic sulfides that are attached to the protein primarily by cysteine residues, although partial ligation by histidine, serine, aspartate and arginine have also been observed. Since the discovery of the first Fe-S cluster-containing proteins, ferredoxins, in the early 1960s, the number of proteins utilizing Fe-S clusters as prosthetic groups (collectively known as Fe-S proteins) has greatly proliferated. Initially, Fe-S clusters were primarily appreciated for their role in mediating biological electron transfer. However the discovery of new types of Fe-S proteins have significantly extended the roles of biological Fe-S clusters beyond the classic electron transfer to include redox and non-redox catalysis, regulation of gene expression and enzymatic activity, disulfide reduction, radical generation, and DNA replication and repair. In addition, major advances in understanding Fe-S cluster biogenesis have been achieved through the critical discovery and identification of three bacterial Fe-S cluster assembly machineries comprising of highly conserved sets of genes that are present in most living organisms.

This literature review will begin with a summary of human diseases and disorders that have been found to be associated with impaired Fe-S cluster biogenesis. This will be followed by a brief introduction of the general structures, properties, physiological functions and biogenesis of biological Fe-S centers. The introduction of biosynthesis of Fe-S clusters will focus on the

current knowledge of three independent bacterial machineries dedicated to the maturation of Fe-S proteins. Monothiol glutaredoxins (Grxs) with CGFS active sites will also be discussed in light of their involvement in Fe-S cluster biogenesis and Fe regulation. In addition, an introduction to the bacterial fumarate and nitrate reduction (FNR) regulatory protein that utilizes an Fe-S cluster in O<sub>2</sub>-sensing will be included, focusing on investigations of its O<sub>2</sub>-sensing mechanism. A summary of the research results presented in this dissertation will be included at the end of this chapter.

### **Human diseases associated with defects in the Fe-S cluster biogenesis**

Because Fe-S clusters play essential roles in various fundamental life processes including respiration and a wide array of metabolic processes, substantial disruption of the assembly and repair of Fe-S clusters would inevitably lead to impairment of numerous basic cellular processes. Thus it is not surprising that defects in genes associated with Fe-S cluster biogenesis have been found as the cause of several human diseases and disorders.

The most well-known disease associated with impaired Fe-S cluster biogenesis is Friedreich's ataxia (FRDA), the most common recessive ataxia. FRDA is a neurodegenerative disease characterized by progressive gait and limb ataxia, dysarthria, muscle weakness, hypertrophic cardiomyopathy as well as diabetes (1). The cause of FRDA is a functional deficiency of a protein called frataxin as a result of unstable expansion of a GAA triplet-repeat in the intronic sequence of FXN gene (1). While the precise role remains controversial, frataxin has been proposed to play a role in the delivery of iron and/or the regulation of mitochondrial Fe-S cluster assembly (2). Consequently, analysis of tissue samples from FRDA patients revealed that enzymatic activities of two mitochondrial Fe-S proteins, aconitase and succinate dehydrogenase, were greatly impaired (3). Moreover, mitochondrial iron overload, a common feature of

disrupted human Fe-S cluster biogenesis, has also been observed in the hearts and brains of FRDA patients (4).

A hereditary myopathy with exercise and acidosis intolerance is another disease caused by disrupted Fe-S cluster biogenesis. Patients afflicted by this disease would develop muscle weakness, exercise-induced acidosis and myoglobinuria (5). Markedly reduced activities of Fe-S cluster-containing proteins from multiple respiratory chains and cytosolic aconitase have been observed in patients' muscle samples (6). Later, biochemical studies revealed that this myopathy was caused by a single point intronic mutation in the gene encoding human ISCU, the primary scaffold protein of mitochondrial Fe-S cluster assembly (7;8).

A fatal infantile encephalopathy and/or pulmonary hypertension affecting ten patients, leading to death before the age of 15 months with symptoms of failure to thrive, pulmonary hypertension, and neurological regression has been attributed to homozygous missense mutation in *NFUI* gene (9). The protein product encoded by *NFUI* gene is a mitochondria protein with an important role in Fe-S cluster biogenesis, and has been suggested to function in the delivery and maturation of a specific subset of mitochondrial Fe-S proteins (10). The biochemical phenotype of this disease revealed that the activities of two Fe-S enzymes, lipoic acid synthase and succinate dehydrogenase, were impaired (9). In addition, defects in the *NFUI* gene along with *BOLA3*, another mitochondrial gene proposed to be involved in Fe-S cluster biogenesis, have recently been identified as the cause of a rare autosomal recessive syndrome associated with severe pyruvate dehydrogenase complex (PDHc) deficiency and defects in multiple mitochondrial respiratory chain enzymes (11).

Sideroblastic anemias constitute a diverse class of inherited hematopoietic disorders characterized by deposition of iron in the mitochondria of red cell precursors (12). Thus far, two

forms of sideroblastic anemias have been associated with defects of Fe-S cluster biogenesis. X-linked sideroblastic anemia with cerebellar ataxia (XLSA/A) results from mutations in gene encoding ABCB7, an ATP-binding cassette transporter of the mitochondrial inner membrane that has a central role in mitochondrial export of a moiety required for assembly of cytosolic Fe-S clusters (13;14). The manifestations of XLSA/A include early onset non-progressive ataxia associated with severe cerebellar hypoplasia (15). Glutaredoxin 5 (Glx5) is a mitochondrial protein required for Fe-S cluster biogenesis, possibly via facilitating transfer of preassembled Fe-S clusters from scaffold proteins to target Fe-S proteins (*vide infra* for a detailed review) (16;17). A mutation in the gene encoding human Glrx5 leading to aberrant splicing was identified as the cause of one human patient with hypochromic, microcytic sideroblastic anemia associated with iron overload (18).

The diseases and disorders introduced above are the ones that have been unambiguously associated with abnormal Fe-S cluster biogenesis. Studies on the chromosomal locations of disease-causing genes and mammalian tissue culture models have suggested that many more diseases are likely to be attributed to defects in Fe-S cluster biogenesis (13;14). Thus understanding the mechanism of Fe-S biogenesis, including the assembly and transfer of Fe-S clusters to specific target proteins as well as the repair of damaged clusters, is of great importance to human health.

### **Structures and properties of biological Fe-S centers**

There are four fundamental types of biological Fe-S centers, namely Fe(SCys)<sub>4</sub>, Fe<sub>2</sub>(μ<sub>2</sub>-S)<sub>2</sub>(SCys)<sub>4</sub>, Fe<sub>3</sub>(μ<sub>2</sub>-S)<sub>3</sub>(μ<sub>3</sub>-S)(SCys)<sub>3</sub> and Fe<sub>4</sub>(μ<sub>3</sub>-S)<sub>4</sub>(SCys)<sub>4</sub> centers (Figure 1.1A, B, D, and E). By convention, they are often written as [2Fe-2S]<sup>2+,+</sup>, [3Fe-4S]<sup>+,0,2-</sup> and [4Fe-4S]<sup>3+,2+,+0</sup> with the superscript indicating the core oxidation states of the clusters. The formal oxidation states of Fe

can be  $\text{Fe}^{3+}$ ,  $\text{Fe}^{2+}$  or  $\text{Fe}^{2.5+}$  depending on the extent of valence (de)localization for the different types of cluster in each accessible redox state, assuming a formal oxidation state of  $-2$  for the bridging sulfides. The combined applications of X-ray absorption, electron paramagnetic resonance (EPR), Mössbauer, UV-visible absorption, circular dichroism (CD), variable-temperature magnetic circular dichroism (VTMCD), saturation magnetization, resonance Raman, nuclear vibrational resonance (NRV) and nuclear magnetic resonance (NMR) spectroscopies have contributed significantly to the characterizations of the electronic, magnetic and vibrational properties of Fe-S centers. A comprehensive understanding of the geometric and electronic structures of Fe-S centers is required for understanding both assembly and structure-function correlations. In this section, the four fundamental types of Fe-S centers are introduced, focusing on the ground state electronic, magnetic and redox properties of each type. The ranges of reported midpoint potentials (mV vs NHE) for the most common Fe-S cluster redox couples are shown in Figure 1.2 and the ground state spin ( $S$ ) and the extent of valence delocalization for each accessible oxidation states of the fundamental types of Fe-S centers are shown in Figure 1.3.

*Mononuclear Fe centers:* Lacking inorganic sulfides and hence not strictly a Fe-S cluster, mononuclear Fe centers with tetrahedral cysteinyl-S coordination (see Figure 1.1A) share fundamental structural, electronic and magnetic properties with Fe-S clusters and are often regarded as the simplest type of Fe-S center. They constitute the sole prosthetic groups of rubredoxins and desulfuredoxins, and as a result often referred to as rubredoxin-type (Rd-type) centers (19). Rd-type centers are often considered high potential centers as they can undergo one electron redox cycling between high-spin ( $S = 5/2$ )  $\text{Fe}^{3+}$  and high-spin ( $S = 2$ )  $\text{Fe}^{2+}$  with midpoint potentials in the range  $+300$  to  $-100$  mV (Figure 1.2).

*[2Fe-2S] clusters:* [2Fe-2S] clusters are the simplest form of Fe-S clusters. Generally, [2Fe-2S] clusters have complete cysteinyl ligation with each Fe atom tetrahedrally coordinated by two bridging inorganic sulfides and two cysteine residues (see Figure 1.1B). However, there are notable examples of [2Fe-2S] clusters with one or two non-cysteinyl ligands. The Rieske-type [2Fe-2S] clusters, shown in Figure 1.1C, are coordinated by two cysteine ligands to one Fe site and two histidyl ligands to the reducible Fe site (20). A subunit-bridging [2Fe-2S] cluster in *S. cerevisiae* Grx3/4-Fra2 complex ligated by two cysteine and one histidine residues has been recently characterized with the nature of the fourth ligand remains unresolved (21). Furthermore, [2Fe-2S] clusters ligated by one histidine and three cysteine ligands have been identified in mitoNEET (22-24) and bacterial transcription factor IscR (25). Other examples of [2Fe-2S] centers with one non-cysteinyl ligand include the aspartate ligand in succinate dehydrogenases (26) and sulfide dehydrogenases (27) and arginine ligand in biotin synthase (28).

Only [2Fe-2S] clusters with 2+ and 1+ core states have been observed under physiological conditions. Redox potentials for the [2Fe-2S]<sup>2+,+</sup> couple range from +100 to -460 mV for all-cysteinyl-ligated centers while Rieske-type centers usually have higher potentials (+380 to -150 mV) due to the presence of more electropositive histidine ligands at the reducible Fe site (Figure 1.2). The redox potentials for the [2Fe-2S]<sup>+,0</sup> couple is ~ 1.0 V lower than the [2Fe-2S]<sup>2+,+</sup> couple (29). Due to the low potential required for its formation, all-cysteine-ligated [2Fe-2S]<sup>0</sup> clusters are unstable under physiological conditions and have only been observed in synthetic analogues (30) and artificially modified protein (31). Thus far, the Rieske-type center provides the only known example of a stable all-ferrous [2Fe-2S]<sup>0</sup> cluster, stabilized by protonation of one of the  $\mu_2$ -sulfides with [2Fe-2S]<sup>+,0</sup> couple redox potential at -0.73 V at pH 7 (29).

The ground state electronic properties of [2Fe-2S] clusters are summarized in Figure 1.3. Both fully oxidized [2Fe-2S]<sup>2+</sup> and fully reduced [2Fe-2S]<sup>0</sup> clusters have a  $S = 0$  ground state as a result of antiferromagnetic exchange between two high-spin ( $S = 5/2$ ) ferric and between two high-spin ( $S = 2$ ) ferrous ions, respectively. In contrast, the one electron reduced [2Fe-2S]<sup>+</sup> clusters can exist in two electronic ground states. All biological [2Fe-2S]<sup>+</sup> clusters present in wild-type proteins exhibit a valence-localized  $S = 1/2$  ground state due to antiferromagnetic coupling of the high-spin ( $S = 5/2$ ) ferric and high-spin ( $S = 2$ ) ferrous sites. In contrast, Cys-to-Ser mutations at the reducible Fe site of the cluster in *Clostridium pasteurianum* 2Fe ferredoxin revealed a valence-delocalized [2Fe-2S]<sup>+</sup> cluster with  $S = 9/2$  ground state that results from ferromagnetic coupling (32-34). It is worth mentioning that the valence-delocalized  $S = 9/2$  [2Fe-2S]<sup>+</sup> units are an important building block of all higher nuclearity clusters.

*[4Fe-4S] clusters:* [4Fe-4S] clusters, depicted in Figure 1.1E, are the most common type of Fe-S clusters. While the majority of biological [4Fe-4S] clusters have complete cysteinyl ligation, there are a few notable exceptions. For example, some ferredoxins have [4Fe-4S] clusters with an aspartate ligand at one Fe site (35) and the [4Fe-4S] clusters in both NiFe and Fe-hydrogenases and nitrate reductases have a single histidine ligand (36-38). In addition, [4Fe-4S] clusters in (de)hydratases (39;40) and radical-SAM enzymes (41;42) all have a unique Fe site that is not protein-bound and functions to bind and active the substrate (see Figures 1.4A and D, respectively).

Biological [4Fe-4S] clusters can exist in 3+, 2+, 1+ and 0 core oxidation states and exhibit wide range of redox potentials (Figures 1.2 and 1.3). The HiPIP (high potential iron-sulfur protein)-type centers cycle between [4Fe-4S]<sup>3+,2+</sup> couple with redox potential ranging between +500 to + 50 mV. The [4Fe-4S]<sup>2+,+</sup> couple usually has a lower redox potential with

midpoint potentials between +80 to -170 mV. The [4Fe-4S] cluster in nitrogenase Fe protein differs from others as it is stable in three redox states 2+, 1+ and 0 and has the ability to serve as a two-electron donor (43-45).

The ground state electronic and magnetic properties of [4Fe-4S] clusters are more complicated than other types of Fe-S clusters and, to some extent, can be interpreted in terms of antiferromagnetic interactions involving one or two  $S = 9/2$  valence-delocalized [2Fe-2S] units (Figure 1.3). The  $S = 0$  ground state of the [4Fe-4S]<sup>2+</sup> cluster results from antiferromagnetic coupling between two  $S = 9/2$  valence-delocalized [2Fe-2S]<sup>+</sup> fragments. However, one valence-localized Fe<sup>3+</sup>Fe<sup>2+</sup> pair has been observed for the [4Fe-4S]<sup>2+</sup> clusters in two-electron reduced ferredoxin-thioredoxin reductase (FTR) (46) and in pyruvate formate-lyase activating enzyme (PFL-AE) (47). For [4Fe-4S]<sup>3+</sup> clusters, the  $S = 1/2$  ground state spin can be considered as a result of coupling between a  $S = 5$  Fe<sup>3+</sup>Fe<sup>3+</sup> pair and a  $S = 9/2$  valence-delocalized Fe<sup>3+</sup>Fe<sup>2+</sup> pair. Similarly, to a first approximation, the  $S = 1/2$  ground-state spin of the [4Fe-4S]<sup>+</sup> cluster can be considered to result from a ferromagnetically coupled  $S = 4$  Fe<sup>2+</sup>Fe<sup>2+</sup> pair coupled to  $S = 9/2$  Fe<sup>3+</sup>Fe<sup>2+</sup> pair. However, NMR studies have indicated the valence-delocalized pair in [4Fe-4S]<sup>3+</sup> clusters can reside on different [2Fe-2S]<sup>+</sup> rhombs, indicating fluxional behavior (48). Furthermore, for the delocalized pair in [4Fe-4S]<sup>3+</sup> and [4Fe-4S]<sup>+</sup> clusters,  $S = 7/2$ , and  $S = 9/2$  and  $7/2$  mixed spin systems have also been observed (49;50). While both [4Fe-4S]<sup>3+</sup> and [4Fe-4S]<sup>+</sup> clusters have  $S = 1/2$  ground spin, they can be distinguished by EPR spectroscopy. The [4Fe-4S]<sup>3+</sup> clusters generally exhibit axial EPR signals with  $g_{\text{ave}} > 2.0$ , whereas the [4Fe-4S]<sup>+</sup> clusters usually have a rhombic EPR signal with  $g_{\text{ave}} < 2.0$ . The rhombic EPR signals of  $S = 1/2$  [4Fe-4S]<sup>+</sup> clusters are fast relaxing and broaden significantly at temperatures above 30 K, thus can be further distinguished from similar EPR signals of  $S = 1/2$  [2Fe-2S]<sup>+</sup> clusters. Finally, for

the  $[4\text{Fe-4S}]^0$  cluster, the ground state has been determined to be  $S = 4$  based on EPR and Mössbauer from studies of the nitrogenase Fe protein (44).

In addition to archetypal  $[4\text{Fe-4S}]$  clusters introduced above, recent crystallography studies have led to identification of a novel type of cluster that contains four irons. Originally identified as a  $[4\text{Fe-4S}]$  cluster with unique properties to physiologically switches between what were then believed to be 3+, 2+, and 1+ oxidation states within a small potential range, the Fe-S cluster located proximal to the active site in the oxygen-tolerant NiFe-hydrogenase has recently proven to be an unprecedented  $[4\text{Fe-3S}]$  cluster (51;52). This  $[4\text{Fe-3S}]$  cluster is coordinated by six cysteine residues with the two additional cysteines ligating three of the four iron atoms at open face resulted from the absence of one bridging sulfide. The biologically accessible oxidation states for the  $[4\text{Fe-3S}]$  cluster have been determined to be +5, +4, and +3.

*[3Fe-4S] clusters:* The majority of  $[3\text{Fe-4S}]$  cluster exist in cubane form shown in Figure 1.1D. However,  $[3\text{Fe-4S}]$  clusters with a linear arrangement have also been reported in proteins. The cuboidal  $[3\text{Fe-4S}]$  cluster can be visualized as a cubane-type  $[4\text{Fe-4S}]$  cluster core minus one Fe. In fact, oxidative degradation of biological cubane-type  $[4\text{Fe-4S}]$  clusters often results in cubane  $[3\text{Fe-4S}]$  centers. However, there are proteins with cubane  $[3\text{Fe-4S}]$  clusters as intrinsic prosthetic groups (53). Unlike  $[2\text{Fe-2S}]$  and  $[4\text{Fe-4S}]$  clusters, all biological cubane  $[3\text{Fe-4S}]$  clusters are ligated exclusively by cysteine residues with tetrahedral coordination at each Fe site. As shown in Figures 1.2 and 1.3, the physiologically relevant cubane  $[3\text{Fe-4S}]^{+,0}$  couple has redox potential ranging from +90 to -460 mV. The 2- redox state of the cubane  $[3\text{Fe-4S}]$  cluster is also accessible with midpoint potential  $\sim -700$  mV at pH 7 for the  $[3\text{Fe-4S}]^{0,2-}$  pair (54). However, this redox potential is strongly pH dependent, requiring uptake of three protons and seems unlikely to be physiologically relevant. In oxidized cuboidal  $[3\text{Fe-4S}]^+$  clusters, the three

high-spin ( $S = 5/2$ ) ferric sites are antiferromagnetically coupled, yielding an  $S = 1/2$  ground state, while in the one-electron-reduced  $[3\text{Fe-4S}]^0$  cluster, the  $S = 2$  ground state arises from antiferromagnetic interaction between an  $S = 9/2$  valence-delocalized  $\text{Fe}^{2+/3+}$  pair and a valence localized high spin ( $S = 5/2$ ) ferric site (Figure 1.3).

The linear-type  $[3\text{Fe-4S}]^+$  cluster is a uncommon type of Fe-S clusters. It was first reported by Hagen and coworkers in 1983 in a systematic study of synthetic analogues of Fe-S clusters (55). The initial observation of a protein-bound linear  $[3\text{Fe-4S}]^+$  cluster occurred a year later via incubation of cubane-type  $[3\text{Fe-4S}]^+$  cluster containing aconitase under alkaline conditions or in the presence of a denaturing agent (56). The linear  $[3\text{Fe-4S}]^+$  cluster in partially unfolded aconitase was definitely identified via combined spectroscopic characterizations and comparison with the synthetic analogue and till now provides the only example of an extensively characterized protein-bound linear  $[3\text{Fe-4S}]^+$  cluster (55-58). While direct structural characterization of a protein-bound linear  $[3\text{Fe-4S}]^+$  cluster is not currently available, it is clearly structurally analogous to the synthetic linear  $[3\text{Fe-4S}]^+$  compound based on its distinctive electronic and magnetic properties. Hence, the linear  $[3\text{Fe-4S}]^+$  cluster from aconitase consists of three Fe atoms each resides in a tetrahedral environment of sulfur atoms with cysteinyl-S completing the coordination at the two terminal Fe sites (55;56). The linear  $[3\text{Fe-4S}]^+$  cluster has only been identified in the 1+ oxidation state. The  $S = 5/2$  ground state spin for linear  $[3\text{Fe-4S}]^+$  cluster is a result of spin-coupling of the three high-spin ( $S = 5/2$ ) ferric sites, with the spin of the central Fe site being antiparallel to those of the two terminal Fe sites (55;56). The coupling has been shown to be highly asymmetric coupling due to the linear structural arrangement, with the central Fe site strongly spin-coupled to both terminal Fe sites and the terminal Fe sites exhibiting only weak exchange interaction among themselves (55;56). Since the discovery of protein-bound

linear  $[3\text{Fe-4S}]^+$  cluster in aconitase, their presence have been reported in reconstituted human cytosolic IRP1 based on EXFAS and EPR evidence (59) and in anaerobically isolated PFL-AE judged by Mössbauer data (60). Moreover, based on absorption data alone, linear  $[3\text{Fe-4S}]^+$  clusters have been reported in several ferredoxins under denaturing conditions. However, definitive evidence for the presence of linear  $[3\text{Fe-4S}]^+$  clusters in these proteins requires further investigation (61-64). Thus far, there has been no evidence of linear  $[3\text{Fe-4S}]^+$  clusters performing any known physiological functions.

*Cluster with higher nuclearity:* The  $[8\text{Fe-7S}]$  P-cluster in the FeMo subunit of the Mo-dependent nitrogenase can be visualized as two  $[4\text{Fe-3S}]$  fragments fused by a  $\mu_6\text{-S}^{2-}$  and two  $\mu_2$ -bridging cysteine residues in the all-ferrous redox state (see Figure 1.1F). The double cubane P-cluster exclusively participates in mediating electron transfer from the  $[4\text{Fe-4S}]$  cluster in the Fe protein subunit of nitrogenase to the FeMo cofactor located in FeMo subunit. The P-cluster can exist in two stable redox states, the all-ferrous  $[8\text{Fe-7S}]^{2+}$  state ( $\text{P}^{\text{N}}$ ) and the two-electron oxidized  $[8\text{Fe-7S}]^{4+}$  state ( $\text{P}^{\text{OX}}$ ) (65;66). In addition, a transient  $[8\text{Fe-7S}]^{3+}$  state has also been observed. The P-cluster differs from other types of Fe-S centers in that the oxidation from  $\text{P}^{\text{N}}$  to  $\text{P}^{\text{OX}}$  is accompanied by a dramatic structural change of the cluster core, which includes cleavage of two Fe- $(\mu_6\text{-S})$  bonds and recruiting a serine residue and a backbone amide nitrogen to maintain the tetracoordinated Fe sites (65). Furthermore, the observation that the  $[8\text{Fe-7S}]^{2+/4+}$  couple is the most stable redox pair raises the possibility that the double cubane P-cluster may have the ability to mediate two-electron transfer (67-69).

### **Cluster conversions**

Fe-S clusters have demonstrated remarkable ability for facile conversion and interconversion in both free and protein-bound conditions. The literature review here focuses on

the biological cluster conversions. The conversions observed for synthetic analogues of Fe-S clusters have been reviewed elsewhere (70). Biological Fe-S clusters can undergo rearrangement into other structural types in response to changes in environmental or intracellular conditions, such as exposure to O<sub>2</sub> or NO, chemical oxidants and reductants, denaturants, or changes in pH. Since the cluster transformations are often accompanied by changes in local protein structures, they sometimes provide means for regulating gene expression or enzymatic activity in response to external stimuli. In addition, cluster interconversions are also of great importance in understanding Fe-S cluster biogenesis. The most common types of cluster conversions include interconversions between [4Fe-4S] and cubane-type [3Fe-4S] clusters, and between [4Fe-4S] and [2Fe-2S] clusters. A summary of the types of cluster conversions observed in Fe-S cluster-containing proteins is presented in Figure 1.4.

Aconitase provides a well-studied example of cluster conversions as it can accommodate a variety of different Fe-S clusters. Aconitase in its active form contains a [4Fe-4S]<sup>2+,+</sup> cluster with a unique Fe site ligated by water or hydroxyl group (39). Aerobic isolation or air-exposure of the [4Fe-4S]<sup>2+,+</sup> cluster-containing aconitase leads to oxidative removal of the unique Fe and results in an inactive enzyme with a cuboidal [3Fe-4S]<sup>+</sup> cluster (71). The catalytically active [4Fe-4S]<sup>2+,+</sup> center can be restored under reducing conditions as the [3Fe-4S]<sup>0</sup> cluster is able to readily incorporate Fe<sup>2+</sup>. In addition to aconitase, this type of reversible conversion between [4Fe-4S] and cuboidal [3Fe-4S] clusters is commonly observed in the presence of O<sub>2</sub> or strong oxidants such as ferricyanide, particularly for proteins containing [4Fe-4S] clusters with noncysteinylligation at a specific Fe site (53). Furthermore, when reduced to 0 oxidation state, the cubane [3Fe-4S] clusters also exhibit the ability to readily bind divalent transitional metal ions other than Fe, to form heterometal [M-3Fe-4S]<sup>2+</sup> cubane clusters (M = Mn, Co, Ni, Zn, Cd),

as demonstrated in bacterial ferredoxins (72;73). In addition, the aconitase cuboidal  $[3\text{Fe-4S}]^+$  cluster is unique as it can undergo rearrangement to generate a linear  $[3\text{Fe-4S}]^+$  cluster when exposed to  $\text{pH} > 9$  or incubated with urea (56). It is remarkable that in the newly formed linear  $[3\text{Fe-4S}]^+$  cluster, two of the original cysteine ligands are retained and two remote cysteine ligands are recruited, necessitating a major protein structural conformational change. Reduction of the linear  $[3\text{Fe-4S}]^+$  cluster leads to the reformation of the active  $[4\text{Fe-4S}]^{2+,+}$  cluster in the presence of  $\text{Fe}^{2+}$  (56). Simultaneously, a significant amount of  $[2\text{Fe-2S}]^{2+}$  cluster was also formed, in addition to linear  $[3\text{Fe-4S}]^+$  cluster, during denaturation of aconitase (~ 30% of original cuboidal  $[3\text{Fe-4S}]^+$  cluster) (56).

The nitrogenase Fe protein is an ATP-binding,  $[4\text{Fe-4S}]$  cluster-containing homodimeric protein. It has been known since 1984 that when exposed to Fe chelators in the presence of MgATP, the  $[4\text{Fe-4S}]^{2+}$  cluster in the nitrogenase Fe protein can be converted to a  $[2\text{Fe-2S}]^{2+}$  cluster (74;75). Later, crystallographic and spectroscopic studies of a mimic of the MgATP-bound form of the Fe protein have revealed a glycerol-induced cleavage of the  $[4\text{Fe-4S}]^{2+}$  cluster into two  $[2\text{Fe-2S}]^+$  fragments (76). The two  $[2\text{Fe-2S}]^+$  units are separated by 5 Å and the coordination is quite unusual with each fragment having one cysteinyl ligand at each Fe site and glycerol molecule serving as a bidentate bridging ligand. The reversible conversion from the two  $[2\text{Fe-2S}]^+$  fragments to form a  $[4\text{Fe-4S}]^+$  cluster occurs on reduction.

A well-documented example of  $[4\text{Fe-4S}]$  to  $[2\text{Fe-2S}]$  cluster conversion without outside intervention, such as addition of chelators, detergents, alkali, or other non-physiological agents, is provided by fumarate and nitrate reduction regulatory protein (FNR). Under strictly anaerobic conditions, FNR exists as homodimer with one  $[4\text{Fe-4S}]^{2+}$  cluster in each subunit. Upon exposure to  $\text{O}_2$ , the  $[4\text{Fe-4S}]^{2+}$  cluster undergoes rapid reversible conversion to a more stable

[2Fe-2S]<sup>2+</sup> cluster (77). Subsequently, O<sub>2</sub>-induced degradation of [4Fe-4S] clusters via a semi-stable [2Fe-2S] cluster intermediate has been observed for numerous proteins, including the SAM-binding [4Fe-4S] cluster in almost all radical-SAM enzymes (78-81). In addition, reductive coupling of [2Fe-2S] clusters to form [4Fe-4S] clusters has also been demonstrated in two primary scaffold proteins in Fe-S cluster biogenesis, namely IscU from *E. coli* and NifU (N-terminal domain) from *A. vinelandii* (82-84). Taken together, the reversible conversion between [4Fe-4S]<sup>2+</sup> and [2Fe-2S]<sup>2+</sup> clusters observed in the proteins mentioned above are of great importance in providing insights into the understanding of the mechanism of oxidative degradation of [4Fe-4S] clusters and of assembly of biological Fe-S clusters.

### **Functions of biological Fe-S centers**

*Electron transfer:* Electron transfer is the most common function of Fe-S centers. It takes advantage of the wide range of physiologically accessible redox potentials of Fe-S centers which depend on the cluster type, specific redox couple and the protein environments, as shown in Figure 1.2. The types of biological Fe-S centers involved in electron transfer include Rd-type center, conventional and Rieske-type [2Fe-2S] clusters, cubane-type [3Fe-4S] clusters, [4Fe-4S] clusters, and double-cubane [8Fe-7S] clusters. The Fe-S center-containing proteins that perform electron transfer roles can usually be classified into mobile electron carrier proteins, membrane-bound enzyme complexes and soluble redox enzymes. Fe-S centers participating in electron transport can often form chains with close proximity (edge-to-edge distances of 4 to 14 Å) to allow efficient tunneling of electrons, thus obviating the need for specific through-bond electron transfer pathways (85). Thus Fe-S centers are major components in the membrane-bound respiratory and photosynthetic electron transport chain, and constitute intramolecular electron transport chains in numerous redox enzymes. A well-characterized example of electron transfer

chain facilitated by Fe-S clusters is the mitochondrial respiratory complex, which contains a total of thirteen Fe-S clusters (one [3Fe-4S] cluster, one Rieske-type and three conventional [2Fe-2S] clusters, and eight [4Fe-4S] clusters) in order to transfer electrons from NADH, succinate, and the  $\beta$ -oxidation of fatty acids to effect the four-electron/four-proton reduction of  $O_2$  to  $H_2O$  (86).

*Enzyme catalysis:* In addition to functioning in directing electron transfer, Fe-S clusters also constitute, in whole or in part, the catalytic active-site center of a number of redox and non-redox enzymes to facilitate substrate binding and activation.

Aconitase, the enzyme that catalyzes the reversible stereospecific isomerization of citrate into isocitrate, provides a classic example of Fe-S cluster serving as the catalytic center. Aconitase belongs to a large family of (de)hydratases that contain a  $[4Fe-4S]^{2+}$  cluster with a unique non-protein-coordinated Fe site that functions as a Lewis acid to assist reversible abstraction of the hydroxyl group and a proton from adjacent carbons on the substrate (see Figure 1.5A) (39;40). A similar approach utilizing a [4Fe-4S] cluster with a unique non-cysteine-ligated Fe as active site is adopted by radical-SAM (*S*-adenosylmethionine) superfamily of enzymes that catalyze diverse array of radical reactions and are heavily involved in the biosynthesis of numerous DNA precursors, vitamins, cofactors and antibiotics (41;87). The active-site structure of radical SAM enzymes is shown in Figure 1.5D. Unlike the clusters in (de)hydratases, which are redox inert, the [4Fe-4S] clusters in radical-SAM enzymes are redox-active and facilitate the reductive cleavage of SAM to yield a highly reactive 5'-deoxyadenosyl radical which then subsequently generates a substrate or protein radical via hydrogen abstraction, in order to initiate a radical reaction.

A different approach for facilitating substrate binding is via incorporation of a heterometal site into Fe-S cluster at the active site of the enzymes. Molybdenum-dependent

nitrogenase is one type of nitrogenase that catalyze the ATP-driven eight-electron and eight-proton reduction of dinitrogen to yield ammonia and hydrogen gas (88). The molybdenum nitrogenase is comprised of two subunits: a [4Fe-4S] cluster containing Fe protein, and a MoFe protein subunit containing the [8Fe-7S] P-cluster and a Fe-S cluster-based FeMo cofactor (FeMo-co). During the catalytic cycle, ATP-dependent electron flow from the [4Fe-4S] cluster in the Fe protein is transferred via the P-cluster to the FeMo-co where substrate binding and reduction takes place (67). The [Mo-7Fe-9S-C] FeMo-co active site, shown in Figure 1.5C, can be visualized as a [4Fe-3S] partial cubane cluster bridged to a [Mo-3Fe-3S] partial cubane center via three ( $\mu_2$ -S) sulfides and one central  $\mu_6$ -carbon atom (89;90). However, the precise role of the Mo site in catalysis has yet to be defined. Another example is the nickel-requiring CO dehydrogenase which catalyzes the reversible reduction of CO<sub>2</sub> to CO. The novel [Ni-4Fe-5S] active center of CO dehydrogenase, which is structurally best considered as a [3Fe-4S] fragment covalently attached to a  $\mu_2$ -S-bridged NiFe fragment via the three  $\mu_3$ -bridging S atoms (Figure 1.5B). In this case, the square planar Ni site provides the site of CO binding (91).

A third method employed to functionalize Fe-S clusters for enzymatic activities involves attaching an additional metal site via a bridging cysteinyl-S to an Fe site in a [4Fe-4S] cluster for substrate binding. In this case the [4Fe-4S] cluster provides the conduit of direct electron transfer to the active site. Examples of enzymes utilizing this approach include sulfite and nitrite reductase which uses a siroheme as the substrate binding site (Figure 1.5E) (92;93), acetyl-CoA synthase which uses a dinickel center to facilitate CO insertion into a Ni-CH<sub>3</sub> bond for formation of an acetyl group (Figure 1.5F) (94-96), and Fe-hydrogenase that utilizes a novel organometallic diiron center to catalyze reversible H<sub>2</sub> production from protons and electrons via a heterolytic mechanism (Figure 1.5G) (37;97).

*Regulation of gene expression and enzymatic activity:* Fe-S clusters in a number of proteins are responsive to a variety of environmental stimuli that results in protein conformational changes, thereby facilitating roles in the regulation of gene expression or enzymatic activity. Encounters with external stimuli usually result in two distinct types of effects on the sensory Fe-S centers in the regulatory proteins (98). The first involves cluster rearrangement or total disassembly, and requires auxiliary agents or enzymes for reversal. The second effect is alternation in oxidation states of the Fe-S cluster core, which is readily reversible, depending on the prevalent redox potential or the specific oxidant present. Nevertheless, each class of regulatory protein utilizes a distinct sensing mechanism.

One of the best characterized Fe-S cluster-containing gene regulatory proteins is the bacterial transcriptional regulator of fumarate and nitrate reduction (FNR) (99;100). FNR regulates the expression of over 100 genes in response to the prevailing O<sub>2</sub> levels via the lability of its [4Fe-4S]<sup>2+</sup> cluster (77). Transcriptionally active FNR exists in a dimeric form containing a [4Fe-4S]<sup>2+</sup> cluster in the sensory domain and binds target promoters with high affinity. Upon exposure to elevated O<sub>2</sub> levels, the FNR [4Fe-4S]<sup>2+</sup> cluster degrades via a [2Fe-2S]<sup>2+</sup> cluster-bound form to an apo form with concomitant dimer-to-monomer conversion and loss of site-specific DNA-binding, thus becoming inactive as a transcriptional regulator. In addition to O<sub>2</sub>, the [4Fe-4S]<sup>2+</sup> cluster in FNR also appears to be degraded by NO with the formation of a dinitrosyl-iron-cysteine complexes and loss of transcriptional regulator activity (101). However, the physiological significance of this reaction remains to be determined. A more detailed introduction to FNR and the mechanism of O<sub>2</sub>-induced [4Fe-4S] degradation will be presented later in this chapter since it constitutes one of the primary goals of this work.

IscR is an Fe-S cluster-containing transcription factor that is able to regulate the expression of more than 40 genes depending on cellular demands for Fe-S cluster biogenesis and oxidative stress (102). *E. coli* IscR can exist in both an apo form devoid of clusters and a holo form containing a [2Fe-2S] cluster that can be reversibly oxidized and reduced (25;103). The [2Fe-2S] cluster-bound IscR functions as a direct negative regulator of the *isc* operon which comprises genes encoding for the housekeeping Fe-S cluster assembly pathway. The proposed feedback regulation mechanism suggests that IscR competes with apo proteins for clusters under conditions that require increased levels of Fe-S cluster biosynthesis, such as oxidative stress, thereby coupling Fe-S cluster assembly to the cellular requirement for cluster synthesis (103). In contrast, the apo form of IscR has an extended role as a global regulator of a number of Fe-S protein genes, including activation of the transcription of the *suf* operon which encodes the bacterial backup Fe-S cluster assembly system under oxidative stress or iron starvation conditions (102). Using the combination of DNase footprinting and bioinformatics methods, Giel and coworkers have demonstrated that the DNA-binding domain in IscR can recognize two different DNA sequences, one of which appears to be specific for repression of the *isc* operon (102).

Similar to IscR, the mammalian cytosolic iron-regulatory protein 1 (IRP1) that functions as a translational regulator in response to cellular iron availability also employs a mechanism involving cluster assembly (39). When iron is limited, IRP1 exists in an apo form devoid of clusters and binds to iron responsive elements (IREs) in the specific stem-loop RNA structures in the untranslated regions of the messenger RNAs of proteins involved in the uptake, storage and export of iron in the cell (104;105). Under Fe-replete conditions, IRP1 acquires a [4Fe-4S] cluster, thereby losing its ability to bind IREs, but enabling it to function as cytosolic aconitase

catalyzing the reversible stereospecific isomerization of citrate into isocitrate via a cis-aconitate intermediate (39). Hence IRP proteins in bacteria and eukaryotes appear to exhibit dual catalytic and regulatory roles (106-109). Although the specific mRNA binding structures recognized by bacterial apo aconitases have not been firmly established, they have been speculated to be similar to the stem-loop structures recognized by eukaryotic IRPs (106-108;110).

NsrR is a dedicated sensor of NO as well as other reactive nitrogen species (111). Thus far, there is no consensus regarding the type of Fe-S cluster in the active form of NsrR, as both [2Fe-2S] and [4Fe-4S] clusters have been observed in NsrR proteins from various organisms (112-114). However, the available evidence suggests that cluster-containing NsrR is the active form functioning as transcriptional repressor by binding specifically to target promoters (112;113). The DNA-binding activity is lost on exposure of NsrR to NO, probably due to the degradation of the cluster and the formation of dinitrosyl iron complexes, thus relieving the repression of genes involved in NO detoxification and NO damage repair.

SoxR is a well-known stress-responsive transcriptional regulator that is activated under oxidative stress conditions. Unlike the aforementioned Fe-S cluster-containing regulatory proteins, SoxR senses the oxidative stress via reversible one-electron oxidation of a [2Fe-2S]<sup>+</sup> cluster (115;116). Upon exposure to O<sub>2</sub><sup>-</sup>, the [2Fe-2S]<sup>2+</sup> cluster-bound SoxR activates the expression of *soxS* gene, which then in turn enhances the expression of a number of genes whose products function in removal of superoxide and repair of oxidative damage (117). Although both apo and the [2Fe-2S]<sup>+</sup> cluster-containing forms of SoxR can bind to *soxS* promoter DNA with the same affinity as the oxidized [2Fe-2S]<sup>2+</sup> cluster-bound SoxR, only the latter form is capable in activating the transcription of *soxS* gene (116). This is attributed, in light of the crystal structure of the SoxR–DNA complex, to redox-dependent structural changes of SoxR and the

target promoter resulted from the asymmetric charge distribution of the [2Fe-2S] cluster environment in SoxR (118).

In addition to regulation of gene expression, there are also a few examples of regulation of enzymatic activity using non-catalytic Fe-S clusters. The best characterized example is the [4Fe-4S] cluster-containing phosphoribosylpyrophosphate (PRPP)-amidotransferase from *Bacillus subtilis* that catalyzes the first step in purine nucleotide biosynthesis (119). The oxygen sensitive [4Fe-4S] cluster is required for the enzymatic activity of PRPP-amidotransferase, and the O<sub>2</sub>-induced destruction of the cluster results in the protein becoming vulnerable towards proteolytic degradation (120). As a result, the [4Fe-4S] cluster in PRPP-amidotransferase is able to function as an O<sub>2</sub> sensor for the regulation of purine biosynthesis. Another example is provided by ferrochelatase, the enzyme that catalyzes the last step of heme biosynthesis. Early studies demonstrated that most bacterial ferrochelatases characterized do not possess Fe-S clusters, while mammalian ferrochelatases contain a [2Fe-2S] cluster that is essential for activity but has no apparent catalytic function (121-123). As the [2Fe-2S] clusters were found to be sensitive to NO-induced degradation, it was suggested that incorporation of the cluster in mammalian ferrochelatases was adapted as a defense mechanism against bacterial infection by preventing pathogens from using heme made by the host (121;124). However, the later discovery that some bacterial ferrochelatases contain [2Fe-2S] cluster appears to call for reevaluation of this hypothesis (125). Recently Albetel and coworkers have demonstrated that the [2Fe-2S] clusters in both eukaryotic and prokaryotic ferrochelatase are degraded by NO at similar rates, and have raised possibility that the [2Fe-2S] centers in ferrochelatases function to sense cellular levels of [2Fe-2S] clusters as part of a general oxidative stress response mechanism (126).

*Disulfide reduction:* While the two-electron reduction of biological disulfides is generally achieved by a family of flavoproteins that use NADPH as two-electron donor, three unique types of  $[4\text{Fe-4S}]^{2+}$  cluster-containing enzymes have been reported to catalyze the cleavage of disulfides in two sequential one-electron steps using a  $[4\text{Fe-4S}]$  active site. Ferredoxin-thioredoxin reductase (FTR), the plant enzyme that catalyzes the light-mediated reduction of thioredoxin disulfides, contains an active site comprising a  $[4\text{Fe-4S}]^{2+}$  cluster and a nearby asymmetrically disposed cysteine disulfide (127;128). The proposed catalytic mechanism for FTR suggests that the cluster center does not directly interact with the substrate disulfide, rather the reduction of the thioredoxin disulfide involves one-electron oxidation of the  $[4\text{Fe-4S}]^{2+}$  cluster, coupled with two-electron oxidation of the FTR disulfide, to yield a  $[4\text{Fe-4S}]^{3+}$  cluster with a specific Fe site ligated by two cysteine residues and the formation of mixed thioredoxin/FTR disulfide (46;127;128). A further one-electron reduction by ferredoxin results in reduction of the  $[4\text{Fe-4S}]^{3+}$  cluster, restoration of the FTR disulfide, and cleavage of the thioredoxin disulfide. Recently, a  $[4\text{Fe-4S}]^{2+}$  cluster with similar environment to that of FTR has been characterized in one of the NiFe-hydrogenase maturation proteins, HypD, which has been suggested to initiate a disulfide redox cascade in a similar fashion to release cyanide from a cysteine thiocyanate for the formation of NiFe-hydrogenase active site (129). In contrast, the active site  $[4\text{Fe-4S}]^{2+}$  cluster in the methanogenic heterodisulfide reductase (HDR), the enzyme that catalyzes the reduction of CoM-S-S-CoB to Coenzyme M (CoM-SH) and Coenzyme B (CoB-SH), directly interacts with the substrate to cleave the CoM-S-S-CoB heterodisulfide via a similar mechanism involving two sequential one-electron steps (130).

*DNA replication and repair:* Recent years have witnessed the discovery of rapidly growing classes of Fe-S cluster-containing enzymes involved in DNA metabolism, including

DNA primases, polymerases, glycosylases and helicases. The Fe-S clusters found in these enzymes do not directly participate in catalysis but have been shown in all cases to be critical for enzymatic activity.

DNA primase catalyzes the synthesis of short RNA primers required to initiate DNA replication. The presence of an Fe-S cluster has been reported in human DNA primases, and has been identified as a HiPIP-like [4Fe-4S] cluster (131). While the presence of the cluster does provide structural stability, its specific function remains unclear. However, a putative role for the cluster in controlling the length of the primer strand has been suggested. Recently, it has also been demonstrated that eukaryotic DNA polymerases contain a [4Fe-4S] cluster (132). The physiological role of the [4Fe-4S] cluster has yet to be defined, but it is essential for stabilizing the DNA polymerase by enabling complex formation within subunits and/or maintaining the catalytic polymerases subunit with its respective accessory proteins. Several Fe-S cluster-containing DNA glycosylases are involved in base excision repair, including MutY, thymine-DNA, endonuclease III, and the family of 4 uracil-DNA glycosylases, and have been shown to contain a redox-active [4Fe-4S]<sup>3+,2+</sup> cluster when bound to DNA (133-135). Initially, the cluster was thought to simply play a structural role, possibly in substrate recognition. However, later studies have revealed that the DNA-mediated cluster redox activity functions in locating damaged DNA bases by mediating electron transfer through the  $\pi$ -stacked base pairs (135). Similar functions have also been suggested for the [4Fe-4S] clusters present in several DNA nucleotide excision repair helicases, including XPD (xeroderma pigmentosum complementation group D) (Rad3 in yeast) and FanJ (Fanconi J cross-link repair helicase) (136-138).

*Iron and/or cluster storage:* Following the discovery of polyferredoxins in methanogenic archaea containing up to 12 [4Fe-4S] clusters in six tandemly repeated 8Fe ferredoxin-like

domains, a role for polyferredoxins and 8Fe ferredoxins in bacterial iron and/or cluster storage has been proposed (139). Further support for this proposal comes from the observation that genes encoding polyferredoxins have been found in operons encoding enzymes with large demands for [4Fe-4S] clusters, such as hydrogenase (140;141). Since the current consensus is that Fe-S clusters are assembled on scaffold proteins from Fe-S cluster biogenesis pathways, it is likely that polyferredoxins and 8Fe ferredoxins provide temporary storage sites for [4Fe-4S] clusters to be used for protein maturation.

*Sulfur donor:* Several radical SAM enzymes, including biotin synthase (BioB) (142;143), lipoic acid synthase (LipA) (144) and MiaB (145), catalyze the thiolation of substrates. However, the nature of the immediate sulfur source is still controversial. These enzymes all contain an additional Fe-S cluster in addition to the [4Fe-4S] cluster involved in mediating reductive cleavage of SAM to yield a 5'-deoxyadenosyl radical. The additional cluster is a [2Fe-2S] cluster in BioB and a [4Fe-4S] cluster in LipA and MiaB. It has been suggested that the additional Fe-S cluster is able to function as a sacrificial S-donor for the sulfur insertion reactions based on studies carried out on BioB, in which the [2Fe-2S] cluster has been shown to act as the immediate sulfur source for biotin formation from dethiobiotin in a single turnover reaction (143).

### **Biogenesis of Fe-S clusters**

In contrast to the above mentioned structural and functional versatility, the chemical composition of the Fe-S cluster core is surprisingly simple, comprising only iron ( $\text{Fe}^{2+/3+}$ ) and inorganic sulfides ( $\text{S}^{2-}$ ). Since the beginning of what is now bioinorganic chemistry, systematic studies on synthetic analogues of naturally occurring Fe-S clusters have been carried out in Richard Holm's laboratory (70). As synthetic analogues demonstrated close resemblance to the

active sites of Fe-S proteins in terms of structural, electronic and magnetic properties and Fe-S clusters could be reconstituted in many apo Fe-S proteins by incubating with  $\text{Fe}^{2+/3+}$  and  $\text{S}^{2-}$ , it was initially assumed that Fe-S clusters assemble spontaneously on proteins in the cell (70;146). However, due to the insolubility of  $\text{Fe}^{3+}$  at neutral pH and the deleterious effects of the high concentrations of free  $\text{Fe}^{2+}$  and  $\text{S}^{2-}$  that are required for spontaneous self-assembly, it soon became apparent that spontaneous self-assembly is unlikely to occur *in vivo* (147). In fact, over the past two decades, it has gradually become evident that the biosynthesis of Fe-S clusters is a highly coordinated process and that several complex multicomponent systems have been developed by living organisms specifically for Fe-S cluster biogenesis (148-150).

Based on genetics, molecular biology and biochemical studies on prokaryotic and eukaryotic model organisms, three distinct types of machineries dedicated to Fe-S cluster biogenesis have been identified, i.e. the NIF (nitrogen fixation), ISC (iron sulfur cluster), and SUF (sulfur utilization factor) systems. Strikingly, the ISC and SUF Fe-S cluster assembly machineries are conserved through evolution, as eukaryotic mitochondria have retained almost all the key components of the bacterial ISC assembly pathway, while plastids have inherited the bacterial SUF system from cyanobacteria. A central theme of Fe-S cluster biosynthesis of all three systems is the scaffold concept that involves *de novo* assembly of clusters on a scaffold protein followed by intact transfer to apo target or carrier proteins. Additionally, maturation of cytosolic and nuclear Fe-S proteins in eukaryotes requires the CIA (cytosolic iron sulfur protein assembly) machinery, which critically depends on the mitochondria ISC machinery and a mitochondrial ISC export system. As my Ph.D. research is focused on elucidating cluster assembly and repair mechanism of bacterial and eukaryotic mitochondrial Fe-S proteins, this literature review will concentrate only on the NIF, ISC and SUF systems. A comparison of the

genetic organizations of genes involved in Fe-S cluster biogenesis in selected prokaryotic organisms is shown in Figure 1.6.

*The NIF system:* Originally identified in the nitrogen-fixing bacteria *Azotobacter vinelandii* by Dean and coworkers, the NIF system was the first Fe-S cluster biogenesis machinery to be discovered and is generally specific for the maturation of Fe-S cluster proteins involved in nitrogen fixation in diazotrophic organisms (151). However, some simple non-diazotrophic pathogenic bacteria such as *Helicobacter pylori* also appear to utilize the NIF system as the sole Fe-S cluster assembly system (152), and a NIF-like system has also been identified in the intestinal parasite *Entamoeba histolytica* (153).

The NIF Fe-S cluster assembly machinery offers the simplest system for the understanding of molecular mechanism of cluster assembly as it comprises only four components, namely NifS, NifU, <sup>Nif</sup>IscA and CysE1 (see Figure 1.6). NifS is a homodimeric pyridoxal phosphate (PLP)-dependent cysteine desulfurase that catalyzes the conversion of L-cysteine to L-alanine with the formation of a cysteine persulfide on a flexible loop (154). The cysteine persulfide is then transferred to a specific active-site cysteine residue of the NifU scaffold protein. Cellular trafficking in sulfane sulfur (S<sup>0</sup>) rather than sulfide minimizes the need to produce potentially toxic “free” sulfides (155). The fourth component encoded in the *nif* operon is CysE1, an *O*-acetylserine synthase catalyzing the rate-limiting step in cysteine biogenesis, which is present to ensure an adequate supply of the cysteine substrate for NifS (156).

The homodimeric modular NifU is the primary scaffold protein of the NIF system on which *de novo* assembly of Fe-S clusters takes place. NifU is a modular protein that consists of three distinct domains, a N-terminal domain that is homologous with the IscU protein from the

ISC system, a central ferredoxin-like domain that contains a permanent redox active  $[2\text{Fe-2S}]^{2+,+}$  cluster, and a C-terminal domain that contains a conserved CXXC motif (84;157). NifS-mediated Fe-S cluster assembly on NifU results in sequential formation of transient  $[2\text{Fe-2S}]^{2+}$  and  $[4\text{Fe-4S}]^{2+}$  clusters on the N-terminal domain and  $[4\text{Fe-4S}]^{2+}$  clusters on the C-terminal domain (84). The  $[4\text{Fe-4S}]^{2+}$  clusters assembled on both scaffolding domains are competent for *in vitro* activation of apo nitrogenase Fe protein via intact transfer of the cluster. It is noteworthy that proteins with sequence homology to the NifU C-terminal domain have been found in both eukaryotic and prokaryotic organisms and are referred to collectively as Nfu proteins (149;158). Nfu proteins have attracted considerable attention as potential alternative scaffold and/or cluster carrier proteins, however the types of cluster assembled on Nfu proteins as well as the phenotypes associated with deficiency of Nfu proteins varies from organism to organism, and remain to be fully established (10;158-160).

The *nif* operon also encodes an A-type Fe-S cluster assembly protein, termed  $^{\text{Nif}}\text{IscA}$ . The precise physiological function(s) of A-type proteins remains elusive and has generated considerable debate in the literature, which will be discussed in more detail in the following section concerning the ISC system. Nevertheless, a role for the A-type protein in the NIF system ( $^{\text{Nif}}\text{IscA}$ ) as an alternative scaffold has been proposed based on the observation that NifS-mediated reconstitution of apo recombinant *A. vinelandii*  $^{\text{Nif}}\text{IscA}$  results in the assembly of one labile  $[4\text{Fe-4S}]^{2+}$  cluster per homodimer via a transient  $[2\text{Fe-2S}]^{2+}$  cluster intermediate (161).

*The ISC system:* In many organisms, the ISC machinery is considered the primary system for the maturation of housekeeping Fe-S proteins under non-stress conditions. In bacteria, the ISC system is encoded by a highly conserved gene cluster, *iscRSUA-hscBA-fdx*, as shown in Figure 1.6. (162;163). With the exception of *iscR*, homologues of genes encoded in bacterial *isc*

operon have also been shown to be critically involved in maturation of eukaryotic mitochondria Fe-S proteins. As mentioned earlier (See “*Functions of biological Fe-S centers*”), IscR is a global transcriptional regulator. In the [2Fe-2S] cluster-containing form, IscR is specific for repression of genes in the *isc* operon (103).

IscS shares high sequence homology with NifS and is also a cysteine desulfurase supplying the inorganic sulfur for cluster assembly on scaffold proteins (162;164;165). In the mitochondria, the functional cysteine desulfurase entity is a complex consisting of the Nfs1, an IscS homologue, and Isd11, an essential eukaryotic protein with no obvious sequence relatives in bacteria (166-168). Although Nfs1 alone exhibits cysteine desulfurase activity *in vitro*, the protein is susceptible to aggregation and degradation in the absence of Isd11 (166-168). Thus, the Nfs1-Isd11 complex is generally regarded as the active mitochondrial cysteine desulfurase with Isd11 assisting in the stabilization of Nfs1.

IscU, the protein corresponds to the N-terminal domain of NifU, is unambiguously the primary scaffold protein of the ISC system and essential for *de novo* assembly of housekeeping Fe-S proteins (148;169;170). In eukaryotic mitochondria, ISCU is the mammalian homologue to bacterial IscU, while yeast contains a functionally redundant protein pair known as Isu1/2. All IscU proteins possess three rigorously conserved cysteine residues (Cys37, Cys63 and Cys106 in *A. vinelandii* and *E. coli* IscU) that provide ligation to Fe-S clusters (148). Time course studies revealed that IscS-mediated *in vitro* cluster reconstitution on *A. vinelandii* IscU proceeds via sequential formation of homodimeric form of IscU containing one [2Fe-2S]<sup>2+</sup>, two [2Fe-2S]<sup>2+</sup> and one [4Fe-4S]<sup>2+</sup> clusters (82;83). While the one [2Fe-2S]<sup>2+</sup> cluster-bound form of IscU is stable and resistant to iron chelators, one of the clusters in the two [2Fe-2S]<sup>2+</sup> cluster-containing IscU is labile and can be selectively removed by EDTA. Furthermore, the two [2Fe-2S]<sup>2+</sup> cluster-

bound form is a viable intermediate on the pathway to forming a  $[4\text{Fe-4S}]^{2+}$  cluster on IscU via two-electron reductive coupling. The resulting  $[4\text{Fe-4S}]^{2+}$  cluster is shown to be sensitive to oxygen and rapidly undergoes oxygen-induced cluster conversion to form IscU containing a single  $[2\text{Fe-2S}]^{2+}$  cluster (83). Thus, the ability of IscU to accommodate either  $[2\text{Fe-2S}]^{2+}$  or  $[4\text{Fe-4S}]^{2+}$  clusters in response to cellular redox status and/or  $\text{O}_2$  levels *in vitro* may be of physiological relevance by providing different types of Fe–S cluster proteins under different cellular conditions. In accord with the scaffold concept, studies on IscU from several organisms have demonstrated that the  $[2\text{Fe-2S}]^{2+}$  clusters assembled on IscU can be transferred intact to apo forms of  $[2\text{Fe-2S}]$  cluster-requiring proteins, such as ferredoxins, to effect maturation (171).

The efficient transfer of the IscU  $[2\text{Fe-2S}]^{2+}$  cluster is specifically assisted by a dedicated chaperon system including HscA and HscB proteins that are also encoded within bacterial *isc* operon (Ssq1 and Jac1 in eukaryotes respectively). HscA/Ssq1 belongs to a family of ATP-dependent molecular chaperones and binds to IscU selectively at a highly conserved LPPVK motif that is unique to IscU proteins (17;172-175). The binding of HscA/Ssq1 to IscU is facilitated by HscB/Jac1, which escorts IscU to HscA/Ssq1 (176). Interaction with IscU greatly enhances the HscA/Ssq1 ATPase activity, and the ATP binding and hydrolysis are coupled with a structural change on IscU that labilizes the bound  $[2\text{Fe-2S}]^{2+}$  cluster and increases the rate of cluster transfer from IscU to apo cluster-requiring proteins. In mitochondria, this process additionally requires the nucleotide exchange factor Mge1 to facilitate efficient replacement of ADP for ATP on Ssq1 which then triggers the dissociation of IscU, the eukaryotic homologue to bacterial IscU, thus rendering Ssq1 ready for the next cycle of reaction (177).

In contrast, the biogenesis of  $[4\text{Fe-4S}]$  clusters is less well understood. IscU is indispensable for the maturation of  $[4\text{Fe-4S}]$  cluster-requiring proteins and the  $[4\text{Fe-4S}]^{2+}$

cluster-bound *A. vinelandii* IscU has been shown to be competent for *in vitro* activation of apo aconitase via intact cluster transfer (178-180). While a [4Fe-4S]<sup>2+</sup> cluster-bound form of mammalian ISCU has recently been characterized *in vitro*, the ability to assemble a [4Fe-4S]<sup>2+</sup> cluster has yet to be determined for IscU proteins from other organisms (181). Most recently, *in vivo* studies carried out on eukaryotic mitochondrial ISC machinery by Lill and coworkers have demonstrated that while Isu1/2 have critical roles for the formation of both [2Fe-2S] and [4Fe-4S] clusters, the maturation of mitochondrial [4Fe-4S] proteins also specifically requires ISC A-type proteins (182;183).

The bacterial *isc* operon encodes an A-type Fe-S cluster assembly protein, IscA. Eukaryotic mitochondria generally contain two proteins related to bacterial IscA, termed Isa1 and Isa2, but only Isa1 is a functional orthologue of bacterial A-type proteins (182). Unfortunately there is currently no consensus concerning the specific physiological role(s) of A-type proteins, including SufA and <sup>Nif</sup>IscA from respective SUF and NIF systems, due to lack of clear phenotypes of single gene knockout except under aerobic or oxidative stress conditions (148;184-186). However, results from research carried out on several model organisms has led to proposals of several putative roles for A-type proteins in Fe-S cluster biogenesis, including a role as carrier proteins for delivery and insertion of preformed clusters to specific recipient proteins (161;187-189), as iron donors to U-type scaffold proteins and/or for the formation of [4Fe-4S] clusters (182-184;190;191). In support of a cluster carrier role, several members of IscA/Isa1 protein family were shown *in vitro* to accommodate a [2Fe-2S]<sup>2+</sup> cluster that can be subsequently transferred to apo acceptor proteins such as ferredoxins (187;188;192;193). Moreover, preliminary cluster transfer data show that *E. coli* IscA can accept a [2Fe-2S]<sup>2+</sup> cluster from IscU *in vitro*, whereas cluster transfer in reverse direction was unsuccessful, indicating a

function for IscA acting downstream of IscU, the primary scaffold protein, possibly as an intermediate Fe-S cluster carrier (189).

Alternatively, several IscA proteins, including *E. coli* IscA (194), *S. cerevisiae* Isa1 and Isa2 (182), and human ISCA1 (195), have been found to have the ability to bind Fe<sup>3+</sup> with high affinity (association constant determined to be  $2.0 \times 10^{19} \text{ M}^{-1}$  for *E. coli* IscA). Early studies demonstrated that the A-type protein-bound Fe<sup>3+</sup> ion can be specifically mobilized by L-cysteine and that the Fe-bound A-type proteins are effective Fe donor for *in vitro* cysteine desulfurase-mediated Fe-S cluster assembly on IscU (194). Consequently, a function for A-type proteins as Fe donors for Fe-S cluster assembly on U-type scaffold proteins has been proposed. However, most recent *in vivo* studies on eukaryotic mitochondria revealed that A-type proteins are dispensable for the formation of Fe-S cluster on Isu and maturation of [2Fe-2S] cluster-requiring proteins (182;183). Nevertheless, both Isa1 and Isa2, together with a partner protein Iba57 which facilitates the release of Fe, were found to be specifically required for the maturation of mitochondrial [4Fe-4S] cluster-requiring proteins under anaerobic conditions (182;183). Moreover, this is also consistent with previous observations that prokaryotic IscA in conjunction with SufA, are essential for the assembly of [4Fe-4S] clusters, but are dispensable for the maturation of [2Fe-2S] cluster protein under aerobic conditions (191). Taken together, these results also suggest that there is a need for reevaluation of the proposal that A-type proteins act as immediate Fe donor to U-type scaffolds.

In this context, it is worth mentioning that the physiological immediate Fe donor for the ISC system remains elusive. In addition to IscA/Isa1, an alternative candidate for immediate Fe donor for *de novo* cluster assembly is human frataxin protein. As mentioned earlier in this chapter, deficiency of human frataxin, a small mitochondrial protein, leads to the

neurodegenerative disease Friedreich's ataxia. Frataxin is a conserved family of proteins, known as Yfh1 in yeast and with the bacterial ortholog termed CyaY. Several lines of evidence suggest that frataxin may act as immediate Fe donor for *de novo* assembly of Fe-S clusters on U-type scaffolds. Firstly, frataxin deficiency in eukaryotes results in impairment of Fe-S cluster biogenesis and mitochondrial Fe overload (3;17;196;197). Secondly, frataxin was shown to physically interact with cysteine desulfurase (IscS/Nfs1) (198;199). In addition, Fe-stimulated frataxin and Isu interaction (198;200;201), and citrate-dependent interaction between frataxin and mitochondrial aconitase (202) have also been observed. Furthermore, several frataxin proteins have demonstrated the ability to bind and donate iron for cluster assembly on IscU *in vitro* (201;203-206). However, deletion of the gene encoding bacterial CyaY alone conferred no phenotype, contradicting the putative role as an Fe donor (207). Alternatively, a role for frataxin as an allosteric regulator for cysteine desulfurase has also been proposed based on the observation that frataxin binding to Isu and Nfs1/Isd11 stimulates desulfurase activity in humans (208).

The ISC Fdx (Yah1 in yeast and FDX2 in mammals) contains a redox active  $[2\text{Fe-2S}]^{2+,+}$  cluster and plays a crucial yet ill-defined role in the Fe-S cluster biogenesis. *In vivo* studies have demonstrated that deletion of yeast Yah1 is lethal and depletion of this gene results in decreased activity of other mitochondrial Fe-S proteins and accumulation of Fe in the mitochondria of higher organisms (17;209;210). In eukaryotes, it has been generally accepted that Yah1/FDX2, together with mitochondrial ferredoxin reductase (Arh1 in yeast and FDXR in mammals) and NADH, constitute an electron transfer chain to provide electron flow for the reduction of sulfane sulfur in cysteine desulfurase to sulfide present in the clusters (170). Interestingly, *in vivo* studies carried out in yeast revealed a mutual requirement of Isu and Yah1 for their conversion into

cluster-bound proteins that are essential for the function of the entire ISC system (17). Thus the ferredoxin in the ISC system is considered an unusual protein in the sense that it is required for its own maturation. Additionally, a potential role for bacterial ISC Fdx in mediating reductive coupling of two adjacent  $[2\text{Fe-2S}]^{2+}$  clusters on IscU to yield one  $[4\text{Fe-4S}]^{2+}$  cluster has also been suggested (83).

*The SUF system:* In many bacteria, the SUF system serves as a backup to the more general ISC system under oxidative stress and/or iron limitation conditions. However, in gram-positive bacteria, cyanobacteria, pathogenic bacteria, plant chloroplast and some thermophilic bacteria and archaea, the SUF system constitutes the sole system for Fe-S cluster biogenesis. Generally, the bacterial *suf* operon comprises genes *sufABCDSE* and has been extensively investigated using *E. coli* as model organism (see Figure 1.6).

The gene product of *sufS* is a cysteine desulfurase protein. However, in contrast to its NifS and IscS homologues in which sulfane sulfur is directly transferred to the scaffold protein, SufS works in concert with SufE, a sulfur transferase also encoded in the *suf* operon (211). Unlike Isd11, which helps in stabilizing Nfs1 in the mitochondria, SufE directly accepts sulfane sulfur from SufS to create a cysteine persulfide that is more accessible to acceptor proteins, and then forwards the sulfane sulfur to the scaffold protein(s) in the SUF system (212;213). The formation of SufSE complex greatly enhances the activity of SufS as a cysteine desulfurase (211).

The products of three genes from the *suf* operon, *sufB*, *sufC* and *sufD*, form a complex with 1:2:1 stoichiometry and the resulting SufBC<sub>2</sub>D complex is generally considered as the primary scaffold of the SUF system (214). SufC is a soluble ATPase and exhibits structural similarity to the ATPase subunits of ABC transporters (ATP binding cassette) (215). The *E. coli* SufB protein contains total of thirteen cysteine residues with four of them being highly

conserved in other organisms (216). SufD is homologous to SufB but lacks the conserved cysteine residues. Physical interaction between SufBC<sub>2</sub>D and the SufSE complex have been shown to further enhance the desulfurase activity of the SufSE complex (213). A series of *in vitro* studies have revealed that in the SufBC<sub>2</sub>D complex, SufB accept sulfur from SufSE and is able to assemble a [4Fe-4S]<sup>2+</sup> cluster via *in vitro* reconstitution and that the resulting [4Fe-4S]<sup>2+</sup> cluster is labile and degrades to a [2Fe-2S]<sup>2+</sup> cluster upon exposure to air (214;216). While interaction with SufC is required for SufB to be competent for accepting sulfur from SufSE (216), both SufC and SufD are required for *in vivo* iron acquisition for cluster assembly on SufB (217). SufBC<sub>2</sub>D has also demonstrated the ability to bind to one molecule of reduced flavin adenine nucleotide (FADH<sub>2</sub>) per complex, as a redox cofactor for mobilizing iron during cluster assembly (214).

SufA is the A-type Fe-S cluster assembly protein in the SUF system and is a homolog of IscA. Like IscA, the specific physiological functions of SufA have not been clearly established. Although there has been report of Fe-bound form of recombinant SufA (184), a role for SufA as an iron donor for the SUF system has not been documented and the nature of the specific iron donor in this system remains elusive (218). Rather, SufA has demonstrated the ability as cluster carrier protein. Native SufA co-expressed *in vivo* with its cognate partner proteins from the *suf* operon (SufBCDSE) under anaerobic conditions was shown to contain a [2Fe-2S]<sup>2+</sup> cluster, possibly as result of intact cluster transfer from Suf BC<sub>2</sub>D (218;219). Moreover, the [2Fe-2S]<sup>2+</sup> cluster-containing form of SufA is competent for *in vitro* maturation of [4Fe-4S]<sup>2+</sup> cluster-requiring proteins in the presence of DTT (189).

Some gram positive bacteria, such as *Enterococcus faecalis*, utilize a different set of *suf* genes that contains *sufBUSDC* and lacks *sufE* and *sufA* (220). The encoded SufU protein is

generally considered as a homologue to IscU and contains all three conserved cysteines. However, SufU lacks the LPPVK motif presented in IscU, consistent with the absence of molecular chaperones in the SUF system. The specific role(s) of SufU in Fe-S biosynthesis remains to be elucidated and is under active investigation. Interestingly, recent studies on *B. subtilis* SufU have suggested that this type of protein is able to function as both a putative scaffold protein and an *in vitro* activator of the cysteine desulfurase SufS (221). In addition, the SUF system of some cyanobacteria also contains a SufR transcriptional regulator (222;223). Characterization of *Synechocystis* sp. PCC 6803 SufR indicates that it harbors two  $[4\text{Fe-4S}]^{2+,+}$  clusters per homodimer rather than the  $[2\text{Fe-2S}]^{2+,+}$  cluster identified in IscR (224). SufR binds to the DNA fragment that contains promoters for *sufR* and the *sufBCDS* operon, and the binding affinity is influenced by the presence and redox state of the  $[4\text{Fe-4S}]^{2+,1+}$  cluster (224). Thus, the  $[4\text{Fe-4S}]^{2+}$  cluster-containing SufR may function as both a transcriptional repressor of the *sufBCDS* operon and as an autoregulator of *sufR*.

### **Roles of monothiol glutaredoxins in Fe-S cluster biogenesis and Fe regulation**

Glutaredoxins (Grxs) are a family of ubiquitous proteins first discovered as glutathione (GSH)-dependent reductases of the disulfides formed in ribonucleotide reductase in viable *E. coli* mutants lacking thioredoxin (Trx) (225;226). This discovery led to the original classification of the Grx family of proteins as oxidoreductases involved in maintaining the cellular redox potential by reducing disulfide bridges and/or glutathiolylated proteins using a NADPH-dependent glutathione reductase and the reducing power of reduced GSH (227-229). Most organisms encode multiple Grxs in various subcellular locations, with photosynthetic organisms being renowned for possessing large number of Grxs (228;230). As the number of sequenced genomes has increased and the evolutionary and functional diversity of Grxs has

emerged, Grxs have now been classified into six classes (Class I to VI) based on phylogeny, domain structures, and both active site and GSH-binding sequences (229;231;232). While Classes I and II Grxs are widespread among all kingdoms of life (see Figure 1.7 for schematic representation of domain structures of Class I and II Grxs), Classes III to VI Grxs are restricted to specific organisms and their specific roles are less understood (229). Class I Grxs, which includes human Grx1 and 2, *S. cerevisiae* Grx1 and 2, and *E. coli* Grx1-3, are known as classic “dithiol” Grxs with CXXC/S active sites and exhibits thiol-disulfide reductase activity. Class II Grxs all contain highly conserved CGFS active-site motifs, thus will be collectively referred to as CGFS-Grxs in this review (other names for CGFS-Grxs include monothiol Grxs). CGFS-Grxs can be further categorized into two groups, namely single-domain CGFS-Grxs and multi-domain CGFS-Grxs. Single-domain CGFS-Grxs are those comprising only one Grx domain and are wide spread in both prokaryotes and eukaryotes with the best characterized members being *S. cerevisiae* mitochondrial Grx5 and *E. coli* Grx4. Whereas multi-domain CGFS-Grxs are modular proteins with a N-terminal Trx-like domain attached to one or more (up to three) Grx domains, and are present only in eukaryotes. Notable members of multi-domain CGFS-Grxs are the functionally redundant *S. cerevisiae* Grx3 and 4 (Grx3/4) with one Grx domain, human Grx3 (also known as the PICOT, for protein kinase C interacting cousin of thioredoxin) with two Grx domains, and plant GrxS17 with three Grx domains. CGFS-Grxs are chemically very different from Class I Grxs as they all lack significant thiol-disulfide reductase activity (233-235). However, overwhelming evidence has linked CGFS-Grxs to Fe homeostasis, especially roles in Fe-S cluster biogenesis and iron regulation, and this section will focus on recent advances in understanding the roles of CGFS-Grxs.

*Structure of [2Fe-2S]<sup>2+</sup> cluster-containing CGFS-Grxs:* A wide variety of recombinant CGFS-Grxs have shown the ability to incorporate a [2Fe-2S]<sup>2+</sup> cluster upon overexpression in *E. coli* and/or when subjected to cysteine desulfurase-mediated reconstitution (21;236-240). Despite the early reservations regarding the physiological relevance of the Fe-S clusters present in Grxs, the existence of cluster-bound Grxs in the native host environment has been confirmed *in vivo* using Grx3/4 from *S. cerevisiae* (241). The [2Fe-2S]<sup>2+</sup> cluster centers in CGFS-Grxs have been shown to be both oxidatively and reductively labile, as evidenced by observations of cluster degradation upon exposure to air as well as immediately following reduction via dithionite under strictly anaerobic conditions (21;237). The nature of the [2Fe-2S]<sup>2+</sup> cluster ligation in CGFS-Grxs was initially assessed by analytical and spectroscopic techniques combined with site-directed cysteine mutagenesis studies (237), and subsequently confirmed and extended by crystallography studies (233;242). The [2Fe-2S]<sup>2+</sup> clusters in CGFS-Grxs have been revealed to reside at the interface of an asymmetric dimeric structure and coordinated by the cysteine residues of two non-covalently bound GSH molecules and the active-site cysteine residues from each CGFS motif (see Figure 1.8A). NMR studies of <sup>15</sup>N-labeled cluster-bound poplar CGFS-type GrxS14 have recently demonstrated that the GSH ligands undergo continuous exchange with free GSH in solution (243). Several Class I Grxs have also found to contain subunit-bridging [2Fe-2S]<sup>2+</sup> clusters with identical ligation scheme to that of CGFS-Grxs' (244;245). However, the clusters in Class I Grxs are more stable and exhibit distinct structural and spectroscopic properties compared to those assembled on CGFS-Grxs (21;237;240;244). Firstly, the relative orientation of the two CGFS-Grx protomers are rotated by approximately 90° compared to that of the [2Fe-2S]<sup>2+</sup> cluster-containing Class I Grxs, as shown in Figure 1.8 (233;242;244;245). Consequently, extensive direct contact is established between the two

CGFS-Grx protomers. Thus the protein structural differences in the vicinity of the cluster are considered to be responsible for the decreased stability along with divergent electronic and vibrational properties displayed by the  $[2\text{Fe-2S}]^{2+}$  clusters in CGFS-Grxs.

Comparison of structures of monomeric apo- and dimeric holo-*E.coli* Grx4 also reveal subtle but important structural differences, see Figure 1.9 (242). Notably, the specific position of  $\beta 1\text{-}\alpha 2$  loop in the dimeric  $[2\text{Fe-2S}]^{2+}$  cluster-containing form, stabilized via interaction with Ser33, would allow adequate positioning of Cys30 to coordinate the Fe in the  $[2\text{Fe-2S}]^{2+}$  cluster, and allow Lys22, which is crucial for cluster binding, to contact the GSH bound to the cluster (236;242). It has been proposed that the conformational changes between apo- and cluster-containing CGFS-Grxs provide the structural and thermodynamic rationale for releasing an intact cluster and imply a role for CGFS-Grxs in mediating cluster delivery from scaffold proteins to apo acceptor proteins (see below).

*CGFS-Grxs in Fe-S cluster biogenesis:* The initial indication of a primary or auxiliary involvement of CGFS-Grxs in Fe-S cluster biogenesis came from gene knockout studies on *S. cerevisiae* mitochondrial Grx5. Although deletion of *grx5* gene in yeast is not lethal, unlike that of most core components of the ISC cluster assembly machinery, the *S. cerevisiae*  $\Delta$ *grx5* strain exhibits phenotypes that can be attributed to disrupted Fe-S cluster biogenesis, notably decreased cluster assembly in at least two mitochondrial Fe-S cluster-requiring enzymes (aconitase and succinate dehydrogenase) and accumulation of iron in the cell, which together lead to increased sensitivity to oxidative stress and defects in respiratory growth (16;246). In a subsequent study,  $^{55}\text{Fe}$  radiolabeled immunoprecipitation of a *S. cerevisiae* *grx5* null mutant demonstrated decreased levels of cluster-bound mitochondrial ferredoxin (Yah1) and biotin synthase (Bio2), and a concomitant marked increase in the Fe content (presumably in the form of bound Fe-S

clusters) on Isu1 (17). Together, these observations suggest that mitochondrial Grx5 participates in a step following *de novo* cluster assembly on Isu1, possibly in facilitating the transfer of preassembled clusters from U-type scaffolds to apo acceptor proteins. Consistent with this hypothesis, the phenotype of  $\Delta grx5$  mutants were found to be partially suppressed by overexpression of Ssq1 which also facilitates dissociation of clusters on Isu1 (16). Furthermore, the involvement of CGFS-Grxs in Fe-S cluster biogenesis appears to be conserved throughout evolution, as yeast Grx5 homologues from various species including *E. coli* (247), *A. thaliana* (237), zebrafish (248) and human (247) all displayed the ability to rescue the phenotypes of the *grx5* deletion strain when targeted to *S. cerevisiae* mitochondria.

Bioinformatics and genetic studies also provided convincing evidence of connections between CGFS-Grxs and Fe-S cluster biogenesis pathways. Phylogenetic profiling demonstrated high evolutionary co-occurrence between CGFS-Grxs and components from ISC machinery, including ferredoxin, U-type and A-type proteins (249). In *S. cerevisiae*, strong interactions between Grx5 and both Ssq1 and Isa1 have been predicted by low-definition protein docking, with the latter further confirmed by *in vivo* yeast two-hybrid analysis (249). Moreover, in another yeast, *S. pombe*, bimolecular fluorescence complementation studies demonstrated *in vivo* interaction between Grx5 and both Isa1 and Isa2 (250). In *E. coli*, genetic interaction between *grxD*, the gene expressing its sole CGFS-Grx, Grx4, and the *isc* operon have been demonstrated by the synthetic lethality of double mutants involving deletion of *grxD* and genes in the *isc* operon (251).

On the basis of the ability to incorporate a labile subunit-bridging  $[2Fe-2S]^{2+}$  cluster, CGFS-Grxs were initially proposed to act as an alternative scaffold for *de novo* biosynthesis of  $[2Fe-2S]$  clusters. *In vitro* cluster transfer experiments demonstrating rapid transfer of intact

[2Fe-2S]<sup>2+</sup> cluster from poplar chloroplast GrxS14 to the apo-form of plant-type ferredoxin (237), provided the initial direct evidence that CGFS-Grxs have the ability to function as Fe-S cluster scaffold or carrier proteins. Recently, intact transfer of a [2Fe-2S]<sup>2+</sup> cluster to apo bacterial ferredoxin has also been reported for *E. coli* Grx4 (cluster transfer rate not available) (238). However, several lines of evidence argue against a scaffolding role for CGFS-Grxs. Most importantly, preliminary results indicate that formation of an Fe-S cluster on *S. cerevisiae* mitochondrial Grx5 is dependent on a functional ISC machinery and in particular requires Isu1 and the molecular co-chaperones (170). Secondly, thus far there is no evidence suggesting CGFS-Grxs physically interact with cysteine desulfurases which provide the sulfur atoms for *de novo* assembly of clusters on scaffold proteins. Hence, the ability to rapidly transfer the labile [2Fe-2S]<sup>2+</sup> cluster to apo acceptor proteins is best interpreted in terms of a role for CGFS-Grxs as carrier proteins involved in trafficking Fe-S clusters assembled on U-type scaffold proteins to specific acceptor proteins. Such a role is also consistent with the observations that the *S. cerevisiae* *Δgrx5* mutant can be partially rescued by overexpressing *ssq1* gene, the molecular chaperone that facilitates transfer of clusters from Isu1, and that Grx5 deficiency can lead to cluster accumulation of Isu1 as demonstrated by yeast immunoprecipitation studies (16;17). The ability of CGFS-Grxs to serve as sensors of cellular Fe levels in yeast (*vide infra*), also suggests a role in cluster storage. As previously noted, roles for CGFS-Grxs in both cluster storage and trafficking are complementary rather than mutually exclusive (237).

To further investigate the putative roles of CGFS-Grxs in cluster trafficking and storage, Chapter 2 of this dissertation reports detailed biochemical and biophysical characterization of the types and properties of Fe-S cluster assembled on recombinant *S. cerevisiae* Grx5. In addition, to facilitate the understanding of specific role(s) of CGFS-Grxs in Fe-S cluster biogenesis, there is a

pressing need to identify the physiological partner proteins of CGFS-Grxs in the trafficking of Fe-S clusters, including cluster donors and recipients, and to elucidate the molecular-level mechanism of cluster exchange involving CGFS-Grxs. Guided by the connections between CGFS-Grxs and Fe-S cluster assembly pathways provided by the aforementioned bioinformatics and genetic studies, Chapter 3 of this dissertation reports that *A. vinelandii* Grx5 is able to serve as an intermediate carrier for  $[2\text{Fe-2S}]^{2+}$  cluster transfer from IscU to IscFdx in the presence of HscA/B co-chaperones and ATP, while Appendix C provides *in vitro* evidence that CGFS-Grxs and A-type Fe-S cluster assembly proteins are partners in cluster trafficking.

*CGFS-Grxs in Fe homeostasis:* In addition to involvements in Fe-S cluster biogenesis, a link between mitochondrial Grx5 deficiency and defects in heme biosynthesis has been discovered in higher eukaryotes. Grx5 deficiency in zebrafish embryos and a human patient has been identified as the cause for developing two different forms of anemia by specifically impairing heme biosynthesis (18;248). The working model suggests that in the event of the impaired mitochondrial ISC machinery as the result of Grx5 deficiency, cytosolic Fe regulatory protein IRP1 will be incorrectly activated due to the loss of its  $[4\text{Fe-4S}]^{2+}$  cluster (see the section in “*Functions of biological Fe-S centers*”). The activated IRP1 then binds to the 5'-IRE on the mRNAs of gene encoding aminolevulinic synthase 2 (ALAS2), a protein required in the early stage of heme biosynthesis, blocking its translation and consequently preventing heme production (248).

Independently, a role for CGFS-Grxs in intracellular iron trafficking has recently been demonstrated. In *S. cerevisiae*, deficiency of cytosolic-nuclear Grx3/4 leads to immediate loss of virtually all cellular iron-requiring reactions despite accumulation of soluble iron in the cytosol, suggesting that Fe is not bioavailable in Grx3/4 depleted cells (241). Site-directed mutagenesis

studies showed that subunit-bridged  $[2\text{Fe-2S}]^{2+}$  cluster in Grx3/4 is crucial for their function in Fe homeostasis, as mutation of the Grx3/4 cluster-coordinating cysteine residue renders the same phenotypes as that observed in Grx3/4-depleted cells (241). Interestingly, the incorporation of the  $[2\text{Fe-2S}]^{2+}$  cluster into Grx3/4 is independent of the cytosolic CIA machinery, but rather requires the mitochondrial ISC assembly and export system (241). The detailed mechanism of how the  $[2\text{Fe-2S}]^{2+}$  cluster-containing Grx3/4 homodimer is involved in mediating intracellular Fe trafficking from the cytosolic labile Fe pool to Fe-dependent proteins and mitochondria remains elusive. However, it has been suggested that the Fe moiety of the cluster in Grx3/4 could be used for insertion into Fe-requiring proteins; alternatively the cluster could act as sensor in activating cytosolic Fe for trafficking in a yet unknown fashion (241). Furthermore, it is not clear yet if such an intracellular Fe delivery role for CGFS-Grxs is conserved in eukaryotes or is unique to *S. cerevisiae*.

Furthermore, CGFS-Grxs, especially the eukaryotic multi-domain CGFS-Grxs, have also been found to participate in Fe regulation. In *S. cerevisiae*, the expression of genes involved in Fe uptake and storage are primarily under the control of the Fe-responsive transcription factors, Aft1 and Aft2. Aft1 is known to undergo nucleocytoplasmic shuttling in a Fe-dependent fashion: under Fe-depleted conditions, Aft1 is located in nucleus where it functions as transcriptional activator of the Fe regulon, whereas Fe-replete conditions promote the translocation of Aft1 into cytosol (252). Although it is currently unclear if Aft1 and Aft2 are Fe-S cluster proteins, Aft1 has been shown to respond to an unknown signal produced and exported by the mitochondrial ISC Fe-S cluster assembly machinery (253;254). In the cells that express low levels of Grx3/4, Aft1 has been shown to be retained in the nucleus in a constitutively active form, demonstrating an important physiological connection between Aft1 and Grx3/4 (255). Moreover, specific protein-

protein interaction between Aft1 and Grx3/4 has been revealed by yeast two-hybrid analysis and co-immunoprecipitation studies (256). Sensing of intracellular Fe levels by Aft1 and the export of Aft1 from nucleus upon Fe sufficiency additionally depends on two cytosolic proteins, the protease-related protein Fra1 and the BolA-like protein Fra2, as deletions of either FRA1 or FRA2 gene lead to translocation of Aft1 from cytosol to nucleus (257). Moreover, *in vivo* evidence of interaction between Grx3/4 and Fra1/2, and *in vitro* biochemical and biophysical studies have showed that Fra2 in particular can form a  $[2\text{Fe-2S}]^{2+}$  cluster-bridged heterodimer with Grx3/4 (21;257). Having Fra2 in place of a Grx causes changes in the cluster coordination scheme, with ligands provided by the cysteine moiety from the CGFS active site of Grx3/4, GSH, and a conserved histidine in Fra2 while the identity of the fourth ligand remains unclear at the present moment (21). Also, the  $[2\text{Fe-2S}]^{2+}$  cluster in the heterodimer exhibit increased stability compared to the cluster in the Grx3/4 homodimer. It has been proposed that the  $[2\text{Fe-2S}]^{2+}$  cluster-containing Grx3/4-Fra2 heterodimer constitutes part of a signaling pathway that senses the cellular Fe status and, in turn, regulates the nucleocytoplasmic shuttling of Aft1 via a yet-unidentified mechanism (21).

The involvement of CGFS-Grxs, especially the eukaryotic cytosolic multi-domain CGFS-Grxs, in regulation of cellular Fe homeostasis has been found to be functionally conserved, even in organisms that utilize different Fe regulatory systems. For instance, the fission yeast *S. pombe* employs a different approach for Fe regulation that includes two transcriptional repressors, Fep1 and Php4, that are involved in controlling Fe acquisition and distribution, respectively (258). Both Fep1 and Php4 are found to interact with and be regulated by *S. pombe* Grx4, a cytosolic multi-domain CGFS-Grx (259;260). Moreover, it is likely that in many organisms, CGFS-Grxs work in concert with a family of BolA-like proteins in order to maintain Fe homeostasis.

Originally identified as a protein that induces round morphology in *E. coli*, the BolA family of proteins has been found to be widespread among all kingdoms of life and to display a strong genomic association with CGFS-Grxs (261;262). In addition to the aforementioned interaction between Fra2, a BolA-like protein, and Grx3/4 in *S. cerevisiae*, physical interactions between BolA proteins and CGFS-Grxs have also been identified in several other organisms (263;264). Although the specific function(s) of BolA proteins in Fe metabolism remains elusive, new evidence has clearly suggested their direct involvement (11). In addition to studies on *S. cerevisiae*, recent *in vitro* investigations carried out on the human multi-domain Grx3 and *E. coli* Grx4 have demonstrated formation of a  $[2\text{Fe-2S}]^{2+}$  cluster-containing Grx-BolA complex with different spectroscopic properties and increased cluster stability compared to that of the  $[2\text{Fe-2S}]^{2+}$  cluster-bridged CGFS-Grxs homodimer, suggesting that interaction with BolA may alter the putative cluster carrier function of CGFS-Grxs (238;240). Nevertheless, the physiological importance of interaction between BolA proteins and CGFS-Grxs require further investigation and remain of great interest to many researchers.

### **Transcriptional regulator FNR**

The fumarate and nitrate reduction (FNR) regulatory protein is an oxygen-responsive global transcriptional regulator that controls the switch between aerobic and anaerobic metabolism in *E. coli* and many other facultative anaerobes in response to cellular oxygen levels (99;265). FNR is present in the cell at relative constant levels under either aerobic or anaerobic growth conditions (266). Under oxygen-limiting conditions, FNR regulates the transcription of > 100 genes to facilitate the adaption to anaerobic respiration using fumarate as the terminal electron acceptor (267;268).

FNR is a member of expanding superfamily of structurally related bacterial transcriptional regulators, including the structurally characterized cyclic-AMP receptor protein (CRP) (269-271). While a three-dimensional structure of FNR is not currently available, based on sequence homology with CRP, it has been predicted that FNR consists of two functionally distinct domains and exists as dimer in its functional form (Figure 1.10). The C-terminal helix-turn-helix domain of FNR is involved in site-specific DNA binding by recognizing the consensus sequence TTGAT-N4-ATCAA in target promoters (272;273). The N-terminal domain of FNR provides the sensory function, and unlike that of CRP, contains five cysteine residues, four of which, i.e. Cys20, 23, 29, and 122 in *E. coli*, are essential for FNR to function *in vivo* and are capable of binding either a  $[4\text{Fe-4S}]^{2+}$  or a  $[2\text{Fe-2S}]^{2+}$  cluster (77;274).

The ability of FNR to sense and respond to cellular oxygen levels critically depends on the presence of a  $[4\text{Fe-4S}]^{2+}$  cluster in the sensory domain. Indeed FNR is only active as a transcriptional regulator under anaerobic conditions when it is in a dimeric form containing one  $[4\text{Fe-4S}]^{2+}$  cluster per subunit. The  $[4\text{Fe-4S}]^{2+}$  cluster induces protein dimerization, which is essential for FNR activity. By analogy to CRP, a dimerization helix in the predicted FNR structure promotes coiled-coil interaction between subunits (270;275). The putative dimerization helix consists mostly of hydrophobic residues with the notable exception of two negatively charged residues, Glu150 and Asp154. Substitution of Asp154 with amino acid residues containing neutral or positive side chains, or replacement of Glu150 with a positively charged residue has been shown to successfully increase dimerization and activity of apo FNR under aerobic conditions in the absence of the  $[4\text{Fe-4S}]^{2+}$  cluster (276-278). Although the location of the  $[4\text{Fe-4S}]^{2+}$  cluster is predicted to be distant from the dimerization helix, comparison of CD spectra of  $[4\text{Fe-4S}]^-$ ,  $[2\text{Fe-2S}]^-$  and apo-FNR reveals small but significant differences in protein

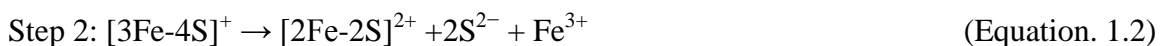
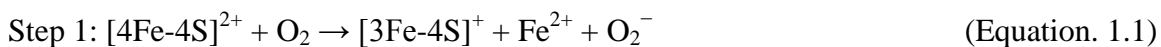
secondary structure (278). As a result, it has been concluded that the  $[4\text{Fe-4S}]^{2+}$  cluster is required to induce a long range conformational change necessary to overcome inter-subunit charge repulsion and to favor dimerization (278). It is worth mentioning that the  $[4\text{Fe-4S}]^{2+}$  cluster in FNR is redox-inert *in vivo* with the redox potential of the  $[4\text{Fe-4S}]^{2+/+}$  couple estimated to be lower than  $-650$  mV (99). FNR samples reduced by deazaflavin-mediated photoreduction exhibit a broad EPR signal at  $g \approx 5$  at 4.3 K and high microwave powers indicating that the  $[4\text{Fe-4S}]^+$  cluster has an  $S = 3/2$  state, while addition of dithionite can only achieve partial reduction to  $[4\text{Fe-4S}]^+$  cluster (77;99). Such a low redox potential suggests that  $[4\text{Fe-4S}]$  cluster in FNR is unlikely to exist in the 1+ oxidation state *in vivo* (99).

However, the  $[4\text{Fe-4S}]^{2+}$  cluster in FNR is very sensitive to oxygen, and thus serves as the sensory site for FNR's  $\text{O}_2$ -sensing function. Mössbauer studies have demonstrated that the  $[4\text{Fe-4S}]^{2+}$  cluster in FNR is converted to a  $[2\text{Fe-2S}]^{2+}$  cluster on exposure to oxygen both *in vivo* and *in vitro* (77;279). Moreover, the cluster conversion is accompanied by a conformational change that leads to dissociation of the protein into monomers and loss of FNR activity (77;280). Both the  $[4\text{Fe-4S}]^{2+}$  and  $[2\text{Fe-2S}]^{2+}$  clusters are ligated by the same four cysteine residues in *E. coli* FNR (Cys20, 23, 29, and 122), as mutating the only other cysteine residue (Cys16) to alanine did not affect neither the presence of  $[4\text{Fe-4S}]^{2+}$  cluster nor the oxygen-induced formation of  $[2\text{Fe-2S}]^{2+}$  cluster (77). Furthermore, the  $[4\text{Fe-4S}]^{2+}$  cluster can be regenerated from the  $[2\text{Fe-2S}]^{2+}$  cluster in oxygen-exposed FNR with restored activity either by *in vitro* cysteine desulfurase-mediated reconstitution under reducing conditions with additional ferrous iron (77), or via shifting the air-exposed cells back to anaerobic growth conditions (279). This suggests that FNR activation/inactivation is a reversible process. Although the oxygen-induced  $[2\text{Fe-2S}]^{2+}$  cluster in FNR is relatively stable in air with half-life at least 12 hours at  $0^\circ\text{C}$  (77) or several

hours at room temperature *in vitro* (266), it is rapidly degraded by superoxide, a byproduct of aerobic metabolism, both *in vitro* and *in vivo* and yields the apo monomeric form of FNR (266). Apo-FNR is also the predominant form of FNR in cells grown under aerobic conditions, due to oxygen-induced degradation of the  $[4\text{Fe-4S}]^{2+}$  cluster (281). The inactive apo-FNR can be then converted back to the  $[4\text{Fe-4S}]^{2+}$  cluster-containing form with restored transcriptional activity upon the onset of anaerobic growth conditions in an ISC machinery-dependent process (282).

While the *in vivo* cycling of FNR between active and inactive states is relatively well understood, the detailed mechanism of oxygen-induced cluster conversion has not been fully elucidated. As mentioned earlier, interconversions between different types of Fe-S clusters are hardly new discovery. However, prior to FNR, a  $[4\text{Fe-4S}]$  to  $[2\text{Fe-2S}]$  cluster conversion had not been observed without addition of chelators, detergents or other non-physiological agents. Hence, the rapid  $[4\text{Fe-4S}]^{2+}$  to  $[2\text{Fe-2S}]^{2+}$  cluster conversion of FNR at a physiological pH simply upon exposure to air merited comprehensive investigations and previous studies have resulted in two fundamentally different proposals involving a sulfur-based or a metal-based oxidation. The  $[4\text{Fe-4S}]^{2+}$  cluster formally contains two  $\text{Fe}^{2+}$  and two  $\text{Fe}^{3+}$  ions while the  $[2\text{Fe-2S}]^{2+}$  clusters contains two  $\text{Fe}^{3+}$  ions. The possibility of a sulfur-based oxidation was first suggested by Sutton and coworkers based on analytical data showing that only 70% of the bridging sulfides originally in the  $[4\text{Fe-4S}]^{2+}$  cluster could be detected following oxygen exposure, leaving 30% of the sulfide unaccounted for and presumed oxidized (77;283). In accord with this hypothesis, two  $\text{Fe}^{2+}$  ions were detected during the  $[4\text{Fe-4S}]^{2+}$  to  $[2\text{Fe-2S}]^{2+}$  cluster conversion by using the  $\text{Fe}^{2+}$ -specific chelator ferene (283), indicating that the ejected  $\text{Fe}^{2+}$  had not been oxidized. However, attempts to detect sulfide oxidation products such as polysulfide or sulfinic acid were unsuccessful and a detailed mechanism was not proposed (283).

The alternative metal-based oxidation mechanism involves the oxidation of one cluster iron and the release of one Fe<sup>3+</sup>, one Fe<sup>2+</sup> and two sulfides. The proposed reaction scheme consists of two steps (284). In the first step, one-electron oxidation of the [4Fe-4S]<sup>2+</sup> cluster results in release of one Fe<sup>2+</sup> and the formation of an intermediate cubane-type [3Fe-4S]<sup>+</sup> cluster that contains three Fe<sup>3+</sup> ions. The formation of intermediate [3Fe-4S]<sup>+</sup> cluster was detected by EPR, which revealed a signal  $g \approx 2.01$  with properties characteristic of  $S = 1/2$  [3Fe-4S]<sup>+</sup> cluster upon limited exposure of [4Fe-4S]-FNR to oxygen (284). The time course of [3Fe-4S]<sup>+</sup> cluster EPR intensity changes fitted well to a double-exponential function, consistent with that of an intermediate species (284). The iron released was determined to be in the 2+ oxidation state (284;285). In addition, the reduction product of oxygen was identified as superoxide (284). The second step involves spontaneous rearrangement of the intermediate [3Fe-4S]<sup>+</sup> cluster to form the [2Fe-2S]<sup>2+</sup> cluster, releasing one Fe<sup>3+</sup> and two sulfide ions. Quantitative detection of sulfides released were reported using DTNB [5,5-dithiobis-(2-nitrobenzoic acid)], a colorimetric reagent of the detection of sulfide (286). Taken together, the proposed metal-based oxidation of FNR [4Fe-4S]<sup>2+</sup> cluster can be written as follows:



The main arguments over the two different mechanisms of oxygen-induced FNR cluster conversion were centered around the inconsistencies of the oxidation states of the released iron reported by the two different research groups (283;284) and whether the [3Fe-4S]<sup>+</sup> cluster was a dead-end or functional intermediate (77;284). Attempts at reconciling the two mechanistic proposals have centered on the observation that Fe<sup>2+</sup> and Fe<sup>3+</sup> chelators can significantly enhance

the rate of step 2 in the metal-based oxidation reaction scheme and influence the final oxidation state of released iron ion (285).

Another major unsolved issue regarding oxygen-sensing by FNR involves the physiological significance of the  $[2\text{Fe-2S}]^{2+}$  cluster-bound form of FNR. The presence of the oxygen-induced  $[2\text{Fe-2S}]^{2+}$  cluster *in vivo*, together with rapid reversible conversion between the  $[4\text{Fe-4S}]^{2+}$  and  $[2\text{Fe-2S}]^{2+}$  clusters indicate that the  $[2\text{Fe-2S}]^{2+}$  cluster-containing form of FNR could be physiologically relevant, possibly to facilitate FNR's ability to respond to fluctuating cellular oxygen levels (77;279). Alternatively, the fact that both  $[2\text{Fe-2S}]^-$  and apo-FNR are in the transcriptionally inactive monomeric forms (280) and the absence of measurable amount of Fe-S clusters in FNR in aerobically grown cells due to the lability of the FNR  $[2\text{Fe-2S}]^{2+}$  cluster to superoxide (266), has raised the possibility that the  $[2\text{Fe-2S}]^{2+}$  cluster-bound form of FNR is just a transient intermediate captured in the conversion of the  $[4\text{Fe-4S}]^{2+}$  cluster-containing transcriptionally active form to the inactive apo-form of FNR.

One objective of the work described in this dissertation was to address these two unresolved issues concerning the mechanism of FNR oxygen-sensing and the physiological relevance of the  $[2\text{Fe-2S}]^{2+}$  cluster-bound form of FNR. The results not only shed light on the mechanism and reversibility of the oxygen-induced  $[4\text{Fe-4S}]^{2+}$ -to- $[2\text{Fe-2S}]^{2+}$  cluster conversion in FNR, but also provide the first insights in the mechanism of repair of oxygen-sensitive biological  $[4\text{Fe-4S}]^{2+}$  clusters in general.

### **Summary of Presented Work**

Chapter 2 reports the spectroscopic characterization of Fe-S cluster-bound forms of recombinant *S. cerevisiae* mitochondrial Grx5 using UV-visible absorption/CD, EPR, resonance Raman, VTVH MCD and Mössbauer spectroscopies. The results show that anaerobic cysteine

desulfurase-mediated cluster reconstitution of *S. cerevisiae* Grx5 can yield a form containing one linear type  $[3\text{Fe-4S}]^+$  cluster per dimer in the presence of GSH and a form containing one cubane  $[4\text{Fe-4S}]^{2+}$  cluster per dimer in the presence of DTT. *In vitro* experiments demonstrate that the  $[4\text{Fe-4S}]^{2+}$  cluster-containing Grx5 is competent for restoring the activity of apo aconitase at physiologically relevant rates.

Chapter 3 investigates the proposed cluster trafficking role of CGFS-Grxs in Fe-S cluster assembly, using *Azotobacter vinelandii* as model organism. *In vitro* cluster transfer studies show that Grx5 can quantitatively and rapidly accept an intact  $[2\text{Fe-2S}]^{2+}$  cluster from  $[2\text{Fe-2S}]\text{-IscU}$  in the presence of the ATP-dependent dedicated HscA and HscB molecular co-chaperone systems. In addition, the results demonstrate that the  $[2\text{Fe-2S}]^{2+}$  cluster in Grx5 can be stoichiometrically transferred to the apo ISC-specific Fdx at a physiologically relevant rate.

Chapter 4 investigates the properties and functions of the two CGFS-type Grxs in *Azotobacter vinelandii*. Analytical and spectroscopic (UV-visible absorption and CD, and resonance Raman) characterization of both the general purpose Grx5 and NIF-specific Grx-nif reveals one oxidatively and reductively labile  $[2\text{Fe-2S}]^{2+}$  cluster with complete cysteinyl ligation per Grx homodimer. *In vitro* cluster transfer experiments carried out under anaerobic conditions show that Grx5 and Grx-nif can accept  $[2\text{Fe-2S}]^{2+}$  clusters from  $[4\text{Fe-4S}]^{2+}$  cluster donors including NfuA, IscU and NifU.

Chapter 5 investigates the oxygen-sensing mechanism of the bacterial global transcriptional regulator FNR. The combination of resonance Raman, UV-visible absorption and CD, and mass spectrometry studies reveals that the oxygen-induced cluster transformation of the FNR  $[4\text{Fe-4S}]^{2+}$  cluster occurs by a sulfur-based oxidation mechanism and the formation of an atypical  $[2\text{Fe-2S}]^{2+}$  cluster with cysteine persulfide-ligation. The results also demonstrate that

cluster conversion is reversible under anaerobic conditions in the presence of a dithiol reagent and a small excess of  $\text{Fe}^{2+}$ . The observation of analogous oxygen-induced  $[\text{4Fe-4S}]^{2+}$ -to- $[\text{2Fe-2S}]^{2+}$  cluster transformations in enzymes with oxygen-sensitive  $[\text{4Fe-4S}]$  clusters suggests that the reverse process may represent a viable repair mechanism for oxygen-damaged biological  $[\text{4Fe-4S}]$  clusters that requires only anaerobic conditions and an  $\text{Fe}^{2+}$  donor.

Appendix A reports spectroscopic characterization (UV-visible absorption, EPR, resonance Raman, VTMCD, VTVH MCD and Mössbauer spectroscopies) of Fe-bound forms of *A. vinelandii*  $\text{Nif}^{\text{IscA}}$ . The studies reveal that  $\text{Nif}^{\text{IscA}}$  is able to bind a rhombic intermediate-spin ( $S = 3/2$ )  $\text{Fe}^{3+}$  center or a rhombic high spin ( $S = 2$ )  $\text{Fe}^{2+}$  center per homodimer. The Fe-bound  $\text{Nif}^{\text{IscA}}$  can undergo reversible redox cycling between  $\text{Fe}^{3+}$  and  $\text{Fe}^{2+}$  forms with a midpoint potential of  $+ 36 \pm 15$  mV at pH 7.8 (NHE), and the Fe in both  $\text{Fe}^{3+}$ - and  $\text{Fe}^{2+}$ -bound forms of  $\text{Nif}^{\text{IscA}}$  can be released by L-cysteine as free  $\text{Fe}^{2+}$ . Possible roles for Fe-bound A-type proteins are discussed.

Appendix B investigates the mechanism of  $[\text{4Fe-4S}]^{2+}$  cluster assembly on *A. vinelandii*  $\text{Nif}^{\text{IscA}}$  and its role in maturation of  $[\text{4Fe-4S}]^{2+}$  proteins *in vitro*. The results show that cluster-bound  $\text{Nif}^{\text{IscA}}$  can undergo rapid and reversible cycling between forms containing one  $[\text{2Fe-2S}]^{2+}$  cluster and one  $[\text{4Fe-4S}]^{2+}$  cluster per homodimer via DTT-induced two-electron reductive coupling of two  $[\text{2Fe-2S}]^{2+}$  clusters and oxygen-induced cleavage of the  $[\text{4Fe-4S}]^{2+}$  cluster in the presence of apo  $\text{Nif}^{\text{IscA}}$ . *In vitro* cluster transfer experiments monitored by UV-visible absorption and CD spectroscopies demonstrate that  $\text{Nif}^{\text{IscA}}$  accepts  $[\text{2Fe-2S}]^{2+}$  cluster from  $[\text{4Fe-4S}]^{2+}$  cluster-containing  $\text{NifU}$  under strict anaerobic conditions. In addition, the  $[\text{4Fe-4S}]^{2+}$  cluster-bound form of  $\text{Nif}^{\text{IscA}}$  is shown to be competent for rapid *in vitro* activation of apo nitrogenase Fe protein.

Appendix C shows that CGFS-Grxs and A-type proteins can function as partners in cellular Fe-S cluster trafficking and repair. Cluster transfer experiments monitored using UV-visible CD spectroscopy reveals rapid, unidirectional and quantitative transfer of intact  $[2\text{Fe-2S}]^{2+}$  clusters from various cluster-bound CGFS-Grxs homodimer (*Av* Grx5, *At* GrxS14 and *Sc* Grx3) to apo A-type proteins (*Av* <sup>Nif</sup>IscA and *At* SufA). The results also show that the direction of cluster transfer can be reversed by the formation of the  $[2\text{Fe-2S}]^{2+}$  cluster-containing heterodimeric yeast Grx3/Fra2 complex.

### Abbreviations

ABC, ATP binding cassette; *A.thaliana*, *At*, *Arabidopsis thaliana*; *A. vinelandii.*, *Av*, *Azotobater vinelandii*; BAN, backbone amide nitrogen; BioB, biotin synthase; *B. subtilis*, *Bs*, *Bacillus subtilis*; CD, circular dichroism; CIA, cytosolic iron sulfur protein assembly; CRP, cyclic-AMP receptor protein; DTNB, 5,5-dithiobis-(2-nitrobenzoic acid; DTT, dithiothreitol; *E. coli*, *Ec*, *Escherichia coli*; EDTA, ethylenediaminetetraacetic acid; EPR, electron paramagnetic resonance; Fdx, ferredoxin; FeMo-co, iron molybdenum cofactor; FNR, fumarate and nitrate reduction; FRDA, Friedreich's ataxia; FTR, ferredoxin-thioredoxin reductase; FXN, frataxin; Grx, glutaredoxin; GSH, glutathione; HDR, heterodisulfide reductase; HiPIP, high potential iron-sulfur protein; Hsc, heat shock cognate; IRE, iron-responsive element; IRP, iron-regulatory protein; ISC, iron sulfur cluster; LipA, lipoyl synthase; MiaB, a tRNA-methylthiotransferase; NADH, nicotinamide adenine dinucleotide (reduced); NHE, normal hydrogen electrode; NIF, nitrogen fixation; NMR, nuclear magnetic resonance; PRPP, phosphoribosylpyrophosphate; SAM, S-adenosylmethionine; *S. cerevisiae*, *Sc*, *Saccharomyces cerevisiae*; *S. pombe*, *Sp*, *Schizosaccharomyces pombe*; SUF, sulfur utilization factor; Trx, thioredoxin; VTMCd, variable-

temperature magnetic circular dichroism; XPD, xeroderma pigmentosum complementation group D.

## References

1. Campuzano, V., Montermini, L., Molto, M. D., Pianese, L., Cossee, M., Cavalcanti, F., Monros, E., Rodius, F., Duclos, F., and Monticelli, A. (1996) Friedreich's ataxia: autosomal recessive disease caused by an intronic GAA triplet repeat expansion, *Science* 271, 1423-1427.
2. Bencze, K. Z., Kondapalli, K. C., Cook, J. D., McMahon, S., Millan-Pacheco, C., Pastor, N., and Stemmler, T. L. (2006) The structure and function of frataxin, *Crit Rev. Biochem. Mol. Biol.* 41, 269-291.
3. Rotig, A., de, L. P., Chretien, D., Foury, F., Koenig, M., Sidi, D., Munnich, A., and Rustin, P. (1997) Aconitase and mitochondrial iron-sulphur protein deficiency in Friedreich ataxia, *Nat. Genet.* 17, 215-217.
4. Michael, S., Petrocine, S. V., Qian, J., Lamarche, J. B., Knutson, M. D., Garrick, M. D., and Koeppen, A. H. (2006) Iron and iron-responsive proteins in the cardiomyopathy of Friedreich's ataxia, *Cerebellum.* 5, 257-267.
5. Larsson, L. E., Linderholm, H., Mueller, R., Ringqvist, T., and Soernaes, R. (1964) Hereditary metabolic myopathy with paroxysmal myoglobinuria due to abnormal glycolysis, *J. Neurol. Neurosurg. Psychiatry* 27, 361-380.
6. Haller, R. G., Henriksson, K. G., Jorfeldt, L., Hultman, E., Wibom, R., Sahlin, K., Areskog, N. H., Gunder, M., Ayyad, K., Blomqvist, C. G., and . (1991) Deficiency of skeletal muscle succinate dehydrogenase and aconitase. Pathophysiology of exercise in a novel human muscle oxidative defect, *J. Clin. Invest.* 88, 1197-1206.
7. Mochel, F., Knight, M. A., Tong, W. H., Hernandez, D., Ayyad, K., Taivassalo, T., Andersen, P. M., Singleton, A., Rouault, T. A., Fischbeck, K. H., and Haller, R. G. (2008) Splice mutation in the iron-sulfur cluster scaffold protein ISCU causes myopathy with exercise intolerance, *Am. J. Hum. Genet.* 82, 652-660.
8. Olsson, A., Lind, L., Thornell, L. E., and Holmberg, M. (2008) Myopathy with lactic acidosis is linked to chromosome 12q23.3-24.11 and caused by an intron mutation in the ISCU gene resulting in a splicing defect, *Hum. Mol. Genet.* 17, 1666-1672.
9. Navarro-Sastre, A., Tort, F., Stehling, O., Uzarska, M. A., Arranz, J. A., Del, T. M., Labayru, M. T., Landa, J., Font, A., Garcia-Villoria, J., Merinero, B., Ugarte, M., Gutierrez-Solana, L. G., Campistol, J., Garcia-Cazorla, A., Vaquerizo, J., Riudor, E., Briones, P., Elpeleg, O., Ribes, A., and Lill, R. (2011) A fatal mitochondrial disease is associated with defective NFU1 function in the maturation of a subset of mitochondrial Fe-S proteins, *Am. J. Hum. Genet.* 89, 656-667.
10. Bandyopadhyay, S., Naik, S., O'Carroll, I. P., Huynh, B. H., Dean, D. R., Johnson, M. K., and Dos Santos, P. C. (2008) A proposed role for the *Azotobacter vienlandii* NfuA protein as an intermediate iron-sulfur cluster carrier, *J. Biol. Chem.* 283, 14092-14099.

11. Cameron, J. M., Janer, A., Levandovskiy, V., Mackay, N., Rouault, T. A., Tong, W. H., Ogilvie, I., Shoubridge, E. A., and Robinson, B. H. (2011) Mutations in iron-sulfur cluster scaffold genes NFU1 and BOLA3 cause a fatal deficiency of multiple respiratory chain and 2-oxoacid dehydrogenase enzymes, *Am. J. Hum. Genet.* 89, 486-495.
12. Bottomley, S. S. (2006) Congenital sideroblastic anemias, *Curr. Hematol. Rep.* 5, 41-49.
13. Rouault, T. A. and Tong, W. H. (2008) Iron-sulfur cluster biogenesis and human disease, *Trends Genet.* 24, 398-407.
14. Sheftel, A., Stehling, O., and Lill, R. (2010) Iron-sulfur proteins in health and disease, *Trends Endocrinol. Metab.* 21, 302-314.
15. Fleming, M. D. (2011) Congenital sideroblastic anemias: iron and heme lost in mitochondrial translation, *Hematology. Am. Soc. Hematol. Educ. Program.* 2011, 525-531.
16. Rodríguez-Manzanque, M. T., Tamarit, J., Bellí, G., Ros, J., and Herrero, E. (2002) Grx5 is a mitochondrial glutaredoxin required for the activity of iron/sulfur enzymes, *Mol. Biol. Cell* 13, 1109-1121.
17. Mühlenhoff, U., Gerber, J., Richhardt, N., and Lill, R. (2003) Components involved in assembly and dislocation of iron-sulfur clusters on the scaffold protein IscU1p, *EMBO J.* 22, 4815-4825.
18. Camaschella, C., Campanelle, A. F. L., Boschetto, L., Merlini, R., Silvestri, L., Levi, S., and Iolascon, A. (2007) The human counterpart of zebrafish *shiraz* shows sideroblastic-like microcytic anemia and iron overload., *Blood* 110, 1353-1358.
19. Romao, M. J. and Archer, M. Structural versatility of proteins containing rubredoxin-type centers. In *Iron Metabolism*; Ferreira, G. C., Moura, J. J. G., and Franco, R.; Wiley-VCH Verlag; 1999; 341-358.
20. Link, T. A. (1999) The structures of Rieske and Rieske-type proteins, *Adv. Inorg. Chem.* 47, 83-157.
21. Li, H., Mapolelo, D. T., Dingra, N. N., Naik, S. G., Lees, N. S., Hoffman, B. M., Riggs-Gelasco, P. J., Huynh, B. H., Johnson, M. K., and Outten, C. E. (2009) The yeast iron regulatory proteins Grx3/4 and Fra2 form heterodimeric complexes containing a [2Fe-2S] cluster with cysteinyl and histidyl ligation, *Biochemistry* 48, 9569-9581.
22. Paddock, M. L., Wiley, S. E., Axelrod, H. L., Cohen, A. E., Roy, M., Abresch, E. C., Capraro, D., Murphy, A. N., Nechushtai, R., Dixon, J. E., and Jennings, P. A. (2007) MitoNEET is a uniquely folded 2Fe-2S outer mitochondrial membrane protein stabilized by pioglitazone, *Proc. Natl. Acad. Sci. USA* 104, 14342-14347.
23. Lin, J., Zhou, T., Ye, K., and Wang, J. (2007) Crystal structure of human mitoNEET reveals distinct groups of iron sulfur proteins, *Proc. Natl. Acad. Sci. USA* 104, 14640-14645.

24. Hou, X., Liu, R., Ross, S., Smart, E. J., Zhu, H., and Gong, W. (2007) Crystallographic studies of human MitoNEET, *J. Biol. Chem.* 282, 33242-33246.
25. Fleischhacker, A. S., Stubna, A., Hsueh, K.-L., Guo, Y., Teter, S. J., Rose, J. C., Brunold, T. C., Markley, J. L., Munck, E., and Kiley, P. J. (2012) Characterization of the [2Fe-2S] Cluster of Escherichia coli Transcription Factor IscR, *Biochemistry* 51, 4453-4462.
26. Yankovskaya, V., Horsefield, R., Törnroth, S., Luna-Chavez, C., Miyoshi, H., Léger, C., Byrne, B., Cecchini, G., and Iwata, S. (2003) Architecture of succinate dehydrogenase and reactive oxygen species generation, *Science* 299, 700-704.
27. Hagen, W. R., Silva, P. J., Amorim, M. A., Hagedoorn, P. L., Wassink, H., Haaker, H., and Robb, F. T. (2000) Novel structure and redox chemistry of the prosthetic groups of the iron-sulfur flavoprotein sulfide dehydrogenase from *Pyrococcus furiosus*; evidence for a [2Fe-2S] cluster with Asp(Cys)<sub>3</sub> ligands, *J. Biol. Inorg. Chem.* 5, 527-534.
28. Berkovitch, F., Nicolet, Y., Wan, J. T., Jarrett, J. T., and Drennan, C. L. (2004) Crystal structure of biotin synthase, an S-adenosylmethionine-dependent radical enzyme, *Science* 303, 76-79.
29. Leggate, E. J., Bill, E., Essigke, T., Ullmann, G. M., and Hirst, J. (2004) Formation and characterization of an all-ferrous Rieske cluster and stabilization of the [2Fe-2S]<sup>0</sup> core by protonation, *Proc. Natl. Acad. Sci. USA* 101, 10913-10918.
30. Mayerle, J. J., Frankel, R. B., Holm, R. H., Ibers, J. A., Phillips, W. D., and Weiher, J. F. (1973) Synthetic analogs of the active sites of iron-sulfur proteins. Structure and properties of bis(o-xylyldithiolato-m<sup>2</sup>-sulfidoferrate (3)), an analog of the 2Fe-2S proteins, *Proc. Natl. Acad. Sci. USA* 70, 2429-2433.
31. Im, S.-C., Kohzuma, T., McFarlane, W., Gaillard, J., and Sykes, A. G. (1997) Formation, properties, and characterization of a fully reduced Fe(II)Fe(II) form of spinach (and parsley) [2Fe-2S] ferredoxin with the macrocyclic complex [Cr(15-aneN<sub>4</sub>)(H<sub>2</sub>O)<sub>2</sub>]<sup>2+</sup> as reductant, *Inorg. Chem.* 36, 1388-1396.
32. Crouse, B. R., Meyer, J., and Johnson, M. K. (1995) Spectroscopic evidence for a reduced Fe<sub>2</sub>S<sub>2</sub> cluster with a S = 9/2 ground state in mutant forms of *Clostridium pasteurianum* 2Fe ferredoxin, *J. Am. Chem. Soc.* 117, 9612-9613.
33. Achim, C., Golinelli, M.-P., Bominaar, E. L., Meyer, J., and Münck, E. (1996) Mossbauer study of Cys56Ser mutant 2Fe ferredoxin from *Clostridium pasteurianum*: Evidence for double exchange in an [Fe<sub>2</sub>S<sub>2</sub>]<sup>+</sup> cluster, *J. Am. Chem. Soc.* 118, 8168-8169.
34. Johnson, M. K., Duin, E. C., Crouse, B. R., Golinelli, M.-P., and Meyer, J. Valence-delocalized [Fe<sub>2</sub>S<sub>2</sub>]<sup>+</sup> clusters. In *Spectroscopic methods in bioinorganic chemistry*; Solomon, E. I. and Hodgson, K. O.; American Chemical Society; 1998; 286-301.
35. Calzolari, L., Gorst, C. M., Zhou, Z.-H., Teng, Q., Adams, M. W. W., and La Mar, G. N. (1995) <sup>1</sup>H-NMR investigation of the electronic and molecular structure of the 4-iron cluster

- ferredoxin from the hyperthermophile *Pyrococcus furiosus* - identification of Asp-14 as a cluster ligand in each of the 4 redox states., *Biochemistry* 34, 11373-11384.
36. Volbeda, A., Charon, M.-H., Piras, C., Hatchikian, E. C., Frey, M., and Fontecilla-Camps, J. C. (1995) Crystal structure of the nickel-iron hydrogenase from *Desulfovibrio gigas*, *Nature* 373, 580-587.
  37. Peters, J. W., Lanzilotta, W. N., Lemon, B. J., and Seefeldt, L. C. (1998) X-ray crystal structure of the Fe-only hydrogenase (Cp1) from *Clostridium pasteurianum* to 1.8 Angstrom resolution, *Science* 282, 1853-1858.
  38. Bertero, M. G., Rothery, R. A., Palak, M., Hou, C., Lim, D., Blasco, F., Weiner, J. H., and Strynadka, N. C. (2003) Insights into the respiratory electron transfer pathway from the structure of nitrate reductase A, *Nat. Struct. Biol.* 10, 681-687.
  39. Beinert, H., Kennedy, M. C., and Stout, C. D. (1996) Aconitase as iron-sulfur protein, enzyme, and iron-regulatory protein, *Chem. Rev.* 96, 2335-2373.
  40. Flint, D. H. and Allen, R. M. (1996) Iron-sulfur proteins with non-redox functions, *Chem. Rev.* 96, 2315-2334.
  41. Frey, P. A., Hegeman, A. D., and Ruzicka, F. J. (2008) The radical SAM superfamily, *Crit. Rev. Biochem. Mol. Biol.* 43, 63-88.
  42. Nicolet, Y., Amara, P., Mouesca, J. M., and Fontecilla-Camps, J. C. (2009) Unexpected electron transfer mechanism upon AdoMet cleavage in radical SAM proteins, *Proc. Natl. Acad. Sci. USA* 106, 14867-14871.
  43. Watt, G. D. and Reddy, K. R. N. (1994) Formation of an all ferrous Fe<sub>4</sub>S<sub>4</sub> cluster in the iron-protein-component of *Azotobacter vinelandii* nitrogenase, *J. Inorg. Biochem.* 53, 281-294.
  44. Angove, H. C., Yoo, S. J., Burgess, B. K., and Münck, E. (1997) Mössbauer and EPR evidence for an all-ferrous Fe<sub>4</sub>S<sub>4</sub> cluster with *S* = 4 in the Fe protein of nitrogenase, *J. Am. Chem. Soc.* 119, 8730-8731.
  45. Strop, P., Takahara, P. M., Chiu, H.-J., Angove, H. C., Burgess, B. K., and Rees, D. C. (2001) Crystal structure of the all-ferrous [4Fe-4S]<sup>0</sup> form of the nitrogenase iron protein from *Azotobacter vinelandii*, *Biochemistry* 40, 651-656.
  46. Walters, E. M., Garcia-Serres, R., Jameson, G. N. L., Glauser, D. A., Bourquin, F., Manieri, W., Schürmann, P., Huynh, B. H., and Johnson, M. K. (2005) Spectroscopic characterization of site-specific [Fe<sub>4</sub>S<sub>4</sub>] cluster chemistry in ferredoxin:thioredoxin reductase: Implications for the catalytic mechanism, *J. Am. Chem. Soc.* 127, 9612-9624.
  47. Yang, J., Naik, S. G., Ortillo, D. O., Garcia-Serres, R., Li, M., Broderick, W. E., Huynh, B. H., and Broderick, J. B. (2009) The iron-sulfur cluster of pyruvate formate-lyase activating

- enzyme in whole cells: cluster interconversion and a valence-localized  $[4\text{Fe-4S}]^{2+}$  state, *Biochemistry* 48, 9234-9241.
48. Banci, L., Bertini, I., Ciurli, S., Ferretti, S., Luchinat, C., and Piccioli, M. (1993) The electronic structure of  $[\text{Fe}_4\text{S}_4]^{3+}$  clusters in proteins. An investigation of the oxidized high-potential iron-sulfur protein II from *Ectothiorhodospira vacuolata*, *Biochemistry* 32, 9387-9397.
  49. Noodleman, L., Case, D. A., and Mouesca, J.-M. (1996) Valence electron delocalization in polynuclear iron-sulfur clusters, *J. Biol. Inorg. Chem.* 1, 177-182.
  50. Mouesca, J.-M., Rius, G., and Lamotte, B. (1993) Single crystal proton ENDOR studies of the  $[\text{Fe}_4\text{S}_4]^{3+}$  cluster: Determination of the spin population distribution and a proposal of a model to interpret the  $^1\text{H}$  NMR paramagnetic shifts in high potential ferredoxins, *J. Am. Chem. Soc.* 115, 4714-4731.
  51. Pandelia, M. E., Nitschke, W., Infossi, P., Giudici-Orticoni, M. T., Bill, E., and Lubitz, W. (2011) Characterization of a unique  $[\text{FeS}]$  cluster in the electron transfer chain of the oxygen tolerant  $[\text{NiFe}]$  hydrogenase from *Aquifex aeolicus*, *Proc. Natl. Acad. Sci. USA* 108, 6097-6102.
  52. Fritsch, J., Scheerer, P., Frielingsdorf, S., Kroschinsky, S., Friedrich, B., Lenz, O., and Spahn, C. M. (2011) The crystal structure of an oxygen-tolerant hydrogenase uncovers a novel iron-sulphur centre, *Nature* 479, 249-252.
  53. Johnson, M. K., Duderstadt, R. E., and Duin, E. C. (1999) Biological and synthetic  $[\text{Fe}_3\text{S}_4]$  clusters, *Adv. Inorg. Chem.* 47, 1-82.
  54. Duff, J. L. C., Breton, J. L., Butt, J. N., Armstrong, F. A., and Thomson, A. J. (1996) Novel redox chemistry of the  $[3\text{Fe-4S}]$  clusters: Electrochemical characterization of the all-Fe(II) form of the  $[3\text{Fe-4S}]$  cluster generated reversibly in various proteins and its spectroscopic investigation in *Sulfolobus acidocaldarius* ferredoxin, *J. Am. Chem. Soc.* 118, 8593-8603.
  55. Hagen, K. S., Watson, A. D., and Holm, R. H. (1983) Synthetic routes to  $\text{Fe}_2\text{S}_2$ ,  $\text{Fe}_3\text{S}_4$ ,  $\text{Fe}_4\text{S}_4$ , and  $\text{Fe}_6\text{S}_9$  clusters from the common precursor  $[\text{Fe}(\text{SC}_2\text{H}_5)_4]^{2-}$ : Structures and properties of  $[\text{Fe}_3\text{S}_4(\text{SR})_4]^{3-}$  and  $[\text{Fe}_6\text{S}_9(\text{SC}_2\text{H}_5)_2]^{4-}$ , examples of the newest types of Fe-S-SR clusters, *J. Am. Chem. Soc.* 105, 3905-3913.
  56. Kennedy, M. C., Kent, T. A., Emptage, M. H., Merkle, H., Beinert, H., and Münck, E. (1984) Evidence for the formation of a linear  $[3\text{Fe-4S}]$  cluster in partially unfolded aconitase, *J. Biol. Chem.* 259, 14463-14471.
  57. Richards, A. J. M., Thomson, A. J., Holm, R. H., and Hagen, K. S. (1990) The magnetic circular dichroism spectra of the linear trinuclear clusters  $[\text{Fe}_3\text{S}_4(\text{SR})_4]^{3-}$  in purple aconitase and in a synthetic model, *Spectrochim. Acta* 46A, 987-993.
  58. Girerd, J.-J., Papaefthymiou, G. C., Watson, A. D., Gamp, E., Hagen, K. S., Edelstein, N., Frankel, R. B., and Holm, R. H. (1984) Electronic properties of the linear

- antiferromagnetically coupled clusters  $[\text{Fe}_3\text{S}_4(\text{SR})_4]^{3-}$ , structural isomers of the  $[\text{Fe}_3\text{S}_4]^+$  unit in iron-sulfur proteins, *J. Am. Chem. Soc.* 106, 5941-5947.
59. Gailer, J., George, G. N., Pickering, I. J., Prince, R. C., Kohlhepp, P., Zhang, D., Walker, F. A., and Winzerling, J. J. (2001) Human Cytosolic Iron Regulatory Protein 1 Contains a Linear Iron-Sulfur Cluster, *J. Am. Chem. Soc.* 123, 10121-10122.
  60. Krebs, C., Henshaw, T. F., Cheek, J., Huynh, B. H., and Broderick, J. B. (2000) Conversion of 3Fe-4S to 4Fe-4S Clusters in Native Pyruvate Formate-Lyase Activating Enzyme: Mössbauer Characterization and Implications for Mechanism, *J. Am. Chem. Soc.* 122, 12497-12506.
  61. Jones, K., Gomes, C. M., Huber, H., Teixeira, M., and Wittung-Stafshede, P. (2002) Formation of a linear [3Fe-4S] cluster in a seven-iron ferredoxin triggered by polypeptide unfolding, *J. Biol. Inorg. Chem.* 7, 357-362.
  62. Griffin, S., Higgins, C. L., Soulimane, T., and Wittung-Stafshede, P. (2003) High thermal and chemical stability of *Thermus thermophilus* seven-iron ferredoxin. Linear clusters form at high pH on polypeptide unfolding, *Eur. J. Biochem.* 270, 4736-4743.
  63. Higgins, C. L. and Wittung-Stafshede, P. (2004) Formation of linear three-iron clusters in *Aquilex aeolicus* two-iron ferredoxins: effect of protein unfolding speed, *Arch. Biochem. Biophys.* 427, 154-163.
  64. Leal, S. S., Teixeira, M., and Gomes, C. M. (2004) Studies on the degradation pathway of iron-sulfur centers during unfolding of a hyperstable ferredoxin: Cluster dissociation, iron release and proteins stability, *J. Biol. Inorg. Chem.* 9, 987-996.
  65. Peters, J. W., Stowell, M. H. B., Soltis, S. M., Finnegan, M. G., Johnson, M. K., and Rees, D. C. (1997) Redox-dependent structural-changes in the nitrogenase P-cluster, *Biochemistry* 36, 1181-1187.
  66. Lee, C. C., Blank, M. A., Fay, A. W., Yoshizawa, J. M., Hu, Y., Hodgson, K. O., Hedman, B., and Ribbe, M. W. (2009) Stepwise formation of P-cluster in nitrogenase MoFe protein, *Proc. Natl. Acad. Sci. USA* 106, 18474-18478.
  67. Burgess, B. K. and Lowe, D. J. (1996) Mechanism of molybdenum nitrogenase, *Chem. Rev.* 96, 2983-3011.
  68. Ohki, Y., Imada, M., Murata, A., Sunada, Y., Ohta, S., Honda, M., Sasamori, T., Tokitoh, N., Katada, M., and Tatsumi, K. (2009) Synthesis, structures, and electronic properties of [8Fe-7S] cluster complexes modeling the nitrogenase P-cluster, *J. Am. Chem. Soc.* 131, 13168-13178.
  69. Hu, Y. and Ribbe, M. W. (2010) Decoding the nitrogenase mechanism: the homologue approach, *Acc. Chem. Res.* 43, 475-484.

70. Rao, P. V. and Holm, R. H. (2004) Synthetic analogues of the active sites of iron-sulfur proteins, *Chem. Rev.* 104, 527-559.
71. Kent, T. A., Dreyer, J.-C., Kennedy, M. C., Huynh, B. H., Emptage, M. H., Beinert, H., and Münck, E. (1982) Mössbauer studies of beef heart aconitase: Evidence for facile interconversions of iron-sulfur clusters, *Proc. Natl. Acad. Sci. USA* 79, 1096-1100.
72. Butt, J. N., Armstrong, F. A., Breton, J., George, S. J., Thomson, A. J., and Hatchikian, E. C. (1991) Investigation of the metal ion uptake reactivities of [3Fe-4S] clusters in proteins: Voltammetry of co-adsorbed ferredoxin-aminocyclitol films at graphite electrodes and spectroscopic identification of transformed clusters, *J. Am. Chem. Soc.* 113, 6663-6670.
73. Finnegan, M. G., Conover, R. C., Park, J.-B., Zhou, Z.-H., Adams, M. W. W., and Johnson, M. K. (1995) Electronic, magnetic, redox, and ligand-binding properties of [MFe<sub>3</sub>S<sub>4</sub>] clusters (M = Zn, Co, Mn) in *Pyrococcus furiosus* ferredoxin, *Inorg. Chem.* 34, 5358-5369.
74. Anderson, G. L. and Howard, J. B. (1984) Reactions with the oxidized iron protein of *Azotobacter vinelandii* nitrogenase: Formation of a 2Fe center., *Biochemistry* 23, 2118-2122.
75. Ryle, M. J., Lanzilotta, W. N., Seefeldt, L. C., Scarrow, R. C., and Jensen, G. M. (1996) Circular dichroism and X-ray spectroscopies of *Azotobacter vinelandii* nitrogenase iron protein., *J. Biol. Chem.* 271, 1551-1557.
76. Sen, S., Igarashi, R., Smith, A. D., Johnson, M. K., Seefeldt, L. C., and Peters, J. W. (2004) A conformational mimic of the MgATP-bound "on state" of the nitrogenase iron protein, *Biochemistry* 43, 1787-1797.
77. Khoroshilova, N., Popescu, C., Münck, E., Beinert, H., and Kiley, P. J. (1997) Iron-sulfur cluster disassembly in the FNR protein of *Escherichia coli* by O<sub>2</sub>: [4Fe-4S] to [2Fe-2S] conversion with loss of biological activity, *Proc. Natl. Acad. Sci. USA* 94, 6087-6092.
78. Broderick, J. B., Duderstadt, R. E., Fernandez, D. C., Wojtuszewski, K., Henshaw, T. F., and Johnson, M. K. (1997) Pyruvate formate-lyase activating enzyme is an iron-sulfur protein, *J. Am. Chem. Soc.* 119, 7396-7397.
79. Ollagnier, S., Meier, C., Mulliez, E., Gaillard, J., Schuenemann, V., Trautwein, A. X., Mattioli, T., Lutz, M., and Fontecave, M. (1999) Assembly of 2Fe-2S and 4Fe-4S clusters in the anaerobic ribonucleotide reductase from *Escherichia coli*, *J. Am. Chem. Soc.* 121, 6344-6350.
80. Pierrel, F., Hernandez, H., Johnson, M. K., Fontecave, M., and Atta, M. (2003) MiaB protein from *Thermotoga maritima*: characterization of an extremely thermophilic tRNA-methylthiotransferase, *J. Biol. Chem.* 278, 29515-29524.
81. Cospér, M. M., Krebs, B., Hernandez, H., Jameson, G., Eidsness, M. K., Huynh, B. H., and Johnson, M. K. (2004) Characterization of the cofactor content of *Escherichia coli* biotin synthase, *Biochemistry* 43, 2007-2021.

82. Agar, J. N., Krebs, B., Frazzon, J., Huynh, B. H., Dean, D. R., and Johnson, M. K. (2000) IscU as a scaffold for iron-sulfur cluster biosynthesis: Sequential assembly of [2Fe-2S] and [4Fe-4S] clusters in IscU, *Biochemistry* 39, 7856-7862.
83. Chandramouli, K., Unciuleac, M.-C., Naik, S., Dean, D. R., Huynh, B. H., and Johnson, M. K. (2007) Formation and properties of [4Fe-4S] clusters on the IscU scaffold protein, *Biochemistry* 46, 6804-6811.
84. Smith, A. D., Jameson, G. N. L., Dos Santos, P. C., Agar, J. N., Naik, S., Krebs, C., Frazzon, J., Dean, D. R., Huynh, B. H., and Johnson, M. K. (2005) NifS-mediated assembly of [4Fe-4S] clusters in the N- and C-terminal domains of the NifU scaffold protein, *Biochemistry* 44, 12955-12969.
85. Page, C. C., Moser, C. C., Chen, X., and Dutton, P. L. (1999) Natural engineering principles of electron tunnelling in biological oxidation-reduction, *Nature* 402, 47-52.
86. Johnson, M. K. and Smith, A. D. Iron-sulfur proteins. In *Encyclopedia of Inorganic Chemistry, Second Edition*; King, R. B.; John Wiley & Sons; 2005; 2589-2619.
87. Challand, M. R., Driesener, R. C., and Roach, P. L. (2011) Radical S-adenosylmethionine enzymes: mechanism, control and function, *Nat. Prod. Rep.* 28, 1696-1721.
88. Dos Santos, P. C., Dean, D. R., Hu, Y., and Ribbe, M. W. (2004) Formation and insertion of the nitrogenase iron-molybdenum cofactor, *Chem. Rev.* 104, 1159-1173.
89. Spatzal, T., Aksoyoglu, M., Zhang, L., Andrade, S. L., Schleicher, E., Weber, S., Rees, D. C., and Einsle, O. (2011) Evidence for interstitial carbon in nitrogenase FeMo cofactor, *Science* 334, 940-940.
90. Lancaster, K. M., Roemelt, M., Ethenhuber, P., Hu, Y., Ribbe, M. W., Neese, F., Bergmann, U., and DeBeer, S. (2011) X-ray emission spectroscopy evidences a central carbon in the nitrogenase iron-molybdenum cofactor, *Science* 334, 974-977.
91. Dobbek, H., Svetlitchnyi, V., Gremer, L., Huber, R., and Meyer, O. (2001) Crystal structure of carbon monoxide dehydrogenase reveals a [Ni-4Fe-5S] cluster, *Science* 293, 1281-1285.
92. Crane, B. R., Siegel, L. M., and Getzoff, E. D. (1995) Sulfite reductase structure at 1.6 Å - Evolution and catalysis for reduction of inorganic anions, *Science* 270, 59-67.
93. Crane, B. R., Siegel, L. M., and Getzoff, E. D. (1997) Structures of the siroheme- and [4Fe-4S]-containing active center of sulfite reductase in different states of oxidation: Heme activation via reduction-gated exogenous ligand exchange, *Biochemistry* 36, 12101-12119.
94. Doukov, T. I., Iverson, T. M., Seravalli, J., Ragsdale, S. W., and Drennan, C. L. (2002) A Ni-Fe-Cu center in a bifunctional carbon monoxide dehydrogenase/acetyl-CoA synthase, *Science* 298, 567-572.

95. Darnault, C., Volbeda, A., Kim, E. J., Legrand, P., Vernède, X., Lindahl, P. A., and Fontecilla-Camps, J. C. (2003) Ni-Zn-[Fe<sub>4</sub>-S<sub>4</sub>] and Ni-Ni-[Fe<sub>4</sub>-S<sub>4</sub>] clusters in closed and open  $\alpha$  subunits of acetyl-CoA synthase/carbon monoxide dehydrogenase, *Nat. Struct. Biol.* 10, 271-279.
96. Svetlitchnyi, V., Dobbek, H., Meyer-Klaucke, W., Meins, T., Thiele, T., Römer, P., Huber, R., and Meyer, O. (2004) A functional Ni-Ni-[4Fe-4S] cluster in the monomeric acetyl-CoA synthase from *Carboxydotherrnus hydrogenoformans*, *Proc. Natl. Acad. Sci. USA* 101, 446-451.
97. Nicolet, Y., Cavazza, C., and Fontecilla-Camps, J. C. (2002) Fe-only hydrogenases: structure, function and evolution, *J. Inorg. Biochem.* 91, 1-8.
98. Beinert, H. and Kiley, P. J. (1999) Fe-S proteins in sensing and regulatory functions, *Curr. Opin. Chem. Biol.* 3, 152-157.
99. Kiley, P. J. and Beinert, H. (1998) Oxygen sensing by the global regulator, FNR: The role of the iron-sulfur cluster, *FEMS Microbiol. Rev.* 22, 341-352.
100. Crack, J. C., Jarvis, A. J., Gaskell, A. A., White, G. F., Green, J., Thomson, A. J., and Le Brun, N. E. (2008) Signal perception by FNR: the role of the iron-sulfur cluster, *Biochem. Soc. Trans.* 36, 1144-1148.
101. Cruz-Ramos, H., Crack, J., Wu, G., Hughes, M. N., Scott, C., Thomson, A. J., Green, J., and Poole, R. K. (2002) NO sensing by FNR: regulation of *E. coli* NO-detoxifying flavohaemoglobin, Hmp, *EMBO J.* 21, 3235-3244.
102. Giel, J. L., Rodionov, D., Liu, M., Blattner, F. R., and Kiley, P. J. (2006) IscR-dependent gene expression links iron-sulphur cluster assembly to the control of O<sub>2</sub>-regulated genes in *Escherichia coli*, *Mol. Microbiol.* 60, 1058-1075.
103. Schwartz, C. J., Giel, J. L., Patschkowski, T., Luther, C., Ruzicka, F. J., Beinert, H., and Kiley, P. J. (2001) IscR, an Fe-S cluster-containing transcription factor, represses expression of *Escherichia coli* genes encoding Fe-S cluster assembly proteins, *Proc. Natl. Acad. Sci. USA* 98, 14895-14900.
104. Walden, W. E., Selezneva, A. I., Dupuy, J., Volbeda, A., Fontecilla-Camps, J. C., Theil, E. C., and Volz, K. (2006) Structure of dual function iron regulatory protein 1 complexed with ferritin IRE-RNA, *Science* 314, 1903-1908.
105. Wallander, M. L., Leibold, E. A., and Eisenstein, R. S. (2006) Molecular control of vertebrate iron homeostasis by iron regulatory proteins, *Biochim. Biophys. Acta* 1763, 668-689.
106. Alen, C. and Sonenshein, A. L. (1999) *Bacillus subtilis* aconitase is an RNA-binding protein, *Proc. Natl. Acad. Sci. USA* 96, 10412-10417.

107. Tang, Y. and Guest, J. R. (1999) Direct evidence for mRNA binding and post-transcriptional regulation by *Escherichia coli* aconitases, *Microbiology* 145, 3069-3079.
108. Tang, Y., Quail, M. A., Artymiuk, P. J., Guest, J. R., and Green, J. (2002) *Escherichia coli* aconitases and oxidative stress: post-transcriptional regulation of sodA expression, *Microbiology* 148, 1027-1037.
109. Tang, Y., Guest, J. R., Artymiuk, P. J., Read, R. C., and Green, J. (2004) Post-transcriptional regulation of bacterial motility by aconitase proteins, *Mol. Microbiol.* 51, 1817-1826.
110. Williams, C. H., Stillman, T. J., Barynin, V. V., Sedelnikova, S. E., Tang, Y., Green, J., Guest, J. R., and Artymiuk, P. J. (2002) *E. coli* aconitase B structure reveals a HEAT-like domain with implications for protein-protein recognition, *Nat. Struct. Biol.* 9, 447-452.
111. Tucker, N. P., Le Brun, N. E., Dixon, R., and Hutchings, M. I. (2010) There's NO stopping NsrR, a global regulator of the bacterial NO stress response, *Trends Microbiol.* 18, 149-156.
112. Tucker, N. P., Hicks, M. G., Clarke, T. A., Crack, J. C., Chandra, G., Le Brun, N. E., Dixon, R., and Hutchings, M. I. (2008) The transcriptional repressor protein NsrR senses nitric oxide directly via a [2Fe-2S] cluster, *PLoS. One.* 3, e3623.
113. Isabella, V. M., Lapek, J. D., Jr., Kennedy, E. M., and Clark, V. L. (2009) Functional analysis of NsrR, a nitric oxide-sensing Rrf2 repressor in *Neisseria gonorrhoeae*, *Mol. Microbiol.* 71, 227-239.
114. Yukl, E. T., Elbaz, M. A., Nakano, M. M., and Moenne-Loccoz, P. (2008) Transcription factor NsrR from *Bacillus subtilis* senses nitric oxide with a 4Fe-4S cluster, *Biochemistry* 47, 13084-13092.
115. Hidalgo, E., Ding, H. G., and Dimple, B. (1997) Redox signal transduction via iron-sulfur clusters in the SoxR transcription activator, *TIBS* 22, 207-210.
116. Gaudu, P. and Weiss, B. (1996) SoxR, a [2Fe-2S] transcription factor, is active only in its oxidized form, *Proc. Natl. Acad. Sci. USA* 93, 10094-10098.
117. Nunoshiba, T. (1996) Two-stage gene regulation of the superoxide stress response soxRS system in *Escherichia coli*, *Crit Rev. Eukaryot. Gene Expr.* 6, 377-389.
118. Watanabe, S., Kita, A., Kobayashi, K., and Miki, K. (2008) Crystal structure of the [2Fe-2S] oxidative-stress sensor SoxR bound to DNA, *Proc. Natl. Acad. Sci. USA* 105, 4121-4126.
119. Smith, J. L., Zaluzec, E. J., Wery, J.-P., Niu, L., Switzer, R. L., Zalkin, H., and Satow, Y. (1994) Structure of the allosteric regulatory enzyme of purine biosynthesis, *Science* 264, 1427-1433.

120. Grandoni, J. A., Switzer, R. L., Marakoff, C. A., and Zalkin, H. (1989) Evidence that the iron-sulfur cluster of *Bacillus subtilis* glutamine phosphoribosylpyrophosphate amidotransferase determines stability of the enzyme to degradation in vivo., *J. Biol. Chem.* 264, 6058-6064.
121. Sellers, V. M., Johnson, M. K., and Dailey, H. A. (1996) Function of the [2Fe-2S] cluster in mammalian ferrochelatase: A possible role as a nitric oxide sensor, *Biochemistry* 35, 2699-2704.
122. Dailey, H. A., Finnegan, M. G., and Johnson, M. K. (1994) Human ferrochelatase is an iron-sulfur protein, *Biochemistry* 33, 403-407.
123. Ferreira, G. C., Franco, R., Lloyd, R. S., Pereira, A. S., Moura, I., Moura, J. J. G., and Huynh, B. H. (1994) Mammalian ferrochelatase, a new addition to the metalloenzyme family, *J. Biol. Chem.* 269, 7062-7065.
124. Wu, C.-K., Dailey, H. A., Rose, J. P., Burden, A., Sellers, V. M., and Wang, B.-C. (2001) The 2.0 Å structure of human ferrochelatase, the terminal enzyme of heme biosynthesis, *Nature Struct. Biol.* 8, 156-160.
125. Shepherd, M., Dailey, T. A., and Dailey, H. A. (2006) A new class of [2Fe-2S]-cluster-containing protoporphyrin (IX) ferrochelatases, *Biochem. J.* 397, 47-52.
126. Albetel, A-N. Role and properties of [2Fe-2S] centers in ferrochelatases. Ph.D. Dissertation, The University of Georgia, 2012.
127. Dai, S., Schwendtmayer, C., Schürmann, P., Ramaswamy, S., and Eklund, H. (2000) Redox signaling in chloroplasts: Cleavage of disulfides by an iron-sulfur cluster, *Science* 287, 655-658.
128. Walters, E. M. and Johnson, M. K. (2004) Ferredoxin:thioredoxin reductase: disulfide reduction catalyzed via novel site-specific [4Fe-4S] cluster chemistry, *Photosynth. Res.* 79, 249-264.
129. Watanabe, S., Matsumi, R., Arai, T., Atomi, H., Imanaka, T., and Miki, K. (2007) Crystal structures of [NiFe] hydrogenase maturation proteins HypC, HypD, and HypE: Insights into cyanation reaction by thiol redox signaling, *Mol. Cell* 27, 29-40.
130. Duin, E. C., Madadi-Kahkesh, S., Hedderich, R., Clay, M. D., and Johnson, M. K. (2002) Heterodisulfide reductase from *Methanothermobacter marburgensis* contains an active-site [4Fe-4S] cluster that is directly involved in mediating heterodisulfide reduction, *FEBS Lett.* 512, 263-268.
131. Weiner, B. E., Huang, H., Dattilo, B. M., Nilges, M. J., Fanning, E., and Chazin, W. J. (2007) An iron-sulfur cluster in the C-terminal domain of the p58 subunit of human DNA primase, *J. Biol. Chem.* 282, 33444-33451.

132. Netz, D. J. A., Stith, C. M., Stümpfig, M., Köpf, G., Vogel, D., Genau, H. M., Stodola, J. L., Lill, R., Burgers, P. M. J., and Pierik, A. J. (2012) Eukaryotic DNA polymerases require an iron-sulfur cluster for the formation of active complexes, *Nature Chem. Biol.* 8, 125-132.
133. Hinks, J. A., Evans, M. C. W., de Miguel, Y., Sartori, A. A., Jiricny, J., and Pearl, L. H. (2002) An iron-sulfur cluster in the family 4 uracil-DNA glycosylases, *J. Biol. Chem.* 277, 16936-16940.
134. Boal, A. K., Yavin, E., Lukianova, O. A., O'Shea, V. L., David, S. S., and Barton, J. K. (2005) DNA-bound redox activity of DNA repair glycosylases containing [4Fe-4S] clusters, *Biochemistry* 44, 8397-8407.
135. Boal, A. K., Genereux, J. C., Sontz, P. A., Gralnick, J. A., Newman, D. K., and Barton, J. K. (2009) Redox signaling between DNA repair proteins for efficient lesion detection, *Proc. Natl. Acad. Sci. USA* 106, 15237-15242.
136. Rudolf, J., Makrantonis, V., Inglede, W. J., Stark, M. J. R., and White, M. F. (2006) The DNA repair helicases XPD and FancJ have essential iron-sulfur domains, *Mol. Cell* 23, 801-808.
137. White, M. F. (2003) Archaeal DNA repair: paradigms and puzzles, *Biochem. Soc. Trans.* 31, 690-693.
138. White, M. F. (2009) Structure, function and evolution of the XPD family of iron-sulfur-containing 5'→3' DNA helicases, *Biochem. Soc. Trans.* 37, 547-551.
139. Thauer, R. K. and Schönheit, P. Iron-sulfur complexes of ferredoxin as a storage form of iron in *Clostridium pasteurianum*. In *Iron-Sulfur Proteins*; Spiro, T. G.; Wiley; 1982; 329-341.
140. Reeve, J. N., Beckler, G. S., Cram, D. S., Hamilton, P. T., Brown, J. W., Krzycki, J. A., Kolodziej, A. F., Alex, L. A., Orme-Johnson, W. H., and Walsh, C. T. (1989) A hydrogenase-linked gene in *Methanobacterium thermoautotrophicum* strain ΔH encodes a polyferredoxin, *Proc. Natl. Acad. Sci. USA* 86, 3031-3035.
141. Hedderich, R., Albracht, S. P. J., Linder, D., Koch, J., and Thauer, R. K. (1992) Isolation and characterization of polyferredoxin from *Methanobacterium thermoautotrophicum*. The *mvhB* gene product of the methylviologen-reducing hydrogenase operon, *FEBS Lett.* 298, 65-68.
142. Tse Sum Bui, B., Florentin, D., Fournier, F., Ploux, O., Méjean, A., and Marquet, A. (1998) Biotin synthase mechanism: on the origin of sulphur, *FEBS Lett.* 440, 226-230.
143. Jameson, G. N. L., Cosper, M. M., Hernández, H. L., Johnson, M. K., and Huynh, B. H. (2004) Role of the [2Fe-2S] cluster in recombinant *Escherichia coli* biotin synthase, *Biochemistry* 43, 2022-2031.

144. Cicchillo, R. M., Lee, K.-H., Baleanu-Gogonea, C., Nesbitt, N. M., Krebs, C., and Booker, S. J. (2004) *Escherichia coli* lipoyl synthase binds two distinct [4Fe-4S] clusters per polypeptide, *Biochemistry* 43, 11770-11781.
145. Hernandez, H., Pierrel, F., Elleingand, E., Garcia-Serres, R., Huynh, B. H., Johnson, M. K., Fontecave, M., and Atta, M. (2007) MiaB, a bifunctional radical-S-adenosylmethionine enzyme involved in the thiolation and methylation of tRNA, contains two essential [4Fe-4S] clusters, *Biochemistry* 46, 5140-5147.
146. Malkin, R. and Rabinowitz, J. C. (1966) The reconstitution of clostridial ferredoxins, *Biochem. Biophys. Res. Commun.* 23, 822-827.
147. Papanikolaou, G. and Pantopoulos, K. (2005) Iron metabolism and toxicity, *Toxicol. Appl. Pharmacol.* 202, 199-211.
148. Johnson, D. C., Dean, D. R., Smith, A. D., and Johnson, M. K. (2005) Structure, function and formation of biological iron-sulfur clusters, *Annu. Rev. Biochem.* 74, 247-281.
149. Bandyopadhyay, S., Chandramouli, K., and Johnson, M. K. (2008) Iron-sulfur cluster biosynthesis, *Biochem. Soc. Trans.* 36, 1112-1119.
150. Lill, R. (2009) Function and biogenesis of iron-sulphur proteins, *Nature* 460, 831-838.
151. Jacobson, M. R., Cash, V. L., Weiss, M. C., Laird, N. F., Newton, W. E., and Dean, D. R. (1989) Biochemical and genetic analysis of the *nifUSVWZM* cluster from *Azotobacter vinelandii*, *Mol. Gen. Genet.* 219, 49-57.
152. Olson, J. W., Agar, J. N., Johnson, M. K., and Maier, R. J. (2000) Characterization of the NifU and NifS Fe-S cluster formation proteins essential for the viability of *Helicobacter pylori*, *Biochemistry* 39, 16213-16219.
153. Ali, V., Shigeta, Y., Tokumoto, U., Takahashi, Y., and Nozaki, T. (2004) An intestinal parasitic protist, *Entamoeba histolytica*, possesses a non-redundant nitrogen fixation-like system for iron-sulfur cluster assembly under anaerobic conditions, *J. Biol. Chem.* 279, 16863-16874.
154. Zheng, L., White, R. H., Cash, V. L., Jack, R. F., and Dean, D. R. (1993) Cysteine desulfurase activity indicates a role for NIFS in metallocluster biosynthesis, *Proc. Natl. Acad. Sci. USA* 90, 2754-2758.
155. Mueller, E. G. (2006) Trafficking in persulfides: delivering sulfur in biosynthetic pathways, *Nat. Chem. Biol.* 2, 185-194.
156. Frazzon, J. and Dean, D. R. (2003) Formation of iron-sulfur clusters in bacteria: An emerging field in bioinorganic chemistry, *Curr. Opin. Chem. Biol.* 7, 166-173.

157. Dos Santos, P. C., Smith, A. D., Frazzon, J., Cash, V. L., Johnson, M. K., and Dean, D. R. (2004) Iron-sulfur cluster assembly: NifU-directed activation of the nitrogenase Fe-protein, *J. Biol. Chem.* 279, 19705-19711.
158. Léon, S., Touraine, B., Ribot, C., Briat, J.-F., and Lobréaux, S. (2003) Iron-sulfur cluster assembly in plants: Distinct NFU proteins in mitochondria and plastids from *Arabidopsis thaliana*, *Biochem. J.* 371, 823-830.
159. Yabe, T., Morimoto, K., Kikuchi, S., Nishio, K., Terashima, I., and Nakai, M. (2004) The arabidopsis chloroplast NifU-like protein CnfU, which can act as an iron-sulfur cluster scaffold protein, is required for the biogenesis of ferredoxin and photosystem I, *Plant Cell* 16, 993-1007.
160. Tong, W.-H., Jameson, G. N. L., Huynh, B. H., and Rouault, T. A. (2003) Subcellular compartmentalization of human Nfu, an iron-sulfur cluster scaffold protein and its ability to assemble a [4Fe-4S] cluster, *Proc. Natl. Acad. Sci. USA* 100, 9762-9767.
161. Krebs, C., Agar, J. N., Smith, A. D., Frazzon, J., Dean, D. R., Huynh, B. H., and Johnson, M. K. (2001) IscA, an alternative scaffold for Fe-S cluster biosynthesis, *Biochemistry* 40, 14069-14080.
162. Zheng, L., Cash, V. L., Flint, D. H., and Dean, D. R. (1998) Assembly of iron-sulfur clusters. Identification of an *iscSUA-hscBA-fdx* gene cluster from *Azotobacter vinelandii*, *J. Biol. Chem.* 273, 13264-13272.
163. Takahashi, Y. and Nakamura, M. (1999) Functional assignment of the ORF2-*iscS-iscA-hscB-hscA-fdx*-ORF3 gene cluster involved in the assembly of Fe-S clusters in *Escherichia coli*, *J. Biochem.* 126, 917-926.
164. Flint, D. H. (1996) *E. coli* contains a protein homologous in function and N-terminal sequence to the protein encoded by the *nifS* gene in *A. vinelandii* and that can participate in the synthesis of the Fe-S cluster of dihydroxy-acid dehydratase, *J. Biol. Chem.* 271, 16068-16074.
165. Smith, A. D., Agar, J. N., Johnson, K. A., Frazzon, J., Amster, I. J., Dean, D. R., and Johnson, M. K. (2001) Sulfur transfer from IscS to IscU: The first step in iron-sulfur cluster biosynthesis, *J. Am. Chem. Soc.* 123, 11103-11104.
166. Muhlenhoff, U., Balk, J., Richhardt, N., Kaiser, J. T., Sipos, K., Kispal, G., and Lill, R. (2004) Functional characterization of the eukaryotic cysteine desulfurase Nfs1p from *Saccharomyces cerevisiae*, *J. Biol. Chem.* 279, 36906-36915.
167. Adam, A. C., Bornhövd, C., Prokisch, H., Neupert, W., and Hell, K. (2006) The Nfs1 interacting protein Isd11 has an essential role in Fe/S cluster biogenesis in mitochondria, *EMBO J.* 25, 174-183.

168. Wiedemann, N., Urzica, E., Guiard, B., Müller, H., Lohaus, C., Meyer, H. E., Ryan, M. T., Meisinger, C., Mühlhoff, U., Lill, R., and Pfanner, N. (2006) Essential role of Isd11 in mitochondrial iron-sulfur cluster synthesis on Isu scaffold proteins, *EMBO J.* 25, 184-195.
169. Lill, R. and Mühlhoff, U. (2006) Iron-sulfur protein biogenesis in eukaryotes: Components and mechanisms, *Annu. Rev. Cell Dev. Biol.* 22, 457-486.
170. Lill, R., Hoffmann, B., Molik, S., Pierik, A. J., Rietzschel, N., Stehling, O., Uzarska, M. A., Webert, H., Wilbrecht, C., and Mühlhoff, U. (2012) The role of mitochondria in cellular iron-sulfur protein biogenesis and iron metabolism, *Biochim. Biophys. Acta* 1823, 1491-1508.
171. Chandramouli, K. and Johnson, M. K. (2006) HscA and HscB stimulate [2Fe-2S] cluster transfer from IscU to apoferredoxin in an ATP-dependent reaction, *Biochemistry* 45, 11087-11095.
172. Hoff, K. G., Ta, D. T., Tapley, T. L., Silberg, J. J., and Vickery, L. E. (2002) Hsc66 substrate specificity is directed toward a discrete region of the iron-sulfur cluster template protein IscU, *J. Biol. Chem.* 277, 27353-27359.
173. Mayer, M. P., Brehmer, D., Gassler, C. S., and Bukau, B. (2001) Hsp70 chaperone machines, *Adv. Protein Chem.* 59, 1-44.
174. Hoff, K. G., Cupp-Vickery, J. R., and Vickery, L. E. (2003) Contributions of the LPPVK motif of the iron-sulfur template protein IscU to interactions with the Hsc66-Hsc20 chaperone system, *J. Biol. Chem.* 278, 37582-37589.
175. Silberg, J. J., Hoff, K. G., Tapley, T. L., and Vickery, L. E. (2001) The Fe/S assembly protein IscU behaves as a substrate for the molecular chaperone Hsc66 from *Escherichia coli*, *J. Biol. Chem.* 276, 1696-1700.
176. Hoff, K. G., Silberg, J. J., and Vickery, L. E. (2000) Interaction of the iron-sulfur cluster assembly protein IscU with the Hsc66/Hsc20 molecular chaperone system of *Escherichia coli*, *Proc. Natl. Acad. Sci. USA* 97, 7790-7795.
177. Kampinga, H. H. and Craig, E. A. (2010) The HSP70 chaperone machinery: J proteins as drivers of functional specificity, *Nat. Rev. Mol. Cell Biol.* 11, 579-592.
178. Johnson, D. C., Unciuleac, M.-C., and Dean, D. R. (2006) Controlled expression and functional analysis of iron-sulfur cluster biosynthetic components within *Azotobacter vinelandii*, *J. Bacteriol.* 188, 7551-7561.
179. Gerber, J., Neumann, K., Prohl, C., Mühlhoff, U., and Lill, R. (2004) The yeast scaffold proteins Isu1p and Isu2p are required inside mitochondria for maturation of cytosolic Fe/S proteins, *Mol. Cell. Biol.* 24, 4848-4857.

180. Unciuleac, M.-C., Chandramouli, K., Naik, S., Mayer, S., Huynh, B. H., Johnson, M. K., and Dean, D. R. (2007) *In vitro* activation of apo-aconitase using a [4Fe-4S] cluster-loaded form of the IscU [Fe-S] cluster scaffolding protein, *Biochemistry* 46, 6812-6821.
181. Colin, F., Martelli, A., Clemancey, M., Latour, J. M., Gambarelli, S., Zeppieri, L., Birck, C., Page, A., Puccio, H., and Ollagnier de, C. S. (2013) Mammalian frataxin controls sulfur production and iron entry during de novo Fe<sub>4</sub>S<sub>4</sub> cluster assembly, *J. Am. Chem. Soc.* 135, 733-740.
182. Mühlenhoff, U., Richter, N., Pines, O., Pierik, A. J., and Lill, R. (2011) Specialized function of yeast Isa1 and Isa2 in the maturation of mitochondrial [4Fe-4S] proteins, *J. Biol. Chem.* 286, 41205-41216.
183. Sheftel, A. D., Wilbrecht, C., Stehling, O., Niggemeyer, B., Elsasser, H. P., Muhlenhoff, U., and Lill, R. (2012) The human mitochondrial ISCA1, ISCA2, and IBA57 proteins are required for [4Fe-4S] protein maturation, *Mol. Biol. Cell* 23, 1157-1166.
184. Lu, J., Yang, J., Tan, G., and Ding, H. (2008) Complementary roles of SufA and IscA in the biogenesis of iron-sulfur clusters in *Escherichia coli*, *Biochem. J.* 409, 535-543.
185. Ayala-Castro, C., Saini, A., and Outten, F. W. (2008) Fe-S cluster assembly pathways in bacteria, *Microbiol. Mol. Biol. Rev.* 72, 110-125.
186. Vinella, D., Brochier-Armanet, C., Loiseau, L., Talla, E., and Barras, F. (2009) Iron-sulfur (Fe/S) protein biogenesis: phylogenomic and genetic studies of A-type carriers, *PLoS. Genet.* 5, e1000497.
187. Morimoto, K., Yamashita, E., Kondou, Y., Lee, S. J., Arisaka, F., Tsukihara, T., and Nakai, M. (2006) The asymmetric IscA homodimer with an exposed [2Fe-2S] cluster suggests the structural basis of the Fe-S cluster biosynthetic scaffold, *J. Mol. Biol.* 360, 117-132.
188. Ollagnier-de-Choudens, S., Mattioli, T., Takahashi, Y., and Fontecave, M. (2001) Iron-sulfur cluster assembly. Characterization of IscA and evidence for a specific functional complex with ferredoxin, *J. Biol. Chem.* 276, 22604-22607.
189. Ollagnier-de-Choudens, S., Sanakis, Y., and Fontecave, M. (2004) SufA/IscA: reactivity studies of a class of scaffold proteins involved with [Fe-S] cluster assembly, *J. Biol. Inorg. Chem.* 9, 828-838.
190. Wang, W., Huang, H., Tan, G., Fan, S., Liu, M., Landry, A. P., and Ding, H. (2010) *In vivo* evidence for the iron-binding activity of an iron-sulfur cluster assembly protein IscA in *Escherichia coli*, *Biochem. J.* 432, 429-436.
191. Tan, G., Lu, J., Bitoun, J. P., Huang, H., and Ding, H. (2009) IscA/SufA paralogues are required for the [4Fe-4S] cluster assembly in enzymes of multiple physiological pathways in *Escherichia coli* under aerobic growth conditions, *Biochem. J.* 420, 463-472.

192. Wu, G., Mansy, S. S., Hemann, C., Hille, R., Surerus, K. K., and Cowan, J. A. (2002) Iron-sulfur cluster biosynthesis: Characterization of *Schizosaccharomyces pombe* Isa1, *J. Biol. Inorg. Chem.* 7, 526-532.
193. Wollenberg, M., Berndt, C., Bill, E., Schwenn, J. D., and Seidler, A. (2003) A dimer of the FeS cluster biosynthesis protein IscA from cyanobacteria binds a [2Fe2S] cluster between two protomers and transfers it to [2Fe2S] and [4Fe4S] apo proteins, *Eur. J. Biochem.* 270, 1662-1671.
194. Ding, H. and Clark, R. J. (2004) Characterization of iron-binding in IscA, an ancient iron-sulfur cluster assembly protein, *Biochem. J.* 379, 433-440.
195. Lu, J., Bitoun, J. P., Tan, G., Wang, W., Min, W., and Ding, H. (2010) Iron-binding activity of human iron-sulfur cluster assembly protein hIscA1, *Biochem. J.* 428, 125-131.
196. Chen, O. S., Hemenway, S., and Kaplan, J. (2002) Inhibition of Fe-S cluster biosynthesis decreases mitochondrial iron export: Evidence that Yfh1p affects Fe-S cluster synthesis, *Proc. Natl. Acad. Sci. USA* 99, 12321-12326.
197. Mühlenhoff, U., Richhardt, N., Ristow, M., Kispal, G., and Lill, R. (2002) The yeast frataxin homolog Yfh1p plays a specific role in the maturation of cellular Fe/S proteins, *Hum. Mol. Genet.* 11, 2025-2036.
198. Gerber, J., Mühlenhoff, U., and Lill, R. (2003) An interaction between frataxin and Isu1/Nfs1 that is crucial for Fe/S cluster synthesis on Isu1, *EMBO Rep.* 4, 907-911.
199. Shan, Y., Napoli, E., and Cortopassi, G. (2007) Mitochondrial frataxin interacts with ISD11 of the NFS1/ISCU complex and multiple mitochondrial chaperones, *Hum. Mol. Genet.* 16, 929-941.
200. Ramazzotti, A., Vanmansart, V., and Foury, F. (2004) Mitochondrial functional interactions between frataxin and Isu1P, the iron-sulfur cluster scaffold protein, in *Saccharomyces cerevisiae*, *FEBS Lett.* 557, 215-220.
201. Yoon, T. and Cowan, J. A. (2003) Iron-sulfur cluster biosynthesis. Characterization of frataxin as an iron donor for assembly of [2Fe-2S] clusters in ISU-type proteins, *J. Am. Chem. Soc.* 125, 6078-6084.
202. Bulteau, A. L., O'Neill, H. A., Kennedy, M. C., Ikeda-Saito, M., Isaya, G., and Szwed, L. I. (2004) Frataxin acts as an iron chaperone protein to modulate mitochondrial aconitase activity, *Science* 305, 242-245.
203. Adamec, J., Rusnak, F., Owen, W. G., Naylor, S., Benson, L. M., Gacy, A. M., and Isaya, G. (2000) Iron-dependent self-assembly of recombinant yeast frataxin: implications for Friedreich ataxia, *Am. J. Hum. Genet.* 67, 549-562.

204. Bou-Abdallah, F., Adinolfi, S., Pastore, A., Laue, T. M., and Dennis, C. N. (2004) Iron binding and oxidation kinetics in frataxin CyaY of *Escherichia coli*, *J. Mol. Biol.* 341, 605-615.
205. Cook, J. D., Bencze, K. Z., Jankovic, A. D., Crater, A. K., Busch, C. N., Bradley, P. B., Stemmler, A. J., Spaller, M. R., and Stemmler, T. L. (2006) Monomeric yeast frataxin is an iron-binding protein, *Biochemistry* 45, 7767-7777.
206. Layer, G., Ollagnier-de-Choudens, S., Sanakis, Y., and Fontecave, M. (2006) Iron-sulfur cluster biosynthesis. Characterization of *Escherichia coli* CyaY as an iron donor for the assembly of [2Fe-2S] clusters in the scaffold IscU, *J. Biol. Chem.* 281, 16256-16263.
207. Li, D. S., Ohshima, K., Jiralerspong, S., Bojanowski, M. W., and Pandolfo, M. (1999) Knock-out of the *cyaY* gene in *Escherichia coli* does not affect cellular iron content and sensitivity to oxidants, *FEBS Lett.* 456, 13-16.
208. Tsai, C. L. and Barondeau, D. P. (2010) Human frataxin is an allosteric switch that activates the Fe-S cluster biosynthetic complex, *Biochemistry* 49, 9132-9139.
209. Lange, H., Kaut, A., Kispal, G., and Lill, R. (2000) A mitochondrial ferredoxin is essential for biogenesis of cellular iron-sulfur proteins, *Proc. Natl. Acad. Sci. USA* 97, 1050-1055.
210. Sheftel, A. D., Stehling, O., Pierik, A. J., Elsasser, H. P., Muhlenhoff, U., Webert, H., Hobler, A., Hannemann, F., Bernhardt, R., and Lill, R. (2010) Humans possess two mitochondrial ferredoxins, Fdx1 and Fdx2, with distinct roles in steroidogenesis, heme, and Fe/S cluster biosynthesis, *Proc. Natl. Acad. Sci. USA* 107, 11775-11780.
211. Loiseau, L., Ollagnier-de-Choudens, S., Nachin, L., Fontecave, M., and Barras, F. (2003) Biogenesis of Fe-S cluster by the bacterial Suf system. SufS and SufE form a new type of cysteine desulfurase, *J. Biol. Chem.* 278, 38352-38359.
212. Ollagnier-de-Choudens, S., Lascoux, D., Loiseau, L., Barras, F., Forest, E., and Fontecave, M. (2003) Mechanistic studies of the SufS-SufE cysteine desulfurase: evidence for S transfer from SufS to SufE, *FEBS Lett.* 555, 263-267.
213. Outten, F. W., Wood, M. J., Muñoz, F. M., and Storz, G. (2003) The SufE protein and the SufBCD complex enhance SufS cysteine desulfurase activity as part of a sulfur transfer pathway for Fe-S cluster assembly in *E. coli*, *J. Biol. Chem.* 278, 45713-45719.
214. Wollers, S., Layer, G., Garcia-Serres, R., Signor, L., Clemancey, M., Latour, J. M., Fontecave, M., and Ollagnier de, C. S. (2010) Iron-sulfur (Fe-S) cluster assembly: the SufBCD complex is a new type of Fe-S scaffold with a flavin redox cofactor, *J. Biol. Chem.* 285, 23331-23341.
215. Kitaoka, S., Wada, K., Hasegawa, Y., Minami, Y., Fukuyama, K., and Takahashi, Y. (2006) Crystal structure of *Escherichia coli* SufC, an ABC-type ATPase component of the SUF iron-sulfur cluster assembly machinery, *FEBS Lett.* 580, 137-143.

216. Layer, G., Gaddam, S. A., Ayala-Castro, C. N., Ollagnier-de-Choudens, S., Lascoux, D., Fontecave, M., and Outten, F. W. (2007) SufE transfers sulfur from SufS to SufB for iron-sulfur cluster assembly, *J. Biol. Chem.* 282, 13342-13350.
217. Saini, A., Mapolelo, D. T., Chahal, H. K., Johnson, M. K., and Outten, F. W. (2010) SufD and SufC ATPase activity are required for iron acquisition during in vivo Fe-S cluster formation on SufB, *Biochemistry* 49, 9402-9412.
218. Chahal, H. K., Dai, Y., Saini, A., Ayala-Castro, C., and Outten, F. W. (2009) The SufBCD Fe-S scaffold complex interacts with SufA for Fe-S cluster transfer, *Biochemistry* 48, 10644-10653.
219. Gupta, V., Sendra, M., Naik, S. G., Chahal, H. K., Huynh, B. H., Outten, F. W., Fontecave, M., and Ollagnier de Choudens, S. (2009) Native *Escherichia coli* SufA, coexpressed with SufBCDSE, purifies as a [2Fe-2S] protein and acts as an Fe-S transporter to Fe-S target enzymes, *J. Am. Chem. Soc.* 131, 6149-6153.
220. Riboldi, G. P., Verli, H., and Frazzon, J. (2009) Structural studies of the *Enterococcus faecalis* SufU [Fe-S] cluster protein, *BMC. Biochem.* 10, 3.
221. Albrecht, A. G., Netz, D. J., Miethke, M., Pierik, A. J., Burghaus, O., Peuckert, F., Lill, R., and Marahiel, M. A. (2010) SufU is an essential iron-sulfur cluster scaffold protein in *Bacillus subtilis*, *J. Bacteriol.* 192, 1643-1651.
222. Yu, J., Shen, G., Wang, T., Bryant, D. A., Golbeck, J. H., and McIntosh, L. (2003) Suppressor mutations in the study of photosystem I biogenesis: sll0088 is a previously unidentified gene involved in reaction center accumulation in *Synechocystis* sp. strain PCC 6803, *J. Bacteriol.* 185, 3878-3887.
223. Wang, T., Shen, G., Balasubramanian, R., McIntosh, L., Bryant, D. A., and Golbeck, J. H. (2004) The sufR gene (sll0088 in *Synechocystis* sp. strain PCC 6803) functions as a repressor of the sufBCDS operon in iron-sulfur cluster biogenesis in cyanobacteria, *J. Bacteriol.* 186, 956-967.
224. Shen, G., Balasubramanian, R., Wang, T., Wu, Y., Hoffart, L. M., Krebs, C., Bryant, D. A., and Golbeck, J. H. (2007) SufR coordinates two [4Fe-4S]<sup>2+,1+</sup> clusters and functions as a transcriptional repressor of the *sufBCDS* operon and an autoregulator of *sufR* in cyanobacteria, *J. Biol. Chem.* 282, 31909-31919.
225. Holmgren, A. (1976) Hydrogen donor system for *Escherichia coli* ribonucleoside-diphosphate reductase dependent upon glutathione, *Proc. Natl. Acad. Sci. USA* 73, 2275-2279.
226. Holmgren, A. (1979) Glutathione-dependent synthesis of deoxyribonucleotides. Purification and characterization of glutaredoxin from *Escherichia coli*, *J. Biol. Chem.* 254, 3664-3671.

227. Herrero, E. and de la Torre-Ruiz, M. A. (2007) Monothiol glutaredoxins: a common domain for multiple functions, *Cell. Mol. Life Sci.* 64, 1518-1530.
228. Lillig, C. H., Berndt, C., and Holmgren, A. (2008) Glutaredoxin systems, *Biochim. Biophys. Acta* 1780, 1304-1317.
229. Rouhier, N., Couturier, J., Johnson, M. K., and Jacquot, J. P. (2010) Glutaredoxins: roles in iron homeostasis, *Trends Biochem. Sci.* 35, 43-52.
230. Rouhier, N. (2010) Plant glutaredoxins: pivotal players in redox biology and iron-sulphur centre assembly, *New Phytol.* 186, 365-372.
231. Rouhier, N., Couturier, J., and Jacquot, J. P. (2006) Genome-wide analysis of plant glutaredoxin systems, *J. Exp. Bot.* 57, 1685-1696.
232. Couturier, J., Jacquot, J. P., and Rouhier, N. (2009) Evolution and diversity of glutaredoxins in photosynthetic organisms, *Cell Mol. Life Sci.* 66, 2539-2557.
233. Johansson, C., Roos, A. K., Montano, S. J., Sengupta, R., Filippakopoulos, P., Guo, K., von, D. F., Holmgren, A., Oppermann, U., and Kavanagh, K. L. (2011) The crystal structure of human GLRX5: iron-sulfur cluster co-ordination, tetrameric assembly and monomer activity, *Biochem. J.* 433, 303-311.
234. Tamarit, J., Belli, G., Cabiscol, E., Herrero, E., and Ros, J. (2003) Biochemical Characterization of Yeast Mitochondrial Grx5 Monothiol Glutaredoxin, *J. Biol. Chem.* 278, 25745-25751.
235. Fernandes, A. P., Fladvad, M., Berndt, C., Andresen, C., Lillig, C. H., Neubauer, P., Sunnerhagen, M., Holmgren, A., and Vlamis-Gardikas, A. (2005) A novel monothiol glutaredoxin (Grx4) from *Escherichia coli* can serve as a substrate for thioredoxin reductase, *J. Biol. Chem.* 280, 24544-24552.
236. Picciocchi, A., Saguez, C., Boussac, A., Cassier-Chauvat, C., and Chauvat, F. (2007) CGFS-type monothiol glutaredoxins from the cyanobacterium *Synechocystis* PCC6803 and other evolutionary distant model organisms possess a glutathione-ligated [2Fe-2S] cluster, *Biochemistry* 46, 15018-15026.
237. Bandyopadhyay, S., Gama, F., Molina-Navarro, M. M., Gualberto, J. M., Claxton, R., Naik, S. G., Huynh, B. H., Herrero, E., Jacquot, J.-P., Johnson, M. K., and Rouhier, N. (2008) Chloroplast monothiol glutaredoxins as scaffold proteins for the assembly and delivery of [2Fe-2S] clusters, *EMBO J.* 27, 1122-1133.
238. Yeung, N., Gold, B., Liu, N. L., Prathapam, R., Sterling, H. J., Williams, E. R., and Butland, G. (2011) The *E. coli* monothiol glutaredoxin GrxD forms homodimeric and heterodimeric FeS cluster containing complexes, *Biochemistry* 50, 8957-8969.
239. Ye, H., Jeong, S. Y., Ghosh, M. C., Kovtunovych, G., Silvestri, L., Ortillo, D., Uchida, N., Tisdale, J., Camaschella, C., and Rouault, T. A. (2010) Glutaredoxin 5 deficiency causes

- sideroblastic anemia by specifically impairing heme biosynthesis and depleting cytosolic iron in human erythroblasts, *J. Clin. Invest.* 120, 1749-1761.
240. Li, H., Mapolelo, D. T., Randeniya, S., Johnson, M. K., and Outten, C. E. (2012) Human Glutaredoxin 3 Forms [2Fe-2S]-Bridged Complexes with Human BolA2, *Biochemistry* 51, 1687-1696.
241. Mühlenhoff, U., Molik, S., Godoy, J. R., Uzarska, M. A., Richter, N., Seubert, A., Zhang, Y., Stubbe, J., Pierrel, F., Herrero, E., Lillig, C. H., and Lill, R. (2010) Cytosolic monothiol glutaredoxins function in intracellular iron sensing and trafficking via their bound iron-sulfur cluster, *Cell Metab.* 12, 373-385.
242. Iwema, T., Picciocchi, A., Traore, D. A., Ferrer, J. L., Chauvat, F., and Jacquamet, L. (2009) Structural basis for delivery of the intact [Fe<sub>2</sub>S<sub>2</sub>] cluster by monothiol glutaredoxin, *Biochemistry* 48, 6041-6043.
243. Wang, L., Ouyang, B., Li, Y., Feng, Y., Jacquot, J. P., Rouhier, N., and Xia, B. (2012) Glutathione regulates the transfer of iron-sulfur cluster from monothiol and dithiol glutaredoxins to apo ferredoxin, *Protein Cell* 3, 714-721.
244. Rouhier, N., Unno, H., Bandyopadhyay, S., Masip, L., Kim, S. K., Hirasawa, M., Gualberto, J. M., Lattard, V., Kusunoki, M., Knaff, D. B., Georgiou, G., Hase, T., Johnson, M. K., and Jacquot, J. P. (2007) Functional, structural, and spectroscopic characterization of a glutathione-ligated [2Fe-2S] cluster in poplar glutaredoxin C1, *Proc. Natl. Acad. Sci. USA* 104, 7379-7384.
245. Johansson, C., Kavanagh, K. L., Gileadi, O., and Oppermann U. (2007) Reversible sequestration of active site cysteines in a 2Fe-2S-bridged dimer provides a mechanism for glutaredoxin 2 regulation in human mitochondria, *J. Biol. Chem.* 282, 3077-3082.
246. Rodríguez-Manzanaque, M. T., Ros, J., Cabrito, I., Sorribas, A., and Herrero, E. (1999) Grx5 glutaredoxin plays a central role in protection against protein oxidative damage in *Saccharomyces cerevisiae*, *Mol. Cell. Biol.* 19, 8180-8190.
247. Molina-Navarro, M. M., Casas, C., Piedrafita, L., Bellí, G., and Herrero, E. (2006) Prokaryotic and eukaryotic monothiol glutaredoxins are able to perform the functions of Grx5 in the biogenesis of Fe/S clusters in yeast mitochondria, *FEBS Lett.* 580, 2273-2280.
248. Wingert, R. A., Galloway, J. L., Barut, B., Foott, H., Fraenkel, P., Axe, J. L., Weber, G. J., Dooley, K., Davidson, A. J., Schmidt, B., Paw, B. H., and Shaw, G. C. (2005) Deficiency of glutaredoxin 5 reveals Fe-S clusters are required for vertebrate haem synthesis, *Nature* 436, 1035-1039.
249. Vilella, F., Alves, R., Rodriguez-Manzanaque, M. T., Belli, G., Swaminathan, S., Sunnerhagen, P., and Herrero, E. (2004) Evolution and cellular function of monothiol glutaredoxins: involvement in iron-sulphur cluster assembly, *Comp. Funct. Genom.* 5, 328-341.

250. Kim, K. D., Chung, W. H., Kim, H. J., Lee, K. C., and Roe, J. H. (2010) Monothiol glutaredoxin Grx5 interacts with Fe-S scaffold proteins Isa1 and Isa2 and supports Fe-S assembly and DNA integrity in mitochondria of fission yeast, *Biochem. Biophys. Res. Commun.* 392, 467-472.
251. Butland, G., Babu, M., az-Mejia, J. J., Bohdana, F., Phanse, S., Gold, B., Yang, W., Li, J., Gagarinova, A. G., Pogoutse, O., Mori, H., Wanner, B. L., Lo, H., Wasniewski, J., Christopolous, C., Ali, M., Venn, P., Safavi-Naini, A., Sourour, N., Caron, S., Choi, J. Y., Laigle, L., Nazarians-Armavil, A., Deshpande, A., Joe, S., Datsenko, K. A., Yamamoto, N., Andrews, B. J., Boone, C., Ding, H., Sheikh, B., Moreno-Hagelseib, G., Greenblatt, J. F., and Emili, A. (2008) eSGA: *E. coli* synthetic genetic array analysis, *Nat. Methods* 5, 789-795.
252. Yamaguchi-Iwai, Y., Ueta, R., Fukunaka, A., and Sasaki, R. (2002) Subcellular localization of Aft1 transcription factor responds to iron status in *Saccharomyces cerevisiae*, *J. Biol. Chem.* 277, 18914-18918.
253. Chen, O. S., Crisp, R. J., Valachovic, M., Bard, M., Winge, D. R., and Kaplan, J. (2004) Transcription of the yeast iron regulon does not respond directly to iron but rather to iron-sulfur cluster biosynthesis, *J. Biol. Chem.* 279, 29513-29518.
254. Rutherford, J. C., Ojeda, L., Balk, J., Muhlenhoff, U., Lill, R., and Winge, D. R. (2005) Activation of the iron regulon by the yeast Aft1/Aft2 transcription factors depends on mitochondrial but not cytosolic iron-sulfur protein biogenesis, *J. Biol. Chem.* 280, 10135-10140.
255. Pujol-Carrion, N., Belli, G., Herrero, E., Nogues, A., and de la Torre-Ruiz MA (2006) Glutaredoxins Grx3 and Grx4 regulate nuclear localisation of Aft1 and the oxidative stress response in *Saccharomyces cerevisiae*, *J. Cell Sci.* 119, 4554-4564.
256. Ojeda, L., Keller, G., Muhlenhoff, U., Rutherford, J. C., Lill, R., and Winge, D. R. (2006) Role of glutaredoxin-3 and glutaredoxin-4 in the iron regulation of the Aft1 transcriptional activator in *Saccharomyces cerevisiae*, *J. Biol. Chem.* 281, 17661-17669.
257. Kumanovics, A., Chen, O., Li, L., Bagley, D., Adkins, E., Lin, H., Dingra, N. N., Outten, C. E., Keller, G., Winge, D., Ward, D. M., and Kaplan, J. (2008) Identification of FRA1 and FRA2 as genes involved in regulating the yeast iron regulon in response to decreased mitochondrial iron-sulfur cluster synthesis, *J. Biol. Chem.* 283, 10276-10286.
258. Kaplan, C. D. and Kaplan, J. (2009) Iron acquisition and transcriptional regulation, *Chem. Rev.* 109, 4536-4552.
259. Mercier, A. and Labbe, S. (2009) Both Php4 function and subcellular localization are regulated by iron via a multistep mechanism involving the glutaredoxin Grx4 and the exportin Crm1, *J. Biol. Chem.* 284, 20249-20262.
260. Jbel, M., Mercier, A., and Labbe, S. (2011) Grx4 monothiol glutaredoxin is required for iron limitation-dependent inhibition of Fep1, *Eukaryot. Cell* 10, 629-645.

261. Aldea, M., Hernandez-Chico, C., de la Campa, A. G., Kushner, S. R., and Vicente, M. (1988) Identification, cloning, and expression of *bolA*, an *ftsZ*-dependent morphogene of *Escherichia coli*, *J. Bacteriol.* 170, 5169-5176.
262. Huynen, M. A., Spronk, C. A., Gabaldon, T., and Snel, B. (2005) Combining data from genomes, Y2H and 3D structure indicates that BolA is a reductase interacting with a glutaredoxin, *FEBS Lett.* 579, 591-596.
263. Giot, L., Bader, J. S., Brouwer, C., Chaudhuri, A., Kuang, B., Li, Y., Hao, Y. L., Ooi, C. E., Godwin, B., Vitols, E., Vijayadamodar, G., Pochart, P., Machineni, H., Welsh, M., Kong, Y., Zerhusen, B., Malcolm, R., Varrone, Z., Collis, A., Minto, M., Burgess, S., McDaniel, L., Stimpson, E., Spriggs, F., Williams, J., Neurath, K., Ioime, N., Agee, M., Voss, E., Furtak, K., Renzulli, R., Aanensen, N., Carrolla, S., Bickelhaupt, E., Lazovatsky, Y., DaSilva, A., Zhong, J., Stanyon, C. A., Finley, R. L., Jr., White, K. P., Braverman, M., Jarvie, T., Gold, S., Leach, M., Knight, J., Shimkets, R. A., McKenna, M. P., Chant, J., and Rothberg, J. M. (2003) A protein interaction map of *Drosophila melanogaster*, *Science* 302, 1727-1736.
264. Butland, G., Peregrin-Alvarez, J. M., Li, J., Yang, W., Yang, X., Canadien, V., Starostine, A., Richards, D., Beattie, B., Krogan, N., Davey, M., Parkinson, J., Greenblatt, J., and Emili, A. (2005) Interaction network containing conserved and essential protein complexes in *Escherichia coli*, *Nature* 433, 531-537.
265. Spiro, S. and Guest, J. R. (1990) FNR and its role in oxygen-regulated gene expression in *Escherichia coli*, *FEMS Microbiol. Rev.* 6, 399-428.
266. Sutton, V. R., Stubna, A., Patschkowski, T., Münck, E., Beinert, H., and Kiley, P. J. (2004) Superoxide destroys the  $[2\text{Fe}-2\text{S}]^{2+}$  cluster of FNR from *E. coli*, *Biochemistry* 43, 791-798.
267. Becker, S., Holighaus, G., Gabrielczyk, T., and Unden, G. (1996)  $\text{O}_2$  as the regulatory signal for FNR-dependent gene regulation in *Escherichia coli*, *J. Bacteriol.* 178, 4515-4521.
268. Salmon, K., Hung, S. P., Mekjian, K., Baldi, P., Hatfield, G. W., and Gunsalus, R. P. (2003) Global gene expression profiling in *Escherichia coli* K12. The effects of oxygen availability and FNR, *J. Biol. Chem.* 278, 29837-29855.
269. Korner, H., Sofia, H. J., and Zumft, W. G. (2003) Phylogeny of the bacterial superfamily of Crp-Fnr transcription regulators: exploiting the metabolic spectrum by controlling alternative gene programs, *FEMS Microbiol. Rev.* 27, 559-592.
270. Schultz, S. C., Shields, G. C., and Steitz, T. A. (1991) Crystal structure of a CAP-DNA complex: the DNA is bent by 90 degrees, *Science* 253, 1001-1007.
271. Shaw, D. J., Rice, D. W., and Guest, J. R. (1983) Homology between CAP and Fnr, a regulator of anaerobic respiration in *Escherichia coli*, *J. Mol. Biol.* 166, 241-247.

272. Bell, A. I., Gaston, K. L., Cole, J. A., and Busby, S. J. (1989) Cloning of binding sequences for the *Escherichia coli* transcription activators, FNR and CRP: location of bases involved in discrimination between FNR and CRP, *Nucleic Acids Res.* 17, 3865-3874.
273. Eiglmeier, K., Honore, N., Iuchi, S., Lin, E. C., and Cole, S. T. (1989) Molecular genetic analysis of FNR-dependent promoters, *Mol. Microbiol.* 3, 869-878.
274. Green, J., Sharrocks, A. D., Green, B., Geisow, M., and Guest, J. R. (1993) Properties of FNR proteins substituted at each of the five cysteine residues, *Mol. Microbiol.* 8, 61-68.
275. Moore, L. J. and Kiley, P. J. (2001) Characterization of the dimerization domain in the FNR transcription factor, *J. Biol. Chem.* 276, 45744-45750.
276. Bates, D. M., Lazazzera, B. A., and Kiley, P. J. (1995) Characterization of FNR\* mutant proteins indicates two distinct mechanisms for altering oxygen regulation of the *Escherichia coli* transcription factor FNR, *J. Bacteriol.* 177, 3972-3978.
277. Kiley, P. J. and Reznikoff, W. S. (1991) Fnr mutants that activate gene expression in the presence of oxygen, *J. Bacteriol.* 173, 16-22.
278. Moore, L. J., Mettert, E. L., and Kiley, P. J. (2006) Regulation of FNR dimerization by subunit charge repulsion, *J. Biol. Chem.* 281, 33268-33275.
279. Popescu, C., Bates, D. M., Beinert, H., Münck, E., and Kiley, P. J. (1998) Mössbauer spectroscopy as a tool for the study of activation/inactivation of the transcription regulator FNR in whole cells of *Escherichia coli*, *Proc. Natl. Acad. Sci. USA* 95, 13431-13435.
280. Lazazzera, B. A., Beinert, H., Khoroshilova, N., Kennedy, M. C., and Kiley, P. J. (1996) DNA-binding and dimerization of the Fe-S-containing FNR protein from *Escherichia coli* are regulated by oxygen, *J. Biol. Chem.* 271, 2762-2768.
281. Bates, D. M., Popescu, C., Khoroshilova, N., Vogt, K., Beinert, H., Münck, E., and Kiley, P. J. (2000) Substitution of leucine 28 with histidine in the *E. coli* transcription factor FNR results in increased stability of the [4Fe-4S]<sup>2+</sup> cluster to oxygen, *J. Biol. Chem.* 275, 6234-6240.
282. Mettert, E. L., Outten, F. W., Wanta, B., and Kiley, P. J. (2008) The impact of O<sub>2</sub> on the Fe-S cluster biogenesis requirements of *Escherichia coli* FNR, *J. Mol. Biol.* 384, 798-811.
283. Sutton, V. R., Mettert, E. L., Beinert, H., and Kiley, P. J. (2004) Kinetic analysis of the oxidative conversion of the [4Fe-4S]<sup>2+</sup> cluster of FNR to a [2Fe-2S]<sup>2+</sup> Cluster, *J. Bacteriol.* 186, 8018-8025.
284. Crack, J. C., Green, J., Cheesman, M. R., Le Brun, N. E., and Thomson, A. J. (2007) Superoxide-mediated amplification of the oxygen-induced switch from [4Fe-4S] to [2Fe-2S] clusters in the transcriptional regulator FNR, *Proc. Natl. Acad. Sci. USA* 104, 2092-2097.

285. Crack, J. C., Gaskell, A. A., Green, J., Cheesman, M. R., Le Brun, N. E., and Thomson, A. J. (2008) Influence of the environment on the [4Fe-4S]<sup>2+</sup> to [2Fe-2S]<sup>2+</sup> cluster switch in the transcriptional regulator FNR, *J. Am. Chem. Soc.* 130, 1749-1758.
286. Crack, J. C., Green, J., Le Brun, N. E., and Thomson, A. J. (2006) Detection of sulfide release from the oxygen-sensing [4Fe-4S] cluster of FNR, *J. Biol. Chem.* 281, 18909-18913.
287. Surerus, K. K., Münck, E., Moura, I., Moura, J. J. G., and LeGall, J. (1987) Evidence for the formation of a ZnFe<sub>3</sub>S<sub>4</sub> cluster in *Desulfovibrio gigas* ferredoxin II, *J. Am. Chem. Soc.* 109, 3805-3807.
288. Breton, J. L., Duff, J. L. C., Butt, J. N., Armstrong, F. A., George, S. J., Petillot, Y., Forest, E., Schafer, G., and Thomson, A. J. (1995) Identification of the iron-sulfur clusters in a ferredoxin from the archaeon *Sulfolobus acidocaldarius*: Evidence for a reduced [3Fe-4S] cluster with pH-dependent electronic properties, *Eur. J. Biochem.* 233, 937-946.
289. Beinert, H., Holm, R. H., and Münck, E. (1997) Iron-sulfur clusters; Nature's modular, multipurpose structures, *Science* 277, 653-659.
290. Guex, N. and Peitsch, M. C. (1997) SWISS-MODEL and the Swiss-PdbViewer: an environment for comparative protein modeling, *Electrophoresis* 18, 2714-2723.

Figure 1.1: Structures of fundamental types of Fe-S centers as determined by X-ray crystallography. Structures are taken from the coordinates deposited in the Protein Data Bank: A. Fe<sup>3+</sup> center in rubredoxin from *Desulfovibrio vulgaris*, PDB ID# 8RXN; B. [2Fe-2S]<sup>2+</sup> cluster in *Anabaena pcc 7120* 2Fe ferredoxin ([2Fe-2S]), PDB ID# 1FRD; C. [2Fe-2S]<sub>R</sub><sup>2+</sup> Rieske-type cluster in *Sulfolobus acidocaldarius* Rieske protein, PDB ID# 1JM1; D. [3Fe-4S]<sup>+</sup> cluster in *Azotobacter vinelandii* 7Fe FdI, PDB ID# 6FDR; E. [4Fe-4S]<sup>2+</sup> cluster in *Azotobacter vinelandii* 7Fe FdI, PDB ID# 6FDR; F. [8Fe-7S]<sup>N</sup> P-cluster in dithionite-reduced *Azotobacter vinelandii* nitrogenase MoFe protein, PDB ID# 1M1N. Color code: magenta, Fe; yellow, S; gray, C; violet, N. Unlabeled S atoms correspond to bridging sulfides. Adapted from reference (86).

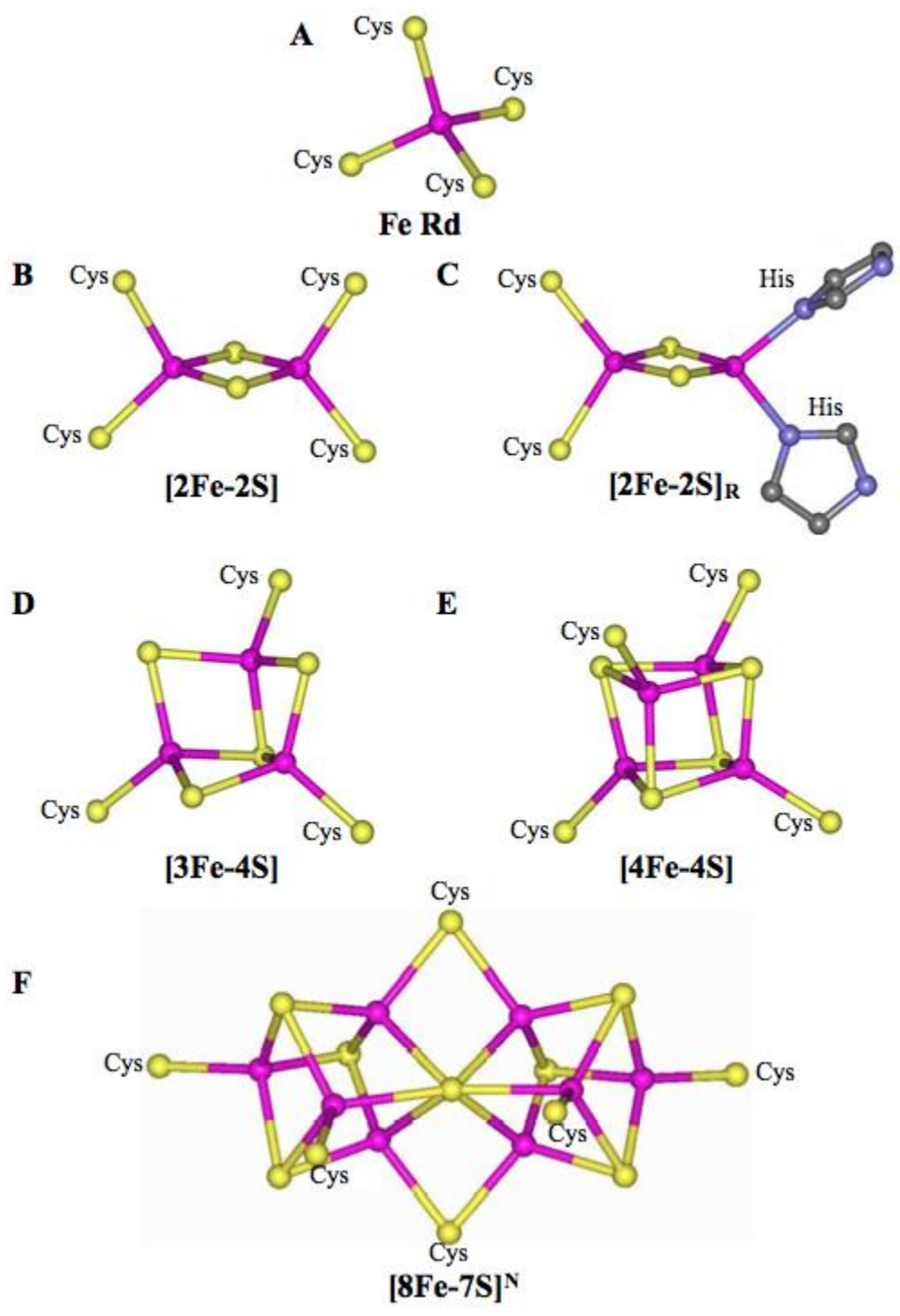


Figure 1.2: Ranges of midpoint potential (mV vs NHE) for the major classes of biological Fe–S centers in their physiologically accessible redox states. Color code: red, Fe<sup>3+</sup>; blue, Fe<sup>2+</sup>; green, Fe<sup>2.5+</sup>, valance-delocalized; yellow, S; cyan, N; grey, C. Adapted from reference (86).

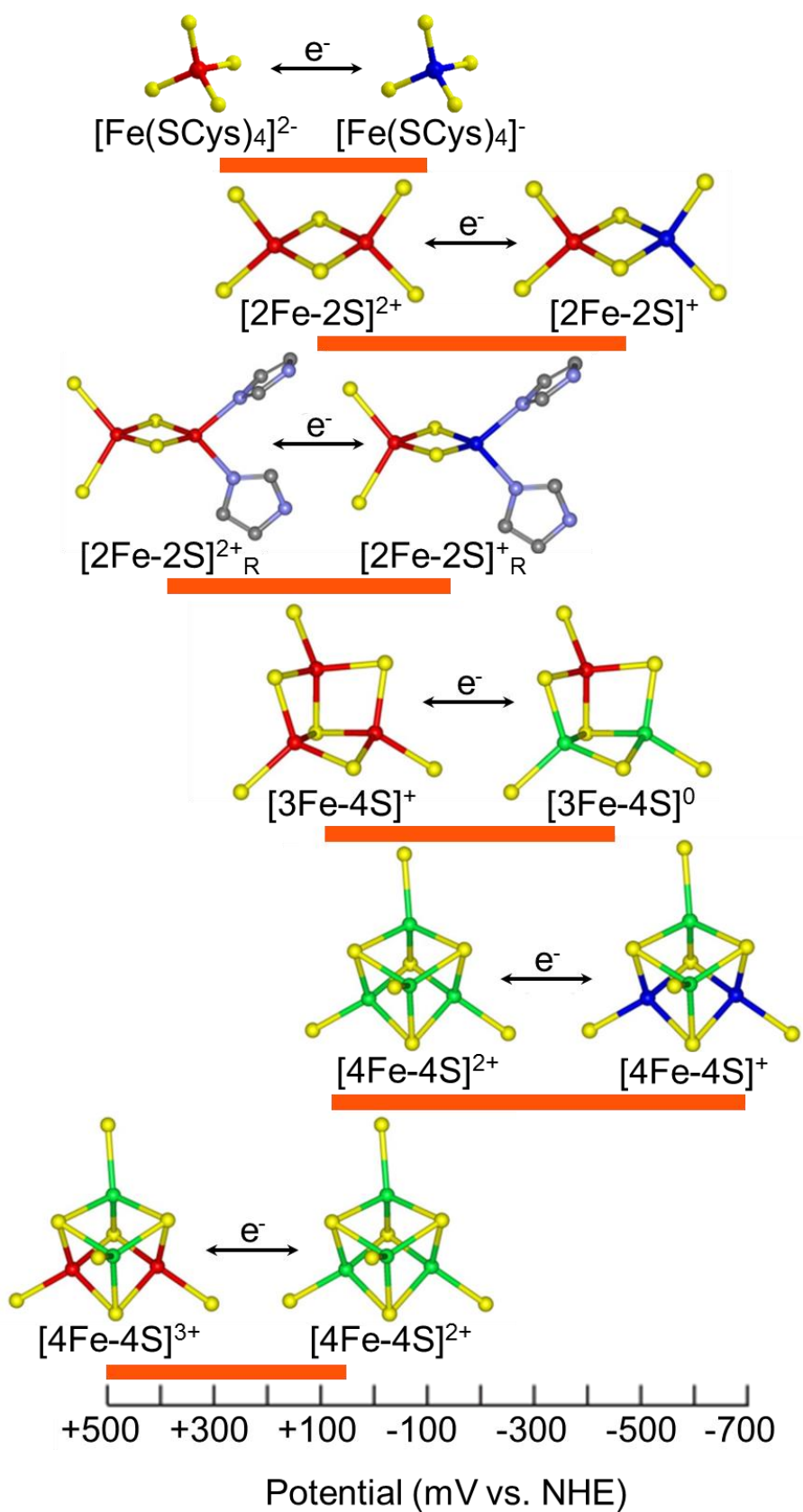


Figure 1.3: Ground state spin ( $S$ ) and valence localization/delocalization patterns for fundamental types of Fe–S centers. Also indicated is the core oxidation state of Fe-S centers. Valence delocalized  $[2\text{Fe-2S}]^+$  clusters with  $S = 9/2$  ground state have only been observed in C56S and C60S variants of *Clostridium pasteurianum* 2Fe ferredoxin (32-34). The  $[3\text{Fe-4S}]^-$  cluster is shown in parenthesis since it has not been observed in any proteins, and only has been identified as fragment in heterometallic cuboidal clusters (287). Three electron reduction of the  $[3\text{Fe-4S}]^+$  cluster to yield the  $[3\text{Fe-4S}]^{2-}$  cluster occurs with the concomitant addition of three protons (288). Color code: red,  $\text{Fe}^{3+}$ ; blue,  $\text{Fe}^{2+}$ ; green,  $\text{Fe}^{2.5+}$ ; yellow, S; grey, O. Adapted from reference (86).

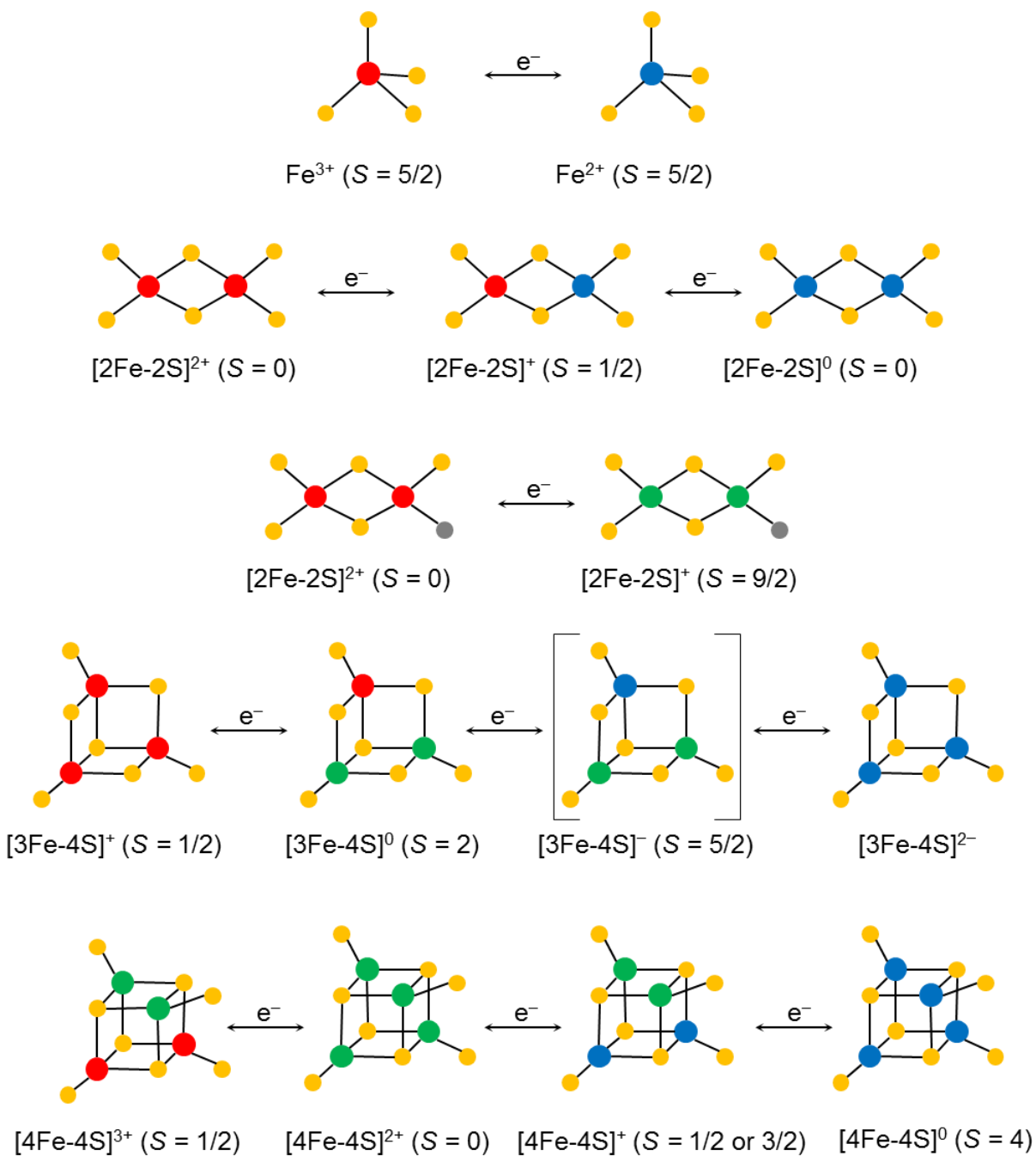


Figure 1.4: Schematic representations summarizing the types of cluster interconversions observed in Fe-S proteins. The charges of Fe-S cluster core are indicated.  $M^{2+} = Cr^{2+}, Mn^{2+}, Co^{2+}, Ni^{2+}, Zn^{2+}, Cd^{2+}$ ;  $M^+ = Cu^+$  and  $Tl^+$ . Adapted from reference (70;289).

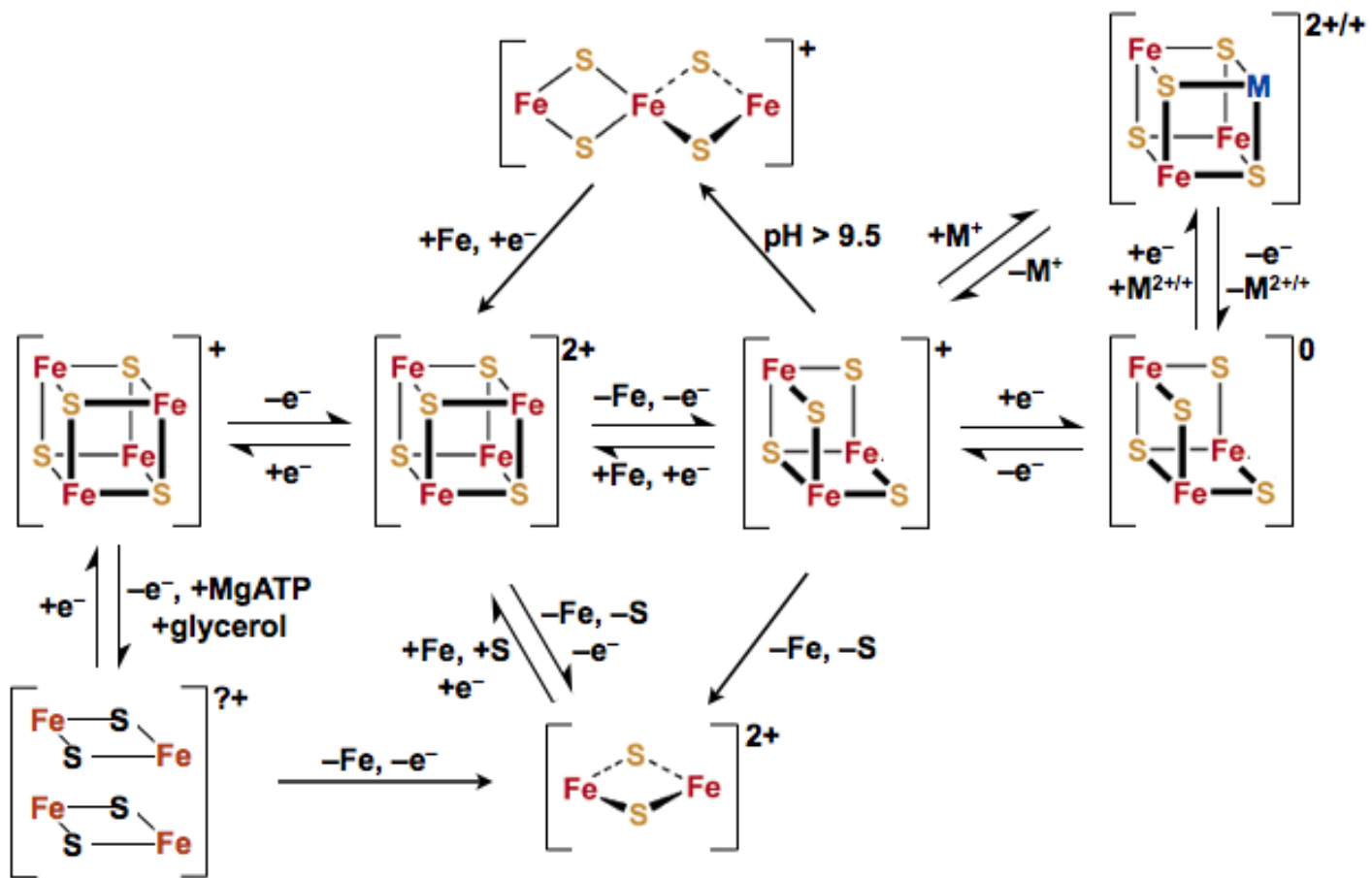


Figure 1.5: Structures of some Fe-S clusters that constitute enzyme active sites. The structures are determined by X-ray crystallography and are taken from coordinates deposited in the Protein Data Bank: (A) [4Fe-4S] + isocitrate, PDB ID# 7ACN, isocitrate-bound form of porcine heart aconitase; (B) [Ni-4Fe-5S], PDB ID# 1SU8, reduced CO dehydrogenase II from *Carboxydotherrmus hydrogenoformans*; (C) [Mo-7Fe-9S-C], PDB ID# 3U7Q, *Azotobacter vinelandii* MoFe protein; (D) [4Fe-4S] + SAM, PDB ID# 1OLT, SAM-bound form of HemN from *Escherichia coli*; (E) siroheme-[4Fe-4S], PDB ID# 2GEP, sulfite-bound form of sulfite reductase from *Escherichia coli*; (F) Ni-Ni-[4Fe-4S], PDB ID# 1RU3, acetyl-CoA synthase from *Carboxydotherrmus hydrogenoformans*; (G) Fe-Fe-[4Fe-4S], PDB ID# 1HFE, *Desulfovibrio desulfuricans* Fe-hydrogenase. Color code: magenta, Fe; yellow S; gray, C; red, O; green, Ni; cyan, Mo; black, unknown low Z atom (O/C/N). Unlabeled S atoms correspond to bridging sulfides and BAN indicates backbone amide N. Adapted from reference (86).

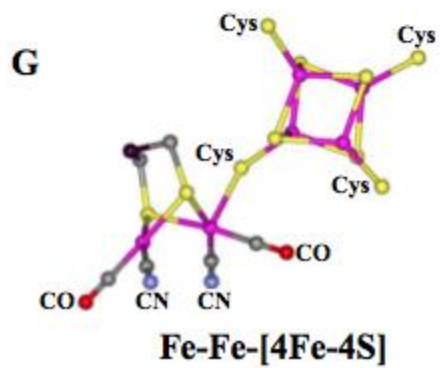
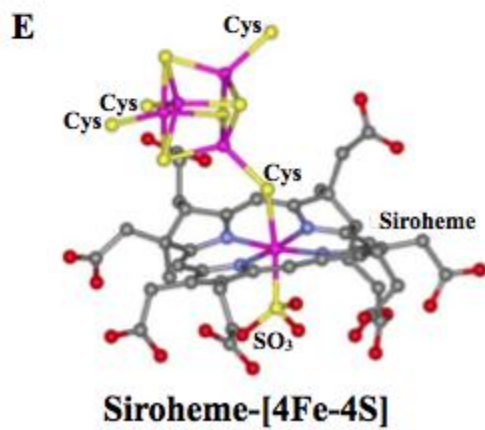
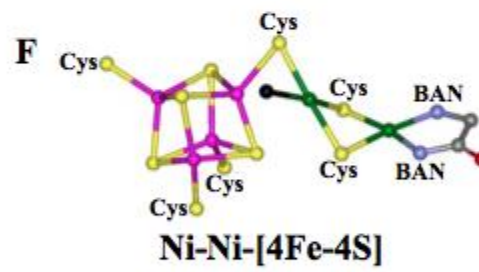
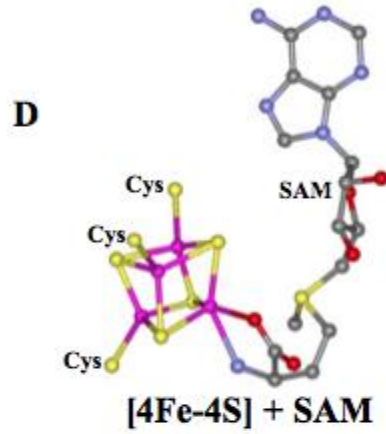
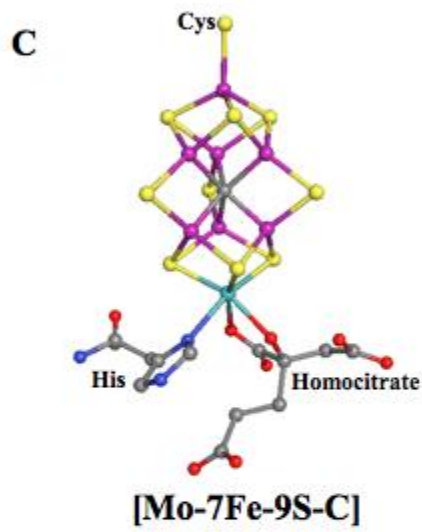
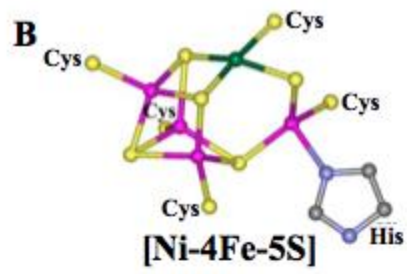
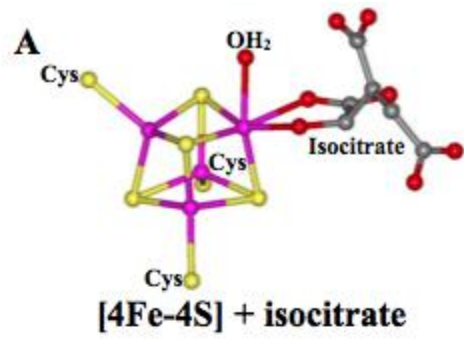
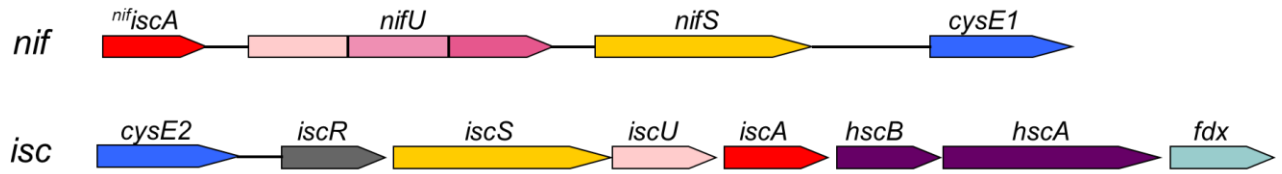
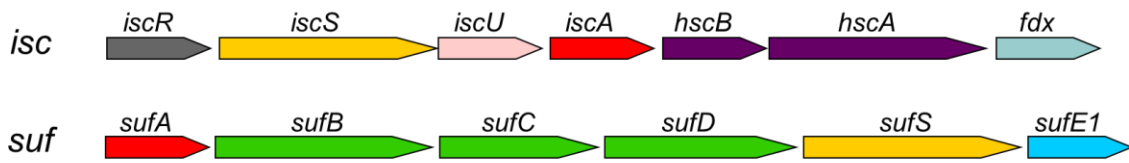


Figure 1.6: Organization of genes involved in *nif*, *isc* and *suf* Fe-S cluster assembly operons in selected prokaryotic organisms. Different colors within *nifU* indicate different modular domains. Genes from different gene clusters or different organisms proposed to encode for protein product with same function are designated in the same color, for instance, *nifS*, *iscS* and *sufS* are all shown in yellow. Genes located within the same operon that encodes proteins proposed to form a functional complex are also denoted in the same color, e.g. *hscA* and *hscB*; and *sufB*, *sufC* and *sufD*.

*Azotobacter vinelandii* (Av)



*Escherichia coli* (Ec)



*Enterococcus faecalis* (Ef)



*Helicobacter pylori* (Hp)

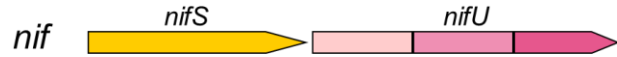


Figure 1.7: Schematic representation of classification and domain organization of classes I and II Grxs. Studies of Grxs from photosynthetic organisms led to classification of Grxs into six classes, which can be extend to non-photosynthetic organisms. Among the six classes of Grxs, classes I and II are the most widespread. Grx domains for selective members of classes I and II are respectively designated in green and purple, with active site sequence labeled accordingly. The mitochondrial/plastid targeting sequences are shown in blue. Additional thioredoxin-like modules are denoted in orange and a domain of unknown function is shown in gray. Adapted from reference (229).

### Class I

Plant GrxC1 to C5, S12, *Hs* Glrx1 and 2,  
*Ec* Grx1 and 3, *Sc* Grx1, 2, 6, 7

CxxC/S

### Class II

*Ec* Grx4

CGFS

GrxS14/S15, *Sc* Grx5, *Hs* Grx5

CGFS

GrxS16 (specific to plants)

CGFS

*Sc* Grx3p, *Sc* Grx4p

Trx CGFS

GrxS17 (lower plants, algae)  
PICOT = *Hs* Grx3

Trx CGFS CGFS

GrxS17 (higher plants)

Trx CGFS CGFS CGFS

Figure 1.8: Comparison of the crystal structures of *E. coli* Grx4 and human Grx2. The [2Fe-2S] cluster-containing dimeric structure of (A) *E. coli* Grx4 (PDB: 2WCI) and (B) human Grx2 (PDB: 2HT9) are presented with one protomer colored by mean of a continuous spectral color scheme. The Fe-S cluster, ligating cysteine residues and GSH molecules are shown in stick representation. Sulfur atoms are shown in yellow and iron atoms are in brown. By placing the bottom protomer in both structures in the same orientation, the top protomer marked by the dashed box in the *E. coli* Grx4 structure is rotated by approximately 90° compare to that of human Grx2. The direct contacts established between two *E. coli* Grx4 protomers as a result of protein conformation are also indicated. Adapted from reference (242).

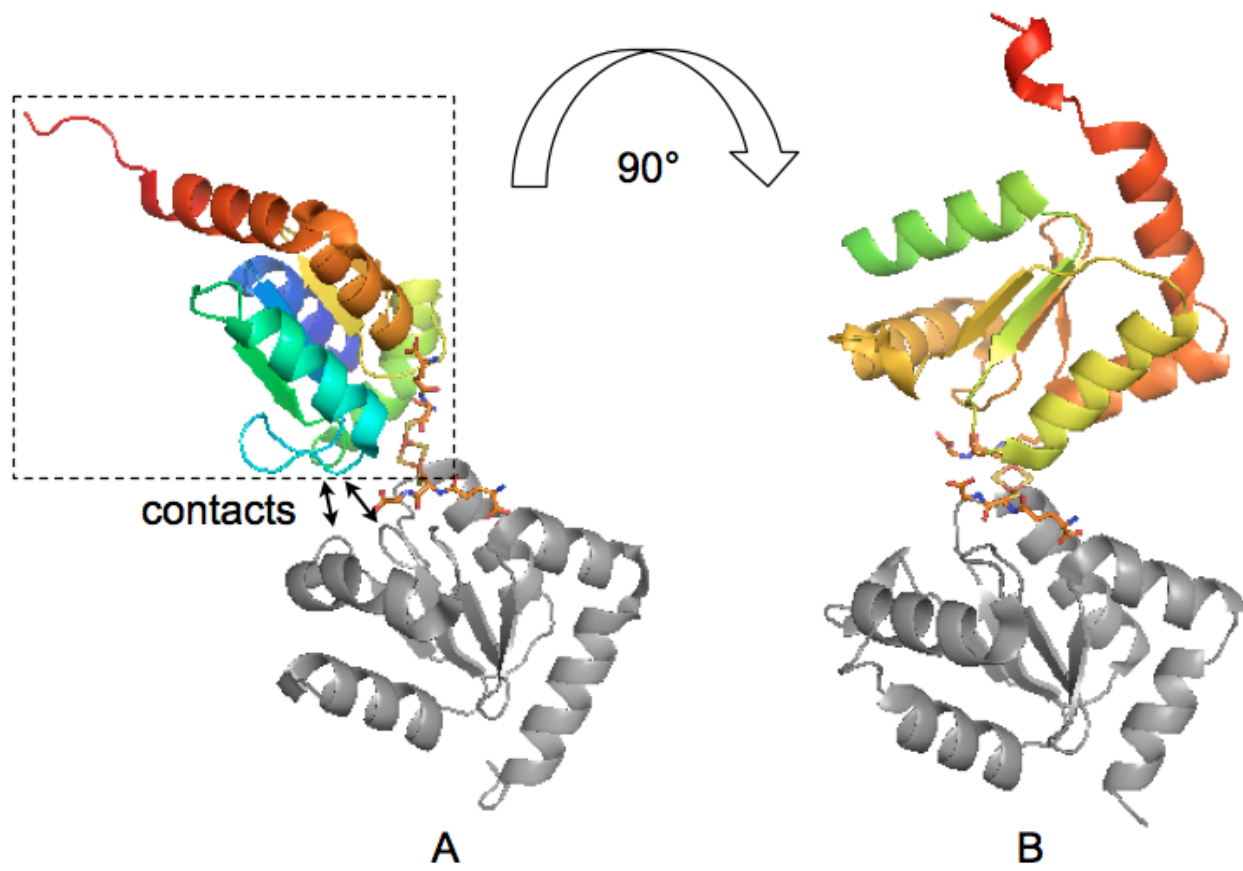


Figure 1.9: Superimposition of apo (orange) and cluster-bound (green) structures of *E. coli* Grx4, PDB ID# 1YKA and 2WCI, respectively). The [2Fe-2S] cluster is represented by grey (iron) and yellow (sulfur) spheres. The GSH molecule in the crystal structure of the cluster-bound Grx4 is shown as stick. The second protomer of the cluster-bound *E. coli* Grx4 structure and its related GSH molecule have been omitted for clarity. The side chains of selected residues are depicted as sticks. The black arrows indicate the major conformational changes between the apo and cluster-bound forms of *E. coli* Grx4. Adapted from reference (242).

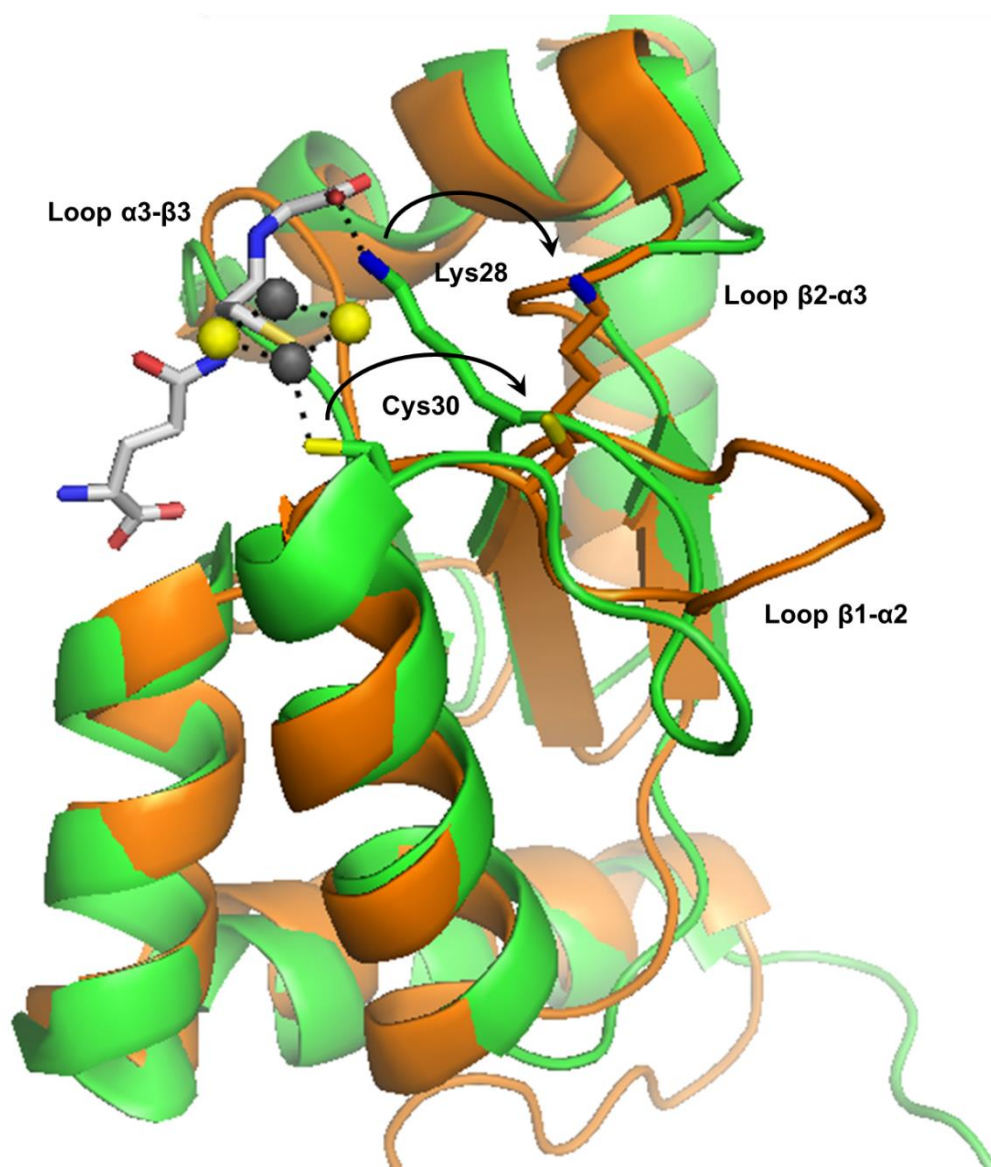
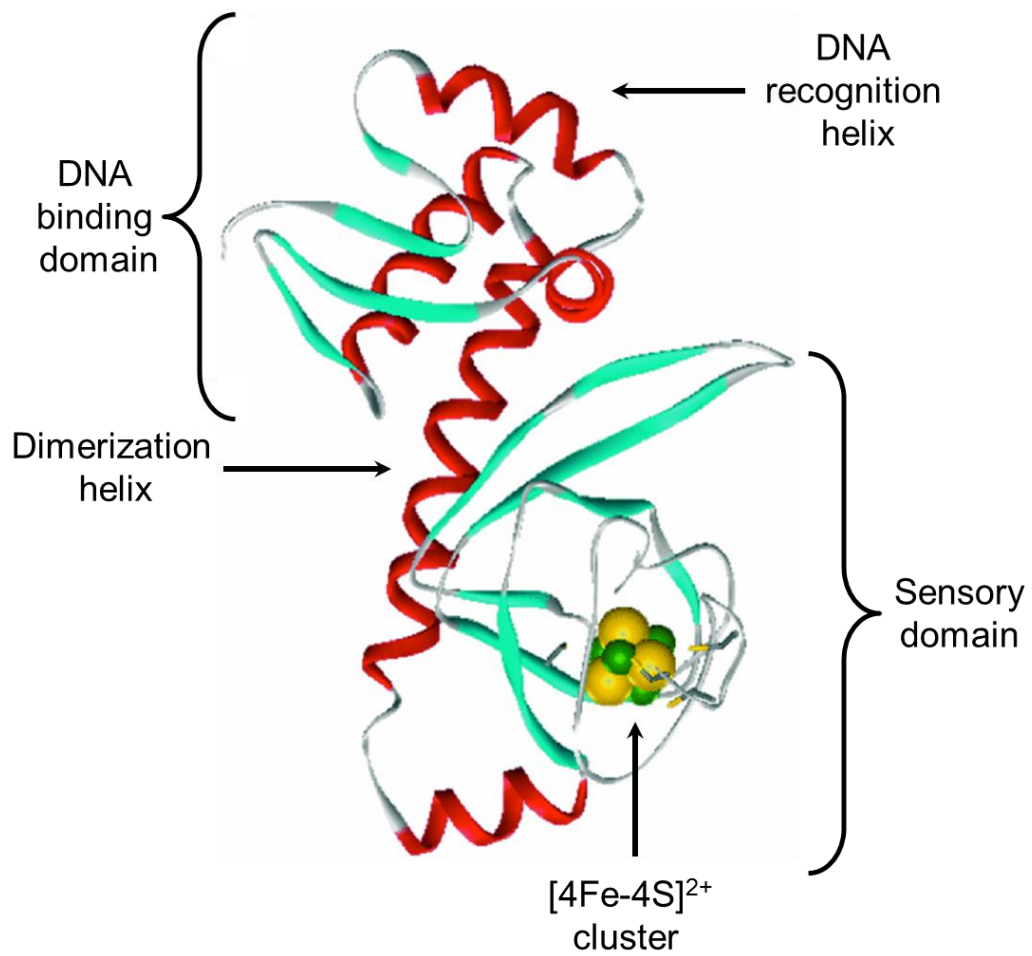


Figure 1.10: The predicted structure of a FNR monomer, based on sequence homology with CRP. The proposed FNR structure was generated by using Swiss-Model and the Swiss-PDB viewer (290) with crystal structure of CRP as a template (270). The two functionally distinct domains in FNR and locations of important features are marked. Adapted from reference (100).



## CHAPTER 2

# ASSEMBLY OF LINEAR [3Fe-4S]<sup>+</sup>, [2Fe-2S]<sup>2+</sup> AND [4Fe-4S]<sup>2+</sup> CLUSTERS IN *SACCHAROMYCES CEREVISIAE* MITOCHONDRIAL GLUTAREDOXIN 5: SPECTROSCOPIC CHARACTERIZATION AND IMPLICATIONS FOR FUNCTIONS

---

Bo Zhang,<sup>a</sup> Sibali Bandyopadhyay,<sup>a</sup> Sunil G. Naik,<sup>b</sup> Boi Hanh Huynh,<sup>b</sup> Jérémy Couturier,<sup>c</sup>  
Nicolas Rouhier,<sup>c</sup> and Michael K. Johnson<sup>a</sup>

*To be submitted to J. Am. Chem. Soc.*

<sup>a</sup>Department of Chemistry and Center for Metalloenzyme Studies, University of Georgia, Athens, Georgia 30602; <sup>b</sup>Department of Physics, Emory University, Atlanta, Georgia 30322, United States; <sup>c</sup>Unité Mixte de Recherches 1136 INRA-Nancy Université, Interactions Arbres Microorganismes, IFR 110, EFABA 54506 Vandoeuvre-lès-Nancy Cedex, France.

**Abbreviations:**

*Saccharomyces cerevisiae*, *Sc*; glutaredoxin, Grx; circular dichroism, CD; variable-temperature magnetic circular dichroism, VTMCD; electron paramagnetic resonance, EPR; dithiothreitol, DTT; tris(2-carboxyethyl)phosphine, TCEP; glutathione, GSH; thioredoxin, Trx.

## Abstract

*Saccharomyces cerevisiae* mitochondrial glutaredoxin 5 (Grx5) belongs to a ubiquitous class of monothiol glutaredoxins with a strictly conserved CGFS active-site sequence (CGFS-Grxs). *In vivo* studies on *S. cerevisiae* Grx5 have revealed an important role for this family of proteins in Fe-S cluster biogenesis which is likely related to the ability of several other members of this family of monothiol CGFS-Grxs to incorporate a labile  $[2\text{Fe-2S}]^{2+}$  cluster that can be rapidly transferred to apo recipient proteins. However, little is known concerning the types and roles of Fe-S clusters that can be assembled on *S. cerevisiae* Grx5. In this work, we show that recombinant *S. cerevisiae* Grx5 lacking the mitochondrial targeting sequence is purified as an apo protein under aerobic or anaerobic conditions when expressed in *E. coli*. However, *in vitro* reconstitution in the presence of glutathione (GSH) results in a form of Grx5 that predominantly contains one linear  $[3\text{Fe-4S}]^+$  cluster per dimer, in addition to minor forms containing  $[2\text{Fe-2S}]^{2+}$  or  $[4\text{Fe-4S}]^{2+}$  clusters. The excited state electronic properties and ground state electronic and vibrational properties of the linear  $[3\text{Fe-4S}]^+$  cluster have been characterized using UV-visible absorption and circular dichroism, variable-temperature magnetic circular dichroism, electron paramagnetic resonance, Mössbauer and resonance Raman spectroscopies. The results reveal a rhombic  $S = 5/2$  linear  $[3\text{Fe-4S}]^+$  cluster ( $E/D = 0.31$ ,  $D = 0.6 \text{ cm}^{-1}$ ), with properties similar to those reported for synthetic linear  $[3\text{Fe-4S}]^+$  clusters and the linear  $[3\text{Fe-4S}]^+$  clusters in purple aconitase. Moreover, the results indicate that the Fe-S cluster content previously reported for many monothiol Grxs has been misinterpreted in terms of  $[2\text{Fe-2S}]$  clusters exclusively rather than mixtures of linear  $[3\text{Fe-4S}]^+$  and  $[2\text{Fe-2S}]^{2+}$  clusters. Our studies also show that in the absence of GSH, anaerobic reconstitution of Grx5 in the presence of DTT yields a dimeric form containing one  $[4\text{Fe-4S}]^{2+}$  cluster that is most likely coordinated by the active-site cysteine and

the partially conserved cysteine residue of Grx5. The  $[4\text{Fe-4S}]^{2+}$  cluster-bound form of Grx5 is competent for *in vitro* activation of apo-aconitase. Potential roles for *S. cerevisiae* Grx5 in scavenging Fe-S clusters released during protein unfolding under oxidative stress conditions and in maturation of  $[4\text{Fe-4S}]^{2+}$  cluster-containing proteins are discussed in light of these results.

## Introduction

Glutaredoxins (Grxs) represent a ubiquitous family of proteins with structural homology to thioredoxins. Based on phylogeny, active site sequence and domain structure, the most widespread Grxs can be classified into two main groups: classic dithiol Grxs with CxxC/S active sites and monothiol Grxs with strictly conserved CGFS active-site sequence (hereafter referred to as CGFS-Grxs) (1). CGFS-Grxs exhibit a higher degree of homology compared to dithiol Grxs and can be further categorized into single-domain Grxs consisting of only one CGFS-Grx domain, and multi-domain Grxs that are modular proteins with a N-terminal Trx-like extension and one to three C-terminal CGFS-Grxs domains. While single-domain CGFS-Grxs are widespread, multi-domain CGFS-Grxs are restricted to eukaryotic organisms (1;2). Initially, Grxs were recognized as thiol-disulfide oxidoreductases based on the ability exhibited by the classic dithiol Grxs to reduce cysteine disulfides particularly on glutathionylated proteins (2). However, none of the CGFS Grxs investigated thus far exhibit significant level of dithiol oxidoreductase activity when tested with standard model substrates for Grxs (3-6). Rather both *in vivo* and *in vitro* studies of CGFS-Grxs have implicated a role for single-domain CGFS-Grxs in Fe-S cluster biogenesis (7-12).

The initial studies that revealed CGFS-Grxs as important components in Fe-S cluster biogenesis were carried out on *S. cerevisiae* mitochondrial Grx5 (*Sc* Grx5), a single domain CGFS-Grx, that has since been employed as model protein in the investigations of biological functions of CGFS-Grxs. A *S. cerevisiae* *grx5* deletion strain exhibited phenotypes that can be attributed to defective Fe-S cluster biogenesis, notably impaired activity of at least two mitochondrial Fe-S enzymes (aconitase and succinate dehydrogenase) and mitochondrial iron accumulation (7). As a result, the cell displayed increased sensitivity to oxidative stress as well

as growth defects in minimal medium. In addition, radiolabeled  $^{55}\text{Fe}$  immunoprecipitation studies revealed that depletion of *Sc* Grx5 results in Fe accumulation on Isu1, the primary scaffold protein for the assembly of Fe-S clusters in the mitochondrial ISC machinery (8). These *in vivo* results suggested that *Sc* Grx5 was required for dissociation of preassembled Fe-S cluster from Isu1 and/or the transfer of clusters from Isu1 to acceptor proteins. Further evidence linking CGFS-Grxs to Fe-S cluster biogenesis came from the observation that the phenotypic defects of *Sc* Grx5 deficiency can be suppressed by overexpression of Ssq1, an essential protein in the ISC assembly machinery involved in releasing Fe-S clusters from Isu1 (8). Moreover, yeast two-hybrid analysis also demonstrated specific *in vivo* interaction between *Sc* Grx5 and *Sc* Isa1, an A-type Fe-S cluster or Fe carrier protein in the mitochondrial iron-sulfur cluster assembly machinery, suggesting participation of *Sc* Grx5 in trafficking of Fe-S clusters (12). The involvement of CGFS-Grxs in Fe-S cluster biogenesis is also evolutionarily conserved, since homologs of *Sc* Grx5 from various species ranging from prokaryotes to eukaryotes have been shown to have the ability to rescue the phenotype of the *grx5* deletion strain when targeted to *S. cerevisiae* mitochondria (9;13;14).

Site-directed mutagenesis studies in *Sc* Grx5 revealed that the active site cysteine residue is essential for its biological function, since mutation of this cysteine results in the same phenotype as observed in the *grx5* deletion strain (15). In addition, both spectroscopic and structural studies of a variety of reconstituted or as-purified recombinant single-domain and multi-domain CGFS-Grxs have shown that the active-site cysteine along with the cysteine of two glutathiones are required to coordinate a  $[\text{2Fe-2S}]^{2+}$  cluster at the subunit interface of the homodimer (4;9;16-18). The  $[\text{2Fe-2S}]^{2+}$  cluster in homodimeric CGFS-Grxs have a homogeneous  $S = 0$  ground state that results from antiferromagnetic coupling of the two high

spin  $S = 5/2$  ferric irons (9;17). However, the  $[2\text{Fe-2S}]^{2+}$  clusters in CGFS-Grxs homodimers are unlikely to be redox active *in vivo* since the cluster is both oxidatively and reductively labile. The cluster gradually degrades upon exposure to air and rapidly degrades, via a semi-stable  $[2\text{Fe-2S}]^+$  intermediate with an  $S = 1/2$  electronic ground state, on anaerobic reduction with small excess of dithionite (17).

The *in vivo* evidence for a role of *Sc* Grx5 in Fe-S cluster biogenesis that is evolutionarily conserved, coupled with the ability of various CGFS-Grxs to ligate a  $[2\text{Fe-2S}]^{2+}$  cluster using the essential active-site cysteine residue, prompted us to carry out detailed spectroscopic characterization of the type and properties of Fe-S clusters that can be assembled on *Sc* Grx5. Thus far, there is only limited information regarding the ability of *Sc* Grx5 to incorporate an Fe-S cluster. Picciocchi and coworkers have reported purification of a cluster-bound form of recombinant *Sc* Grx5 and the type of the cluster was interpreted as  $[2\text{Fe-2S}]$  cluster on the basis of UV-visible absorption data alone (19). Here we report that recombinant *Sc* Grx5 purifies as an apo protein under both aerobic and anaerobic conditions. However, using the combination of UV-visible absorption, circular dichroism (CD) and variable-temperature magnetic circular dichroism (VTMCD), electron paramagnetic resonance (EPR), Mössbauer and resonance Raman spectroscopies, we demonstrate that cysteine desulfurase-mediated cluster assembly on recombinant *Sc* Grx5 primarily results in the formation of linear  $[3\text{Fe-4S}]^+$  clusters in the presence of GSH and  $[4\text{Fe-4S}]^{2+}$  clusters in the absence of GSH. The ligation of the assembled Fe-S clusters and the significance of the presence of linear  $[3\text{Fe-4S}]^+$  and  $[4\text{Fe-4S}]^{2+}$  clusters in *S. cerevisiae* Grx5 are discussed in light of these new results.

## Experimental procedures

*Plasmid constructions:* The sequence coding for the mature form of *S. cerevisiae* Grx5 devoid of the first 29 amino acids, corresponding to the mitochondrial targeting sequence, was cloned into the pET3d plasmid between NcoI and BamHI restriction sites using the following forward and reverse primers described in Table 2.1. Owing to the use of NcoI for cloning, an alanine codon was added to keep the sequence in frame. The C90S variant, where the cysteine at position 90 was substituted by a serine residue, was also cloned by PCR into pET3d using two complementary primers (Table 2.1). All plasmids were verified by sequencing.

*Protein Expression and Purification:* Recombinant *Sc* Grx5 was heterologously expressed in the *E. coli* BL21(DE3) strain in the presence of the pSBET plasmid. Cells harboring the Grx5 plasmid were cultivated at 37 °C in LB media supplemented with ampicillin (100 µg/ml) and kanamycin (30 µg/ml). Protein expression was induced with isopropyl-1-thio-β-D-galactopyranoside (IPTG) to a final concentration of 100 µg/ml when OD<sub>600</sub> was between 0.4 and 0.8. The culture was then further cultivated at 34 °C for 4 hours and harvested by centrifugation and stored at -80 °C until further use. For aerobic purification, cells expressing recombinant Grx5 was thawed and resuspended in 100mM Tris-HCl, pH 7.8 buffer containing 1mM GSH (buffer A) with addition of 10µg/mL phenylmethylsulphonyl fluoride (PMSF), 15µg/ml DNase and 5×10<sup>-3</sup>µg/ml RNase. Cells were disrupted by intermittent sonication on ice, and centrifuged at 17,000 rpm at 4 °C for 1 hour to remove the cell debris. The cell-free extract was then precipitated with 40% of ammonium sulfate and pelleted by centrifugation. The resulting pellet was resuspended in minimal volume of buffer A, loaded onto a phenyl-sepharose High-Performance Fast-Flow (Pharmacia) column, previously equilibrated with 100mM Tris-HCl, pH 7.8, containing 1mM GSH and 1M ammonium sulfate (buffer B) and eluted using a

decreasing linear gradient of 100-0% ammonium sulfate. The purest fractions judged by SDS-PAGE analysis were combined and concentrated down to approximate 3 mL using YM10 membrane and then applied to a HiTrap<sup>M</sup> Q-HP anion-exchange column (GE Healthcare) previously equilibrated with buffer A and the elution was achieved with an increasing linear gradient of 0 - 100% NaCl. The purest fractions containing apo *Sc* Grx5, as judged by SDS-PAGE analysis, were pooled and dialyzed into 100mM Tris-HCl, pH 7.8 buffer by Amicon ultrafiltration using a YM10 membrane and stored in liquid nitrogen. Anaerobic purification of *Sc* Grx5 was carried out in a glove box under argon atmosphere ( $O_2 < 2$  ppm) using the same protocol described above, except that lysis of the cells containing overexpressed *Sc* Grx5 was achieved by incubation with Ready-Lyse<sup>TM</sup> (Epicentre).

The *Sc* Grx5 C90S mutant was expressed in the *E. coli* BL21(DE3) strain in the presence of the pSBET plasmid and purified following procedures previously described for *Arabidopsis* chloroplastic glutaredoxin C5 (20). Briefly, after cell lysis, the protein fraction was precipitated from the cell-free extract between 40 and 80% ammonium sulphate saturation. And the Grx5 C90S was purified aerobically using an ACA44 gel filtration column and followed by a DEAE ion exchange column. The purified proteins were finally stored in Tris buffer (30 mM Tris-HCl, pH 8.0) in liquid nitrogen.

*In vitro* Reconstitution of *Sc* Grx5 in the Presence of GSH: Prior to use, as-purified *Sc* Grx5 protein samples were incubated with 40 mM tris(2-carboxyethyl)phosphine (TCEP) under anaerobic conditions to cleave disulfides, followed by anaerobic removal of TCEP by buffer exchange using Amicon ultrafiltration with a YM10 membrane. Reconstitution was achieved by incubation of TCEP-treated *Sc* Grx5 with 20-fold excess of ferrous ammonium sulfate, 20-fold excess of L-cysteine, catalytic amount of NifS and 3 mM of GSH under strictly anaerobic

conditions (< 2 ppm O<sub>2</sub>) at room temperature for 2.5 hours. Excess reagents were then removed by passing the reconstitution mixture through a Hi-Trap Q-Sepharose column (GE Healthcare) with an increasing linear gradient of 0-100% NaCl. The colored fractions eluted were pooled and concentrated using a YM10 membrane. Samples for resonance Raman isotopic labeling studies were reconstituted with Na<sub>2</sub>S (natural abundance S) or Na<sub>2</sub><sup>34</sup>S (>95% <sup>34</sup>S enrichment) in place of L-cysteine and NifS. <sup>57</sup>Fe-enriched ferrous ammonium sulfate (>95% <sup>57</sup>Fe enrichment) was used in place of natural abundance Fe for the preparation of Mössbauer samples. The same reconstitution procedure described above was used for the *Sc Grx5 C90S* mutant.

*In vitro Reconstitution of Sc Grx5 in the Presence of DTT:* As-purified *Sc Grx5* was incubated with 20-fold excess of ferrous ammonium sulfate, 20-fold excess of L-cysteine, catalytic amount of NifS and 5 mM of DTT under strictly anaerobic conditions (< 2 ppm O<sub>2</sub>). The same procedure for removing of excess reagents was performed as that described above. Mössbauer samples were prepared with <sup>57</sup>Fe-enriched ferrous ammonium sulfate (>95% enrichment). The same reconstitution procedure was used for the *Sc Grx5 C90S* mutant.

*Analytical and Spectroscopic Analyses:* Protein concentrations were determined using the DCTM Protein Assay (Bio-Rad) with bovine serum albumin as the standard. Iron concentrations were determined colorimetrically using method described by Fish after digestion of protein samples in KMnO<sub>4</sub>/HCl (21). Mass spectrometry analysis was carried out by University of Georgia Proteomic and Mass Spectrometry Core Facility. All samples for spectroscopic studies were prepared in a Vacuum Atmosphere glove box under argon atmosphere (O<sub>2</sub> < 2 ppm). UV-visible absorption spectra were recorded in sealed 1 mm quartz cuvettes at room temperature using a Shimadzu UV-3101 PC scanning spectrophotometer. Resonance Raman samples were in the form of 20-μL frozen droplet mounted on the cold finger of an Air Products Displex Model

CSA-202E closed cycle refrigerator and Resonance Raman spectra were recorded as previously described, using an Instrument SA Ramanor U1000 scanning spectrometer coupled with a Coherent Sabre argon or krypton ion laser (22). X-band (~9.6 GHz) EPR spectra were recorded using a ESP-300D spectrometer (Bruker, Billerica, MA) equipped with a dual-mode ER-4116 cavity and an ESR 900 helium flow cryostat (Oxford Instruments, Concord, MA). Room temperature circular dichroism (CD) spectra were recorded in sealed 1 mm quartz cuvettes using a Jasco J-715 spectropolarimeter. Variable temperature magnetic circular dichroism (VTMCD) spectra were recorded on samples containing 50% (v/v) ethylene glycol using the same spectropolarimeter mated to an Oxford Instruments Spectromag 4000 (0-7 T) split-coil superconducting magnet (1.5-300 K). Mössbauer spectra of  $^{57}\text{Fe}$ -enriched samples were recorded using the previously described instrumentation, and analyzed using WMOSS software (Web Research) (23).

*Activation of Apo-aconitase Using  $[4\text{Fe-4S}]^{2+}$  cluster-bound Sc Grx5:* Purification of recombinant *Azotobacter vinelandii* aconitase with a polyhistidine tag was carried out as previously described (24). The apo form of aconitase was obtained by incubation as-purified aconitase sample with EDTA and potassium ferricyanide using method described by Kenney and Beinert (25). Activation mixtures contained 100 mM Tris-HCl (pH 7.8), 1mM DTT, 4 $\mu\text{M}$  apo aconitase and 12  $\mu\text{M}$  of  $[4\text{Fe-4S}]^{2+}$  cluster-bound Sc Grx5. The molar concentration corresponds to the concentration of the  $[4\text{Fe-4S}]^{2+}$  cluster calculated by using the molar absorption coefficient of  $\epsilon_{400} = 16.9 \text{ mM}^{-1} \text{ cm}^{-1}$  per  $[4\text{Fe-4S}]^{2+}$  cluster. Activation mixtures were incubated at room temperature under strict anaerobic conditions, and 10- $\mu\text{L}$  aliquots of sample were taken at different time points and assayed for aconitase activity as previously described (24;26). Briefly, the activity of aconitase was measured spectrophotometrically at 240 nm at room temperature by

following the formation of *cis*-aconitate from citrate or isocitrate, using a molar absorption coefficient  $\epsilon_{240}$  of  $3400 \text{ mM}^{-1} \text{ cm}^{-1}$  for *cis*-aconitate (27). Anaerobically reconstituted samples of *A. vinelandii* aconitase containing one  $[\text{4Fe-4S}]^{2+}$  cluster per monomer exhibited maximal specific activity (corresponding to 100% activity) of 25 units/mg using citrate and 79 units/mg using isocitrate (24). The time course of holo aconitase formation at room temperature was analyzed by fitting to second-order kinetics, based on the initial concentrations of apo aconitase and  $[\text{4Fe-4S}]^{2+}$  clusters on *Sc* Grx5, using the Chemical Kinetics Simulator software package (IBM).

## Results

*Sc* Grx5 was purified exclusively as an apo-protein: The mature form of *S. cerevisiae* Grx5 lacking the mitochondria targeting sequences was heterologously expressed in *E. coli* and purified to homogeneity. Due to the requirement of GSH to coordinate the  $[\text{2Fe-2S}]^{2+}$  clusters in CGFS-type Grxs, 1 mM of GSH was added throughout the purification process (4;16). The molecular mass of the purified *Sc* Grx5 sample was determined by electrospray mass spectrometry to be 13418 Da, in agreement with the predicted monomer molecular mass based on the expressed construct (Figure 2.1). Mass analysis of *Sc* Grx5 also identified two additional peaks at 13723 and 14028 Da, which correspond to the addition of one and two GSH molecules, respectively. This observed glutathiolation of *Sc* Grx5 is consistent with previously reported biochemical characterization results (3). Surprisingly, as-purified *Sc* Grx5 was exclusively in the apo-form devoid of any type of bound Fe-S cluster, as judged by the absence of bands associated with the characteristic S-to-Fe(III) charge transfer transitions in the visible absorption spectrum (data not shown). Moreover, the absence of Fe-S clusters in as-purified *Sc* Grx5 was not due to

the presence of oxygen, as purification carried out under strictly anaerobic conditions inside the glovebox did not result in any Fe-S cluster-bound form of *Sc* Grx5.

*In vitro* assembly of Fe-S clusters in *Sc* Grx5 in the presence of GSH: In order to address the ability of *S. cerevisiae* Grx5 to incorporate Fe-S clusters, anaerobic cysteine desulfurase-mediated cluster reconstitution experiments were carried out in the presence of 3 mM of GSH, since all of the spectroscopically and crystallographically characterized  $[2\text{Fe-2S}]^{2+}$  clusters in other CGFS-Grxs are ligated by GSH molecules in addition to the Grx active-site cysteine residues (4;9;16-18). After removal of excess reagents using chromatography, a cluster-loaded form of *Sc* Grx5 with strong absorption in the visible range was obtained (Figure 2.2, blue spectrum). The  $[2\text{Fe-2S}]^{2+}$  centers in CGFS-Grxs all exhibit very similar UV-visible absorption and CD spectra (9;17;18), that are quite distinct to those observed for cluster-bound *Sc* Grx5, see Figure 2.2. Notably, the UV-visible absorption spectrum of the Fe-S cluster in the reconstituted *Sc* Grx5 exhibits two additional pronounced bands at 566 and 513 nm and the dominant band at 400 nm is blue-shifted by approximately 10 nm compared to the equivalent band of the  $[2\text{Fe-2S}]^{2+}$  clusters. Furthermore, the CD spectrum of the cluster-bound *Sc* Grx5 and the  $[2\text{Fe-2S}]^{2+}$  cluster-bound *Sc* Grx3 exhibit major differences with the former exhibiting an intense positive band at 580 nm and a small positive feature at 418 nm that is not observed in any  $[2\text{Fe-2S}]^{2+}$  cluster-containing homodimeric CGFS-Grxs (Figure 2.2). Surprisingly, the absorption features of the cluster-bound *Sc* Grx5 in the visible range are strikingly similar to those previously reported for the linear  $[3\text{Fe-4S}]^+$  clusters in synthetic complexes and in alkaline (purple) aconitase (28;29). On the basis of the theoretical and experimental  $\epsilon_{280}$  values for the apo protein ( $8.6 \text{ mM}^{-1} \text{ cm}^{-1}$ ), the  $\epsilon_{280}$  and  $\epsilon_{403}$  values for the linear  $[3\text{Fe-4S}]^+$  cluster in *Sc* Grx5 are estimated to be 28.4 and  $20.0 \text{ mM}^{-1} \text{ cm}^{-1}$ , respectively, and the  $A_{403}/A_{280}$  is found to be 0.44. Protein and Fe analysis

revealed that a sample with  $A_{403}/A_{280} = 0.37$  contains  $1.1 \pm 0.1$  Fe per Grx5 monomer. Taken together, the absorption and analytical data are consistent with approximately one linear  $[3\text{Fe-4S}]^+$  cluster per dimeric *Sc* Grx5. This stoichiometry is also indicated based on the extinction coefficients at 280 and  $\sim 410$  nm ( $\sim 30$  and  $\sim 20$   $\text{mM}^{-1}\text{cm}^{-1}$ , respectively) established for synthetic and protein-bound linear  $[3\text{Fe-4S}]^+$  clusters (28;29). Hence, Mössbauer, EPR, VT-MCD, and resonance Raman spectroscopic studies were undertaken to investigate the electronic, magnetic and vibrational properties of the linear  $[3\text{Fe-4S}]^+$  cluster present in *Sc* Grx5.

More definitive and quantitative assessment of the type of Fe-S cluster(s) present in *Sc* Grx5 was provided by Mössbauer studies of a sample reconstituted with  $^{57}\text{Fe}$ . Figure 2.3A shows a 4.2 K Mössbauer spectrum of *Sc* Grx5 reconstituted in the presence of 3 mM GSH, recorded in a weak magnetic field of 50 mT parallel to the  $\gamma$ -radiation. Four components are discernible in this complex spectrum. The major component, which accounts for 72% of total  $^{57}\text{Fe}$ , exhibits paramagnetic hyperfine structure (shown in orange). This component is identified as a linear  $[3\text{Fe-4S}]^+$  cluster based on simulated parameters for spectra obtained at different applied magnetic fields (*vide infra*). The remaining three components contained in this sample are a  $S = 0$   $[2\text{Fe-2S}]^{2+}$  cluster that accounts for 11% of the total  $^{57}\text{Fe}$  absorption (shown in red), a  $S = 0$   $[4\text{Fe-4S}]^{2+}$  cluster accounting for 6% of the total  $^{57}\text{Fe}$  (shown in blue), and a mononuclear  $S = 2$   $\text{Fe}^{2+}$  species, estimated to account for 11% of the total  $^{57}\text{Fe}$  absorption (shown in green). The solid black line overlaid on the experimental spectrum in Figure 2.3A is the composite spectrum that includes all four components. The agreement between the simulated spectrum and the experimental data supports the above assessment of the composition of Fe species in the sample.

Removal of the contributions from the minor components ( $[2\text{Fe-2S}]^{2+}$  cluster,  $[4\text{Fe-4S}]^{2+}$  cluster and  $\text{Fe}^{2+}$  species) reveals the experimental spectrum arising solely from the linear  $[3\text{Fe-}$

4S]<sup>+</sup> cluster (black spectrum in Figure 2.3B). To better characterize the linear [3Fe-4S]<sup>+</sup> cluster in *Sc Grx5*, Mössbauer spectra were recorded at 4.2 K with 4 T and 8 T parallel fields and the contributions from the [2Fe-2S]<sup>2+</sup> cluster, [4Fe-4S]<sup>2+</sup> cluster and Fe<sup>2+</sup> species were again removed from the raw data (black spectra in Figure 2.3C and 2.3D, respectively). The Mössbauer spectra of the linear [3Fe-4S]<sup>+</sup> cluster in *Sc Grx5* with 50 mT, 4 T and 8 T are all simulated to a good approximation using the parameters shown in Table 2.2, shown as orange lines overlaying the experimental spectra in Figure 2.3A–D. The theoretical spectra are computed with equal intensity for each Fe site using the parameters listed in Table 2.2, and a rhombic  $S = 5/2$  ground state with  $E/D = 0.31$  and  $D = 2.0 \text{ cm}^{-1}$ , i.e. analogous spin Hamiltonian parameters to those used in simulating the Mössbauer spectrum of the linear [3Fe-4S]<sup>+</sup> cluster in aconitase (29).

The Mössbauer spectra of the linear [3Fe-4S]<sup>+</sup> cluster in *Sc Grx5* exhibit a well-resolved six-line pattern of magnetic hyperfine interactions and are analogous to the Mössbauer spectra reported for the linear [3Fe-4S]<sup>+</sup> cluster in partially-unfolded, alkaline aconitase (29). The field-dependence of the magnetic hyperfine splitting pattern can be interpreted using the spin coupling model established for the linear [3Fe-4S]<sup>+</sup> cluster in aconitase and the synthetic complexes (29-31). The Mössbauer spectra can be decomposed into contributions from three equal intensity high-spin ferric sites, each in a tetrahedral environment of sulfur atoms, that are spin-coupled to form a  $S = 5/2$  ground state with the spin of the central Fe (site 3) antiparallel to both terminal Fe sites (sites 1 and 2). The observed magnetic hyperfine splitting is dependent on the magnitude of the effective field at each Fe site, which is the sum of the applied and internal magnetic field, and can be written as  $|\mathbf{B}_{\text{eff}}| = |\mathbf{B}_{\text{int}} + \mathbf{B}|$ . The internal magnetic field of each Fe site can be expressed as  $\mathbf{B}_{\text{int}} = -A\langle\mathbf{S}\rangle/g_n\beta_n$ , where  $\langle\mathbf{S}\rangle$  is the expectation value of the electronic spin for the lowest energy doublet of the  $S = 5/2$  ground state manifold and  $A$  is the magnetic hyperfine

coupling constant. Thus the direction of the internal field of each Fe site is dictated by the sign of  $A$ , and depending on the sign, the effective field will either increase or decrease with an increasing applied field. For the  $S = 5/2$  linear  $[3\text{Fe-4S}]^+$  cluster, the lower Kramers doublet is magnetically uniaxial, with  $g_y = 9.6$ ,  $g_x, g_z < 1$ , thus  $\langle \mathbf{S} \rangle \approx \pm g_y/4$ , to a good approximation. In the weak applied field of 50 mT, the magnetic hyperfine splitting is dominated by the magnitude of the internal magnetic field of each Fe site which are 32.9, 31.7, and 23.8 T, respectively for site 1, 2, and 3, as determined by the analysis of the Mössbauer spectra for the linear  $[3\text{Fe-4S}]^+$  cluster in *Sc Grx5*. As all three internal fields differ in magnitude, superposition of the magnetic splitting of the three high-spin Fe sites results in the broad and complex spectrum shown in Figure 2.3B. In strong applied magnetic fields (4 T and 8 T), only the “spin down” state with  $\langle \mathbf{S} \rangle < 0$  of the lower Kramers doublet is appreciably populated at 4.2 K. Thus, the internal magnetic field of the terminal Fe sites with  $A/g_n\beta_n < 0$  are opposite to the applied field whereas that of the central Fe site is parallel to the applied field. At 4 T, the magnitudes of the effective field perceived at site 1 and 2 become 28.9 and 27.7 T, respectively, with decreased magnetic splitting compared to that of low applied field; while that of site 3 becomes 27.8 T with increased magnetic splitting. With the magnitudes of the effective magnetic fields for all three Fe sites close to each other, the magnetic hyperfine splitting of these three sites almost overlap, and the resulting Mössbauer spectrum exhibits much simplified splitting pattern with stronger intensity, as shown in Figure 2.3C. With the applied field further increased to 8 T, the magnitudes of the effective fields at the terminal and central Fe sites become different again, with those at site 1 and 2 further decreasing to 24.8 and 23.7 T, respectively, and that at site 3 further increasing to 31.8 T. Consequently, the hyperfine absorption lines attributed to the terminal Fe sites and the central Fe site become separated and resolved again resulting in decreased absorption intensity in

the Mössbauer spectrum, as observed in Figure 2.3D. The above analysis on the field-dependent behavior is consistent with a linear  $[3\text{Fe-4S}]^+$  cluster (29;31;32).

The linear  $[3\text{Fe-4S}]^+$  cluster in *Sc Grx5* was also investigated by EPR spectroscopy to further assess the electronic ground state properties. On the basis of the parallel Mössbauer studies on the same sample, approximately 30% of the cluster-bound *Sc Grx5* sample was shown to contain  $[2\text{Fe-2S}]^{2+}$  cluster,  $[4\text{Fe-4S}]^{2+}$  cluster, and a mononuclear high-spin ( $S = 2$ ) ferrous species. However, both  $[2\text{Fe-2S}]^{2+}$  and  $[4\text{Fe-4S}]^{2+}$  clusters in the 2+ oxidation state have diamagnetic ground states and the high-spin  $S = 2$  ferrous species does not exhibit an observable EPR signal using perpendicular or parallel mode X-band EPR. Therefore, the presence of these additional components does not interfere with the EPR characterization of the linear  $[3\text{Fe-4S}]^+$  cluster in *Sc Grx5*. The X-band EPR spectra of the linear  $[3\text{Fe-4S}]^+$  cluster-containing form of *Sc Grx5* recorded at 4.3, 10, and 20 K display a sharp derivative-shaped resonance at  $g = 4.3$  and broad absorption-shaped low-field features centered at  $g = 8.7$  and 5.3 (Figure 2.4). The  $g = 4.3$  component is consistent with the  $S = 5/2$  spin Hamiltonian used to interpret the Mössbauer and MCD saturation magnetization data (*vide infra*), i.e.  $E/D = 0.31$  and  $D = 2.0 \text{ cm}^{-1}$ , which predicts  $g$ -values at 4.42, 4.27, and 4.15 for the middle doublet of the ground state manifold and a weak low-field absorption shaped component at  $g \sim 9.6$  arising from the lowest doublet. The broad absorption-shaped low-field features centered at  $g = 8.7$  and 5.3 are interpreted in terms of substantial  $D$ -strain (33), i.e. distributed  $D$  and  $E$  values resulting from inhomogeneity in the linear  $[3\text{Fe-4S}]^+$  clusters in the frozen solution. Similar  $D$ -strain effects on the observed EPR spectrum have been reported for the aconitase and synthetic linear  $[3\text{Fe-4S}]^+$  clusters in alkaline aconitase (29;34).

VTMCD spectroscopy provides a selective probe of the electronic transitions and ground state properties of paramagnetic chromophores as well as useful method for assessing cluster type for paramagnetic Fe-S clusters. Mössbauer studies have shown ~70% of the Fe is in the form of paramagnetic linear  $[3\text{Fe-4S}]^+$  clusters with the remaining Fe in the form of  $S = 0$   $[2\text{Fe-2S}]^{2+}$  and  $[4\text{Fe-4S}]^{2+}$  clusters and a high-spin  $S = 2$   $\text{Fe}^{2+}$  species. However, since the former two types of clusters are diamagnetic and the  $\text{Fe}^{2+}$  species would not be expected to exhibit significant VTMCD intensity in the visible region, their presence does not interfere with low-temperature MCD characterization of the paramagnetic linear  $[3\text{Fe-4S}]^+$  cluster in *Sc Grx5* in the visible region. VTMCD spectra recorded at 6 T for temperatures in the range 1.7 to 50 K consist of three consecutive negative features between 300 to 400 nm, three consecutive pronounced positive bands in the region between 400 and 550 nm, and multiple less intense features with alternative negative and positive signs with decreasing energy (Figure 2.5). These temperature-dependent MCD bands facilitate resolution of the overlapping S-to-Fe(III) charge transfer transitions that comprise the UV-visible absorption spectrum. More importantly, the pattern and intensity of the low-temperature MCD spectra of the linear  $[3\text{Fe-4S}]^+$  cluster in *Sc Grx5* are strikingly similar to those previously reported for synthetic and protein-bound linear  $[3\text{Fe-4S}]^+$  clusters (34), and are distinct from other structurally well-defined biological Fe-S clusters.

Information on the ground-state electronic properties of the linear  $[3\text{Fe-4S}]^+$  cluster in *Sc Grx5* was provided by the VTVH MCD magnetization studies. In accord with an  $S = 5/2$  ground-state spin, the VTVH MCD saturation magnetization data collected at 415 nm is comprised of a nested set of field-dependent plots at fixed temperatures, that results from differential Boltzmann population and field-induced mixing of zero-field components, see Figure 2.6 (35). The VTVH MCD saturation magnetization data collected at 415 nm were fit to a rhombic  $S = 5/2$  ground

state ( $E/D = 0.31$ ) by varying the transition polarizations and magnitude of the axial zero-field splitting parameter,  $D$ . The best fit, shown in Figure 2.6, was obtained for a predominantly y-polarized electronic transition (36%  $M_{xy}$ ; 6%  $M_{xz}$ ; 58%  $M_{yz}$ ) with  $D = 0.6 \text{ cm}^{-1}$ . The Mössbauer spectra of the linear  $[3\text{Fe-4S}]^+$  cluster in *Sc Grx5* were analyzed using a value of  $2.0 \text{ cm}^{-1}$  for the axial zero-field splitting parameter  $D$ . However, VTVH MCD saturation magnetization data are quite sensitive to the values of  $D$ , with satisfactory fits only possible with  $D = 0.6 \pm 0.2 \text{ cm}^{-1}$ , whereas Mössbauer is quite insensitive to the value of  $D$ . This value of  $D$  is similar to those determined using VTVH MCD saturation magnetization for the aconitase linear  $[3\text{Fe-4S}]^+$  cluster,  $D = 1.5 \pm 0.2 \text{ cm}^{-1}$ , and the synthetic analog complex,  $D = 0.7 \pm 0.2 \text{ cm}^{-1}$  (34).

To our knowledge, the vibrational properties of linear-type  $[3\text{Fe-4S}]^+$  centers have not been previously investigated. As the UV-visible absorption, EPR, VTMCD and Mössbauer results presented above provide compelling evidence for a linear  $[3\text{Fe-4S}]^+$  cluster as the predominant type of Fe-S cluster in *Sc Grx5*, the Fe-S stretching modes of the linear  $[3\text{Fe-4S}]^+$  cluster were assessed by resonance Raman spectroscopy using visible excitation into S-to-Fe(III) charge transfer bands. Resonance Raman spectra of the linear  $[3\text{Fe-4S}]^+$  cluster-bound *Sc Grx5* in the Fe-S stretching region, using 406.7, 457.9, 487.9, and 514.5-nm excitation, are shown in Figure 2.7. To facilitate assignment of normal modes primarily involving Fe-S<sup>b</sup> and Fe-S<sup>t</sup> stretching, resonance Raman spectra of samples reconstituted with natural abundance ( $\sim 95\%$   $^{32}\text{S}$ ,  $\sim 4\%$   $^{34}\text{S}$ ) and isotopically enriched ( $> 95\%$ )  $^{34}\text{S}$  bridging sulfides are compared in Figure 2.8. Significantly, the resonance Raman enhancement profiles and frequencies are quite distinct compared to those of other types of biological Fe-S clusters, including  $[2\text{Fe-2S}]^{2+}$ ,  $[4\text{Fe-4S}]^{2+}$  and cubane-type  $[3\text{Fe-4S}]^+$  clusters. Under idealized  $D_{2d}$  symmetry the  $\text{Fe}_3\text{S}^b_4\text{S}^t_4$  cluster is expected to have 6 predominantly Fe-S<sup>b</sup> stretching modes ( $2A_1$ ,  $2B_2$ ,  $2E$ ) and three

predominantly Fe-S<sup>t</sup> stretching modes ( $A_1$ ,  $B_2$ ,  $E$ ). Definitive band assignments based on normal mode calculations have not been carried out thus far, because of possible contributions from the minority  $[2\text{Fe}-2\text{S}]^{2+}$  and  $[4\text{Fe}-4\text{S}]^{2+}$  clusters that are present in the samples. Nevertheless, based on the large magnitude of the  $^{34}\text{S}/^{32}\text{S}$  isotope shifts ( $\sim 5 \text{ cm}^{-1}$ ), the intense band at  $388 \text{ cm}^{-1}$  is primarily attributed to the  $A_1$  symmetric breathing mode of the  $\text{Fe}(\mu\text{-S}^b)_2\text{Fe}(\mu\text{-S}^b)_2\text{Fe}$  core with the S motions along the x and y directions (i.e. perpendicular to the Fe-Fe-Fe axis) and the band at  $279 \text{ cm}^{-1}$  is primarily attributed to the  $A_1$  symmetric breathing mode of the  $\text{Fe}(\mu\text{-S}^b)_2\text{Fe}(\mu\text{-S}^b)_2\text{Fe}$  core with the S motions along the z direction (parallel to the Fe-Fe-Fe axis). The latter is downshifted  $\sim 100 \text{ cm}^{-1}$ , since it requires significant movement of the outer Fe atoms. The former occurs at a similar frequency to that of the symmetric breathing mode of the  $\text{Fe}(\mu\text{-S}^b)_2\text{Fe}$  core in biological and synthetic  $[2\text{Fe}-2\text{S}]^{2+}$  clusters ( $A_{1g}$  under idealized  $D_{2h}$  symmetry) which occur in the range  $387\text{-}401 \text{ cm}^{-1}$  (36-38).

*In vitro* assembly of a  $[4\text{Fe}-4\text{S}]^{2+}$  cluster in *Sc Grx5*: To further explore the types and properties of Fe-S clusters assembled in *Sc Grx5*, *in vitro* cysteine desulfurase-mediated cluster reconstitution was carried out with 5 mM DTT in place of GSH. This change in reconstitution conditions resulted in the formation of a Fe-S center that is different from the linear  $[3\text{Fe}-4\text{S}]^+$  cluster as evidenced by the combination of UV-visible absorption, Mössbauer and resonance Raman spectroscopic studies. The absorption spectrum of the Fe-S cluster assembled in the absence of GSH (red line in Figure 2.2) exhibits a broad band in the visible region centered at 400 nm ( $A_{400}/A_{280}=0.43$ ) that is characteristic of a  $[4\text{Fe}-4\text{S}]^{2+}$  cluster (39). Protein and Fe analyses indicated  $2.5 \pm 0.3$  Fe per *Sc Grx5* monomer, suggesting approximate one  $[4\text{Fe}-4\text{S}]^{2+}$  cluster per *Sc Grx5* homodimer. Moreover, the extinction coefficient at 400 nm,  $16.9 \text{ mM}^{-1}\text{cm}^{-1}$ , based on the *Sc Grx5* dimer concentration, is indicative of approximately one  $[4\text{Fe}-4\text{S}]^{2+}$  cluster

per *Sc* Grx5 dimer (26;39;40). The CD spectrum of the  $[4\text{Fe-4S}]^{2+}$  cluster in the UV-visible region is very weak and featureless, which is also characteristic of biological  $[4\text{Fe-4S}]^{2+}$  clusters (see Appendix B).

Mössbauer analysis of  $^{57}\text{Fe}$ -reconstituted *Sc* Grx5 in the absence of GSH provided more definite confirmation of the presence of a  $[4\text{Fe-4S}]^{2+}$  cluster in *Sc* Grx5. The 4.2 K Mössbauer spectrum recorded with a parallel applied field of 50 mT can be best simulated as the sum of two equal intensity quadrupole doublets with the following parameters:  $\Delta E_Q = 1.05$  mm/s,  $\delta = 0.41$  mm/s,  $\Gamma = 0.45$  mm/s for doublet 1 and  $\Delta E_Q = 1.16$  mm/s,  $\delta = 0.49$  mm/s,  $\Gamma = 0.36$  mm/s for doublet 2 (Figure 2.9). The parameters are consistent of a cysteine ligated  $[4\text{Fe-4S}]^{2+}$  cluster with an  $S = 0$  ground state resulting from antiferromagnetic interaction between two valence delocalized  $[2\text{Fe-2S}]^+$  fragments (41;42). Analysis of the Mössbauer spectrum revealed that 92% of the  $^{57}\text{Fe}$  in the sample is presented in the form of  $[4\text{Fe-4S}]^{2+}$  cluster while the remaining 8% of  $^{57}\text{Fe}$  can be attributed to adventitiously bound  $\text{Fe}^{2+}$  species. The presence of other Fe-containing species was not detected.

The vibrational properties of the  $[4\text{Fe-4S}]^{2+}$  cluster in *Sc* Grx5 were also investigated by low temperature resonance Raman spectroscopy. Cubane-type  $[4\text{Fe-4S}]^{2+}$  clusters are known to exhibit lower resonance enhancement compared to other types of biological Fe-S clusters. Shown in Figure 2.10, the resonance Raman spectrum obtained using 487.9 nm excitation in the Fe-S stretching region ( $240\text{--}450\text{ cm}^{-1}$ ) is characteristic of a  $[4\text{Fe-4S}]^{2+}$  cluster and the Raman band observed for  $[4\text{Fe-4S}]$ -Grx5 can be reasonably assigned by comparison to  $[4\text{Fe-4S}]$ -ferredoxins and appropriate analog complexes (43). Based on extensive spectroscopic studies on biological and synthetic  $[4\text{Fe-4S}]$  clusters, the frequency of the totally symmetric Fe and bridging S breathing mode can be used to indicate cluster ligation,  $333\text{--}339\text{ cm}^{-1}$  for a  $[4\text{Fe-4S}]$

cluster with complete cysteinyl ligation, and 340-343  $\text{cm}^{-1}$  for a [4Fe-4S] cluster with an unique Fe site with OH<sup>-</sup>, serinate or aspartate ligation (44;45). Thus the frequency of the totally symmetric breathing mode at 338  $\text{cm}^{-1}$  observed for the [4Fe-4S]<sup>2+</sup> cluster in *Sc* Grx5 suggests complete cysteinyl ligation for the [4Fe-4S]<sup>2+</sup> cluster. The Raman band at 352  $\text{cm}^{-1}$  is assigned to an asymmetric Fe-S(Cys) stretching mode, however the intensity of the corresponding band in [4Fe-4S]-Grx5 is anomalously high compared to that of other biological [4Fe-4S]<sup>2+</sup> clusters (43). An analogous spectrum with essentially the same frequencies and relative band intensities was obtained with 457.9-nm excitation (data not shown), indicating that this atypical property of the [4Fe-4S]<sup>2+</sup> center in *Sc* Grx5 is unlikely to be attributed to anomalous excitation profiles for discrete bands. One possible explanation is that the high intensity of the 352  $\text{cm}^{-1}$  band is due to perturbation of the symmetry of the cuboidal [4Fe-4S]<sup>2+</sup> core. This possibility is tentatively supported by the resonance Raman studies on the subunit-bridging [4Fe-4S]<sup>2+</sup> cluster in the MgATP-bound nitrogenase Fe protein from *A. vinelandii* (46). The [4Fe-4S]<sup>2+</sup> cluster in the MgATP-bound nitrogenase Fe protein can exist in a cleaved form involving two [2Fe-2S] fragments separated by  $\sim 5 \text{ \AA}$  in the oxidized state (46). A nitrogenase Fe protein sample containing both the [4Fe-4S]<sup>2+</sup> cluster and the [2Fe-2S] fragments exhibited a resonance Raman spectrum very similar to that obtained for [4Fe-4S]-Grx5, in terms of band frequencies and relative intensities of corresponding bands (46). Since the [4Fe-4S]<sup>2+</sup> cluster in *Sc* Grx5 is likely to reside at the dimer interface (*vide infra*), it is conceivable that the increased intensity of the asymmetric terminal Fe-S stretching mode of the cluster is a result of distortions of the [4Fe-4S]<sup>2+</sup> cluster core and/or the cluster environment.

*Activation of apo aconitase using [4Fe-4S]<sup>2+</sup> cluster-bound Sc Grx5:* To investigate the possibility that the [4Fe-4S]<sup>2+</sup> cluster-bound form of *Sc* Grx5 is competent for *in vitro* activation

of apo-aconitase, 4 $\mu$ M apo-aconitase was incubated with three-fold excess of [4Fe-4S]-Grx5 (12 $\mu$ M in [4Fe-4S]<sup>2+</sup> clusters) and aconitase enzymatic activity was accessed periodically over a 90 min time period. Figure 2.11 shows the time-dependent apo-aconitase activation when it is mixed with [4Fe-4S]-Grx5. Analysis based on second-order kinetics and the initial concentrations of [4Fe-4S]<sup>2+</sup> clusters in *Sc* Grx5 and apo-aconitase, indicate a second-order rate constant of 6.0 $\times$ 10<sup>3</sup> M<sup>-1</sup>min<sup>-1</sup> at room temperature, which implies activation by intact cluster transfer, since it is at least an order of magnitude greater than the rate of aconitase activation with equivalent amounts of Fe<sup>2+</sup> and S<sup>2-</sup> ions. The rate constant for [4Fe-4S]-Grx5 aconitase activation is comparable to that observed under analogous conditions using a [4Fe-4S]<sup>2+</sup> cluster-loaded form of *A. vinelandii* IscU, 1.1  $\times$ 10<sup>4</sup> M<sup>-1</sup>min<sup>-1</sup>, but is an order of magnitude slower than that reported using [4Fe-4S]-NfuA from *A. vinelandii* as the cluster donor, 6.0 $\times$ 10<sup>4</sup> M<sup>-1</sup>min<sup>-1</sup> (24;26). Taken together, these results indicate that the [4Fe-4S]<sup>2+</sup> cluster-bound form of *Sc* Grx5 is competent for activation of apo-aconitase *in vitro* via intact [4Fe-4S] cluster transfer.

*Investigation of cluster ligation in Sc Grx5:* As the spectroscopic properties reported herein indicate that both the linear [3Fe-4S]<sup>+</sup> and [4Fe-4S]<sup>2+</sup> clusters assembled in *Sc* Grx5 are best interpreted in terms of complete cysteinyl-ligation, site-directed mutagenesis studies were undertaken to address the specific cysteines involved in cluster ligation, as *Sc* Grx5 possesses two cysteine residues at positions 33 and 90 (recombinant *S. cerevisiae* Grx5 numbering). The active-site cysteine (Cys33) is conserved in all monothiol CGFS-Grxs and is involved in ligating [2Fe-2S]<sup>2+</sup> clusters, whereas Cys90 is conserved in some but not all CGFS-type Grxs (1;15). In order to address the cluster ligation in *Sc* Grx5, a C90S mutant was generated to investigate the ability of this variant to incorporate Fe-S clusters. When subjected to *in vitro* cysteine desulfurase-mediated Fe-S cluster reconstitution in the presence of 3 mM GSH, the *Sc* Grx5

C90S variant is found able to accommodate a linear  $[3\text{Fe-4S}]^+$  cluster, as evidenced by the identical UV-visible absorption characteristics compared to that of the linear  $[3\text{Fe-4S}]^+$  cluster center in the wild type *Sc Grx5* (Figure 2.12). However, the C90S mutant failed to assemble a  $[4\text{Fe-4S}]^{2+}$  cluster during cysteine desulfurase-mediated Fe-S cluster reconstitution in the presence of 5 mM DTT, as evidenced by the lack of any visible absorption bands after removal of the excess reagents in the reconstitution mixture by anaerobic gel filtration (data not shown). Thus the site-directed mutagenesis studies suggest that the partially conserved cysteine is required for the incorporation of the  $[4\text{Fe-4S}]^{2+}$  cluster in *Sc Grx5* but not the linear  $[3\text{Fe-4S}]^+$  cluster. Coupled with the analytical data that indicates approximately one  $[4\text{Fe-4S}]^{2+}$  cluster per *Sc Grx5* homodimer, the data suggest that the ligation of the  $[4\text{Fe-4S}]^{2+}$  cluster in *S. cerevisiae* Grx5 involves both the active site cysteine and the partially conserved cysteine of two *Sc Grx5* monomers. Based on the ability of the C90S mutant to accommodate a linear  $[3\text{Fe-4S}]^+$  cluster and the requirement of GSH for the cluster formation, we conclude that the linear  $[3\text{Fe-4S}]^+$  cluster in *Sc Grx5* is coordinated by the active-site cysteine of two CGFS-Grx monomers and two external GSH molecules, similar to the ligation of the  $[2\text{Fe-2S}]^{2+}$  cluster in other CGFS Grxs (4;16).

## Discussion

The widely accepted and evolutionarily conserved role for CGFS-Grxs in facilitating the transfer and insertion of preassembled Fe-S clusters was revealed using *S. cerevisiae* mitochondrial Grx5 as a model protein (7;8). While the majority of CGFS-Grxs investigated thus far have demonstrated the ability to incorporate a  $[2\text{Fe-2S}]^{2+}$  at the Grxs dimer interface (4;16), the ability of *S. cerevisiae* mitochondrial Grx5 to accommodate an Fe-S cluster had not been addressed prior to this work. Using a combination of UV-visible absorption, CD and VTMCD,

EPR, Mössbauer and resonance Raman spectroscopic techniques, we have demonstrated that recombinant *S. cerevisiae* mitochondrial Grx5 is a versatile Fe-S protein able to accommodate linear  $[3\text{Fe-4S}]^+$ , cubane-type  $[4\text{Fe-4S}]^{2+}$ , and  $[2\text{Fe-2S}]^{2+}$  clusters.

Previously, Chauvat and coworkers have reported purification of a recombinant form of *Sc* Grx5 with a bound Fe-S cluster (19). The type of the cluster was interpreted as  $[2\text{Fe-2S}]$  cluster solely on the basis of the UV-visible absorption spectrum comprising a band at ~410 nm that could equally be attributed, at least in part, to a minor heme impurity (19). In contrast, we have been unable to express and purify a cluster-bound form of recombinant *Sc* Grx5 in this study, despite having tried both aerobic and strictly anaerobic purification conditions. In the previous study and this work, both constructs used to over-produce *Sc* Grx5 in *E. coli* strain were generated to express the mature form of *Sc* Grx5 that does not contain the N-terminal mitochondria targeting sequence. The purity of the *Sc* Grx5 sample used in this work was accessed by SDS-PAGE analysis, and ESI-MS was used to ensure that the correct mature form of *Sc* Grx5 was obtained. Furthermore, despite extensive efforts, we have failed to obtain a form of *Sc* Grx5 containing predominantly  $[2\text{Fe-2S}]^{2+}$  clusters using established *in vitro* cluster reconstitution protocols for CGFS-Grxs  $[2\text{Fe-2S}]^{2+}$  cluster assembly (9;17;18).

Linear-type  $[3\text{Fe-4S}]^+$  clusters were initially characterized as synthetic complexes (28), and the first protein-bound linear  $[3\text{Fe-4S}]^+$  cluster was later discovered in partially unfolded beef heart aconitase via incubation under alkaline conditions (pH > 9.5) or treating with high concentrations of urea (4-8 M) (29). The only other well-documented examples of protein-bound linear  $[3\text{Fe-4S}]^+$  clusters prior to this study were reconstituted human cytosolic iron-responsive protein 1 (IRP1) at pH 7.5 (47) and as one of the many types of clusters in the as-isolated form of the pyruvate formate lyase activating enzyme (PFL-AE) (32). We have demonstrated in this

work that anaerobic cluster reconstitution of *Sc* Grx5 in the presence of GSH yields a form containing a linear [3Fe-4S]<sup>+</sup> cluster as the dominant Fe-containing species. The excited state and ground state electronic properties of the linear [3Fe-4S]<sup>+</sup> cluster in *Sc* Grx5 have been characterized in detail using UV-visible absorption, CD and VTMCD, EPR and Mössbauer spectroscopies. The results are strikingly similar to those obtained for structurally-characterized synthetic linear [3Fe-4S]<sup>+</sup> clusters and protein-bound linear [3Fe-4S]<sup>+</sup> clusters and are consistent with a  $S = 5/2$  linear [3Fe-4S]<sup>+</sup> cluster in a rhombic ( $E/D = 0.31$ ) environment (28;29;31;34).

The nature of the ligation of the linear [3Fe-4S]<sup>+</sup> cluster in *Sc* Grx5 have yet to be definitively determined. Nevertheless, the cluster stoichiometry of ~ 1 linear [3Fe-4S]<sup>+</sup> cluster per dimer and the observation that GSH and only the active-site CGFS cysteine are required for assembly of the linear [3Fe-4S]<sup>+</sup> cluster suggest complete-cysteinyl ligation involving the active-site cysteine residues from two *Sc* Grx5 monomers and the cysteines of two GSH molecules. An analogous ligation scheme has been reported for [2Fe-2S]<sup>2+</sup> clusters in structurally characterized CGFS-Grxs (4;16). Furthermore, it is also important to note that judged by the distinctive UV-visible absorption and/or Mössbauer properties of linear [3Fe-4S]<sup>+</sup> clusters, it is evident that a number of recombinant CGFS-Grxs, including human Glrx5 and Glrx3, *E. coli* Grx4, *Synechocystis* Grx3, *A. thaliana* Grx5, and *G. violaceus* Grx3, contain linear [3Fe-4S]<sup>+</sup> cluster in either their as-isolated or reconstituted forms (11;19;48;49). The presence of linear [3Fe-4S]<sup>+</sup> clusters in other CGFS-Grxs indicate that the ability to incorporate a linear [3Fe-4S]<sup>+</sup> cluster is not unique to *S. cerevisiae* Grx5, but is a common attribute to many, if not all, CGFS-Grxs. However, definitive evidence for linear [3Fe-4S]<sup>+</sup> clusters generally requires the use of more discriminating spectroscopic techniques, in addition to UV-visible absorption.

To our knowledge, linear-type  $[3\text{Fe-4S}]^+$  clusters are not associated with any physiological functions. Thus the significance of the presence of linear  $[3\text{Fe-4S}]^+$  clusters in CGFS-Grxs remains to be established. It may be related to the stability of linear  $[3\text{Fe-4S}]^+$  clusters and their established ability to undergo cluster conversions based initially on the studies of synthetic clusters (28). Moreover, the elegant and comprehensive studies carried out on aconitase have demonstrated that the linear  $[3\text{Fe-4S}]^+$  clusters are stable in the presence of air in alkaline pH, but are also able to lose  $\text{Fe}^{3+}$  and  $\text{S}^{2-}$  ions to form  $[2\text{Fe-2S}]^{2+}$  clusters, or to undergo reorganization to quantitatively yield  $[4\text{Fe-4S}]^{2+}$  cluster in the presence of additional  $\text{Fe}^{2+}$  ions under reducing conditions (29). Furthermore, on the basis of the close resemblance in the UV-visible absorption properties to those of synthetic linear  $[3\text{Fe-4S}]^+$  complexes, the formation of linear  $[3\text{Fe-4S}]^+$  clusters have also been observed during unfolding of ferredoxins under oxidative conditions (50-53), as well as during  $\text{O}_2$ -induced inactivation of *E. coli* dihydroxy-acid dehydratase (54). Thus the ability to accommodate linear  $[3\text{Fe-4S}]^+$  clusters in the presence of GSH implies a role for CGFS-Grxs in scavenging and recycling Fe-S clusters released during protein unfolding under oxidative conditions to avoid potential toxicity caused by Fe accumulation in the cell. This is also consistent with the phenotype effect of mitochondrial iron overload as a result of *Sc* Grx5 deficiency (7).

Reconstitution of *Sc* Grx5 in the absence of GSH yielded a homogeneous form containing one  $[4\text{Fe-4S}]^{2+}$  cluster per homodimer, as evidenced by protein and Fe analyses, as well as UV-visible absorption, Mössbauer and resonance Raman spectroscopic results. In addition, the mutagenesis studies presented in this work implicate Cys90 as a potential ligand for the  $[4\text{Fe-4S}]^{2+}$  cluster. Taken together, the spectroscopic, mutagenesis and analytical data indicate one  $[4\text{Fe-4S}]^{2+}$  cluster per *Sc* Grx5 dimer that is coordinated at the subunit interface by

both the active-site and semi-conserved intrinsic cysteine residues of *Sc* Grx5. In a previous study, biochemical characterization of apo *Sc* Grx5 revealed that Cys90 is capable of forming an intra-protein disulfide with the active site cysteine residue, Cys33 (3). Although the additional cysteine residue at the C-terminal moiety is not strictly conserved in all CGFS-Grxs, it is present in *E. coli* Grx4 and human mitochondrial Glrx5, which both have high resolution structures available for the  $[2\text{Fe-2S}]^{2+}$  cluster-containing forms (4;16). In both structures, the corresponding additional cysteine residue resides at the beginning of helix  $\alpha_4$  and is separated from the active site cysteine by a sulfur-to-sulfur distance of approximately 8 Å (7.6 – 8.4 Å for human Glrx5). Furthermore, the backbone nitrogen of the semi-conserved cysteine residues forms a hydrogen bond with the glutamate carboxylate group of the GSH molecules coordinating the  $[2\text{Fe-2S}]^{2+}$  cluster in both *E. coli* Grx4 and human mitochondrial Glrx5. Taking into consideration of the flexibility of  $\beta_1$ - $\alpha_2$  loop on which the active-site cysteine residue is located and the close proximity of the C-terminal semi-conserved cysteine to the Fe-S cluster-binding site, it is certainly possible for the C-terminal cysteine residue to participate in  $[4\text{Fe-4S}]^{2+}$  cluster coordination without involving major perturbation of protein structural conformation. Alternatively, it is possible that the inability of the *Sc* Grx5 C90S mutant to accommodate a  $[4\text{Fe-4S}]^{2+}$  cluster is due to the particular conformation adopted by the C90S variant which may prevent the incorporation of a  $[4\text{Fe-4S}]^{2+}$  cluster. In this case, the nature of the two remaining ligands remains unclear. Nevertheless, crystallographic studies are required to elucidate detailed ligation arrangement of the  $[4\text{Fe-4S}]^{2+}$  cluster in *S. cerevisiae* Grx5.

Consistent with the *in vivo* studies carried out on *S. cerevisiae* that demonstrated the requirement of Grx5 in maintaining mitochondrial aconitase enzymatic activity (7), we have shown in this work that the  $[4\text{Fe-4S}]^{2+}$  cluster-bound form of *Sc* Grx5 is competent for restoring

the activity of apo aconitase protein *in vitro* via intact cluster transfer. This observation, coupled with the intrinsic cysteinyl-ligation scheme for the  $[4\text{Fe-4S}]^{2+}$  cluster in *Sc Grx5*, raises the possibility of CGFS-Grxs participating in the maturation of  $[4\text{Fe-4S}]^{2+}$  cluster-containing proteins in mitochondria in a GSH-independent fashion, possibly as a carrier protein to mediate the transfer of preassembled  $[4\text{Fe-4S}]^{2+}$  clusters to target proteins. This hypothesis is in agreement of the discovery that GSH is not required for the maturation of mitochondrial Fe-S proteins (55). However, two lines of evidence argue strongly against physiological relevance for the  $[4\text{Fe-4S}]^{2+}$  cluster-bound form of *Sc Grx5*, if the C-terminal semi-conserved cysteine residue is indeed a cluster ligand. First, the C-terminal cysteine is not essential for the biological activity of *Sc Grx5* as mutation at this site failed to cause any phenotypic effects (15). Secondly, the C-terminal cysteine is only partially conserved in CGFS-Grxs and CGFS-Grxs that lack the C-terminal cysteine residue can partially rescue the defects of the *S. cerevisiae grx5* null mutant (56).

Thus far, the majority of CGFS-Grxs characterized were found to contain a subunit-bridged  $[2\text{Fe-2S}]^{2+}$  cluster ligated by the active-site cysteine of two Grx monomers and two GSH molecules. However, we have yet to obtain an homogenous  $[2\text{Fe-2S}]^{2+}$  cluster-containing form of *Sc Grx5*. Mössbauer studies of *Sc Grx5* sample reconstituted in the presence of GSH revealed a minor contribution (11% of total Fe) of a quadrupole doublet that can be attributed to protein-bound  $[2\text{Fe-2S}]^{2+}$  cluster, in addition to the major component (72% of total Fe) that constitutes the linear  $[3\text{Fe-4S}]^+$  cluster. The coexistence of linear  $[3\text{Fe-4S}]^+$  and  $[2\text{Fe-2S}]^{2+}$  clusters in synthetic and biological samples is not a new phenomenon. For example  $[2\text{Fe-2S}]^{2+}$  clusters are byproducts of the synthetic route to generate complexes with linear  $[3\text{Fe-4S}]^+$  cores (28;31). In both aconitase and PFL-AE, protein-bound  $[2\text{Fe-2S}]^{2+}$  clusters are generated under conditions

that induce the formation of linear  $[3\text{Fe-4S}]^+$  clusters (29;32). Thus the ability of *Sc* Grx5 to accommodate solely  $[2\text{Fe-2S}]^{2+}$  clusters cannot be ruled out and the conditions for obtaining a homogeneous  $[2\text{Fe-2S}]^{2+}$  cluster-containing *Sc* Grx5 require further investigation. Furthermore, oxygen-induced degradation of protein-bound  $[4\text{Fe-4S}]$  clusters can often result in a semi-stable  $[2\text{Fe-2S}]^{2+}$  intermediate ((40;41), Chapter 5 and Appendix B). Although our preliminary data obtained by monitoring the stability of the  $[4\text{Fe-4S}]^{2+}$  cluster in *Sc* Grx5 under oxygenated conditions using UV-visible absorption spectroscopy suggests that the degradation of the  $[4\text{Fe-4S}]^{2+}$  cluster does not involve a  $[2\text{Fe-2S}]^{2+}$  cluster intermediate (data not shown), further experiments using more discriminating spectroscopic techniques are planned to provide detailed investigation of the stability and degradation pathway of the  $[4\text{Fe-4S}]^{2+}$  clusters in *Sc* Grx5. One possible route to obtain a  $[2\text{Fe-2S}]^{2+}$  cluster-bound *Sc* Grx5 may involve BolA proteins, a ubiquitous family of proteins that often partner with CGFS-Grxs in Fe-S cluster biogenesis and in Fe homeostasis (1;57). Recent *in vitro* studies revealed that BolA proteins can replace one CGFS-Grx monomer in the  $[2\text{Fe-2S}]^{2+}$  cluster coordination and this change in cluster environment was found to stabilize the labile  $[2\text{Fe-2S}]^{2+}$  clusters found in CGFS-Grxs homodimer (17). In support of this proposal, *S. cerevisiae* possesses two BolA proteins with mitochondrial localization (57), and using one of these two proteins, we have recently characterized a  $[2\text{Fe-2S}]^{2+}$  cluster-bound Grx5-BolA complex (B. Zhang, A. Dlouhy, C. E. Outten, and M. K. Johnson, unpublished results).

CGFS-Grxs are clearly attracting increasing attention due to their involvement in Fe-S cluster biogenesis and in Fe-trafficking and regulation in eukaryotes (1;9;10;57;58). The investigation of the Fe-S cluster-bound forms of recombinant *Sc* Grx5 reported in this work has uncovered the ability of CGFS-Grxs to accommodate three different types of Fe-S clusters, linear

[3Fe-4S]<sup>+</sup>, [4Fe-4S]<sup>2+</sup> and [2Fe-2S]<sup>2+</sup> clusters. Thus there is clearly a pressing need to identify the physiologically relevant Fe-S cluster bound forms of CGFS-Grxs and to investigate the Fe-S cluster structure-function relationships of CGFS-Grxs in specific organisms.

## References

1. Rouhier, N., Couturier, J., Johnson, M. K., and Jacquot, J. P. (2010) Glutaredoxins: roles in iron homeostasis, *Trends Biochem. Sci.* 35, 43-52.
2. Lillig, C. H., Berndt, C., and Holmgren, A. (2008) Glutaredoxin systems, *Biochim. Biophys. Acta.* 1780, 1304-1317.
3. Tamarit, J., Belli, G., Cabiscol, E., Herrero, E., and Ros, J. (2003) Biochemical Characterization of Yeast Mitochondrial Grx5 Monothiol Glutaredoxin, *J. Biol. Chem.* 278, 25745-25751.
4. Johansson, C., Roos, A. K., Montano, S. J., Sengupta, R., Filippakopoulos, P., Guo, K., von, D. F., Holmgren, A., Oppermann, U., and Kavanagh, K. L. (2011) The crystal structure of human GLRX5: iron-sulfur cluster co-ordination, tetrameric assembly and monomer activity, *Biochem. J.* 433, 303-311.
5. Zaffagnini, M., Michelet, L., Massot, V., Trost, P., and Lemaire, S. D. (2008) Biochemical characterization of glutaredoxins from *Chlamydomonas reinhardtii* reveals the unique properties of a chloroplastic CGFS-type glutaredoxin, *J. Biol. Chem.* 283, 8868-8876.
6. Fernandes, A. P., Fladvad, M., Berndt, C., Andresen, C., Lillig, C. H., Neubauer, P., Sunnerhagen, M., Holmgren, A., and Vlamis-Gardikas, A. (2005) A novel monothiol glutaredoxin (Grx4) from *Escherichia coli* can serve as a substrate for thioredoxin reductase, *J. Biol. Chem.* 280, 24544-24552.
7. Rodríguez-Manzaneque, M. T., Tamarit, J., Bellí, G., Ros, J., and Herrero, E. (2002) Grx5 is a mitochondrial glutaredoxin required for the activity of iron/sulfur enzymes, *Mol. Biol. Cell* 13, 1109-1121.
8. Mühlenhoff, U., Gerber, J., Richhardt, N., and Lill, R. (2003) Components involved in assembly and dislocation of iron-sulfur clusters on the scaffold protein IscUlp, *EMBO J.* 22, 4815-4825.
9. Bandyopadhyay, S., Gama, F., Molina-Navarro, M. M., Gualberto, J. M., Claxton, R., Naik, S. G., Huynh, B. H., Herrero, E., Jacquot, J.-P., Johnson, M. K., and Rouhier, N. (2008) Chloroplast monothiol glutaredoxins as scaffold proteins for the assembly and delivery of [2Fe-2S] clusters, *EMBO J.* 27, 1122-1133.
10. Shakamuri, P., Zhang, B., and Johnson, M. K. (2012) Monothiol Glutaredoxins Function in Storing and Transporting [Fe(2)S(2)] Clusters Assembled on IscU Scaffold Proteins, *J. Am. Chem. Soc.* 134, 15213-15216.
11. Yeung, N., Gold, B., Liu, N. L., Prathapam, R., Sterling, H. J., Willams, E. R., and Butland, G. (2011) The *E. coli* monothiol glutaredoxin GrxD forms homodimeric and heterodimeric FeS cluster containing complexes, *Biochemistry* 50, 8957-8969.

12. Vilella, F., Alves, R., Rodriguez-Manzanaque, M. T., Belli, G., Swaminathan, S., Sunnerhagen, P., and Herrero, E. (2004) Evolution and cellular function of monothiol glutaredoxins: involvement in iron-sulphur cluster assembly, *Comp. Funct. Genom.* 5, 328-341.
13. Wingert, R. A., Galloway, J. L., Barut, B., Foott, H., Fraenkel, P., Axe, J. L., Weber, G. J., Dooley, K., Davidson, A. J., Schmidt, B., Paw, B. H., and Shaw, G. C. (2005) Deficiency of glutaredoxin 5 reveals Fe-S clusters are required for vertebrate haem synthesis, *Nature* 436, 1035-1039.
14. Molina-Navarro, M. M., Casas, C., Piedrafita, L., Bellí, G., and Herrero, E. (2006) Prokaryotic and eukaryotic monothiol glutaredoxins are able to perform the functions of Grx5 in the biogenesis of Fe/S clusters in yeast mitochondria, *FEBS Lett.* 580, 2273-2280.
15. Belli, G., Polaina, J., Tamarit, J., De La Torre, M. A., Rodriguez-Manzanaque, M. T., Ros, J., and Herrero, E. (2002) Structure-function analysis of yeast Grx5 monothiol glutaredoxin defines essential amino acids for the function of the protein, *J. Biol. Chem.* 277, 37590-37596.
16. Iwema, T., Picciocchi, A., Traore, D. A., Ferrer, J. L., Chauvat, F., and Jacquamet, L. (2009) Structural basis for delivery of the intact [Fe<sub>2</sub>S<sub>2</sub>] cluster by monothiol glutaredoxin, *Biochemistry* 48, 6041-6043.
17. Li, H., Mapolelo, D. T., Dingra, N. N., Naik, S. G., Lees, N. S., Hoffman, B. M., Riggs-Gelasco, P. J., Huynh, B. H., Johnson, M. K., and Outten, C. E. (2009) The yeast iron regulatory proteins Grx3/4 and Fra2 form heterodimeric complexes containing a [2Fe-2S] cluster with cysteinyl and histidyl ligation, *Biochemistry* 48, 9569-9581.
18. Li, H., Mapolelo, D. T., Randeniya, S., Johnson, M. K., and Outten, C. E. (2012) Human Glutaredoxin 3 Forms [2Fe-2S]-Bridged Complexes with Human BolA2, *Biochemistry* 51, 1687-1696.
19. Picciocchi, A., Saguez, C., Boussac, A., Cassier-Chauvat, C., and Chauvat, F. (2007) CGFS-type monothiol glutaredoxins from the cyanobacterium *Synechocystis* PCC6803 and other evolutionary distant model organisms possess a glutathione-ligated [2Fe-2S] cluster, *Biochemistry* 46, 15018-15026.
20. Couturier, J., Stroher, E., Albetel, A. N., Roret, T., Muthuramalingam, M., Tarrago, L., Seidel, T., Tsan, P., Jacquot, J. P., Johnson, M. K., Dietz, K. J., Didierjean, C., and Rouhier, N. (2011) Arabidopsis chloroplastic glutaredoxin C5 as a model to explore molecular determinants for iron-sulfur cluster binding into glutaredoxins, *J. Biol. Chem.* 286, 27515-27527.
21. Fish, W. W. (1988) Rapid colorimetric micromethod for the quantitation of complexed iron in biological samples, *Meth. Enzymol.* 158, 357-364.

22. Coper, M. M., Krebs, B., Hernandez, H., Jameson, G., Eidsness, M. K., Huynh, B. H., and Johnson, M. K. (2004) Characterization of the cofactor content of *Escherichia coli* biotin synthase, *Biochemistry* 43, 2007-2021.
23. Ravi, N., Bollinger, J. M., Huynh, B. H., Edmondson, D. E., and Stubbe, J. (1994) Mechanism of assembly of the tyrosyl radical-diiron(III) cofactor of *E. coli* ribonucleotide reductase. 1. Mössbauer characterization of the diferric radical precursor, *J. Am. Chem. Soc.* 116, 8007-8014.
24. Unciuleac, M.-C., Chandramouli, K., Naik, S., Mayer, S., Huynh, B. H., Johnson, M. K., and Dean, D. R. (2007) *In vitro* activation of apo-aconitase using a [4Fe-4S] cluster-loaded form of the IscU [Fe-S] cluster scaffolding protein, *Biochemistry* 46, 6812-6821.
25. Kennedy, M. C. and Beinert, H. (1988) The state of cluster SH and S<sup>2-</sup> of aconitase during cluster interconversions and removal. A convenient preparation of apoenzyme., *J. Biol. Chem.* 263, 8194-8198.
26. Bandyopadhyay, S., Naik, S., O'Carroll, I. P., Huynh, B. H., Dean, D. R., Johnson, M. K., and Dos Santos, P. C. (2008) A proposed role for the *Azotobacter vinelandii* NfuA protein as an intermediate iron-sulfur cluster carrier, *J. Biol. Chem.* 283, 14092-14099.
27. Saas, J., Ziegelbauer, K., von Haeseler, A., Fast, B., and Boshart, M. (2005) *J. Biol. Chem.* 275, 2745-2755.
28. Hagen, K. S., Watson, A. D., and Holm, R. H. (1983) Synthetic routes to Fe<sub>2</sub>S<sub>2</sub>, Fe<sub>3</sub>S<sub>4</sub>, Fe<sub>4</sub>S<sub>4</sub>, and Fe<sub>6</sub>S<sub>9</sub> clusters from the common precursor [Fe(SC<sub>2</sub>H<sub>5</sub>)<sub>4</sub>]<sup>2-</sup>: Structures and properties of [Fe<sub>3</sub>S<sub>4</sub>(SR)<sub>4</sub>]<sup>3-</sup> and [Fe<sub>6</sub>S<sub>9</sub>(SC<sub>2</sub>H<sub>5</sub>)<sub>2</sub>]<sup>4-</sup>, examples of the newest types of Fe-S-SR clusters, *J. Am. Chem. Soc.* 105, 3905-3913.
29. Kennedy, M. C., Kent, T. A., Emptage, M. H., Merkle, H., Beinert, H., and Münck, E. (1984) Evidence for the formation of a linear [3Fe-4S] cluster in partially unfolded aconitase, *J. Biol. Chem.* 259, 14463-14471.
30. Münck, E. Aspects of <sup>57</sup>Fe Mössbauer spectroscopy. In *Physical methods in bioinorganic chemistry. Spectroscopy and magnetism*; Que, L., Jr.; University Science Books; 2000; 287-319.
31. Girerd, J.-J., Papaefthymiou, G. C., Watson, A. D., Gamp, E., Hagen, K. S., Edelstein, N., Frankel, R. B., and Holm, R. H. (1984) Electronic properties of the linear antiferromagnetically coupled clusters [Fe<sub>3</sub>S<sub>4</sub>(SR)<sub>4</sub>]<sup>3-</sup>, structural isomers of the [Fe<sub>3</sub>S<sub>4</sub>]<sup>+</sup> unit in iron-sulfur proteins, *J. Am. Chem. Soc.* 106, 5941-5947.
32. Krebs, C., Henshaw, T. F., Cheek, J., Huynh, B. H., and Broderick, J. B. (2000) Conversion of 3Fe-4S to 4Fe-4S Clusters in Native Pyruvate Formate-Lyase Activating Enzyme: Mössbauer Characterization and Implications for Mechanism, *J. Am. Chem. Soc.* 122, 12497-12506.
33. Hagen, W. R. In *Biomolecular EPR Spectroscopy*; CRC press; 2008; 204-205.

34. Richards, A. J. M., Thomson, A. J., Holm, R. H., and Hagen, K. S. (1990) The magnetic circular dichroism spectra of the linear trinuclear clusters  $[\text{Fe}_3\text{S}_4(\text{SR})_4]^{3-}$  in purple aconitase and in a synthetic model, *Spectrochim. Acta.* 46A, 987-993.
35. Johnson, M. K. CD and MCD Spectroscopy. In *Physical methods in bioinorganic chemistry. Spectroscopy and magnetism*; Que, L., Jr.; University Science Books; 2000; 233-286.
36. Han, S., Czernuszewicz, R. S., and Spiro, T. G. (1989) Vibrational spectra and normal mode analysis for [2Fe-2S] protein analogues using  $^{34}\text{S}$ ,  $^{54}\text{Fe}$ , and  $^2\text{H}$  substitution: Coupling of Fe-S stretching and S-C-C bending modes, *J. Am. Chem. Soc.* 111, 3496-3504.
37. Han, S., Czernuszewicz, R. S., Kimura, T., Adams, M. W. W., and Spiro, T. G. (1989)  $\text{Fe}_2\text{S}_2$  protein resonance Raman revisited: Structural variations among adrenodoxin, ferredoxin, and red paramagnetic protein, *J. Am. Chem. Soc.* 111, 3505-3511.
38. Fu, W., Drozdowski, P. M., Davies, M. D., Sligar, S. G., and Johnson, M. K. (1992) Resonance Raman and magnetic circular dichroism studies of reduced [2Fe-2S] proteins, *J. Biol. Chem.* 267, 15502-15510.
39. Agar, J. N., Krebs, B., Frazzon, J., Huynh, B. H., Dean, D. R., and Johnson, M. K. (2000) IscU as a scaffold for iron-sulfur cluster biosynthesis: Sequential assembly of [2Fe-2S] and [4Fe-4S] clusters in IscU, *Biochemistry* 39, 7856-7862.
40. Chandramouli, K., Unciuleac, M.-C., Naik, S., Dean, D. R., Huynh, B. H., and Johnson, M. K. (2007) Formation and properties of [4Fe-4S] clusters on the IscU scaffold protein, *Biochemistry* 46, 6804-6811.
41. Khoroshilova, N., Popescu, C., Münck, E., Beinert, H., and Kiley, P. J. (1997) Iron-sulfur cluster disassembly in the FNR protein of *Escherichia coli* by  $\text{O}_2$ : [4Fe-4S] to [2Fe-2S] conversion with loss of biological activity, *Proc. Natl. Acad. Sci. USA* 94, 6087-6092.
42. Beinert, H., Holm, R. H., and Münck, E. (1997) Iron-sulfur clusters; Nature's modular, multipurpose structures, *Science* 277, 653-659.
43. Czernuszewicz, R. S., Macor, K. A., Johnson, M. K., Gewirth, A., and Spiro, T. G. (1987) Vibrational mode structure and symmetry in proteins and analogues containing  $\text{Fe}_4\text{S}_4$  clusters: Resonance Raman evidence for different degrees of distortion in HiPIP and ferredoxin, *J. Am. Chem. Soc.* 109, 7178-7187.
44. Conover, R. C., Kowal, A. T., Fu, W., Park, J.-B., Aono, S., Adams, M. W. W., and Johnson, M. K. (1990) Spectroscopic characterization of the novel iron-sulfur cluster in *Pyrococcus furiosus* ferredoxin, *J. Biol. Chem.* 265, 8533-8541.
45. Brereton, P. S., Duderstadt, R. E., Staples, C. R., Johnson, M. K., and Adams, M. W. W. (1999) Effect of serinate ligation at each of the iron sites of the  $[\text{Fe}_4\text{S}_4]$  cluster of *Pyrococcus furiosus* ferredoxin on the redox, spectroscopic and biological properties, *Biochemistry* 38, 10594-10605.

46. Sen, S., Igarashi, R., Smith, A. D., Johnson, M. K., Seefeldt, L. C., and Peters, J. W. (2004) A conformational mimic of the MgATP-bound "on state" of the nitrogenase iron protein, *Biochemistry* 43, 1787-1797.
47. Gailer, J., George, G. N., Pickering, I. J., Prince, R. C., Kohlhepp, P., Zhang, D., Walker, F. A., and Winzerling, J. J. (2001) Human cytosolic iron regulatory protein 1 contains a linear iron-sulfur cluster, *J. Am. Chem. Soc.* 123, 10121-10122.
48. Ye, H., Jeong, S. Y., Ghosh, M. C., Kovtunovych, G., Silvestri, L., Ortillo, D., Uchida, N., Tisdale, J., Camaschella, C., and Rouault, T. A. (2010) Glutaredoxin 5 deficiency causes sideroblastic anemia by specifically impairing heme biosynthesis and depleting cytosolic iron in human erythroblasts, *J. Clin. Invest.* 120, 1749-1761.
49. Haunhorst, P., Berndt, C., Eitner, S., Godoy, J. R., and Lillig, C. H. (2010) Characterization of the human monothiol glutaredoxin 3 (PICOT) as iron-sulfur protein, *Biochem. Biophys. Res. Commun.* 394, 372-376.
50. Leal, S. S., Teixeira, M., and Gomes, C. M. (2004) Studies on the degradation pathway of iron-sulfur centers during unfolding of a hyperstable ferredoxin: Cluster dissociation, iron release and proteins stability, *J. Biol. Inorg. Chem.* 9, 987-996.
51. Jones, K., Gomes, C. M., Huber, H., Teixeira, M., and Wittung-Stafshede, P. (2002) Formation of a linear [3Fe-4S] cluster in a seven-iron ferredoxin triggered by polypeptide unfolding, *J. Biol. Inorg. Chem.* 7, 357-362.
52. Griffin, S., Higgins, C. L., Soulimane, T., and Wittung-Stafshede, P. (2003) High thermal and chemical stability of *Thermus thermophilus* seven-iron ferredoxin. Linear clusters form at high pH on polypeptide unfolding, *Eur. J. Biochem.* 270, 4736-4743.
53. Higgins, C. L. and Wittung-Stafshede, P. (2004) Formation of linear three-iron clusters in *Aquilex aeolicus* two-iron ferredoxins: effect of protein unfolding speed, *Arch. Biochem. Biophys.* 427, 154-163.
54. Flint, D. H., Emptage, M. H., Finnegan, M. G., Fu, W., and Johnson, M. K. (1993) The role and properties of the iron-sulfur cluster in *Escherichia coli* dihydroxy-acid dehydratase, *J. Biol. Chem.* 268, 14732-14742.
55. Sipos, K., Lange, H., Fekete, Z., Ullmann, P., Lill, R., and Kispal, G. (2002) Maturation of cytosolic iron-sulfur proteins requires glutathione, *J. Biol. Chem.* 277, 26944-26949.
56. Molina, M. M., Belli, G., De La Torre, M. A., Rodriguez-Manzanique, M. T., and Herrero, E. (2004) Nuclear monothiol glutaredoxins of *Saccharomyces cerevisiae* can function as mitochondrial glutaredoxins, *J. Biol. Chem.* 279, 51923-51930.
57. Li, H. and Outten, C. E. (2012) Monothiol CGFS Glutaredoxins and BolA-like Proteins: [2Fe-2S] Binding Partners in Iron Homeostasis, *Biochemistry* 51, 4377-4389.

58. Mühlhoff, U., Molik, S., Godoy, J. R., Uzarska, M. A., Richter, N., Seubert, A., Zhang, Y., Stubbe, J., Pierrel, F., Herrero, E., Lillig, C. H., and Lill, R. (2010) Cytosolic monothiol glutaredoxins function in intracellular iron sensing and trafficking via their bound iron-sulfur cluster, *Cell Metab.* 12, 373-385.
59. Neese, F. and Solomon, E. I. (1999) MCD *C*-term signs, saturation behavior, and determination of band polarizations in randomly oriented systems with spin  $S \geq 1/2$ . Applications to  $S = 1/2$  and  $S = 5/2$ , *Inorg. Chem.* 38, 1847-1865.

Table 2.1: Primers used for *S. cerevisiae* Grx5 cloning and mutagenesis. Mutated codons are shown in bold.

Primer name	Primer sequence	Destination Vector
Grx5 FOR	5'CCCCCATGGCTTTGAGCACAGAGATAAGA 3'	pET3d
Grx5 REV	5'CCCCGGATCCTCAACGATCTTTGGTTTC 3'	pET3d
Grx5 C90S FOR	5'GAATTCATTGGTGGAA <b>AG</b> TGATGTTATTACAAGT 3'	pET3d
Grx5 C90S REV	5'ACTTGTAATAACATCA <b>ACT</b> TCCACCAATGAATTC 3'	pET3d

Table 2.2: Mössbauer parameters for the linear  $[3\text{Fe-4S}]^+$  cluster in *Sc Grx5*.

Site	$A/g_n\beta_n$ (T)	$eQV_{yy}$ (mm/s)	$\delta$ (mm/s)	$\Gamma$
1	-13.7	-0.05	0.28	0.35
2	-13.2	-0.10	0.28	0.35
3	+9.9	-0.40	0.38	0.35

The Mössbauer data were analyzed for an  $S = 5/2$  ground state with  $E/D = 0.31$ ,  $D = 2.0 \text{ cm}^{-1}$ ,  $g_x = g_y = g_z = 2.0$  (29). The simulated Mössbauer spectra were generated with equal intensity from each of the three iron sites.

Figure 2.1: Reconstructed ESI-quadrupole mass spectra of as-isolated apo-Grx5. The peak at 13418 Da corresponds to the monomer molecular ion peak of recombinant *S. cerevisiae* Grx5, and the peaks at 13723 and 14028 Da correspond to the addition of one and two covalently bound GSH molecules, respectively.

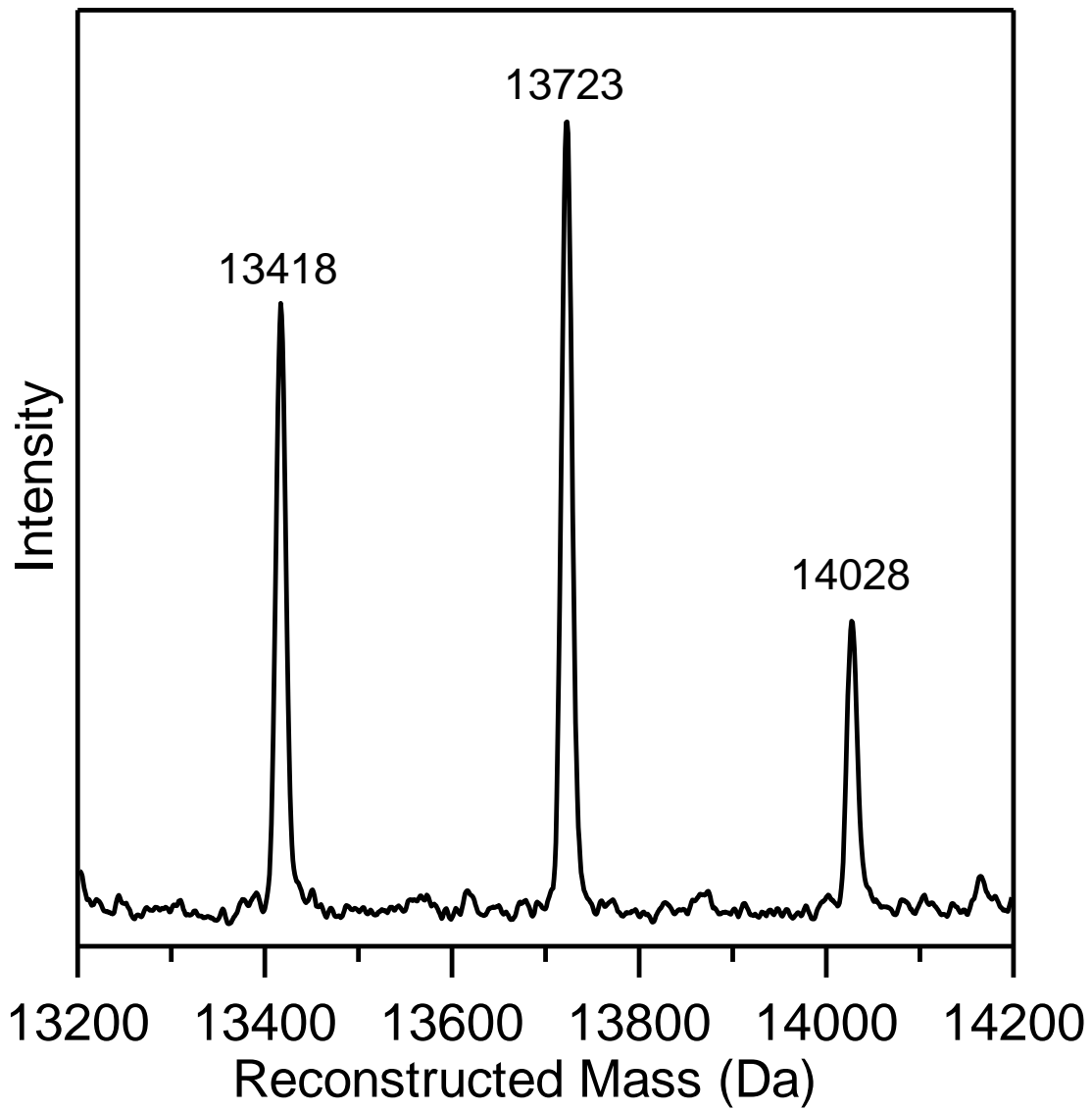


Figure 2.2: Comparison of UV–visible absorption and visible CD spectra of the linear  $[3\text{Fe-4S}]^+$  cluster-bound (blue line) and  $[4\text{Fe-4S}]^{2+}$  cluster-bound (red line) forms of *S. cerevisiae* Grx5 and the  $[2\text{Fe-2S}]^{2+}$  cluster-bound *S. cerevisiae* Grx3 homodimer (black line). Spectra were recorded under anaerobic conditions in sealed 0.1 cm cuvettes in 100 mM Tris-HCl buffer with 1 mM GSH at pH 7.8 for linear  $[3\text{Fe-4S}]$ -Grx5, in 100 mM Tris-HCl buffer with 1 mM DTT at pH 7.8 for  $[4\text{Fe-4S}]$ -Grx5 and in 100 mM Tris-HCl buffer with 250 mM NaCl at pH 7.8 for  $[2\text{Fe-2S}]$ -Grx3. The  $\epsilon$  and  $\Delta\epsilon$  values are based on the *Sc* Grx5 and *Sc* Grx3 protein homodimer concentrations. The spectra of *S. cerevisiae* Grx3 are taken from reference (18).

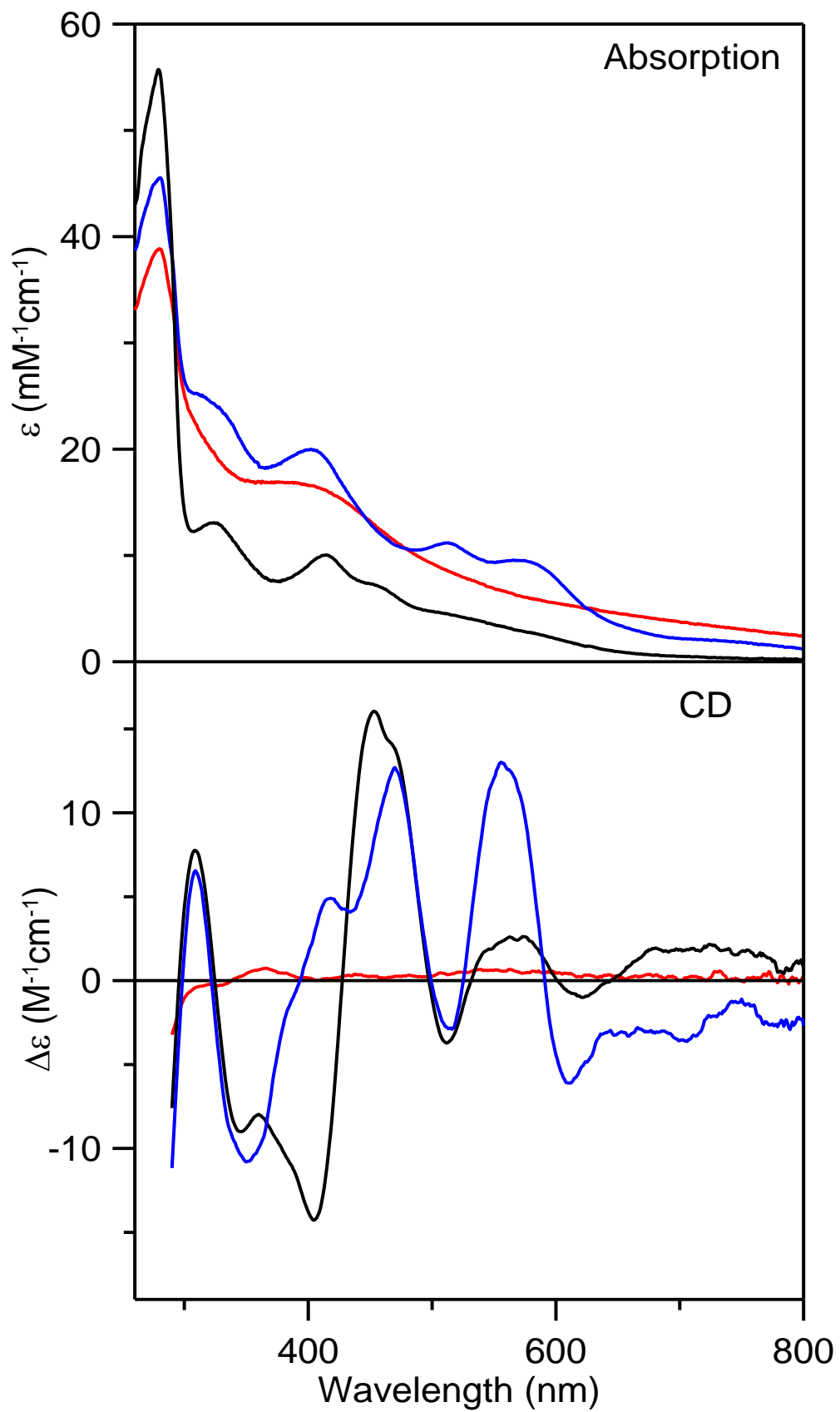


Figure 2.3: Mössbauer evidence for linear  $[3\text{Fe-4S}]^+$  clusters in *Sc Grx5* reconstituted with  $^{57}\text{Fe}$  in the presence of GSH. The sample was approximately 4 mM in  $^{57}\text{Fe}$  and was in 100 mM Tris-HCl buffer, pH 7.8 with 1 mM GSH. The spectra were recorded at 4.2 K with a weak field (50 mT in A, B) and high fields (4T in C and 8T in D) applied parallel to the  $\gamma$ -radiation. The solid orange lines in all spectra are theoretical spectra for the linear  $[3\text{Fe-4S}]^+$  cluster in *S. cerevisiae Grx5* computed with the parameters listed in Table 1. The solid black line overlaid on the experimental spectrum in A is the composite spectrum generated by adding the simulated spectra of the linear  $[3\text{Fe-4S}]^+$  cluster (scaled to 72% of the total iron absorption) and  $[2\text{Fe-2S}]^{2+}$  cluster (11% of the total iron absorption, red line),  $[4\text{Fe-4S}]^{2+}$  cluster (6% of the total iron absorption, blue line) and adventitiously bound  $\text{Fe}^{2+}$  (11% of the total iron absorption, green line). The parameters used to simulate the  $[2\text{Fe-2S}]^{2+}$  cluster are the same as those used to simulate the  $[2\text{Fe-2S}]^{2+}$  cluster in poplar GrxS14 (9). The parameters used to simulate the  $[4\text{Fe-4S}]^{2+}$  cluster are the same as those used to simulate the  $[4\text{Fe-4S}]^{2+}$  cluster in *Sc Grx5* reconstituted in the presence of DTT, see text for details. The spectra in B, C, D were obtained by subtracting the contribution of the  $[2\text{Fe-2S}]^{2+}$ ,  $[4\text{Fe-4S}]^{2+}$  clusters and the adventitiously bound  $\text{Fe}^{2+}$  species from the raw spectra recorded at 50 mT, 4 T and 8 T, respectively.

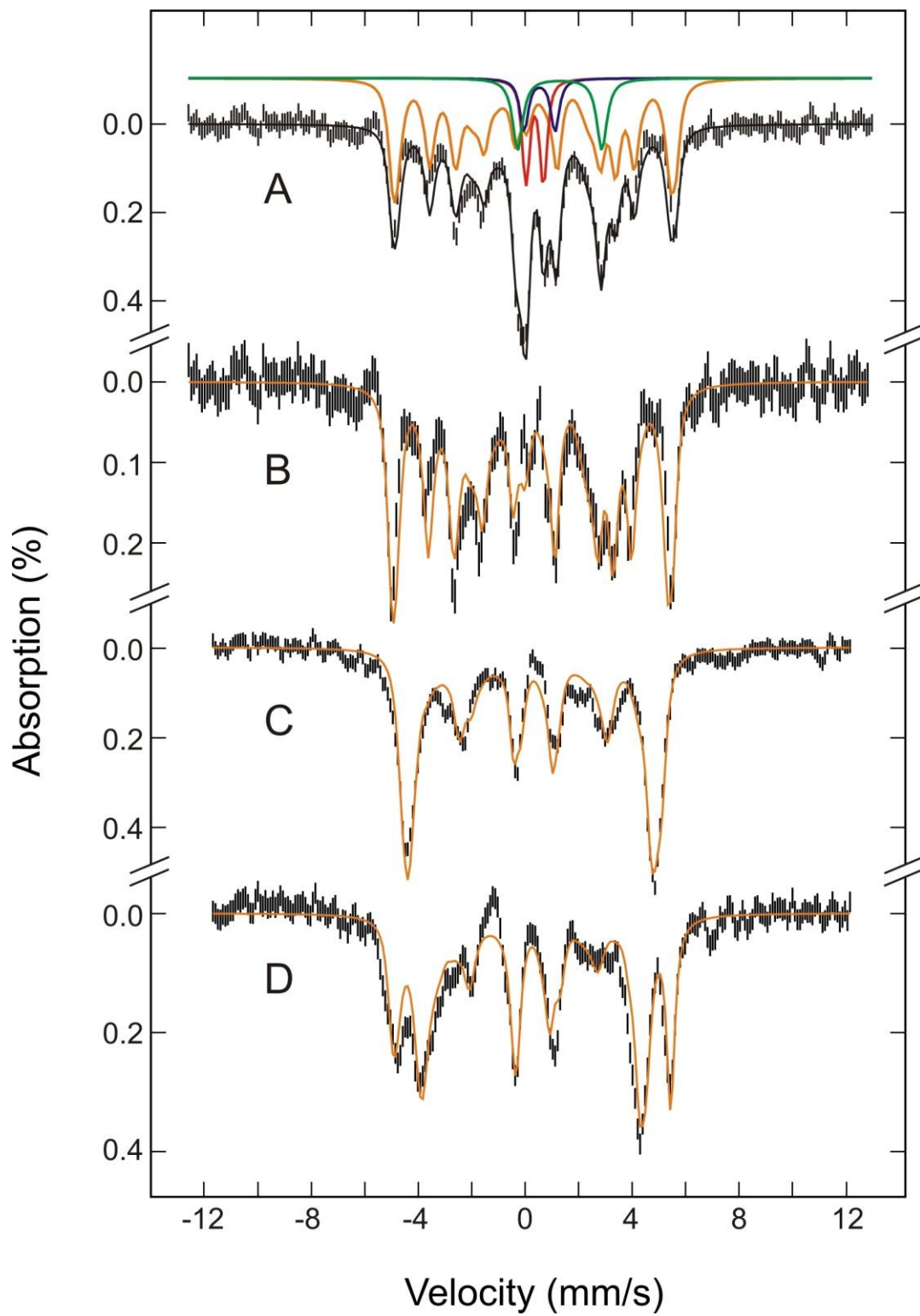


Figure 2.4: X-band EPR evidence for linear  $[3\text{Fe-4S}]^+$  clusters in *Sc Grx5*. The conditions were microwave frequency, 9.60 GHz; modulation frequency, 100 kHz; modulation amplitude, 0.65 mT and microwave power, 4 mW; temperature 4.3 K for the top panel, microwave power, 10 mW; temperature, 10.0 K for the middle panel, and microwave power, 10 mW; temperature, 20.0 K for the bottom panel.

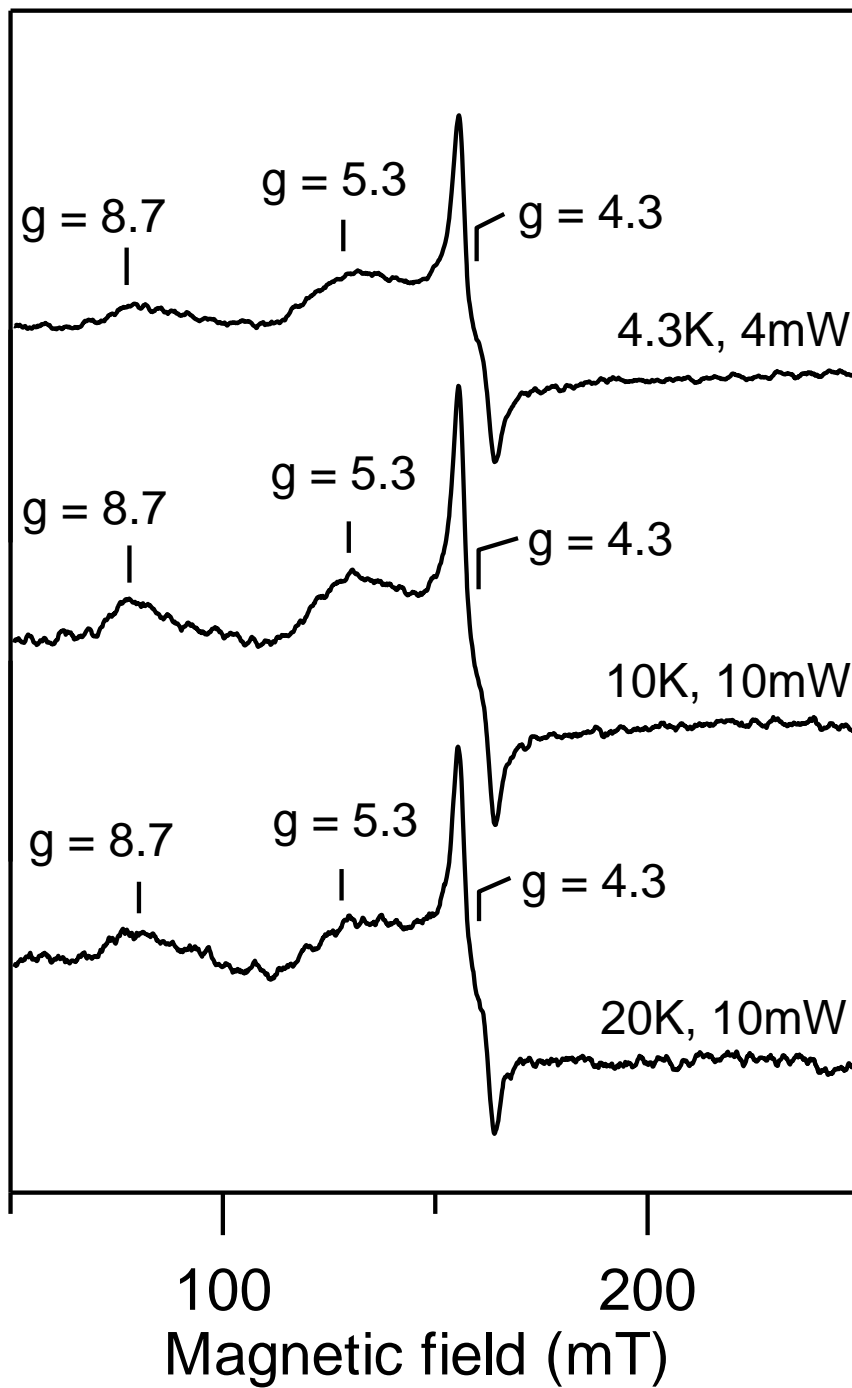


Figure 2.5: VTMCD spectra of linear  $[3\text{Fe-4S}]^+$  cluster in *Sc Grx5*. The sample was in 100 mM Tris-HCl buffer with 1 mM GSH at pH 7.8, with 50% v/v ethylene glycol. Spectra were recorded for sample in 1 mm cuvette at 1.70, 4.22, 10.0, 25.0 and 50.0 K in a magnetic field of 6 T. All MCD bands for linear  $[3\text{Fe-4S}]^+$  cluster-bound *Sc Grx5* increase in intensity with decreasing temperature.

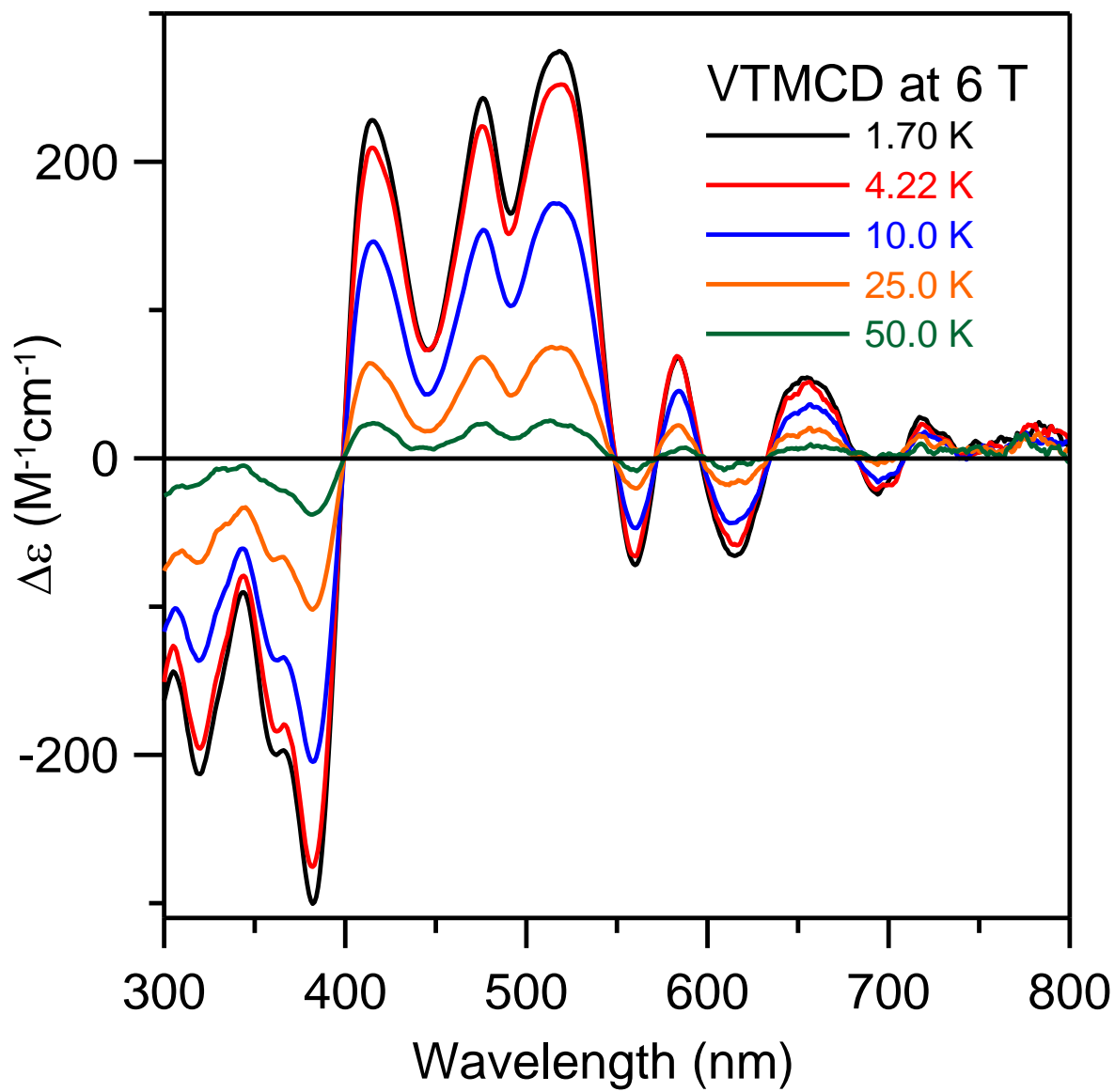


Figure 2.6: VHVT MCD saturation magnetization data for the linear  $[3\text{Fe-4S}]^+$  center in *S. cerevisiae* Grx5. Sample is as described in Fig. 2.5. MCD intensity at 415 nm was monitored as a function of magnetic field, from 0 to 6 T, at temperatures of 1.70 K (●), 4.22 K (■), 10.0 K (▲) and 25.0 K (◆). Solid lines are theoretical fits for a rhombic  $S = 5/2$  ground state with zero-field splitting parameters  $D = +0.6 \text{ cm}^{-1}$  and  $E/D = 0.31$ , an isotropic real  $g$ -value of 2.0023, and a predominantly  $y$ -polarized electronic transition (36%  $M_{xy}$ ; 6%  $M_{xz}$ ; 58%  $M_{yz}$ ). The fitting procedure used was that developed by Neese and Solomon (59).

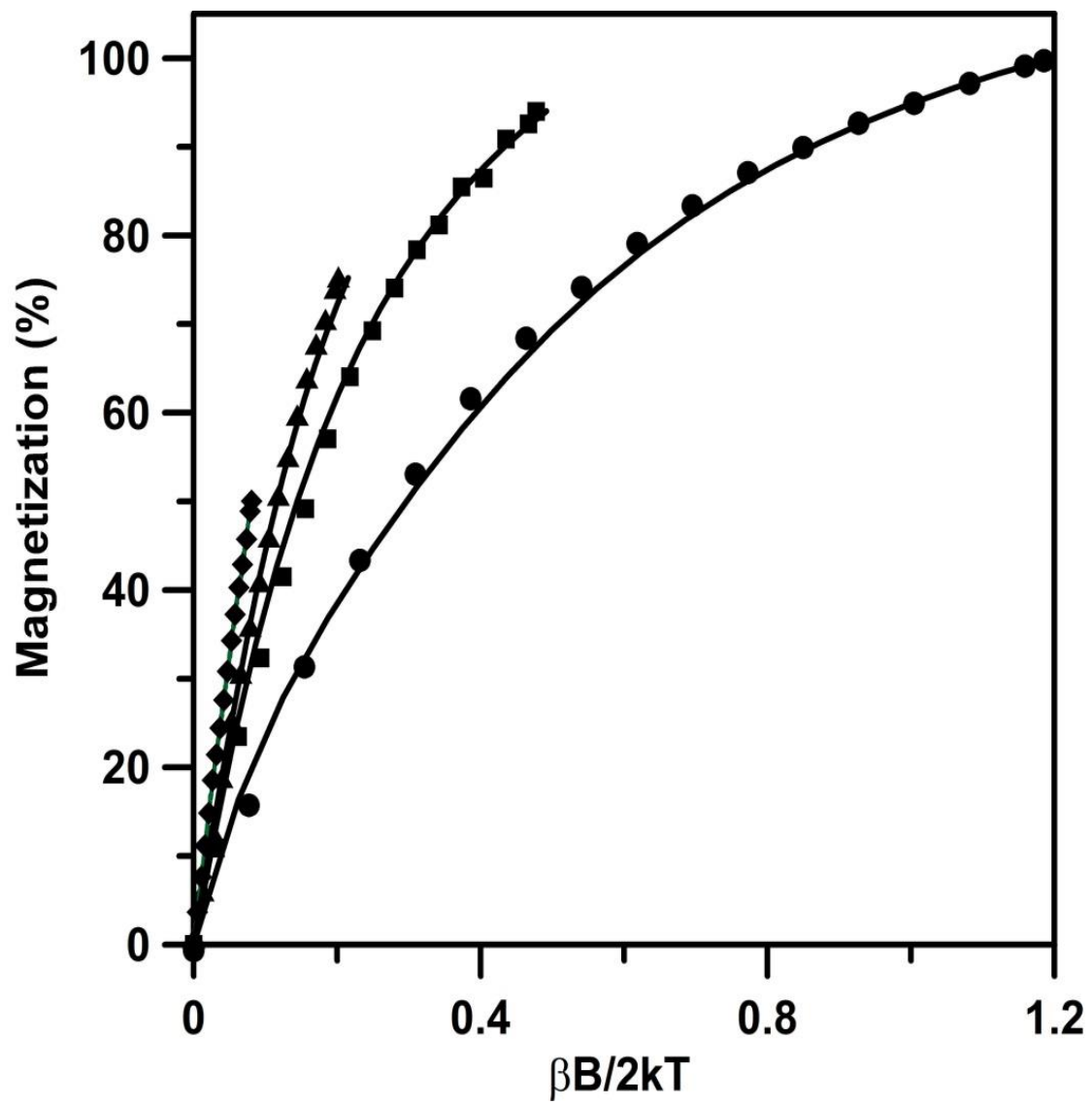


Figure 2.7: Resonance Raman spectra of linear  $[3\text{Fe-4S}]^+$  cluster-bound *Sc* Grx5 with 406.7, 457.9, 487.9 and 514.5 nm laser excitations. The sample contained  $\sim 2$  mM of linear  $[3\text{Fe-4S}]^+$  cluster in 100 mM Tris-HCl buffer with 1 mM GSH at pH 7.8 and was in the form of a frozen droplet at 17 K. Each spectrum is the sum of 100 individual scans with each scan involving photon counting for 1 s at  $0.5\text{ cm}^{-1}$  increment with  $7\text{ cm}^{-1}$  spectral resolution. Bands due to ice lattice modes have been subtracted from all spectra.

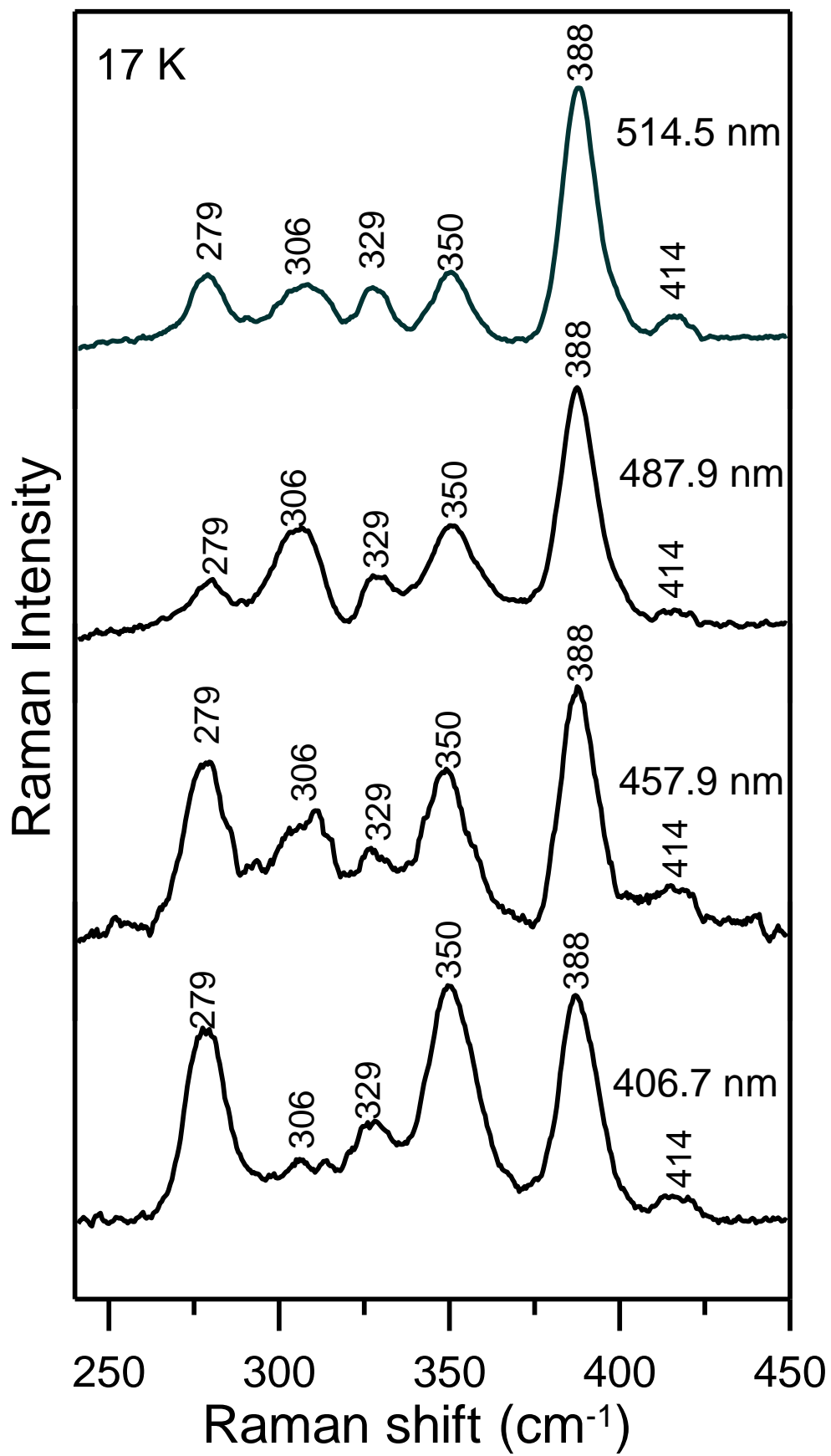


Figure 2.8: Resonance Raman spectra of the  $^{32}\text{S}^{\text{b}}$ - and  $^{34}\text{S}^{\text{b}}$ -reconstituted linear  $[\text{3Fe-4S}]^+$  cluster in *Sc Grx5* showing  $^{34}\text{S}/^{32}\text{S}$  isotopic shifts. Spectra were obtained with 457.9, 487.9 and 514.5 nm laser excitations. The conditions were the same as in Figure 2.7.

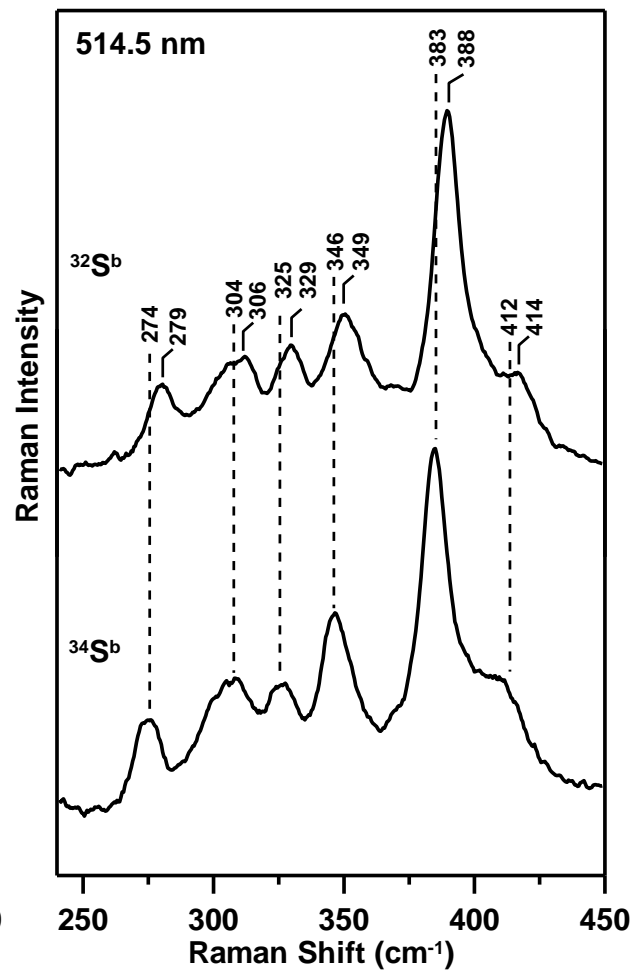
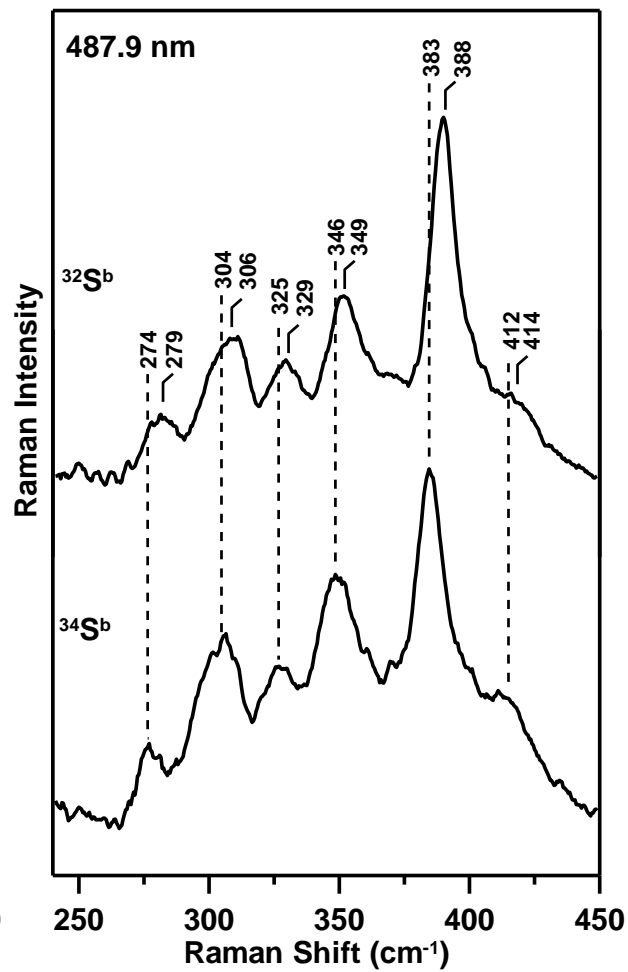
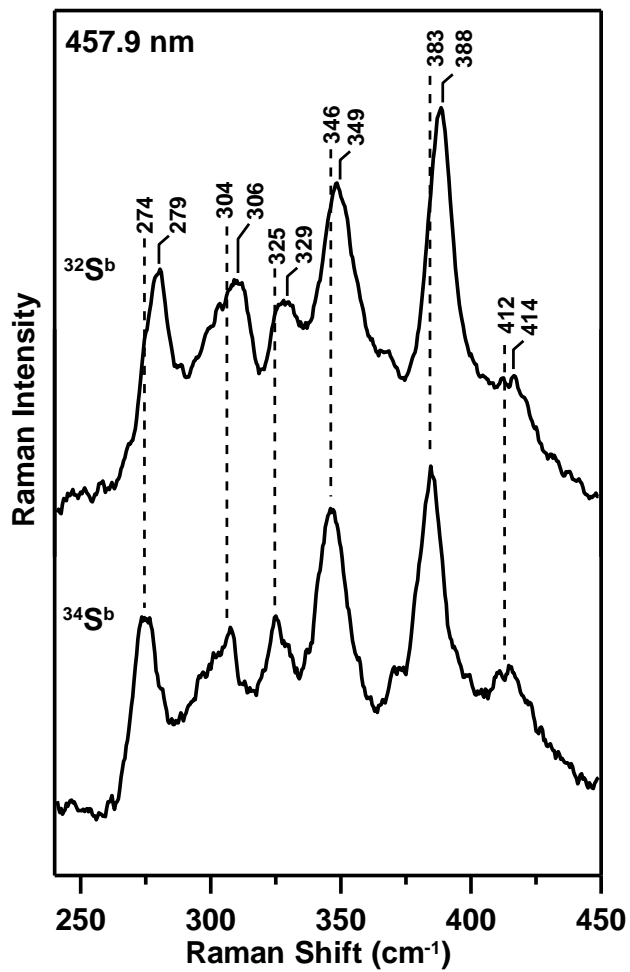


Figure 2.9: Mössbauer spectrum of  $[4\text{Fe-4S}]^{2+}$  cluster-bound *Sc Grx5*. The spectrum was recorded at 4.2 K with an applied field of 50 mT parallel to the  $\gamma$ -radiation. The solid blue line is a theoretical simulation of 92% of  $[4\text{Fe-4S}]^{2+}$  with two overlapping quadrupole doublets of the following parameters:  $\Delta E_Q = 1.05$  mm/s,  $\delta = 0.41$  mm/s,  $\Gamma = 0.45$  mm/s for doublet 1 and  $\Delta E_Q = 1.16$  mm/s,  $\delta = 0.49$  mm/s,  $\Gamma = 0.36$  mm/s for doublet 2.

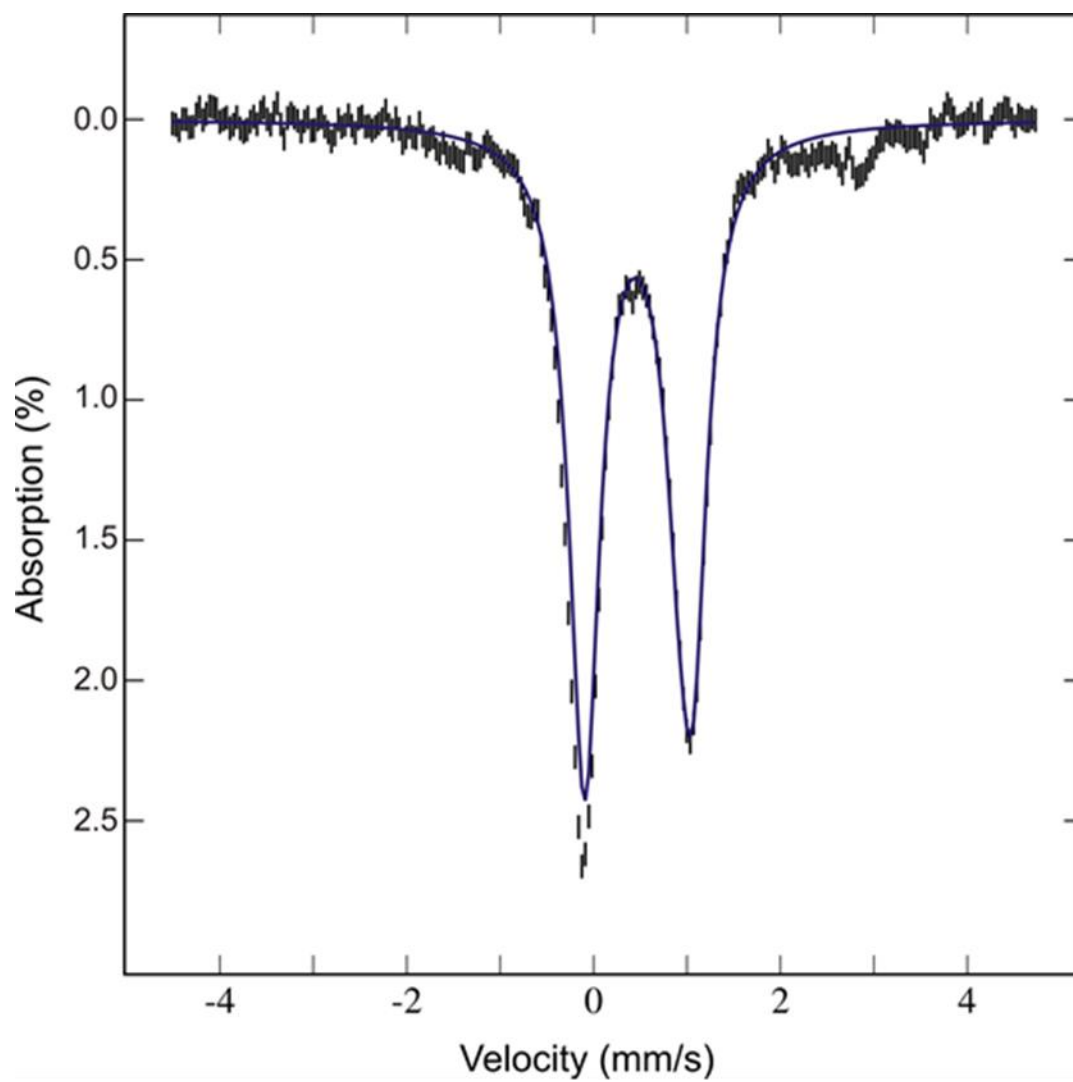


Figure 2.10: Resonance Raman spectrum of  $[4\text{Fe-4S}]^{2+}$  cluster-bound *Sc Grx5* with 487.9 nm laser excitation. The sample contained  $\sim 2$  mM of  $[4\text{Fe-4S}]^{2+}$  cluster in 100 mM Tris-HCl buffer with 1 mM DTT at pH 7.8 and was in the form of a frozen droplet at 17 K. The spectrum is the sum of 100 individual scans with each scan involving photon counting for 1 s at  $0.5\text{ cm}^{-1}$  increment with  $7\text{ cm}^{-1}$  spectral resolution. Bands due to ice lattice modes have been subtracted.

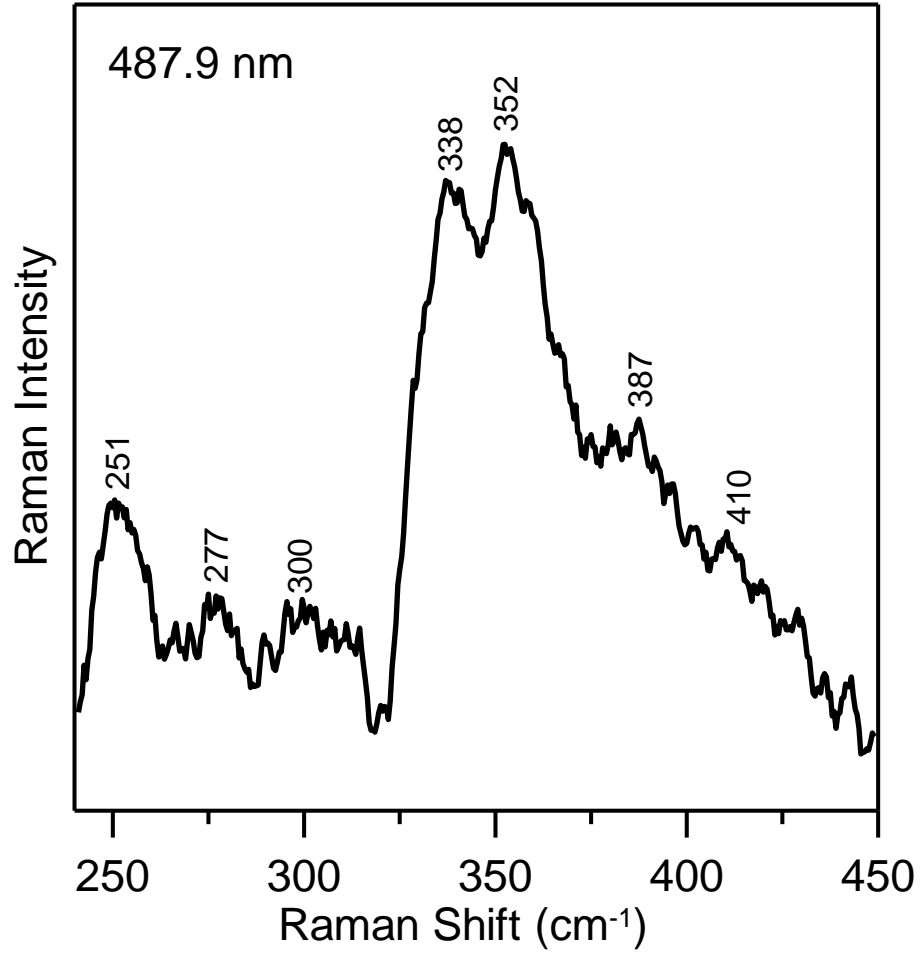


Figure 2.11: Activation of apo-aconitase using  $[4\text{Fe-4S}]^{2+}$  cluster-bound *Sc* Grx5. Apo-aconitase (4  $\mu\text{M}$ ) was incubated with  $[4\text{Fe-4S}]^{2+}$  cluster-bound *Sc* Grx5 (12  $\mu\text{M}$  in  $[4\text{Fe-4S}]^{2+}$  cluster concentration) at room temperature under anaerobic conditions. Aliquots were withdrawn after 2, 6, 10, 30, 45, 60, 75, and 90 min and aconitase activity was immediately measured. The solid line is best fit to second-order kinetics with rate constant of  $6.0 \times 10^3 \text{ M}^{-1} \text{ min}^{-1}$ .

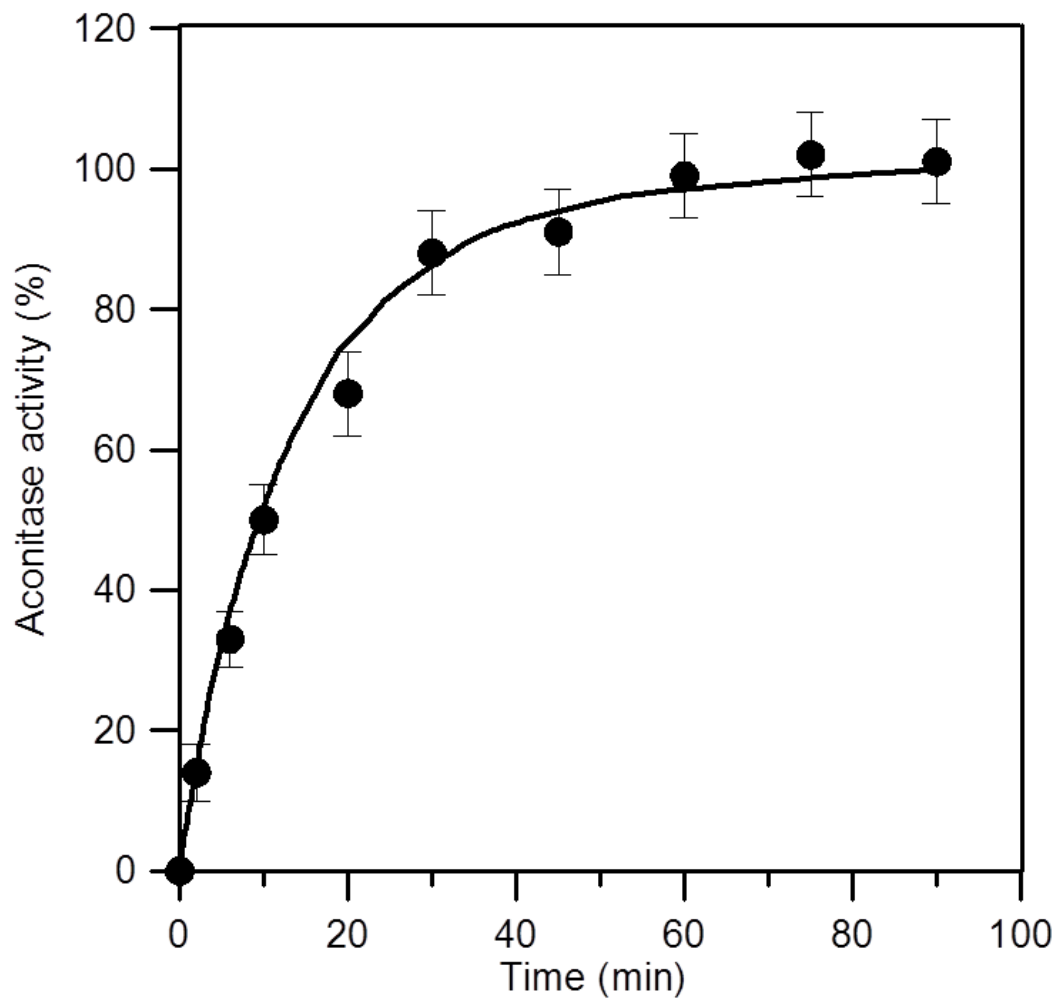
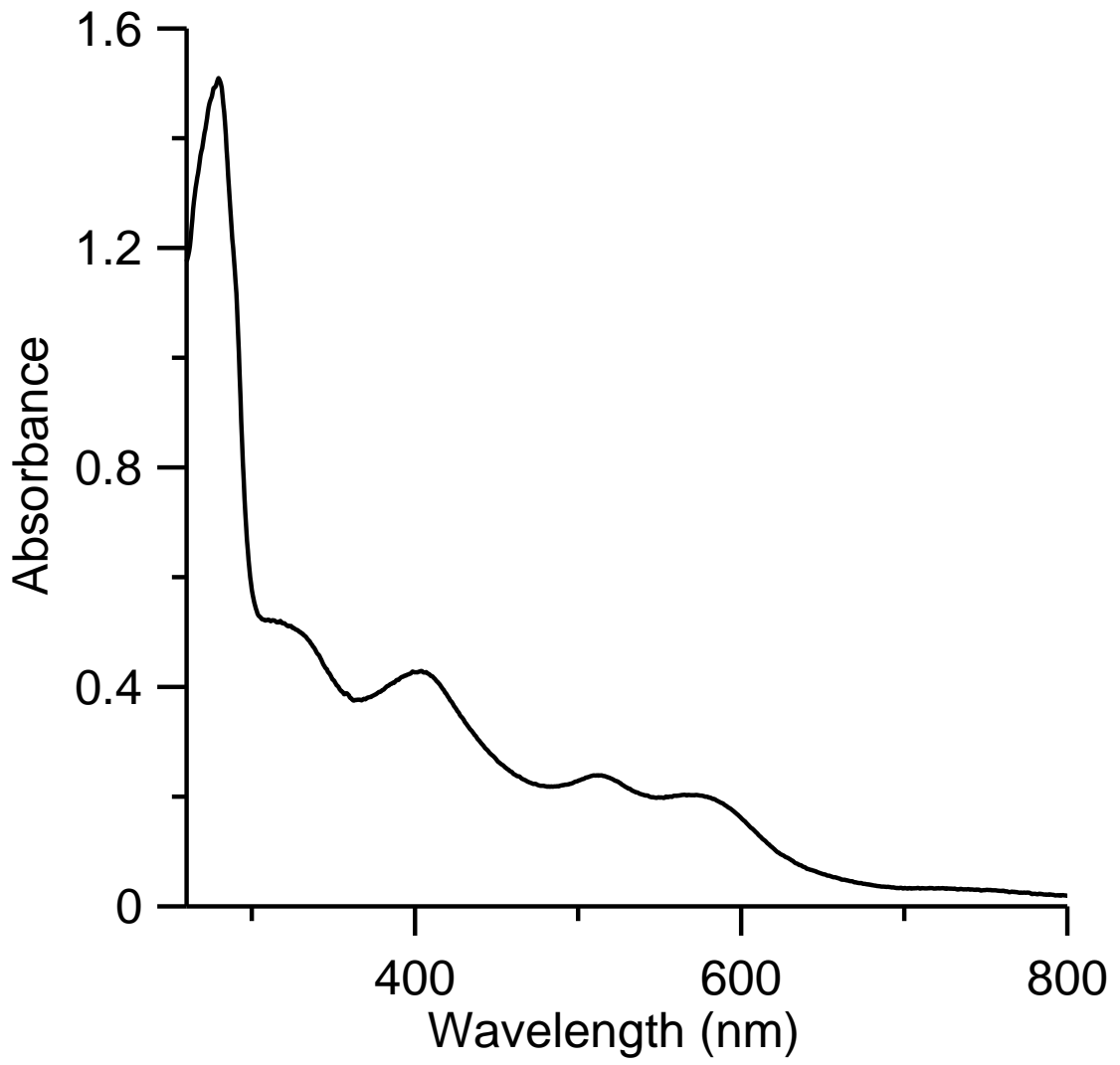


Figure 2.12: UV–visible absorption spectrum of the linear  $[3\text{Fe-4S}]^+$  cluster-bound *Sc* Grx5 C90S mutant. The sample was reconstituted under anaerobic conditions in the presence of 3 mM GSH and excess reagents were removed chromatographically. The spectrum was recorded under anaerobic conditions in sealed 0.1 cm cuvettes in 100 mM Tris-HCl buffer with 1 mM GSH at pH 7.8.



CHAPTER 3  
MONOTHIOGLUTAREDOXINS FUNCTION IN STORING AND TRANSPORTING  
[Fe<sub>2</sub>S<sub>2</sub>] CLUSTERS ASSEMBLED ON ISCU SCAFFOLD PROTEINS

---

Priyanka Shakamuri, Bo Zhang, and Johnson, M. K.

*J. Am. Chem. Soc.* **2012**, *134*, 15213-15216.

Reprinted here with permission of the publisher.

Department of Chemistry and Center for Metalloenzyme Studies, University of Georgia; Athens,  
Georgia 30602

**Abbreviations:** iron-sulfur cluster, ISC; ferredoxin, Fdx; glutaredoxin, Grx; glutathione, GSH; circular dichroism, CD; isopropyl  $\beta$ -D-thiogalactoside, IPTG.

## Abstract

In the bacterial ISC system for iron-sulfur cluster assembly, IscU acts as a primary scaffold protein, and the molecular co-chaperones HscA and HscB specifically interact with IscU to facilitate ATP-driven cluster transfer. In this work, cluster transfer from *Azotobacter vinelandii*  $[\text{Fe}_2\text{S}_2]^{2+}$  cluster-bound IscU to apo-Grx5, a general purpose monothiol glutaredoxin in *A. vinelandii*, was monitored by circular dichroism spectroscopy, in the absence and in the presence of HscA/HscB/Mg-ATP. The results indicate a 700-fold enhancement in the rate of  $[\text{Fe}_2\text{S}_2]^{2+}$  cluster transfer in the presence of the co-chaperones and Mg-ATP, yielding a second-order rate constant of  $20000 \text{ M}^{-1} \text{ min}^{-1}$  at 23 °C. Thus, HscA and HscB are required for efficient ATP-dependent  $[\text{Fe}_2\text{S}_2]^{2+}$  cluster transfer from IscU to Grx5. The results support a role for monothiol Grxs in storing and transporting  $[\text{Fe}_2\text{S}_2]^{2+}$  clusters assembled on IscU and illustrate the limitations of interpreting *in vitro* cluster transfer studies involving  $[\text{Fe}_2\text{S}_2]$ -IscU in the absence of the dedicated HscA/HscB co-chaperone system.

## Introduction

The ubiquitous and essential IscU protein serves as the primary scaffold for cysteine desulfurase-mediated iron-sulfur cluster assembly in the ISC machinery for cluster biogenesis that is used by many bacteria and in eukaryotic mitochondria (1-3). Under reconstitution conditions, the initial product is a stable form containing one  $[\text{Fe}_2\text{S}_2]^{2+}$  cluster per homodimer,  $[\text{Fe}_2\text{S}_2]$ -IscU, which is slowly converted under strictly anaerobic conditions into a form containing one  $[\text{Fe}_4\text{S}_4]^{2+}$  cluster per homodimer,  $[\text{Fe}_4\text{S}_4]$ -IscU, via reductive coupling of two  $[\text{Fe}_2\text{S}_2]^{2+}$  clusters at the subunit interface (4;5). *In vivo* studies have shown that IscU-type proteins have critical roles in the maturation of both  $[\text{Fe}_2\text{S}_2]$  and  $[\text{Fe}_4\text{S}_4]$  cluster containing proteins under aerobic and anaerobic conditions (6). Taken together with recent structural evidence that the initial product of IscS/IscU cluster biosynthesis is an IscU monomer with a solvent-exposed  $[\text{Fe}_2\text{S}_2]$  cluster (3), there is little doubt that the stable  $[\text{Fe}_2\text{S}_2]$ -IscU dimer is physiologically relevant for initiating cellular  $[\text{Fe}_2\text{S}_2]$  cluster trafficking. Moreover, the bacterial *isc* operon also contains an essential and dedicated molecular co-chaperone system, HscA/HscB in bacteria (Ssq1/Jac1 in yeast mitochondria), which serves to specifically enhance the rate of  $[\text{Fe}_2\text{S}_2]^{2+}$  cluster transfer from the  $[\text{Fe}_2\text{S}_2]$ -IscU dimer to apo acceptor proteins such as Isc ferredoxin (Fdx) in an ATP-dependent reaction (7;8). However, it is currently unclear if IscU transfers clusters directly to acceptor proteins or via proposed intermediate cluster carrier proteins such as the A-type (9;10), Nfu-type (11;12), or monothiol glutaredoxins (Grxs) (13;14).

*In vivo* studies in *Saccharomyces cerevisiae* have demonstrated an important role for Grx5 in Fe-S cluster biogenesis (15). Yeast Grx5 is a member of a ubiquitous and well-defined class of monothiol Grxs with CGFS active sites that exhibit low glutathione-dependent thiol-disulfide oxidoreductase activity (14). Rather,  $^{55}\text{Fe}$ -radiolabeled immunoprecipitation studies

have indicated a role in facilitating transfer of Fe-S clusters assembled on Isu1, a yeast homologue of IscU (16). Moreover, spectroscopic and structural studies have shown that monothiol Grxs can bind subunit-bridging  $[\text{Fe}_2\text{S}_2]^{2+}$  clusters, ligated by the active-site cysteines of each monomer and two glutathiones, that can be rapidly transferred to physiologically relevant acceptor proteins (13;17;18). However, there is currently no direct evidence for  $[\text{Fe}_2\text{S}_2]^{2+}$  cluster transfer from IscU to apo monothiol Grxs. In this work, we present direct spectroscopic evidence for rapid, ATP-driven,  $[\text{Fe}_2\text{S}_2]^{2+}$  cluster transfer from  $[\text{Fe}_2\text{S}_2]$ -IscU to apo-Grx5 in the presence of HscA and HscB using recombinant proteins from *Azotobacter vinelandii*. The results demonstrate the critical role that HscA and HscB play in facilitating cluster transfer from  $[\text{Fe}_2\text{S}_2]$ -IscU to monothiol Grxs and suggest an important role for monothiol Grxs in the trafficking of  $[\text{Fe}_2\text{S}_2]^{2+}$  clusters assembled on IscU.

## Experimental Procedures

*Materials:* All chemicals were purchased from Sigma-Aldrich, Fisher or Invitrogen, unless otherwise stated. The plasmids for overexpression of *A. vinelandii* IscU, HscA, HscB, and Grx5 were provided by Dr. Dennis Dean (Virginia Polytechnic Institute and State University). The recombinant plasmid pDB1686 that contains *A. vinelandii* *grx5* gene with 347 bp fragment was cloned into NdeI-BamHI sites of pET-16b vector for production of *A. vinelandii* Grx5 with an N-terminal histidine-tag. The cloning of *grx5* gene to pET-16b vector was performed by GenScript USA Inc. and nucleotide sequence was confirmed by DNA sequencing analyses performed by the University of Georgia Genomics Facility. Anaerobic experiments were conducted under argon in a Vacuum Atmospheres glove box at oxygen levels of < 2 ppm. Protein concentrations were determined by the DC protein assay (Bio-Rad), using BSA as a

standard. Fe concentrations were determined colorimetrically using bathophenanthroline under reducing conditions, after  $\text{KMnO}_4/\text{HCl}$  protein digestion (19).

*Overexpression and purification of A. vinelandii HscA and HscB:* The plasmids pDB1303 and 1036, which overexpress HscA and HscB, respectively, were transformed into the *E. coli* host BL21(DE3) gold and 1 or 2 colonies were directly added to LB (Lysogeny broth) media containing 100  $\mu\text{g}/\text{mL}$  ampicillin and allowed to grow at 37 °C. When the cultures reached an OD600 between 0.8-1.0, isopropyl 1-thio- $\beta$ -D-galactopyranoside (IPTG) was added to a final concentration of 0.8 mM, and the bacterial cultures were further cultivated at 28 °C for 20 hours. The cells were harvested at 9000 g for 5 min at 4 °C and stored at -80 °C until further use.

*A. vinelandii* HscA and HscB were purified under aerobic conditions essentially as previously described (7). The cell paste (25 g) was thawed and resuspended in 75 mL of 100 mM Tris-HCl buffer, pH 7.8 containing 1 mM dithiothreitol (DTT) (buffer A). To this mixture phenylmethanesulfonyl fluoride (PMSF) (13 mg), 10  $\mu\text{g}/\text{mL}$  DNase I (Roche), and 10  $\mu\text{g}/\text{mL}$  RNase A (Roche) were added. The cells were broken by intermittent sonication for 45 min, and the cell debris was removed by centrifugation at 39700 g for 1 hour at 4 °C. The cell free extract containing HscA or HscB was loaded onto a 110-mL Q-sepharose column previously equilibrated with Buffer A. Elution was achieved with a 0 to 1 M NaCl gradient using buffer A. Based on SDS gel analysis, the purest fractions were combined. These pure fractions were dialyzed into 100 mM Tris-HCl, pH 7.8, containing 1 mM DTT and 1 M ammonium sulfate by ultracentrifugation using YM30 membrane for HscA or YM10 membrane for HscB. The protein was further purified by loading into a 75-ml phenyl sepharose column and eluting with 1 to 0 M ammonium sulfate gradient using buffer A. The fractions were collected, assessed by the SDS-PAGE analysis, and the purest fractions were combined, concentrated by Amicon ultrafiltration

using a YM30 or YM10 membrane and further purified on a size exclusion column (Superdex 200 in case of HscA and Superdex 75 for HscB) previously equilibrated with 100 mM Tris-HCl buffer, 200 mM NaCl, pH 7.8. The purified proteins were concentrated and exchanged anaerobically with buffer A and stored in liquid nitrogen until future use.

*Overexpression and anaerobic purification of His-tagged A. vinelandii Grx5:* The *E. coli* expression strain C41(DE3) was transformed with *A. vinelandii* Grx5 plasmid containing the helper vector pET-16b. LB cultures were grown at 37°C and induced in exponential phase by adding IPTG (final concentration of 0.8 mM) and the bacterial cultures were further cultivated at 34 °C for 4 hours. The reddish-brown cells were harvested by centrifugation at 5000 g for 15 min at 4 °C and stored at –80 °C until further use. For purification, 8 g of cells were thawed and resuspended in 50 mM Tris-HCl buffer at pH 7.8 with 1 mM glutathione (GSH). 10 µg/mL PMSF, 15 µg/mL DNase and 5 µg/mL RNase were added to the mixture. The cells were lysed by sonication, and cell debris was removed by centrifugation at 39700 g for 1 hour at 4 °C. The reddish-brown cell-free extract containing Av Grx5 was loaded onto a 3x5-mL His-Trap HP column (GE Healthcare) previously equilibrated with binding buffer (50 mM Tris-HCl, pH 7.8, containing 1 mM GSH, 0.5 M NaCl, 20 mM imidazole). The column was washed with 10 column volumes of binding buffer before the protein of interest was eluted with a 20-500 mM imidazole gradient. The purest fractions containing apo- and holo- *A. vinelandii* Grx5 were collected separately and imidazole was removed by Amicon ultrafiltration using an YM10 membrane. Based on Fe and protein determinations, coupled with resonance Raman and UV-visible absorption and CD studies, holo *A. vinelandii* Grx5 was found to contain  $1.0 \pm 0.1$  [Fe<sub>2</sub>S<sub>2</sub>]/dimer.

*Preparation of A. vinelandii [Fe<sub>2</sub>S<sub>2</sub>]-IscU and [Fe<sub>2</sub>S<sub>2</sub>]-IscFdx:* IscU samples containing 0.9 [Fe<sub>2</sub>S<sub>2</sub>]<sup>2+</sup> clusters/dimer were prepared as described previously (4). The [Fe<sub>2</sub>S<sub>2</sub>]<sup>2+</sup> cluster concentrations of *A. vinelandii* [Fe<sub>2</sub>S<sub>2</sub>]-IscU used in this work were based on the experimentally determined extinction coefficient per [Fe<sub>2</sub>S<sub>2</sub>]<sup>2+</sup> cluster,  $\epsilon_{456} = 9.2 \text{ mM}^{-1}\text{cm}^{-1}$ , as assessed by Mössbauer spectroscopy and Fe and protein determinations (4). The holo- and apo- forms of IscFdx were prepared as previously described, and the holo protein contained  $1.0 \pm 0.1$  [Fe<sub>2</sub>S<sub>2</sub>]<sup>2+</sup> cluster per monomer based on iron and protein determinations (7).

*HscA ATPase activity assays:* The HscA ATPase activity in the presence and absence of HscB and apo-IscU was determined by measuring the phosphate released in a coupled enzyme assay using an Enzchek phosphate assay kit at 23 °C. The ATPase activity of *A. vinelandii* HscA alone is low (0.042 mol of ATP hydrolysed (mol of HscA)<sup>-1</sup> min<sup>-1</sup>). However, in the presence of 100-fold excess of HscB, the activity was enhanced 12-fold and in the presence of 100-fold excess of HscB and apo-IscU, the ATPase activity was enhanced 24-fold. Previous work has shown that K<sup>+</sup> ions are required for the optimal ATPase activity of Hsp70 molecular chaperones (20), thus activities were also assessed in the presence of 150 mM KCl, the cytoplasmic concentration of K<sup>+</sup>, as well as 100-fold excess of HscB and IscU. Under these conditions, the ATPase activity of HscA was enhanced 85-fold. These results are in good agreement with previously published data (7), which reported 13-, 25-, and 100-fold increases in *A. vinelandii* HscA ATPase activity under analogous conditions on addition of HscB, HscB/IscU, and HscB/IscU/KCl, respectively.

*Cluster transfer experiments:* The time course of cluster transfer from *A. vinelandii* [Fe<sub>2</sub>S<sub>2</sub>]-IscU to apo-Grx5 was monitored under anaerobic conditions at 23 °C using UV-visible CD spectroscopy in small volume 1-cm cuvettes. Reactions were carried out in 100 mM Tris-

HCl buffer, pH 7.8, with 3 mM GSH. The final reaction mixture (800  $\mu$ L) was 0.15 mM in apo Grx5 monomer and 0.10 mM in IscU monomer with 0.9  $[\text{Fe}_2\text{S}_2]^{2+}$  clusters/dimer to give a final IscU  $[\text{Fe}_2\text{S}_2]^{2+}$  cluster concentration of 0.045 mM. The zero time point corresponds to the addition of Grx5 to the reaction mixture. Reactions were also carried out in the presence of 0.10 mM *A. vinelandii* HscA and HscB, 40 mM  $\text{MgCl}_2$ , 2 mM ATP, 150 mM KCl, and 3 mM GSH. The zero time point for these experiments corresponds to the addition of ATP to the reaction mixture. The cluster content for the repurified  $[\text{Fe}_2\text{S}_2]$ -Grx5 formed by cluster transfer was determined to be  $1.0 \pm 0.1$   $[\text{Fe}_2\text{S}_2]$  cluster/dimer based on Fe and protein determinations. In addition, the  $[\text{Fe}_2\text{S}_2]$  centers in  $[\text{Fe}_2\text{S}_2]$ -Grx5 as purified and prepared by cluster transfer were indistinguishable based resonance Raman and UV-visible absorption and CD spectra.

The time course of cluster transfer from *A. vinelandii*  $[\text{Fe}_2\text{S}_2]$ -Grx5 (32  $\mu$ M in  $[\text{Fe}_2\text{S}_2]^{2+}$  clusters) to apo-IscFdx was monitored under anaerobic conditions 23°C using UV-visible CD spectroscopy in small volume 1-cm cuvettes. Reactions were carried out in 100 mM Tris-HCl buffer, pH 7.8, with 2 mM dithiothreitol. The final reaction mixture (800  $\mu$ L) was 32  $\mu$ M in *A. vinelandii* Grx5  $[\text{Fe}_2\text{S}_2]^{2+}$  clusters and 48  $\mu$ M in apo-IscFdx. The zero time point corresponds to the addition of apo IscFdx to the reaction mixture. The holo *A. vinelandii* IscFdx repurified from the reaction mixture contained  $1.0 \pm 0.1$   $[\text{Fe}_2\text{S}_2]$  cluster per monomer and exhibited identical EPR and UV-visible absorption/CD spectra to those of holo *A. vinelandii* IscFdx as purified (21).

The kinetics for both types of cluster transfer reaction were analyzed by fitting to second order kinetics, based on the initial concentrations of  $[\text{Fe}_2\text{S}_2]$  clusters on the donor proteins and the concentration of the cluster-accepting form of the acceptor protein using the Chemical Kinetics Simulator software package (IBM). Intact cluster transfer for both types of cluster

transfer reaction was confirmed by the absence of any significant change in the rate of cluster transfer in parallel experiments carried in the presence of 2 mM EDTA.

*Spectroscopic measurements:* UV-visible absorption and CD spectra were recorded using a Shimadzu UV-3101PC spectrophotometer and a Jasco J715 spectropolarimeter, respectively. X-band (~ 9.6 GHz) EPR spectra were recorded using a ESP-300D spectrometer (Bruker, Billerica, MA) equipped with an ER-4116 dual mode cavity and an ESR 900 flow cryostat (Oxford Instruments, Concord, MA).

## Results and Discussion

The marked differences in the CD spectra of the  $[\text{Fe}_2\text{S}_2]^{2+}$  centers in *A. vinelandii* IscU and Grx5, red and blue spectra, respectively, in Figure 3.1, make this the method of choice for monitoring cluster transfer between these two proteins. No cluster transfer was observed from  $[\text{Fe}_2\text{S}_2]$ -Grx5 to apo-IscU over a period of 3 h using a 2-fold excess of  $[\text{Fe}_2\text{S}_2]$  clusters per apo-IscU dimer, in the presence of physiologically relevant levels of glutathione (3 mM). However, the reverse reaction involving cluster transfer from  $[\text{Fe}_2\text{S}_2]$ -IscU to apo-Grx5 does occur, albeit very slowly, in the presence of 3 mM glutathione. This is shown in Figure 3.1, which indicates ~30% cluster transfer over a period of 3 h, using IscU containing 0.9  $[\text{Fe}_2\text{S}_2]^{2+}$  cluster per homodimer and a 1.7-fold excess of dimeric Grx5 per IscU  $[\text{Fe}_2\text{S}_2]$  cluster. In contrast, in the presence of HscA, HscB, Mg-ATP, and KCl (required for optimal ATPase activity of HscA), the CD spectrum of  $[\text{Fe}_2\text{S}_2]$ -IscU is perturbed by binding to HscA and HscB, as previously observed (7), and the rate of cluster transfer from  $[\text{Fe}_2\text{S}_2]$ -IscU to apo-Grx5 is dramatically enhanced, going to completion within 6 min of initiating the reaction by the addition of Mg-ATP, see Figure 3.2.

Rate constants for  $[\text{Fe}_2\text{S}_2]$ -IscU to apo-Grx5 cluster transfer in the absence and in the presence of the co-chaperones, Mg-ATP and KCl, were quantitatively assessed by fitting CD intensities as a function of time to second-order kinetics based on the initial concentrations of donor and acceptor, see Figure 3.3. The rate constant increases  $\sim 700$ -fold, from 30 to 20000  $\text{M}^{-1} \text{min}^{-1}$ , on addition of the co-chaperones, Mg-ATP and KCl. This is much greater than the  $\sim 20$ -fold increase (from 36 to 800  $\text{M}^{-1} \text{min}^{-1}$ ) in the rate of cluster transfer from  $[\text{Fe}_2\text{S}_2]$ -IscU to apo-IscFdx that occurs on addition of the same cochaperones (7). This suggests that  $[\text{Fe}_2\text{S}_2]$ -IscU is unlikely to be the immediate  $[\text{Fe}_2\text{S}_2]$  cluster donor for maturation of IscFdx, which functions as an essential electron donor for ISC mediated cluster assembly in *A. vinelandii* (22). Rather, as discussed below, IscFdx may receive  $[\text{Fe}_2\text{S}_2]$  clusters directly from Grx5.

The ability of Grx5 to rapidly and quantitatively accept  $[\text{Fe}_2\text{S}_2]^{2+}$  clusters from  $[\text{Fe}_2\text{S}_2]$ -IscU in the presence of the cochaperones, in an ATP-dependent reaction, supports a physiological role for monothiol Grxs in the trafficking of  $[\text{Fe}_2\text{S}_2]^{2+}$  clusters that are assembled on IscU. Monothiol Grxs therefore have the capacity to store and/or deliver  $[\text{Fe}_2\text{S}_2]^{2+}$  clusters assembled on U-type scaffold proteins. Interestingly, slow and reversible  $[\text{Fe}_2\text{S}_2]$  cluster exchange via direct protein interaction between human Isu and Grx2, in the absence of the human Fe-S cluster biogenesis co-chaperone system (HSPA9 and HSC20) (23;24) and Mg-ATP, has recently been reported by monitoring loss or gain in disulfide oxidoreductase activity and isothermal titration calorimetry (25). Although human Grx2 (CSYC active site) is a dithiol Grx and has not been implicated in Fe-S cluster biogenesis, it has been shown to exist in a mononuclear apo form with high disulfide oxidoreductase activity and a  $[\text{Fe}_2\text{S}_2]^{2+}$  cluster-bridged dimer, ligated by the first active-site cysteine of each Grx2 monomer and two glutathiones, which lacks disulfide oxidoreductase activity (26). In light of the stability of the cluster-bound

form with respect to cluster transfer and sensitivity to oxidative stress, the  $[\text{Fe}_2\text{S}_2]^{2+}$  cluster on human Grx2 has been proposed to function as a sensor that responds to oxidative stress by activating the disulfide oxidoreductase activity via cluster degradation (27).

A  $[\text{Fe}_2\text{S}_2]^{2+}$  cluster storage function for monothiol Grxs may be required under Fe-replete conditions, and the extent of cluster loading may be an important sensor of the cellular Fe-S cluster status. This latter hypothesis is supported by the accumulating evidence that the Fe regulon in yeast is controlled by the extent of  $[\text{Fe}_2\text{S}_2]$  cluster-loading of the cytosolic Grx3 and Grx4 monothiol glutaredoxins (28-30). In *S. cerevisiae*, the sensing mechanism involves interaction of the  $[\text{Fe}_2\text{S}_2]^{2+}$  cluster-bound form of the Grx3 or Grx4 homodimer with a BolA-type protein, termed Fra2, to form a less labile  $[\text{Fe}_2\text{S}_2]^{2+}$  cluster-bound Grx3/4-Fra2 heterodimer that prevents accumulation of the Aft transcription factor in the nucleus, where it functions in activating Fe uptake systems. A related Fe or Fe-S cluster regulatory function may also occur in bacteria since a stable  $[\text{Fe}_2\text{S}_2]^{2+}$  cluster-bound Grx4/BolA heterodimer has been reported in *Escherichia coli*, where Grx4 is the sole monothiol Grx (31). A homologous BolA protein is also present in *A. vinelandii*. Alternatively, either the  $[\text{Fe}_2\text{S}_2]^{2+}$  cluster-bound monothiol Grx homodimer or the Grx-BolA heterodimer may serve to regulate Fe-S cluster biogenesis in bacteria by acting as the  $[\text{Fe}_2\text{S}_2]^{2+}$  cluster donor for IscR, which acts as a transcriptional repressor of the entire *isc* operon in its  $[\text{Fe}_2\text{S}_2]^{2+}$  cluster-bound form (32).

In addition to a potential  $[\text{Fe}_2\text{S}_2]^{2+}$  cluster storage or sensing role for monothiol Grxs, the available evidence for rapid cluster transfer to physiologically relevant acceptor proteins suggests a role as a delivery system for clusters assembled on primary scaffold proteins. This was first demonstrated in plant chloroplasts, in which  $[\text{Fe}_2\text{S}_2]^{2+}$  cluster-bound monothiol GrxS14 was found to rapidly and quantitatively transfer its  $[\text{Fe}_2\text{S}_2]$  cluster to apo plant Fdx with a second-

order rate constant of  $20000 \text{ M}^{-1} \text{ min}^{-1}$  at  $23 \text{ }^\circ\text{C}$  (13). Subsequently, cluster transfer from  $[\text{Fe}_2\text{S}_2]$ -Grx4 to apo-IscFdx in *E. coli* was demonstrated, although the rate constant was not determined (31). Based on the CD studies shown in Figure 3.4, intact and quantitative cluster transfer from  $[\text{Fe}_2\text{S}_2]$ -Grx5 to apo-IscFdx also occurs in *A. vinelandii*, with a second-order rate constant of  $2100 \text{ M}^{-1} \text{ min}^{-1}$  at  $23 \text{ }^\circ\text{C}$ . This rate constant is 2-3 times larger than that reported for co-chaperone-assisted  $[\text{Fe}_2\text{S}_2]$  cluster transfer from IscU ( $800 \text{ M}^{-1} \text{ min}^{-1}$  at  $23 \text{ }^\circ\text{C}$ ) (7), indicating that Grx5 is a viable intermediate carrier protein for delivering  $[\text{Fe}_2\text{S}_2]$  clusters assembled on IscU to apo-IscFdx.

Much work needs to be done to identify specific cluster acceptor proteins for  $[\text{Fe}_2\text{S}_2]^{2+}$  cluster-bound forms of monothiol Grxs. These could be other proposed carrier proteins such as A-type and Nfu-type proteins and/or specific apo Fe-S proteins and enzymes. Identifying the specificity of  $[\text{Fe}_2\text{S}_2]$  cluster-bound forms of monothiol Grxs with respect to acceptor proteins is under active investigation in our laboratory. In addition, since IscU functions as a catalyst for Fe-S cluster assembly (33), it is clearly important to develop a robust *in vitro* catalytic system that includes the co-chaperones for investigating cluster assembly on target proteins using Fe(II) and cysteine as the primary substrates.

### **Acknowledgments**

We thank Dr. Dennis Dean and coworkers for providing plasmids for the recombinant expression of *A. vinelandii* IscU, HscA, HscB, and Grx5. This work was supported by a grant from the NIH (GM62542 to M.K.J).

## References

1. Johnson, D. C., Dean, D. R., Smith, A. D., and Johnson, M. K. (2005) Structure, function and formation of biological iron-sulfur clusters, *Annu. Rev. Biochem.* 74, 247-281.
2. Lill, R. (2009) Function and biogenesis of iron-sulphur proteins, *Nature* 460, 831-838.
3. Marinoni, E. N., de Oliveira, J. S., Nicolet, Y., Raulfs, E. C., Amara, P., Dean, D. R., and Fontecilla-Camps, J. C. (2012) (IscS-IscU)<sub>2</sub> complex structures provide insights into Fe<sub>2</sub>S<sub>2</sub> biogenesis and transfer, *Angew. Chem., Int. Ed.* 51, 5439-5442.
4. Agar, J. N., Krebs, B., Frazzon, J., Huynh, B. H., Dean, D. R., and Johnson, M. K. (2000) IscU as a scaffold for iron-sulfur cluster biosynthesis: Sequential assembly of [2Fe-2S] and [4Fe-4S] clusters in IscU, *Biochemistry* 39, 7856-7862.
5. Chandramouli, K., Unciuleac, M.-C., Naik, S., Dean, D. R., Huynh, B. H., and Johnson, M. K. (2007) Formation and properties of [4Fe-4S] clusters on the IscU scaffold protein, *Biochemistry* 46, 6804-6811.
6. Mühlenhoff, U., Richter, N., Pines, O., Pierik, A. J., and Lill, R. (2011) Specialized function of yeast Isa1 and Isa2 in the maturation of mitochondrial [4Fe-4S] proteins, *J. Biol. Chem.* 286, 41205-41216.
7. Chandramouli, K. and Johnson, M. K. (2006) HscA and HscB stimulate [2Fe-2S] cluster transfer from IscU to apoferredoxin in an ATP-dependent reaction, *Biochemistry* 45, 11087-11095.
8. Vickery, L. E. and Cupp-Vickery, J. R. (2007) Molecular chaperones HscA/Ssq1 and HscB/Jac1 and their roles in iron-sulfur protein maturation, *Crit. Rev. Biochem. Mol. Biol.* 42, 95-111.
9. Ollagnier-de-Choudens, S., Sanakis, Y., and Fontecave, M. (2004) SufA/IscA: reactivity studies of a class of scaffold proteins involved with [Fe-S] cluster assembly, *J. Biol. Inorg. Chem.* 9, 828-838.
10. Vinella, D., Brochier-Armanet, C., Loiseau, L., Talla, E., and Barras, F. (2009) Iron-sulfur (Fe/S) protein biogenesis: phylogenomic and genetic studies of A-type carriers, *PLoS. Genet.* 5, e1000497.
11. Bandyopadhyay, S., Naik, S., O'Carroll, I. P., Huynh, B. H., Dean, D. R., Johnson, M. K., and Dos Santos, P. C. (2008) A proposed role for the *Azotobacter vinelandii* NfuA protein as an intermediate iron-sulfur cluster carrier, *J. Biol. Chem.* 283, 14092-14099.
12. Angelini, S., Gerez, C., Ollagnier-de-Choudens, S., Sanakis, Y., Fontecave, M., Barras, F., and Py, B. (2008) NfuA, a new factor required for maturing Fe/S proteins in *Escherichia coli* under oxidative stress and iron starvation conditions, *J. Biol. Chem.* 289, 14084-14091.

13. Bandyopadhyay, S., Gama, F., Molina-Navarro, M. M., Gualberto, J. M., Claxton, R., Naik, S. G., Huynh, B. H., Herrero, E., Jacquot, J.-P., Johnson, M. K., and Rouhier, N. (2008) Chloroplast monothiol glutaredoxins as scaffold proteins for the assembly and delivery of [2Fe-2S] clusters, *EMBO J.* 27, 1122-1133.
14. Rouhier, N., Couturier, J., Johnson, M. K., and Jacquot, J. P. (2010) Glutaredoxins: roles in iron homeostasis, *Trends Biochem. Sci.* 35, 43-52.
15. Rodríguez-Manzanegue, M. T., Tamarit, J., Bellí, G., Ros, J., and Herrero, E. (2002) Grx5 is a mitochondrial glutaredoxin required for the activity of iron/sulfur enzymes, *Mol. Biol. Cell* 13, 1109-1121.
16. Mühlenhoff, U., Gerber, J., Richhardt, N., and Lill, R. (2003) Components involved in assembly and dislocation of iron-sulfur clusters on the scaffold protein Isc1p, *EMBO J.* 22, 4815-4825.
17. Picciocchi, A., Saguez, C., Boussac, A., Cassier-Chauvat, C., and Chauvat, F. (2007) CGFS-type monothiol glutaredoxins from the cyanobacterium *Synechocystis* PCC6803 and other evolutionary distant model organisms possess a glutathione-ligated [2Fe-2S] cluster, *Biochemistry* 46, 15018-15026.
18. Iwema, T., Picciocchi, A., Traore, D. A., Ferrer, J. L., Chauvat, F., and Jacquamet, L. (2009) Structural basis for delivery of the intact [Fe<sub>2</sub>S<sub>2</sub>] cluster by monothiol glutaredoxin, *Biochemistry* 48, 6041-6043.
19. Fish, W. W. (1988) Rapid colorimetric micromethod for the quantitation of complexed iron in biological samples, *Meth. Enzymol.* 158, 357-364.
20. O'Brien, M. C. and McKay, D. B. (1995) How potassium affects the activity of the molecular chaperone Hsc70. I. Potassium is required for optimal ATPase activity, *J. Biol. Chem.* 270, 2247-2250.
21. Jung, Y.-S., Gao-Sheridan, H. S., Christiansen, J., Dean, D. R., and Burgess, B. K. (1999) Purification and biophysical characterization of a new [2Fe-2S] ferredoxin from *Azotobacter vinelandii*, a putative [Fe-S] cluster assembly/repair protein, *J. Biol. Chem.* 274, 32402-32410.
22. Johnson, D. C., Unciuleac, M.-C., and Dean, D. R. (2006) Controlled expression and functional analysis of iron-sulfur cluster biosynthetic components within *Azotobacter vinelandii*, *J. Bacteriol.* 188, 7551-7561.
23. Uhrigshardt, H., Singh, A., Kovtunovych, G., Ghosh, M., and Rouault, T. A. (2010) Characterization of the human HSC20, an unusual DnaJ type III protein, involved in iron-sulfur cluster biogenesis, *Hum. Mol. Genet.* 19, 3816-3834.
24. Rouault, T. A. and Tong, W. H. (2008) Iron-sulfur cluster biogenesis and human disease, *Trends Genet.* 24, 398-407.

25. Qi, W. and Cowan, J. A. (2011) Mechanism of glutaredoxin-ISU [2Fe-2S] cluster exchange, *Chem. Commun.* 47, 4989-4991.
26. Johansson, C., Kavanagh, K. L., Gileadi, O., and Oppermann U. (2007) Reversible sequestration of active site cysteines in a 2Fe-2S-bridged dimer provides a mechanism for glutaredoxin 2 regulation in human mitochondria, *J. Biol. Chem.* 282, 3077-3082.
27. Lillig, C. H., Berndt, C., Vergnolle, O., Lönn, M. E., Hudemann, C., Bill, E., and Holmgren, A. (2005) Characterization of human glutaredoxin 2 as an iron-sulfur protein: A possible role as a redox sensor, *Proc. Natl. Acad. Sci. USA* 102, 8168-8173.
28. Ojeda, L., Keller, G., Muhlenhoff, U., Rutherford, J. C., Lill, R., and Winge, D. R. (2006) Role of glutaredoxin-3 and glutaredoxin-4 in the iron regulation of the Aft1 transcriptional activator in *Saccharomyces cerevisiae*, *J. Biol. Chem.* 281, 17661-17669.
29. Li, H., Mapolelo, D. T., Dingra, N. N., Naik, S. G., Lees, N. S., Hoffman, B. M., Riggs-Gelasco, P. J., Huynh, B. H., Johnson, M. K., and Outten, C. E. (2009) The yeast iron regulatory proteins Grx3/4 and Fra2 form heterodimeric complexes containing a [2Fe-2S] cluster with cysteinyl and histidyl ligation, *Biochemistry* 48, 9569-9581.
30. Li, H., Mapolelo, D. T., Dingra, N. N., Keller, G., Riggs-Gelasco, P. J., Winge, D. R., Johnson, M. K., and Outten, C. E. (2011) Histidine 103 in Fra2 is an iron-sulfur cluster ligand in the [2Fe-2S] Fra2-Grx3 complex and is required for in vivo iron signaling in yeast, *J. Biol. Chem.* 286, 867-876.
31. Yeung, N., Gold, B., Liu, N. L., Prathapam, R., Sterling, H. J., Williams, E. R., and Butland, G. (2011) The *E. coli* monothiol glutaredoxin GrxD forms homodimeric and heterodimeric FeS cluster containing complexes, *Biochemistry* 50, 8957-8969.
32. Schwartz, C. J., Giel, J. L., Patschkowski, T., Luther, C., Ruzicka, F. J., Beinert, H., and Kiley, P. J. (2001) IscR, an Fe-S cluster-containing transcription factor, represses expression of *Escherichia coli* genes encoding Fe-S cluster assembly proteins, *Proc. Natl. Acad. Sci. USA* 98, 14895-14900.
33. Bonomi, F., Iametti, S., Ta, D. T., and Vickery, L. E. (2005) Multiple turnover transfer of [2Fe2S] clusters by the iron-sulfur cluster assembly scaffold proteins IscU and IscA, *J. Biol. Chem.* 280, 29513-29518.

Figure 3.1: Time course of cluster transfer from *A. vinelandii* [Fe<sub>2</sub>S<sub>2</sub>]-IscU (45 μM in [Fe<sub>2</sub>S<sub>2</sub>]<sup>2+</sup> clusters) to apo-Grx5 (150 μM in monomer) monitored by UV-visible CD spectroscopy at 23 °C. (A) CD spectra recorded at 0, 7, 20, 40, 60, 80, 120, and 180 min after adding [Fe<sub>2</sub>S<sub>2</sub>]-IscU to apo-Grx5 in 100 mM Tris-HCl buffer, pH 7.8, with 3 mM glutathione. (B) Simulated CD spectra corresponding to quantitative [Fe<sub>2</sub>S<sub>2</sub>]<sup>2+</sup> cluster transfer from [Fe<sub>2</sub>S<sub>2</sub>]-IscU to apo-Grx5 in 10% increments. Δε values are based on the [Fe<sub>2</sub>S<sub>2</sub>]<sup>2+</sup> cluster concentration, and the path length was 1 cm.

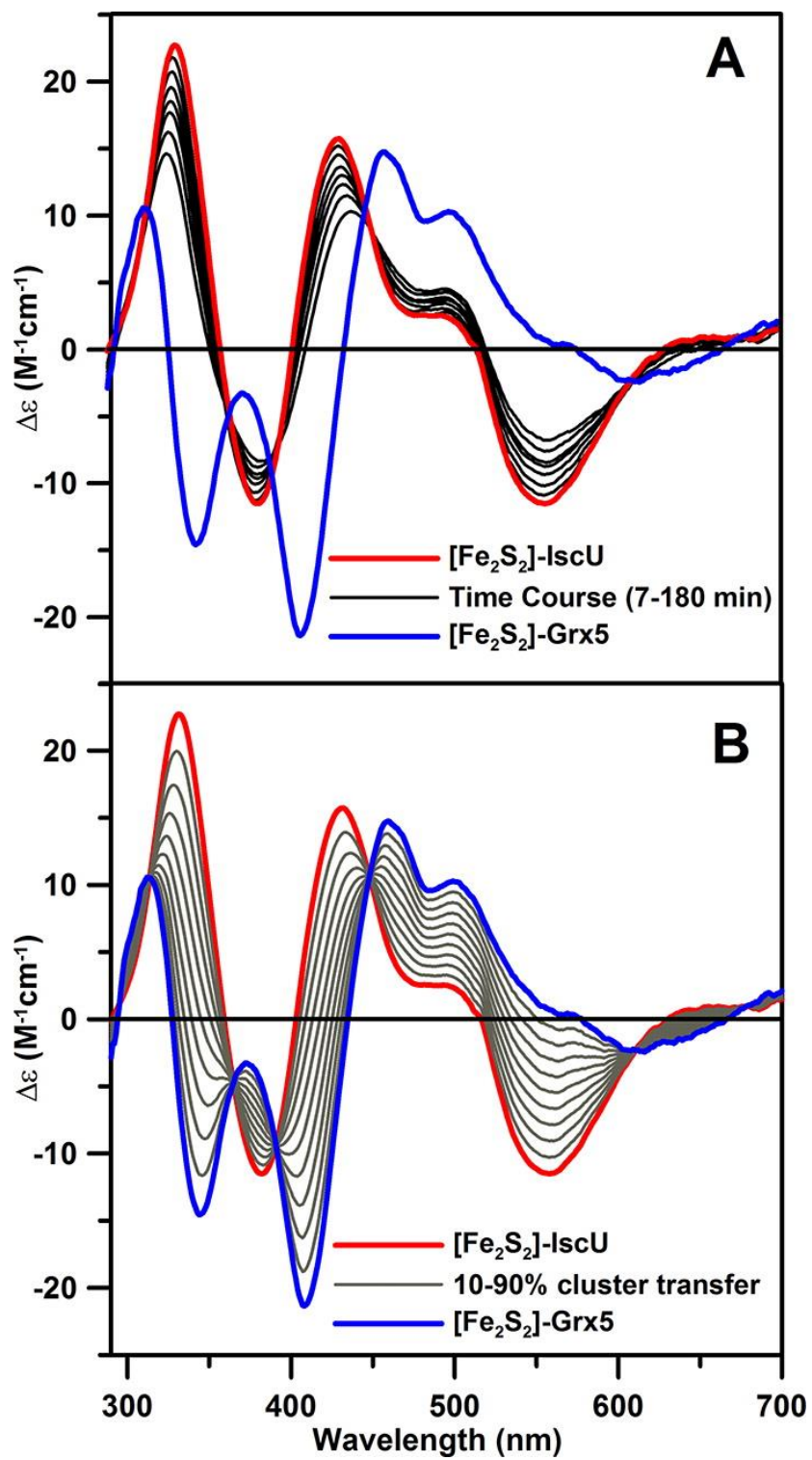


Figure 3.2: Time course of cluster transfer from *A. vinelandii* [Fe<sub>2</sub>S<sub>2</sub>]-IscU to apo-Grx in the presence of 0.10 mM *A. vinelandii* HscA and HscB, 40 mM MgCl<sub>2</sub>, 2 mM ATP, and 150 mM KCl monitored by UV-visible CD spectroscopy at room temperature. CD spectra were recorded at 3, 6, 10, 14, 18, 22, 26, 30, 40, 50, and 60 min after the addition of Mg-ATP to the reaction mixture. All other conditions are the same as described in Figure 3.1.

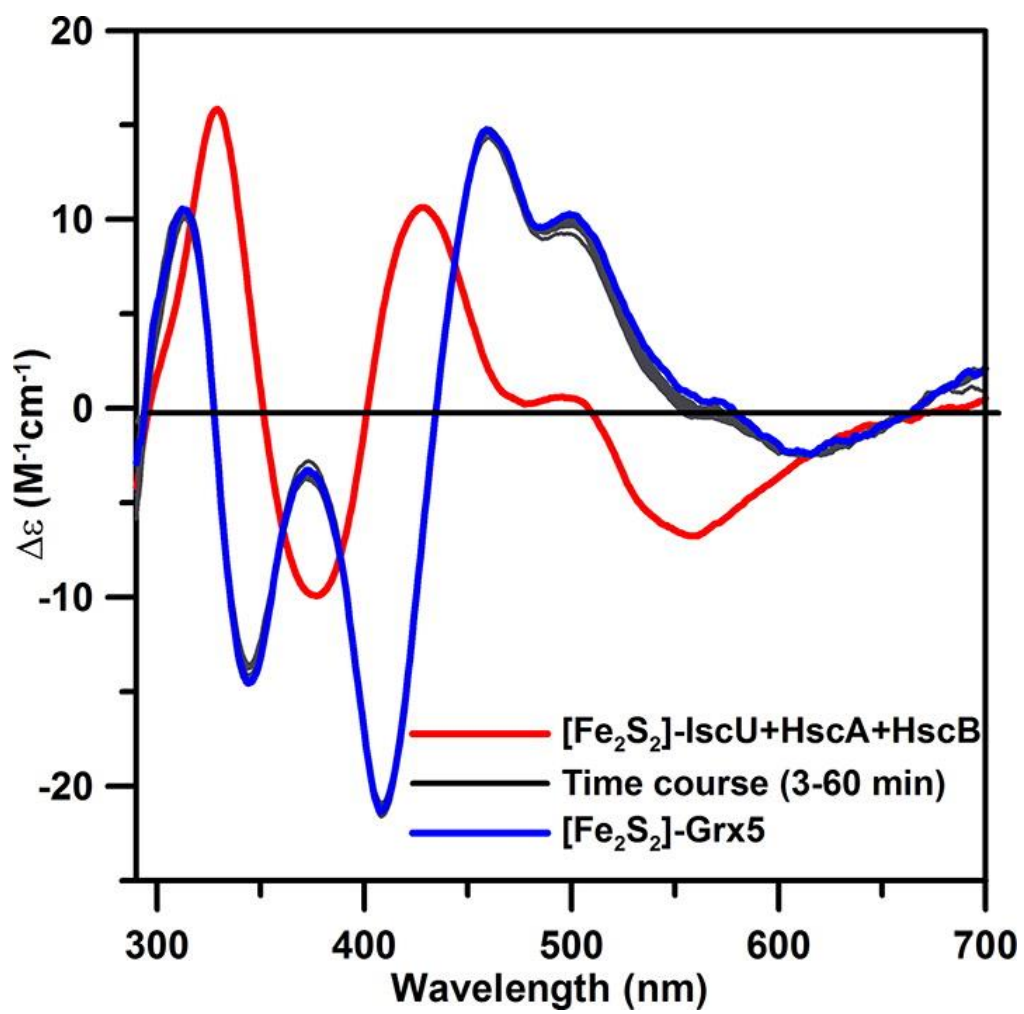


Figure 3.3: Comparison of the kinetics of cluster transfer from *A. vinelandii* [Fe<sub>2</sub>S<sub>2</sub>]-IscU to apo-Grx5 in the presence and in the absence of HscA/HscB/ATP. All conditions are the same as described in Figures 3.1 and 3.2. The data in the presence of HscA/HscB/ATP (■) were obtained by continuously monitoring the CD intensity at 460 nm after initiation of the reaction with Mg-ATP, and the solid line is a best-fit simulation to second-order kinetics with a rate constant of 20000 M<sup>-1</sup> min<sup>-1</sup>. The data in the absence of HscA/HscB/ATP (•) were obtained by monitoring the difference in the CD intensity at 457 and 408 nm, and the solid line is a best-fit simulation to second-order kinetics with a rate constant of 30 M<sup>-1</sup> min<sup>-1</sup>.

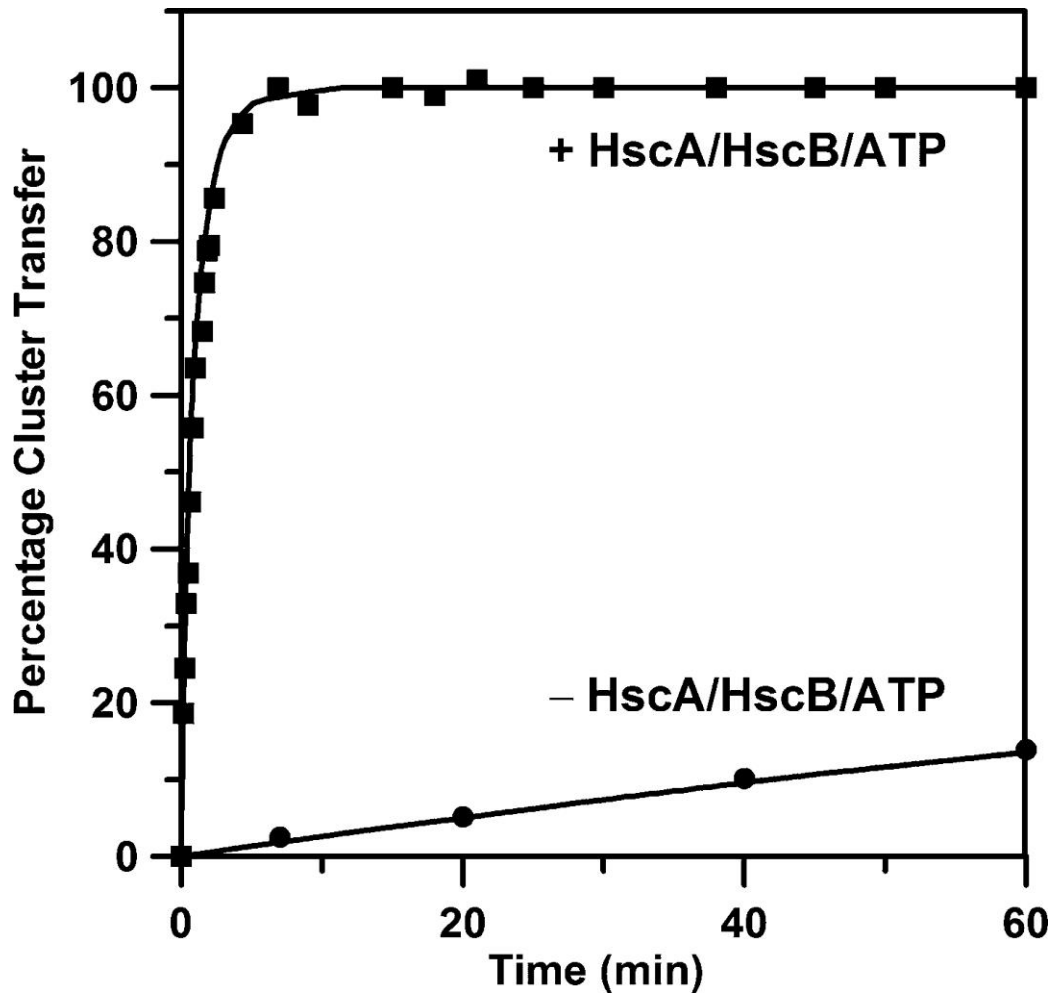
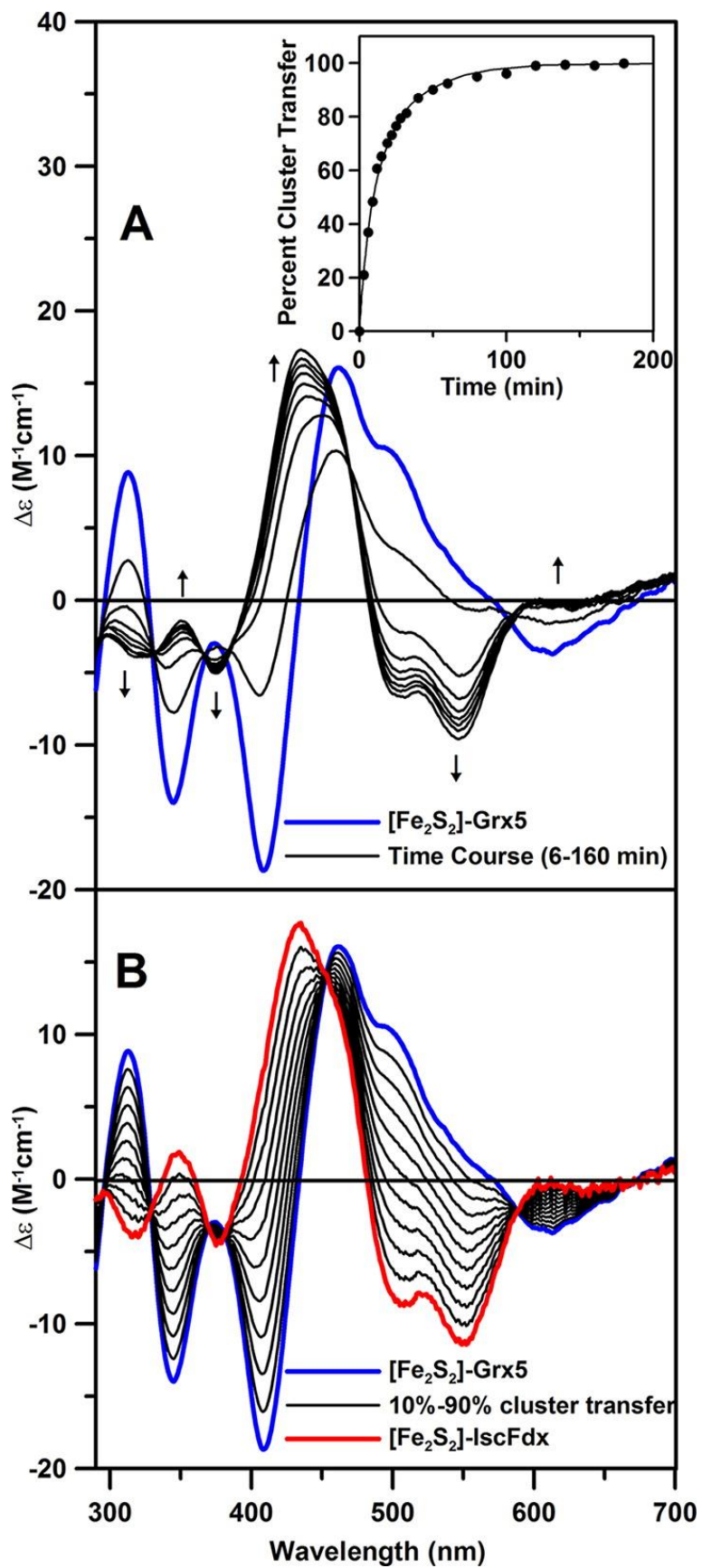


Figure 3.4: Time course of cluster transfer from *A. vinelandii* [Fe<sub>2</sub>S<sub>2</sub>]-Grx5 (32 μM in [Fe<sub>2</sub>S<sub>2</sub>]<sup>2+</sup> clusters) to apo-IscFdx (48 μM) monitored by UV-visible CD spectroscopy at 23 °C. (A) CD spectra recorded at 6, 20, 40, 60, 80, 100, 120, and 160 min after adding [Fe<sub>2</sub>S<sub>2</sub>]-Grx5 to apo-IscFdx in 100 mM Tris-HCl buffer, pH 7.8, with 2 mM dithiothreitol. The arrows indicate the direction of intensity change with increasing time at selected wavelengths. Inset shows kinetic data for the cluster transfer measured at 434 nm, and the solid line is a best-fit simulation to second-order kinetics with a rate constant of 2100 M<sup>-1</sup>min<sup>-1</sup>. (B) Simulated CD spectra corresponding to quantitative [Fe<sub>2</sub>S<sub>2</sub>]<sup>2+</sup> cluster transfer from [Fe<sub>2</sub>S<sub>2</sub>]-Grx5 to apo-IscFdx in 10% increments. Δε values are based on the [Fe<sub>2</sub>S<sub>2</sub>]<sup>2+</sup> cluster concentration, and the path length was 1 cm.



## CHAPTER 4

### POTENTIAL ROLES FOR *AZOTOBACTER VINELANDII* MONOTHIOL GLUTAREDOXINS IN [2Fe-2S] CLUSTER TRAFFICKING AND STORAGE

---

Bo Zhang and Michael K. Johnson

*To be submitted to J. Biol. Inorg. Chem.*

Department of Chemistry and Center for Metalloenzyme Studies, University of Georgia, Athens,  
Georgia 30602

**Abbreviations:** iron-sulfur cluster, ISC; nitrogen fixation, NIF; ferredoxin, Fdx; glutaredoxin, Grx; glutathione, GSH; circular dichroism, CD; isopropyl  $\beta$ -D-thiogalactoside, IPTG; *A. vinelandii*, Av.

## Abstract

Monothiol glutaredoxins with highly conserved CGFS active-site motifs (CGFS-Grxs) are versatile Fe-S cluster-binding proteins. While the majority of CGFS-Grxs are able to incorporate a labile subunit-bridging  $[2\text{Fe-2S}]^{2+}$  cluster utilizing the active-site cysteine residues and two GSH molecules, linear  $[3\text{Fe-4S}]^+$  and  $[4\text{Fe-4S}]^{2+}$  cluster-bound forms of CGFS-Grxs have also been reported. Recent studies of CGFS-Grxs from eukaryotes have implicated a role for this family of proteins in both Fe-S cluster biogenesis and the regulation of cellular iron homeostasis. However, the precise molecular functions of prokaryotic CGFS-Grxs are less well understood. *Azotobacter vinelandii* possesses two CGFS-Grxs: a general purpose Grx5, and a *nif*-specific Grx-nif. In this study, the nature and properties of the clusters in the heterologously expressed Grx5 and Grx-nif were assessed using UV-visible absorption/circular dichroism and resonance Raman spectroscopies together with analytical studies. The results reveal that the coordination environment and properties of the  $[2\text{Fe-2S}]^{2+}$  cluster in Grx5 and Grx-nif are analogous to that of spectroscopically and structurally characterized  $[2\text{Fe-2S}]^{2+}$  clusters in other CGFS-Grxs. Additionally, both Grx5 and Grx-nif are found to be able to accommodate a complete cysteinyl-ligated linear  $[3\text{Fe-4S}]^+$  cluster as a minor cluster component, but not a  $[4\text{Fe-4S}]^{2+}$  cluster. Recent studies have demonstrated the ability of Grx5 and Grx-nif to accept a  $[2\text{Fe-2S}]^{2+}$  cluster from the IscU primary scaffold protein in the presence of the dedicated co-chaperones and ATP, and to deliver  $[2\text{Fe-2S}]^{2+}$  clusters to apo acceptor proteins via intact cluster transfer, providing *in vitro* evidence for their involvements in Fe-S cluster biogenesis. In this study, UV-visible CD-monitored anaerobic cluster transfer experiments indicate that Grx5 and Grx-nif are unable to accept  $[4\text{Fe-4S}]^{2+}$  clusters from the  $[4\text{Fe-4S}]^{2+}$  cluster-bound forms of IscU, NfuA and NifU. Rather,  $[2\text{Fe-2S}]^{2+}$  clusters are assembled on apo Grx5 and Grx-nif in the presence of  $[4\text{Fe-4S}]^{2+}$

cluster-bound forms of NfuA and NifU, respectively. Taken together, these results suggest that the CGFS-Grxs in *A. vinelandii* are primarily involved with  $[2\text{Fe-2S}]^{2+}$  cluster trafficking under oxidative stress conditions.

## Introduction

The biogenesis of Fe-S clusters in the nitrogen-fixing bacteria *Azotobacter vinelandii* is primarily carried out by two dedicated multicomponent Fe-S cluster assembly machineries, designated the ISC (iron sulfur cluster) and NIF (nitrogen-fixation-specific) systems (1-3). While the NIF system is specific for the maturation of Fe-S proteins involved in the nitrogen fixation process, the ISC system is responsible for the generation of clusters to be used in general Fe-S protein biogenesis (2;4). Despite the differences in physiological target specificity, both systems share several key components and a common basic mechanism for the biosynthesis of Fe-S clusters that can be separated into two main steps: *de novo* assembly of Fe-S clusters on scaffold proteins and insertion of preformed cluster into apo proteins. The initial assembly of  $[2\text{Fe-2S}]^{2+}$  and  $[4\text{Fe-4S}]^{2+}$  clusters in both systems involves a cysteine desulfurase protein (IscS and NifS) that serves as the immediate S donor for Fe-S cluster formation by catalyzing the conversion of L-cysteine to L-alanine, and a primary scaffold protein (IscU and NifU) that provides the platform for the *de novo* assembly of Fe-S clusters (5;6). Although *in vitro* studies have demonstrated that the subsequent delivery and insertion of the preassembled clusters to apo proteins can be achieved either through direct cluster transfer from the scaffold proteins or via the involvement of intermediate cluster carrier proteins, the latter may be favored *in vivo* for effective maturation of specific target proteins or the *in situ* repair of oxygen-damaged Fe-S clusters (7-10). In either case, the first step in intact cluster transfer is the release of assembled Fe-S clusters from the scaffold proteins; and in the ISC system, this process is facilitated by the molecular co-chaperones HscA and HscB that are specifically required to release the  $[2\text{Fe-2S}]^{2+}$  clusters from IscU in an ATP-driven process (8).

Recent studies of monothiol glutaredoxins with strictly conserved CGFS active-site motifs (CGFS-Grxs) have demonstrated the ability of this family of proteins to function as intermediate cluster carrier and/or storage proteins. Deletion of the gene encoding *Saccharomyces cerevisiae* Grx5, a mitochondrial CGFS-Grx, leads to phenotypes that can be attributed to disrupted Fe-S cluster biogenesis (11;12). Furthermore, <sup>55</sup>Fe radiolabeled immunoprecipitation studies on the  $\Delta$ grx5 mutant revealed a marked increase in the Fe-S cluster content of *S. cerevisiae* Isu1 (analogous to bacterial IscU) (13). Consequently, a role for Grx5 in facilitating the transfer of preassembled clusters from U-type scaffold proteins to acceptor proteins has been suggested (13). More importantly, the involvement of CGFS-Grxs in Fe-S cluster biogenesis is found to be conserved throughout evolution, as Grx5 homologues from various species including *E. coli* (14), *A. thaliana* (15), zebrafish (16) and human (14) have been reported to be able to complement the  $\Delta$ grx5 strain when targeted to *S. cerevisiae* mitochondria.

A role for CGFS-Grxs in Fe-S cluster biogenesis is also implicated by their ability to serve as versatile Fe-S cluster-binding proteins, able to accommodate [2Fe-2S]<sup>2+</sup>, linear [3Fe-4S]<sup>+</sup> as well as [4Fe-4S]<sup>2+</sup> clusters. The majority of CGFS-Grxs can exist in both a monomeric apo form and a homodimeric [2Fe-2S]<sup>2+</sup> cluster-bound form when heterologously expressed in *E. coli* (15;17-20). The presence of the [2Fe-2S]<sup>2+</sup> cluster-bound form of CGFS-Grxs in the native host environment has been subsequently demonstrated, thereby confirming its physiological significance (21;22). The initial understanding of the nature and coordination properties of [2Fe-2S]<sup>2+</sup> center in CGFS-Grxs benefited greatly from intensive spectroscopic and mutagenesis studies. Extensive spectroscopic and analytical analyses of the [2Fe-2S]<sup>2+</sup> center revealed one [2Fe-2S]<sup>2+</sup> cluster with complete cysteinyl ligation per dimer, and mutagenesis studies indicated the involvement of the active-site CGFS and glutathione (GSH) cysteines as

cluster ligands (15). Hence the cluster was proposed to be coordinated by the active site cysteine residue from two monomers and the cysteine moiety of two external GSH molecules (15;18). Such a structural arrangement for  $[2\text{Fe-2S}]^{2+}$  cluster-bound CGFS-Grxs was later confirmed by crystallography studies of *E. coli* Grx4 and human Grx5 (23;24). Several structural details of the cluster-bound CGFS-Grxs provided a plausible hypothesis for their ability to accept and release  $[2\text{Fe-2S}]^{2+}$  clusters (23). First, the subtle differences between the conformation of the  $[2\text{Fe-2S}]^{2+}$  cluster-bound form and apo form allows the positioning of several important residues to coordinate the Fe atoms in the cluster or to form direct contact with coordinating GSH molecules. In addition, the relative orientation of CGFS-Grx protomers leads to contact between protomers, and this structural arrangement has been proposed to contribute to the lability of cluster and to provide the driving force for cluster release. Thus the observed structural differences in the vicinity of the Fe-S cluster binding site of apo and cluster-bound CGFS-Grxs indicate that the CGFS-Grxs undergo conformational changes, probably triggered by interactions with physiological partner proteins, to release the  $[2\text{Fe-2S}]^{2+}$  cluster. Moreover, *in vitro* cluster transfer experiments have demonstrated that poplar chloroplast GrxS14 and *E. coli* Grx4 can rapidly transfer intact  $[2\text{Fe-2S}]^{2+}$  clusters to the apo-forms of plant-type and *E. coli* ferredoxins, respectively (15;20).

In contrast, both the structural and function of the linear  $[3\text{Fe-4S}]^+$  and  $[4\text{Fe-4S}]^{2+}$  cluster-bound CGFS-Grxs are less well understood. Spectroscopic and mutagenesis studies of different cluster-bound forms of *S. cerevesiae* Grx5 suggest that the linear  $[3\text{Fe-4S}]^+$  cluster is likely to be analogous to that of the  $[2\text{Fe-2S}]^{2+}$  center in CGFS-Grxs while the  $[4\text{Fe-4S}]^{2+}$  cluster require both the active site cysteine and a semi-conserved cysteine residue from two monomers to complete the cluster ligation (see Chapter 2).

The genome of *A. vinelandii* encodes for two CGFS-Grxs, termed Grx5 and Grx-nif (25). While the gene encoding for *Av* Grx5 is not associated with the genes involved in the Fe-S cluster assembly systems, the genomic location of *grx-nif* gene is adjacent to a fragment of the *nif* operon that contains genes required for cofactor biosynthesis of Mo-dependent nitrogenase and Mo trafficking (25). Furthermore, the deletion of *Av grx-nif* gene has been reported to result in a 50% decrease in the activity of nitrogenase Fe protein, a [4Fe-4S] cluster-requiring protein, indicating strong connection between *Av* Grx-nif and the NIF Fe-S cluster assembly system (25). Most recently, via UV-visible circular dichroism (CD) spectroscopy-monitored *in vitro* cluster transfer experiments, we have demonstrated that *Av* Grx5 is able to mediate quantitative and rapid transfer of a [2Fe-2S]<sup>2+</sup> cluster from [2Fe-2S]-IscU to apo IscFdx, a [2Fe-2S] cluster-containing protein essential for the function of the whole ISC system (3). Moreover, the observations that *Av* Grx5 can only quantitatively accept the [2Fe-2S]<sup>2+</sup> cluster from IscU at physiologically cluster transfer relevant rates in the presence of the dedicated molecular chaperone system (HscA, HscB and Mg-ATP), and that the cluster transfer from [2Fe-2S]-Grx5 to apo IscFdx is 2-3 times faster than that from chaperone-facilitated [2Fe-2S]-IscU, strongly support a role for *Av* Grx5 as an intermediate carrier protein working directly downstream from IscU for the insertion of preassembled [2Fe-2S] clusters to specific Fe-S proteins (see Chapter 3). In addition, we have reported that the [2Fe-2S]<sup>2+</sup> cluster-bound form of *Av* Grx-nif can act as cluster donor to *Av* <sup>Nif</sup>IscA by rapid and intact [2Fe-2S] cluster transfer (Appendix C). Taken together, these recent results further support the proposed roles for CGFS-Grxs in facilitating the transfer of [2Fe-2S]<sup>2+</sup> for the maturation or repair of target proteins and in storing [2Fe-2S]<sup>2+</sup> clusters, possibly under Fe-replete and/or oxidative conditions.

To complement our previous functional studies of CGFS-Grxs from *A. vinelandii*, we present in this study characterizations of the electronic and vibrational properties of the Fe-S cluster-bound forms of *Av* Grx5 and Grx-nif using UV-visible absorption, circular dichroism (CD) and resonance Raman spectroscopies. The results present in this work show that the [2Fe-2S]<sup>2+</sup> cluster centers in *Av* Grx5 and Grx-nif are analogous to those found in other CGFS-Grxs. Additionally, we present *in vitro* evidence in further support of a storage role for CGFS-Grxs by demonstrating that both *Av* Grx5 and Grx-nif can accept [2Fe-2S]<sup>2+</sup> cluster from [4Fe-4S]<sup>2+</sup> cluster-containing proteins under strictly anaerobic conditions. The results suggest that CGFS-Grxs have the potential to act as a cluster reservoir, transferring preassembled [2Fe-2S]<sup>2+</sup> clusters for protein maturation or repair and storing clusters in the form of [2Fe-2S]<sup>2+</sup> clusters under Fe-replete and/or oxidative stress conditions to minimized the toxic effects of cellular Fe accumulation.

## **Experimental procedures**

*Overexpression and purification of His-tagged Av Grx5 and Grx-nif:* The plasmids that overexpress N-terminal histidine-tagged *Av* Grx5 and Grx-nif were separately transformed into the *E. coli* expression strain C41(DE3). Colonies containing Grx5 or Grx-nif plasmids were grown at 37 °C in Lysogeny Broth (LB) media. The culture was induced at exponential phase by adding isopropyl-β-D-thiogalactopyranoside (IPTG) (final concentration of 0.8 mM), and the bacterial cultures were further cultivated at 34 °C for 4 hours. The reddish-brown cells were harvested by centrifugation at 5000 g for 15 min at 4 °C and stored at -80 °C until further use.

For aerobic purification of proteins, 8 g of cell paste were thawed and resuspended in 50 mM Tris-HCl buffer at pH 7.8 with 1 mM glutathione (GSH). 10 μg/mL phenylmethylsulphonyl fluoride (PMSF), 15 μg/mL DNase and 5 μg/mL RNase were added to the mixture. The cells

were lysed by sonication, and cell debris was removed by centrifugation at 39700 g for 1 hour at 4 °C. The reddish-brown colored cell-free extract containing Av Grx5 or Grx-nif was loaded onto a 3x5 mL His-Trap HP column (GE Healthcare) previously equilibrated with binding buffer (50 mM Tris-HCl, pH 7.8, containing 1 mM GSH, 0.5 M NaCl, 20 mM imidazole). The column was washed with 10 column volumes of binding buffer before the protein of interest was eluted with a linear gradient of 20 to 500 mM of imidazole. The purest fractions containing Av Grx5 or Grx-nif were collected separately and imidazole was removed by Amicon ultrafiltration using an YM10 membrane. The same procedure was used for anaerobic purification, except that the sonication and chromatographic purification processes were carried out inside a glove box ( $O_2 < 2$  ppm), and that the buffers used were rigorously degassed to remove oxygen.

*Preparation of apo forms of Av Grx5 and Grx-nif.* Apo forms of Av Grx5 and Grx-nif was prepared by incubating as-isolated protein samples containing low levels of bound Fe-S clusters with 50-fold excess of EDTA and 20-fold excess of potassium ferricyanide on ice for 60 minutes under strictly anaerobic conditions. The protein was then buffer exchanged into 50 mM Tris-HCl, pH 7.8 buffer using a 2x5 mL desalting column (GE Healthcare) and the resulting apo-protein was concentrated via Amicon ultrafiltration using a YM10 membrane.

*Reconstitution of Fe-S clusters on Av Grx5 and Grx-nif.* Anaerobic cluster reconstitution experiments were carried out by incubating apo forms of Grx5 or Grx-nif with 10-fold excess of ferrous ammonium sulfate, 10-fold excess of L-cysteine, and catalytic amount of cysteine desulfurase (IscS for Grx5 and NifS for Grx-nif) in the presence of 3 mM GSH. Excess reagents were subsequently removed by passing the reaction mixture through Hi-Trap Q-Sepharose column and the eluted colored fractions containing Fe-S cluster-bound protein samples were collected separately and concentrated by ultrafiltration using an Amicon YM10 membrane.

*[4Fe-4S]-IscU to apo Grx5 cluster transfer.* Anaerobic reconstitution and repurification of the  $[4\text{Fe-4S}]^{2+}$  cluster-bound Av IscU sample was carried out following the published procedure (5). The cluster transfer from the  $[4\text{Fe-4S}]\text{-IscU}$  to apo Av Grx5 were performed in 100 mM Tris-HCl buffer at pH 7.8 in the presence of 3 mM GSH. The time course of cluster transfer was monitored under anaerobic conditions in a sealed 1 cm cuvette at room temperature using UV-visible CD spectroscopy.

*[4Fe-4S]-NfuA to apo Grx5 cluster transfer.* Av NfuA containing  $\sim 0.8 [4\text{Fe-4S}]^{2+}$  clusters/dimer ( $A_{400}/A_{280} = 0.17$ ) was prepared as previously described (7), and the content of the  $[4\text{Fe-4S}]^{2+}$  cluster in the sample used for cluster transfer experiment was assessed by quantitative comparison of the UV-visible absorption spectrum with that of Av NfuA sample with Mössbauer-defined  $[4\text{Fe-4S}]^{2+}$  cluster content (7). The experimental conditions for the cluster transfer from  $[4\text{Fe-4S}]\text{-NfuA}$  to apo Av Grx5 were the same as described above for  $[4\text{Fe-4S}]\text{-IscU}$  to apo Av Grx5 cluster transfer.

*Cluster transfer from [4Fe-4S] cluster-bound wild-type and truncated forms of NifU to apo Grx-nif.*  $[4\text{Fe-4S}]^{2+}$  cluster-bound holo forms of NifU, NifU1 (N-terminal domain fragment of NifU) and NifU2 (central and C-terminal domain fragments of NifU) were prepared according to published procedures (6;26). The experimental conditions for the cluster transfer were the same as described above for  $[4\text{Fe-4S}]\text{-IscU}$  to apo Av Grx5 cluster transfer

*Analytical and spectroscopic methods.* Protein concentrations were determined by the DC protein assay (Bio-Rad) using bovine serum albumin (Roche) as standard. Iron concentrations were determined colorimetrically using bathophenanthroline under reducing conditions after digestion of proteins in 0.8%  $\text{KMnO}_4/0.2 \text{ M HCl}$  (27). Standard solutions of known Fe concentrations were prepared using 1000 ppm atomic absorption iron standard (Fluka).

Preparation and handling of anaerobic samples for spectroscopic studies and cluster transfer experiments were carried out inside a Vacuum Atmosphere glove box under argon atmosphere with oxygen level lower than 2 ppm. UV-visible absorption spectra were recorded in sealed quartz cuvettes at room temperature using a Shimadzu-3101PC spectrophotometer. Room temperature UV-visible CD spectra were recorded in sealed quartz cuvettes using a Jasco J-715 spectropolarimeter. Resonance Raman samples were in the form of 18- $\mu$ L frozen droplet mounted on the cold finger of an Air Products Displex Model CSA-202E closed cycle refrigerator (28) and resonance Raman spectra were recorded using an Instrument SA Ramanor U1000 scanning spectrometer coupled with a Coherent Sabre argon ion laser.

## Results

*Purification and spectroscopic characterization of cluster-containing forms of A. vinelandii Grx5 and Grx-nif:* A series of recent studies on recombinant CGFS-Grxs from various species have revealed their ability to accommodate a labile subunit-bridging  $[2\text{Fe-2S}]^{2+}$  cluster ligated by the active site cysteine residues of two Grx monomers and two GSH molecules at homodimer interface (15;18-20;23;24). To investigate the nature and properties of the Fe-S clusters assembled on the two CGFS-Grxs from *A. vinelandii*, recombinant N-terminal histidine tagged Grx5 and Grx-nif were expressed in *E. coli* and purified to homogeneity. GSH (1 mM) was present throughout the purification process due to its requirement in ligating and stabilizing the Grx-bound  $[2\text{Fe-2S}]^{2+}$  and linear  $[3\text{Fe-4S}]^+$  clusters ((15) and Chapter 2). Similar to what has been observed for poplar GrxS14 and *S. cerevisiae* Grx3/4 (15;18), aerobically purified Grx5 and Grx-nif contained low but measurable levels of protein-bound  $[2\text{Fe-2S}]^{2+}$  clusters that gradually degraded during prolonged aerobic handling. Substantially higher amounts of  $[2\text{Fe-2S}]^{2+}$  cluster-bound Grx5 and Grx-nif were obtained via anaerobic purification carried out under

an Ar atmosphere using rigorously degassed buffers. Anaerobic cluster reconstitution experiments were also undertaken to obtain homogeneous samples and thereby facilitate the spectroscopic and biochemical characterization of the type(s) and stoichiometry of the Fe-S clusters assembled on Grx5 and Grx-nif. Since identical spectroscopic properties have been reported for Fe-S clusters presented in both as-purified and reconstituted samples of several CGFS-Grxs (15;18;20), studies were carried out only on Grx5 and Grx-nif samples subjected to cysteine desulfurase-mediated reconstitution followed by repurification.

The cluster-bound forms of Grx5 and Grx-nif exhibit almost identical UV-visible absorption and CD spectra, as shown in Figure 4.1. The absorption spectra comprise several overlapping features in the visible and near UV region with dominant peaks at 322 and 403 nm as a result of the S-to-Fe (III) charge transfer transactions and share close similarity to the spectra reported for bridging  $[2\text{Fe-2S}]^{2+}$  clusters in CGFS-Grxs (15;18;19;23). The corresponding UV-visible CD spectra are also indicative of a  $[2\text{Fe-2S}]^{2+}$  center and are very similar to the published spectra for  $[2\text{Fe-2S}]^{2+}$  cluster-bridged CGFS-Grxs with slight variations only in terms of CD intensity (15;18;19). Iron and protein determinations performed on cluster-loaded samples indicate 1.1 Fe per monomer for both Grx5 and Grx-nif, a value in agreement with previous reports (15;18;19) and can be translated to a stoichiometry of approximate one  $[2\text{Fe-2S}]^{2+}$  cluster per homodimer for both Grx5 and Grx-nif. On the basis of analytical analysis and absorption intensity, the extinction coefficients for the  $[2\text{Fe-2S}]^{2+}$  cluster in Grx5 and Grx-nif are estimated to be  $\epsilon_{403} = 13.6 \pm 1.0 \text{ mM}^{-1} \text{ cm}^{-1}$  and  $\epsilon_{403} = 12.1 \pm 1.0 \text{ mM}^{-1} \text{ cm}^{-1}$ , respectively. We note that the extinction coefficient values determined for the  $[2\text{Fe-2S}]^{2+}$  cluster in Grx5 and Grx-nif are slightly higher than the established values for the corresponding band of biological  $[2\text{Fe-2S}]^{2+}$  clusters, which typically range between 8.0 – 11.0  $\text{mM}^{-1} \text{ cm}^{-1}$  for the dominant absorption band

in the 390 – 430 nm region (15;19;29). However, taken together with the analytical data, the results are consistent with no more than one  $[2\text{Fe-2S}]^{2+}$  cluster per CGFS-Grx monomer.

The vibrational properties of the clusters in Grx5 and Grx-nif were investigated using resonance Raman spectroscopy to further address the ligation environment of the  $[2\text{Fe-2S}]^{2+}$  center, as the resonance Raman results of  $[2\text{Fe-2S}]^{2+}$  cluster containing proteins are extremely sensitive to the nature of coordinating ligands as well as the Fe-S-C-C dihedral angles of the coordinated cysteine ligands (30). Resonance Raman spectra for Grx5 (solid line) and Grx-nif (broken line) acquired using 457, 488 and 514 nm laser excitation wavelengths are compared in Figure 4.2. The spectra are identical within experimental error for the cluster-containing Grx5 and Grx-nif with resonantly enhanced Fe-S stretching modes at 289, 325, 345, 366, 400 and 421  $\text{cm}^{-1}$  in the Fe-S stretching region. The vibrational frequencies and relative intensities are both indicative of  $[2\text{Fe-2S}]^{2+}$  centers with complete cysteinyl ligation (30;31). Moreover, the spectra closely resemble those reported and assigned for the  $[2\text{Fe-2S}]^{2+}$  clusters in other CGFS-Grxs (15;18;19). Taken together, the analytical and spectroscopic results demonstrate that the  $[2\text{Fe-2S}]^{2+}$  clusters in both *Av* Grx5 and Grx-nif are analogous to those found in other  $[2\text{Fe-2S}]^{2+}$  cluster containing CGFS-Grx homodimers (15;18;19;23;24).

Recently, spectroscopic studies of the reconstituted *S. cerevisiae* mitochondrial Grx5 have demonstrated the incorporation of one all-cysteinyl-ligated linear  $[3\text{Fe-4S}]^+$  cluster per dimer that is ligated by the active site cysteine residues of the CGFS-Grxs and external GSH molecules (see Chapter 2). In this study, we have also observed the presence of linear  $[3\text{Fe-4S}]^+$  cluster, in addition to  $[2\text{Fe-2S}]^{2+}$  clusters, in both aerobically isolated and anaerobically reconstituted *Av* CGFS-Grxs. As shown in Figure 4.3, the evidence for linear  $[3\text{Fe-4S}]^+$  cluster is provided by the distinctive absorption bands at 566 and 513 nm, as reported for structurally and

spectroscopically characterized linear  $[3\text{Fe-4S}]^+$  clusters ((32;33) and Chapter 2). Fortunately, the linear  $[3\text{Fe-4S}]^+$  cluster-containing fraction of *Av* CGFS-Grxs can be chromatographically separated from the  $[2\text{Fe-2S}]^{2+}$  cluster-bound forms from the cysteine desulfurase-mediated reconstitution mixture, thus enabling the spectroscopic and functional studies of the exclusively  $[2\text{Fe-2S}]^{2+}$  cluster-bound forms of *Av* CGFS-Grxs (Figure 4.3).

Besides the strictly conserved active-site cysteine, a number of CGFS-Grxs also possess an additional cysteine residue at a position in the C-terminal domain that is 50 to 55 amino acids away from the active-site cysteine, but in close spatial proximity based on apo CGFS Grx structures (23;34;35). We have recently demonstrated that the recombinant *S. cerevisiae* mitochondrial Grx5 can reconstitute one cubane-type  $[4\text{Fe-4S}]^{2+}$  cluster per homodimer in the absence of GSH (see Chapter 2). Based on cysteine mutagenesis studies, the semi-conserved C-terminal cysteine residue in *Sc* Grx5 was proposed to coordinate the  $[4\text{Fe-4S}]^{2+}$  cluster at the subunit interface along with the strictly conserved cysteine (see Chapter 2). In the present study, we were interested in knowing whether Grx5 and Grx-nif from *A. vinelandii* are capable of accommodating a  $[4\text{Fe-4S}]^{2+}$  cluster *in vitro*, especially considering the potential involvements of Grx-nif in nitrogen fixation which specifically requires single and double cubane clusters. Therefore, *in vitro* anaerobic cysteine desulfurase-mediated reconstitution in the presence of DTT rather than GSH were carried out on both *Av* Grx5 and Grx-nif, duplicating the reaction conditions to obtain  $[4\text{Fe-4S}]^{2+}$  cluster-bound *Sc* Grx5 (see Chapter 2). After chromatographic removal of excess reagents, we failed to observe cluster-bound forms of neither *Av* Grx5 nor Grx-nif, indicating that both *Av* CGFS-Grxs are unable to accommodate a  $[4\text{Fe-4S}]^{2+}$  cluster (data not shown). As neither of the two *Av* CGFS-Grxs possess the additional cysteine residue,

the result is in agreement with our hypothesis that the semi-conserved cysteine is essential for the coordination of a  $[4\text{Fe-4S}]^{2+}$  cluster in CGFS-Grxs.

*In vitro* cluster transfer from  $[4\text{Fe-4S}]^{2+}$  cluster-bound scaffold and carrier proteins to apo Av CGFS-Grxs: Results from both *in vivo* and *in vitro* studies on several members of CGFS-Grxs, including Av Grx5 and Grx-nif, have provided compelling evidence supporting roles for this family of proteins in storage and mediating the intracellular transport of preassembled  $[2\text{Fe-2S}]^{2+}$  clusters ((13;15;20;23), Chapter 3, and Appendix C). In light of the recent report that Av  $\text{Nif}^{\text{IscA}}$  is competent to accept a  $[2\text{Fe-2S}]^{2+}$  cluster from  $[4\text{Fe-4S}]^{2+}$  cluster-loaded NifU, (see Appendix B), we were interested in determining if CGFS-Grxs has the potential to accept preassembled  $[4\text{Fe-4S}]^{2+}$  clusters or to participate in cluster storage of oxygen-sensitive  $[4\text{Fe-4S}]^{2+}$  clusters as  $[2\text{Fe-2S}]^{2+}$  clusters in a similar fashion to  $\text{Nif}^{\text{IscA}}$ . The experimental strategy was to monitor the time course of cluster transfer from  $[4\text{Fe-4S}]^{2+}$  cluster donors to apo-forms of Av Grx5 and Grx-nif using UV-visible CD spectroscopy. Due to the sensitivity of CD spectroscopy to the chirality induced by the protein folding in the vicinity of the biological Fe-S clusters, marked differences in CD spectra are usually observed for the same type cluster in different Fe-S cluster-containing proteins, making it the method of choice for monitoring the time course of cluster transfer experiments ((8;15), Chapter 3, and Appendices B and C). However, since protein-bound  $[4\text{Fe-4S}]^{2+}$  clusters, including  $[4\text{Fe-4S}]$  cluster-bound CGFS-Grxs (see Chapter 2), often exhibit low or negligible CD intensity, CD spectroscopy primarily facilitates the assessment of the extent of  $[2\text{Fe-2S}]^{2+}$  cluster formation on CGFS-Grxs in this study.

Cluster transfer experiments using apo Av Grx5 as the acceptor were carried out using  $[4\text{Fe-4S}]$ -IscU and  $[4\text{Fe-4S}]$ -NfuA as cluster donor. The essential IscU protein serves as the

primary scaffold for the ISC Fe-S cluster assembly machinery. *In vitro* anaerobic cysteine desulfurase-mediated cluster assembly leads to sequential formation of homodimeric IscU containing one  $[2\text{Fe-2S}]^{2+}$ , two  $[2\text{Fe-2S}]^{2+}$ , and one  $[4\text{Fe-4S}]^{2+}$  clusters (5;36). Quantitative comparison of UV-visible absorption and CD spectra of the  $[4\text{Fe-4S}]^{2+}$  cluster-containing IscU samples used for cluster transfer studies with those of homogeneous  $[2\text{Fe-2S}]^{2+}$  and  $[4\text{Fe-4S}]^{2+}$  cluster-bound forms of IscU, as assessed by Mössbauer studies, indicates that  $[4\text{Fe-4S}]^{2+}$  and  $[2\text{Fe-2S}]^{2+}$  clusters account for approximately 67 % and 33 %, respectively, of the total cluster content.

The room-temperature cluster transfer reaction from  $[4\text{Fe-4S}]$ -IscU (72  $\mu\text{M}$  in  $[4\text{Fe-4S}]^{2+}$  clusters) was carried out under anaerobic conditions in the presence of 3 mM of GSH using a 1:4 donor  $[4\text{Fe-4S}]$ :acceptor monomer stoichiometry. Since the  $[4\text{Fe-4S}]$ -IscU does not exhibit significant CD intensity, the CD spectrum before cluster transfer is dominated by the  $[2\text{Fe-2S}]$ -IscU (36  $\mu\text{M}$  in  $[2\text{Fe-2S}]^{2+}$  clusters) in the sample (Figure 4.4). The time course of cluster transfer from  $[4\text{Fe-4S}]$ -IscU to apo Grx5 is shown in Figure 4.4, and the marked changes observed in the CD spectra are consistent with loss of IscU  $[2\text{Fe-2S}]^{2+}$  clusters with concomitant formation of  $[2\text{Fe-2S}]^{2+}$  cluster-bound  $A_v$  Grx5. On the basis of the  $\Delta\epsilon$  values of the  $[2\text{Fe-2S}]$ -Grx5 determined in this study, quantitative analysis of the final CD spectra of the cluster transfer experiment revealed the formation of approximate 57  $\mu\text{M}$  of  $[2\text{Fe-2S}]$ -Grx5. Previous *in vitro*  $[2\text{Fe-2S}]$ -IscU to apo  $A_v$  Grx5 cluster transfer experiments carried out in the absence of chaperones and ATP, with a 3.4-fold excess of monomeric Grx5 per IscU  $[2\text{Fe-2S}]^{2+}$  cluster indicated ~ 30% cluster transfer over a period of 3 hours (see Chapter 3). Taking into consideration the much larger excess of apo  $A_v$  Grx5 monomer to  $[2\text{Fe-2S}]$ -IscU (8-fold excess) in the reaction mixture used in this study, which will certainly shift the reaction equilibrium

towards the [2Fe-2S]-Grx5 formation, coupled with the clean isobestic points observed in the CD spectra obtained for the cluster transfer time course (see Figure 4.4), it would appear that the majority of the [2Fe-2S]<sup>2+</sup> clusters (~36 μM) that were originally in IscU have been transferred intact to Av Grx5 after 2 hours of reaction. Based on studies of the stability of the [4Fe-4S]<sup>2+</sup> clusters on IscU under analogous conditions over a 2-hour time period, the remaining 21 μM of [2Fe-2S]-Grx5 that is formed is attributed primarily to free iron and sulfides released upon [4Fe-4S]<sup>2+</sup> cluster degradation during the course of the cluster transfer. However, we cannot rule out the possibility of some [4Fe-4S]<sup>2+</sup> cluster transfer followed by rapid oxidative cleavage to form [2Fe-2S]-Grx5, as observed for cluster transfer from [4Fe-4S]-NfuA (*vide infra*).

Although not encoded in the *A. vinelandii* Fe-S cluster biogenesis operon, the modular protein Av NfuA is proposed to function as intermediate cluster carrier. The N-terminal domain of NfuA shares sequence homology to IscA but lacks the cysteine residues essential for the function of A-type proteins, while the C-terminal domain shares sequence similarity to the C-terminal region of NifU (7). A [4Fe-4S]<sup>2+</sup> cluster can be assembled within a dimeric form of NfuA on its C-terminal domain, and the [4Fe-4S]<sup>2+</sup> cluster containing-NfuA has been shown to be competent for rapid *in vitro* activation of apo aconitase via intact transfer of a [4Fe-4S]<sup>2+</sup> cluster (7).

Cluster transfer experiments from [4Fe-4S]-NfuA to apo-Grx5 were initiated by adding 200 μM apo monomeric form of Av Grx5 to [4Fe-4S]-NfuA (50 μM in [4Fe-4S]<sup>2+</sup> cluster concentration) in the presence of 3 mM GSH under strictly anaerobic conditions. The CD spectrum of the [4Fe-4S]<sup>2+</sup> cluster in NfuA facilitates the direct monitoring of the cluster transfer from [4Fe-4S]-NfuA to apo Grx5 (Figure 4.5A). Simulated CD data were generated based on weighted averages of the CD spectra of [4Fe-4S]-NfuA and [2Fe-2S]-Grx5, and assuming

formation of two  $[2\text{Fe-2S}]^{2+}$  clusters on Grx5 from a single  $[4\text{Fe-4S}]^{2+}$  cluster on NfuA (Figure 4.5B). The agreement between the experimental and simulated data suggests intact cluster transfer. Moreover, a control CD study showed  $\sim 20\%$  degradation of the  $[4\text{Fe-4S}]^{2+}$  cluster on NfuA under identical reaction conditions in the absence of Grx5 (data not shown). This observation further supports our conclusion of intact cluster transfer and at same time argues strongly against cluster degradation and reassembly on apo-Grx5. Quantitative analysis of the final CD spectra of the cluster transfer experiment revealed the formation of approximate  $76 \mu\text{M}$  of  $[2\text{Fe-2S}]\text{-Grx5}$  from  $[4\text{Fe-4S}]\text{-NfuA}$  ( $50 \mu\text{M}$  in  $[4\text{Fe-4S}]^{2+}$  cluster concentration). Taken together, the results of cluster transfer from  $[4\text{Fe-4S}]\text{-NfuA}$  to apo-Grx5 are most consistent with Grx5 facilitating  $[4\text{Fe-4S}]^{2+} \rightarrow 2 [2\text{Fe-2S}]^{2+}$  conversion, probably via initial transfer of a  $[4\text{Fe-4S}]^{2+}$  cluster, followed by oxidative cleavage into two  $[2\text{Fe-2S}]^{2+}$  clusters in the presence of excess Grx5 and GSH.

For cluster transfer experiments involving *Av* Grx-nif, the holo form of *Av* NifU was selected as a potential cluster donor as *grx-nif* is part of one of the two *nif* operons in *A. vinelandii* (25). NifU is a modular protein comprising an IscU-like N-terminal domain that is able to sequentially assemble a  $[2\text{Fe-2S}]^{2+}$  and  $[4\text{Fe-4S}]^{2+}$  cluster, a central  $[2\text{Fe-2S}]^{2+,+}$  cluster-containing ferredoxin-like domain, and a C-terminal Nfu-like domain that can accommodate a  $[4\text{Fe-4S}]^{2+}$  cluster (6). The dimeric holo form of NifU that results from NifS-mediated anaerobic reconstitution contains one subunit-bridging  $[4\text{Fe-4S}]^{2+}$  cluster in the N-terminal and C-terminal domains and one permanent redox-active  $[2\text{Fe-2S}]^{2+,+}$  cluster in the central domain (6). The CD spectrum of the holo NifU has been shown to be dominated by the permanent, redox-active  $[2\text{Fe-2S}]^{2+}$  cluster which does not participate in the cluster transfer, while the  $[4\text{Fe-4S}]^{2+}$  cluster

centers in both N-terminal and C-terminal domains have negligible contribution to the CD intensity (Appendix B), see Figure 4.6A.

For the cluster transfer experiment, 144  $\mu\text{M}$  of apo-Grx-nif monomer was added to 14  $\mu\text{M}$  holo NifU (14  $\mu\text{M}$  in both  $[\text{4Fe-4S}]^{2+}$  and permanent  $[\text{2Fe-2S}]^{2+}$  clusters), in the presence of 3 mM GSH. Marked changes in the CD spectra were observed upon addition of apo Grx-nif over a 60-minute time period, notably the continuous increases in CD intensity at 308, 346, and 460 nm (Figure 4.6A). Consequently, subtraction of the CD spectrum of the permanent  $[\text{2Fe-2S}]^{2+}$  cluster on NifU central domain enables the time course of  $[\text{2Fe-2S}]$ -Grx-nif formation to be assessed (Figure 4.6B). On the basis of  $\Delta\epsilon_{461} = 14.0 \pm 1.0 \text{ M}^{-1}\text{cm}^{-1}$  for the  $[\text{2Fe-2S}]^{2+}$  cluster in Grx-nif and the initial concentration of NifU  $[\text{4Fe-4S}]^{2+}$  clusters (14  $\mu\text{M}$ ), the final resultant CD spectrum corresponds to formation of 13  $\mu\text{M}$  of  $[\text{2Fe-2S}]^{2+}$  clusters on Grx-nif. Taken at face value, the amount of  $[\text{2Fe-2S}]$ -Grx-nif might suggest that the cluster transfer is accompanied by  $[\text{4Fe-4S}]^{2+} \rightarrow [\text{2Fe-2S}]^{2+}$  cluster conversion with loss of iron and sulfide. However, the results are not conclusive with respect to quantitative assessment of the extent of cluster transfer, as it is also possible that some or all of the  $[\text{2Fe-2S}]$ -Grx-nif could have resulted from degradation of  $[\text{4Fe-4S}]^{2+}$  clusters in NifU.

The presence of two  $[\text{4Fe-4S}]^{2+}$  cluster-binding domain in the full-length NifU additionally raises the question concerning whether the cluster transfer exclusively involves only one of the two domains, or that both the IscU- and Nfu-like domains can transfer clusters to Grx-nif. To address this question, we performed cluster transfer experiments using truncated forms of NifU comprising individual scaffolding domains as  $[\text{4Fe-4S}]^{2+}$  cluster donors. The truncated forms of NifU used were holo NifU1 which comprises only the N-terminal domain fragment of NifU and contains one  $[\text{4Fe-4S}]^{2+}$  cluster per dimer and holo NifU2 which contains both central

and C-terminal domain fragments of NifU and contains two permanent  $[2\text{Fe-2S}]^{2+}$  clusters and one  $[4\text{Fe-4S}]^{2+}$  cluster per dimer (6). The results showed that Grx-nif is able to accept  $[2\text{Fe-2S}]^{2+}$  clusters from both  $[4\text{Fe-4S}]$ -NifU1 and holo-NifU2 (with  $[4\text{Fe-4S}]^{2+}$  cluster in the C-terminal domain), with similar rates of cluster transfer, but not from  $[2\text{Fe-2S}]$ -NifU1 (data not shown). Thus both of the two cluster scaffolding domains on NifU appear to be competent for effecting the formation of  $[2\text{Fe-2S}]$ -Grx-nif.

## Discussion

Glutaredoxins with the signature CGFS active-site motif constitute a class of Grxs that are critically involved in several important aspects of Fe metabolism and homeostasis, such as Fe-S cluster biogenesis, intracellular iron trafficking as well as Fe-sensing and regulation (12;15;18;21;37). These proposed functions of CGFS-Grxs have been shown to be closely associated with their ability to ligate a subunit-bridging  $[2\text{Fe-2S}]^{2+}$  cluster at the homodimer interface coordinated by the CGFS active-site cysteine residue of each monomer and the cysteine moiety of two glutathione molecules, and to transfer the clusters to apo acceptor proteins ((15;23;24), see also Chapter 3 and Appendix C). In this work, we have investigated the nature and properties of the Fe-S clusters assembled on recombinant *Av* Grx5 and Grx-nif. Using a combination of spectroscopic and analytical techniques, we demonstrate that both *Av* Grx5 and Grx-nif can form a  $[2\text{Fe-2S}]^{2+}$  cluster-containing homodimer. The close resemblance of the electronic and vibrational properties of the  $[2\text{Fe-2S}]^{2+}$  centers in *Av* CGFS-Grxs to those reported of spectroscopically and structurally characterized CGFS-Grxs from other organisms, suggests complete cysteinyl ligation of the  $[2\text{Fe-2S}]^{2+}$  cluster that is analogous to that observed in other  $[2\text{Fe-2S}]^{2+}$  cluster containing CGFS-Grx homodimers (15;18;19;23;24).

An alternative Fe-S cluster scaffold function was initially proposed for CGFS-Grxs based on their ability to incorporate a labile  $[2\text{Fe-2S}]^{2+}$  cluster via cysteine desulfurase-mediated cluster assembly and to rapidly transfer the cluster to physiologically relevant proteins (15). However, a scaffolding role of CGFS-Grxs seems unlikely as there is currently no evidence indicating functional interaction between CGFS-Grxs and cysteine desulfurases. Consequently, the identity of the physiological cluster donor to CGFS-Grxs needs to be addressed. Recently, we have reported extremely rapid and quantitative cluster transfer from  $[2\text{Fe-2S}]$ -IscU to apo *Av* Grx5 only in the presence of the dedicated HscA/HscB co-chaperone system and Mg-ATP (see Chapter 3). Coupled with the *in vivo* evidence of Fe accumulation on yeast *S. cerevisiae* mitochondrial Isu1 in  $\Delta\text{grx5}$  strains (13), the  $[2\text{Fe-2S}]^{2+}$  cluster-bound form of IscU is most likely the cluster donor to *Av* Grx5 under physiological conditions. On the other hand, the nature of the physiological  $[2\text{Fe-2S}]^{2+}$  cluster source to Grx-nif remains unclear. In this study, we failed to observe cluster transfer from  $[2\text{Fe-2S}]$ -NifU1, the IscU-like N-terminal domain of NifU, to apo *Av* Grx-nif. This may be attributed to small conformational differences between the wild-type and truncated form of NifU that could subsequently affect physical interactions with Grx-nif. However, the means by which *Av* Grx-nif obtains its  $[2\text{Fe-2S}]^{2+}$  cluster remain to be elucidated.

Following the results of *in vivo* and *in vitro* studies, it has been generally accepted that CGFS-Grxs provide a cluster storage or transfer role for the  $[2\text{Fe-2S}]^{2+}$  clusters assembled on IscU scaffold protein ((13), Chapter 3 and Appendix C). Inspired by this proposal, one of the initial objectives of this work was to investigate whether such a cluster storage role can be extended to include  $[4\text{Fe-4S}]^{2+}$  clusters assembled on U-type or Nfu-type proteins. To date we have found no evidence that *Av* Grx5 or Grx-nif can assemble  $[4\text{Fe-4S}]^{2+}$  clusters via cysteine

desulfurase-mediated reconstitution in the absence of GSH or cluster transfer from  $[4\text{Fe-4S}]^{2+}$  cluster-loaded forms of IscU or NifU.

In contrast, the work presented herein demonstrates that Grx5 can accept  $[2\text{Fe-2S}]^{2+}$  clusters from  $[4\text{Fe-4S}]$ -NfuA, via a process that appears to involve  $[4\text{Fe-4S}]^{2+}$  transfer followed by oxidative  $[4\text{Fe-4S}]^{2+}$  cleavage to yield two  $[2\text{Fe-2S}]^{2+}$  cluster-bound Grx5 homodimers, in the presence of excess Grx5 and GSH. Cluster transfer experiments involving  $[4\text{Fe-4S}]^{2+}$  cluster loaded IscU and NifU with apo Grx5 and Grx-nif, respectively, also indicate some formation of  $[2\text{Fe-2S}]^{2+}$  cluster-bound Grx5 and Grx-nif. However, the extent to which this is occurring via  $[4\text{Fe-4S}]^{2+}$  cluster transfer followed by loss of iron and sulfide or  $[4\text{Fe-4S}]^{2+}$  cluster degradation and assembly of  $[2\text{Fe-2S}]^{2+}$  clusters on Grx5 and Grx-nif from the released iron and sulfide has yet to be definitively established. Precedents for cluster transfers that result in  $[4\text{Fe-4S}]^{2+}$  to 2  $[2\text{Fe-2S}]^{2+}$  cluster conversions are provided by  $[4\text{Fe-4S}]^{2+}$  cluster-bound *E. coli* SufBCD acting as a cluster donor to form  $[2\text{Fe-2S}]^{2+}$  cluster-bound *E. coli* SufA (38) and  $[4\text{Fe-4S}]^{2+}$  cluster-loaded *A. vinlandii* NifU acting as a cluster donor to form  $[2\text{Fe-2S}]^{2+}$  cluster-bound <sup>Nif</sup>IscA (see Appendix B). In both cases the reaction proceeds without significant loss of iron and sulfide, as is the case for the  $[4\text{Fe-4S}]^{2+}$  cluster-bound *Av* NfuA to  $[2\text{Fe-2S}]^{2+}$  cluster-bound Grx5 reported in this work. The detailed mechanism of cluster transfer accompanied by cluster conversion is not yet clear. However, in light of the ability of <sup>Nif</sup>IscA to cycle between  $[2\text{Fe-2S}]^{2+}$  and  $[4\text{Fe-4S}]^{2+}$  cluster-containing forms (see Appendix B), it has been postulated that the mechanism for cluster transfer to A-type proteins involves  $[4\text{Fe-4S}]^{2+}$  cluster transfer followed by oxidative cleavage to yield two homodimeric  $[2\text{Fe-2S}]^{2+}$  cluster-bound A-type proteins in the presence of excess A-type protein. However, the molecular mechanism of cluster transfer from  $[4\text{Fe-4S}]$ -

NfuA to Av apo-Grx5 may be different than that previously proposed for A-type proteins, as Av Grx5 does not appear to accommodate a stable  $[4\text{Fe-4S}]^{2+}$  cluster in the homodimeric form.

UV-visible CD spectroscopy has been shown to be very effective for investigating the time course of interprotein cluster transfer experiments *in vitro* ((8;15), Chapter 3, and Appendices B and C). However, the studies described in this work have underlined the limitations of this approach in studying cluster transfer experiment involving samples that do not exhibit significant CD intensity, e.g. most protein-bound  $[4\text{Fe-4S}]^{2+}$  clusters. As other biophysical techniques frequently used in the Fe-S protein characterization, including UV-visible absorption, X-ray absorption, EPR and Mössbauer spectroscopies, are not sensitive to the protein secondary structure in the vicinity of the bound Fe-S clusters, a more selective experimental method needs to be developed to enable the mechanistic and kinetic studies of  $[4\text{Fe-4S}]^{2+}$  cluster transfers that do not involve either changes in the cluster coordination environment and/or increase or loss of enzymatic activities.

Taking into consideration that biological  $[4\text{Fe-4S}]^{2+}$  clusters are often susceptible to oxygen-induced degradation, with  $[2\text{Fe-2S}]^{2+}$  cluster being major cluster break-down product (5;36;39;40), the results of the *in vitro* cluster transfer reactions presented herein nevertheless suggest a potential role for CGFS-Grxs in cluster storage under oxidative stress conditions, in addition to storing pre-assembled  $[2\text{Fe-2S}]^{2+}$  clusters under Fe-replete conditions as previously demonstrated (see Chapter 3). Such a role is consistent with the Fe accumulation and increased sensitivity to oxidative stress displayed by the *S. cerevisiae*  $\Delta\text{grx5}$  mutant (11). Studies of cysteine desulfurase-mediated assembly of  $[4\text{Fe-4S}]^{2+}$  clusters on IscU (36) and the functions of A-type proteins in Fe-S cluster assembly (see Appendices A and B), coupled with recent studies of the oxygen-sensing mechanism of bacterial fumarate and nitrate reduction transcriptional

regulatory protein (FNR) (see Chapter 5) have led to discovery of two potential mechanisms for the assembly or repair of oxygen-damaged [4Fe-4S] cluster using components of the ISC and NIF systems. One being the reductive coupling of two [2Fe-2S]<sup>2+</sup> clusters, and the other involving formation of cysteine persulfide-ligated [2Fe-2S]<sup>2+</sup> cluster and Fe<sup>2+</sup> insertion (see Chapter 5 and Appendix B). Moreover, the formation of protein-bound persulfides or polysulfides has been demonstrated by Kennedy and Beinert via controlled oxidation-induced damage of [4Fe-4S]<sup>2+</sup> cluster in aconitase (41). In light of these findings, it is possible that CGFS-Grxs may also contribute indirectly to the repair of [4Fe-4S]<sup>2+</sup> cluster by intact transfer of [2Fe-2S]<sup>2+</sup> cluster to proteins that are able to reductively convert [2Fe-2S]<sup>2+</sup> to [4Fe-4S]<sup>2+</sup> clusters or to yield [2Fe-2S]<sup>2+</sup> clusters with cysteine persulfide ligands in an early step for [4Fe-4S]<sup>2+</sup> cluster repair. Thus the decreased activity of the nitrogenase Fe-protein observed in the strain lacking *grx-nif* gene might be interpreted as a result of a deficiency in the repair of its [4Fe-4S]<sup>2+</sup> cluster due to the inactivation of *grx-nif* gene (25). This is further supported by recent demonstration of rapid and quantitative transfer of a [2Fe-2S]<sup>2+</sup> cluster from Grx-nif to Nif<sup>+</sup>IscA, which can then undergo reversible cycling between [2Fe-2S]<sup>2+</sup> and [4Fe-4S]<sup>2+</sup> cluster-bound forms in response to cellular redox status and effect maturation of the nitrogenase Fe-protein *in vitro* using the [4Fe-4S]<sup>2+</sup> cluster-containing form (see Appendices B and C). Alternatively, the involvement of *Av* Grx-nif in the NIF system may lie in its proposed role as a [2Fe-2S]<sup>2+</sup> cluster carrier (see Appendix C). One of the mechanisms that *Azotobacter* species employ to protect nitrogenase from oxygen damage involves association of FeSII, a [2Fe-2S] cluster-containing protective protein, with nitrogenase during oxidative stress conditions (42-44). FeSII binding protects nitrogenase from irreversible loss of activity under elevated oxygen levels (42;43). Therefore, *Av* Grx-nif may serve as immediate [2Fe-2S] cluster donor for FeSII and thereby be

indirectly involve in the protection mechanism against oxygen damage. However, more work is needed to verify that the ability to accept a  $[2\text{Fe-2S}]^{2+}$  clusters from  $[4\text{Fe-4S}]$  cluster donor proteins is a shared feature by CGFS-Grxs.

In this study, we have also reported the presence of linear  $[3\text{Fe-4S}]^+$  clusters in both aerobically purified and anaerobically reconstituted *Av* CGFS-Grxs on the basis of the distinctive absorption features of linear  $[3\text{Fe-4S}]^+$  clusters in the 500 – 600 nm region in the UV-visible absorption spectra (32;33). The observation of linear  $[3\text{Fe-4S}]^+$  cluster-bound forms of *Av* CGFS-Grxs inevitably raises the question regarding the origin of this species. This work demonstrates that linear  $[3\text{Fe-4S}]^+$  cluster-bound forms of CGFS-Grxs can be generated by reconstitution of the apo protein under rigorous anaerobic conditions and by aerobic purification of the recombinant protein, but not by anaerobic purification of the recombinant protein. Based on the available evidence, it would appear that different CGFS-Grxs vary significantly in their propensity to incorporate  $[2\text{Fe-2S}]^{2+}$  and/or linear  $[3\text{Fe-4S}]^+$  clusters during anaerobic reconstitution in the presence of GSH (see chapter 2). We tentatively attribute this to small structural differences in CGFS-Grxs. However, the observation that linear  $[3\text{Fe-4S}]^+$  clusters are only observed in as-purified recombinant CGFS-Grxs when the purification is carried out under aerobic conditions, implicates a role for oxygen in generating linear  $[3\text{Fe-4S}]^+$  cluster-bound forms of CGFS-Grxs *in vivo*. In light of the evidence for the formation of linear  $[3\text{Fe-4S}]^+$  clusters during  $\text{O}_2$ -induced degradation of  $[2\text{Fe-2S}]^{2+}$ , cubane-type  $[3\text{Fe-4S}]^+$ , and  $[4\text{Fe-4S}]^{2+}$  clusters under protein denaturation conditions (33;45-49), this suggests a potential role for CGFS-Grxs in scavenging linear  $[3\text{Fe-4S}]^+$  clusters released due to protein unfolding under oxidative stress conditions. The observation of linear  $[3\text{Fe-4S}]^+$  cluster-bound forms of *Av* CGFS-Grxs suggests that the ability to accommodate this type of cluster may be a common

attribute to this family of proteins, although the significance of this result remains to be fully elucidated (see Chapter 2).

### **Acknowledgements**

We thank Dr. Dennis Dean and his coworkers at Virginia Tech for supplying the plasmids for the proteins used in this work.

## References

1. Frazzon, J. and Dean, D. R. (2003) Formation of iron-sulfur clusters in bacteria: An emerging field in bioinorganic chemistry, *Curr. Opin. Chem. Biol.* 7, 166-173.
2. Johnson, D. C., Dean, D. R., Smith, A. D., and Johnson, M. K. (2005) Structure, function and formation of biological iron-sulfur clusters, *Annu. Rev. Biochem.* 74, 247-281.
3. Johnson, D. C., Unciuleac, M.-C., and Dean, D. R. (2006) Controlled expression and functional analysis of iron-sulfur cluster biosynthetic components within *Azotobacter vinelandii*, *J. Bacteriol.* 188, 7551-7561.
4. Dos Santos, P. C., Johnson, D. C., Ragle, B. E., Unciuleac, M.-C., and Dean, D. R. (2007) Controlled expression of *nif* and *isc* iron-sulfur protein maturation components reveals target specificity and limited functional replacement between the two systems, *J. Bacteriol.* 189, 2854-2862.
5. Agar, J. N., Krebs, B., Frazzon, J., Huynh, B. H., Dean, D. R., and Johnson, M. K. (2000) IscU as a scaffold for iron-sulfur cluster biosynthesis: Sequential assembly of [2Fe-2S] and [4Fe-4S] clusters in IscU, *Biochemistry* 39, 7856-7862.
6. Smith, A. D., Jameson, G. N. L., Dos Santos, P. C., Agar, J. N., Naik, S., Krebs, C., Frazzon, J., Dean, D. R., Huynh, B. H., and Johnson, M. K. (2005) NifS-mediated assembly of [4Fe-4S] clusters in the N- and C-terminal domains of the NifU scaffold protein, *Biochemistry* 44, 12955-12969.
7. Bandyopadhyay, S., Naik, S., O'Carroll, I. P., Huynh, B. H., Dean, D. R., Johnson, M. K., and Dos Santos, P. C. (2008) A proposed role for the *Azotobacter vinelandii* NfuA protein as an intermediate iron-sulfur cluster carrier, *J. Biol. Chem.* 283, 14092-14099.
8. Chandramouli, K. and Johnson, M. K. (2006) HscA and HscB stimulate [2Fe-2S] cluster transfer from IscU to apoferredoxin in an ATP-dependent reaction, *Biochemistry* 45, 11087-11095.
9. Unciuleac, M.-C., Chandramouli, K., Naik, S., Mayer, S., Huynh, B. H., Johnson, M. K., and Dean, D. R. (2007) *In vitro* activation of apo-aconitase using a [4Fe-4S] cluster-loaded form of the IscU [Fe-S] cluster scaffolding protein, *Biochemistry* 46, 6812-6821.
10. Dos Santos, P. C., Smith, A. D., Frazzon, J., Cash, V. L., Johnson, M. K., and Dean, D. R. (2004) Iron-sulfur cluster assembly: NifU-directed activation of the nitrogenase Fe-protein, *J. Biol. Chem.* 279, 19705-19711.
11. Rodríguez-Manzanegue, M. T., Ros, J., Cabrito, I., Sorribas, A., and Herrero, E. (1999) Grx5 glutaredoxin plays a central role in protection against protein oxidative damage in *Saccharomyces cerevisiae*, *Mol. Cell. Biol.* 19, 8180-8190.

12. Rodríguez-Manzanares, M. T., Tamarit, J., Bellí, G., Ros, J., and Herrero, E. (2002) Grx5 is a mitochondrial glutaredoxin required for the activity of iron/sulfur enzymes, *Mol. Biol. Cell* 13, 1109-1121.
13. Mühlhoff, U., Gerber, J., Richhardt, N., and Lill, R. (2003) Components involved in assembly and dislocation of iron-sulfur clusters on the scaffold protein Isc1p, *EMBO J.* 22, 4815-4825.
14. Picciocchi, A., Saguez, C., Boussac, A., Cassier-Chauvat, C., and Chauvat, F. (2007) CGFS-type monothiol glutaredoxins from the cyanobacterium *Synechocystis* PCC6803 and other evolutionary distant model organisms possess a glutathione-ligated [2Fe-2S] cluster, *Biochemistry* 46, 15018-15026.
15. Bandyopadhyay, S., Gama, F., Molina-Navarro, M. M., Gualberto, J. M., Claxton, R., Naik, S. G., Huynh, B. H., Herrero, E., Jacquot, J.-P., Johnson, M. K., and Rouhier, N. (2008) Chloroplast monothiol glutaredoxins as scaffold proteins for the assembly and delivery of [2Fe-2S] clusters, *EMBO J.* 27, 1122-1133.
16. Wingert, R. A., Galloway, J. L., Barut, B., Foott, H., Fraenkel, P., Axe, J. L., Weber, G. J., Dooley, K., Davidson, A. J., Schmidt, B., Paw, B. H., and Shaw, G. C. (2005) Deficiency of glutaredoxin 5 reveals Fe-S clusters are required for vertebrate haem synthesis, *Nature* 436, 1035-1039.
17. Ye, H., Jeong, S. Y., Ghosh, M. C., Kovtunovych, G., Silvestri, L., Ortillo, D., Uchida, N., Tisdale, J., Camaschella, C., and Rouault, T. A. (2010) Glutaredoxin 5 deficiency causes sideroblastic anemia by specifically impairing heme biosynthesis and depleting cytosolic iron in human erythroblasts, *J. Clin. Invest.* 120, 1749-1761.
18. Li, H., Mapolelo, D. T., Dingra, N. N., Naik, S. G., Lees, N. S., Hoffman, B. M., Riggs-Gelasco, P. J., Huynh, B. H., Johnson, M. K., and Outten, C. E. (2009) The yeast iron regulatory proteins Grx3/4 and Fra2 form heterodimeric complexes containing a [2Fe-2S] cluster with cysteinyl and histidyl ligation, *Biochemistry* 48, 9569-9581.
19. Li, H., Mapolelo, D. T., Randeniya, S., Johnson, M. K., and Outten, C. E. (2012) Human Glutaredoxin 3 Forms [2Fe-2S]-Bridged Complexes with Human BolA2, *Biochemistry* 51, 1687-1696.
20. Yeung, N., Gold, B., Liu, N. L., Prathapam, R., Sterling, H. J., Williams, E. R., and Butland, G. (2011) The *E. coli* monothiol glutaredoxin GrxD forms homodimeric and heterodimeric FeS cluster containing complexes, *Biochemistry* 50, 8957-8969.
21. Mühlhoff, U., Molik, S., Godoy, J. R., Uzarska, M. A., Richter, N., Seubert, A., Zhang, Y., Stubbe, J., Pierrel, F., Herrero, E., Lillig, C. H., and Lill, R. (2010) Cytosolic monothiol glutaredoxins function in intracellular iron sensing and trafficking via their bound iron-sulfur cluster, *Cell Metab.* 12, 373-385.

22. Haunhorst, P., Berndt, C., Eitner, S., Godoy, J. R., and Lillig, C. H. (2010) Characterization of the human monothiol glutaredoxin 3 (PICOT) as iron-sulfur protein, *Biochem. Biophys. Res. Commun.* 394, 372-376.
23. Iwema, T., Picciocchi, A., Traore, D. A., Ferrer, J. L., Chauvat, F., and Jacquamet, L. (2009) Structural basis for delivery of the intact [Fe<sub>2</sub>S<sub>2</sub>] cluster by monothiol glutaredoxin, *Biochemistry* 48, 6041-6043.
24. Johansson, C., Roos, A. K., Montano, S. J., Sengupta, R., Filippakopoulos, P., Guo, K., von, D. F., Holmgren, A., Oppermann, U., and Kavanagh, K. L. (2011) The crystal structure of human GLRX5: iron-sulfur cluster co-ordination, tetrameric assembly and monomer activity, *Biochem. J.* 433, 303-311.
25. Setubal, J. C., dos, S. P., Goldman, B. S., Ertesvag, H., Espin, G., Rubio, L. M., Valla, S., Almeida, N. F., Balasubramanian, D., Cromes, L., Curatti, L., Du, Z., Godsy, E., Goodner, B., Hellner-Burris, K., Hernandez, J. A., Houmiel, K., Imperial, J., Kennedy, C., Larson, T. J., Latreille, P., Ligon, L. S., Lu, J., Maerk, M., Miller, N. M., Norton, S., O'Carroll, I. P., Paulsen, I., Raulfs, E. C., Roemer, R., Rosser, J., Segura, D., Slater, S., Stricklin, S. L., Studholme, D. J., Sun, J., Viana, C. J., Wallin, E., Wang, B., Wheeler, C., Zhu, H., Dean, D. R., Dixon, R., and Wood, D. (2009) Genome sequence of *Azotobacter vinelandii*, an obligate aerobe specialized to support diverse anaerobic metabolic processes, *J. Bacteriol.* 191, 4534-4545.
26. Yuvaniyama, P., Agar, J. N., Cash, V. L., Johnson, M. K., and Dean, D. R. (2000) NifS-directed assembly of a transient [2Fe-2S] cluster within the NifU protein, *Proc. Natl. Acad. Sci. USA* 97, 599-604.
27. Fish, W. W. (1988) Rapid colorimetric micromethod for the quantitation of complexed iron in biological samples, *Meth. Enzymol.* 158, 357-364.
28. Drozdowski, P. M. and Johnson, M. K. (1988) A simple anaerobic cell for low temperature Raman spectroscopy, *Appl. Spectrosc.* 42, 1575-1577.
29. Dailey, H. A., Finnegan, M. G., and Johnson, M. K. (1994) Human ferrochelatase is an iron-sulfur protein, *Biochemistry* 33, 403-407.
30. Han, S., Czernuszewicz, R. S., Kimura, T., Adams, M. W. W., and Spiro, T. G. (1989) Fe<sub>2</sub>S<sub>2</sub> protein resonance Raman revisited: Structural variations among adrenodoxin, ferredoxin, and red paramagnetic protein, *J. Am. Chem. Soc.* 111, 3505-3511.
31. Fu, W., Drozdowski, P. M., Davies, M. D., Sligar, S. G., and Johnson, M. K. (1992) Resonance Raman and magnetic circular dichroism studies of reduced [2Fe-2S] proteins, *J. Biol. Chem.* 267, 15502-15510.
32. Hagen, K. S., Watson, A. D., and Holm, R. H. (1983) Synthetic routes to Fe<sub>2</sub>S<sub>2</sub>, Fe<sub>3</sub>S<sub>4</sub>, Fe<sub>4</sub>S<sub>4</sub>, and Fe<sub>6</sub>S<sub>9</sub> clusters from the common precursor [Fe(SC<sub>2</sub>H<sub>5</sub>)<sub>4</sub>]<sup>2-</sup>: Structures and properties of [Fe<sub>3</sub>S<sub>4</sub>(SR)<sub>4</sub>]<sup>3-</sup> and [Fe<sub>6</sub>S<sub>9</sub>(SC<sub>2</sub>H<sub>5</sub>)<sub>2</sub>]<sup>4-</sup>, examples of the newest types of Fe-S-SR clusters, *J. Am. Chem. Soc.* 105, 3905-3913.

33. Kennedy, M. C., Kent, T. A., Emptage, M. H., Merkle, H., Beinert, H., and Münck, E. (1984) Evidence for the formation of a linear [3Fe-4S] cluster in partially unfolded aconitase, *J. Biol. Chem.* 259, 14463-14471.
34. Herrero, E. and de la Torre-Ruiz, M. A. (2007) Monothiol glutaredoxins: a common domain for multiple functions, *Cell. Mol. Life Sci.* 64, 1518-1530.
35. Fladvad, M., Bellanda, M., Fernandes, A. P., Mammi, S., Vlamis-Gardikas, A., Holmgren, A., and Sunnerhagen, M. (2005) Molecular mapping of functionalities in the solution structure of reduced Grx4, a monothiol glutaredoxin from *Escherichia coli*, *J. Biol. Chem.* 280, 24553-24561.
36. Chandramouli, K., Unciuleac, M.-C., Naik, S., Dean, D. R., Huynh, B. H., and Johnson, M. K. (2007) Formation and properties of [4Fe-4S] clusters on the IscU scaffold protein, *Biochemistry* 46, 6804-6811.
37. Li, H. and Outten, C. E. (2012) Monothiol CGFS Glutaredoxins and BolA-like Proteins: [2Fe-2S] Binding Partners in Iron Homeostasis, *Biochemistry* 51, 4377-4389.
38. Chahal, H. K., Dai, Y., Saini, A., Ayala-Castro, C., and Outten, F. W. (2009) The SufBCD Fe-S scaffold complex interacts with SufA for Fe-S cluster transfer, *Biochemistry* 48, 10644-10653.
39. Johnson, M. K. and Smith, A. D. Iron-sulfur proteins. In *Encyclopedia of Inorganic Chemistry, Second Edition*; King, R. B.; John Wiley & Sons; 2005; 2589-2619.
40. Khoroshilova, N., Popescu, C., Münck, E., Beinert, H., and Kiley, P. J. (1997) Iron-sulfur cluster disassembly in the FNR protein of *Escherichia coli* by O<sub>2</sub>: [4Fe-4S] to [2Fe-2S] conversion with loss of biological activity, *Proc. Natl. Acad. Sci. USA* 94, 6087-6092.
41. Beinert, H. (1983) Semi-micro methods for analysis of labile sulfide and of labile sulfide plus sulfane sulfur in unusually stable iron-sulfur proteins, *Anal. Biochem.* 131, 373-378.
42. Moshiri, F., Kim, J. W., Fu, C., and Maier, R. J. (1994) The FeSII protein of *Azotobacter vinelandii* is not essential for aerobic nitrogen fixation, but confers significant protection to oxygen-mediated inactivation of nitrogenase in vitro and in vivo, *Mol. Microbiol.* 14, 101-114.
43. Robson, R. L. (1979) Characterization of an oxygen-stable nitrogenase complex isolated from *Azotobacter chroococcum*, *Biochem. J.* 34, 569-575.
44. Moshiri, F., Crouse, B. R., Johnson, M. K., and Maier, R. J. (1995) The "nitrogenase-protective" FeSII protein of *Azotobacter vinelandii*: overexpression, characterization and crystallization, *Biochemistry* 34, 12973-12982.
45. Krebs, C., Henshaw, T. F., Cheek, J., Huynh, B. H., and Broderick, J. B. (2000) Conversion of 3Fe-4S to 4Fe-4S Clusters in Native Pyruvate Formate-Lyase Activating

Enzyme: Mössbauer Characterization and Implications for Mechanism, *J. Am. Chem. Soc.* 122, 12497-12506.

46. Jones, K., Gomes, C. M., Huber, H., Teixeira, M., and Wittung-Stafshede, P. (2002) Formation of a linear [3Fe-4S] cluster in a seven-iron ferredoxin triggered by polypeptide unfolding, *J. Biol. Inorg. Chem.* 7, 357-362.
47. Leal, S. S., Teixeira, M., and Gomes, C. M. (2004) Studies on the degradation pathway of iron-sulfur centers during unfolding of a hyperstable ferredoxin: Cluster dissociation, iron release and proteins stability, *J. Biol. Inorg. Chem.* 9, 987-996.
48. Higgins, C. L. and Wittung-Stafshede, P. (2004) Formation of linear three-iron clusters in *Aquilex aeolicus* two-iron ferredoxins: effect of protein unfolding speed, *Arch. Biochem. Biophys.* 427, 154-163.
49. Griffin, S., Higgins, C. L., Soulimane, T., and Wittung-Stafshede, P. (2003) High thermal and chemical stability of *Thermus thermophilus* seven-iron ferredoxin. Linear clusters form at high pH on polypeptide unfolding, *Eur. J. Biochem.* 270, 4736-4743.

Figure 4.1: UV-visible absorption and visible CD spectra of [2Fe-2S]-Grx5 (solid lines) and [2Fe-2S]-Grx-nif (broken lines). Spectra were recorded under anaerobic conditions in sealed 0.1 cm cuvettes in 100 mM Tris-HCl buffer with 1 mM GSH at pH 7.8. The  $\epsilon$  and  $\Delta\epsilon$  values are based on the [2Fe-2S]<sup>2+</sup> cluster concentrations.

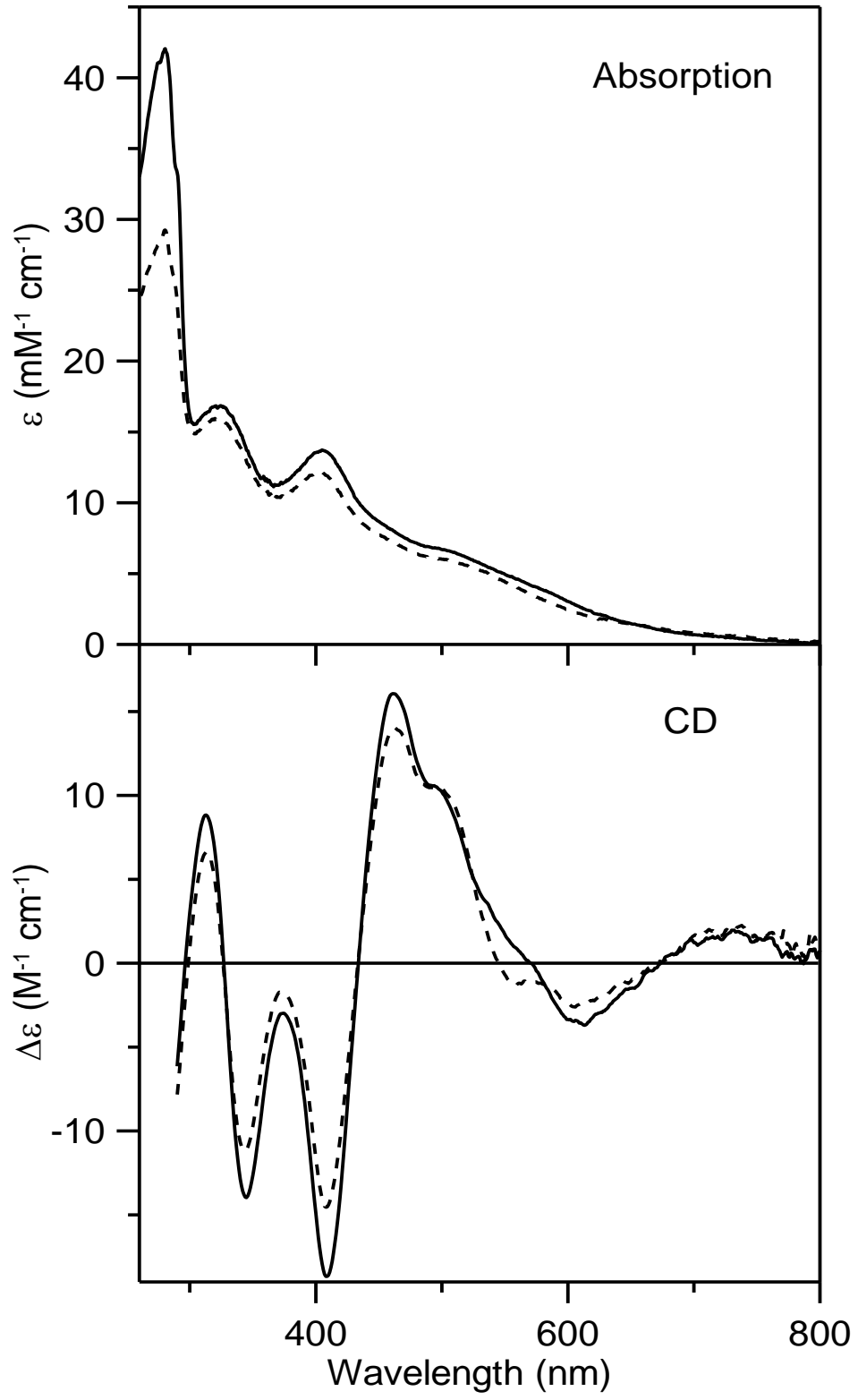


Figure 4.2: Resonance Raman spectra of [2Fe-2S]-Grx5 (solid lines) and [2Fe-2S]-Grx-nif (broken lines) with 457.9, 487.9 and 514.5 nm laser excitations. The sample contained ~ 2 mM of [2Fe-2S]<sup>2+</sup> cluster in 100 mM Tris-HCl buffer with 1 mM GSH at pH 7.8 and was in the form of a frozen droplet at 17 K. Each spectrum is the sum of 100 individual scans with each scan involving photon counting for 1 s at 0.5 cm<sup>-1</sup> increment with 7 cm<sup>-1</sup> spectral resolution. Bands due to ice lattice modes have been subtracted from all spectra.

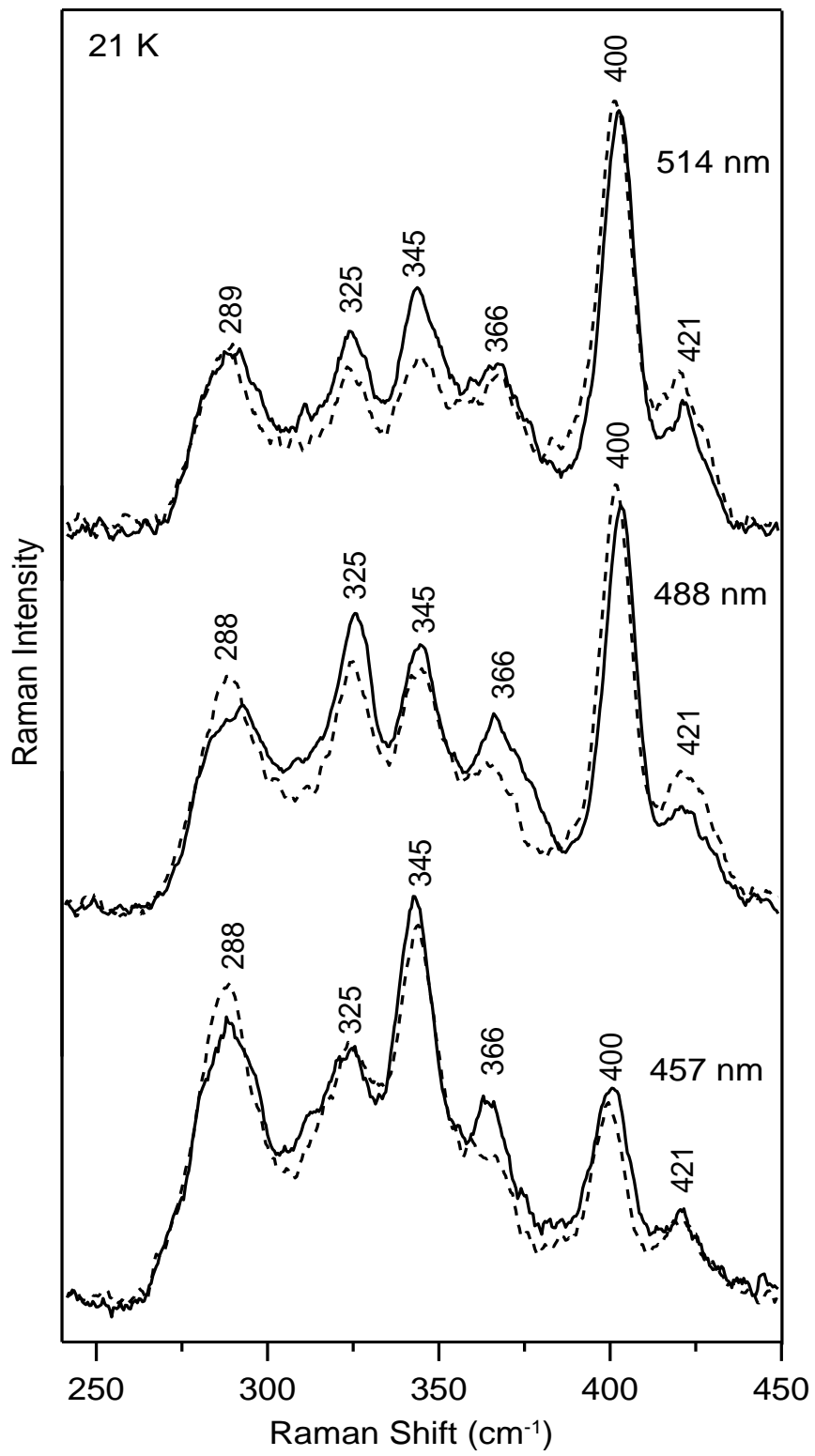


Figure 4.3: UV-visible absorption spectra of chromatographically resolved fractions of cluster-bound forms of Grx5. Inset shows the elution profile of Grx5 fractions contained in the cysteine desulfurase-mediated Fe-S cluster assembly mixture. The reconstitution mixture was loaded onto a 5-mL Q-sepharose column after a reaction time of 140 min under anaerobic conditions. The absorption spectrum in solid line corresponds to fraction 1, which contains only  $[2\text{Fe-2S}]^{2+}$  cluster-bound Grx5, and spectrum in broken line corresponds to fraction 2 additionally contains linear  $[3\text{Fe-4S}]^+$  cluster-bound Grx5 as a minor component. Spectra were recorded under anaerobic conditions in sealed 0.1 cm cuvettes in 100 mM Tris-HCl buffer with 1 mM GSH at pH 7.8.

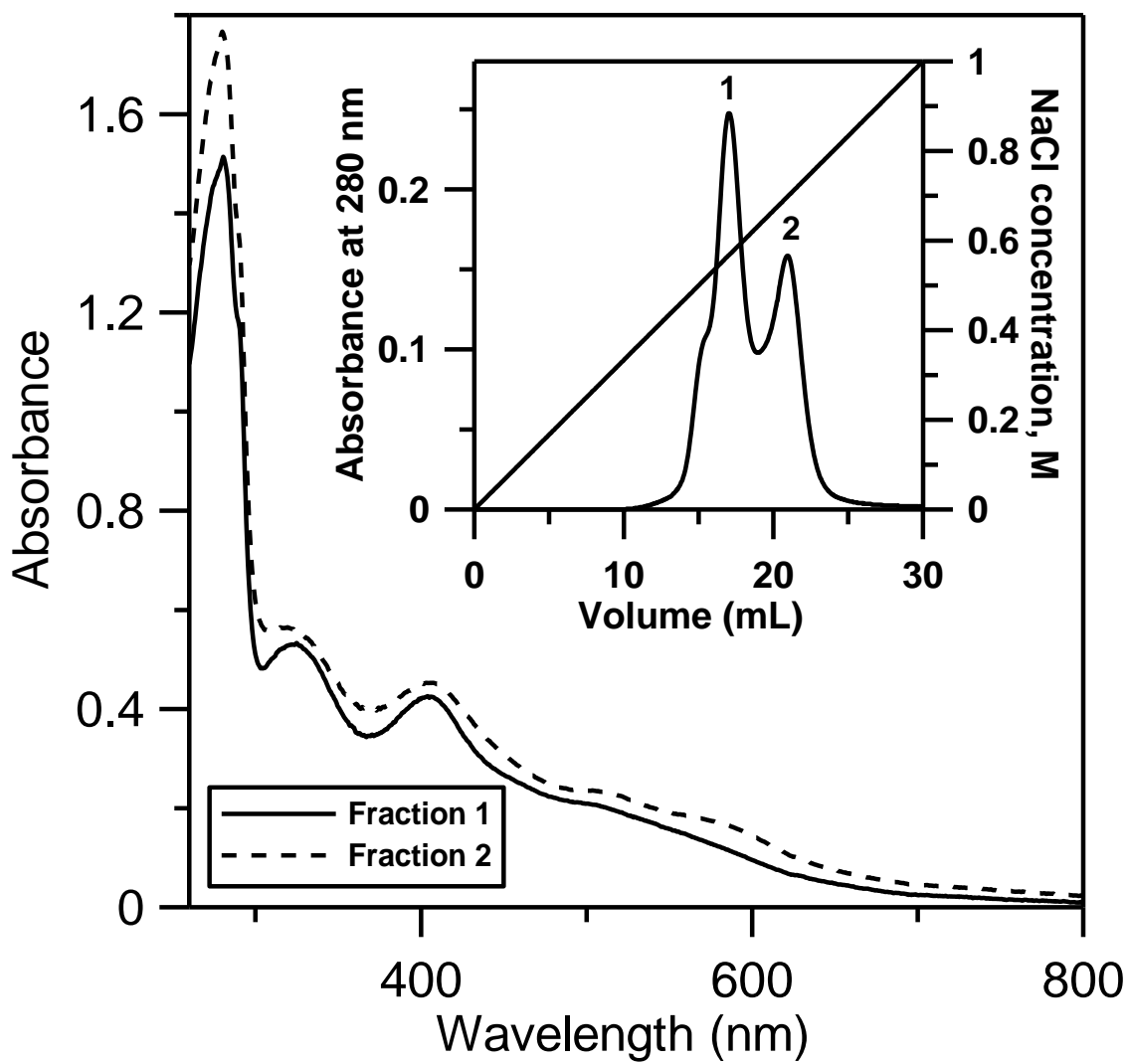


Figure 4.4: Time course of cluster transfer from *A.vinelandii* [4Fe-4S]-IscU to apo Grx5 monitored by UV-visible CD spectroscopy. The thick line corresponds to the CD spectrum of the holo-form of IscU used as cluster donor to apo Grx5 (72  $\mu\text{M}$  in [4Fe-4S]<sup>2+</sup> and 36  $\mu\text{M}$  in [2Fe-2S]<sup>2+</sup> clusters). The CD spectrum is dominated by the [2Fe-2S]<sup>2+</sup> cluster in IscU whereas the [4Fe-4S]<sup>2+</sup> cluster-bound IscU does not exhibit significant CD intensity. The thin lines correspond to CD spectra recorded at 3, 20, 40, 60, 80, 100 and 120 min after the addition of apo Grx5. The arrows indicate the direction of intensity change with increasing amount of time at selected wavelengths. The cluster transfer reaction was carried out under anaerobic conditions at room temperature in 100 mM Tris-HCl buffer at pH 7.8 in the presence of 3 mM GSH.

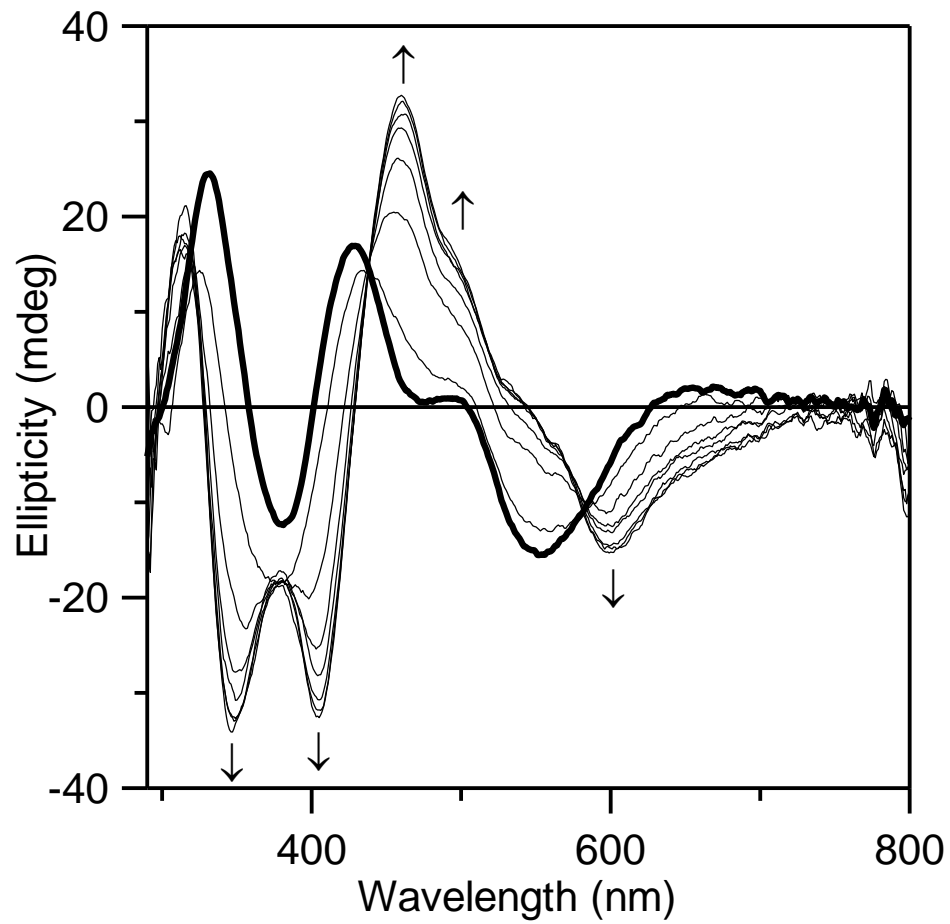


Figure 4.5: Time course of cluster transfer from *A.vinelandii* [4Fe-4S]-NfuA to apo Grx5 monitored by UV-visible CD spectroscopy. (A) CD spectra of the cluster transfer reaction mixture that was initially 50  $\mu\text{M}$  in NfuA [4Fe-4S]<sup>2+</sup> clusters and 200  $\mu\text{M}$  in apo Grx5 monomer. The thick line corresponds to [4Fe-4S]-NfuA recorded before addition of apo Grx5 and the thin lines correspond to CD spectra recorded at 5, 60, 120, 180, 240 and 265 min after the addition of apo Grx5. The arrows indicate the direction of intensity change with increasing amount of time at selected wavelengths. The cluster transfer reaction was carried out under anaerobic conditions at room temperature in 100 mM Tris-HCl buffer with 3 mM GSH at pH 7.8. (B) Predicted changes in the CD spectra for quantitative cluster transfer. Thick lines correspond to [4Fe-4S]-NfuA and [2Fe-2S]-Grx5 and thin lines represent simulated CD spectra corresponding to 90 – 10% loss of [4Fe-4S] cluster on NfuA in 10% decrement and concomitant [2Fe-2S]<sup>2+</sup> cluster formation on Grx5. The simulation is based on formation of two [2Fe-2S]<sup>2+</sup> clusters from one [4Fe-4S]<sup>2+</sup> cluster. The  $\Delta\epsilon$  values are based on Grx5 [2Fe-2S]<sup>2+</sup> and NfuA [4Fe-4S]<sup>2+</sup> clusters.

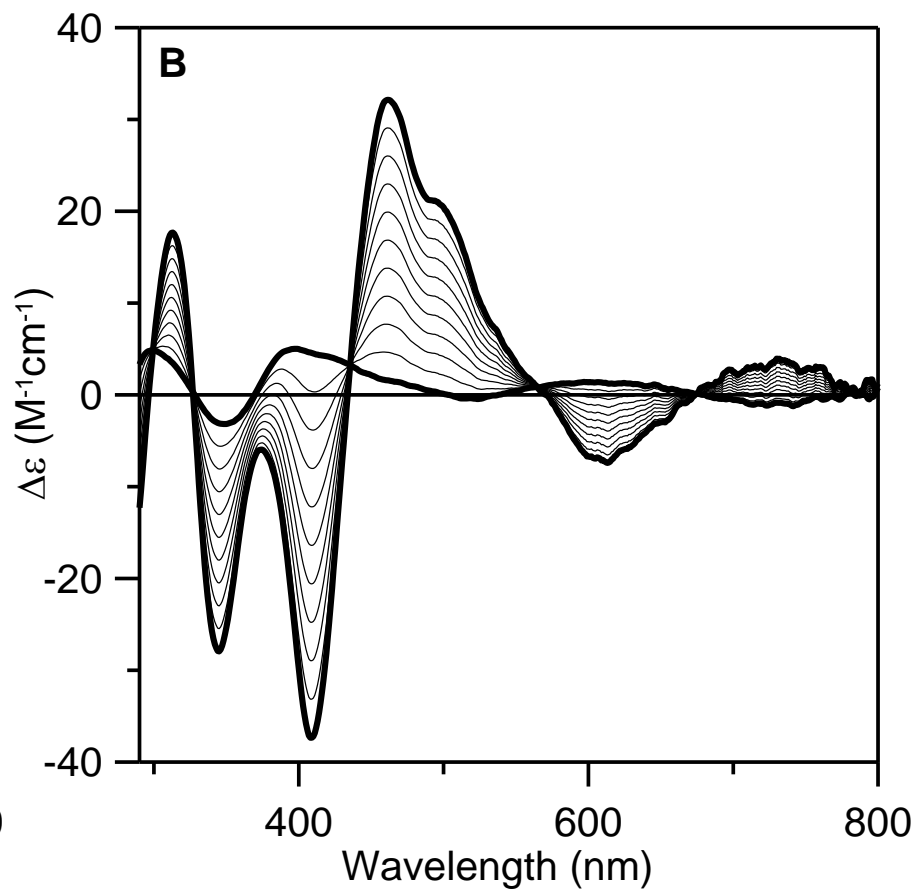
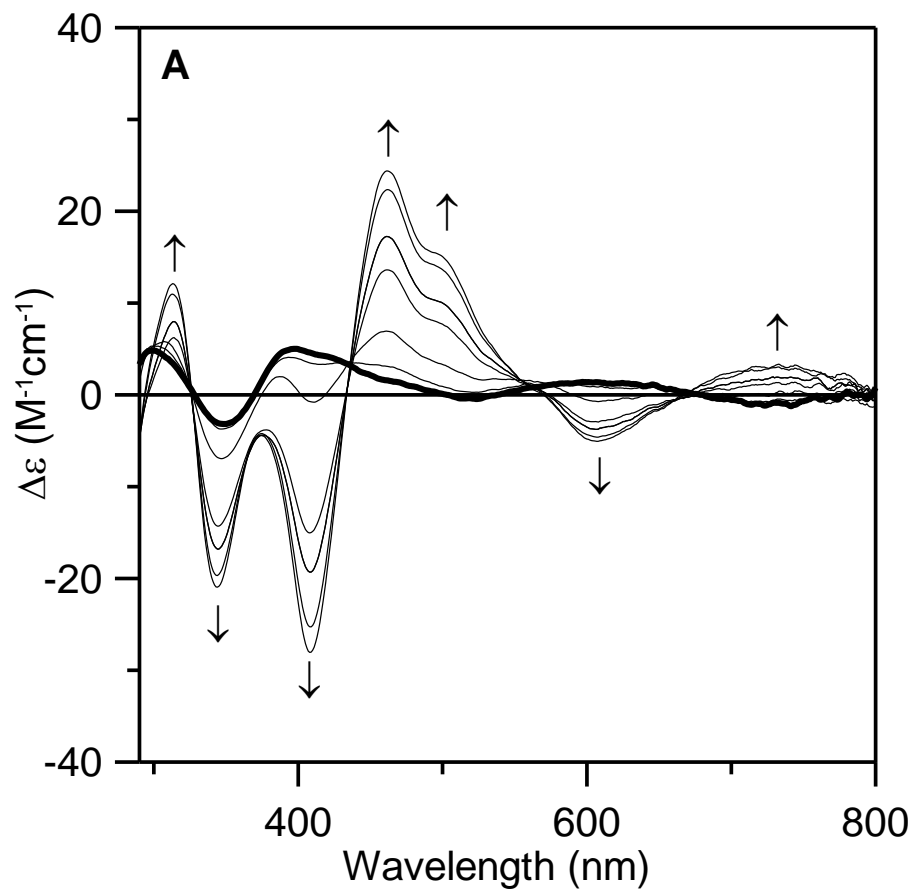
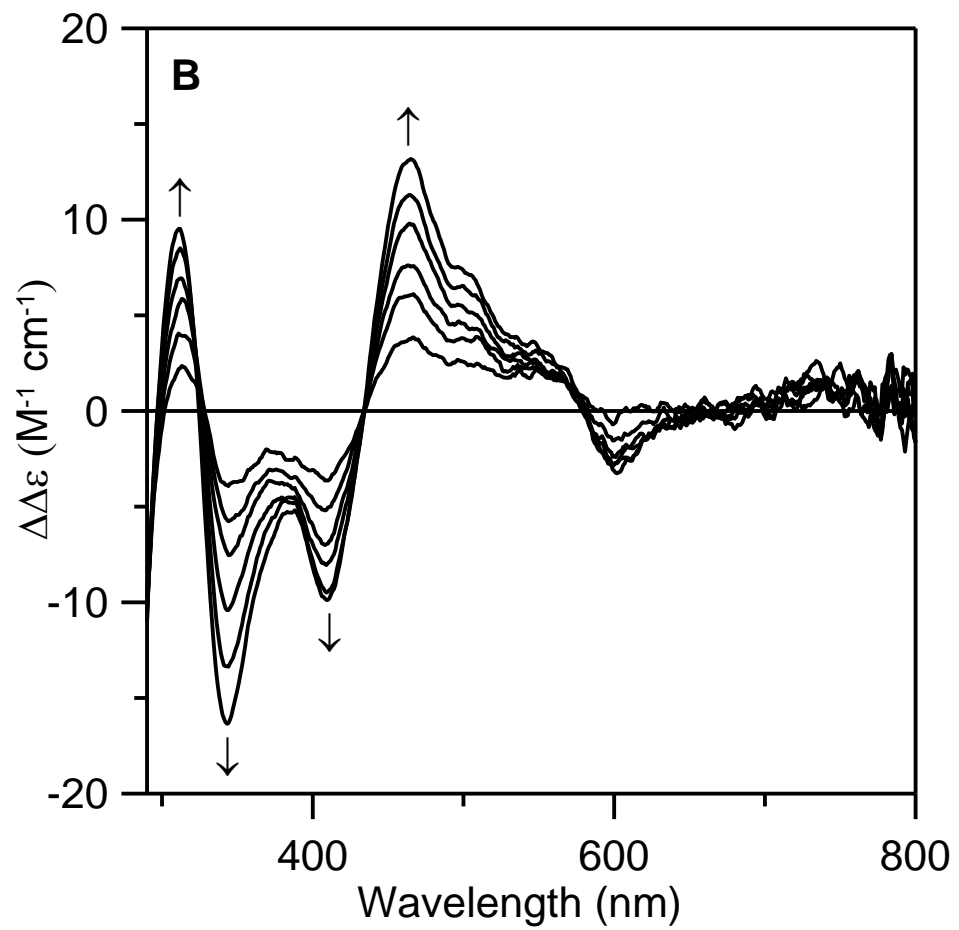
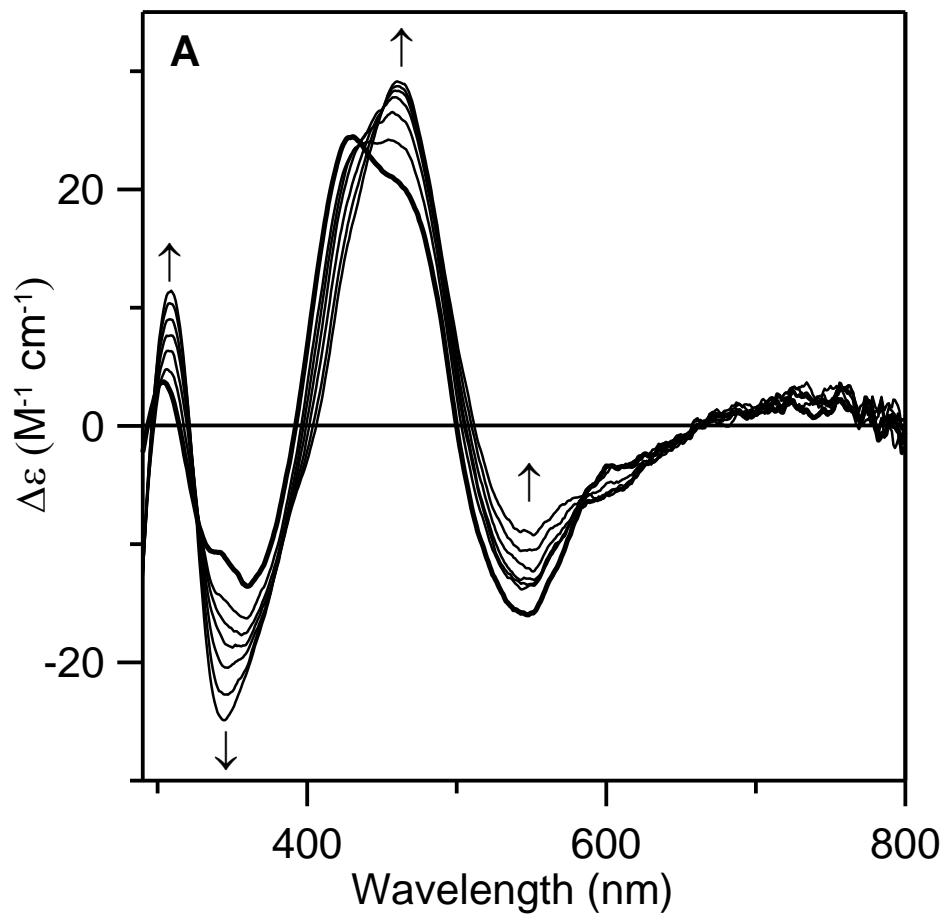


Figure 4.6: Time course of cluster transfer from [4Fe-4S]-containing NifU to apo-Grx-nif monitored by UV-visible CD spectroscopy. (A) CD spectra of the cluster transfer reaction mixture that was initially 14  $\mu\text{M}$  in NifU monomer (with one [4Fe-4S]<sup>2+</sup> cluster and one permanent [2Fe-2S]<sup>2+</sup> cluster per NifU monomer) and 144  $\mu\text{M}$  in apo-Grx-nif monomer. The thick line corresponds to NifU recorded before addition of apo Grx-nif and the thin lines correspond to CD spectra recorded at 5, 10, 15, 25, 40 and 60 min after the addition of apo Grx-nif. The arrows indicate the direction of intensity change with increasing amount of time at selected wavelengths. The cluster transfer reaction was carried out under anaerobic conditions at room temperature in 100 mM Tris-HCl buffer with 3 mM GSH at pH 7.8. (B) The resulting CD spectra of [2Fe-2S]<sup>2+</sup> cluster transfer to Grx-nif from subtraction of the CD spectrum of the permanent [2Fe-2S]<sup>2+</sup> cluster in NifU. The arrows indicate the direction of intensity change with increasing amount of time at selected wavelengths. The  $\Delta\epsilon$  and  $\Delta\Delta\epsilon$  values are expressed per NifU monomer.



## CHAPTER 5

### REVERSIBLE CYCLING BETWEEN CYSTEINE PERSULFIDE-LIGATED [2Fe-2S] AND CYSTEINE-LIGATED [4Fe-4S] CLUSTERS IN THE FNR REGULATORY PROTEIN

---

Bo Zhang,<sup>a</sup> Jason C. Crack,<sup>c</sup> Sowmya Subramanian,<sup>a</sup> Jeffrey Green,<sup>c</sup> Andrew J. Thomson,<sup>b</sup> Nick  
E. Le Brun,<sup>b</sup> and Michael K. Johnson<sup>a</sup>

*Proc. Natl. Acad. Sci. USA* **2012**, *109*, 15734-15739.

Reprinted with permission of the publisher.

<sup>a</sup>Department of Chemistry and Center for Metalloenzyme Studies, University of Georgia; Athens, Georgia 30602; <sup>b</sup>Center for Molecular and Structural Biochemistry, School of Chemistry, University of East Anglia, Norwich NR4 7TJ, United Kingdom; and <sup>c</sup>Department of Molecular Biology and Biotechnology, University of Sheffield, Sheffield S10 2TN, United Kingdom

**Abbreviations:** fumarate and nitrate reduction, FNR; Cyclic-AMP receptor protein, CRP; dithiothreitol, DTT; glutathione, GSH; liquid chromatography electrospray ionization mass spectrometry, LC-ESI MS; 5,5-dithiobis-(2-nitrobenzoic acid), DTNB.

## Abstract

Fumarate and nitrate reduction (FNR) regulatory proteins are O<sub>2</sub>-sensing bacterial transcription factors that control the switch between aerobic and anaerobic metabolism. Under anaerobic conditions [4Fe-4S]<sup>2+</sup>-FNR exists as a DNA-binding homodimer. In response to elevated oxygen levels, the [4Fe-4S]<sup>2+</sup> cluster undergoes a rapid conversion to a [2Fe-2S]<sup>2+</sup> cluster, resulting in a dimer-to-monomer transition and loss of site-specific DNA binding. In this work, resonance Raman and UV-visible absorption/CD spectroscopies and MS were used to characterize the interconversion between [4Fe-4S]<sup>2+</sup> and [2Fe-2S]<sup>2+</sup> clusters in *Escherichia coli* FNR. Selective <sup>34</sup>S labeling of the bridging sulfides in the [4Fe-4S]<sup>2+</sup> cluster-bound form of FNR facilitated identification of resonantly enhanced Cys<sup>32</sup>S-<sup>34</sup>S stretching modes in the resonance Raman spectrum of the O<sub>2</sub>-exposed [2Fe-2S]<sup>2+</sup> cluster-bound form of FNR. This result indicates O<sub>2</sub>-induced oxidation and retention of bridging sulfides in the form of [2Fe-2S]<sup>2+</sup> cluster-bound cysteine persulfides. MS also demonstrates that multiple cysteine persulfides are formed on O<sub>2</sub> exposure of [4Fe-4S]<sup>2+</sup>-FNR. The [4Fe-4S]<sup>2+</sup> cluster in FNR can also be regenerated from the cysteine persulfide-coordinated [2Fe-2S]<sup>2+</sup> cluster by anaerobic incubation with DTT and Fe<sup>2+</sup> ion in the absence of exogenous sulfide. Resonance Raman data indicate that this type of cluster conversion involving sulfide oxidation is not unique to FNR, because it also occurs in O<sub>2</sub>-exposed forms of O<sub>2</sub>-sensitive [4Fe-4S] clusters in radical S-adenosylmethionine enzymes. The results provide fresh insight into the molecular mechanism of O<sub>2</sub>-sensing by FNR and iron-sulfur cluster conversion reactions in general, and suggest unique mechanisms for the assembly or repair of biological [4Fe-4S] clusters.

## Introduction

Facultative anaerobic bacteria respond to environmental O<sub>2</sub> levels to promote optimal cell growth under aerobic and anaerobic conditions. The best-characterized O<sub>2</sub>-sensing transcriptional regulator is the *Escherichia coli* fumarate and nitrate reduction (FNR) protein, which controls the switch between aerobic and anaerobic metabolism by regulating the transcription of hundreds of genes in response to cellular O<sub>2</sub> levels (1-3), and has been the subject of several recent reviews (4-7). Although there is currently no crystallographic structure for *E. coli* FNR, the protein shares sequence homology with the structurally characterized cyclic-AMP receptor class of proteins (8), which comprise a C-terminal helix-turn-helix DNA-binding domain and an N-terminal sensory domain and binds to DNA as a homodimer. However, the sensor domain in *E. coli* FNR contains five cysteines and mutagenesis studies indicate that four of these cysteines (C20, C23, C29, and C122) are essential for *in vivo* function (9) and serve as ligands to the [4Fe-4S] and [2Fe-2S] clusters that function in the O<sub>2</sub>-sensing mechanism (10;11).

A large part of our current understanding of the mechanism of O<sub>2</sub>-sensing by FNR comes from the early biochemical and spectroscopic studies of Kiley and colleagues (10;12-16) (Figure 5.1). *In vivo* and *in vitro* Mössbauer studies demonstrated the presence of a [4Fe-4S]<sup>2+</sup> cluster under anaerobic conditions that is converted to a [2Fe-2S]<sup>2+</sup> cluster (60–65% yield *in vitro*) on exposure to air (10;12). This cluster conversion is accompanied by a dimer-to-monomer transition and inability of FNR to bind DNA (13;14). The [4Fe-4S]<sup>2+</sup> cluster can be reformed *in vitro* by anaerobic incubation with excess Fe<sup>2+</sup> and cysteine in the presence of catalytic amounts of the cysteine desulfurase, IscS (10). The [2Fe-2S]<sup>2+</sup> cluster-bound form of FNR is stable in air for at least 1 h *in vitro*, but is more rapidly degraded *in vivo* by superoxide, a byproduct of aerobic metabolism, to yield monomeric apo-FNR (15). Hence, the dominant forms of FNR

under anaerobic and aerobic growth conditions are the  $[4\text{Fe-4S}]^{2+}$  cluster-containing dimer and the apo monomer, respectively. *E. coli* has two primary machineries for Fe-S cluster assembly, the iron-sulfur cluster (ISC) system for general Fe-S cluster biosynthesis and the sulfur utilization factor (SUF) system, which operates under oxidative stress and iron-limitation conditions. *In vivo* studies have clearly demonstrated that the ISC system, but not the SUF system, is required for converting apo-FNR back to  $[4\text{Fe-4S}]^{2+}$  cluster-bound FNR upon the onset of anaerobic growth conditions (16).

There are two major unresolved issues involving the mechanism of  $\text{O}_2$ -sensing by FNR. The first concerns the mechanism of  $\text{O}_2$ -induced  $[4\text{Fe-4S}]^{2+}$  to  $[2\text{Fe-2S}]^{2+}$  cluster conversion and centers on the question of whether the reaction involves metal-based oxidation, sulfur-based oxidation, or a combination of the two. The metal-based oxidation mechanism involves oxidation and release of two cluster irons to yield a  $[2\text{Fe-2S}]^{2+}$  cluster, one  $\text{Fe}^{3+}$  and one  $\text{Fe}^{2+}$  and two  $\text{S}^{2-}$  ions, proceeding via a  $[3\text{Fe-4S}]^+$  cluster intermediate (4;17-20). A sulfur-based oxidation mechanism was proposed based on analytical data showing that only 70% of the sulfide in the original  $[4\text{Fe-4S}]^{2+}$  cluster was detectable following  $\text{O}_2$  exposure, leading to the suggestion that ~30% had become oxidized (10). However, attempts to detect sulfur oxidation products, such as polysulfide, cysteine persulfide, or sulfinic acid, were unsuccessful (21). The second issue involves the significance of the  $[2\text{Fe-2S}]^{2+}$  cluster-bound form of FNR; that is, is it just an intermediate in the conversion of the transcriptionally active  $[4\text{Fe-4S}]$ -FNR to the transcriptional inactive apo-FNR or can  $[4\text{Fe-4S}]^{2+} \leftrightarrow [2\text{Fe-2S}]^{2+}$  cluster interconversion occur *in vivo* and, hence, play a role as a sensor of dynamic changes in cellular  $\text{O}_2$  levels?

Here we report on resonance Raman, UV-visible absorption and CD, and MS studies of the  $\text{O}_2$ -induced  $[4\text{Fe-4S}]^{2+}$  to  $[2\text{Fe-2S}]^{2+}$  cluster conversion in *E. coli* FNR. The results clearly

show sulfur-based oxidation and the formation of  $[2\text{Fe-2S}]^{2+}$  clusters with one or two cysteine persulfide ligands. In addition, the cluster conversion is shown to be reversible on addition of  $\text{Fe}^{2+}$  under anaerobic conditions in the presence of dithiol reagents and the absence of  $\text{S}^{2-}$ . This result suggests that facile  $[4\text{Fe-4S}]^{2+} \leftrightarrow [2\text{Fe-2S}]^{2+}$  cluster interconversion can occur, implying that FNR can be responsive to dynamic changes in cellular  $\text{O}_2$  levels. Moreover, our observation that  $\text{O}_2$ -induced, sulfur-based oxidation of  $[4\text{Fe-4S}]^{2+}$  clusters to yield semi-stable cysteine persulfide-ligated  $[2\text{Fe-2S}]^{2+}$  clusters also occurs in other  $\text{O}_2$ -sensitive Fe-S proteins, raises the possibility that formation of  $[4\text{Fe-4S}]^{2+}$  clusters by the addition of  $\text{Fe}^{2+}$  to cysteine persulfide-ligated  $[2\text{Fe-2S}]^{2+}$  clusters in the presence of dithiol reagents may provide a major mechanism for the repair or de novo biosynthesis of  $[4\text{Fe-4S}]^{2+}$  clusters.

## Experimental procedures

*Purification and reconstitution of [4Fe-4S]-FNR with natural abundance and  $^{34}\text{S}$  bridging sulfides:* FNR samples were prepared as previously described (17). Isotopically enriched  $[4\text{Fe-4S}]^{2+}$  clusters were prepared using  $^{34}\text{S}$ -cysteine synthesized using a thermostable cysteine synthase (22), o-acetylserine and  $^{34}\text{S}^{2-}$  (CIL Inc). Samples for spectroscopic studies were in 25 mM Hepes buffer with 2.5 mM  $\text{CaCl}_2$ , 100 mM NaCl, 100 mM  $\text{NaNO}_3$ , at pH 7.5, except resonance Raman samples, which also contained 500 mM KCl. Samples, containing  $[2\text{Fe-2S}]$ -FNR, were prepared essentially as described previously (18), except the protein fraction from the PD10 column (GE Healthcare) was collected (taking care to ensure no contamination with low molecular weight components), and centrifuged at  $14,000 \times g$  for 2 min. The  $[4\text{Fe-4S}]^{2+}$  cluster concentration of reconstituted FNR and the  $[2\text{Fe-2S}]^{2+}$  cluster concentration of air exposed FNR were determined using  $\epsilon_{406} = 16.22 (\pm 0.14) \text{ mM}^{-1} \cdot \text{cm}^{-1}$  (23) and  $\epsilon_{420} = 7.95 (\pm 0.06) \text{ mM}^{-1} \cdot \text{cm}^{-1}$ , respectively. The latter was determined by assaying  $[2\text{Fe-}$

2S] FNR samples for protein, acid-labile sulfide, and iron as previously described (18;24;25). These determinations revealed 2.1 and 2.0 iron and sulfide per protein, respectively, consistent with the stoichiometric nature of cluster conversion.

*Reconstitution of [4Fe-4S]<sup>2+</sup> centers in E. coli BioB:* BioB containing one [4Fe-4S]<sup>2+</sup> cluster per BioB monomer was prepared under strictly anaerobic conditions in 50 mM Hepes buffer, pH 7.5 following the procedure described by Cosper et al. (26). The [4Fe-4S]<sup>2+</sup> cluster concentration was based on  $\epsilon_{410} = 15.6 \text{ mM}^{-1} \cdot \text{cm}^{-1}$ .

*Spectroscopic methods:* All samples were prepared and handled under Ar or N<sub>2</sub> in a glove box at oxygen levels < 2 ppm, unless otherwise stated. Absorption and CD measurements were made using a Jasco V550 UV-visible spectrophotometer and Jasco J-810 spectropolarimeter, respectively. Raman samples (~2 mM in [4Fe-4S] clusters) were placed onto the sample holder inside the glove box under Ar atmosphere. For the oxygen-exposed samples, the [4Fe-4S]<sup>2+</sup> cluster-containing FNR and biotin synthase (BioB) Raman samples were thawed under an Ar atmosphere before being taken outside the glove box and exposed to air for 20 min with gentle mixing using a syringe. Resonance Raman samples were in the form of a 20- $\mu\text{L}$  frozen droplet mounted on the cold finger of an Displex Model CSA-202E closed-cycle refrigerator (Air Products) and resonance Raman spectra were recorded using a Ramanor U1000 scanning spectrometer (Instrument SA) coupled with a Sabre argon ion laser (Coherent), as previously described (26;27). MS was used to investigate the formation of cysteine persulfides on FNR as a function of time of oxygen exposure. Five-microliter aliquots of FNR (~1 mM in [4Fe-4S]<sup>2+</sup> clusters) were exposed to air for time intervals between 0 and 60 min. Immediately after exposure to air, the samples were mixed with 20  $\mu\text{L}$  of a 1% (vol/vol) aqueous solution of formic acid (solvent A) and injected into the LC-ESI-MS. The samples were

purified using a BioBasic-4 column, as previously described (28), using solvent A and acetonitrile with 1% formic acid as solvent B, except that both solvents were rigorously degassed before use. The HPLC flow rate was 50  $\mu\text{L}/\text{min}$  and samples were injected in 25- $\mu\text{L}$  aliquots into 10% solvent B and solvent B was increased to 95% over 20 min and maintained at 95% for 5 min before reaching 100% using an Applied Biosystems 140B solvent delivery system. The effluent was analyzed using a single quadrupole MS equipped with an ESI source (PE Sciex API I plus) and the mass spectrum was scanned from 700–1600  $m/z$ . The reported masses are accurate to  $\pm 0.1\%$ .

## Results

*Resonance Raman characterization of the  $[4\text{Fe-4S}]^{2+} \leftrightarrow [2\text{Fe-2S}]^{2+}$  cluster interconversion in FNR:* Resonance Raman spectra of the  $[4\text{Fe-4S}]^{2+}$  center in FNR anaerobically reconstituted with natural abundance ( $\sim 95\%$   $^{32}\text{S}$ ,  $\sim 4\%$   $^{34}\text{S}$ ) and isotopically enriched ( $>95\%$ )  $^{34}\text{S}$  bridging sulfides are shown in Figure 5.2A. The Fe-S stretching frequencies, relative intensities of Raman bands with 458-nm excitation, and the  $^{34}\text{S}$ -bridging downshifts are all characteristic of an all cysteine-ligated  $[4\text{Fe-4S}]^{2+}$  cluster and are very similar to those reported and assigned by normal-mode analysis for  $[4\text{Fe-4S}]$ -ferredoxins and appropriate analog complexes (29). To a first approximation, the Fe-S stretching modes can be assigned under effective  $D_{2d}$  symmetry as predominantly Fe-S(bridging) and Fe-S(Cys) stretching modes based on the magnitude of the  $^{34}\text{S}$ -bridging downshifts, 2–7  $\text{cm}^{-1}$  and  $<1 \text{ cm}^{-1}$ , respectively (Table 5.1).

After exposure to air for 20 min, the cluster is converted into a  $[2\text{Fe-2S}]^{2+}$  center with an atypical resonance Raman spectrum in the Fe-S stretching region (240 – 450  $\text{cm}^{-1}$ ); that is, 10- to 20- fold lower resonance enhancement and three broad and poorly resolved bands centered near

293, 345, and 395  $\text{cm}^{-1}$ , compared with  $[\text{2Fe-2S}]^{2+}$  cluster-containing ferredoxins, which have six or seven well-resolved and strongly resonantly enhanced bands (30-32) (Figure 5.2B). In addition, the  $[\text{2Fe-2S}]^{2+}$  center in  $\text{O}_2$ -exposed FNR has a band at 498  $\text{cm}^{-1}$  in the S-S stretching region that is resonantly enhanced with visible excitation into the S-to- $\text{Fe}^{3+}$  charge transfer transitions of the  $[\text{2Fe-2S}]^{2+}$  cluster, suggesting assignment to the S-S stretching mode of one or more coordinated cysteine persulfides. Definitive confirmation of a cysteine persulfide-ligated  $[\text{2Fe-2S}]^{2+}$  center in  $\text{O}_2$ -exposed FNR is provided by selective  $^{34}\text{S}$  labeling of the bridging sulfides in the  $[\text{4Fe-4S}]^{2+}$  cluster-bound form of FNR. In contrast to the parent  $[\text{4Fe-4S}]^{2+}$  center, bands involving primarily Fe-S(Cys) or Fe-S(bridging) stretching of the  $[\text{2Fe-2S}]$  center both undergo significant  $^{34}\text{S}/^{32}\text{S}$  isotope shifts, implying oxidation of some of the bridging sulfides to form  $\text{Fe-}^{34}\text{S-S(Cys)}$  ligands. Moreover, the 7- $\text{cm}^{-1}$   $^{34}\text{S}/^{32}\text{S}$  isotope shift of the 498  $\text{cm}^{-1}$  band is consistent with the 7–8  $\text{cm}^{-1}$  isotope shifts predicted for a mixed  $^{34}\text{S-}^{32}\text{S}$  stretching mode based on a simple diatomic oscillator approximation. The Raman data, therefore, demonstrate the presence of cysteine persulfide ligation to the  $[\text{2Fe-2S}]$  center in  $\text{O}_2$ -exposed FNR and indicate that the cysteine persulfide results from  $\text{O}_2$ -induced  $\text{S}^{2-}$  to  $\text{S}^0$  oxidation.

The effect of GSH and DTT on the formation of the cysteine persulfide-ligated  $[\text{2Fe-2S}]^{2+}$  center in FNR by air exposure of  $[\text{4Fe-4S}]$ -FNR was investigated by measuring resonance Raman spectra in the absence and presence of 3 mM GSH, which approximates to cellular GSH concentration or 8 mM DTT, after 20 min of air exposure (Figure 5.3). The close similarity in the spectra and the presence of the S-S stretching mode of the ligating cysteine persulfides in all three spectra demonstrate that the  $\text{O}_2$ -induced  $[\text{4Fe-4S}]^{2+}$  to  $[\text{2Fe-2S}]^{2+}$  cluster conversion process is independent of the presence of DTT or GSH (Figure 5.3). Moreover, the time course of  $\text{O}_2$ -induced  $[\text{4Fe-4S}]^{2+}$  to  $[\text{2Fe-2S}]^{2+}$  cluster conversion in FNR was monitored by resonance Raman

at 457 nm and 488 nm for samples frozen between 30 s and 60 min after exposure to air (Figure 5.4). The results indicate that the overwhelming majority of the  $[4\text{Fe-4S}]^{2+}$  cluster are converted to a cysteine persulfide-ligated  $[2\text{Fe-2S}]^{2+}$  center within the first 30 s of air exposure. However, the spectra from the resultant cysteine persulfide-ligated  $[2\text{Fe-2S}]^{2+}$  cluster continue to undergo increased broadening and small frequency shifts for specific bands (e.g., 288–296  $\text{cm}^{-1}$  and 392–397  $\text{cm}^{-1}$ ) as the air-exposure time is increased from 30 s to 60 min (Figure 5.4). This finding suggests that the  $[2\text{Fe-2S}]^{2+}$  cluster ligation changes and becomes less homogeneous with prolonged air exposure. As discussed below, MS and CD data indicate that this is most likely a consequence of formation of  $[2\text{Fe-2S}]^{2+}$  clusters with one and two cysteine persulfide ligands, with the latter becoming more prevalent as the air-exposure time increases.

Previous electron-paramagnetic-resonance studies have shown that a transient  $[3\text{Fe-4S}]^+$  cluster intermediate is formed in the generation of  $[2\text{Fe-2S}]^{2+}$ -FNR (17;19;23). Formation of the  $[3\text{Fe-4S}]^+$  cluster is  $\text{O}_2$ -dependent ( $k = 250 \text{ M}^{-1}\cdot\text{s}^{-1}$ ), but its conversion to the  $[2\text{Fe-2S}]^{2+}$  cluster product is spontaneous, occurring at a rate ( $k = 0.008 \text{ s}^{-1}$ ) that is  $\text{O}_2$ -independent. A small amount (<10%) of  $[3\text{Fe-4S}]^+$  cluster fails to convert and is detected as a dead-end product. The lower resonance enhancement of the  $[2\text{Fe-2S}]^{2+}$  cluster Raman spectrum with 488-nm excitation facilitates observation of a cubane-type  $[3\text{Fe-4S}]^+$  cluster. Cubane-type  $[3\text{Fe-4S}]^+$  clusters have intense Raman spectra with 458- and 488-nm excitation that are dominated by a band at  $\sim 347 \text{ cm}^{-1}$  that is attributed primarily to the  $\text{Fe}_3\text{-(}\mu_3\text{-S)}$  symmetric stretching mode, as indicated by the resonance Raman spectrum of the well-characterized cubane-type  $[3\text{Fe-4S}]^+$  cluster in *Pyrococcus furiosus* ferredoxin (33-37). Hence, it seems likely that the  $347\text{-cm}^{-1}$  band that is clearly observed with 488-nm excitation when the cysteine persulfide-ligated  $[2\text{Fe-2S}]^{2+}$  center in FNR is less resonantly enhanced (Figure 5.4) arises from a cubane  $[3\text{Fe-4S}]^+$  cluster.

However, this must be a trace amount of  $[3\text{Fe-4S}]^+$  cluster (certainly  $<10\%$ ), because the resonance enhancement for cubane-type  $[3\text{Fe-4S}]^+$  clusters, such as the one on *Pyrococcus furiosus* ferredoxin shown in Figure 5.4, is  $\sim 30$ -times greater than that of the cysteine persulfide-ligated  $[2\text{Fe-2S}]^{2+}$  cluster in FNR with 488-nm excitation. Notably, the relative amount of these two types of cluster does not change significantly for 0.5- to 60-min air exposure, suggesting that this is the dead-end product that is resistant to further rearrangement, possibly because of the loss of an Fe from a different subsite. It is likely that the  $[3\text{Fe-4S}]^+$  cluster intermediate is formed and degraded within the first 30 s of exposure of the highly concentrated Raman sample to air.

Of particular interest is our observation that  $\text{O}_2$ -induced  $[4\text{Fe-4S}]^{2+}$  to cysteine persulfide-ligated  $[2\text{Fe-2S}]^{2+}$  cluster conversion in FNR is reversed under anaerobic conditions in the presence of DTT and excess  $\text{Fe}^{2+}$ . This result is illustrated by resonance Raman studies of FNR in the presence of 3 mM GSH (Figure 5.5). After generating the cysteine persulfide-ligated  $[2\text{Fe-2S}]^{2+}$  cluster-bound form (Figure 5.5B) by exposing the  $[4\text{Fe-4S}]^{2+}$  cluster-bound form ( $\sim 2$  mM in  $[4\text{Fe-4S}]^{2+}$  clusters) (Figure 5.5A) to air for 20 min, the sample was thawed under anaerobic conditions inside a glove box and incubated for 20 min with 8 mM DTT and  $\text{Fe}^{2+}$  before refreezing on the Raman probe. The resulting spectrum (Figure 5.5C) indicates substantial conversion back to the original  $[4\text{Fe-4S}]^{2+}$  center.

It is not possible to be more quantitative about the extent of the conversion based on Raman data, as the photon counts that dictate Raman intensity are very dependent on sample alignment. Therefore, the characteristic UV-visible absorption and CD spectra of  $[2\text{Fe-2S}]^{2+}$  and  $[4\text{Fe-4S}]^{2+}$  cluster-bound forms of FNR (23) were used to provide a quantitative assessment of the extent of  $[2\text{Fe-2S}]^{2+}$  to  $[4\text{Fe-4S}]^{2+}$  cluster conversion in the presence of 3 mM DTT and the presence or absence of an eightfold excess  $\text{Fe}^{2+}$ , both before and after repurification of  $[2\text{Fe-2S}]$ -

FNR formed by O<sub>2</sub>-exposure of [4Fe-4S]-FNR for 2 min. An initial set of experiments was carried out with samples of [2Fe-2S]<sup>2+</sup>-FNR prepared by exposing [4Fe-4S]<sup>2+</sup>-FNR to O<sub>2</sub> for 2 min without repurification to remove breakdown products (Figures 5.6). No reaction occurred in the absence of DTT, but the conversion to the characteristic absorption and CD spectrum of [4Fe-4S]<sup>2+</sup>-FNR (23) proceeds rapidly on addition of 3 mM DTT using the Fe<sup>2+</sup> released during [4Fe-4S]<sup>2+</sup> to [2Fe-2S]<sup>2+</sup> cluster conversion. The reaction starts to slow down after about 20 min, but after 109 min, addition of an eightfold excess of Fe<sup>2+</sup> (compared with the initial [2Fe-2S]<sup>2+</sup>-FNR concentration) results in a small additional increase in intensity of the spectra attributed to [4Fe-4S]<sup>2+</sup>-FNR. The reaction was complete within 10 min for samples that were treated with 3 mM DTT and an eightfold excess of Fe<sup>2+</sup> at the start of the reaction, and in both sets of experiments the recovered yield of [4Fe-4S]<sup>2+</sup> clusters was ~75%, based on the published absorption and CD extinction coefficients (23). Parallel experiments after anaerobic removal of cluster degradation products via gel filtration after exposing [4Fe-4S]<sup>2+</sup>-FNR to O<sub>2</sub> for 2 min are shown in Figure 5.7. Little reconversion to [4Fe-4S]<sup>2+</sup>-FNR was observed during exposure to 3 mM DTT for 50 min. However, rapid reconversion to [4Fe-4S]<sup>2+</sup>-FNR with a ~63% yield was observed on addition of an eightfold excess of Fe<sup>2+</sup> (compared with the initial [2Fe-2S]<sup>2+</sup>-FNR concentration). A slightly higher yield (~70%) was obtained after 10 min of reaction when 3 mM DTT and an eightfold excess of Fe<sup>2+</sup> were added together at the start of the reaction, suggesting some DTT-induced cluster degradation occurs in the absence of Fe<sup>2+</sup>. Taken together, the results reveal that DTT is required for [2Fe-2S]<sup>2+</sup> to [4Fe-4S]<sup>2+</sup> cluster conversion, and that ≥70% of the original [4Fe-4S]<sup>2+</sup> clusters are restored within 10 min of addition of an eightfold excess of Fe to the [2Fe-2S]-FNR, even after repurification to remove free sulfides. In contrast, no significant [2Fe-2S]-FNR to [4Fe-4S]-FNR conversion occurred using 3 mM GSH and an

eightfold excess of  $\text{Fe}^{2+}$ . The implication is that DTT facilitates reductive cleavage of two bound cysteine persulfides ligated to the  $[\text{2Fe-2S}]^{2+}$  center in  $\text{O}_2$ -exposed FNR under reducing conditions in the presence of  $\text{Fe}^{2+}$  to reform a  $[\text{4Fe-4S}]^{2+}$  cluster in situ:



The less-than-quantitative yield of  $[\text{4Fe-4S}]^{2+}$  centers in these experiments is likely to be a consequence of  $[\text{2Fe-2S}]^{2+}$  centers in  $\text{O}_2$ -exposed FNR that are ligated by one cysteine persulfide. In this case,  $[\text{4Fe-4S}]^{2+}$  cluster formation in the presence of DTT and  $\text{Fe}^{2+}$  would likely require complete cluster degradation and reassembly from  $\text{Fe}^{2+}$  and  $\text{S}^{2-}$ , which is a slow (>2 h) and incomplete (<40%) process in FNR. Hence, we conclude that inter-cluster cannibalization cannot be responsible for the rapid 70–75%  $[\text{4Fe-4S}]^{2+}$  cluster recovery observed in these experiments.

*MS characterization of the  $[\text{4Fe-4S}]^{2+}$  to  $[\text{2Fe-2S}]^{2+}$  cluster conversion in FNR:* Although liquid-chromatography electrospray ionization (LC-ESI)-quadrupole MS studies of Fe-S proteins invariably result in loss of the Fe-S cluster, our previous studies have demonstrated that cysteine persulfides or covalently attached polysulfides remain intact (28). Hence, this technique provides a direct method for investigating  $\text{O}_2$ -induced  $\text{S}^0$  generation on  $[\text{4Fe-4S}]^{2+}$ -FNR as a function of time. The results are shown in Figure 5.8. Before air exposure, the reconstructed mass spectrum is dominated by the FNR monomer molecular ion peak at 29,165 Da (theoretical mass of 29,165 Da based on the primary sequence). Based on protein and Fe/acid-labile S determinations, the anaerobically reconstituted samples of FNR used in this work contained 0.85–0.99  $[\text{4Fe-4S}]^{2+}$  clusters per monomer immediately after purification. However, the cluster content decreased by up to 10% on anaerobic freezing/thawing and concentration of samples. Hence, the peak at 29,165 Da that persists throughout the air-exposure

time course is attributed to the small component of apo-FNR. The time-course experiment indicates that the form of FNR with one cysteine persulfide dominates after 2 and 10 min of air exposure. However, the form of FNR with two cysteine persulfides gradually increases with prolonged air exposure and dominates after 60 min. Hence, the MS data support the resonance Raman data by demonstrating O<sub>2</sub>-induced S<sup>2-</sup> to S<sup>0</sup> oxidation to form cysteine persulfides and suggest that increased heterogeneity occurs with increasing air exposure, arising primarily from a mixture of [2Fe-2S]<sup>2+</sup> clusters with one and two cysteine persulfide ligands.

*Resonance Raman evidence for analogous O<sub>2</sub>-induced [4Fe-4S]<sup>2+</sup> to [2Fe-2S]<sup>2+</sup> cluster conversions in other proteins:* Anomalous resonance Raman spectra similar to those of the O<sub>2</sub>-generated [2Fe-2S]<sup>2+</sup> clusters in FNR have also been reported for aerobically purified or air-exposed [4Fe-4S]<sup>2+</sup> centers in radical S-adenosylmethionine (SAM) enzymes, such as pyruvate formate lyase and ribonucleotide reductase-activating enzymes (38;39), and biotin synthase (26). In each case the resonance Raman spectra have been attributed to a [2Fe-2S]<sup>2+</sup> cluster based on parallel Mössbauer studies. However, these spectra were generally only scanned in the Fe-S stretching region, 200–450 cm<sup>-1</sup>. Therefore, we have reinvestigated over a wider spectral range the resonance Raman spectrum of air-exposed biotin synthase (BioB), containing only the [4Fe-4S]<sup>2+</sup> cluster that is responsible for reductive cleavage of SAM (Figure 5.9). The spectrum is almost identical to that of the cysteine persulfide-ligated [2Fe-2S]<sup>2+</sup> center in air-exposed [4Fe-4S]-FNR, and exhibits a resonantly enhanced 498-cm<sup>-1</sup> band that is the hallmark of a coordinated cysteine persulfide. Moreover, the spectrum is completely different from that of the [2Fe-2S]<sup>2+</sup> cluster in the second cluster binding site, which is present in as-purified recombinant BioB (26). Hence, it is likely that the SAM-binding [4Fe-4S]<sup>2+</sup> cluster common to all radical

SAM enzymes undergoes the same O<sub>2</sub>-induced [4Fe-4S]<sup>2+</sup> to cysteine persulfide-ligated [2Fe-2S]<sup>2+</sup> cluster transformation on exposure to O<sub>2</sub>.

## Discussion

*Implications for the molecular mechanism of O<sub>2</sub>-sensing by FNR:* The resonance Raman and LC-ESI MS results presented herein clearly point to oxidation of bridging sulfides to generate one or two cysteine persulfide ligands during the reaction of O<sub>2</sub> with the [4Fe-4S]<sup>2+</sup> cluster in FNR to form a [2Fe-2S]<sup>2+</sup> cluster. Such unusual ligation of [2Fe-2S]<sup>2+</sup> clusters would appear to be difficult to detect by Mössbauer spectroscopy, based on the similarity of the observed isomer shift ( $\delta = 0.28$  mm/s) and quadrupole splitting ( $\Delta E_Q = 0.58$  mm/s) (10) to those of all cysteinyl-ligated [2Fe-2S]<sup>2+</sup> clusters. However, this conclusion is consistent with the original analytical and spectroscopic data, which indicated that only 70% of the sulfide in the original [4Fe-4S]<sup>2+</sup> cluster was detectable following O<sub>2</sub> exposure to give a 60–65% yield of [2Fe-2S]<sup>2+</sup> clusters, leaving 30% unaccounted for (10). Indeed, these data led to the original conclusion that the [4Fe-4S]<sup>2+</sup> to [2Fe-2S]<sup>2+</sup> conversion primarily involved sulfide oxidation, even though there was no direct analytical evidence for S<sup>0</sup> (21). Subsequently, this conclusion was challenged by studies that showed that one Fe<sup>2+</sup>, one Fe<sup>3+</sup>, and two sulfide ions are released upon stoichiometric O<sub>2</sub>-induced [4Fe-4S]<sup>2+</sup> to [2Fe-2S]<sup>2+</sup> cluster conversion (18;19;23), leading to the conclusion that conversion occurs via an iron-based oxidation mechanism. In these experiments, released sulfide ion was detected using DTNB [5,5-dithiobis-(2-nitrobenzoic acid)] (Ellman's reagent), based on the established observation that DTNB reacts with one S<sup>2-</sup>, generating sulfane (S<sup>0</sup>) plus the release of two TNB<sup>-</sup> ions (40). This assay accurately detects sulfide that becomes available for oxidation during or following cluster conversion, distinguishing it from sulfide still bridging iron in the cluster. However, in interpreting the data,

we did not consider the possibility that a bridging sulfide and a nearby cysteine might undergo DTNB-induced two-electron oxidation to produce two TBN<sup>-</sup> ions and a cysteine persulfide, which has now been shown to occur during the oxidative degradation of the [4Fe-4S]<sup>2+</sup> cluster in FNR.

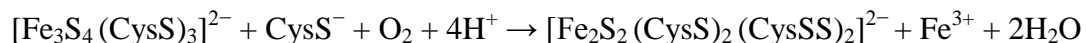
The identification of the fate of the sulfide in the O<sub>2</sub>-induced [4Fe-4S]<sup>2+</sup> to [2Fe-2S]<sup>2+</sup> cluster transformation in FNR necessitates a reassessment of the mechanism of cluster conversion, in which [2Fe-2S]<sup>2+</sup> clusters with one or two cysteine persulfide ligands can be formed. We have previously described the mechanism as a two-step reaction, in which the [4Fe-4S]<sup>2+</sup> cluster first undergoes an O<sub>2</sub>-dependent one-electron oxidation resulting in the formation of a transient cubane-type [3Fe-4S]<sup>+</sup> cluster intermediate (17;19;23), with release of Fe<sup>2+</sup> and the formation of superoxide, O<sub>2</sub><sup>-</sup> (10;19). This first step remains as previously proposed, as there is no oxidation of bridging sulfide during this step. The second step involves the conversion of the [3Fe-4S]<sup>+</sup> cluster to the persulfide-coordinated [2Fe-2S]<sup>2+</sup> form and is therefore more complex than previously envisaged, and may itself involve multiple steps, depending on whether release of iron and sulfide from the cluster occurs simultaneously with sulfide oxidation. It was previously shown that the iron released in this step is Fe<sup>3+</sup>, although its final oxidation state is influenced by the chelating and redox active species present in the reaction mixture (23). The electrons from sulfide oxidation (either two or four electrons for one and two sulfides, respectively) most likely reduce, directly or indirectly, O<sub>2</sub> to either H<sub>2</sub>O<sub>2</sub> or H<sub>2</sub>O. The overall reactions for the formation of the singly or doubly persulfide-coordinated [2Fe-2S]<sup>2+</sup> cluster from the initial [3Fe-4S]<sup>+</sup> intermediate and the nearby free cysteine that are generated in the first step can be written as Scheme 1:

**Scheme 1.** Overall one persulfide ligand reaction:



Reaction 5.2

Overall two persulfide ligand reaction:



Reaction 5.3

The timescale of the appearance of the persulfide coordinated  $[\text{2Fe-2S}]^{2+}$  cluster suggests that the oxidation of at least one sulfide occurs simultaneously with release of  $\text{Fe}^{3+}$  and sulfide from the  $[\text{3Fe-4S}]^+$  intermediate. The formation of a cysteine persulfide by oxidative coupling a  $\mu_2\text{-S}^{2-}$  from the trisulfide face of a  $[\text{Fe}_3\text{S}_4(\text{CysS})_3]^{2-}$  cluster with a nearby free cysteine is clearly a plausible mechanism, with parallels in  $\text{O}_2$ -induced disulfide formation. However, as the rate of degradation of  $[\text{3Fe-4S}]^+$  intermediate to yield a  $[\text{2Fe-2S}]^{2+}$  cluster has been shown to be  $\text{O}_2$ -independent (19), this reaction appears to involve multiple steps with the rate-determining step involving loss of  $\text{Fe}^{3+}/\text{S}^{2-}$  from the intermediate. The overall two-persulfide ligand reaction would most likely result in the four-electron/four-proton reduction of  $\text{O}_2$  to  $\text{H}_2\text{O}$  using two cluster sulfides as the electron donors, and the results presented herein suggest that this is likely to occur via a single cysteine persulfide-ligated intermediate with the production of  $\text{H}_2\text{O}_2$ , which could provide the oxidizing equivalents for the generation of the second cysteine persulfide.

The observation that  $[\text{4Fe-4S}]^{2+}$ -to- $[\text{2Fe-2S}]^{2+}$  cluster conversion is rapidly reversed, under anaerobic conditions and in the absence of exogenous sulfide, on addition of  $\text{Fe}^{2+}$  and DTT to the  $[\text{2Fe-2S}]^{2+}$  cluster-bound form of FNR containing two cysteine persulfide ligands, has important implications both for understanding the FNR mechanism and the mechanism of assembly or repair of  $\text{O}_2$ -sensitive biological  $[\text{4Fe-4S}]^{2+}$  clusters in general. For FNR this

provides the ability to respond rapidly to changes in cellular O<sub>2</sub> levels in a dithiol/disulfide redox-buffering medium. Under aerobic conditions, FNR is inactivated as a transcriptional regulator by O<sub>2</sub>-induced degradation of the [4Fe-4S]<sup>2+</sup> cluster to form a [2Fe-2S]<sup>2+</sup> cluster with two cysteine persulfide ligands. However, in many environments encountered by facultative anaerobes, O<sub>2</sub> is only transiently available and the data presented herein indicate that the persulfide-coordinated [2Fe-2S]<sup>2+</sup> cluster-bound form of FNR could be rapidly reactivated by Fe<sup>2+</sup> and dithiol species without needing the intervention of the entire ISC Fe-S cluster biogenesis system. Consequently, [2Fe-2S]-FNR appears to play a key role in the O<sub>2</sub>-sensing mechanism, as a check point from which the regulator can go back to its transcriptionally active [4Fe-4S]<sup>2+</sup> cluster-bound form, or on to its apo-form, depending on the prevailing O<sub>2</sub> level. Clearly, the [2Fe-2S]<sup>2+</sup> cluster-bound form of FNR should no longer be considered as a passive intermediate in the O<sub>2</sub>-induced transition from [4Fe-4S]-FNR to apo-FNR.

*Implications for the assembly or repair of O<sub>2</sub>-sensitive biological [4Fe-4S]<sup>2+</sup> clusters:* Resonance Raman and structural studies indicate that the O<sub>2</sub>-degradation of [4Fe-4S]<sup>2+</sup> clusters to cysteine persulfide-ligated [2Fe-2S]<sup>2+</sup> clusters also occurs in radical-SAM enzymes and is not limited to FNR. Moreover, sulfur oxidation on oxidative degradation of Fe-S enzymes is not confined to FNR and radical-SAM enzymes. Kennedy and Beinert first reported multiple (up to three) S<sup>0</sup> in the form of persulfides or polysulfides in apo-aconitase on careful ferricyanide oxidation in 1988 (41). Little is currently known about [4Fe-4S]<sup>2+</sup> cluster biogenesis. *In vitro* studies carried out under strictly anaerobic conditions have demonstrated the formation of [4Fe-4S]<sup>2+</sup> clusters on the IscU and NifU scaffold proteins, via reductive coupling of two [2Fe-2S]<sup>2+</sup> clusters, that can be transferred intact to the apo-forms of aconitase and nitrogenase Fe protein, respectively (42-45). However, currently it is not known how [4Fe-4S]<sup>2+</sup> clusters can be

assembled under aerobic conditions or repaired in response to oxidative damage. This work suggests an alternative strategy for assembling  $[4\text{Fe-4S}]^{2+}$  clusters that has the potential to work under aerobic or microaerobic conditions by trafficking in the more  $\text{O}_2$ -tolerant  $[2\text{Fe-2S}]^{2+}$  clusters and for repairing  $\text{O}_2$ -damaged  $[4\text{Fe-4S}]^{2+}$  clusters that have been degraded to cysteine persulfide-ligated  $[2\text{Fe-2S}]^{2+}$  clusters. For assembly, the first step would be cysteine desulfurase catalyzed cysteine persulfide formation on two active-site cysteine residues of the acceptor protein. The second step would then involve transfer of a  $[2\text{Fe-2S}]^{2+}$  cluster to yield a  $[2\text{Fe-2S}]^{2+}$  cluster with two cysteine persulfide ligands. The third step, which would mimic the repair mechanism, would involve incorporation of two  $\text{Fe}^{2+}$  ions coupled with dithiol-mediated cysteine-persulfide reduction for generating the  $[4\text{Fe-4S}]^{2+}$  cluster on the acceptor protein *in situ*.

Much work needs to be done to test the above hypothesis and identify the putative  $\text{Fe}^{2+}$  donor. However, the A-type Fe-S cluster assembly proteins ( $\text{IscA}$ ,  $^{\text{Nif}}\text{IscA}$ , and  $\text{SufA}$ ), which are specifically required for the maturation of the  $[4\text{Fe-4S}]^{2+}$  cluster under aerobic or oxidative stress conditions (46;47), are good candidates because they are capable of binding  $\text{Fe}^{3+}$  under aerobic conditions and releasing  $\text{Fe}^{2+}$  in the presence of cysteine under more reducing conditions (48). Moreover, support for the above hypothesis and the use of A-type proteins as  $\text{Fe}^{2+}$  donors comes from recent *in vivo* studies in *Saccharomyces cerevisiae* (47). In this work, Mühlenhoff et al. demonstrated that the A-type proteins in yeast mitochondria ( $\text{Isa1}$  and  $\text{Isa2}$ ) bind Fe rather than an Fe-S cluster *in vivo* and are required along with  $\text{Iba57}$  (a tetrahydrofolate-dependent protein required for Fe release) and the U-type scaffold proteins ( $\text{Isu1}$  and  $\text{Isu2}$ ) for the maturation of protein-bound  $[4\text{Fe-4S}]^{2+}$  centers in a step that occurs after cluster assembly on the U-type scaffold proteins (47).

## **Acknowledgements**

We thank Nick Cull and Dr. Dennis Phillips for technical assistance and Dr. Claudio Vásquez for the gift of CysK. This work was supported by National Institutes of Health Grant GM62524 (to M.K.J.) and Biotechnology and Biological Sciences Research Council Grants BB/G019347/1 and BB/G018960/1 (to N.E.L.B., A.J.T., and J.G.).

## References

1. Spiro, S. and Guest, J. R. (1990) FNR and its role in oxygen-regulated gene expression in *Escherichia coli*, *FEMS Microbiol. Rev.* 6, 399-428.
2. Guest, J. R., Green, J., Irvine, A. S., and Spiro, S. In *Regulation of Gene Expression in Escherichia coli*; Lin, E. C. C. and Lynch, A. S.; R. G. Landes; 1996; 317-342.
3. Constantinidou, C., Hobman, J. L., Griffiths, L., Patel, M. D., Penn, C. W., Cole, J. A., and Overton, T. W. (2006) A reassessment of the FNR regulon and transcriptomic analysis of the effects of nitrate, nitrite, NarXL, and NarQP as *Escherichia coli* K12 adapts from aerobic to anaerobic growth, *J. Biol. Chem.* 281, 4802-4815.
4. Crack, J. C., Jervis, A. J., Gaskell, A. A., White, G. F., Green, J., Thomson, A. J., and Le Brun, N. E. (2008) Signal perception by FNR: the role of the iron-sulfur cluster, *Biochem. Soc. Trans.* 36, 1144-1148.
5. Green, J., Crack, J. C., Thomson, A. J., and LeBrun, N. E. (2009) Bacterial sensors of oxygen, *Curr. Opin. Microbiol.* 12, 145-151.
6. Kiley, P. J. and Beinert, H. (2003) The role of Fe-S proteins in sensing and regulation in bacteria, *Curr. Opin. Microbiol.* 6, 181-185.
7. Fleischhacker, A. S. and Kiley, P. J. (2011) Iron-containing transcription factors and their roles as sensors, *Curr. Opin. Chem. Biol.* 15, 335-341.
8. Shaw, D. J., Rice, D. W., and Guest, J. R. (1983) Homology between CAP and Fnr, a regulator of anaerobic respiration in *Escherichia coli*, *J. Mol. Biol.* 166, 241-247.
9. Green, J., Sharrocks, A. D., Green, B., Geisow, M., and Guest, J. R. (1993) Properties of FNR proteins substituted at each of the five cysteine residues, *Mol. Microbiol.* 8, 61-68.
10. Khoroshilova, N., Popescu, C., Münck, E., Beinert, H., and Kiley, P. J. (1997) Iron-sulfur cluster disassembly in the FNR protein of *Escherichia coli* by O<sub>2</sub>: [4Fe-4S] to [2Fe-2S] conversion with loss of biological activity, *Proc. Natl. Acad. Sci. USA* 94, 6087-6092.
11. Kiley, P. J. and Beinert, H. (1998) Oxygen sensing by the global regulator, FNR: The role of the iron-sulfur cluster, *FEMS Microbiol. Rev.* 22, 341-352.
12. Popescu, C., Bates, D. M., Beinert, H., Münck, E., and Kiley, P. J. (1998) Mössbauer spectroscopy as a tool for the study of activation/inactivation of the transcription regulator FNR in whole cells of *Escherichia coli*, *Proc. Natl. Acad. Sci. USA* 95, 13431-13435.
13. Lazazzera, B. A., Bates, D. M., and Kiley, P. J. (1993) The activity of the *Escherichia coli* transcription factor FNR is regulated by a change in oligomeric state, *Genes Dev.* 7, 1993-2005.

14. Lazazzera, B. A., Beinert, H., Khoroshilova, N., Kennedy, M. C., and Kiley, P. J. (1996) DNA-binding and dimerization of the Fe-S-containing FNR protein from *Escherichia coli* are regulated by oxygen, *J. Biol. Chem.* 271, 2762-2768.
15. Sutton, V. R., Stubna, A., Patschkowski, T., Münck, E., Beinert, H., and Kiley, P. J. (2004) Superoxide destroys the  $[2\text{Fe-2S}]^{2+}$  cluster of FNR from *E. coli*, *Biochemistry* 43, 791-798.
16. Mettert, E. L., Outten, F. W., Wanta, B., and Kiley, P. J. (2008) The impact of  $\text{O}_2$  on the Fe-S cluster biogenesis requirements of *Escherichia coli* FNR, *J. Mol. Biol.* 384, 798-811.
17. Crack, J., Green, J., and Thomson, A. J. (2004) Mechanism of oxygen sensing by the bacterial transcriptional factor fumarate-nitrate reduction (FNR), *J. Biol. Chem.* 279, 9278-8286.
18. Crack, J. C., Green, J., Le Brun, N. E., and Thomson, A. J. (2006) Detection of sulfide release from the oxygen-sensing  $[4\text{Fe-4S}]$  cluster of FNR, *J. Biol. Chem.* 281, 18909-18913.
19. Crack, J. C., Green, J., Cheesman, M. R., Le Brun, N. E., and Thomson, A. J. (2007) Superoxide-mediated amplification of the oxygen-induced switch from  $[4\text{Fe-4S}]$  to  $[2\text{Fe-2S}]$  clusters in the transcriptional regulator FNR, *Proc. Natl. Acad. Sci. USA* 104, 2092-2097.
20. Jervis, A. J., Crack, J. C., White, G., Artymiuk, P. J., Cheesman, M. R., Thomson, A. J., Le Brun, N. E., and Green, J. (2009) The  $\text{O}_2$  sensitivity of the transcription factor FNR is controlled by Ser24 modulating the kinetics of  $[4\text{Fe-4S}]$  to  $[2\text{Fe-2S}]$  conversion, *Proc. Natl. Acad. Sci. USA* 106, 4659-4664.
21. Sutton, V. R., Mettert, E. L., Beinert, H., and Kiley, P. J. (2004) Kinetic analysis of the oxidative conversion of the  $[4\text{Fe-4S}]^{2+}$  cluster of FNR to a  $[2\text{Fe-2S}]^{2+}$  Cluster, *J. Bacteriol.* 186, 8018-8025.
22. Saavedra, C. P., Encinas, M. V., Araya, M. A., Perez, J. M., Tantalean, J. C., Fuentes, D. E., Calderon, I. L., Pichuantes, S. E., and Vasquez, C. C. (2004) Biochemical characterization of a thermostable cysteine synthase from *Geobacillus stearothermophilus* V, *Biochimie* 86, 481-485.
23. Crack, J. C., Gaskell, A. A., Green, J., Cheesman, M. R., Le Brun, N. E., and Thomson, A. J. (2008) Influence of the environment on the  $[4\text{Fe-4S}]^{2+}$  to  $[2\text{Fe-2S}]^{2+}$  cluster switch in the transcriptional regulator FNR, *J. Am. Chem. Soc.* 130, 1749-1758.
24. Bradford, M. M. (1976) A rapid and sensitive method for the quantitation of microgram quantities of protein utilizing the principle of protein-dye binding, *Anal. Biochem.* 72, 248-254.
25. Beinert, H. (1983) Semi-micro methods for analysis of labile sulfide and of labile sulfide plus sulfane sulfur in unusually stable iron-sulfur proteins, *Anal. Biochem.* 131, 373-378.

26. Coper, M. M., Krebs, B., Hernandez, H., Jameson, G., Eidsness, M. K., Huynh, B. H., and Johnson, M. K. (2004) Characterization of the cofactor content of *Escherichia coli* biotin synthase, *Biochemistry* 43, 2007-2021.
27. Drozdowski, P. M. and Johnson, M. K. (1988) A simple anaerobic cell for low temperature Raman spectroscopy, *Appl. Spectrosc.* 42, 1575-1577.
28. Smith, A. D., Agar, J. N., Johnson, K. A., Frazzon, J., Amster, I. J., Dean, D. R., and Johnson, M. K. (2001) Sulfur transfer from IscS to IscU: The first step in iron-sulfur cluster biosynthesis, *J. Am. Chem. Soc.* 123, 11103-11104.
29. Czernuszewicz, R. S., Macor, K. A., Johnson, M. K., Gewirth, A., and Spiro, T. G. (1987) Vibrational mode structure and symmetry in proteins and analogues containing Fe<sub>4</sub>S<sub>4</sub> clusters: Resonance Raman evidence for different degrees of distortion in HiPIP and ferredoxin, *J. Am. Chem. Soc.* 109, 7178-7187.
30. Han, S., Czernuszewicz, R. S., and Spiro, T. G. (1989) Vibrational spectra and normal mode analysis for [2Fe-2S] protein analogues using <sup>34</sup>S, <sup>54</sup>Fe, and <sup>2</sup>H substitution: Coupling of Fe-S stretching and S-C-C bending modes, *J. Am. Chem. Soc.* 111, 3496-3504.
31. Han, S., Czernuszewicz, R. S., Kimura, T., Adams, M. W. W., and Spiro, T. G. (1989) Fe<sub>2</sub>S<sub>2</sub> protein resonance Raman revisited: Structural variations among adrenodoxin, ferredoxin, and red paramagnetic protein, *J. Am. Chem. Soc.* 111, 3505-3511.
32. Fu, W., Drozdowski, P. M., Davies, M. D., Sligar, S. G., and Johnson, M. K. (1992) Resonance Raman and magnetic circular dichroism studies of reduced [2Fe-2S] proteins, *J. Biol. Chem.* 267, 15502-15510.
33. Duderstadt, R. E., Staples, C. R., Brereton, P. S., Adams, M. W. W., and Johnson, M. K. (1999) Effects of mutations in aspartate 14 on the spectroscopic properties of the [Fe<sub>3</sub>S<sub>4</sub>]<sup>+0</sup> clusters in *Pyrococcus furiosus* ferredoxin, *Biochemistry* 38, 10585-10593.
34. Johnson, M. K., Czernuszewicz, R. S., Spiro, T. G., Fee, J. A., and Sweeney, W. V. (1983) Resonance Raman spectroscopic evidence for a common [3Fe-4S] structure among proteins containing three-iron clusters, *J. Am. Chem. Soc.* 103, 6671-6678.
35. Duderstadt, R. E., Brereton, P. S., Adams, M. W. W., and Johnson, M. K. (1998) Spectroscopic evidence for a new type of [Fe<sub>3</sub>S<sub>4</sub>] cluster in a mutant form of *Pyrococcus furiosus* ferredoxin, *J. Am. Chem. Soc.* 120, 8525-8526.
36. Conover, R. C., Kowal, A. T., Fu, W., Park, J.-B., Aono, S., Adams, M. W. W., and Johnson, M. K. (1990) Spectroscopic characterization of the novel iron-sulfur cluster in *Pyrococcus furiosus* ferredoxin, *J. Biol. Chem.* 265, 8533-8541.
37. Johnson, M. K., Duderstadt, R. E., and Duin, E. C. (1999) Biological and synthetic [Fe<sub>3</sub>S<sub>4</sub>] clusters, *Adv. Inorg. Chem.* 47, 1-82.

38. Broderick, J. B., Duderstadt, R. E., Fernandez, D. C., Wojtuszewski, K., Henshaw, T. F., and Johnson, M. K. (1997) Pyruvate formate-lyase activating enzyme is an iron-sulfur protein, *J. Am. Chem. Soc.* 119, 7396-7397.
39. Ollagnier, S., Meier, C., Mulliez, E., Gaillard, J., Schuenemann, V., Trautwein, A. X., Mattioli, T., Lutz, M., and Fontecave, M. (1999) Assembly of 2Fe-2S and 4Fe-4S clusters in the anaerobic ribonucleotide reductase from *Escherichia coli*, *J. Am. Chem. Soc.* 121, 6344-6350.
40. Nashef, A. S., Osuga, D. T., and Feeney, R. E. (1977) Determination of hydrogen sulfide with 5,5'-dithiobis-(2-nitrobenzoic acid), N-ethylmaleimide, and parachloromercuribenzoate, *Anal. Biochem.* 79, 394-405.
41. Kennedy, M. C. and Beinert, H. (1988) The state of cluster SH and S<sup>2-</sup> of aconitase during cluster interconversions and removal. A convenient preparation of apoenzyme., *J. Biol. Chem.* 263, 8194-8198.
42. Unciuleac, M.-C., Chandramouli, K., Naik, S., Mayer, S., Huynh, B. H., Johnson, M. K., and Dean, D. R. (2007) *In vitro* activation of apo-aconitase using a [4Fe-4S] cluster-loaded form of the IscU [Fe-S] cluster scaffolding protein, *Biochemistry* 46, 6812-6821.
43. Chandramouli, K., Unciuleac, M.-C., Naik, S., Dean, D. R., Huynh, B. H., and Johnson, M. K. (2007) Formation and properties of [4Fe-4S] clusters on the IscU scaffold protein, *Biochemistry* 46, 6804-6811.
44. Smith, A. D., Jameson, G. N. L., Dos Santos, P. C., Agar, J. N., Naik, S., Krebs, C., Frazzon, J., Dean, D. R., Huynh, B. H., and Johnson, M. K. (2005) NifS-mediated assembly of [4Fe-4S] clusters in the N- and C-terminal domains of the NifU scaffold protein, *Biochemistry* 44, 12955-12969.
45. Dos Santos, P. C., Smith, A. D., Frazzon, J., Cash, V. L., Johnson, M. K., and Dean, D. R. (2004) Iron-sulfur cluster assembly: NifU-directed activation of the nitrogenase Fe-protein, *J. Biol. Chem.* 279, 19705-19711.
46. Tan, G., Lu, J., Bitoun, J. P., Huang, H., and Ding, H. (2009) IscA/SufA paralogues are required for the [4Fe-4S] cluster assembly in enzymes of multiple physiological pathways in *Escherichia coli* under aerobic growth conditions, *Biochem. J.* 420, 463-472.
47. Mühlenhoff, U., Richter, N., Pines, O., Pierik, A. J., and Lill, R. (2011) Specialized function of yeast Isa1 and Isa2 in the maturation of mitochondrial [4Fe-4S] proteins, *J. Biol. Chem.* 286, 41205-41216.
48. Ding, H. and Clark, R. J. (2004) Characterization of iron-binding in IscA, an ancient iron-sulfur cluster assembly protein, *Biochem. J.* 379, 433-440.

Table 5.1: Comparison of the resonance Raman Fe-S frequencies ( $\text{cm}^{-1}$ ), assignments, and  $^{32}\text{S}/^{34}\text{S}$ -bridging isotope shifts ( $\text{cm}^{-1}$ ) for  $[\text{4Fe-4S}]^{2+}$  centers in a synthetic analog complex, *C. pasteurianum* ferredoxin, and *Escherichia coli* FNR.

$D_{2d} (T_d)$ Assignment	Solid cube <sup>a</sup>	Fd <sup>b</sup>	FNR
Mainly Fe-S(Cys) stretching			
A <sub>1</sub>	391 (1) <sup>c</sup>	395 (4)	392 (0)
B <sub>2</sub> (T <sub>2</sub> )	367 (1)	351 (1)	366 (0)
E(T <sub>2</sub> )	359 (1)	363 (2)	354 (0)
Mainly Fe-S(bridging) stretching			
B <sub>2</sub> (T <sub>2</sub> )	385 (6)	380 (6)	392 (3)
E(T <sub>2</sub> )			
A <sub>1</sub>	335 (8)	338 (7)	335 (6)
A <sub>1</sub> (E)	298 (5)	298 (5)	300 (3)
B <sub>1</sub> (E)	283 (4)	276 (4)	286 (3)
E(T <sub>1</sub> )	283 (4)		
A <sub>2</sub> (T <sub>1</sub> )	270 (3)	266 (4)	274 (2)
B <sub>2</sub> (T <sub>2</sub> )	249 (6)		
E(T <sub>2</sub> )	243 (5)	251 (6)	254 (4)

<sup>a</sup>  $(\text{Et}_4\text{N})_2[\text{Fe}_4\text{S}_4(\text{SCH}_2\text{Ph})_4]$  in KCl pellet at 77 K. Data from Ref (29).

<sup>b</sup> *C. pasteurianum* 8Fe ferredoxin as a frozen solution at 77 K. Data from Ref (29).

<sup>c</sup> Numbers in parenthesis are downshifts on  $^{34}\text{S}$  substitution of bridging S atoms, all values are  $\pm 1 \text{ cm}^{-1}$ .

Figure 5.1: Summary of the in vivo and in vitro cluster and oligomeric state interconversions reported for *E. coli* FNR.

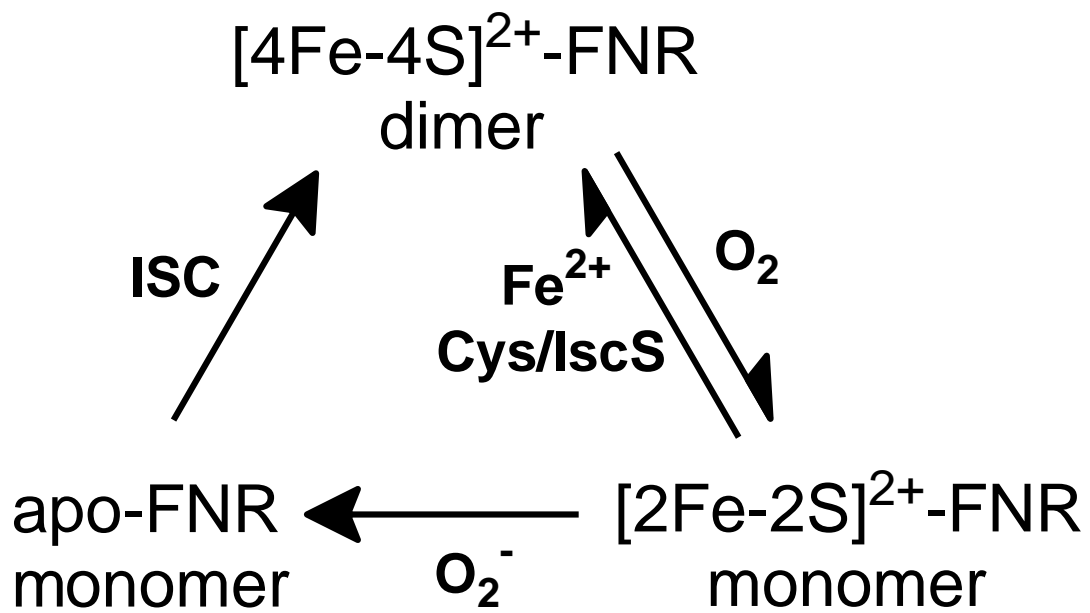


Figure 5.2: Resonance Raman spectra of the O<sub>2</sub>-induced [4Fe-4S]<sup>2+</sup> to [2Fe-2S]<sup>2+</sup> cluster conversion of FNR with natural abundance (black spectra) and <sup>34</sup>S-labeled (red spectra) bridging sulfides. (A) [4Fe-4S]-FNR prepared by anaerobic reconstitution. (B) [2Fe-2S]-FNR obtained by exposing the [4Fe-4S]<sup>2+</sup>-FNR to air for 20 min. The resonance Raman spectra were recorded for samples at 21 K with 140 mW of 457.9-nm laser excitation at the sample, using samples that were <2 mM in [4Fe-4S]<sup>2+</sup> clusters. Each spectrum is the sum of <100 individual scans with each scan involving photon counting for 1 s at a 0.5-cm<sup>-1</sup> increment with 7-cm<sup>-1</sup> spectral resolution. Bands caused by ice lattice modes have been subtracted from all spectra.

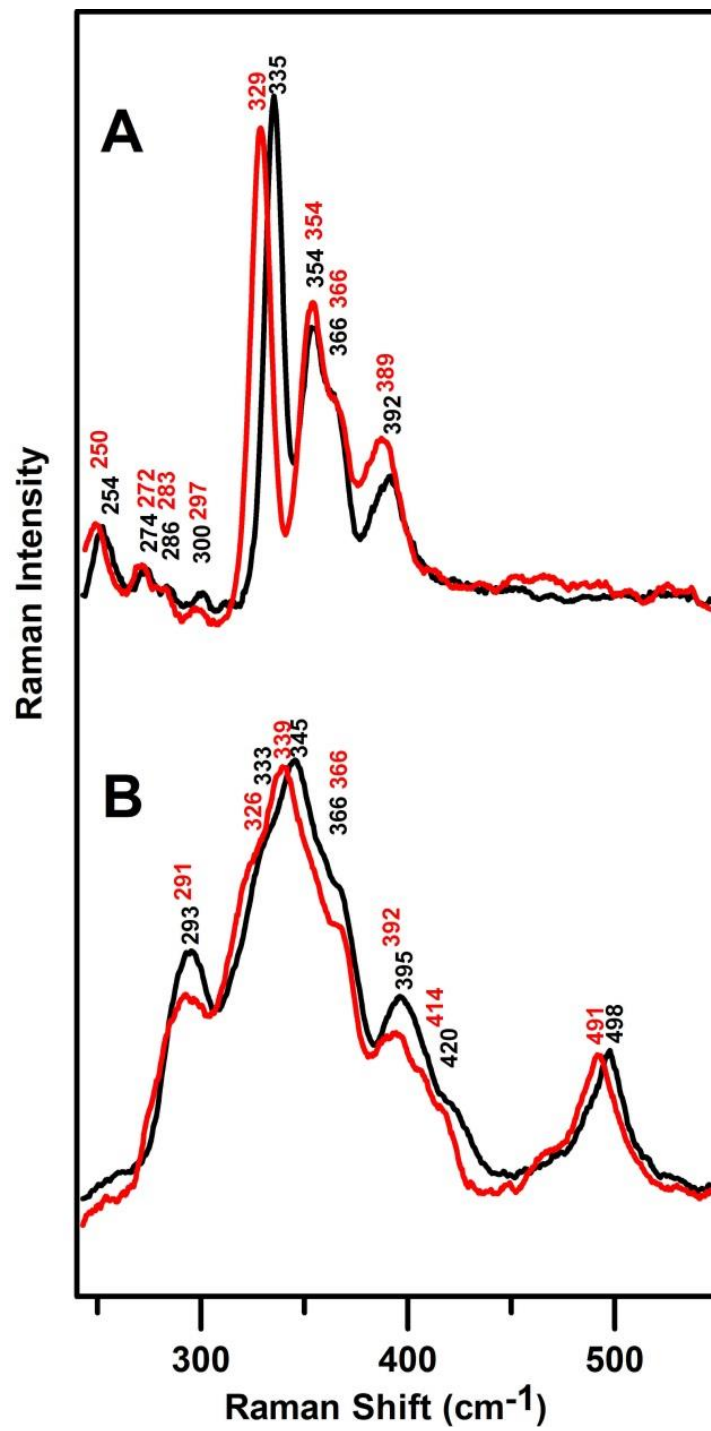


Figure 5.3: Comparison of the resonance Raman spectra of air-exposed FNR obtained in the absence (black spectra) and presence of GSH (green spectra) or DTT (blue spectra). The FNR samples were  $< 2$  mM in  $[4\text{Fe-4S}]^{2+}$  clusters and were incubated with a final concentration of 3 mM GSH or 8 mM DTT under anaerobic conditions before air exposure for 20 min. The Raman experimental conditions are the same as described in Figure 5.2.

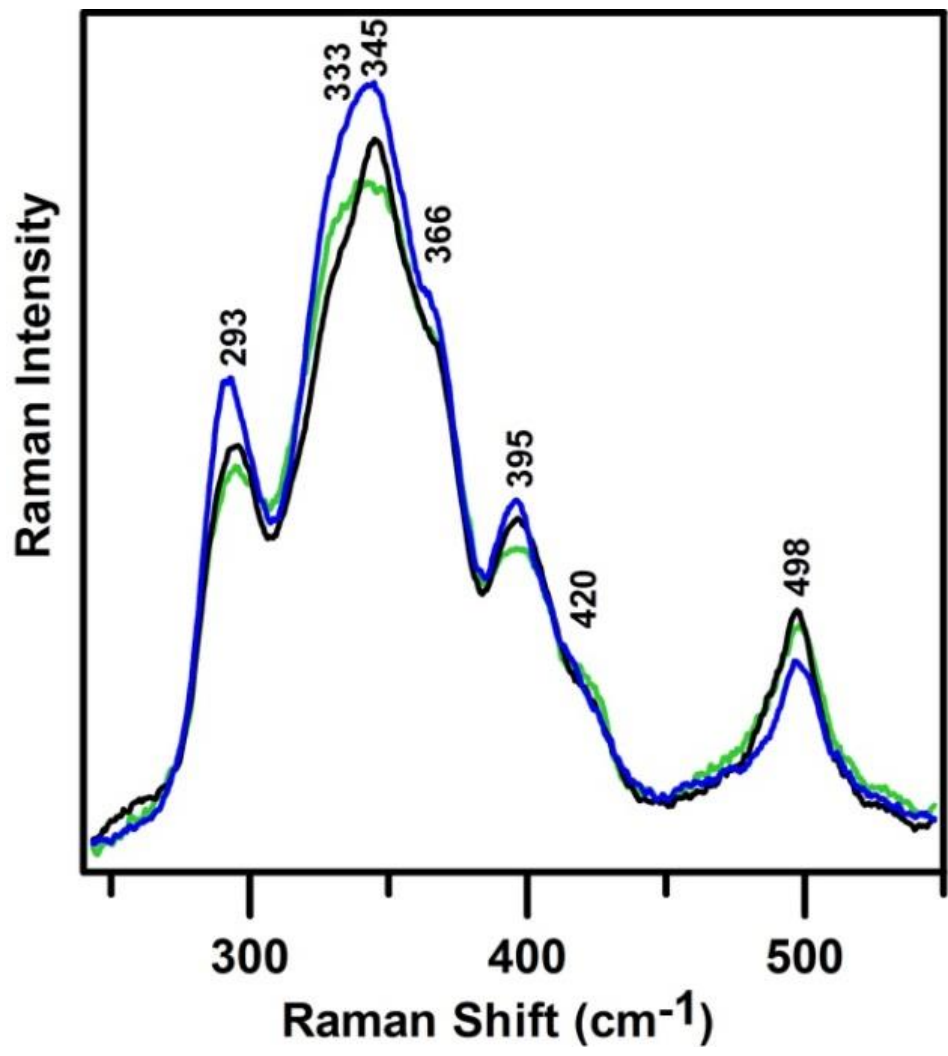


Figure 5.4: Time course of the resonance Raman spectrum of FNR after exposure to air (0–60 min). Samples were exposed to air in the absence of DTT or GSH. The resonance Raman experimental conditions are the same as described in Figure 5.2 and the excitation wavelengths and sample temperatures are shown on each set of spectra. The resonance Raman spectrum of the [3Fe-4S]<sup>+</sup> cluster in *P. furiosus* ferredoxin is shown for comparison with the data collected at 488 nm.

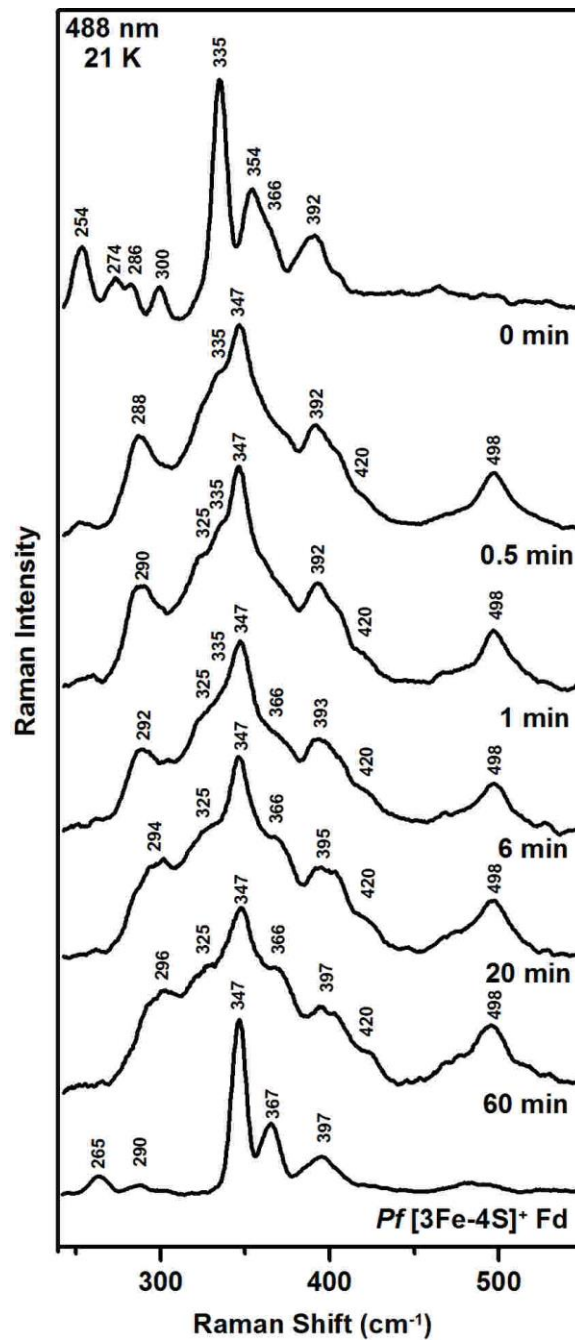
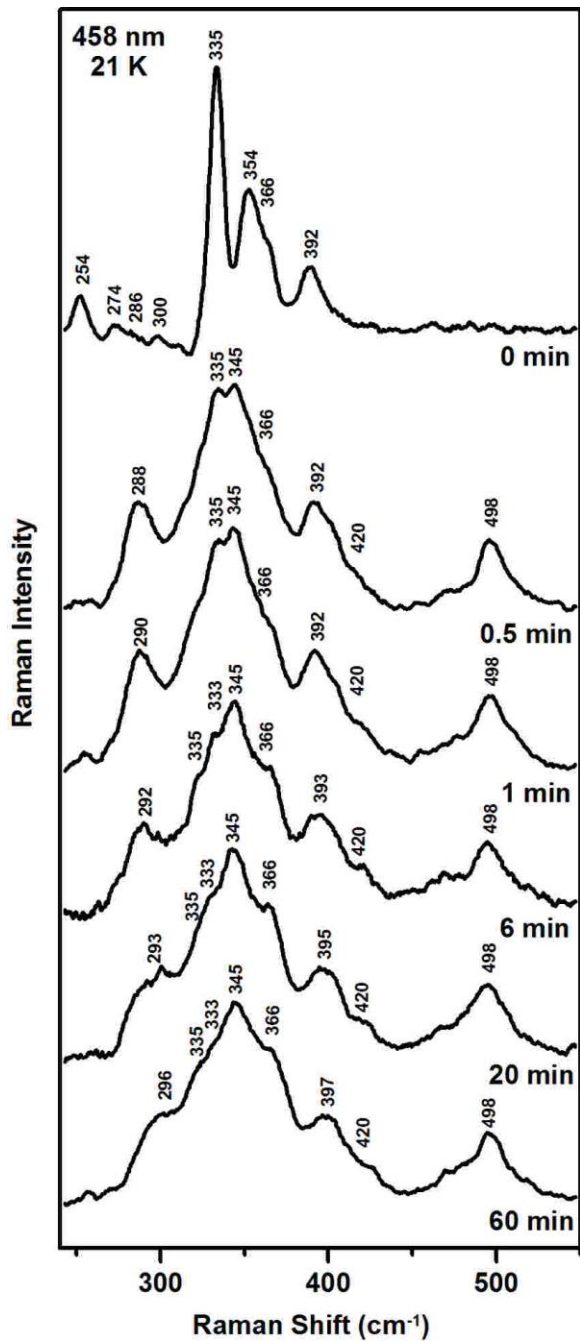


Figure 5.5: Resonance Raman studies of the interconversion between  $[4\text{Fe-4S}]^{2+}$  and  $[2\text{Fe-2S}]^{2+}$  clusters in FNR. (A) Reconstituted  $[4\text{Fe-4S}]^{2+}$ -FNR ( $<2$  mM in  $[4\text{Fe-4S}]^{2+}$  clusters) in the presence of 3 mM GSH. (B)  $[2\text{Fe-2S}]^{2+}$ -FNR obtained by exposing the sample (A) to air for 20 min. (C) After incubation of the sample (B) with 8 mM DTT and 8 mM ferrous ammonium sulfate under anaerobic conditions for 20 min. The Raman experimental conditions are the same as described in Figure 5.2.

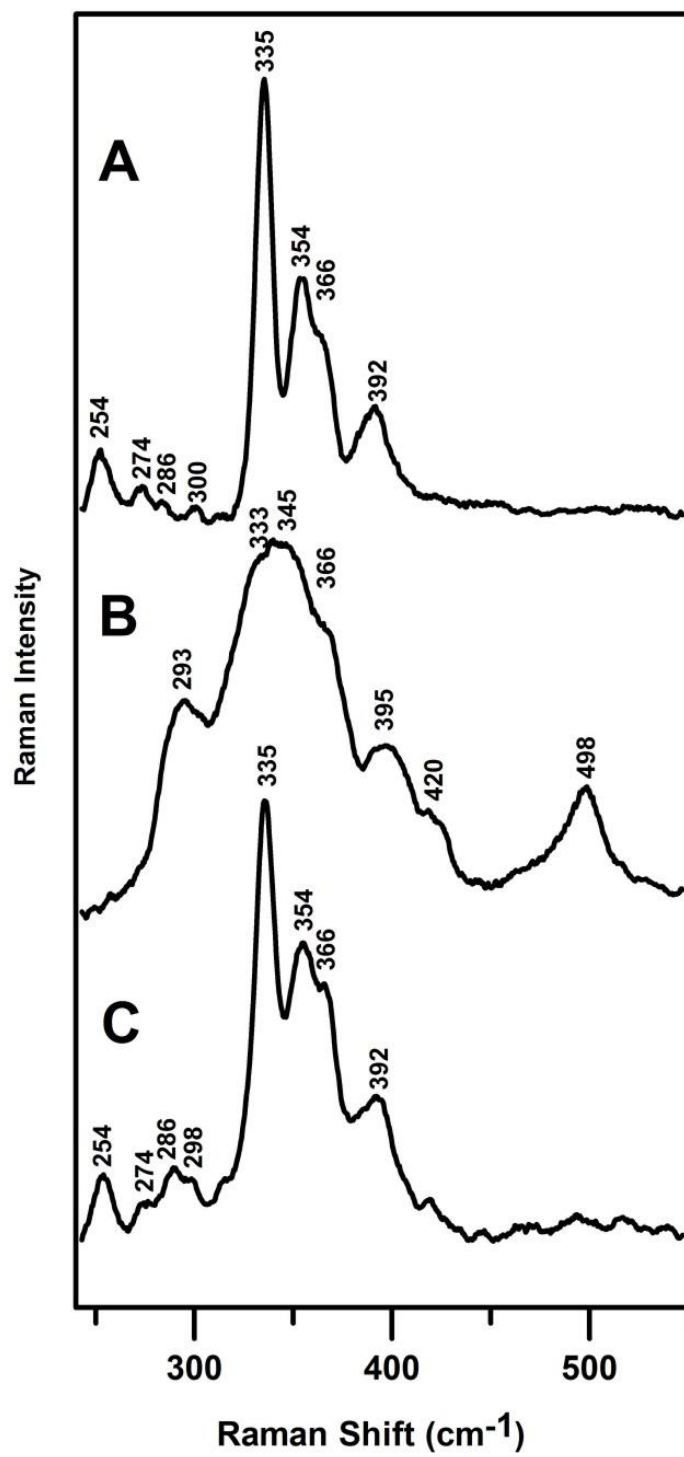


Figure 5.6: UV-visible absorption and CD time course of  $[2\text{Fe-2S}]^{2+}$  to  $[4\text{Fe-4S}]^{2+}$  cluster conversion in FNR without repurification of  $[2\text{Fe-2S}]^{2+}$ -FNR. Sample of  $[2\text{Fe-2S}]^{2+}$ -FNR was obtained by exposing  $[4\text{Fe-4S}]^{2+}$ -FNR to  $\text{O}_2$  for 2 min and the concentration of  $[2\text{Fe-2S}]^{2+}$  centers in FNR was  $57 \mu\text{M}$ . The samples were treated with 3 mM DTT at 0 min and an eightfold excess of ferrous ammonium sulfate was added after 109 min under anaerobic conditions inside a glove box. (Top) Absorption spectra recorded after 0, 109, 114, and 149 min; arrows indicate the direction of changes of absorption intensity as a function of time at discrete wavelengths. (Middle) CD spectra (gray lines) recorded between 0 and 149 min (bold lines); arrows indicate the direction of change of CD intensity as a function of time at discrete wavelengths. (Bottom) Plot of CD intensity at 295, 424, and 480 nm as a function of time.

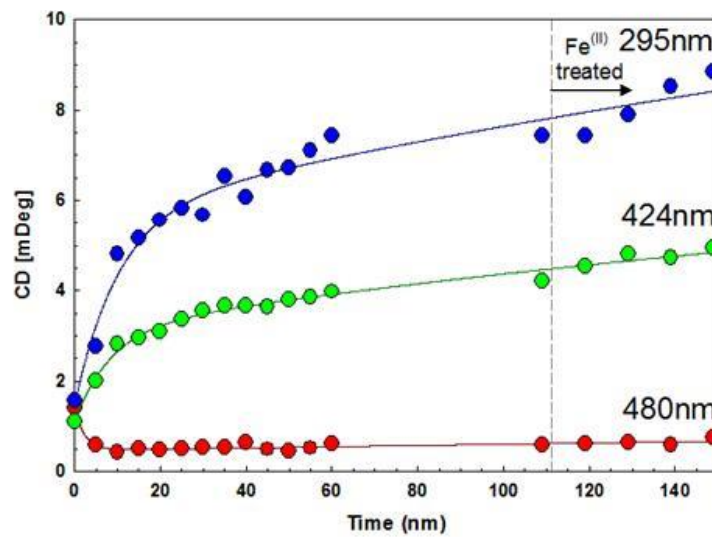
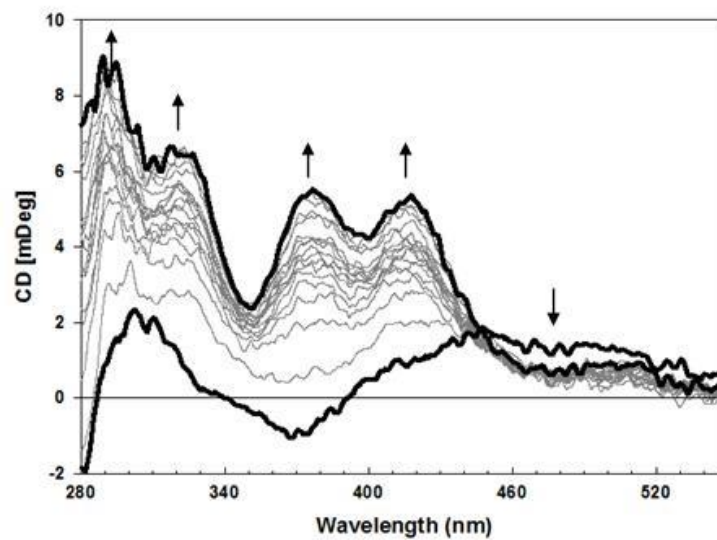
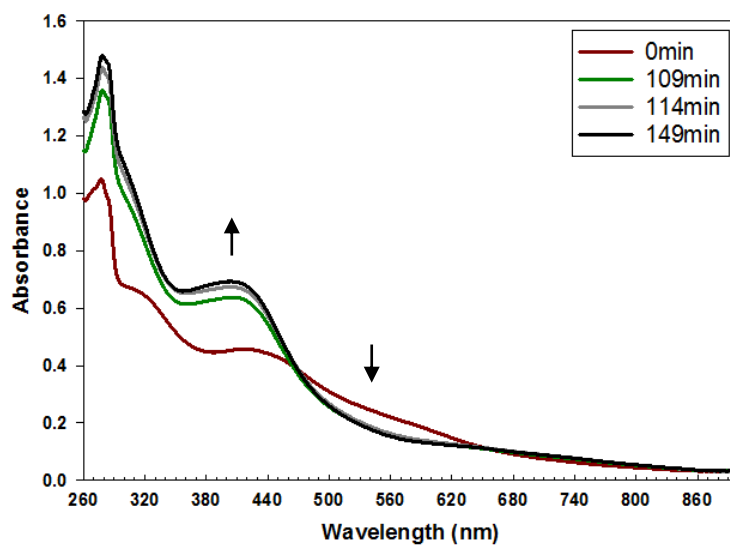


Figure 5.7: UV-visible absorption and CD time course of  $[2\text{Fe-2S}]^{2+}$  to  $[4\text{Fe-4S}]^{2+}$  cluster conversion in FNR after repurification of  $[2\text{Fe-2S}]^{2+}$ -FNR. A sample of  $[2\text{Fe-2S}]^{2+}$ -FNR was obtained by exposing  $[4\text{Fe-4S}]^{2+}$ -FNR to  $\text{O}_2$  for 2 min and repurified using a gel-filtration column (PD10; GE Healthcare). The concentration of  $[2\text{Fe-2S}]^{2+}$  centers in FNR was 50  $\mu\text{M}$ . The samples were treated with 3 mM DTT at 0 min and a fourfold excess of ferrous ammonium sulfate was added after 50 min under anaerobic conditions inside a glove box. (Top) Absorption spectra recorded after 0, 50, 60 and 166 min; arrows indicate the direction of change of absorption intensity as a function of time at discrete wavelengths. (Middle) CD spectra (gray lines) recorded between 0, 50 and 166 min (bold lines); arrows indicate the direction of change of CD intensity as a function of time at discrete wavelengths. (Bottom) Plot of CD intensity at 295, 424, and 480 nm as a function of time.

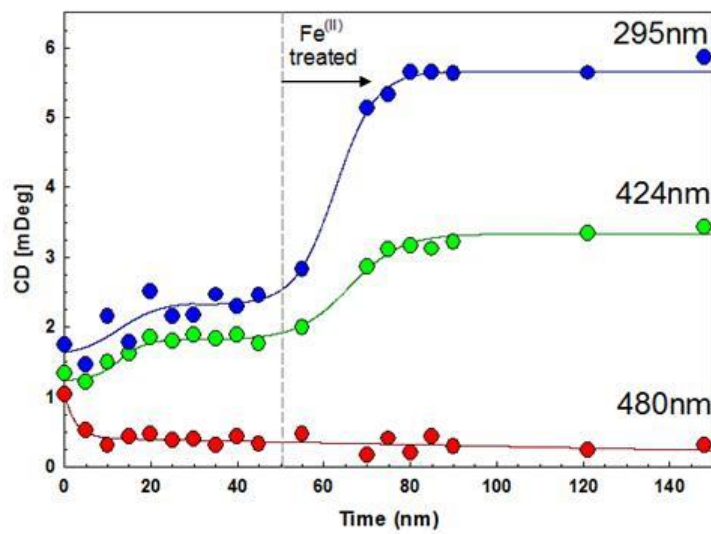
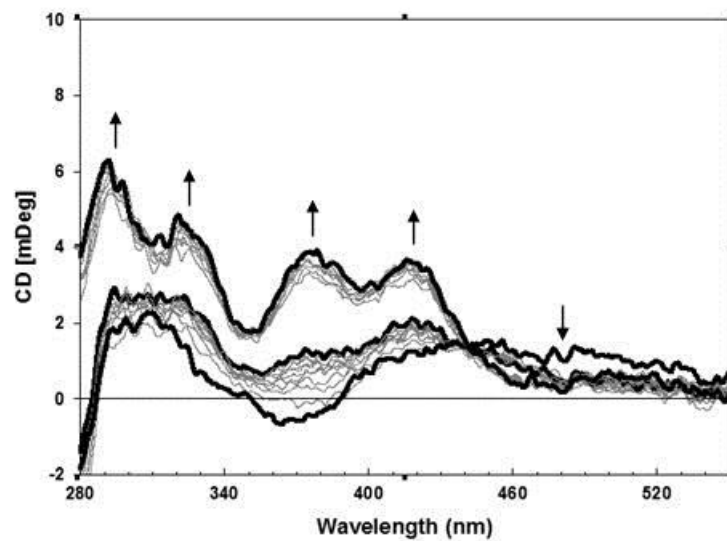
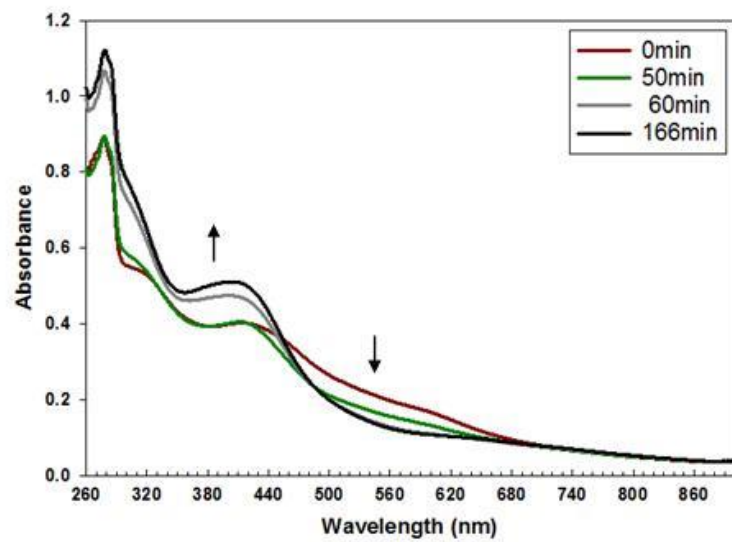


Figure 5.8: Time course of air-exposure of [4Fe-4S]-FNR monitored by MS. Anaerobically reconstituted FNR (<1 mM in [4Fe-4S]<sup>2+</sup> clusters) was exposed to air for 0, 2, 10, 30, and 60 min before analysis using LC-ESI-quadrupole MS. The peak at 29,165 Da corresponds to the monomer molecular ion peak of FNR and the peaks at +32, +64, +96, and +128 Da correspond to the addition of one, two, three, and four covalently bound sulfur atoms, respectively.

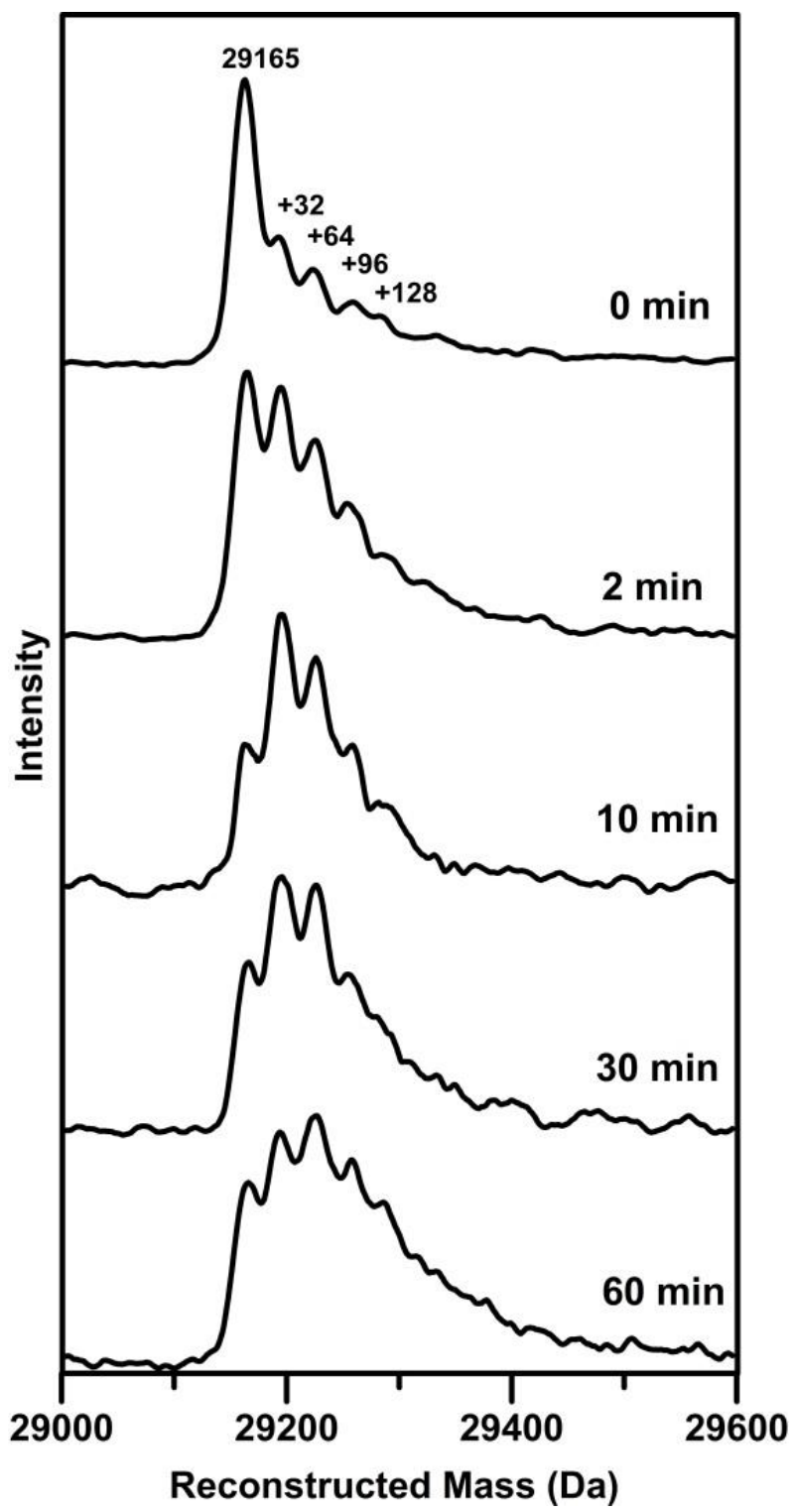
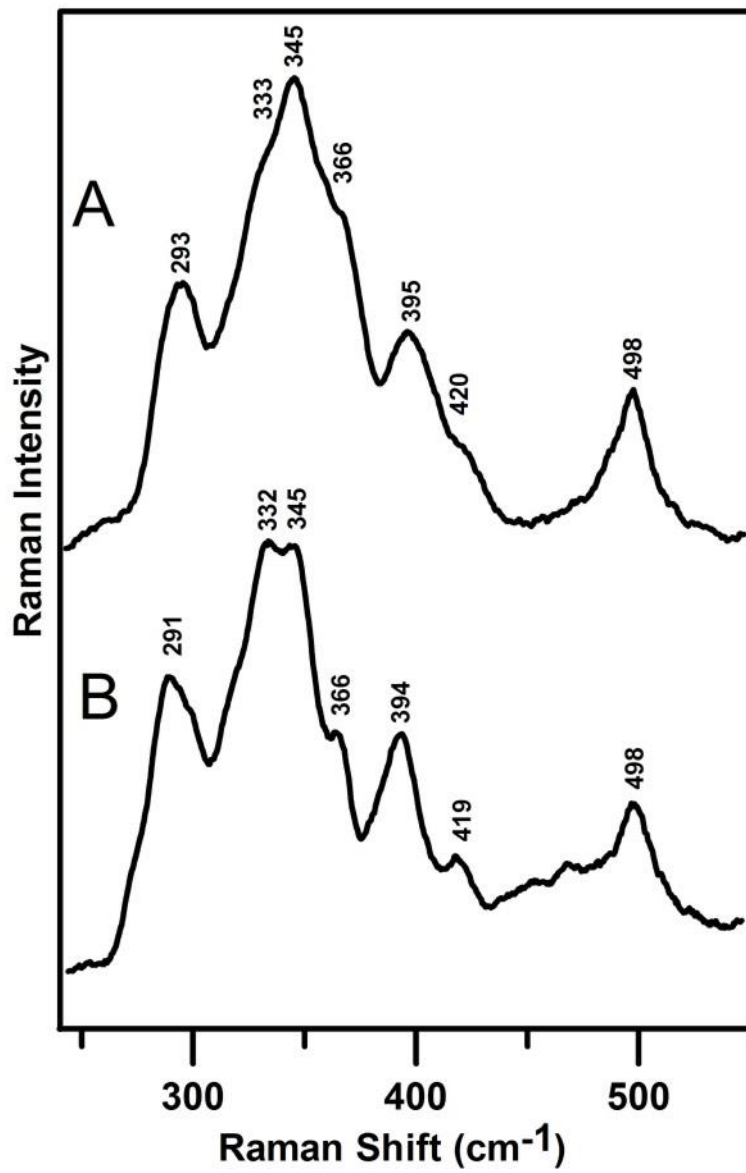


Figure 5.9: Comparison of the resonance Raman spectra of the air-exposed samples of [4Fe-4S]<sup>2+</sup> cluster-containing FNR (A) and BioB (B). The experimental conditions for sample preparation, air exposure, and resonance Raman are the same as described in Figure 5.2, except that samples of BioB were in 50 mM Hepes buffer, pH 7.5.



## CONCLUSIONS AND FUTURE DIRECTIONS

The overall objectives of this work were to establish the role(s) of monothiol glutaredoxins with strict CGFS active-site (CGFS-Grxs) in the Fe-S cluster biogenesis and to understand the mechanism of O<sub>2</sub>-sensing by bacterial fumarate and nitrate reduction (FNR) transcriptional regulatory protein.

Following the genetic and biochemical studies of *S. cerevisiae* (*Sc*) Grx5, a yeast mitochondrial CGFS-Grx (1;2), an evolutionarily conserved role for this family of proteins in mediating the trafficking of preassembled Fe-S clusters has been proposed (3-6). Closely associated with such a role, a variety of CGFS-Grxs have demonstrated the ability to incorporate a labile subunit-bridging [2Fe-2S]<sup>2+</sup> cluster utilizing the active-site cysteine residues and two glutathione (GSH) molecules, and to transfer preassembled clusters to Fe-S cluster-requiring proteins (7). Previously, Picciocchi and coworkers have reported isolation of an Fe-S cluster-containing form of recombinant *Sc* Grx5 and the type of the cluster has been identified as a [2Fe-2S] cluster on the basis of UV-visible absorption characterization alone. However definite evidence of the nature and properties of the bound cluster was not available prior to this work (8). Chapter 2 reports a comprehensive investigation of the Fe-S cluster-bound forms of recombinant *Sc* Grx5 using UV-visible absorption/CD, VTMCD, EPR, resonance Raman, and Mössbauer spectroscopies in combination with analytical and mutagenesis studies. In contrast to published data, recombinant *Sc* Grx5 was isolated exclusively in apo-form devoid of bound clusters. However, we were able to obtain various Fe-S cluster-bound forms of *Sc* Grx5 via *in vitro* anaerobic cysteine desulfurase-mediated reconstitution experiments. In the presence of

GSH, the reaction resulted in a dimeric form of *Sc* Grx5, containing primarily linear  $[3\text{Fe-4S}]^+$  clusters with minor amounts of  $[2\text{Fe-2S}]^{2+}$  and  $[4\text{Fe-4S}]^{2+}$  clusters. In contrast, *in vitro* cluster reconstitution on *Sc* Grx5 leads to the formation of a  $[4\text{Fe-4S}]^{2+}$  cluster-bound dimer in the absence of GSH. Based on the results of the C90S mutagenesis studies, and the requirement of GSH for assembly of linear  $[3\text{Fe-4S}]^+$  cluster, the ligation of the Fe-S clusters observed in *Sc* Grx5 can be reasonably interpreted in terms of the linear  $[3\text{Fe-4S}]^+$  cluster being coordinated at the subunit interface of a homodimer by the active-site cysteines of *Sc* Grx5 and two GSH molecules, in a similar fashion to the structurally characterized  $[2\text{Fe-2S}]^{2+}$  clusters in other CGFS-Grxs, and the  $[4\text{Fe-4S}]^{2+}$  cluster being coordinated at the subunit interface of the homodimer by the active-site cysteine and Cys90, a semi-conserved cysteine residue found in a number of CGFS-Grxs (9). Nevertheless, definitive determination of the coordination environments of the linear  $[3\text{Fe-4S}]^+$  and  $[4\text{Fe-4S}]^{2+}$  clusters in *Sc* Grx5 will require crystallographic investigation.

Consistent with the low aconitase activity observed in the *S. cerevisiae* *grx5* deletion strain (1), the  $[4\text{Fe-4S}]^{2+}$  cluster-bound form of *Sc* Grx5 is competent for restoring the activity of apo aconitase *in vitro*, at rates comparable to those reported using  $[4\text{Fe-4S}]$ -IscU (10). However, the relatively slow cluster transfer rate, coupled with *in vivo* studies which indicate that Cys90 is not required for observing the phenotype associated with *grx5* deletion (11), argue against a role for *Sc* Grx5 in maturation of  $[4\text{Fe-4S}]^{2+}$  cluster-requiring proteins *in vivo*. Currently there is no indication that linear  $[3\text{Fe-4S}]^+$  clusters are functional components of any Fe-S protein. However linear  $[3\text{Fe-4S}]^+$  clusters have been observed in partially unfolded proteins under denaturing or oxidative stress conditions (12-16) and have shown to undergo reductive conversion to yield  $[2\text{Fe-2S}]^{2+}$  and  $[4\text{Fe-4S}]^{2+}$  clusters (12). Consequently, the ability to bind linear  $[3\text{Fe-4S}]^+$

clusters may indicate a role for *Sc* Grx5 in scavenging and recycling damaged Fe-S clusters released during protein unfolding under oxidative stress conditions. Hence future experiments should be designed to see if linear  $[3\text{Fe-4S}]^+$  clusters can be transferred to apo Fe-S proteins and converted to  $[4\text{Fe-4S}]^{2+}$  or  $[2\text{Fe-2S}]^{2+}$  clusters *in situ*, as has been shown to be the case in aconitase (12).

Although Mössbauer analysis revealed a minor contribution from a  $[2\text{Fe-2S}]^{2+}$  cluster (~10% of total Fe) in *Sc* Grx5 reconstituted in the presence of GSH (see Chapter 2), we have been unsuccessful in obtaining a homogenous  $[2\text{Fe-2S}]^{2+}$  cluster-bound form of *Sc* Grx5. This is surprising in light of the compelling evidence that the  $[2\text{Fe-2S}]^{2+}$  cluster-bound form is the dominant, if not exclusive, functional cluster-containing form of CGFS-Grxs (6;17;18). At present, we tentatively propose that the preference for a linear  $[3\text{Fe-4S}]^+$  cluster over  $[2\text{Fe-2S}]^{2+}$  cluster in *Sc* Grx5 is attributed to small structural differences compared to other CGFS-Grxs. This hypothesis certainly will require further structural investigation of *Sc* Grx5. In addition, it will clearly be of great interest to investigate the ability and requirement of *Sc* Grx5 to incorporate an Fe-S cluster *in vivo*. Nevertheless, as well as providing the first reliable evidence on the nature of Fe-S clusters that can be assembled in recombinant *Sc* Grx5, the results presented in Chapter 2 clearly show the potential for CGFS-Grxs to act as versatile Fe-S cluster-binding proteins that are able to accommodate  $[2\text{Fe-2S}]^{2+}$ ,  $[4\text{Fe-4S}]^{2+}$  and linear  $[3\text{Fe-4S}]^+$  clusters. Indeed, as judged by the distinctive properties of linear  $[3\text{Fe-4S}]^+$  clusters showed by UV-visible absorption/CD and Mössbauer spectroscopies, it is evident that the ability to incorporate this unusual type of Fe-S center is a common attribute of many CGFS-Grxs (3;8;18).

The genome of *A. vinelandii* encodes two orthologs of *Sc* Grx5, termed *Av* Grx5 and *Av* Grx-nif. The *grx-nif* gene is located closely to the *nif* gene cluster, and its inactivation can lead to

a 50% decrease in the activity of the Fe protein (19). In Chapter 4, we have demonstrated that the properties and coordination environment of the  $[2\text{Fe-2S}]^{2+}$  cluster in *Av* Grx5 and Grx-nif homodimers are nearly identical to the Mössbauer- and crystallography-defined subunit-bridging  $[2\text{Fe-2S}]^{2+}$  clusters in CGFS-Grxs from other organisms (3;6;18;20;21). Subsequently, in order to elucidate the detailed roles of CGFS-Grxs in Fe-S cluster trafficking and storage, especially in terms of their functional relationship with essential components of the Fe-S cluster assembly pathways; we have carried out the first systematic investigation on cluster exchange between CGFS-Grxs and physiologically relevant proteins selected based on results from *in vivo* studies (2;22). This work is collectively presented in Chapters 3, 4 and Appendix C. The most pertinent results of the *in vitro* CD-monitored cluster transfer experiments can be summarized as follows: (1) *Av* Grx5 can rapidly and quantitatively accept an intact  $[2\text{Fe-2S}]^{2+}$  cluster from the primary scaffold protein IscU only in the presence of the dedicated co-chaperones (HscA and HscB) in an ATP-dependent reaction; (2) *Av*  $[2\text{Fe-2S}]$ -Grx5 is a more effective *in vitro* cluster donor to the ISC-specific ferredoxin (IscFdx) than  $[2\text{Fe-2S}]$ -IscU (23); (3) *Av*  $[2\text{Fe-2S}]$ -Grx-nif is an effective cluster donor to  $\text{Nif}^+$ IscA (an A-type protein with a dual role as Fe donor and cluster carrier); (4) *Av* Grx5 was shown to quantitatively accept  $[2\text{Fe-2S}]^{2+}$  clusters from *Av*  $[4\text{Fe-4S}]$ -NfuA, a cluster carrier protein, under anaerobic conditions via a yet-to-be-identified mechanism.

The results of cluster transfer from *Av*  $[2\text{Fe-2S}]$ -IscU to apo *Av* Grx5 were of particular interest, as they provided the first *in vitro* evidence demonstrating CGFS-Grxs as the immediate cluster acceptor to the U-type scaffold proteins and permitted rationalization of the accumulation of Fe on *S. cerevisiae* mitochondrial Isu (ortholog to bacterial IscU) upon deletion of the gene encoding the mitochondrial Grx5 (2). Taken together, the *in vitro* cluster transfer results provided compelling evidence in support of the proposal that CGFS-Grxs function as

intermediate  $[2\text{Fe-2S}]^{2+}$  cluster carrier proteins in both the ISC and NIF cluster assembly systems. CGFS-Grxs clearly serve as key intermediate carrier proteins facilitating the transfer of preassembled  $[2\text{Fe-2S}]^{2+}$  clusters from U-type scaffold proteins to a specific subset of physiological relevant acceptor proteins for their maturation as well the distribution of  $[2\text{Fe-2S}]^{2+}$  clusters assembled on IscU to other carrier proteins such as the A-type proteins. While the physiological significance of the ability of *Av* Grx5 to accept a  $[2\text{Fe-2S}]^{2+}$  cluster from  $[4\text{Fe-4S}]^{2+}$  cluster-containing protein remains unclear and requires further investigation, it nevertheless implicates a  $[2\text{Fe-2S}]^{2+}$  cluster storage function for CGFS-Grxs under oxidative stress conditions to avoid Fe accumulation and to assist in the repair of damaged  $[4\text{Fe-4S}]^{2+}$  clusters. The latter hypothesis for the involvement of CGFS-Grxs in  $[4\text{Fe-4S}]^{2+}$  cluster repair is proposed in light of the ability of  $^{\text{Nif}}$ IscA, a  $[2\text{Fe-2S}]^{2+}$  cluster acceptor for  $[2\text{Fe-2S}]\text{-Grx-nif}$ , to reversibly cycle between  $[2\text{Fe-2S}]^{2+}$  and  $[4\text{Fe-4S}]^{2+}$  cluster-bound forms in response to cellular redox conditions, in order to effect maturation of  $[4\text{Fe-4S}]^{2+}$  cluster proteins (see Appendix B). A model demonstrating these proposed functions of CGFS-Grxs in  $[2\text{Fe-2S}]^{2+}$  cluster trafficking and storage is illustrated schematically in Figure 6.1. At the present moment, there is still a pressing need to identify physiological partners of CGFS-Grxs in Fe-S cluster biogenesis. Future genetic studies, including two-hybrid screening, of CGFS-Grxs from a wide range of organisms and/or organelles will certainly be helpful in providing guidance to future *in vitro* cluster transfer studies between CGFS-Grxs and a wider range of potential partner proteins. Moreover, as this proposed model is largely built on evidence obtained for the ISC and NIF Fe-S cluster assembly systems, future studies should also be directed towards elucidating the functions of CGFS-Grxs in the SUF system.

The research presented in this dissertation has only addressed the nature and putative functions of Fe-S cluster-bound forms of CGFS-Grxs homodimers. Bioinformatics analysis and genetic studies have indicated conserved physical and functional interactions between CGFS-Grxs and BolA proteins, another widely distributed family of proteins (24-26). In *S. cerevisiae*, a BolA-like protein termed Fra2 can form a  $[2\text{Fe-2S}]^{2+}$  cluster-bridged heterodimer with the cytosolic CGFS-Grxs (Grx3/4) with cluster coordination provided by the active-site cysteine from Grx3/4, a conserved histidine from Fra2, the cysteine moiety from a GSH molecule, with the fourth ligand yet to be determined (27). Subsequently, formation of a  $[2\text{Fe-2S}]^{2+}$  cluster-bound heterodimer has been characterized for human Glrx3-BolA2 (28) and *E. coli* Grx4-BolA (3) complexes. Interestingly, whereas the  $[2\text{Fe-2S}]^{2+}$  cluster-bound yeast Fra2-Grx3/4 and human Glrx3-BolA2 complexes share almost identical spectroscopic properties (27;28), the  $[2\text{Fe-2S}]^{2+}$  cluster in the *E. coli* Grx4-BolA complex exhibits significant spectroscopic differences (S. Randeniya, A. Dlouhy, C. E. Outten, and M. K. Johnson, unpublished results), indicative of differences in the cluster coordination environment. Both *S. cerevisiae* and *A. vinelandii* genome possess BolA and BolA-like proteins (Aim1 and Yal044w-a in *S. cerevisiae* mitochondria, and BolA and YrbA in *A. vinelandii*) that can potentially interact respectively with *Sc* Grx5 and the two *Av* CGFS-Grxs. We have obtained preliminary results indicating a possible  $[2\text{Fe-2S}]^{2+}$  cluster-containing *Sc* Grx5-Aim1 complex (B. Zhang, A. Dlouhy, C. E. Outten, and M. K. Johnson, unpublished results), and most recently, Yal044w-a has been purified by our collaborators from University of South Carolina and can be readily used to investigate the potential interaction with *Sc* Grx5. No doubt, detailed biophysical and biochemical investigations of the potential Grx-BolA complexes from *A. vinelandii* and *S. cerevisiae* in the future would

certainly benefit the understanding of specific molecular interactions between these two families of proteins.

For *S. cerevisiae* cytosolic Grx3/4, interaction with Fra2 transforms their functions from intracellular Fe trafficking to regulation of cellular Fe homeostasis (27;29). In light of this discovery, we hypothesize that a number of CGFS-Grxs, especially those with single Grx domain, might be able to assume a similar role in assessing and regulating cellular Fe-S cluster status upon interaction with BolA proteins, possibly via the extent of cluster-loading in Grx-BolA heterodimer. In support of this tentative proposal, *E. coli* [2Fe-2S]<sup>2+</sup> cluster-bound Grx4-BolA complex has been shown to be much less effective a cluster donor to IscFdx than the [2Fe-2S]<sup>2+</sup> cluster-bound Grx4 homodimer (3). To evaluate this hypothesis, it will be important to determine whether bacterial CGFS-Grxs functionally interact with IscR, which functions as a transcriptional repressor of the ISC system in its [2Fe-2S]<sup>2+,+</sup> cluster-bound form (30). We have tentatively conclude that [2Fe-2S]<sup>2+</sup> cluster-bound *Av* Grx5 homodimer is unlikely a cluster donor to apo IscR based on the results of *in vitro* cluster transfer experiments (B. Zhang and M. K. Johnson, unpublished results). The question remains whether the putative [2Fe-2S]<sup>2+</sup> cluster-bound Grx-BolA complex is able to function as cluster donor to IscR. Furthermore, *Sc* Grx5 homologues in higher eukaryotes are likely to be part of a yet-to-be identified mechanism that directs the utilization of bioavailable Fe for Fe-S cluster maturation and heme biosynthesis (5;18). Also unknown is whether mitochondrial BolA-like proteins are components of this pathway. Alternatively, single-domain CGFS-Grxs may function together with BolA proteins to ensure correct insertion of Fe-S clusters into very specific target proteins, possibly including components of respiratory chain and/or lipoate synthase (31). Hence a comprehensive understanding of the cellular functions of CGFS-Grxs and BolA proteins will be essential for

developing treatments for anemia caused by Grx5 deficiency (5) and multiple mitochondrial dysfunctions syndrome caused by BolA3 mutations (31). Future genetic and biophysics studies should be very informative in this regard.

The specific objective in respect to the research project on FNR was to address the O<sub>2</sub>-sensing mechanism. Through a series of elegant spectroscopic and biochemical studies, it has been shown that inactivation of FNR upon reaction with molecular oxygen involves the transformation of a protein-bound oxidatively labile [4Fe-4S]<sup>2+</sup> cluster into a semi-stable [2Fe-2S]<sup>2+</sup> cluster (32). However, there was no consensus on whether the cluster conversion involved primarily iron or sulfide oxidization (33-35). Using the combination of resonance Raman spectroscopy and mass spectrometry, we were able to demonstrate in Chapter 5 that the [2Fe-2S]<sup>2+</sup> clusters in the O<sub>2</sub>-exposed FNR were in fact coordinated by one or two cysteine persulfide ligands. This discovery has unequivocally shown for the first time that the O<sub>2</sub>-sensing by FNR is primarily a sulfur-based oxidation that involves the oxidation and retention of bridging sulfides of the [4Fe-4S]<sup>2+</sup> cluster in the form of [2Fe-2S]<sup>2+</sup> cluster-bound cysteine persulfides. In light of the new findings, a revised overall FNR O<sub>2</sub>-sensing mechanism was presented in Chapter 5.

The fact that both [2Fe-2S]<sup>2+</sup> cluster-containing FNR and apo-FNR are inactive as transcriptional regulator raised questions concerning the physiological relevance of the [2Fe-2S]<sup>2+</sup> cluster-bound FNR. Previous studies have revealed that the [4Fe-4S]<sup>2+</sup> cluster in FNR can be readily restored from the O<sub>2</sub>-induced [2Fe-2S]<sup>2+</sup> cluster-bound form by incubation under reducing conditions with Fe<sup>2+</sup> ion and sulfide (generated *in situ* by L-Cys and cysteine desulfurase). In Chapter 5, we additionally showed that Fe<sup>2+</sup> ion and a dithiol reagent, but not sulfide, are required under anaerobic conditions to effect conversion of the cysteine persulfide ligated [2Fe-2S]<sup>2+</sup> cluster back to the all-cysteinylligated [4Fe-4S]<sup>2+</sup> cluster in FNR. Hence our

results indicate that  $[2\text{Fe-2S}]^{2+}$  cluster-bound FNR is functionally relevant for facilitating a rapid response to dynamic changes in cellular  $\text{O}_2$  levels via the facile reversible cycling between cysteine-ligated  $[4\text{Fe-4S}]^{2+}$  and cysteine persulfide-ligated  $[2\text{Fe-2S}]^{2+}$  clusters.

As we pointed out in Chapter 5, formation of cysteine persulfide-ligated  $[2\text{Fe-2S}]^{2+}$  cluster is likely a common pathway of  $\text{O}_2$ -induced degradation of biological  $[4\text{Fe-4S}]^{2+}$  clusters. In this study, the assignment of the resonance Raman band observed at  $498\text{ cm}^{-1}$  to the cluster-bound CysS-S stretching mode, together with the anomalous resonance Raman features in the Fe-S stretching region, enabled us to confirm the presence of cysteine persulfide-ligated  $[2\text{Fe-2S}]^{2+}$  cluster generated by  $\text{O}_2$ -exposure of the radical-SAM  $[4\text{Fe-4S}]^{2+}$  cluster in BioB (see Chapter 5). Similar resonance Raman results have also been obtained for the crystallographically identified cysteine persulfide-ligated  $[2\text{Fe-2S}]^{2+}$  cluster in the non-radical SAM cluster binding site of HydE (36) and (B. Zhang, Y. Nicolet, J. Fontecilla-Camps, and M. K. Johnson, unpublished results). Systematic resonance Raman reinvestigations of  $\text{O}_2$ -induced  $[4\text{Fe-4S}]^{2+}$  to  $[2\text{Fe-2S}]^{2+}$  cluster conversions over a wider spectral range have been planned in our laboratory to identify  $[4\text{Fe-4S}]^{2+}$  clusters that convert to this distinct type of  $[2\text{Fe-2S}]^{2+}$  cluster on reaction with  $\text{O}_2$ . However, due to the limitations of resonance Raman spectroscopy and difficulty of performing reliable biochemical assays for sulfane sulfur, quantitative analysis of cysteine persulfide formation will present challenges for future studies.

In addition to providing new information concerning the  $\text{O}_2$ -sensing mechanism of FNR, the novel type of cluster interconversion presented in this dissertation provides a new mechanism for the assembly or repair of  $\text{O}_2$ -damaged  $[4\text{Fe-4S}]^{2+}$  clusters. Previous biophysical studies have provided compelling evidence for *de novo*  $[4\text{Fe-4S}]^{2+}$  cluster biosynthesis at the subunit interface of U-type- and A-type-type proteins via the reductive coupling of two adjacent  $[2\text{Fe-2S}]^{2+}$

clusters to generate one  $[4\text{Fe-4S}]^{2+}$  cluster ((37) and Appendix B). The discovery of cysteine persulfide-ligated  $[2\text{Fe-2S}]^{2+}$  clusters that can be readily converted to  $[4\text{Fe-4S}]^{2+}$  clusters under anaerobic conditions raises the possibility that instead of insertion of a fully assembled  $[4\text{Fe-4S}]$  cluster, maturation of  $[4\text{Fe-4S}]$  cluster-requiring proteins may occur *in situ* via trafficking  $[2\text{Fe-2S}]^{2+}$  cluster to apo proteins containing cysteine persulfides, followed by  $\text{Fe}^{2+}$  insertion coupled with dithiol-mediated cysteine-persulfide reduction. The attractive aspect of this putative cluster assembly mechanism is that it avoids the trafficking of the  $[4\text{Fe-4S}]^{2+}$  clusters that are often oxidatively labile, and therefore would have advantages for the assembly or repair of biological  $[4\text{Fe-4S}]^{2+}$  clusters under semi-aerobic conditions. A proposed model for the biosynthesis or repair of  $\text{O}_2$  sensitive  $[4\text{Fe-4S}]^{2+}$  cluster is summarized in Figure 6. 2.

The initial formation of protein-bound cysteine persulfide in the proposed mechanism is inspired by the observation of persulfides or polysulfides in apo-aconitase that result from careful ferricyanide oxidization (38). Although it is not yet known exactly how cysteine persulfides and/or polysulfides can be formed in apo proteins under normal conditions, our preliminary ESI-MS results have demonstrated that IscS cysteine desulfurase is able to transfer multiple (up to four)  $\text{S}^0$  to apo-FNR (B. Zhang and M. K. Johnson, unpublished data), suggesting that cysteine desulfurase-catalyzed cysteine persulfide and/or polysulfide formation on cysteine residues is a plausible mechanism. In the schematic proposal illustrated in Figure 6.2, the immediate  $[2\text{Fe-2S}]^{2+}$  cluster donor for *in situ*  $[4\text{Fe-4S}]^{2+}$  cluster assembly is shown as  $[2\text{Fe-2S}]^{2+}$  cluster-bound form of A-type proteins for the sake of clarity. While this is possible for  $[4\text{Fe-4S}]^{2+}$  cluster formation in prokaryotes, it should be stressed that there is currently no *in vivo* or *in vitro* evidence that eukaryotic mitochondrial A-type proteins bind Fe-S clusters (39;40). Hence other  $[2\text{Fe-2S}]^{2+}$  cluster carrier proteins, including CGFS-Grxs, could be involved in this

step to ensure efficient trafficking of  $[2\text{Fe-2S}]^{2+}$  clusters from U-type scaffolds to specific proteins on which  $[4\text{Fe-4S}]^{2+}$  clusters are to be assembled. In light of discovery that Fe-bound A-type proteins can undergo cysteine-mediated release of free  $\text{Fe}^{2+}$  ((41) and see Appendix A) and that in eukaryotic mitochondria Fe-bound A-type proteins (Isa1 and Isa2) and Iba57 are specifically required for  $[4\text{Fe-4S}]^{2+}$  cluster maturation following the *de novo*  $[2\text{Fe-2S}]^{2+}$  cluster assembly on U-type scaffold proteins (39;40), we expect that Fe-bound A-type proteins may have the potential to serve as the immediate  $\text{Fe}^{2+}$  source for the *in situ* formation and/or repair of  $[4\text{Fe-4S}]^{2+}$  cluster from the cysteine persulfide-ligated  $[2\text{Fe-2S}]^{2+}$  cluster precursor. In an attempt to test this hypothesis, *in vitro* experiments involving using CD spectroscopy to monitor whether the  $[4\text{Fe-4S}]^{2+}$  cluster in FNR can be regenerated from the cysteine persulfide-ligated  $[2\text{Fe-2S}]^{2+}$  cluster using Fe-bound *Ec* IscA in place of ferrous ammonium sulfate as Fe source have been designed. However, assessing whether  $\text{Fe}^{2+}$  is donated via direct interprotein transfer or first released in the form of free Fe before being utilized will be a difficult task. Attempts may be made by comparing the kinetics of  $[4\text{Fe-4S}]^{2+}$  cluster formation using ferrous ammonium sulfate and Fe-bound IscA as different Fe sources. However, should the CD spectra of this process become too complicated to interpret, experiments can be carried out using  $^{57}\text{Fe}$ -labeled Fe-bound IscA in the presence of excess amount of natural abundance Fe. Mössbauer spectroscopy can then be used to monitor the time-course of this process and provide quantitative analysis of Fe content in the final  $[4\text{Fe-4S}]^{2+}$  cluster. Alternatively the bacterial Iba57 homologs will be incorporated into these experiments, since Iba57 has been shown to be required for efficient Fe release from Isa1/Isa2 for  $[4\text{Fe-4S}]^{2+}$  cluster assembly in eukaryotes (39;40).

In summary, the two major research projects undertaken in this work are linked together through the insights provided towards the understanding of Fe-S cluster biogenesis. In particular,

the work presented herein has revealed that the assembly and repair mechanisms of biological [4Fe-4S] clusters are likely to be much more diverse and complicated than previously envisioned. While [4Fe-4S] clusters are usually sensitive towards oxidative stress conditions, they are one of the most abundant types of biological prosthetic group and [4Fe-4S] cluster-containing proteins are critically involved in almost all fundamental life processes. Therefore a thorough understanding of the mechanism of [4Fe-4S] cluster maturation and repair may lead to therapeutic breakthroughs for human diseases including several neurodegenerative diseases and cancers.

## References

1. Rodríguez-Manzanaque, M. T., Tamarit, J., Bellí, G., Ros, J., and Herrero, E. (2002) Grx5 is a mitochondrial glutaredoxin required for the activity of iron/sulfur enzymes, *Mol. Biol. Cell* 13, 1109-1121.
2. Mühlenhoff, U., Gerber, J., Richhardt, N., and Lill, R. (2003) Components involved in assembly and dislocation of iron-sulfur clusters on the scaffold protein Isc1p, *EMBO J.* 22, 4815-4825.
3. Yeung, N., Gold, B., Liu, N. L., Prathapam, R., Sterling, H. J., Williams, E. R., and Butland, G. (2011) The *E. coli* monothiol glutaredoxin GrxD forms homodimeric and heterodimeric FeS cluster containing complexes, *Biochemistry* 50, 8957-8969.
4. Molina-Navarro, M. M., Casas, C., Piedrafita, L., Bellí, G., and Herrero, E. (2006) Prokaryotic and eukaryotic monothiol glutaredoxins are able to perform the functions of Grx5 in the biogenesis of Fe/S clusters in yeast mitochondria, *FEBS Lett.* 580, 2273-2280.
5. Wingert, R. A., Galloway, J. L., Barut, B., Foott, H., Fraenkel, P., Axe, J. L., Weber, G. J., Dooley, K., Davidson, A. J., Schmidt, B., Paw, B. H., and Shaw, G. C. (2005) Deficiency of glutaredoxin 5 reveals Fe-S clusters are required for vertebrate haem synthesis, *Nature* 436, 1035-1039.
6. Bandyopadhyay, S., Gama, F., Molina-Navarro, M. M., Gualberto, J. M., Claxton, R., Naik, S. G., Huynh, B. H., Herrero, E., Jacquot, J.-P., Johnson, M. K., and Rouhier, N. (2008) Chloroplast monothiol glutaredoxins as scaffold proteins for the assembly and delivery of [2Fe-2S] clusters, *EMBO J.* 27, 1122-1133.
7. Rouhier, N., Couturier, J., Johnson, M. K., and Jacquot, J. P. (2010) Glutaredoxins: roles in iron homeostasis, *Trends Biochem. Sci.* 35, 43-52.
8. Picciocchi, A., Saguez, C., Boussac, A., Cassier-Chauvat, C., and Chauvat, F. (2007) CGFS-type monothiol glutaredoxins from the cyanobacterium *Synechocystis* PCC6803 and other evolutionary distant model organisms possess a glutathione-ligated [2Fe-2S] cluster, *Biochemistry* 46, 15018-15026.
9. Herrero, E. and de la Torre-Ruiz, M. A. (2007) Monothiol glutaredoxins: a common domain for multiple functions, *Cell. Mol. Life Sci.* 64, 1518-1530.
10. Unciuleac, M.-C., Chandramouli, K., Naik, S., Mayer, S., Huynh, B. H., Johnson, M. K., and Dean, D. R. (2007) *In vitro* activation of apo-aconitase using a [4Fe-4S] cluster-loaded form of the IscU [Fe-S] cluster scaffolding protein, *Biochemistry* 46, 6812-6821.
11. Belli, G., Polaina, J., Tamarit, J., De La Torre, M. A., Rodríguez-Manzanaque, M. T., Ros, J., and Herrero, E. (2002) Structure-function analysis of yeast Grx5 monothiol glutaredoxin defines essential amino acids for the function of the protein, *J. Biol. Chem.* 277, 37590-37596.

12. Kennedy, M. C., Kent, T. A., Emptage, M. H., Merkle, H., Beinert, H., and Münck, E. (1984) Evidence for the formation of a linear [3Fe-4S] cluster in partially unfolded aconitase, *J. Biol. Chem.* 259, 14463-14471.
13. Jones, K., Gomes, C. M., Huber, H., Teixeira, M., and Wittung-Stafshede, P. (2002) Formation of a linear [3Fe-4S] cluster in a seven-iron ferredoxin triggered by polypeptide unfolding, *J. Biol. Inorg. Chem.* 7, 357-362.
14. Higgins, C. L. and Wittung-Stafshede, P. (2004) Formation of linear three-iron clusters in *Aquilex aeolicus* two-iron ferredoxins: effect of protein unfolding speed, *Arch. Biochem. Biophys.* 427, 154-163.
15. Griffin, S., Higgins, C. L., Soulimane, T., and Wittung-Stafshede, P. (2003) High thermal and chemical stability of *Thermus thermophilus* seven-iron ferredoxin. Linear clusters form at high pH on polypeptide unfolding, *Eur. J. Biochem.* 270, 4736-4743.
16. Leal, S. S., Teixeira, M., and Gomes, C. M. (2004) Studies on the degradation pathway of iron-sulfur centers during unfolding of a hyperstable ferredoxin: Cluster dissociation, iron release and proteins stability, *J. Biol. Inorg. Chem.* 9, 987-996.
17. Pujol-Carrion, N., Belli, G., Herrero, E., Nogues, A., and de la Torre-Ruiz MA (2006) Glutaredoxins Grx3 and Grx4 regulate nuclear localisation of Aft1 and the oxidative stress response in *Saccharomyces cerevisiae*, *J. Cell Sci.* 119, 4554-4564.
18. Ye, H., Jeong, S. Y., Ghosh, M. C., Kovtunovych, G., Silvestri, L., Ortillo, D., Uchida, N., Tisdale, J., Camaschella, C., and Rouault, T. A. (2010) Glutaredoxin 5 deficiency causes sideroblastic anemia by specifically impairing heme biosynthesis and depleting cytosolic iron in human erythroblasts, *J. Clin. Invest.* 120, 1749-1761.
19. Setubal, J. C., dos, S. P., Goldman, B. S., Ertesvag, H., Espin, G., Rubio, L. M., Valla, S., Almeida, N. F., Balasubramanian, D., Cromes, L., Curatti, L., Du, Z., Godsy, E., Goodner, B., Hellner-Burris, K., Hernandez, J. A., Houmiel, K., Imperial, J., Kennedy, C., Larson, T. J., Latreille, P., Ligon, L. S., Lu, J., Maerk, M., Miller, N. M., Norton, S., O'Carroll, I. P., Paulsen, I., Raulfs, E. C., Roemer, R., Rosser, J., Segura, D., Slater, S., Stricklin, S. L., Studholme, D. J., Sun, J., Viana, C. J., Wallin, E., Wang, B., Wheeler, C., Zhu, H., Dean, D. R., Dixon, R., and Wood, D. (2009) Genome sequence of *Azotobacter vinelandii*, an obligate aerobic specialized to support diverse anaerobic metabolic processes, *J. Bacteriol.* 191, 4534-4545.
20. Iwema, T., Picciocchi, A., Traore, D. A., Ferrer, J. L., Chauvat, F., and Jacquamet, L. (2009) Structural basis for delivery of the intact [Fe<sub>2</sub>S<sub>2</sub>] cluster by monothiol glutaredoxin, *Biochemistry* 48, 6041-6043.
21. Johansson, C., Roos, A. K., Montano, S. J., Sengupta, R., Filippakopoulos, P., Guo, K., von, D. F., Holmgren, A., Oppermann, U., and Kavanagh, K. L. (2011) The crystal structure of human GLRX5: iron-sulfur cluster co-ordination, tetrameric assembly and monomer activity, *Biochem. J.* 433, 303-311.

22. Vilella, F., Alves, R., Rodriguez-Manzanque, M. T., Belli, G., Swaminathan, S., Sunnerhagen, P., and Herrero, E. (2004) Evolution and cellular function of monothiol glutaredoxins: involvement in iron-sulphur cluster assembly, *Comp. Funct. Genom.* 5, 328-341.
23. Chandramouli, K. and Johnson, M. K. (2006) HscA and HscB stimulate [2Fe-2S] cluster transfer from IscU to apoferredoxin in an ATP-dependent reaction, *Biochemistry* 45, 11087-11095.
24. Giot, L., Bader, J. S., Brouwer, C., Chaudhuri, A., Kuang, B., Li, Y., Hao, Y. L., Ooi, C. E., Godwin, B., Vitols, E., Vijayadamodar, G., Pochart, P., Machineni, H., Welsh, M., Kong, Y., Zerhusen, B., Malcolm, R., Varrone, Z., Collis, A., Minto, M., Burgess, S., McDaniel, L., Stimpson, E., Spriggs, F., Williams, J., Neurath, K., Ioime, N., Agee, M., Voss, E., Furtak, K., Renzulli, R., Aanensen, N., Carrolla, S., Bickelhaupt, E., Lazovatsky, Y., DaSilva, A., Zhong, J., Stanyon, C. A., Finley, R. L., Jr., White, K. P., Braverman, M., Jarvie, T., Gold, S., Leach, M., Knight, J., Shimkets, R. A., McKenna, M. P., Chant, J., and Rothberg, J. M. (2003) A protein interaction map of *Drosophila melanogaster*, *Science* 302, 1727-1736.
25. Huynen, M. A., Spronk, C. A., Gabaldon, T., and Snel, B. (2005) Combining data from genomes, Y2H and 3D structure indicates that BolA is a reductase interacting with a glutaredoxin, *FEBS Lett.* 579, 591-596.
26. Ito, T., Tashiro, K., Muta, S., Ozawa, R., Chiba, T., Nishizawa, M., Yamamoto, K., Kuhara, S., and Sakaki, Y. (2000) Toward a protein-protein interaction map of the budding yeast: A comprehensive system to examine two-hybrid interactions in all possible combinations between the yeast proteins, *Proc. Natl. Acad. Sci. USA* 97, 1143-1147.
27. Li, H., Mapolelo, D. T., Dingra, N. N., Naik, S. G., Lees, N. S., Hoffman, B. M., Riggs-Gelasco, P. J., Huynh, B. H., Johnson, M. K., and Outten, C. E. (2009) The yeast iron regulatory proteins Grx3/4 and Fra2 form heterodimeric complexes containing a [2Fe-2S] cluster with cysteinyl and histidyl ligation, *Biochemistry* 48, 9569-9581.
28. Li, H., Mapolelo, D. T., Randeniya, S., Johnson, M. K., and Outten, C. E. (2012) Human Glutaredoxin 3 Forms [2Fe-2S]-Bridged Complexes with Human BolA2, *Biochemistry* 51, 1687-1696.
29. Mühlenhoff, U., Molik, S., Godoy, J. R., Uzarska, M. A., Richter, N., Seubert, A., Zhang, Y., Stubbe, J., Pierrel, F., Herrero, E., Lillig, C. H., and Lill, R. (2010) Cytosolic monothiol glutaredoxins function in intracellular iron sensing and trafficking via their bound iron-sulfur cluster, *Cell Metab.* 12, 373-385.
30. Schwartz, C. J., Giel, J. L., Patschkowski, T., Luther, C., Ruzicka, F. J., Beinert, H., and Kiley, P. J. (2001) IscR, an Fe-S cluster-containing transcription factor, represses expression of *Escherichia coli* genes encoding Fe-S cluster assembly proteins, *Proc. Natl. Acad. Sci. USA* 98, 14895-14900.

31. Cameron, J. M., Janer, A., Levandovskiy, V., Mackay, N., Rouault, T. A., Tong, W. H., Ogilvie, I., Shoubridge, E. A., and Robinson, B. H. (2011) Mutations in iron-sulfur cluster scaffold genes NFU1 and BOLA3 cause a fatal deficiency of multiple respiratory chain and 2-oxoacid dehydrogenase enzymes, *Am. J. Hum. Genet.* 89, 486-495.
32. Crack, J. C., Jervis, A. J., Gaskell, A. A., White, G. F., Green, J., Thomson, A. J., and Le Brun, N. E. (2008) Signal perception by FNR: the role of the iron-sulfur cluster, *Biochem. Soc. Trans.* 36, 1144-1148.
33. Khoroshilova, N., Popescu, C., Münck, E., Beinert, H., and Kiley, P. J. (1997) Iron-sulfur cluster disassembly in the FNR protein of *Escherichia coli* by O<sub>2</sub>: [4Fe-4S] to [2Fe-2S] conversion with loss of biological activity, *Proc. Natl. Acad. Sci. USA* 94, 6087-6092.
34. Sutton, V. R., Mettert, E. L., Beinert, H., and Kiley, P. J. (2004) Kinetic analysis of the oxidative conversion of the [4Fe-4S]<sup>2+</sup> cluster of FNR to a [2Fe-2S]<sup>2+</sup> Cluster, *J. Bacteriol.* 186, 8018-8025.
35. Crack, J. C., Green, J., Cheesman, M. R., Le Brun, N. E., and Thomson, A. J. (2007) Superoxide-mediated amplification of the oxygen-induced switch from [4Fe-4S] to [2Fe-2S] clusters in the transcriptional regulator FNR, *Proc. Natl. Acad. Sci. USA* 104, 2092-2097.
36. Nicolet, Y., Amara, P., Mouesca, J. M., and Fontecilla-Camps, J. C. (2009) Unexpected electron transfer mechanism upon AdoMet cleavage in radical SAM proteins, *Proc. Natl. Acad. Sci. USA* 106, 14867-14871.
37. Chandramouli, K., Unciuleac, M.-C., Naik, S., Dean, D. R., Huynh, B. H., and Johnson, M. K. (2007) Formation and properties of [4Fe-4S] clusters on the IscU scaffold protein, *Biochemistry* 46, 6804-6811.
38. Kennedy, M. C. and Beinert, H. (1988) The state of cluster SH and S<sup>2-</sup> of aconitase during cluster interconversions and removal. A convenient preparation of apoenzyme., *J. Biol. Chem.* 263, 8194-8198.
39. Mühlenhoff, U., Richter, N., Pines, O., Pierik, A. J., and Lill, R. (2011) Specialized function of yeast Isa1 and Isa2 in the maturation of mitochondrial [4Fe-4S] proteins, *J. Biol. Chem.* 286, 41205-41216.
40. Sheftel, A. D., Wilbrecht, C., Stehling, O., Niggemeyer, B., Elsasser, H. P., Mühlenhoff, U., and Lill, R. (2012) The human mitochondrial ISCA1, ISCA2, and IBA57 proteins are required for [4Fe-4S] protein maturation, *Mol. Biol. Cell* 23, 1157-1166.
41. Ding, H. and Clark, R. J. (2004) Characterization of iron-binding in IscA, an ancient iron-sulfur cluster assembly protein, *Biochem. J.* 379, 433-440.

Figure 6.1: Proposed model for the cluster carrier and storage roles of CGFS-Grxs in Fe-S cluster biogenesis. Color scheme: Fe<sup>3+</sup> (red); Fe<sup>2.5+</sup> (green), S (yellow). See text for details.

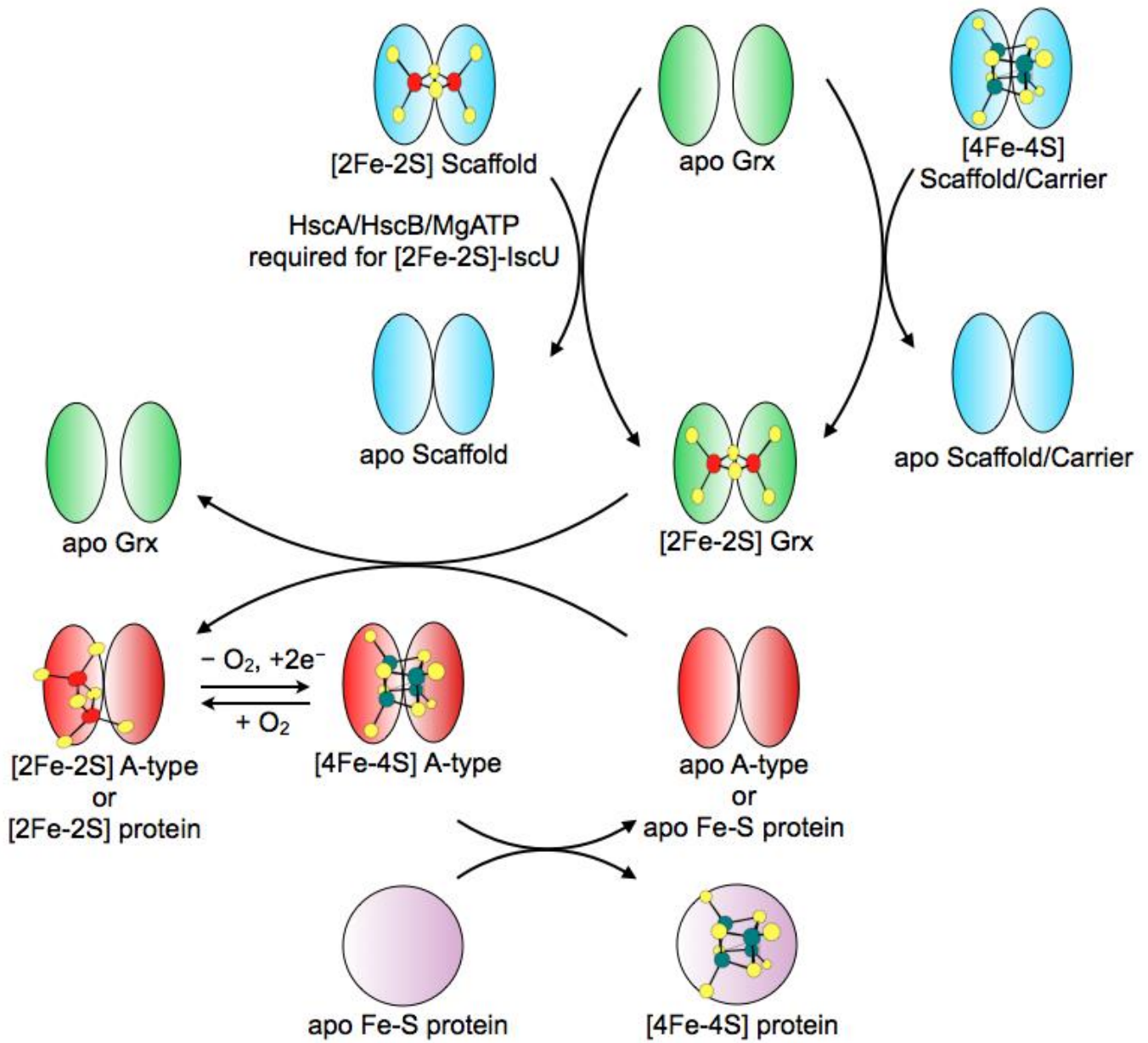
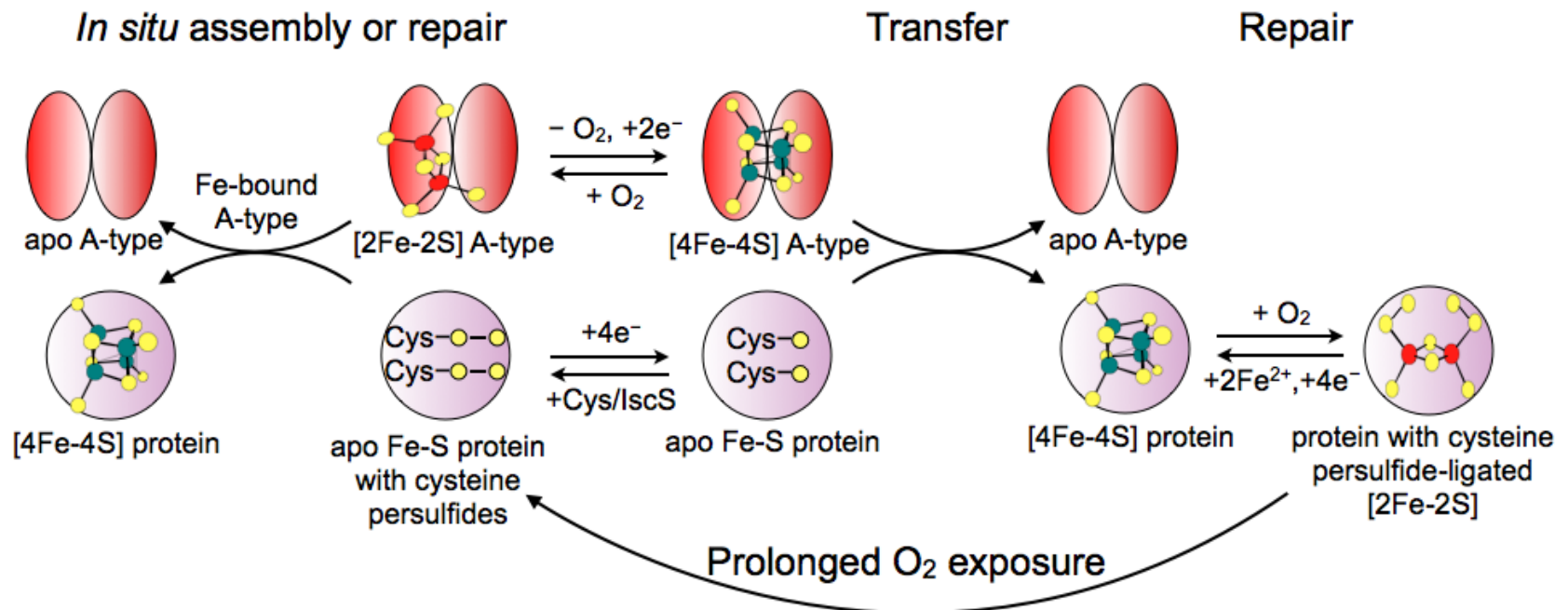


Figure 6.2: Schematic representation of the proposed mechanisms for the maturation and repair of oxygen sensitive  $[4\text{Fe-4S}]^{2+}$  cluster-requiring proteins. The potential involvement of Fe-bound,  $[2\text{Fe-2S}]^{2+}$  cluster-bound and  $[4\text{Fe-4S}]^{2+}$  cluster-bound forms of A-type proteins in the repair and biosynthesis of  $[4\text{Fe-4S}]^{2+}$  clusters is highlighted in this model. See text for details.



APPENDIX A

SPECTROSCOPIC AND FUNCTIONAL CHARACTERIZATION OF IRON-BOUND  
FORMS OF *AZOTOBACTER VINELANDII*<sup>NIF</sup> ISCA

---

Daphne T. Mapolelo,<sup>a</sup> Bo Zhang,<sup>a</sup> Sunil G. Naik,<sup>b</sup> Boi Hanh Huynh,<sup>b</sup> and Michael K. Johnson<sup>a</sup>

*Biochemistry* **2012**, *51*, 8056–8070

Reprinted with permission of the publisher.

<sup>a</sup>Department of Chemistry and Center for Metalloenzyme Studies, University of Georgia; Athens, Georgia 30602; <sup>b</sup>Department of Physics, Emory University, Atlanta, Georgia 30322

**Abbreviations:** VTMCD, variable-temperature magnetic circular dichroism; VTVH MCD, variable-temperature and variable-field magnetic circular dichroism; DTT, dithiothreitol; THP, tris(hydroxypropyl)phosphine; ICP-AES, inductively coupled plasma atomic emission spectroscopy; ICP-MS, inductively coupled plasma mass spectroscopy; EPR, electron paramagnetic resonance; FNR, fumarate nitrate reduction regulatory protein.

## Abstract

The ability of *Azotobacter vinelandii*  $^{57}\text{Fe}$ -IscA to bind Fe has been investigated to assess the role of Fe-bound forms in NIF-specific Fe–S cluster biogenesis.  $^{57}\text{Fe}$ -IscA is shown to bind one Fe(III) or one Fe(II) per homodimer and the spectroscopic and redox properties of both the Fe(III)- and Fe(II)-bound forms have been characterized using the UV–visible absorption, circular dichroism, and variable-temperature magnetic circular dichroism, electron paramagnetic resonance, Mössbauer and resonance Raman spectroscopies. The results reveal a rhombic intermediate-spin ( $S = 3/2$ ) Fe(III) center ( $E/D = 0.33$ ,  $D = 3.5 \pm 1.5 \text{ cm}^{-1}$ ) that is most likely 5-coordinate with two or three cysteinate ligands and a rhombic high-spin ( $S = 2$ ) Fe(II) center ( $E/D = 0.28$ ,  $D = 7.6 \text{ cm}^{-1}$ ) with properties similar to reduced rubredoxins or rubredoxin variants with three cysteinate and one or two oxygenic ligands. Iron-bound  $^{57}\text{Fe}$ -IscA undergoes reversible redox cycling between the Fe(III)/Fe(II) forms with a midpoint potential of  $+36 \pm 15 \text{ mV}$  at pH 7.8 (versus NHE). L-Cysteine is effective in mediating release of free Fe(II) from both the Fe(II)- and Fe(III)-bound forms of  $^{57}\text{Fe}$ -IscA. Fe(III)-bound  $^{57}\text{Fe}$ -IscA was also shown to be a competent iron source for *in vitro* NifS-mediated [2Fe-2S] cluster assembly on the N-terminal domain of NifU, but the reaction occurs via cysteine-mediated release of free Fe(II) rather than direct iron transfer. The proposed roles of A-type proteins in storing Fe under aerobic growth conditions and serving as iron donors for cluster assembly on U-type scaffold proteins or maturation of biological [4Fe-4S] centers are discussed in light of these results.

## Introduction

Iron–sulfur cluster biosynthesis in bacteria involves three distinct types of biosynthetic machinery termed the nitrogen fixation (NIF), iron–sulfur cluster (ISC), and sulfur utilizing factor (SUF) systems (1-4). The NIF system (NifS, NifU, and <sup>Nif</sup>IscA) is a specialized system for maturation of the Fe–S proteins involved with nitrogen fixation (5), while the ISC system (IscR, IscS, IscU, IscA, HscAB, Fdx, IscX) is responsible for general or housekeeping Fe–S cluster biosynthesis (6). In contrast, the SUF system (SufA, SufBCD, SufSE) appears to be a backup system that functions under Fe limitation or oxidative stress conditions in many bacteria, although it is the only system for Fe–S cluster biogenesis in cyanobacteria and in many archaea (7). In accord with evolutionary and O<sub>2</sub>-tolerance considerations, the ISC and SUF systems form the basis of eukaryotic mitochondrial and plastid Fe–S cluster biogenesis machineries, respectively. The primary components of each of these systems were initially indicated based on the organization of genes in the *nif*, *isc*, and *suf* operons and each appears to involve cysteine desulfurase (NifS, IscS, and SufSE)-mediated Fe–S cluster assembly on a primary scaffold protein (NifU, IscU, and SufB) followed by intact cluster transfer to apo forms of acceptor Fe–S proteins (8-16). While the cysteine desulfurase is clearly the S donor, many questions remain concerning the nature of the Fe donor, the mechanism of cluster assembly and transfer to wide variety of acceptor proteins, and the role of the ubiquitous A-type Fe–S cluster biogenesis proteins which are present in the NIF, ISC, and SUF systems (<sup>Nif</sup>IscA, IscA, and SufA).

The A-type proteins are small proteins, approximately 110 amino acids in bacterial proteins and eukaryotic proteins that lack targeting sequences, with three highly conserved cysteine residues in a C-X<sub>n</sub>-C-G-C sequence motif (n is usually 63–65, but is increased by a 21-residue insert in some eukaryotic proteins such as *Saccharomyces cerevisiae* Isa2). All three of

the conserved cysteine residues are essential for function based on *in vivo* yeast mutagenesis studies (17;18). Crystal structures have been reported for the apo forms of *Escherichia coli* IscA (19;20) and SufA (21) and an NMR structure has been reported for *Aquifex aeolicus* IscA (22). The structures all show a novel protein fold, but were of limited utility for addressing the site for Fe or Fe–S cluster binding as the N-terminal C-G-C motif was generally not observed, presumably because of conformational flexibility. Moreover, the *E. coli* IscA structures were homotetramers rather than the homodimeric forms that predominate in solution. Only the *E. coli* SufA crystallized in a dimeric form with the C-G-C motif observable in one subunit in an arrangement that suggested that the two C-G-C motifs would be in close proximity at the subunit interface and hence be available for Fe or Fe–S cluster ligation (21). More recently, the crystal structure of a [2Fe-2S] cluster-bound form of *Thermosynechococcus elongatus* IscA revealed an asymmetric tetramer involving similar  $\alpha$  subunits and domain-swapped  $\beta$  subunits with two subunit bridging [2Fe-2S] clusters (23). The domain swapping has been attributed to a crystallization artifact and molecular modeling studies suggest that the asymmetric cluster ligation, involving the three conserved cysteines from the  $\alpha$  subunit and the N-terminal conserved cysteine of the  $\beta$  subunit, is most likely retained in a functional asymmetric  $\alpha\beta$  dimer. Such asymmetric cluster ligation provides an attractive mechanism for cluster assembly/incorporation and release (23).

A variety of different functions have been proposed for A-type proteins in Fe–S cluster biogenesis based on a combination of *in vivo* and *in vitro* evidence. These include roles as alternative scaffold proteins for *de novo* cluster biosynthesis (24;25), carrier proteins for delivery of clusters preassembled on scaffold proteins (16;26;27), regulatory proteins for iron homeostasis and the sensing of redox stress (28), and specific Fe-donors for cluster assembly on

U-type scaffold proteins (29) or maturation of mitochondrial [4Fe-4S] centers (30). In large part, the lack of a current consensus concerning function stems from the fact that the effects of single gene knockouts in bacteria are generally minor except for growth under elevated levels of O<sub>2</sub> (31) and that multiple A-type proteins exhibiting considerable functional redundancy are present in many organisms (27;32). However, recent *in vivo* studies involving functional characterization of multiple gene deletions of bacterial A-type proteins have revealed strong phenotypes. For example, *E. coli* *iscA* and *sufA* double mutants have demonstrated an essential role for A-type proteins in the maturation of [4Fe-4S] centers under aerobic growth conditions (27;32;33). Moreover, individual gene knockouts of *S. cerevisiae* *Isa1* and *Isa2* and human *ISCA1* and *ISCA2* displayed severe phenotypes that are associated with ineffective maturation of mitochondrial [4Fe-4S] cluster-containing enzymes (30;34).

The work presented herein was designed to assess the proposal that A-type proteins function as specific Fe donors for Fe–S cluster assembly on U-type scaffold proteins by investigating the ability of <sup>Nif</sup>IscA to bind Fe and to assess if Fe-bound forms can function as specific Fe donors for Fe–S cluster assembly on NifU. Through *in vitro* studies of *E. coli* *IscA* and *SufA* and human *ISCA1*, Ding and co-workers have shown that A-type Fe–S cluster biogenesis proteins are competent Fe donors for cluster assembly on the U-type class of primary scaffold proteins (29;32;35-41). The conserved C-terminal CGC cysteines of A-type proteins have been shown to be essential for high affinity binding of Fe(III) which can be specifically mobilized by L-cysteine for *in vitro* assembly on *IscU* (29;32;35-37). Further support for an Fe donor role comes from the ability of A-type proteins to recruit iron for Fe–S cluster biosynthesis *in vitro* from the iron-storage protein ferritin in the presence of the thioredoxin reductase system

(38) or under conditions of limited accessible free-iron (37) and to store Fe(III) in an accessible form for cluster assembly under aerobic growth conditions (32;42).

However, spectroscopic characterization of Fe-bound forms of A-type proteins have been limited to UV–visible absorption and EPR and, notably, Mössbauer studies have failed to confirm high affinity iron binding to the conserved cysteine residues of *E. coli* SufA (43). In addition, the lack of an observable phenotype for double *iscA* and *sufA* mutant strains under anaerobic conditions (27;32), coupled with the *in vivo* evidence that Fe–S cluster formation on Isu1 and Isu2 in yeast mitochondria does not require Isa1 or Isa2 (30), indicate that A-type proteins cannot be the sole Fe donors for cluster assembly on U-type proteins.

The recent comprehensive *in vivo* studies of the role of Isa1/Isa2 in yeast Fe–S cluster biogenesis have raised the possibility of an alternative, albeit ill-defined, role for Fe-bound A-type proteins (30). This work provides compelling evidence that an Fe-bound form of the *S. cerevisiae* Isa1-Isa2 complex is present *in vivo* and is specifically required, along with Iba57 (which releases the Fe) and Isu1/Isu2, for the general maturation of mitochondrial [4Fe-4S] cluster-containing proteins, rather than functioning as a specific Fe donor for cluster assembly on the Isu1/Isu2 scaffold proteins (30).

In principal, the simplicity of the NIF system for Fe–S cluster biogenesis, which comprises only NifS (S-donor), NifU (scaffold for cluster assembly), and <sup>Nif</sup>IscA, and is limited to the maturation of single and double cubane [4Fe-4S] centers in nitrogen fixation proteins, makes <sup>Nif</sup>IscA an excellent candidate for elucidating the function of A-type proteins. Hence, the objectives of this study were to prepare and investigate the detailed electronic, magnetic, redox, and vibrational properties of iron-bound forms of *Azotobacter vinelandii* (*Av*) <sup>Nif</sup>IscA, as a precursor to understanding the role of <sup>Nif</sup>IscA in NIF-specific Fe–S cluster biogenesis. Thus far

spectroscopic characterization of Fe-bound forms of A-type Fe–S cluster biogenesis proteins have been limited to UV–visible absorption and EPR studies of ferric-bound *E. coli* IscA and SufA and human ISCA1 (29;32;35). In this work, the spectroscopic and redox properties of both the Fe(III)- and Fe(II)-bound forms of  $Av^{Nif}$ IscA have been investigated by the combination of UV–visible absorption, circular dichroism (CD) and variable-temperature magnetic circular dichroism (VTMCD), electron paramagnetic resonance (EPR), resonance Raman and Mössbauer spectroscopies. The results provide insight into the ground and excited state properties and ligation of both the Fe(III)- and Fe(II)-bound forms, demonstrate that the Fe in both forms is released by L-cysteine, and facilitate determination of the one-electron redox potential for Fe(III)/Fe(II)-bound  $Nif$ IscA. In addition, Fe(III)-bound  $Nif$ IscA is shown to be an effective but nonspecific Fe donor for [2Fe-2S] cluster assembly on the N-terminal IscU-like domain of NifU. Overall, the results support the view that A-type proteins provide a means of storing Fe(III) under aerobic growth conditions in an accessible form for use in Fe–S cluster biogenesis and possible roles are discussed.

## Experimental procedures

*Materials:* Materials used in this work were of reagent grade and were purchased from Fischer Scientific, Sigma-Alrich Chemical Co, Invitrogen, or VWR International, unless otherwise stated.

*Expression and purification of  $Av^{Nif}$ IscA and NifU-1:* The *A. vinelandii Nif*:*iscA* gene, encoding the  $Nif$ IscA protein, was amplified by PCR and inserted into the expression plasmid pT<sub>7-7</sub> as previously described (24). The resulting plasmid, pDB570, was transformed into the *E. coli* host BL21(DE3) and induced for high level expression of  $Av^{Nif}$ IscA according to the published procedure (24).  $Av^{Nif}$ IscA was purified under aerobic conditions by suspending cell

paste (60.0 g) in 120 mL of 50 mM Tris-HCl buffer pH 7.8 (buffer A) containing 2 mM  $\beta$ -mercaptoethanol and disrupting the cells by sonication on ice for 45 min. After centrifugation at 17 000 rpm for 1 h at 4 °C, the crude extract was treated with 1% (w/v) streptomycin sulfate and incubated at room temperature for 5 min before recentrifugation. The supernatant was then precipitated with 40% ammonium sulfate and the pellet was resuspended in buffer A and then loaded on a Q-Sepharose (Pharmacia) column (50 mm inner diameter, 110 mL) equilibrated with buffer A. Elution was achieved with a 0.0–1.0 M NaCl gradient in buffer A, with  $^{Nif}$ IscA eluting between 0.49 and 0.53 M NaCl and pooled as single fraction. This fraction was then concentrated down to 3 mL using Amicon ultrafiltration with a YM10 membrane and loaded on a 200 mL Superdex S75 gel-filtration column previously equilibrated with 100 mM Tris-HCl buffer pH 7.8, with 150 mM NaCl. On the basis of gel electrophoresis analysis, the last fraction to elute from the Superdex-75 column was concentrated as above and frozen as pellets in liquid nitrogen until used. The purity of this fraction was estimated to be approximately 95% based on gel electrophoresis. The yield of  $^{Nif}$ IscA from 60 g of cells was approximately 50 mg. Expression and purification of *A. vinelandii* NifU-1, a truncated form of NifU containing only the N-terminal U-type domain, was carried out as previously described (44;45).

*Chemical analyses:*  $^{Nif}$ IscA protein concentrations were determined using bovine serum albumin as a standard (Roche) with BioRad Dc protein assay in conjunction with the microscale modified procedure of Brown *et al* (46). The purity and concentration of  $^{Nif}$ IscA samples were also assessed by direct amino acid analyses conducted at Texas A&M University using samples dialyzed against water in a YM10 centricon to remove Tris base which interferes with the assay. On the basis of parallel direct amino acid analyses and BioRad Dc protein assays on identical samples, the BioRad Dc protein assay was found to overestimate the protein concentration of

<sup>Nif</sup>IscA by 17%. All <sup>Nif</sup>IscA concentrations are based on protein monomer unless otherwise stated. Iron concentrations were determined after KMnO<sub>4</sub>/HCl protein digestion as described by Fish (47), using a 1000 ppm atomic absorption iron standard to prepare standard solutions of known Fe concentration (Fluka). Metal analyses of as purified <sup>Nif</sup>IscA samples were carried in the ICP-MS facility in Dr. Michael Adams laboratory at the University of Georgia.

*Preparation of Fe-bound <sup>Nif</sup>IscA:* All sample preparation procedures were carried out under strictly anaerobic conditions inside a Vacuum Atmospheres glovebox under argon (<2 ppm O<sub>2</sub>), unless otherwise noted. Ferric-bound <sup>Nif</sup>IscA was prepared by treating <sup>Nif</sup>IscA (0.8 mM) in 100 mM Tris-HCl buffer, pH 7.8, with 150 mM NaCl with 800 mM Tris(hydroxypropyl)phosphine (THP) to cleave disulfides followed by titration with ferric ammonium citrate at room temperature. The Fe-loaded <sup>Nif</sup>IscA was then passed through a 50 mL desalting column to remove any adventitiously bound iron. The fraction which contained the Fe-bound <sup>Nif</sup>IscA was concentrated by Amicon ultrafiltration using a YM10 membrane. Ferrous-bound <sup>Nif</sup>IscA was prepared by reducing purified ferric-bound <sup>Nif</sup>IscA with a 5-fold excess of sodium dithionite under anaerobic conditions. Both the ferric-bound and ferrous-bound <sup>Nif</sup>IscA were analyzed for Fe and protein before being spectroscopically characterized.

*EPR-monitored redox titrations:* EPR redox titrations were performed at ambient temperature (25–27 °C) inside the glovebox under anaerobic conditions using 0.4 mM Fe-bound <sup>Nif</sup>IscA in a 50 mM Tris-HCl buffer, pH 7.8. THP was completely removed by repeated dialysis prior to conducting redox titrations. Mediator dyes were added, each to a concentration of ca. 50 μM, in order to cover the desired range of redox potentials, i.e., 1,4-benzioquinone (+274 mV), 1,2-naphtho-4-sulfonate (+215 mV), 1,2-naphthoquinone (+134 mV), 1,4-naphthoquinone (+69 mV), methylene blue (+11 mV), indigo-disulphonate (–125 mV), anthraquinone-1,5-

disulphonate (-170 mV), phenosafranin (-252 mV), safranin O (-289 mV), and neutral red (-325 mV). Samples were first oxidized with a minimal excess of potassium ferricyanide followed by reductive titration with sodium dithionite and reoxidation to the starting potential with ferricyanide to check for reversibility. After equilibration at the desired potential, a 0.25-mL aliquot was transferred to a calibrated EPR tube and immediately frozen in liquid nitrogen. Potentials were measured using a platinum working electrode and a saturated Ag/AgCl reference electrode. All redox potentials are reported relative to the normal hydrogen electrode (NHE). The EPR signal intensities from samples collected at different potentials were fitted to a one-electron Nernst equation.

*Determination of the oligomeric state of apo and Fe-bound <sup>Nif</sup>IscA:* The oligomeric state of apo and Fe-bound forms of <sup>Nif</sup>IscA were assessed by gel-filtration chromatography using a 25 mL Superdex G-75 10/300 column (Pharmacia Biotech), equilibrated with 50 mM Tris-HCl buffer with 100 mM KCl (pH 7.6) and using a flow rate of 0.4 mL/min. The molecular weight standards used were aprotinin (Mr 6500), albumin (Mr 66 000), blue dextran (Mr 2 000 000), carbonic anhydrase (Mr 29 000), and cytochrome c (Mr 12 400) (Sigma-Aldrich).

*Spectroscopic methods:* All samples for spectroscopic investigations were prepared under an argon atmosphere in the glovebox unless otherwise noted. UV-visible absorption and CD spectra were recorded in sealed anaerobic 1 mm quartz cuvettes at room temperature, using a Shimadzu UV-3101 PC scanning spectrophotometer and a Jasco J-715 spectropolarimeter, respectively. Resonance Raman spectra were recorded at 17 K on frozen droplets of sample mounted on the coldfinger of a Displex model CSA-202E closed cycle refrigerator (Air Products, Allentown, PA) as previously described (48), using a Ramanor U1000 scanning spectrometer (Instruments SA, Edison, NJ) coupled with a Sabre argon-ion laser (Coherent, Santa Clara, CA).

VTMCD spectra were recorded on anaerobically prepared samples containing 55% (v/v) ethylene glycol to enable the formation of good optical-quality glasses upon rapid freezing. Spectra were recorded with Jasco J-715 spectropolarimeter (Jasco, Easton, MD) mated to an Oxford Instruments Spectromag 4000 cryostat/magnet capable of generating magnetic fields of up to 7 T and maintaining sample temperatures in the range 1.5–300 K, using the protocols described elsewhere (49;50). VHVT MCD saturation magnetization data at discrete wavelengths were collected by increasing the field from 0 to 6 T at fixed temperatures of 1.73, 4.22, 10.0, and 25.0 K and analyzed according to the published procedures using software supplied by Edward I Solomon (Stanford University) (51). X-band (9.6 GHz) EPR spectra were recorded using a ESP-300D spectrometer (Bruker, Billerica, MA) equipped with an ER-4116 dual mode cavity and an ESR 900 flow cryostat (Oxford Instruments, Concord, MA). Mössbauer spectra of  $^{57}\text{Fe}$ -enriched samples in the presence of weak and strong applied magnetic fields were recorded using the instrumentation previously described (52), and analyzed using WMOSS software (Web Research).

## Results

*Fe binding to A. vinelandii Nif<sup>+</sup>IscA*: In previous studies of iron-binding by  $A_v$  Nif<sup>+</sup>IscA, there was no evidence for bound iron in as-purified recombinant samples based on ICP-AES and no evidence for ferric binding in titration experiments monitored by UV–visible absorption, VTMCD and Mössbauer spectroscopies (24). Substoichiometric ferrous binding in a rubredoxin-type environment was observed in samples treated with a 4–10 fold excess of Fe(II) based on UV–visible absorption, VTMCD and Mössbauer studies. However, the bound iron was lost during gel filtration to remove excess iron, indicating low binding affinity. These experiments were all conducted under strictly anaerobic conditions in samples that were pretreated with DTT

to cleave disulfides and then repurified under anaerobic conditions to remove DTT. This was necessary because DTT forms a complex with both ferric and ferrous ions in aqueous solution as evident by UV-visible absorption, VTMCD and Mössbauer spectroscopies. Hence, our initial reaction to the reports by Ding *et al* (29) of ferric binding to *E. coli* IscA on aerobic addition of Fe(II) in the presence of DTT was that the Fe(III)-bound IscA complex may involve exogenous DTT. This possibility was subsequently discounted based on the ability to form the same species in *E. coli* IscA using the thioredoxin reductase system in place of DTT (39). Nevertheless we were still unable to induce high affinity ferric or ferrous binding to  $Av^{Nif}$ IscA even in the presence of DTT under aerobic or anaerobic conditions.

The origin of the inability of  $Av^{Nif}$ IscA to bind iron in a high affinity ferric site was suggested by the observation that the protein is purified in the apo form essentially devoid of bound Fe (<0.02 Fe/monomer), as judged by ICP-MS analysis, even though samples invariably exhibit a 320 nm band that has been attributed to the Fe(III)-bound forms of *E. coli* IscA and SufA (29;32). Furthermore, addition of EDTA or DTT did not decrease the intensity of the 320-nm band. However, the addition of tris(hydroxypropyl)phosphine (THP), an alternative, non-thiol-based disulfide/polysulfide cleaving reagent, resulted in substantial loss of the 320-nm band suggesting that it originates from polysulfides that are not accessible or reducible by DTT. Moreover,  $Av^{Nif}$ IscA was found to bind Fe(III) in the presence of THP under both aerobic and anaerobic conditions. This is illustrated in Figure A.1 which shows a titration of  $Av^{Nif}$ IscA with ferric ammonium citrate under aerobic conditions in the presence of 100 mM THP. The results demonstrate tight binding of Fe(III) with a stoichiometry of 0.5 Fe/ $Av^{Nif}$ IscA monomer which corresponds to 1.0 Fe/ $Av^{Nif}$ IscA dimer, since the apo protein and the Fe(III)-bound form were both determined to be dimers in aqueous solution based on quantitative gel filtration studies (data not

shown). The absorption and CD properties of Fe(III)-bound  $\text{Nif}^{\text{IscA}}$  were also unchanged after exchange into the equivalent aerobic buffer solution containing 2 mM DTT. On the basis of absorption and CD intensity, partially oxidized samples were obtained for analogous Fe(III) titrations of  $\text{Nif}^{\text{IscA}}$  carried out under strictly anaerobic conditions in the presence of THP, indicating partial reduction in the absence of  $\text{O}_2$ . The UV–visible absorption characteristics and the Fe(III) binding stoichiometry are in good agreement with the results of Ding et al. for Fe(II) addition to *E. coli* IscA under aerobic conditions in the presence of DTT or thioredoxin/thioredoxin reductase (29;39). However, in contrast to recombinant *E. coli* IscA, the Fe-bound form of recombinant *Av*  $\text{Nif}^{\text{IscA}}$  was not observed for samples isolated from aerobically grown cells and purified under aerobic or strictly anaerobic conditions. Moreover, UV–visible absorption and CD studies of a reconstituted form of *Av*  $\text{Nif}^{\text{IscA}}$  containing one  $[\text{2Fe-2S}]^{2+}$  cluster per dimer revealed that the Fe(III)-bound form is not a product of  $\text{O}_2$ -induced  $[\text{2Fe-2S}]$  cluster degradation during purification; see Figure A.2. The results show a gradual loss of the cluster on exposure to air over a 12-h time period, without any evidence for the concomitant appearance of the characteristic absorption or CD spectrum associated with Fe(III)-bound  $\text{Nif}^{\text{IscA}}$ . Some Fe(III)-bound  $\text{Nif}^{\text{IscA}}$  is however formed during the  $\text{O}_2$ -induced  $[\text{4Fe-4S}]$  to  $[\text{2Fe-2S}]$  cluster conversion on  $\text{Nif}^{\text{IscA}}$ ; see Appendix B.

*Spectroscopic characterization of Fe-bound A. vinelandii Nif<sup>IscA</sup>*: The Fe(III)-bound form of  $\text{Nif}^{\text{IscA}}$  formed by titration with ferric ammonium citrate in the presence of THP can be purified aerobically without loss of Fe and reduced stoichiometrically with sodium dithionite under anaerobic conditions without loss of Fe based on Fe determinations. Moreover, samples can be repeatedly reduced by dithionite and reoxidized by air without significant loss of Fe based on near-quantitative restoration of the visible absorption spectrum on aerial oxidation, see Figure

A.3. The electronic, vibrational and redox properties of the Fe(III)- and Fe(II)-bound forms were therefore investigated using the combination of UV–visible absorption and VTMCD, EPR, Mössbauer, and resonance Raman spectroscopies.

*Electronic excited state properties:* The electronic excited state properties of Fe(III)- and Fe(II)-bound <sup>Nif</sup>IscA were investigated using UV–visible absorption and VTMCD spectroscopies; see Figure A.4, panels A and B, respectively. The absorption spectrum of Fe(III)-bound <sup>Nif</sup>IscA comprises broad CysS-to-Fe(III) charge transfer bands centered near 320, 440, and 520 nm. VTMCD spectra show that the broad and ill-defined absorption spectrum in the CysS-to-Fe(III) charge transfer region results from at least six overlapping *C*-terms, exhibiting + + – + – – signs with increasing energy. Without structural information concerning the Fe(III) coordination environment, it is not possible to make detailed assignments. However, based on the observation that somewhat similar absorption and VTMCD spectra have been observed for single Cys-to-Ser or Cys-to-Asp variants of oxidized rubredoxin (53) and a trigonal bipyramidal Fe(III) complex with two equatorial thiolate and three nitrogen ligands (54), the data are most consistent with two or three cysteine ligands.

The visible absorption is bleached on reduction and the absorption spectrum of the Fe(II)-bound <sup>Nif</sup>IscA comprises a band centered at 315 nm, with a low-energy shoulder centered near 340 nm. These absorption bands correlate with temperature-dependent MCD bands: positive band centered at 335 nm and negative band centered at 305 nm with a shoulder at 280 nm (Figure A.4B). Both the absorption and VTMCD spectra are very similar to those observed for reduced rubredoxin and metallothionein with <4 equiv of Fe(II) bound (55), which are attributed to charge transfer transitions associated with a tetrahedrally coordinated high-spin ( $S = 2$ ) Fe(II) center with complete cysteinate ligation. However, the VTMCD  $\Delta\epsilon$  values are 2 orders of

magnitude lower than those of reduced rubredoxins with all-cysteinate-ligated high-spin Fe(II) centers in a distorted tetrahedral coordination geometry. In contrast, analogous absorption and VTMCD spectra with  $\Delta\epsilon$  values similar to observed for Fe(II)-bound  $^{Nif}$ IscA are exhibited by Cys-to-Asp variants of reduced rubredoxin, which have 4- or 5-coordinate Fe(II) sites involving three cysteinate and a monodentate or bidentate aspartate ligand (53). Hence the absorption and VTMCD data for the Fe(II)-bound  $^{Nif}$ IscA are most consistent with a 4- or 5-coordinate paramagnetic ferrous site with one or two non-cysteinate ligands.

*Electronic ground state properties:* The ground state electronic and magnetic properties of the Fe(III)- and Fe(II)-bound forms of  $^{Nif}$ IscA were investigated by EPR and Mössbauer spectroscopies, and VTVH MCD saturation magnetization studies. The X-band EPR spectrum of Fe(III)-bound  $^{Nif}$ IscA comprises a broad low-field absorption-shaped component with a maximum at  $g = 5.5$  and a broad derivative-shaped component centered at  $g = 2.0$ ; see Figure A.5A. On the basis of a conventional  $S = 3/2$  spin Hamiltonian, the spectrum is consistent with a rhombic ( $E/D = 0.33$ )  $S = 3/2$  ground state with an isotropic real  $g$ -value of 2.0, which predicts effective  $g$  values of 5.46, 2.00, and 1.46 for both of the two quantum mechanically mixed Kramers doublets of the  $S = 3/2$  manifold. The breadth of the spectrum and the inability to clearly observe the high-field negative absorption-shaped component at  $g = 1.46$  is attributed to  $g$ -strain originating from heterogeneity in Fe(III) coordination environment. Hence the EPR data indicates a novel intermediate-spin,  $S = 3/2$ , rhombic Fe(III) center in Fe(III)-bound  $^{Nif}$ IscA. This result is in agreement with EPR studies of the Fe-bound forms of *E. coli* IscA and SufA and human ISCA1 which reported weak and ill-defined resonances in the  $g = 4-5$  region that were interpreted in terms of an  $S = 3/2$  Fe(III) center (29;32;35).

Additional evidence for a rhombic  $S = 3/2$  ground state for Fe(III)-bound  $^{57}\text{Fe}$ -NifHscA came from Mössbauer and VTVH MCD saturation magnetization studies. The Mössbauer spectrum of a partially reduced sample, prepared by adding excess Fe(III) under anaerobic conditions in the presence of THP and repurifying under anaerobic conditions, is shown in Figure A.6 (top panel). The spectrum was recorded at 4.2 K with a weak magnetic field of 50 mT applied parallel to  $\gamma$ -beam. It shows a mixture of the oxidized and reduced forms with 45% of the absorption associated with a quadrupole doublet (green line) from the rubredoxin-type high-spin ( $S = 2$ ) Fe(II) species that is present in dithionite-reduced Fe(II)-bound  $^{57}\text{Fe}$ -NifHscA (see below and Figure A.7) and the remainder exhibiting magnetic hyperfine structures indicative of a Fe(III) species. To better characterize the Fe(III) species, we also recorded spectra at 4.2 K in 50 mT perpendicular field and in 4 and 8 T parallel fields (data not shown). We then removed the contribution of the rubredoxin-type high-spin Fe(II) species from the raw data by using theoretical simulations (solid lines in Figure A.7) of the Fe(II)-bound  $^{57}\text{Fe}$ -NifHscA spectra (Figure A.7) recorded at the same applied magnetic fields. The resulting spectra (Figure A.6, bottom panel) represent the 4.2 K Mössbauer spectra of the Fe(III) species in 50 mT parallel (A) and perpendicular (C) applied magnetic fields, and in 4 T (C) and 8 T (D) parallel applied fields. The fact that the parallel and perpendicular 50 mT spectra are different indicates nonuniaxial ground state doublets, as expected from the EPR study. Further, in agreement with the EPR results, all four spectra are fit to a good approximation by spin Hamiltonian parameters (listed in Table A.1) for a rhombic  $S = 3/2$  ground state with  $E/D = 0.33$ . The values of the zero field splitting parameter,  $D$ , and the magnetic hyperfine interaction component,  $A_{zz}$ , are highly correlated. It is therefore difficult to get a precise value for one without knowing the other. Nevertheless it is not possible to fit the spectra with  $D < 2 \text{ cm}^{-1}$ .

Using the Mössbauer and EPR-determined ground-state spin Hamiltonian parameters, VTVH MCD saturation magnetization data for Fe(III)-bound  $^{57}\text{Fe}$ IscA collected at discrete wavelengths can be fit to a good approximation by varying the transition polarizations. This is illustrated for the intense positive MCD band at 458 nm in Figure A.8A which shows that the 0 – 6 T magnetization data collected at 1.73, 4.22, 10.0, and 25 K are well fit by a predominantly  $xz$ -polarized transition with effective  $xy$ ,  $xz$ , and  $yz$  transition dipole moments,  $M_{xy}$ ,  $M_{xz}$ ,  $M_{yz}$ , in the ratio 0.2:1.0:0.2. As for the Mossbauer data, the VTVH MCD saturation magnetization data are not very sensitive to the values of  $D$  with satisfactory fits possible with  $D$  between 1 and 5  $\text{cm}^{-1}$ . Taken together, the Mössbauer and VTVH MCD saturation magnetization data confirm a rhombic intermediate spin  $S = 3/2$  Fe(III) center in  $^{57}\text{Fe}$ IscA with  $E/D = 0.33$  and  $D$  between 2 and 5  $\text{cm}^{-1}$ .

The dithionite-reduced Fe(II)-bound  $^{57}\text{Fe}$ IscA did not exhibit an X-band EPR signal in parallel or perpendicular mode, but the ground state properties of the paramagnetic ferrous center can be assessed by high-field Mössbauer measurements, see Figure A.7, and VTVH MCD saturation magnetization data; see Figure A.8B. The 4.2 K Mössbauer spectra recorded with 50 mT, 4 and 8 T magnetic fields applied parallel to the  $\gamma$ -ray beam are very similar to those observed for reduced rubredoxins which have rhombic high-spin ( $S = 2$ ) Fe(II) centers with large zero-field splitting in accord with highly distorted tetrahedral ligation by four cysteinate ligand (56;57). In fact, the Mössbauer spectra at all three applied fields can be fit to a good approximation by assuming a rhombic  $S = 2$  electronic ground state that is identical to that of reduced *C. pasteurianum* rubredoxin (56) with slightly modified parameters for the quadrupole and magnetic hyperfine interactions; see Table A.1. Likewise the VTVH MCD saturation magnetization data collected at 335 nm (Figure A.8B) is very similar to that observed for

reduced *C. pasteurianum* rubredoxin (55) and is fit to a good approximation using the Mössbauer-determined spin Hamiltonian parameters by varying the transition polarization. The best fit was obtained for a predominantly *xy*-polarized transition, i.e.,  $M_{xy}$ ,  $M_{xz}$ ,  $M_{yz}$ , in the ratio 1.0:0.2:0.2; see Figure A.8B. Clearly both the Mössbauer and VTVH MCD saturation magnetization data indicate ground state properties for Fe(II)-bound  $^{57}\text{Fe}$ -IscA that are very similar to those of reduced rubredoxin. However, since the detailed ground state properties of Cys-to-Asp variants of reduced rubredoxin have yet to be determined, the observed ground state properties may also be consistent with a 4- or 5-coordinate Fe(II) sites involving three cysteinate and one or two oxygenic ligands as suggested by the anomalously low intensity and form of the VT-MCD spectra (see above).

*Vibrational properties:* Resonance Raman was used to investigate Fe–S stretching modes in Fe(III)-bound  $^{57}\text{Fe}$ -IscA using visible excitation into CysS-to-Fe(III) charge transfer bands. The resonance Raman spectrum of Fe(III)-bound  $^{57}\text{Fe}$ -IscA in the Fe–S stretching region using 457.9-nm excitation is quite distinct compared to oxidized rubredoxins (58) and comprises a weak cysteine  $\delta(\text{S–C–C})$  bending mode at  $296\text{ cm}^{-1}$  and symmetric and asymmetric Fe–S(Cys) stretching modes at  $338$  and  $397\text{ cm}^{-1}$ , respectively; see Figure A.9. Oxidized rubredoxins exhibit much greater resonance enhancement (at least 50-fold), with an intense symmetric breathing mode of the rhombically distorted tetrahedral Fe-(S(Cys))<sub>4</sub> unit between  $312$  and  $318\text{ cm}^{-1}$ , three weak resolved asymmetric Fe-S(Cys) modes between  $336$  and  $380\text{ cm}^{-1}$ , and internal bending modes of the coordinated cysteines at  $290$  and  $410\text{ cm}^{-1}$  (53;58). As shown in Figure A.9, the resonance Raman spectrum of Fe(III)-bound  $^{57}\text{Fe}$ -IscA is much more similar to Cys-to-Asp rubredoxin variants that are coordinated by three cysteines and one monodentate or bidentate aspartate. For example, *C. pasteurianum* C6D rubredoxin exhibits a symmetric Fe–S(Cys)

stretching mode at  $335\text{ cm}^{-1}$  and an unresolved asymmetric Fe–S(Cys) stretching mode at  $385\text{ cm}^{-1}$ , along with internal bending modes of the coordinated cysteines at  $301$  and  $411\text{ cm}^{-1}$  (53). Clearly the resonance Raman spectrum of Fe(III)-bound  $\text{Nif}^{\text{IscA}}$  can be interpreted in terms of a similar coordination environment to C6D rubredoxin, i.e., 4-coordinate with one noncysteine ligand or 5-coordinate with two noncysteine ligands or in terms symmetric and asymmetric Fe–S stretching involving two coordinated cysteine residues.

*Redox properties of Fe-bound  $\text{Nif}^{\text{IscA}}$ :* Since Fe(II)-bound  $\text{Nif}^{\text{IscA}}$  did not exhibit an X-band EPR spectrum in either parallel or perpendicular mode, monitoring the EPR intensity at  $g = 5.5$  of samples frozen during dye-mediated redox titrations was used to determine the midpoint potential of the Fe(III)/Fe(II) couple. The results of reductive titration are shown in Figure A.5B, and indicate a one-electron redox potential of  $+36 \pm 15\text{ mV}$  at pH 7.8 (versus NHE). Reversibility was demonstrated by restoration of  $80 \pm 10\%$  of the initial intensity at  $g = 5.5$  on oxidation to the initial starting potential. A similar level of reversibility (75%) was observed using UV–visible absorption to monitor redox cycling using dithionite as the reductant and air as the oxidant, see Figure A.2. Our inability to achieve full reversibility is likely to a consequence of greater lability for the Fe(II)-bound form. Although the cellular redox potential is primarily determined by two-electron dithiol/disulfide redox couples which are generally slow and inefficient in effecting one-electron redox processes, the high redox potential suggests that Fe-bound  $\text{Nif}^{\text{IscA}}$  will predominantly or exclusively be in the Fe(II)-bound state in a cellular environment under anaerobic growth conditions. However, the observation of Fe(III)-bound *A. vinelandii*  $\text{Nif}^{\text{IscA}}$  in aerobic solutions containing THP or DTT (this work) and in Fe(III)-bound *E. coli* *IscA* in aerobic solutions containing DTT and thioredoxin/thioredoxin (29;39), indicates that Fe(III)-bound of  $\text{Nif}^{\text{IscA}}$  and *IscA* is likely to be present in the cell under aerobic growth

conditions. Hence both the Fe(III)- and Fe(II)-bound forms may be physiologically relevant with the oxidized form present primarily under aerobic growth conditions.

*Cysteine-mediated release of Fe from Fe-bound <sup>Nif</sup>IscA:* Previous studies by Ding and co-workers have demonstrated that the iron center in Fe(III)-bound *E. coli* IscA is tightly bound with an association constant of  $3.0 \times 10^{19} \text{ M}^{-1}$ , but is specifically mobilized by cysteine when Fe(III)-bound IscA is used as the Fe donor for Fe–S cluster assembly on IscU (36). In accord with this result, addition of a 20-fold excess of L-cysteine to Fe(III)-bound <sup>Nif</sup>IscA under anaerobic conditions resulted in complete loss of the CysS-to-Fe(III) charge transfer bands associated with Fe(III)-bound <sup>Nif</sup>IscA within 20 min at 22 °C (data not shown). To address the possibility that cysteine is also competent to release Fe from Fe(II)-bound <sup>Nif</sup>IscA, we utilized the ability of VTMCD to selectively and quantitatively monitor Fe(II)-bound <sup>Nif</sup>IscA; see Appendix Figure A.10. The results indicate near complete release of Fe(II) from the Fe(II)-bound <sup>Nif</sup>IscA within 5 min of adding a 20-fold excess of L-cysteine, based on the close similarity of the resultant VTMCD spectra compared to that obtained using the same concentration of ferrous ammonium sulfate in the presence of the same excess of L-cysteine under identical conditions. Moreover, analogous VTMCD spectra were observed for the products of L-cysteine-mediated release of Fe from Fe(III)-bound measurements using Fe(III)-bound <sup>Nif</sup>IscA indicating that the Fe is released as Fe(II). We conclude that cysteine is competent to release Fe(II) from both the Fe(III)- and Fe(II)-bound forms of <sup>Nif</sup>IscA.

*<sup>Nif</sup>IscA as an Fe donor for cluster assembly on NifU:* Previous studies of the time course of cysteine desulfurase-mediated  $[2\text{Fe-2S}]^{2+}$  cluster assembly on U-type proteins using A-type proteins as Fe donors have been monitored by UV–visible absorption (29;35;37), which is of limited utility compared to UV–visible CD for distinguishing between  $[2\text{Fe-2S}]^{2+}$  clusters in

different protein environments or between  $[2\text{Fe-2S}]^{2+}$  and  $[4\text{Fe-4S}]^{2+}$  cluster formation. Moreover these studies have been carried out under conditions which favor rapid release of  $\text{Fe}^{2+}$  from Fe-bound A-type proteins (i.e., 37 °C and a 10–20 fold excess of L-cysteine) and hence are of limited use in assessing if A-type proteins function as Fe-donors by direct interprotein Fe transfer or cysteine-mediated release of free  $\text{Fe}^{2+}$ .

In this work, the ability of Fe-bound  $^{\text{Nif}}$ IscA to function as an Fe donor for cluster assembly on NifU was assessed by using UV–visible CD spectroscopy to compare the rates of NifS-mediated  $[2\text{Fe-2S}]$  cluster assembly on the N-terminal IscU-like domain of NifU, termed NifU-1, using equivalent amounts of free  $\text{Fe}^{2+}$  ion and Fe-bound  $^{\text{Nif}}$ IscA as the Fe source, under L-cysteine-limiting conditions at 22 °C; see Figure A.11. Our previous spectroscopic studies of NifS-mediated cluster assembly on full-length homodimeric NifU and NifU-1 have demonstrated that cluster assembly is initiated by  $[2\text{Fe-2S}]^{2+}$  cluster assembly on the N-terminal IscU-like domain of each monomer, which leads to  $[4\text{Fe-4S}]^{2+}$  cluster formation at the dimer interface and subsequent  $[4\text{Fe-4S}]^{2+}$  cluster incorporation in the C-terminal domain (9). Hence NifU-1 was used for these studies to avoid interference from the permanent redox-active  $[2\text{Fe-2S}]^{2+,+}$  cluster which exhibits intense CD spectra in both redox states (see accompanying paper). The time course of CD changes in a reaction mixture comprising 13  $\mu\text{M}$  NifU-1, 108  $\mu\text{M}$  Fe(III)-bound  $^{\text{Nif}}$ IscA (based on Fe concentration), 0.34  $\mu\text{M}$  NifS, and 384  $\mu\text{M}$  L-cysteine is shown in Figure A.11A, with the red spectrum showing the CD spectrum of Fe(III)-bound  $^{\text{Nif}}$ IscA before the addition of L-cysteine to initiate the reaction. The marked differences in the UV–visible CD spectra of Fe(III)-bound  $^{\text{Nif}}$ IscA and the  $[2\text{Fe-2S}]^{2+}$  cluster-bound forms of NifU-1 and  $^{\text{Nif}}$ IscA (Figure A.11E) facilitate simultaneous monitoring of the release of Fe(II) from Fe(III)-bound  $^{\text{Nif}}$ IscA (Figure A.11B) and the formation of  $[2\text{Fe-2S}]^{2+}$  centers on both NifU-1 and  $^{\text{Nif}}$ IscA; see

Figure A.11C. Notably, the CD spectra corresponding to  $[2\text{Fe-2S}]^{2+}$  center formation change with time and can only be simulated assuming initial formation of  $[2\text{Fe-2S}]^{2+}$ -NifU-1 and subsequent formation of  $[2\text{Fe-2S}]^{2+}$ -NifIscA; see Figure A.11D.

Quantitation of each component as a function of time based on the  $\Delta\varepsilon$  values shown in Figure A.11E, is shown in Figure A.11F. The results show a pronounced lag in  $[2\text{Fe-2S}]^{2+}$  cluster assembly on NifU-1 that correlates with a lag in cysteine-mediated release of  $\text{Fe}^{2+}$  from Fe(III)-bound NifIscA. Moreover, parallel experiments using identical conditions and the equivalent concentration of free  $\text{Fe}^{2+}$  in place of Fe(III)-bound NifIscA show no lag phase and proceed at a rate comparable to that observed after the lag phase with Fe(III)-bound NifIscA as the Fe source. Taken together, these results indicate that the ability of Fe-bound NifIscA to function as an Fe donor for  $[2\text{Fe-2S}]$  cluster assembly on NifU-1 requires L-cysteine-mediated release of free Fe(II), implying that it is a nonspecific Fe donor rather than a specific Fe donor that functions by direct interprotein Fe transfer.

Figure A.11F also indicates that the generation of apo-NifIscA influences the final products of NifS-mediated cluster assembly on NifU-1 using Fe(III)-bound NifIscA as the Fe donor. In accord with previous Mössbauer studies of the time course of NifS-mediated cluster assembly on NifU-1 using a 9-fold excess of  $\text{Fe}^{2+}$  (9), CD results under analogous conditions indicate the initial formation of the  $[2\text{Fe-2S}]^{2+}$  cluster-bound form which maximizes at 1  $[2\text{Fe-2S}]$  cluster/homodimer and subsequently decreases; see Figure A.11F. Mössbauer studies have shown that the decrease results from the formation of  $[4\text{Fe-4S}]^{2+}$  clusters, which exhibit negligible UV-visible CD intensity (see Appendix B), via reductive coupling of  $[2\text{Fe-2S}]^{2+}$  clusters assembled at the subunit interface of the homodimers (9). In contrast, when apo-NifIscA is generated by using Fe(III)-bound NifIscA as the Fe donor, the reaction yields fully loaded

NifU-1 containing 2 [2Fe-2S] clusters/homodimer (corresponding to 32% of the Fe released from Fe-bound  $\text{Nif}^{\text{IscA}}$ ) and a major contribution of  $[2\text{Fe-2S}]^{2+}$  cluster-bound  $\text{Nif}^{\text{IscA}}$  (corresponding to 45% of the Fe released from Fe-bound  $\text{Nif}^{\text{IscA}}$ ). There are two possibilities for the formation of  $[2\text{Fe-2S}]^{2+}$  cluster-bound  $\text{Nif}^{\text{IscA}}$ . The first is that it occurs via NifS-mediated cluster assembly on apo- $\text{Nif}^{\text{IscA}}$  (24) once NifU-1 is almost replete with [2Fe-2S] clusters. The second is that a [2Fe-2S] cluster is directly transferred from NifU-1 to apo- $\text{Nif}^{\text{IscA}}$ . At present it is not possible to assess if one or both of these processes are occurring. However, direct [2Fe-2S] cluster transfer is supported by the observation that the second [2Fe-2S] cluster assembled on the IscU homodimer has been shown to be much more labile than the first cluster (10), and that cluster incorporation on  $\text{Nif}^{\text{IscA}}$  only starts to occur when NifU-1 contains 0.5 clusters/homodimer; see Figure A.11F. Furthermore, evidence for cluster transfer from NifU to  $\text{Nif}^{\text{IscA}}$  is presented in the accompanying paper. Hence it is possible that  $\text{Nif}^{\text{IscA}}$  is functioning as both a nonspecific Fe donor for [2Fe-2S] cluster assembly on NifU-1 and an acceptor of [2Fe-2S] clusters generated on NifU-1 in this *in vitro* reaction.

## Discussion

The iron binding studies of *A. vinelandii*  $\text{Nif}^{\text{IscA}}$  presented in this work complement and extend the studies carried out by Ding and co-workers with *E. coli* IscA and SufA and human ISCA1. However, prior to this work, there was no evidence for a high-affinity Fe(III)-bound form of  $\text{Nif}^{\text{IscA}}$ . By using THP rather than DTT to cleave disulfides or polysulfides on  $\text{Nif}^{\text{IscA}}$ , we were able to demonstrate high affinity Fe(III) binding and to obtain homogeneous samples of Fe(III)-bound  $\text{Nif}^{\text{IscA}}$  containing one intermediate spin ( $S = 3/2$ ) Fe(III) center per  $\text{Nif}^{\text{IscA}}$  dimer in accord with the published results obtained for *E. coli* IscA and SufA and human ISCA1 (29;32;35). Moreover, the excited state electronic properties and the ground state electronic and

vibrational properties of this novel intermediate-spin Fe(III) center have been characterized in detail using UV–visible absorption, CD and VTMCD, EPR, Mössbauer and resonance Raman spectroscopies. The results indicate the first example of a rhombic ( $E/D = 0.33$ ) intermediate-spin ( $S = 3/2$ ) Fe(III) center with thiolate ligation. Pure intermediate-spin Fe(III) complexes are uncommon and the majority are axial 5-coordinate square pyramidal complexes with porphyrin, dithiocarbamate, or macrocyclic tetraamido ligands (59). Since the overwhelming majority of intermediate spin Fe(III) complexes are five coordinate and the resonance Raman and UV–visible absorption and VTMCD results for Fe(III)-bound  $^{Nif}$ IscA are best interpreted in terms of two or three cysteinate ligands, this suggests the presence of two or three noncysteinylligands.

This work also demonstrates one-electron redox cycling between Fe(III)/(II)-bound forms of  $^{Nif}$ IscA with a redox potential of  $+36 \pm 15$  mV at pH 7.8 (vs NHE). A well-defined Fe(II)-bound form of other A-type proteins has not been reported. This is probably a consequence of lower binding affinity for Fe(II) compared to Fe(III) and the fact that the Fe(II)-bound form is more difficult to detect than the Fe(III)-bound form since it does not exhibit an X-band EPR signal and is only evident in the UV–visible absorption spectrum by a band at 320 nm, the same wavelength as the most intense absorption of the Fe(III)-bound form and of bound polysulfides. Nevertheless the Fe(II)-bound form is stable in solution under anaerobic conditions and readily detected and characterized using VTMCD and Mössbauer spectroscopies. The results indicate a rhombic high-spin ( $S = 2$ ) Fe(II) species with properties similar to reduced rubredoxins or rubredoxin variants with three cysteinate and one or two oxygenic ligands. Although the one-electron redox potential for the Fe(III)/(II)-bound forms of  $^{Nif}$ IscA indicates that Fe(II)-bound form is likely to be the dominant Fe-bound form in cells under anaerobic growth conditions, the observation of the Fe(III)-bound forms of  $^{Nif}$ IscA and IscA in aerobic dithiol/disulfide buffering

media indicates that the oxidized form is likely to be present in the cell under aerobic growth conditions. Moreover, the observation that L-cysteine mediates Fe(II) release from both the Fe(III)- and Fe(II)-bound forms of <sup>Nif</sup>IscA indicates that both forms have the potential to function as Fe donors to U-type scaffold proteins with the former functioning under aerobic growth conditions and the later functioning under anaerobic growth conditions. This observation also argues against the possibility that the Fe-bound forms, particularly the Fe(II)-bound form, constitute the initial precursors for de novo cysteine desulfurase-mediated cluster biosynthesis on A-type proteins, since the cysteine substrate which supplies the S for cluster assembly would also promote release of bound Fe.

The inability of other research groups to observe high affinity Fe(III) binding in three archetypical A-type proteins, *A. vinelandii* <sup>Nif</sup>IscA (24) and *E. coli* IscA and SufA (40;60) had previously raised doubts concerning the biological significance of the Fe-bound A-type proteins reported by Ding and co-workers. For *A. vinelandii* <sup>Nif</sup>IscA, the current work demonstrates that the initial failure to observe high-affinity Fe(III) binding was a consequence of the inability of DTT to reduce disulfide or polysulfides involving the Fe-binding cysteine residues. In addition, the close similarity in the absorption and EPR properties of the novel mononuclear  $S = 3/2$  Fe(III) center in *A. vinelandii* <sup>Nif</sup>IscA compared to those previously reported for mononuclear  $S = 3/2$  Fe(III) centers in *E. coli* IscA and SufA and human ISCA1 (29;32;35), leaves little doubt that high affinity Fe(III) binding is a common property of A-type proteins.

The question that therefore needs to be addressed is whether or not Fe-bound A-type proteins are present *in vivo*. A definitive answer is currently not available, since, to our knowledge, this question has yet to be addressed for any organism under normal growth conditions. Moreover, it is unclear if physiologically relevant levels of Fe-bound A-type proteins

can exist in the presence of normal cellular levels of L-cysteine, which have been estimated to be in the 0.1– 0.2 mM range in *E. coli* (61). However, *in vivo* characterization of recombinant proteins in *S. cerevisiae* has provided convincing evidence for a Fe-bound rather than Fe–S cluster-bound form of a Isa1/Isa2/Iba57 complex (30). Iba57 is a tetrahydrofolate-dependent protein with bacterial homologues (YgfZ in *E. coli*) that appears to play a key role in facilitating Fe release from the Isa1/Isa2 to appropriate acceptor proteins (30). Hence it is possible that Iba57 and its bacterial homologue protect against indiscriminate cysteine-dependent Fe release for A-type proteins in both yeast and bacteria.

In contrast the situation is far from clear when the *in vivo* status is inferred from the composition of recombinant overexpressed bacterial A-type proteins as purified. The majority, including *A. vinelandii* investigated herein and *E. coli* IscA and SufA (25;26), are purified under aerobic conditions as apo proteins. This is surprising if they function as Fe storage or donor proteins *in vivo* in view of the high binding affinity for Fe(III). While the origin of this discrepancy has yet to be fully resolved, it may be a consequence of lack of coexpression of the Iba57 homologue or aerobic overexpression of recombinant proteins that are unable to bind Fe due to oxidative dithiol or polysulfide formation involving the active site cysteines, as demonstrated for <sup>Nif</sup>IscA in this work. In contrast, Ding and co-workers have purified Fe(III)-bound forms of recombinant human ISCA1 and *E. coli* IscA/SufA under aerobic conditions (29;32;35) and shown that Fe incorporation increases when the aerobic growth medium was supplemented with ferrous ammonium sulfate (35) and ferric citrate (42), respectively. These results demonstrate the potential for recombinant, overexpressed A-type proteins to store Fe(III) in an accessible form for Fe–S cluster assembly under aerobic growth conditions.

It is also important to note that a few recombinant A-type proteins contain Fe–S clusters as purified, i.e., the structurally characterized *T. elongatus* IscA (23) and *E. coli* SufA (when coexpressed with SufBCDSE) (16) which both contain [2Fe-2S] clusters and *Acidithiobacillus ferrooxidans* IscA which contains a [4Fe-4S] cluster (62). Indeed, the observation that *E. coli* SufA is purified as a [2Fe-2S]-containing protein when coexpressed with the other components of the *suf* operon provides compelling evidence for the physiological relevance of cluster-bound forms of A-type proteins. As discussed below and in the following chapter, the ability of A-type proteins to bind Fe–S clusters is best rationalized in terms of a role as cluster carriers for delivering clusters assembled on the U-type and SufB-type scaffold proteins to acceptor proteins. Since the results presented herein argue strongly against the possibility that Fe(III)-bound A-type proteins are the products of aerial oxidation of cluster-bound forms during purification, the available data are consistent with the possibility that both Fe- and cluster-bound A-type proteins are functional forms that are present *in vivo*.

The above discussion demonstrates that there is a growing body of *in vitro* and *in vivo* evidence suggesting a physiological role for Fe-bound forms of bacterial and eukaryotic A-type proteins. Hence the next question that needs to be addressed is whether or not Fe-bound A-type proteins serve as Fe donors for cluster assembly on U-type scaffold proteins as proposed by the work of Ding and co-workers. The results presented herein using Fe-bound <sup>Nif</sup>IscA, coupled with the previously published studies using human ISCA1 and *E. coli* IscA and SufA (29;32;35), clearly demonstrate that A-type proteins are competent Fe donors for *in vitro* cysteine desulfurase-mediate cluster assembly on the appropriate U-type scaffold proteins. However, CD-monitored cluster assembly on NifU-1 using Fe(III)-bound <sup>Nif</sup>IscA is shown here to occur by L-cysteine-mediated release of free Fe(II) rather than by direct interprotein Fe transfer. This

suggests that Fe-bound A-type proteins are not specific Fe donors for U-type proteins, but have the potential to contribute to a pool of free Fe(II) that may be available for cluster assembly on scaffold proteins. While this is possible, it should be stressed that there is currently no *in vivo* evidence in support of a role for A-type proteins as Fe donors to primary scaffold proteins. In *A. vinelandii*, no growth phenotype has been reported for <sup>Nif</sup>iscA knockouts and a null-growth phenotype has only been observed for depletion of IscA for growth under elevated O<sub>2</sub> (31). However, the lack of a phenotype for individual *Av*<sup>Nif</sup>IscA and IscA knockouts under normal aerobic growth conditions may be a consequence of functional redundancy, as has been shown to the case of IscA and SufA in *E. coli* (27;32). In yeast, where there is *in vivo* evidence for an Fe-bound form of Isa1/Isa2, <sup>55</sup>Fe-immunoprecipitation studies indicated that depletion of Isa1 and Isa2 results in a slight increase in Fe associated with Isu1, indicating that the Fe-bound Isa1/Isa2 complex cannot be the sole Fe donor for cluster assembly on Isu1 (30).

The only other candidate for the immediate Fe donor to U-type scaffold proteins is frataxin (yeast Yfh1) and the bacterial homologue CyaY. Physical interactions and structural studies have implicated involvement of the frataxin in the yeast Nfs1/Isd11/IscU1 and bacterial IscS/IscU Fe–S cluster assembly complexes (63;64) and recent *in vitro* studies implicate a role as an allosteric regulator of these biosynthetic complexes (65;66). Moreover, Yfh1 deficiency does result in defective Fe–S cluster biosynthesis on Isu1 (67), which is consistent with a role as an Fe donor. However, neither Yfh1 nor CyaY are essential for viability in yeast and *E. coli*, respectively (68), and the Fe binding affinity is weak (micromolar range) and associated with surface carboxylates (69;70), which argues against a role in cellular Fe trafficking. Nevertheless, it is possible that frataxin and CyaY function as immediate Fe donors for cluster assembly on

Isu1 and IscU, respectively, by functioning as Fe(II)-dependent allosteric regulators that trigger sulfur delivery and channel Fe to the assembly site in the complex.

The recent *in vivo* evidence that A-type proteins are specifically required for the maturation of [4Fe-4S] proteins but are not required for the maturation of [2Fe-2S] proteins, is also difficult to reconcile with a role as a primary Fe-donor to U-type proteins which are required for the maturation of both [2Fe-2S] and [4Fe-4S] proteins. The *iscA* and *sufA* double knockouts in *E. coli* have demonstrated an essential and specific role for A-type proteins in the maturation of [4Fe-4S] centers under aerobic growth conditions (27;32;33), and *S. cerevisiae* Isa1/Isa2 and human ISCA1/ISCA2 have been shown to be specifically required for effective maturation of mitochondrial [4Fe-4S] proteins (30;34). In bacteria this *in vivo* function of A-type proteins has been interpreted in terms of roles as specific cluster carriers for the delivery of clusters assembled on U-type or SufB-type primary scaffold proteins. The cluster carrier hypothesis is supported by *in vitro* studies which indicate that IscA can accept Fe–S clusters from IscU (26) and that SufA can accept Fe–S clusters from the SufBCD complex (71), and by recent phylogenomic and genetic studies of the interdependence of the three A-type proteins in *E. coli*, *i.e.*, IscA, SufA, and ErpA (4;27). A cluster carrier role for <sup>Nif</sup>IscA is also demonstrated in the following chapter which provides *in vitro* evidence that <sup>Nif</sup>IscA has the ability to function as an oxygen-tolerant Fe–S cluster carrier protein for the delivery of clusters assembled on NifU in nitrogen fixation-specific Fe–S cluster biogenesis.

An alternative role for Fe-bound A-type proteins that is implicated by the recent *in vivo* studies of *S. cerevisiae* Isa1 and Isa2 (30) is that they function downstream of U-type or SufB-type primary scaffold proteins as specific Fe donors for the maturation of [4Fe-4S] clusters on acceptor proteins. *In vitro* studies have demonstrated assembly of [4Fe-4S]<sup>2+</sup> clusters on bacterial

U-type proteins via reductive coupling of two  $[2\text{Fe-2S}]^{2+}$  clusters at the subunit interface proteins (9;13) and intact transfer of these  $[4\text{Fe-4S}]$  clusters to acceptor proteins (8;9;11). However, the assembly and transfer of U-type  $[4\text{Fe-4S}]$  clusters in bacteria are only viable under strictly anaerobic conditions due to the acute oxygen sensitivity of the  $[4\text{Fe-4S}]$  center. Consequently an alternative mechanism is required in the presence of oxygen and the *in vivo* knockout data clearly implicate a role for A-type proteins in the maturation or repair of  $[4\text{Fe-4S}]$  clusters under aerobic growth conditions (27;33). Since U-type proteins are required under both aerobic and anaerobic growth conditions and do not require A-type proteins for the assembly of the more oxygen-tolerant  $[2\text{Fe-2S}]$  centers, it seems likely that they are initial source of the  $[2\text{Fe-2S}]$  units for  $[4\text{Fe-4S}]$  cluster assembly under both aerobic and anaerobic conditions. Hence under aerobic conditions it is possible that bacterial  $[4\text{Fe-4S}]$  clusters are assembled on acceptor proteins *in situ* using  $[2\text{Fe-2S}]$  clusters initially formed on U-type proteins and Fe provided by A-type proteins. On the basis of the available data, an analogous  $[4\text{Fe-4S}]$  cluster assembly pathway appears to have been adopted under both aerobic and anaerobic growth conditions in yeast (30). This begs the question as to the source of the additional S.

One possibility that has emerged from our recent studies of the Fumarate Nitrate Reduction (FNR) regulatory protein is that the additional S is present in the form of partial cysteine persulfide ligation of the bound  $[2\text{Fe-2S}]$  cluster (see Chapter 5). Resonance Raman and mass spectrometry studies of FNR have demonstrated that  $\text{O}_2$ -induced degradation of the  $[4\text{Fe-4S}]^{2+}$  cluster results in a  $[2\text{Fe-2S}]^{2+}$  cluster with two cysteine persulfide ligands that can be reconverted back to initial  $[4\text{Fe-4S}]^{2+}$  cluster under anaerobic conditions by addition of Fe(II) in the presence of a dithiol reagent. Moreover, resonance Raman has provided evidence that analogous cysteine persulfide-ligated  $[2\text{Fe-2S}]^{2+}$  clusters are formed by  $\text{O}_2$ -induced degradation

of  $[4\text{Fe-4S}]^{2+}$  centers in radical-SAM enzymes. Hence Fe-bound A-type proteins could be specific Fe donors for cysteine persulfide-ligated  $[2\text{Fe-2S}]^{2+}$  clusters, formed by IscU-generated  $[2\text{Fe-2S}]^{2+}$  cluster binding to cysteine desulfurase-generated cysteine persulfides or by  $\text{O}_2$ -induced degradation  $[4\text{Fe-4S}]^{2+}$  clusters, for the *in situ* repair or maturation of  $[4\text{Fe-4S}]$  centers on acceptor proteins. As discussed in the following chapter, the IscU-generated  $[2\text{Fe-2S}]^{2+}$  clusters are likely to be delivered to acceptor proteins by  $[2\text{Fe-2S}]^{2+}$  cluster-bound A-type proteins. In addition, Fe-bound A-type proteins may function in the repair of cubane-type  $[3\text{Fe-4S}]^+$  that are initially generated by  $\text{O}_2$ -exposure of the site-differentiated  $[4\text{Fe-4S}]^{2+}$  centers in radical-SAM, (de)hydratases and IspG/IspH enzymes (72-75). In dithiol/disulfide buffering media these clusters can be reduced to the  $[3\text{Fe-4S}]^0$  forms which avidly incorporates Fe(II) to generate the original  $[4\text{Fe-4S}]^{2+}$  cluster (73). These proposed roles for Fe-bound A-type proteins in the assembly and repair of biological  $[4\text{Fe-4S}]$  clusters are summarized schematically in Figure A.12. Future experiments are planned to investigate these intriguing possibilities.

### **Acknowledgement**

We thank Dr. Dennis Dean and co-workers for providing plasmids for the recombinant expression of *A. vinelandii*  $\text{Nif}^{\text{IscA}}$  and Dr. Michael Adams for access to the ICP-MS facility.

## References

1. Johnson, D. C., Dean, D. R., Smith, A. D., and Johnson, M. K. (2005) Structure, function and formation of biological iron-sulfur clusters, *Annu. Rev. Biochem.* 74, 247-281.
2. Ayala-Castro, C., Saini, A., and Outten, F. W. (2008) Fe-S cluster assembly pathways in bacteria, *Microbiol. Mol. Biol. Rev.* 72, 110-125.
3. Lill, R. (2009) Function and biogenesis of iron-sulphur proteins, *Nature* 460, 831-838.
4. Py, B. and Barras, F. (2010) Building Fe-S proteins: bacterial strategies, *Nat. Rev. Microbiol.* 8, 436-446.
5. Jacobson, M. R., Cash, V. L., Weiss, M. C., Laird, N. F., Newton, W. E., and Dean, D. R. (1989) Biochemical and genetic analysis of the *nifUSVWZM* cluster from *Azotobacter vinelandii*, *Mol. Gen. Genet.* 219, 49-57.
6. Zheng, L., Cash, V. L., Flint, D. H., and Dean, D. R. (1998) Assembly of iron-sulfur clusters. Identification of an *iscSUA-hscBA-fdx* gene cluster from *Azotobacter vinelandii*, *J. Biol. Chem.* 273, 13264-13272.
7. Takahashi, Y. and Tokumoto, U. (2002) A third bacterial system for the assembly of iron-sulfur clusters with homologs in archaea and plastids, *J. Biol. Chem.* 277, 28380-28383.
8. Dos Santos, P. C., Smith, A. D., Frazzon, J., Cash, V. L., Johnson, M. K., and Dean, D. R. (2004) Iron-sulfur cluster assembly: NifU-directed activation of the nitrogenase Fe-protein, *J. Biol. Chem.* 279, 19705-19711.
9. Smith, A. D., Jameson, G. N. L., Dos Santos, P. C., Agar, J. N., Naik, S., Krebs, C., Frazzon, J., Dean, D. R., Huynh, B. H., and Johnson, M. K. (2005) NifS-mediated assembly of [4Fe-4S] clusters in the N- and C-terminal domains of the NifU scaffold protein, *Biochemistry* 44, 12955-12969.
10. Agar, J. N., Krebs, B., Frazzon, J., Huynh, B. H., Dean, D. R., and Johnson, M. K. (2000) IscU as a scaffold for iron-sulfur cluster biosynthesis: Sequential assembly of [2Fe-2S] and [4Fe-4S] clusters in IscU, *Biochemistry* 39, 7856-7862.
11. Unciuleac, M.-C., Chandramouli, K., Naik, S., Mayer, S., Huynh, B. H., Johnson, M. K., and Dean, D. R. (2007) *In vitro* activation of apo-aconitase using a [4Fe-4S] cluster-loaded form of the IscU [Fe-S] cluster scaffolding protein, *Biochemistry* 46, 6812-6821.
12. Chandramouli, K. and Johnson, M. K. (2006) HscA and HscB stimulate [2Fe-2S] cluster transfer from IscU to apoferredoxin in an ATP-dependent reaction, *Biochemistry* 45, 11087-11095.
13. Chandramouli, K., Unciuleac, M.-C., Naik, S., Dean, D. R., Huynh, B. H., and Johnson, M. K. (2007) Formation and properties of [4Fe-4S] clusters on the IscU scaffold protein, *Biochemistry* 46, 6804-6811.

14. Loiseau, L., Ollagnier-de-Choudens, S., Nachin, L., Fontecave, M., and Barras, F. (2003) Biogenesis of Fe-S cluster by the bacterial Suf system. SufS and SufE form a new type of cysteine desulfurase, *J. Biol. Chem.* 278, 38352-38359.
15. Layer, G., Gaddam, S. A., Ayala-Castro, C. N., Ollagnier-de-Choudens, S., Lascoux, D., Fontecave, M., and Outten, F. W. (2007) SufE transfers sulfur from SufS to SufB for iron-sulfur cluster assembly, *J. Biol. Chem.* 282, 13342-13350.
16. Gupta, V., Sendra, M., Naik, S. G., Chahal, H. K., Huynh, B. H., Outten, F. W., Fontecave, M., and Ollagnier de Choudens, S. (2009) Native *Escherichia coli* SufA, coexpressed with SufBCDSE, purifies as a [2Fe-2S] protein and acts as an Fe-S transporter to Fe-S target enzymes, *J. Am. Chem. Soc.* 131, 6149-6153.
17. Jensen, L. T. and Culotta, V. C. (2000) Role of *Saccharomyces cerevisiae* Isa1 and Isa2 in iron homeostasis, *Mol. Cell. Biol.* 20, 3918-3927.
18. Kaut, A., Lange, H., Diekert, K., Kispal, G., and Lill, R. (2000) Isa1p is a component of the mitochondrial machinery for maturation of cellular iron-sulfur proteins and requires conserved cysteine residues for function, *J. Biol. Chem.* 275, 15955-15961.
19. Bilder, P. W., Ding, H., and Newcomer, M. E. (2004) Crystal structure of the ancient Fe-S scaffold IscA reveals a novel protein fold, *Biochemistry* 43, 133-139.
20. Cupp-Vickery, J. R., Silberg, J. J., Ta, D. T., and Vickery, L. E. (2004) Crystal structure of IscA, an iron-sulfur cluster assembly protein from *E. coli*, *J. Mol. Biol.* 338, 127-137.
21. Wada, K., Hasegawa, Y., Gong, Z., Minami, Y., Fukuyama, K., and Takahashi, Y. (2005) Crystal structure of *Escherichia coli* SufA involved in biosynthesis of iron-sulfur clusters: Implications for a functional dimer, *FEBS Lett.* 579, 6543-6548.
22. Xu, D., Liu, G., Xiao, R., Acton, T., Goldsmith-Fischman, S., Honig, B., Montelione, G. T., and Szyperski, T. (2004) NMR structure of the hypothetical protein AQ-1857 encoded by the Y157 gene from *Aquifex aeolicus* reveals a novel protein fold, *Proteins:Struct. Func. Bioinform.* 54, 794-796.
23. Morimoto, K., Yamashita, E., Kondou, Y., Lee, S. J., Arisaka, F., Tsukihara, T., and Nakai, M. (2006) The asymmetric IscA homodimer with an exposed [2Fe-2S] cluster suggests the structural basis of the Fe-S cluster biosynthetic scaffold, *J. Mol. Biol.* 360, 117-132.
24. Krebs, C., Agar, J. N., Smith, A. D., Frazzon, J., Dean, D. R., Huynh, B. H., and Johnson, M. K. (2001) IscA, an alternative scaffold for Fe-S cluster biosynthesis, *Biochemistry* 40, 14069-14080.
25. Ollagnier-de-Choudens, S., Mattioli, T., Takahashi, Y., and Fontecave, M. (2001) Iron-sulfur cluster assembly. Characterization of IscA and evidence for a specific functional complex with ferredoxin, *J. Biol. Chem.* 276, 22604-22607.

26. Ollagnier-de-Choudens, S., Sanakis, Y., and Fontecave, M. (2004) SufA/IscA: reactivity studies of a class of scaffold proteins involved with [Fe-S] cluster assembly, *J. Biol. Inorg. Chem.* 9, 828-838.
27. Vinella, D., Brochier-Armanet, C., Loiseau, L., Talla, E., and Barras, F. (2009) Iron-sulfur (Fe/S) protein biogenesis: phylogenomic and genetic studies of A-type carriers, *PLoS. Genet.* 5, e1000497.
28. Balasubramanian, R., Shen, G., Bryant, D. A., and Golbeck, J. H. (2006) Regulatory roles for IscA and SufA in iron homeostasis and redox stress responses in the cyanobacterium *Synechococcus* sp. strain PCC 7002, *J. Bacteriol.* 188, 3182-3191.
29. Ding, H. and Clark, R. J. (2004) Characterization of iron-binding in IscA, an ancient iron-sulfur cluster assembly protein, *Biochem. J.* 379, 433-440.
30. Mühlenhoff, U., Richter, N., Pines, O., Pierik, A. J., and Lill, R. (2011) Specialized function of yeast Isa1 and Isa2 in the maturation of mitochondrial [4Fe-4S] proteins, *J. Biol. Chem.* 286, 41205-41216.
31. Johnson, D. C., Unciuleac, M.-C., and Dean, D. R. (2006) Controlled expression and functional analysis of iron-sulfur cluster biosynthetic components within *Azotobacter vinelandii*, *J. Bacteriol.* 188, 7551-7561.
32. Lu, J., Yang, J., Tan, G., and Ding, H. (2008) Complementary roles of SufA and IscA in the biogenesis of iron-sulfur clusters in *Escherichia coli*, *Biochem. J.* 409, 535-543.
33. Tan, G., Lu, J., Bitoun, J. P., Huang, H., and Ding, H. (2009) IscA/SufA paralogues are required for the [4Fe-4S] cluster assembly in enzymes of multiple physiological pathways in *Escherichia coli* under aerobic growth conditions, *Biochem. J.* 420, 463-472.
34. Sheftel, A. D., Wilbrecht, C., Stehling, O., Niggemeyer, B., Elsasser, H. P., Mühlenhoff, U., and Lill, R. (2012) The human mitochondrial ISCA1, ISCA2, and IBA57 proteins are required for [4Fe-4S] protein maturation, *Mol. Biol. Cell* 23, 1157-1166.
35. Lu, J., Bitoun, J. P., Tan, G., Wang, W., Min, W., and Ding, H. (2010) Iron-binding activity of human iron-sulfur cluster assembly protein hIscA1, *Biochem. J.* 428, 125-131.
36. Ding, B., Smith, E. S., and Ding, H. (2005) Mobilization of the iron centre in IscA for the iron-sulfur cluster assembly in IscU, *Biochem. J.* 389, 797-802.
37. Ding, H., Clark, R. J., and Ding, B. (2004) IscA mediates iron delivery for assembly of iron-sulfur clusters in IscU under limited "free" iron conditions, *J. Biol. Chem.* 279, 37499-37504.
38. Bitoun, J. P., Wu, G., and Ding, H. (2008) *Escherichia coli* FtnA acts as an iron buffer for re-assembly of iron-sulfur clusters in response to hydrogen peroxide, *BioMetals* 21, 693-703.

39. Ding, H., Harrison, K., and Lu, J. (2005) Thioredoxin reductase system mediates iron binding in IscA and iron-delivery for the iron-sulfur cluster assembly in IscU, *J. Biol. Chem.* 280, 30432-30437.
40. Yang, J., Bitoun, J. P., and Ding, H. (2006) Interplay of IscA and IscU in biogenesis of iron-sulfur clusters, *J. Biol. Chem.* 281, 27956-27963.
41. Ding, H., Yang, J., Coleman, L. C., and Yeung, S. (2007) Distinct iron binding property of two putative iron donors for the iron-sulfur cluster assembly: IscA and the bacterial frataxin ortholog CyaY under physiological and oxidative stress conditions, *J. Biol. Chem.* 282, 7997-8004.
42. Wang, W., Huang, H., Tan, G., Fan, S., Liu, M., Landry, A. P., and Ding, H. (2010) *In vivo* evidence for the iron-binding activity of an iron-sulfur cluster assembly protein IscA in *Escherchia coli*, *Biochem. J.* 432, 429-436.
43. Sendra, M., Ollagnier de Choudens, S., Lascoux, D., Sanakis, Y., and Fontecave, M. (2007) The SUF iron-sulfur cluster biosynthetic machinery: Sulfur transfer from the SUFS-SUFE complex to SUFA, *FEBS Lett.* 581, 1362-1368.
44. Yuvaniyama, P., Agar, J. N., Cash, V. L., Johnson, M. K., and Dean, D. R. (2000) NifS-directed assembly of a transient [2Fe-2S] cluster within the NifU protein, *Proc. Natl. Acad. Sci. USA* 97, 599-604.
45. Agar, J. N., Yuvaniyama, P., Jack, R. F., Cash, V. L., Smith, A. D., Dean, D. R., and Johnson, M. K. (2000) Modular organization and identification of a mononuclear iron-binding site within the NifU protein, *J. Biol. Inorg. Chem.* 5, 167-177.
46. Brown, R. E., Jarvis, K. L., and Hyland, K. J. (1989) Protein measurement using bicinchoninic acid: elimination of interfering substances, *Anal. Biochem.* 180, 136-139.
47. Fish, W. W. (1988) Rapid colorimetric micromethod for the quantitation of complexed iron in biological samples, *Meth. Enzymol.* 158, 357-364.
48. Drozdowski, P. M. and Johnson, M. K. (1988) A simple anaerobic cell for low temperature Raman spectroscopy, *Appl. Spectrosc.* 42, 1575-1577.
49. Johnson, M. K. Variable-temperature magnetic circular dichroism of metalloproteins. In *Metal clusters in proteins*; Que, L., Jr.; American Chemical Society; 1988; 326-342.
50. Thomson, A. J., Cheesman, M. R., and George, S. J. (1993) Variable-temperature magnetic circular dichroism, *Meth. Enzymol.* 226, 199-232.
51. Neese, F. and Solomon, E. I. (1999) MCD C-term signs, saturation behavior, and determination of band polarizations in randomly oriented systems with spin  $S \geq 1/2$ . Applications to  $S = 1/2$  and  $S = 5/2$ , *Inorg. Chem.* 38, 1847-1865.

52. Ravi, N., Bollinger, J. M., Huynh, B. H., Edmondson, D. E., and Stubbe, J. (1994) Mechanism of assembly of the tyrosyl radical-diiron(III) cofactor of *E. coli* ribonucleotide reductase. 1. Mössbauer characterization of the diferric radical precursor, *J. Am. Chem. Soc.* 116, 8007-8014.
53. Staples, C. R. Structure-function relationships in iron-sulfur proteins. Ph.D. Dissertation, University of Georgia, 1997.
54. Kennepohl, P., Neese, F., Schweitzer, D., Jackson, H. L., Kovacs, J. A., and Solomon, E. I. (2005) Spectroscopy of a non-heme iron thiolate complexes: Insight into the electronic structure of the low-spin active site of nitrile hydratase, *Inorg. Chem.* 44, 1826-1836.
55. Werth, M. T. and Johnson, M. K. (1989) Magnetic circular dichroism and electron paramagnetic resonance studies of Fe(II)-metallothionein, *Biochemistry* 28, 3982-3988.
56. Schulz, C. and Debrunner, P. G. (1976) Rubredoxin, a simple iron-sulfur protein: Its spin Hamiltonian and hyperfine parameters, *J. Phys. Colloques* 37, C6-153-C6-158.
57. Vrajmasu, V. V., Bominaar, E. L., Meyer, J., and Münck, E. (2002) Mössbauer study of reduced rubredoxin as purified and in whole cells. Structural correlation analysis of spin Hamiltonian parameters, *Inorg. Chem.* 41, 6358-6371.
58. Czernuszewicz, R. S., LeGall, J., Moura, I., and Spiro, T. G. (1986) Resonance Raman spectra of rubredoxin: new assignments and vibrational coupling mechanism from iron-54/iron-56 isotope shifts and variable-wavelength excitation, *Inorganic Chemistry* 25, 696-700.
59. Kostka, K. L., Fox, B. G., Hendrich, M. P., Collins, T. J., Rickard, C. E. F., Wright, L. J., and Munck, E. (1993) High-valent transition metal chemistry. Mössbauer and EPR studies of high-spin ( $S = 2$ ) iron(IV) and intermediate-spin ( $S = 3/2$ ) iron(III) complexes with a macrocyclic tetraamido-N ligand, *J. Am. Chem. Soc.* 115, 6746-6757.
60. Fontecave, M. and Ollagnier-de-Choudens, S. (2008) Iron-sulfur cluster biosynthesis in bacteria: Mechanisms of cluster assembly and transfer, *Arch. Biochem. Biophys.* 474, 226-237.
61. Park, S. and Imlay, J. A. (2003) High levels of intracellular cysteine promote oxidative DNA damage by driving the fenton reaction, *J. Bacteriol.* 185, 1942-1950.
62. Zeng, J., Geng, M., Jiang, H., Liu, Y., Liu, J., and Qiu, G. (2007) The IscA from *Acidithiobacillus ferrooxidans* is an iron-sulfur protein which assemble the  $[Fe_4S_4]$  cluster with intracellular iron and sulfur, *Arch. Biochem. Biophys.* 463, 237-244.
63. Gerber, J., Mühlhoff, U., and Lill, R. (2003) An interaction between frataxin and Isu1/Nfs1 that is crucial for Fe/S cluster synthesis on Isu1, *EMBO Rep.* 4, 907-911.

64. Shi, R., Proteau, A., Villarroya, M., Moukadiri, I., Zhang, L., Trempe, J. F., Matte, A., Armengod, M. E., and Cygler, M. (2010) Structural basis for Fe-S cluster assembly and tRNA thiolation mediated by IscS protein-protein interactions, *PLoS. Biol.* 8, e1000354.
65. Adinolfi, S., Iannuzzi, C., Prischi, F., Pastore, C., Iametti, S., Martin, S. R., Bonomi, F., and Pastore, A. (2009) Bacterial frataxin CyaY is the gatekeeper of iron-sulfur cluster formation catalyzed by IscS, *Nat. Struct. Mol. Biol.* 16, 390-396.
66. Tsai, C. L. and Barondeau, D. P. (2010) Human frataxin is an allosteric switch that activates the Fe-S cluster biosynthetic complex, *Biochemistry* 49, 9132-9139.
67. Mühlenhoff, U., Gerber, J., Richhardt, N., and Lill, R. (2003) Components involved in assembly and dislocation of iron-sulfur clusters on the scaffold protein Iscu1p, *EMBO J.* 22, 4815-4825.
68. Li, D. S., Ohshima, K., Jiralerspong, S., Bojanowski, M. W., and Pandolfo, M. (1999) Knock-out of the *cyaY* gene in *Escherichia coli* does not affect cellular iron content and sensitivity to oxidants, *FEBS Lett.* 456, 13-16.
69. Cook, J. D., Bencze, K. Z., Jankovic, A. D., Crater, A. K., Busch, C. N., Bradley, P. B., Stemmler, A. J., Spaller, M. R., and Stemmler, T. L. (2006) Monomeric yeast frataxin is an iron-binding protein, *Biochemistry* 45, 7767-7777.
70. Stemmler, T. L., Lesuisse, E., Pain, D., and Dancis, A. (2010) Frataxin and mitochondrial FeS cluster biogenesis, *J. Biol. Chem.* 285, 26737-26743.
71. Chahal, H. K., Dai, Y., Saini, A., Ayala-Castro, C., and Outten, F. W. (2009) The SufBCD Fe-S scaffold complex interacts with SufA for Fe-S cluster transfer, *Biochemistry* 48, 10644-10653.
72. Beinert, H., Kennedy, M. C., and Stout, C. D. (1996) Aconitase as iron-sulfur protein, enzyme, and iron-regulatory protein, *Chem. Rev.* 96, 2335-2373.
73. Johnson, M. K., Duderstadt, R. E., and Duin, E. C. (1999) Biological and synthetic [Fe<sub>3</sub>S<sub>4</sub>] clusters, *Adv. Inorg. Chem.* 47, 1-82.
74. Johnson, M. K. and Smith, A. D. Iron-sulfur proteins. In *Encyclopedia of Inorganic Chemistry, Second Edition*; King, R. B.; John Wiley & Sons; 2005; 2589-2619.
75. Grawert, T., Kaiser, J., Zepeck, F., Laupitz, R., Hecht, S., Amslinger, S., Schramek, N., Schleicher, E., Weber, S., Haslbeck, M., Buchner, J., Rieder, C., Arigoni, D., Bacher, A., Eisenreich, W., and Rohdich, F. (2004) IspH protein of *Escherichia coli*: studies on iron-sulfur cluster implementation and catalysis, *J. Am. Chem. Soc.* 126, 12847-12855.

Table A.1: Spin Hamiltonian Parameters for the Fe(III)-Bound and Fe(II)-Bound Forms of *A. vinelandii* <sup>Nif</sup>IscA as Assessed by Mössbauer Spectroscopy.

	Fe(III)-bound <sup>Nif</sup> IscA	Fe(II)-bound <sup>Nif</sup> IscA	<i>C. pasterianum</i> Fe(II) rubredoxin <sup>a</sup>
$S$	3/2	2	2
$D$ (cm <sup>-1</sup> )	2-5	7.6 <sup>a</sup>	7.6
$E/D$	0.33	0.28 <sup>a</sup>	0.28
$g_{xx}$	2	2.11 <sup>a</sup>	2.11
$g_{yy}$	2	2.19 <sup>a</sup>	2.19
$g_{zz}$	2	2.00 <sup>a</sup>	2.00
$A_{xx}/g_n\beta_n$ (T)	-11	-17.5	-20.1
$A_{yy}/g_n\beta_n$ (T)	-21	-7.5	-8.3
$A_{zz}/g_n\beta_n$ (T)	-1	-30.1	-30.1
$\delta$ (mm/s)	0.31	0.72	0.7
$\Delta E_Q$ (mm/s)	2.83	-3.33	-3.25
$\eta$	-0.2	0.85	0.65

<sup>a</sup>Taken from Ref 56.

Figure A.1: Fe(III) binding to  $^{NiFe}$ IscA monitored by UV–visible absorption spectroscopy. A  $^{NiFe}$ IscA (0.8 mM) was titrated with ferric ammonium citrate under aerobic conditions in 100 mM Tris/HCl buffer, pH 7.8, in the presence of 100 mM THP. The inset shows a plot of the extinction coefficient at 500 nm as a function of the Fe(III)/ $^{NiFe}$ IscA monomer ratio. All  $\epsilon$  values are based on the concentration of  $^{NiFe}$ IscA monomer.

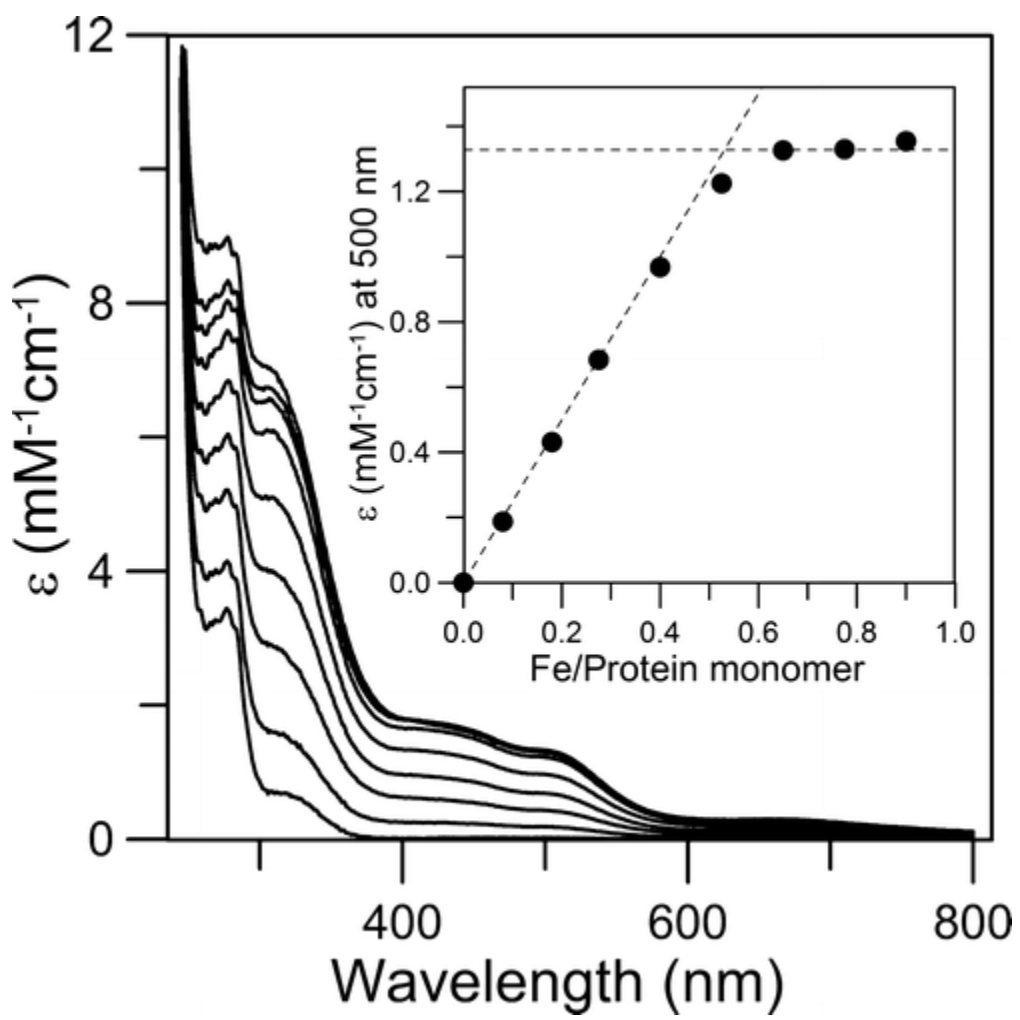


Figure A.2: Fe(III)-bound <sup>Nif</sup>IscA does not form via cluster degradation on exposure of [2Fe-2S]<sup>2+</sup> cluster-bound <sup>Nif</sup>IscA to air as evidenced by UV-visible absorption and CD spectroscopy. The spectra shown are [2Fe-2S]<sup>2+</sup> cluster-bound <sup>Nif</sup>IscA before exposure to air (black line) and after exposed to air for 12 hr (red line). No indication of the formation of Fe(III)-bound <sup>Nif</sup>IscA (blue line) was observed during the time period of the experiment. Samples were at room temperature in 100 mM Tris/HCl buffer at pH 7.8 in 1 cm quartz cuvette. All  $\epsilon$  and  $\Delta\epsilon$  values are based on <sup>Nif</sup>IscA dimer concentration.

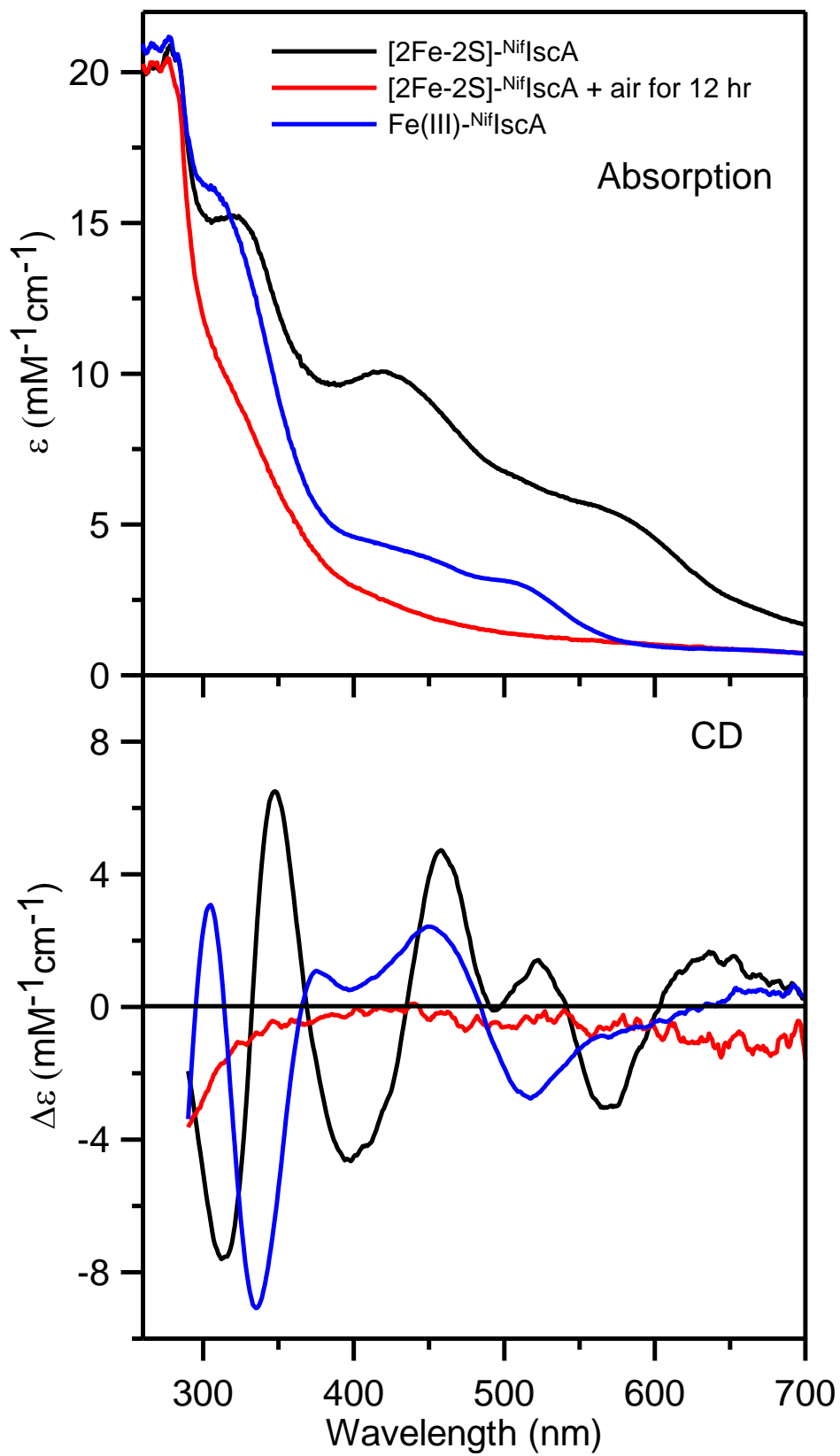


Figure A.3: Redox cycling of Fe-bound  $\text{Nif}^{\text{IscA}}$  monitored by UV-visible absorption spectroscopy. The black spectrum correspond to 95  $\mu\text{M}$  Fe(III)-bound  $\text{Nif}^{\text{IscA}}$  in 100 mM Tris/HCl buffer, pH 7.8, in the presence of 100 mM THP obtained from titrating apo  $\text{Nif}^{\text{IscA}}$  with ferric ammonium citrate under aerobic conditions and. The Fe(III)-bound bound  $\text{Nif}^{\text{IscA}}$  was treated with 114  $\mu\text{M}$  dithionite under anaerobic conditions to yield Fe(II)-bound  $\text{Nif}^{\text{IscA}}$  (red line). After exposing the dithionite-reduced Fe(II)-bound  $\text{Nif}^{\text{IscA}}$  to air for 22 min, Fe(III)-bound  $\text{Nif}^{\text{IscA}}$  was restored with 75 % yield (blue line). Samples were at room temperature in 1 cm quartz cuvette. The  $\epsilon$  values are based on the concentration of  $\text{Nif}^{\text{IscA}}$  monomer.

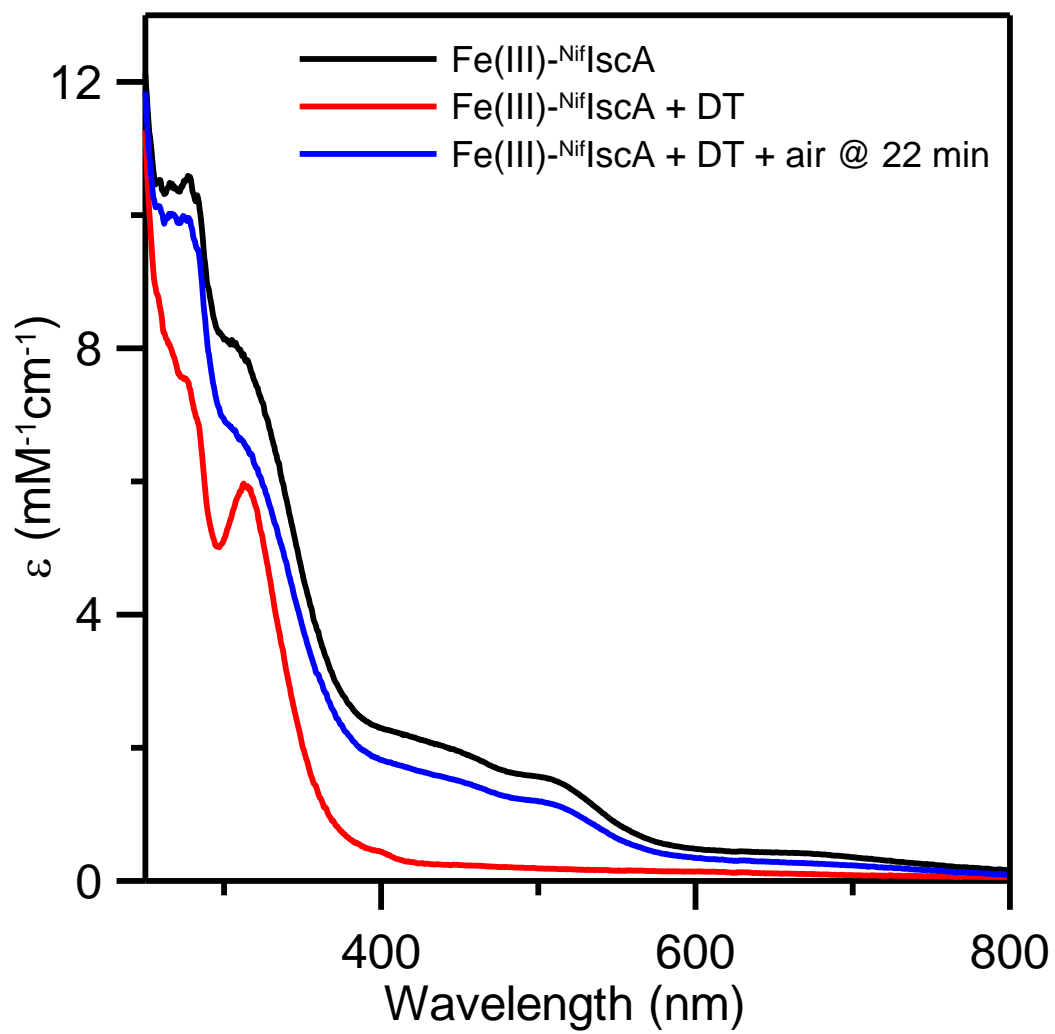


Figure A.4: UV–visible absorption and VTMCD spectra for Fe(III)- and Fe(II)-bound NifIscA. All  $\epsilon$  and  $\Delta\epsilon$  values are based on the concentration of  $^{Nif}$ IscA monomer. (A) Room-temperature absorption and VTMCD spectra of repurified Fe(III)-bound  $^{Nif}$ IscA (0.9 mM in  $^{Nif}$ IscA monomer) in 100mM Tris/HCl buffer, pH 7.8, with 55% v/v ethylene glycol. MCD spectra were recorded for samples in 1 mm cuvettes with a magnetic field of 6 T and at temperatures of 1.73, 4.22, 10, 25, 50, and 100 K. (B) Room-temperature absorption and VTMCD spectra of Fe(II)-bound  $^{Nif}$ IscA (0.8 mM in  $^{Nif}$ IscA monomer and reduced under strictly anaerobic conditions with stoichiometric sodium dithionite) in 100 mM Tris/HCl buffer, pH 7.8, 55% v/v ethylene glycol. MCD spectra were recorded for samples in 1 mm cuvettes with a magnetic field of 6 T and at temperatures of 1.73, 4.22, 10, 25, and 60 K. All MCD bands for Fe(III)- and Fe(II)-bound  $^{Nif}$ IscA increase in intensity with decreasing temperature.

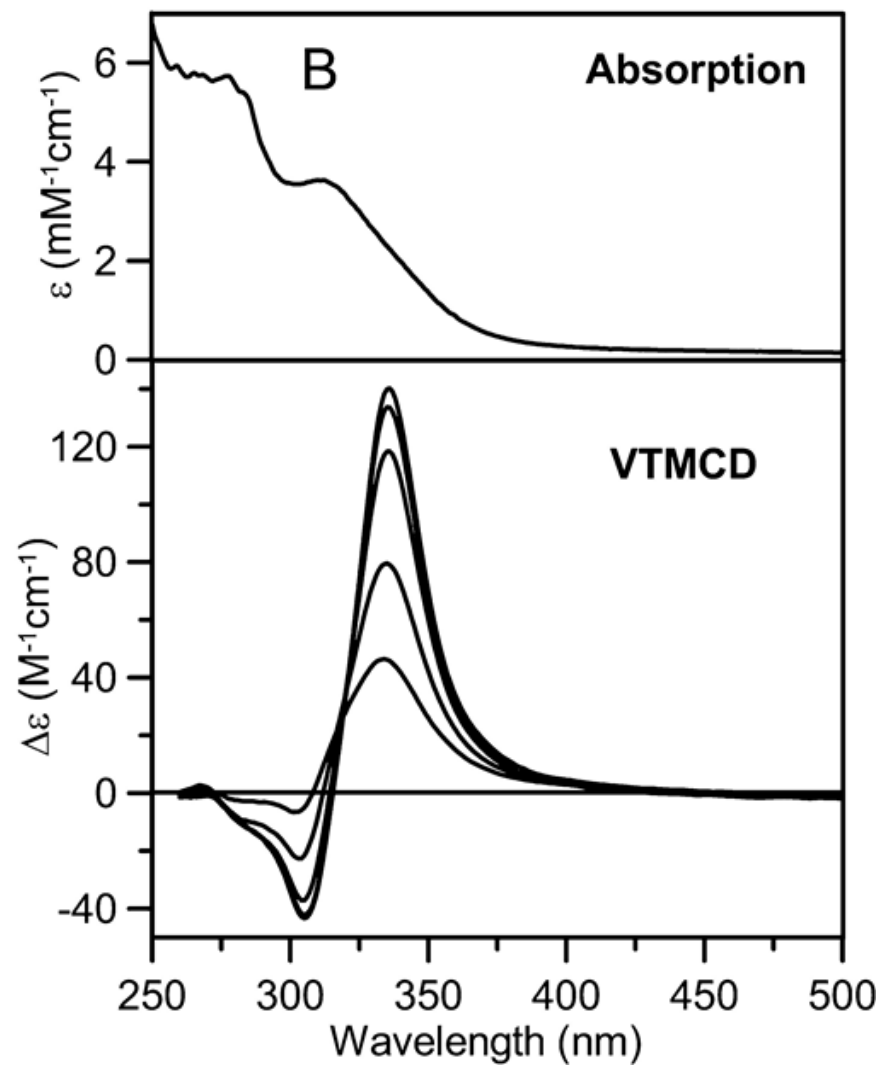
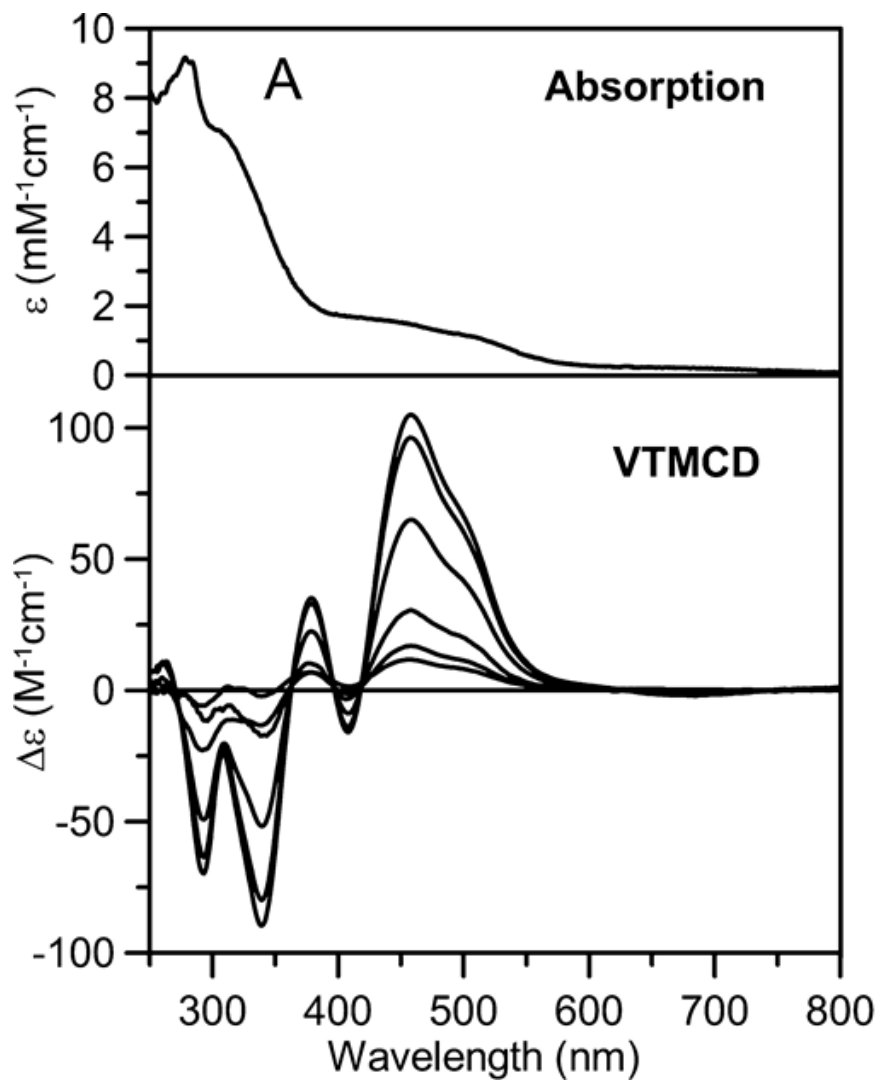


Figure A.5: X-band EPR spectrum of Fe(III)-bound  $\text{Nif}^{\text{IscA}}$  and EPR monitored redox titration. Sample is the same as that described in Figure A.2A. (A) EPR spectrum recorded at 4.9 K at a microwave frequency of 9.60 GHz, with a modulation amplitude = 0.65 mT and a microwave power of 20 mW. (B) Dye-mediated redox titration of Fe-bound  $\text{Nif}^{\text{IscA}}$  monitored by EPR. Solid line is a best fit to a one electron Nernst plot with a midpoint potential of +36 mV versus NHE.

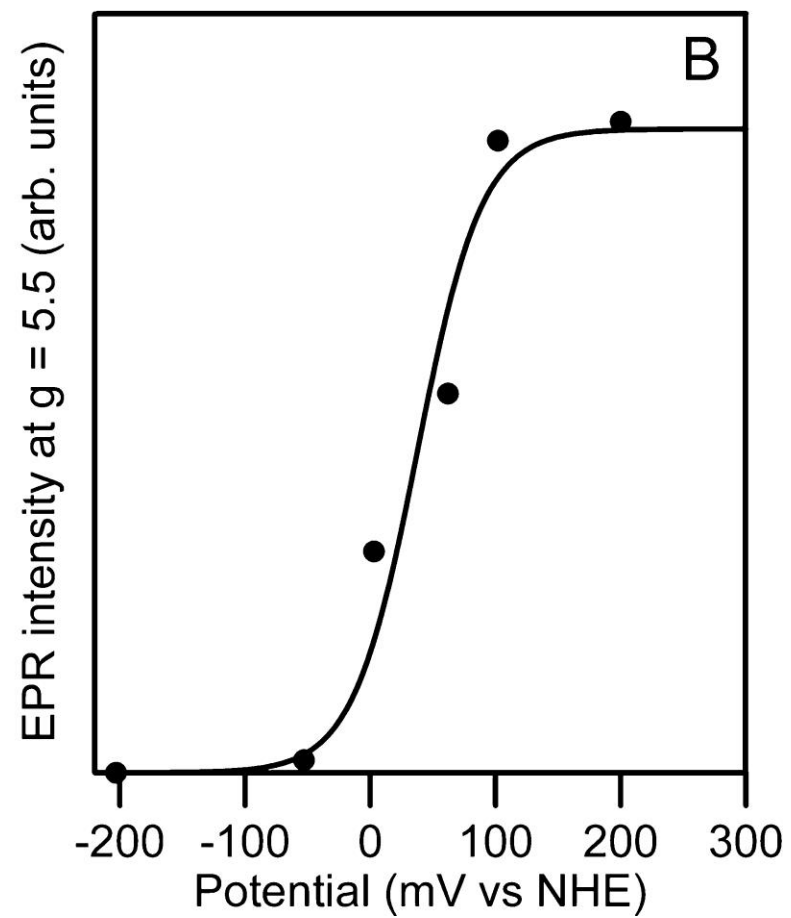
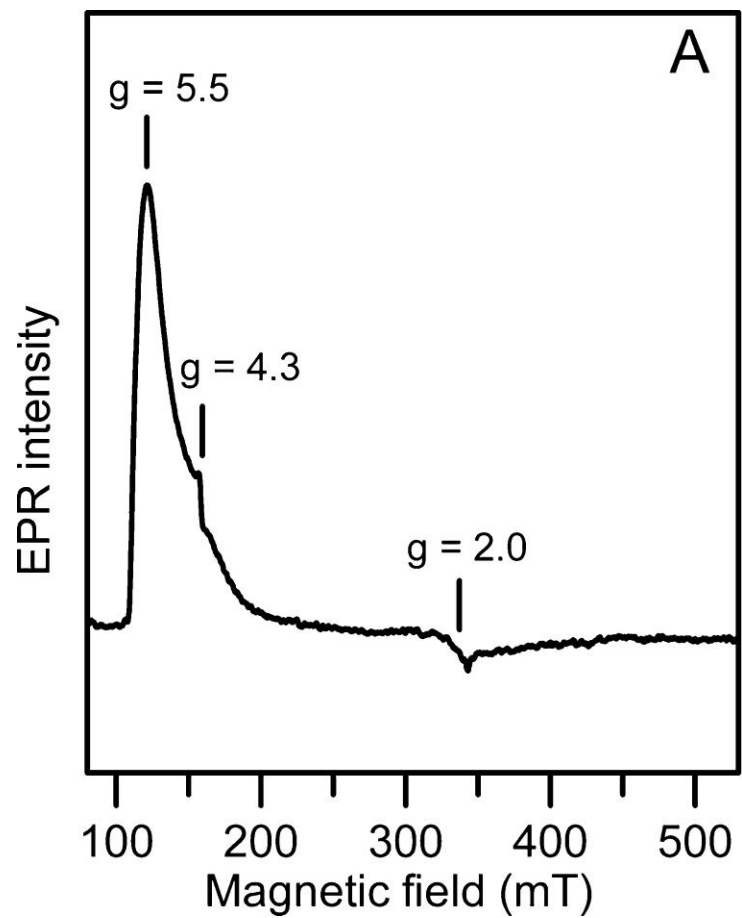


Figure A.6: Mössbauer spectra of  $^{57}\text{Fe}$ -bound forms of  $^{\text{Nif}}\text{IscA}$ . Top panel: Mössbauer spectrum of a partially reduced  $^{57}\text{Fe}$ -bound  $^{\text{Nif}}\text{IscA}$  sample containing both Fe(III)- and Fe(II)-bound forms of the enzyme. The spectrum was recorded at 4.2 K with a field of 50 mT applied parallel to the  $\gamma$ -beam. The solid green line is a quadrupole doublet ( $|\Delta E_{\text{Q}}| = 3.33$  mm/s and  $\delta = 0.72$  mm/s) representing the rubredoxin-type Fe(II)-bound  $^{\text{Nif}}\text{IscA}$  and accounts for 45% of total absorption. Bottom panel: Prepared Mössbauer spectra of Fe(III)-bound  $^{\text{Nif}}\text{IscA}$  after removal of the contribution of the Fe(II)-bound  $^{\text{Nif}}\text{IscA}$  from the raw data (see text). The spectra were recorded at 4.2 K with a field of 50 mT applied parallel (A), 50 mT applied perpendicular (B), 4 T applied parallel (C), and 8 T applied parallel (D) to the  $\gamma$ -beam. Red lines are simulations using parameters (listed in Table A.1) that are consistent with an intermediate spin  $S = 3/2$  Fe(III) species.

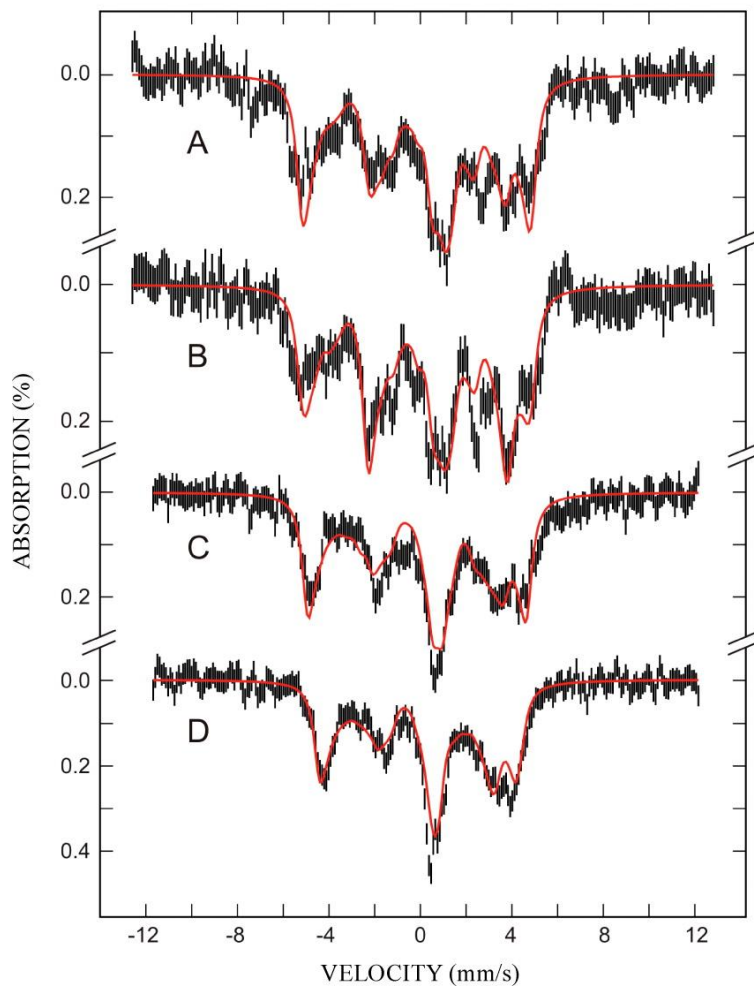
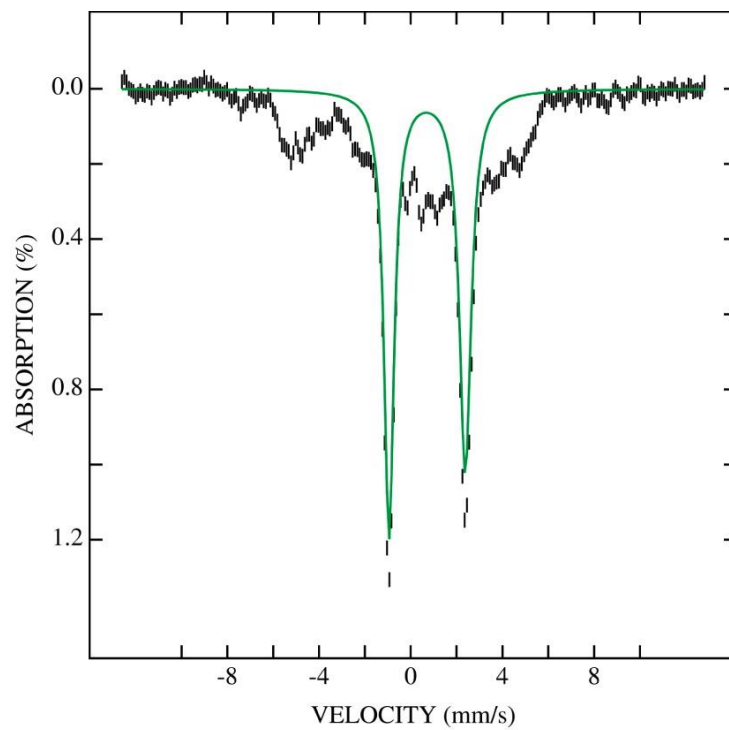


Figure A.7: Mössbauer spectra of  $^{57}\text{Fe(II)}$ -bound  $^{\text{Nif}}$ IscA. Sample was prepared by dithionite reduction of the sample used in Figure A.6. Spectra were recorded at 4.2 K with a magnetic field of 50 mT (A), 4 T (B), and 8 T (C) applied parallel to the  $\gamma$ -beam. The solid green lines overlaid on the experimental spectra are theoretical simulations of a rubredoxin-type Fe(II) species using the parameters listed in Table A.1.

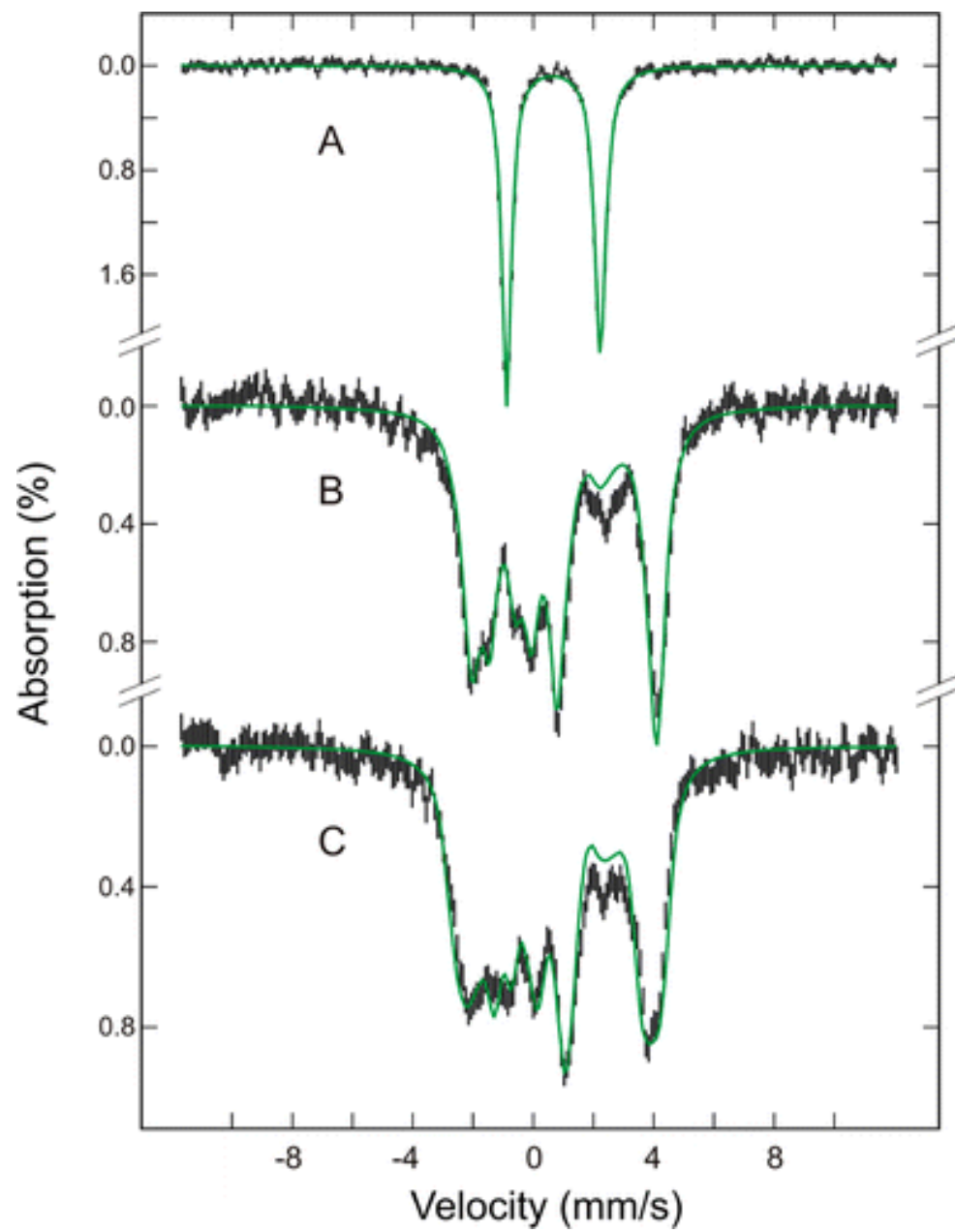


Figure A.8: VHVT MCD saturation magnetization data for Fe(III)- and Fe(II)-bound  $^{NiF}IscA$ . Samples are as described in Figure A.4. (A) VHVT MCD saturation magnetization data for Fe(III)-bound  $^{NiF}IscA$  collected at 458 nm for magnetic fields between 0 and 6 T at temperatures of 1.73 K (●), 4.22 K (▲), 10.0 K (■), and 25.0 K (◆). Solid lines are theoretical fits for a predominantly  $xz$ -polarized electronic transition ( $5M_{xy} = M_{xz} = 5M_{yz}$ ) from a rhombic  $S = 3/2$  ground state with zero-field splitting parameters  $D = +3.0 \text{ cm}^{-1}$  and  $E/D = 0.33$ , and an isotropic real  $g$ -value of 2.0. (B) VHVT MCD saturation magnetization data for Fe(II)-bound  $^{NiF}IscA$  collected at 335 nm for magnetic fields between 0 and 6 T at temperatures of 1.73 K (●), 4.22 K (▲), 10.0 K (■), and 25.0 K (◆). Solid lines are theoretical fits for a predominantly  $xy$  polarized electronic transition ( $M_{xy} = 5M_{xz} = 5M_{yz}$ ) from an  $S = 2$  ground state with zero-field splitting parameters  $D = +7.6 \text{ cm}^{-1}$  and  $E/D = 0.26$ , and real  $g$ -values of  $g_x = 2.11$ ,  $g_y = 2.19$ , and  $g_z = 2.00$ .

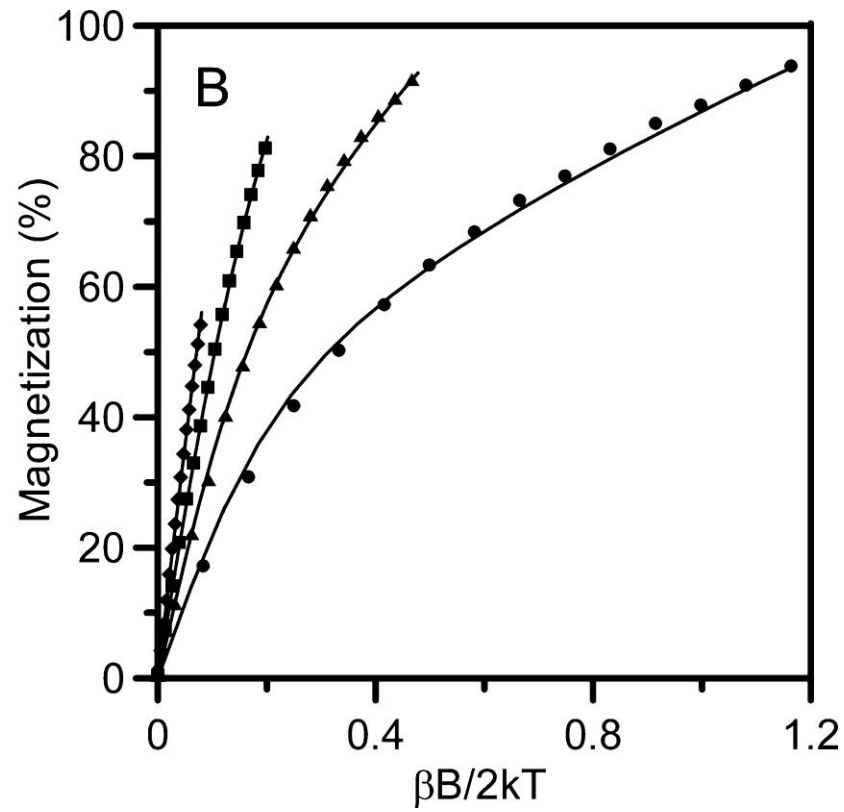
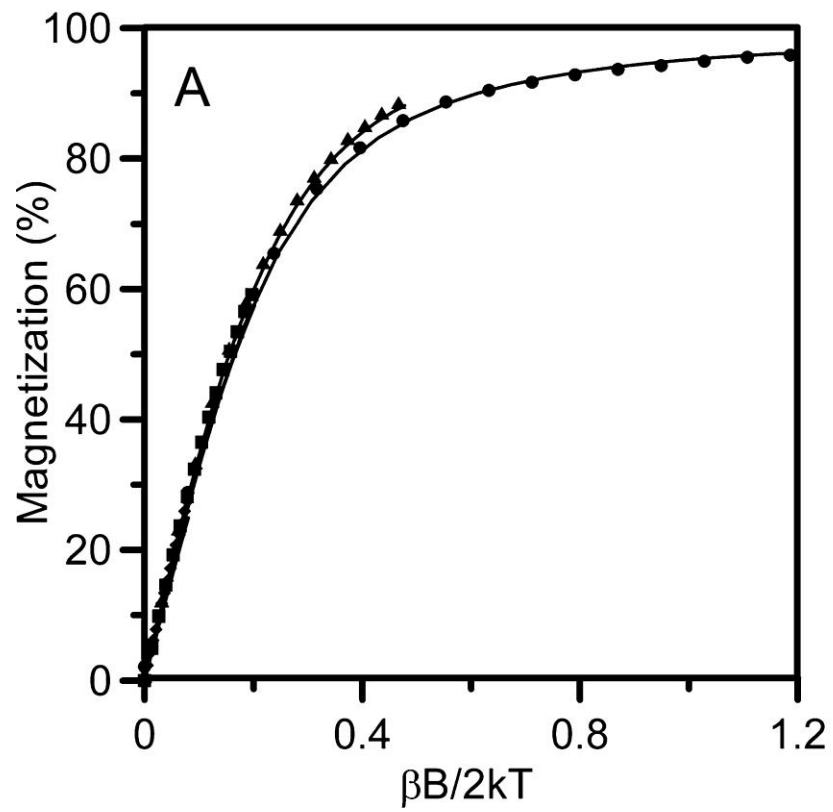


Figure A.9: Comparison of the resonance Raman spectra of *C.pasteurianum* C6D rubredoxin (488-nm excitation) and Fe(III)-bound <sup>Nif</sup>IscA (458-nm excitation). Spectra were recorded at 17 K using samples that were 3–4 mM in protein monomer. Each spectrum is the sum of 100 scans, with each scan involving photon counting for 1 s every 0.5 cm<sup>-1</sup> with a spectral bandwidth of 7 cm<sup>-1</sup>. Raman bands originating from the frozen buffer solution have been subtracted from both spectra.

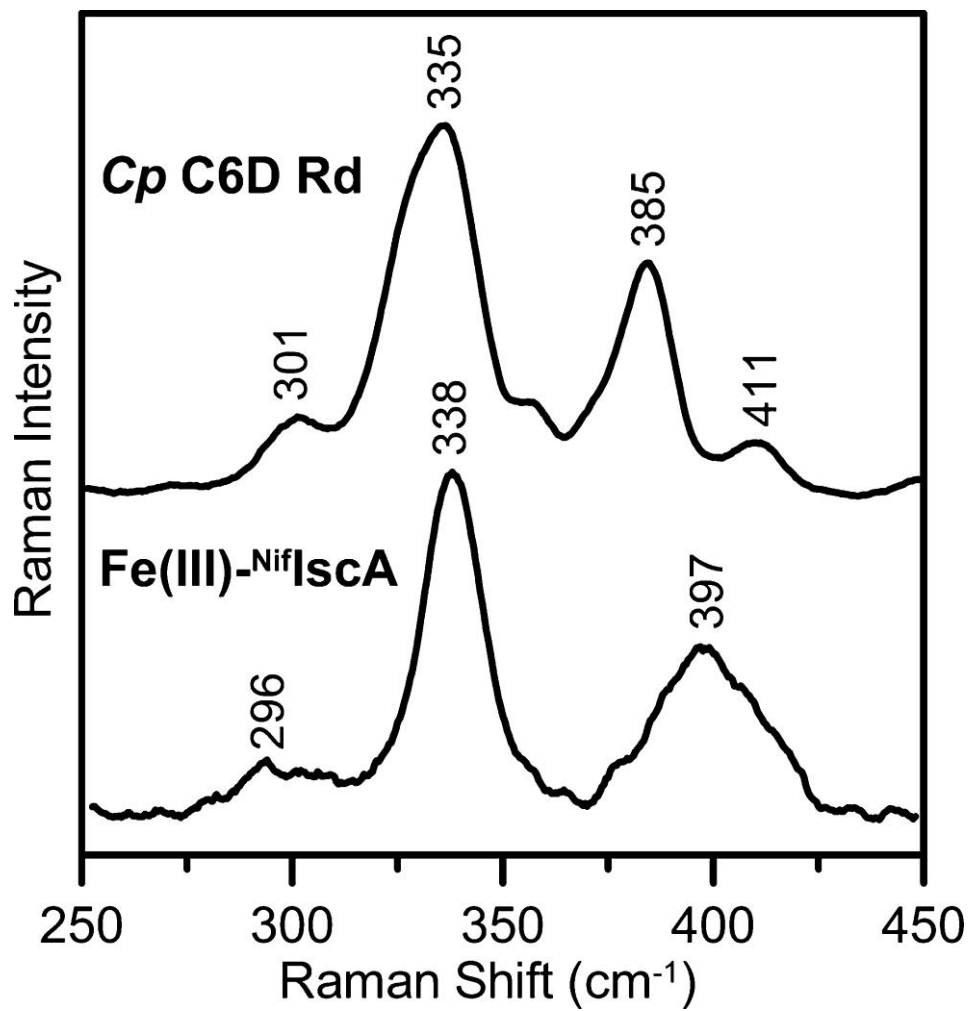


Figure A.10: VTMCD evidence for Fe(II) release from Fe(II)-bound  $^{Nif}$ IscA in the presence of L-cysteine. All samples were in 100 mM Tris/HCl buffer, pH 7.8, with 55% v/v ethylene glycol, and were handled under anaerobic conditions. (Top) MCD spectra of Fe(II)- $^{Nif}$ IscA recorded at 4.22 K with a magnetic field of 6 T. Sample was prepared by reducing a sample of Fe(III)-bound  $^{Nif}$ IscA (0.53 mM in  $^{Nif}$ IscA monomer with 0.5 Fe/monomer) with 0.3 mM sodium dithionite. (Middle) VTMCD spectra of the Fe(II)- $^{Nif}$ IscA sample used in A after addition of a 20-fold excess of L-cysteine and incubating for 5 min prior to freezing for VTMCD studies. Spectra recorded at 4.22 K, 10.0K, 25.0 K, and 50.0 K with a magnetic field of 6 T. (Bottom) VTMCD spectra of 0.12 mM ferrous ammonium sulfate in the presence of a 20-fold excess of L-cysteine and 0.2 mM sodium dithionite. Spectra recorded at 4.22 K, 10.0 K, 25.0 K, and 50.0 K with a magnetic field of 6 T. All MCD bands increase in intensity with decreasing temperature and  $\Delta\epsilon$  values for all MCD spectra are based on Fe(II) concentration.

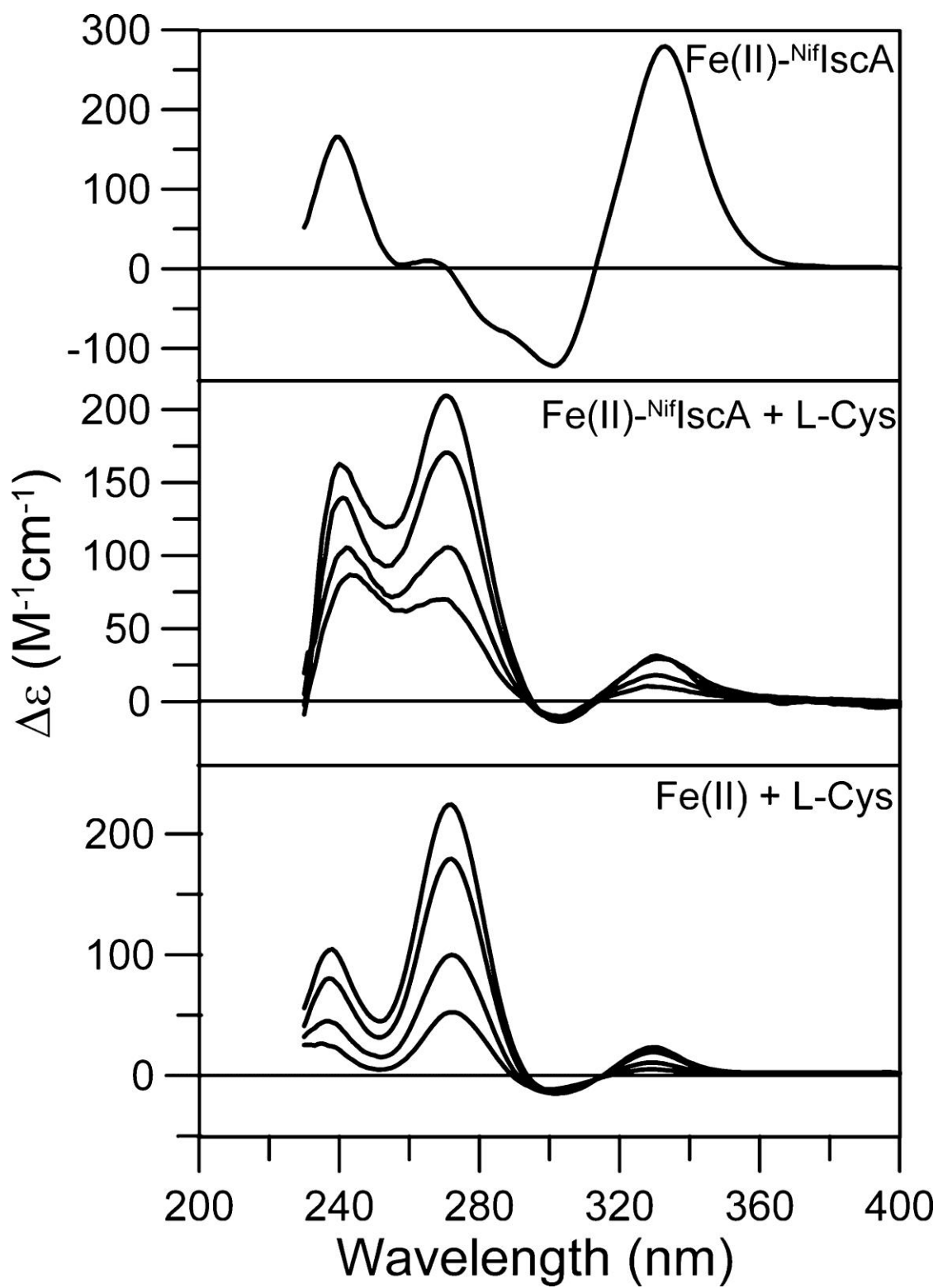


Figure A.11: CD studies of [2Fe-2S] cluster assembly on NifU-1 using Fe(III)-bound <sup>Nif</sup>IscA as the iron donor. (A) CD time course of a reaction mixture (volume 600  $\mu$ M in 1 cm cuvette) comprising 13  $\mu$ M NifU-1, 108  $\mu$ M Fe(III)-bound <sup>Nif</sup>IscA (based on Fe concentration), 0.34  $\mu$ M NifS, and 384  $\mu$ M L-cysteine in 100 mM Tris-HCl buffer, pH 7.5, at 22 °C. Spectra were recorded at 0, 15, 28, 40, 50, 58, 68, 80, and 92 min after initiating the reaction by the addition of L-cysteine. The red spectrum corresponds to the zero-time spectrum, i.e., 108  $\mu$ M Fe(III)-bound <sup>Nif</sup>IscA in the same volume of reaction mixture without NifU-1, NifS, and L-cysteine. The arrows indicate the direction of change in CD intensity with increasing time at discrete wavelengths. Spectra at each time point were resolved into decreasing contributions from the Fe(III)-bound <sup>Nif</sup>IscA component (B) and an increasing combined contribution from the [2Fe-2S] cluster-bound forms of NifU-1 and <sup>Nif</sup>IscA (C). The 0 and 15 min spectra in C have negligible CD intensity and have been omitted for clarity. (D) Simulation of the CD spectra in C based on contributions from the CD spectra of [2Fe-2S] cluster-bound forms of NifU-1 and <sup>Nif</sup>IscA. The individual contributions from the [2Fe-2S] cluster-bound forms of NifU-1 and <sup>Nif</sup>IscA that were used to simulate the 92 min spectrum in C are shown as green and blue lines, respectively. (E) CD spectra for Fe(III)-bound <sup>Nif</sup>IscA (red), [2Fe-2S] cluster-bound NiU-1 (green), and [2Fe-2S] cluster-bound <sup>Nif</sup>IscA (blue) with  $\Delta\epsilon$  values based on Fe or [2Fe-2S] cluster concentration. (F) Computed changes in the concentrations of Fe(III)-bound <sup>Nif</sup>IscA (red), [2Fe-2S] cluster-bound NiU-1 (green), and [2Fe-2S] cluster-bound <sup>Nif</sup>IscA (blue) in the reaction mixture, based on the CD  $\Delta\epsilon$  values shown in E. The black data points and line correspond to the concentration of [2Fe-2S] cluster-bound NifU-1 as a function of time in a control CD experiment using the same reaction mixture with 108  $\mu$ M ferrous ammonium sulfate in place of 108  $\mu$ M Fe(III)-bound <sup>Nif</sup>IscA.

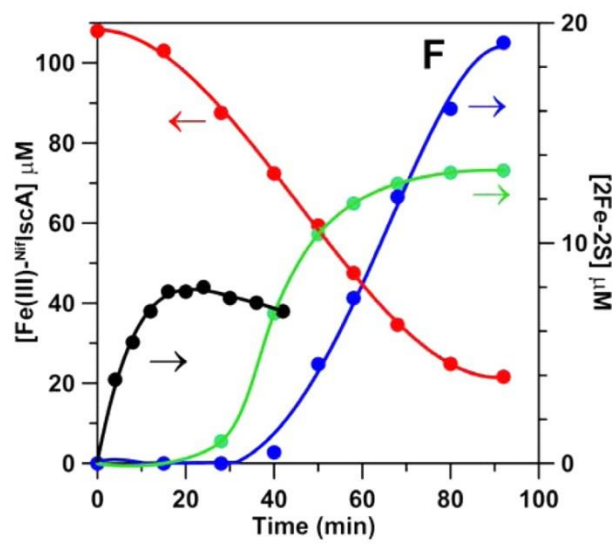
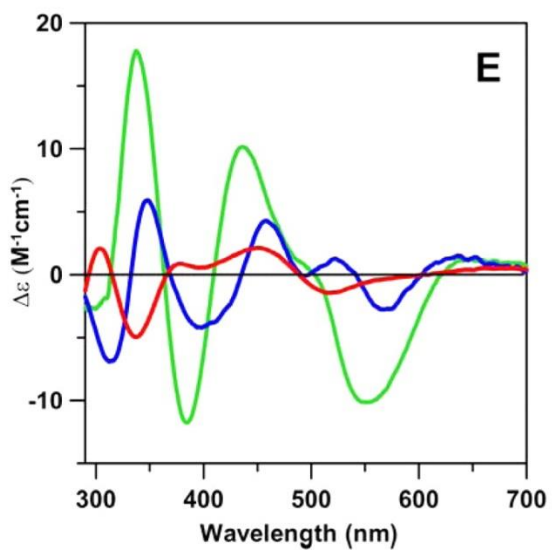
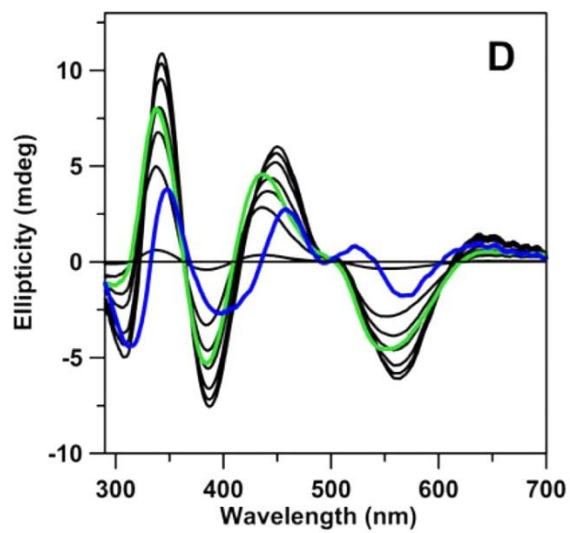
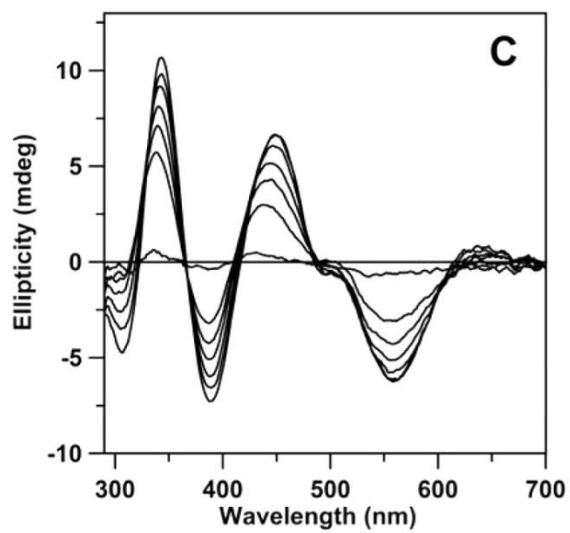
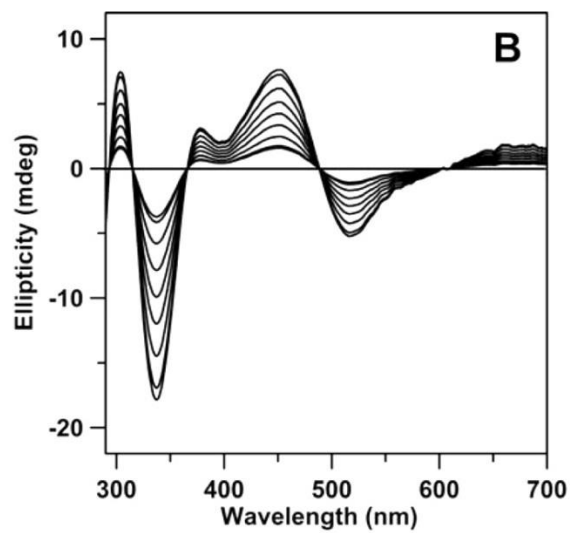
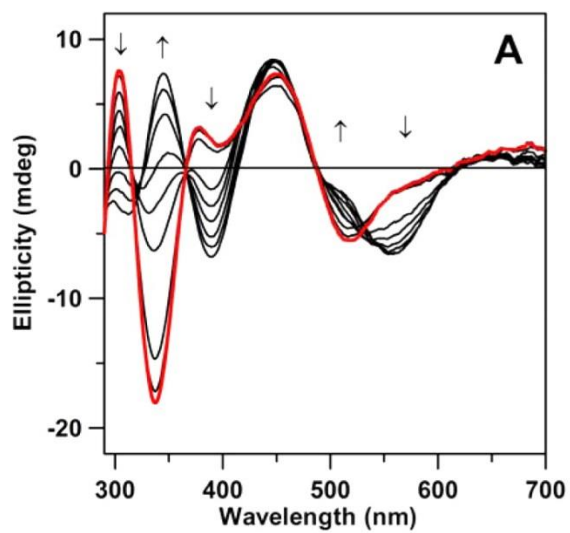
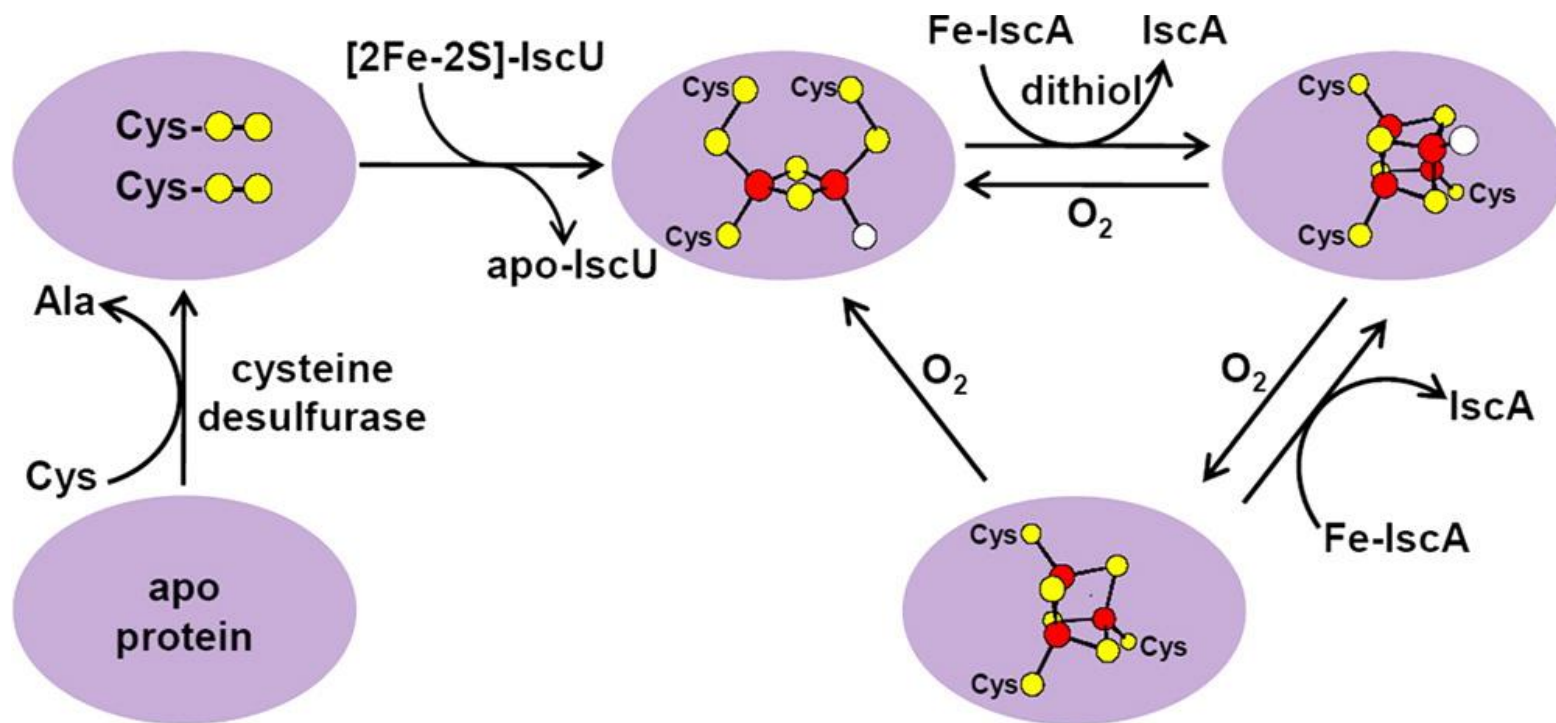


Figure A.12: Schematic representation of the proposed role of the Fe-bound form of A type proteins (Fe-IscA) in the maturation of [4Fe-4S] clusters and the *in situ* repair of oxygen-damaged [4Fe-4S] clusters. Color scheme: Fe (red); S (yellow); cysteinyl S or non-S ligating atom (white). See text for details.



APPENDIX B

SPECTROSCOPIC AND FUNCTIONAL CHARACTERIZATION OF IRON–SULFUR  
CLUSTER-BOUND FORMS OF *AZOTOBACTER VINELANDII*<sup>NIF</sup> ISCA

---

Daphne T. Mapolelo,<sup>a</sup> Bo Zhang,<sup>a</sup> Sunil G. Naik,<sup>b</sup> Boi Hanh Huynh,<sup>b</sup> and Michael K. Johnson<sup>a</sup>

*Biochemistry* **2012**, *51*, 8071–8084.

Reprinted here with permission of the publisher.

<sup>a</sup>Department of Chemistry and Center for Metalloenzyme Studies, University of Georgia;

Athens, Georgia 30602; <sup>b</sup>Department of Physics, Emory University, Atlanta, Georgia 30322

**Abbreviations:** TCEP, tris(2-carboxyethyl)phosphine hydrochloride; DTT, dithiothreitol; FNR, fumarate nitrate reduction regulatory protein; PLP, pyridoxal phosphate; EPR, electron paramagnetic resonance; GSH, glutathione.

## Abstract

The mechanism of [4Fe-4S] cluster assembly on A-type Fe-S cluster assembly proteins, in general, and the specific role of <sup>Nif</sup>IscA in the maturation of nitrogen fixation proteins are currently unknown. To address these questions, *in vitro* spectroscopic studies (UV-visible absorption/CD, resonance Raman and Mössbauer) have been used to investigate the mechanism of [4Fe-4S] cluster assembly on *Azotobacter vinelandii* <sup>Nif</sup>IscA, and the ability of <sup>Nif</sup>IscA to accept clusters from NifU and to donate clusters to the apo form of the nitrogenase Fe-protein. The results show that <sup>Nif</sup>IscA can rapidly and reversibly cycle between forms containing one [2Fe-2S]<sup>2+</sup> and one [4Fe-4S]<sup>2+</sup> cluster per homodimer via DTT-induced two-electron reductive coupling of two [2Fe-2S]<sup>2+</sup> clusters and O<sub>2</sub>-induced [4Fe-4S]<sup>2+</sup> oxidative cleavage. This unique type of cluster interconversion in response to cellular redox status and oxygen levels is likely to be important for the specific role of A-type proteins in the maturation of [4Fe-4S] cluster-containing proteins under aerobic growth or oxidative stress conditions. Only the [4Fe-4S]<sup>2+</sup>-<sup>Nif</sup>IscA was competent for rapid activation of apo nitrogenase Fe protein under anaerobic conditions. Apo <sup>Nif</sup>IscA was shown to accept clusters from [4Fe-4S] cluster-bound NifU via rapid intact cluster transfer, indicating a potential role as a cluster carrier for delivery of clusters assembled on NifU. Overall the results support the proposal that A-type proteins can function as carrier proteins for clusters assembled on U-type proteins and suggest that they are likely to supply [2Fe-2S] clusters rather than [4Fe-4S] for the maturation of [4Fe-4S] cluster-containing proteins under aerobic or oxidative stress growth conditions.

## Introduction

Iron sulfur (Fe–S) clusters are essential and versatile biological cofactors that are found in all organisms and are utilized in a wide range of physiological processes, functioning not only in electron transport and as enzyme active sites, but also in DNA repair and sensing of ambient conditions for regulatory processes (1-4). Although Fe–S clusters are implicated in a wide range of biochemical processes, the detailed molecular mechanisms underlying their biosynthesis and repair remain to be elucidated. Ongoing studies on Fe–S cluster biosynthesis in eukaryotes and prokaryotes have led to the identification of highly conserved sets of genes which encode for proteins that are involved in the assembly of Fe–S clusters and their insertion into target apo-proteins (3;5-9). Besides the nitrogen fixation (NIF) system which is dedicated to maturation of the Fe–S proteins involved with nitrogen fixation in azototrophic bacteria, many bacteria contain the more general purpose iron-sulfur cluster (ISC) and sulfur utilizing factor (SUF) systems (5;7;8;10;11). In *Escherichia coli*, the ISC system is utilized under normal growth conditions (12), while the SUF system is utilized under iron limitation and oxidative stress conditions (8;13-15). The bacterial ISC and SUF systems also constitute the major components of the Fe–S cluster biogenesis systems in mitochondria and chloroplasts, respectively (3;6;9).

A-type Fe–S cluster assembly proteins (<sup>Nif</sup>IscA, IscA, SufA) are encoded by specific genes in the bacterial *nif*, *isc*, and *suf* operons and constitute a homologous class of proteins with three rigorously conserved cysteine residues in a C-X<sub>63-65</sub>-C-G-C sequence motif. *In vitro* studies have shown that the conserved cysteines are competent to ligate monomeric Fe<sup>2+,3+</sup> ions, [2Fe-2S]<sup>2+</sup> clusters or [4Fe-4S]<sup>2+</sup> clusters at the subunit interface of recombinant homodimers (16-18). However, the specific functions of A-type proteins in Fe–S cluster biogenesis have remained elusive, due in large part to the lack of a well-defined phenotype. Except for the A-type ErpA

protein which has been shown to play a specific and essential role in the maturation of the key [4Fe-4S] cluster-containing enzymes (IspH and IspG) in the bacterial isoprenoid biosynthesis pathway (19), genetic studies indicate that A-type proteins often exhibit functional redundancy and are generally only required under aerobic or oxidative stress conditions. In *A. vinelandii*, which contains the NIF and ISC systems, deletion of <sup>Nif</sup>IscA (aka orf6) was found to have no effect on Mo-dependent diazotropic growth (20) and deletion of IscA was shown to be lethal only under elevated oxygen conditions (21). In *E. coli*, knockouts of either IscA or SufA have only a mild effect on cell growth, while deletion of both IscA and SufA results in a null-growth phenotype in minimal medium under aerobic conditions (22;23). This has led to the discovery of specific roles for IscA/SufA in the maturation of bacterial [4Fe-4S]<sup>2+</sup> centers under aerobic growth conditions (24;25). A similar role has also been demonstrated in *S. cerevisiae*, where Isa1 and Isa2 have recently been shown to form an Fe-bound complex that is required, along with the tetrahydrofolate-dependent Iba57 and Isu1/Isu2, for the maturation of mitochondrial [4Fe-4S] proteins (26). However, a molecular level understanding of how A-type proteins facilitate [4Fe-4S] cluster maturation and whether this involves the mononuclear Fe or Fe-S cluster bound forms are still unresolved.

The objectives of this work and that of the accompanying manuscript were to address the role of mononuclear Fe- and Fe-S cluster-bound forms of *Azotobacter vinelandii* (*Av*) <sup>Nif</sup>IscA in NIF-specific Fe-S cluster biosynthesis using *in vitro* spectroscopic approaches. The simplicity of the NIF system, comprising NifS (cysteine desulfurase S-donor), NifU (primary scaffold protein), and <sup>Nif</sup>IscA, and its exclusive role in the maturation of nitrogen fixation proteins containing double or single [4Fe-4S] cubane clusters, make NIF an attractive system for investigating how A-type proteins facilitate [4Fe-4S] cluster maturation. Appendix A

characterizes and addresses the role of mononuclear Fe-bound forms of *A. vinelandii* <sup>Nif</sup>IscA. This work focuses on characterizing and investigating the properties of Fe–S cluster-bound forms of *A. vinelandii* <sup>Nif</sup>IscA and addressing their role in [4Fe-4S] cluster maturation. The results demonstrate that <sup>Nif</sup>IscA can function as a carrier protein for clusters assembled on NifU and an effective cluster donor for maturation of the nitrogenase Fe protein under anaerobic conditions. Moreover the cluster-bound form of <sup>Nif</sup>IscA is shown to be reversibly dependent on medium conditions, with the dithiol reagent DTT favoring the [4Fe-4S]<sup>2+</sup> cluster-bound homodimer under anaerobic conditions and O<sub>2</sub> exposure resulting in conversion to the [2Fe-2S]<sup>2+</sup> cluster-bound homodimer. The mechanism of the cluster interconversion and the potential importance of both the [4Fe-4S]<sup>2+</sup> and [2Fe-2S]<sup>2+</sup> cluster-bound forms of A-type proteins for the maturation of [4Fe-4S] cluster-containing proteins under anaerobic, aerobic, or oxidative stress conditions are discussed in light of these results.

## **Experimental procedures**

*Materials:* Materials used in this work were of reagent grade and were purchased from Fischer Scientific, Sigma-Aldrich Chemical Co, Invitrogen, VWR International, unless otherwise stated.

*Expression and purification of Av<sup>Nif</sup>IscA:* The procedures used for the heterologous expression and purification of *A. vinelandii* <sup>Nif</sup>IscA are described in the accompanying manuscript. All samples used in this work were >95% pure based on gel electrophoresis and direct amino acid analyses conducted at Texas A&M University.

*Biochemical analyses:* Protein and iron assays of Fe–S cluster-bound forms of Av<sup>Nif</sup>IscA were carried out as described in Appendix A of this dissertation. Protein concentrations of Av<sup>Nif</sup>IscA were assessed using the BioRad Dc protein assay and corrected for a 17% overestimation

based on direct amino acid analysis (see Appendix A). The oligomeric state of  $[2\text{Fe-2S}]^{2+}$  cluster-bound  $^{\text{Nif}}\text{IscA}$  was determined by analytical gel-filtration chromatography using a 25-mL Superdex G-75 10/300 column (Pharmacia Biotech), as described in Appendix A.

*Spectroscopic methods:* Samples for all spectroscopic investigations were prepared under argon atmosphere in a glovebox (Vacuum Atmosphere, Hawthorne, CA) at oxygen levels <1 ppm. UV-visible absorption spectra were recorded under anaerobic conditions in septum-sealed 1 mm quartz cuvettes or small-volume 1 cm cuvettes at room temperature, using a Shimadzu UV-3101 PC scanning spectrophotometer fitted with a TCC-260 temperature controller. CD spectra were also recorded under anaerobic conditions in the same cuvettes using a JASCO J-715 spectropolarimeter (Jasco, Easton, MD). Resonance Raman spectra were recorded at 17 K as previously described (27), using a Ramanor U1000 spectrometer (Instruments SA, Edison, NJ) coupled with a Sabre argon ion laser (Coherent, Santa Clara, CA), with 20- $\mu\text{L}$  frozen droplets of sample mounted on the coldfinger of a Displex model CSA-202E closed cycle refrigerator (Air Products, Allentown, PA). X-band (9.6 GHz) EPR spectra were recorded using a ESP-300E spectrometer (Bruker, Billerica, MA), equipped with an ER-4116 dual mode cavity and an ESR-900 helium flow cryostat (Oxford Instruments, Concord, MA). Mössbauer spectra in the presence of applied magnetic fields were recorded using previously described instrumentation (28), and the data were analyzed with the WMOSS program (Web Research).

*NifS-mediated Fe-S cluster assembly on  $^{\text{Nif}}\text{IscA}$ :* Cluster-bound  $^{\text{Nif}}\text{IscA}$  was prepared by first pretreating as-purified apo  $^{\text{Nif}}\text{IscA}$  in 100 mM Tris-HCl buffer at pH 7.8 (buffer A) with 20-fold excess of tris(2-carboxyethyl)phosphine hydrochloride (TCEP) for 30 min in order to cleave disulfides/polysulfides. The protein was then exchanged into buffer A containing 150 mM NaCl using a 50 mL G-25 desalting column (GE Healthcare) previously equilibrated with the same

buffer. The eluted protein was concentrated using a YM10 Amicon. TCEP-treated  $^{57}\text{Fe}$ - $^{60}\text{Ni}$ -IscA (1 mM) was incubated with NifS (6.27  $\mu\text{M}$ ), ferrous ammonium sulfate (4 mM) and L-cysteine (16 mM) in the same buffer for 45 min in an ice bath under anaerobic conditions in a Vacuum Atmospheres glovebox under argon (<1 ppm  $\text{O}_2$ ). Protein concentrations of  $^{60}\text{Ni}$ -IscA and NifS are reported as monomers. For Mössbauer samples,  $^{57}\text{Fe}$ -enriched ferrous ammonium sulfate (>95% enrichment) was used in the reconstitution mixture in place of natural abundance ferrous ammonium sulfate. Mössbauer studies of the time course of Fe–S cluster assembly on  $^{60}\text{Ni}$ -IscA were carried out by taking out aliquots of the reaction mixture at different time intervals, placing in Mössbauer cups and freezing in liquid nitrogen. For Mössbauer control experiments, samples were prepared as above except that  $^{60}\text{Ni}$ -IscA was omitted from the reaction mixture. UV–visible absorption and CD studies of the time course of Fe–S cluster assembly were carried out by taking spectra at different time intervals on one sample under anaerobic conditions in septum-sealed 1 mm quartz cuvettes at room temperature. Purification of cluster-bound  $^{60}\text{Ni}$ -IscA to remove excess reagents was achieved by loading the reconstitution mixture onto  $2 \times 5$  mL High-trap Q-Sepharose column (GE Healthcare) previously equilibrated with buffer A and eluted with a 0–100% NaCl gradient from buffer A containing 1 M NaCl. The  $[\text{2Fe-2S}]^{2+}$  cluster-bound form of  $^{60}\text{Ni}$ -IscA eluted between 0.45 and 0.55 M NaCl and was concentrated using a YM10 Amicon. Incubation of  $[\text{2Fe-2S}]^{2+}$  cluster-bound  $^{60}\text{Ni}$ -IscA with 2 mM DTT under anaerobic conditions in buffer A for 15 min yielded the  $[\text{4Fe-4S}]^{2+}$  cluster-bound form of  $^{60}\text{Ni}$ -IscA.

*Holo  $^{60}\text{Ni}$ -IscA to apo ADP-bound nitrogenase Fe protein cluster transfer:* The apo form of ADP-bound *A. vinelandii* nitrogenase Fe protein was prepared as previously described (29). Reactions were carried out in buffer A and  $[\text{2Fe-2S}]^{2+}$  cluster-bound  $^{60}\text{Ni}$ -IscA was incubated with 2 mM DTT in the same buffer for 15 min prior to use in cluster transfer experiments. The time

course of cluster transfer from 2 mM DTT treated  $[2\text{Fe-2S}]^{2+}$  cluster-bound  $^{\text{Nif}}\text{IscA}$  to apo ADP-bound nitrogenase Fe protein was monitored under anaerobic conditions in small-volume 1 cm cuvettes at room temperature using UV–visible absorption and CD spectroscopies. After 50 min, the cluster transfer mixture was loaded onto a  $2 \times 5$  mL High-trap Q-Sepharose column (GE Healthcare) pre-equilibrated with buffer A. The columns were then washed with 3 bed volumes of the same buffer. Both proteins eluted with a 0–100% NaCl gradient from buffer A containing 1 M NaCl with apo  $^{\text{Nif}}\text{IscA}$  and holo Fe protein eluting between 0.45–0.55 and 0.65–0.70 M NaCl, respectively. The greenish-brown fractions of the Fe protein were concentrated using a YM30 Amicon and used for EPR studies after anaerobic addition of 50% (v/v) ethylene glycol and reduction with sodium dithionite and rapid freezing in liquid nitrogen.

*Holo NifU to apo  $^{\text{Nif}}\text{IscA}$  cluster transfer:* Reactions were carried out in buffer A and  $[4\text{Fe-4S}]$  cluster-bound NifU was prepared as described previously (30). The time course of cluster transfer from  $[4\text{Fe-4S}]^{2+}$  cluster-bound NifU to TCEP-pretreated apo- $^{\text{Nif}}\text{IscA}$  in the absence and presence of DTT was monitored under anaerobic conditions in septum-sealed small-volume 1 cm cuvettes at room temperature using UV–visible absorption and CD spectroscopies.

## Results

*NifS-mediated Fe–S cluster assembly on  $^{\text{Nif}}\text{IscA}$ :* UV–visible absorption/CD and Mössbauer spectroscopies were used to investigate the time course of NifS-catalyzed cluster assembly on  $^{\text{Nif}}\text{IscA}$ . The UV–visible absorption and CD spectra of apo  $^{\text{Nif}}\text{IscA}$  and of the reconstitution mixture taken after 5 min, 20 min, and 65 min of NifS-mediated cluster reconstitution are shown in Figure B.1. No significant visible absorption or CD that can be attributed to S-to-Fe(III) charge-transfer transitions of an Fe–S cluster is observed after 5 min. However, after 20 min, the characteristic visible absorption and CD spectrum of  $^{\text{Nif}}\text{IscA}$

containing one  $[2\text{Fe-2S}]^{2+}$  cluster per homodimer is observed (see below). On the basis of the CD  $\Delta\epsilon$  values per  $[2\text{Fe-2S}]^{2+}$  cluster that were determined for dimeric  $^{\text{Nif}}\text{IscA}$  samples of known  $[2\text{Fe-2S}]^{2+}$  cluster content, as determined by analytical and Mössbauer (see below), it is estimated that the reconstitution mixture contains 30–40% of the  $^{\text{Nif}}\text{IscA}$  in a form containing one  $[2\text{Fe-2S}]^{2+}$  cluster per homodimer. As the reaction proceeds, the UV–visible absorption intensity increases and after 65 min is dominated by a broad shoulder centered at 420 nm which is more characteristic of a  $[4\text{Fe-4S}]^{2+}$  cluster (31). Concomitantly, the UV–visible CD of the  $[2\text{Fe-2S}]^{2+}$  center decreases and is almost completely lost after 65 min. As shown below,  $[4\text{Fe-4S}]^{2+}$  centers on  $^{\text{Nif}}\text{IscA}$  exhibit negligible CD intensity compare to  $[2\text{Fe-2S}]^{2+}$  centers. Consequently, the UV–visible CD and absorption data are consistent with  $[2\text{Fe-2S}]^{2+}$  to  $[4\text{Fe-4S}]^{2+}$  cluster conversion, but this clearly requires confirmation using Mössbauer spectroscopy which provides positive identification and quantitation of both  $[2\text{Fe-2S}]^{2+}$  and  $[4\text{Fe-4S}]^{2+}$  clusters in a reaction mixture.

Mössbauer spectroscopy was used in a previous study to characterize the time course of steady state NifS-mediated cluster assembly on  $^{\text{Nif}}\text{IscA}$  (17). The same approach was used in this study to complement the UV–visible absorption and CD results discussed above. The major differences were that the samples of apo  $^{\text{Nif}}\text{IscA}$  used in this work were pretreated with TCEP rather than DTT to cleave disulfides and were taken from the reaction at different time intervals and frozen for Mössbauer studies, rather than being subjected to cycles of thawing and freezing to generate Mössbauer samples at different time intervals. Figure B.2, left panel, shows Mössbauer spectra (dotted lines) of samples taken from NifS-mediated reconstitution of  $^{\text{Nif}}\text{IscA}$  reaction mixture at 2 min (A), 20 min (B), and 60 min (C). The Mössbauer spectra of control samples taken from an identical reaction mixture that lacked  $^{\text{Nif}}\text{IscA}$  at the same time intervals are shown in the right panel of Figure B.2. The colored lines are theoretical simulations for the

individual Fe species using the Mössbauer parameters listed in Table B.1, with the three high-spin Fe(II) components, termed  $\text{Fe}^{\text{II}}\text{Cys}_4$ ,  $\text{Fe}^{\text{II}}_{-3.5}$ , and  $\text{Fe}^{\text{II}}_{-4.1}$ , shown in green and  $[\text{2Fe-2S}]^{2+}$  clusters and  $[\text{4Fe-4S}]^{2+}$  clusters shown in red and blue, respectively. They are plotted in accord with the percentage absorptions listed in Table B.2. The solid black lines overlaid with the experimental spectra are the composites of these simulated spectra. The labeling of the three high-spin ferrous ions is adapted from Krebs *et al.* (17), where  $\text{Fe}^{\text{II}}\text{Cys}_4$  is tetrahedral sulfur coordinated  $\text{Fe}^{2+}$  ion and  $\text{Fe}^{\text{II}}_{-3.5}$  and  $\text{Fe}^{\text{II}}_{-4.1}$  are labeled according to their quadrupole splitting parameters ( $\Delta E_Q$ ),  $\Delta E_{Q1} = 3.5$  mm/s and  $\Delta E_{Q2} = 4.1$  mm/s, respectively.

Analysis of the Mössbauer data shows that after 2 min of the  $^{57}\text{Fe}$   $\text{Nif}^{\text{IscA}}$  reconstitution reaction, an overwhelming majority (98%) of the Fe is present as high-spin ferrous species while a small minority (2%) is present as  $[\text{4Fe-4S}]^{2+}$  cluster (Figure B.2A and Table B.2). However similar data, with 2% of the Fe present as  $[\text{4Fe-4S}]^{2+}$  cluster, were observed in the control experiment without  $^{57}\text{Fe}$   $\text{Nif}^{\text{IscA}}$  (Figure B.2D and Table B.2), indicating that the  $[\text{4Fe-4S}]^{2+}$  clusters are bound by exogenous cysteine rather than  $^{57}\text{Fe}$   $\text{Nif}^{\text{IscA}}$ . As the reaction progresses to 20 min, the  $^{57}\text{Fe}$   $\text{Nif}^{\text{IscA}}$  reconstitution sample shows formation of  $[\text{2Fe-2S}]^{2+}$  and  $[\text{4Fe-4S}]^{2+}$  clusters with percentage iron absorptions of 9% and 11% respectively, with the rest of the Fe attributed to high-spin ferrous species (Figure B.2B and Table B.2). On the basis of the  $^{57}\text{Fe}$  ferrous ammonium sulfate concentration of 4 mM and the monomeric  $^{57}\text{Fe}$   $\text{Nif}^{\text{IscA}}$  concentration of 1 mM, this translates to  $[\text{2Fe-2S}]^{2+}$  and  $[\text{4Fe-4S}]^{2+}$  cluster concentrations of 0.18 mM and 0.11 mM, respectively, or 36% of the  $^{57}\text{Fe}$   $\text{Nif}^{\text{IscA}}$  was present in a form containing one  $[\text{2Fe-2S}]^{2+}$  per homodimer and 22% of the  $^{57}\text{Fe}$   $\text{Nif}^{\text{IscA}}$  present in a form containing one  $[\text{4Fe-4S}]^{2+}$  per homodimer. The control sample indicates that  $[\text{4Fe-4S}]^{2+}$  concentration is likely to be an overestimate, as 5% of the Fe in the reaction mixture without  $^{57}\text{Fe}$   $\text{Nif}^{\text{IscA}}$  was found to be present as exogenous cysteine-

ligated  $[4\text{Fe-4S}]^{2+}$  clusters (Figure B.2E and Table B.2), which translates to a  $[4\text{Fe-4S}]^{2+}$  cluster concentration of 0.05 mM. With a longer reaction time of 60 min, the accumulation of  $[4\text{Fe-4S}]^{2+}$  clusters increases to 41% of the total Fe (Figure B.2C and Table B.2) which corresponds to a  $[4\text{Fe-4S}]^{2+}$  cluster concentration of 0.41 mM or 82% of the  $^{\text{Nif}}\text{IscA}$  present in a form containing one  $[4\text{Fe-4S}]^{2+}$  per homodimer, along with concomitant decrease in the  $[2\text{Fe-2S}]^{2+}$  cluster contribution to 3% of the total Fe (0.06 mM in  $[2\text{Fe-2S}]^{2+}$  clusters or 12% of the  $^{\text{Nif}}\text{IscA}$  present in a form containing one  $[2\text{Fe-2S}]^{2+}$  per homodimer). The concentration of  $[4\text{Fe-4S}]^{2+}$  clusters in the control sample without  $^{\text{Nif}}\text{IscA}$  remains approximately constant at 6% of the total Fe or 0.06 mM in exogenous cysteine-ligated  $[4\text{Fe-4S}]^{2+}$  clusters (Figure B.2F and Table B.2). Hence, 70% of the  $^{\text{Nif}}\text{IscA}$  was present in a form containing one  $[4\text{Fe-4S}]^{2+}$  per homodimer. In agreement with previous results (17), the Mössbauer and UV-visible absorption and CD data presented herein suggest that a form of  $^{\text{Nif}}\text{IscA}$  containing one  $[4\text{Fe-4S}]^{2+}$  cluster per homodimer is assembled via a species containing one  $[2\text{Fe-2S}]^{2+}$  cluster per homodimer under steady state conditions of NifS-mediated cluster assembly. The only major difference between the two sets of results is slower rates of  $[2\text{Fe-2S}]^{2+}$  cluster assembly in the present study which is attributed to lower PLP content and hence activity for the NifS samples used in this work. The present work also demonstrates that CD can be effectively used as a convenient, selective and quantitative monitor of the  $[2\text{Fe-2S}]^{2+}$  cluster-bound form of  $^{\text{Nif}}\text{IscA}$ .

The mechanism of NifS-mediated  $[4\text{Fe-4S}]^{2+}$  cluster assembly on  $^{\text{Nif}}\text{IscA}$  via a  $[2\text{Fe-2S}]^{2+}$  intermediate under reconstitution conditions has yet to be determined. However the ability of DTT to effect  $[2\text{Fe-2S}]^{2+}$  to  $[4\text{Fe-4S}]^{2+}$  cluster conversion on  $^{\text{Nif}}\text{IscA}$  in the absence of  $\text{O}_2$  suggests two-electron reductive coupling of two  $[2\text{Fe-2S}]^{2+}$  at the subunit interface of a homodimer (see below). This raises the question of the source of reducing equivalents during

NifS-mediated reconstitution in the absence of DTT. The most likely candidate is disulfide formation by the cysteines that are released during reductive coupling.

*Purification and characterization of [2Fe-2S]<sup>2+</sup> cluster-bound <sup>Nif</sup>IscA:* In accord with the results of Krebs *et al.* (17) attempts to purify homogeneous samples of the [4Fe-4S]<sup>2+</sup> cluster-bound form of <sup>Nif</sup>IscA from the NifS-mediated reconstitution mixture after 65 min of reaction were unsuccessful. Despite numerous attempts using anaerobic conditions (<1 ppm O<sub>2</sub> inside the glovebox) and low temperatures (10 °C), the [4Fe-4S]<sup>2+</sup> cluster-bound form of the <sup>Nif</sup>IscA was found to revert back partially or completely to the [2Fe-2S]<sup>2+</sup> cluster-bound form during purification using a Q-sepharose column in the absence of DTT. Based on the results discussed below, this is most likely a consequence of traces of O<sub>2</sub> in the buffer solutions that were degassed outside the glovebox and used to wash and elute <sup>Nif</sup>IscA from the column. However, many of the resultant [2Fe-2S]<sup>2+</sup> cluster-bound forms of <sup>Nif</sup>IscA, were more homogeneous than previously characterized samples (17) and hence more conducive to detailed analytical and spectroscopic characterization. The UV–visible absorption and CD spectra of anaerobically purified <sup>Nif</sup>IscA are shown in Figure B.3. The UV–visible spectrum of cluster-bound <sup>Nif</sup>IscA is dominated in the 300- to-600-nm region by bands centered at 331 and 425 nm with the latter having a shoulder at 463 nm and an unresolved broad band centered at 555 nm. These absorption bands correlate with UV–visible CD bands: positive bands centered at 348, 456, 522, and 630 nm and negative bands centered at 318, 395, and 566 nm. Both the UV–visible absorption and CD spectra are characteristic of a [2Fe-2S]<sup>2+</sup> cluster (32;33). Quantitative gel filtration chromatography revealed a molecular mass of 25 kDa for apo- and [2Fe-2S]-<sup>Nif</sup>IscA. Since the predicted molecular mass of *A<sub>v</sub>* <sup>Nif</sup>IscA is 11,047 Da, this suggests that both the apo- and [2Fe-2S]<sup>2+</sup> cluster-bound forms of <sup>Nif</sup>IscA are present as a dimers in solution. Fe and protein analytical data from six different

preparations indicated that the reconstituted samples contained  $0.79 \pm 0.10$  Fe per  ${}^{\text{Nif}}\text{IscA}$  monomer. Since Mössbauer data for these samples reveal that all the Fe in these sample is present as  $[\text{2Fe-2S}]^{2+}$  clusters (see below), the Fe and protein analytical data correspond to  $0.79 \pm 0.10$   $[\text{2Fe-2S}]^{2+}$  clusters per homodimeric  ${}^{\text{Nif}}\text{IscA}$ . Although we have yet been able to prepare samples with 1.0  $[\text{2Fe-2S}]^{2+}$  clusters per homodimeric  ${}^{\text{Nif}}\text{IscA}$ , taken together with the crystallographic data for *T. elongatus* IscA (18), the analytical data clearly supports a maximal stoichiometry of one  $[\text{2Fe-2S}]^{2+}$  cluster per homodimeric  ${}^{\text{Nif}}\text{IscA}$ . Since the UV–visible absorption spectra of these samples indicate a molar extinction coefficient at 425 nm ( $\epsilon_{425}$ ) of  $4.03 \pm 0.20$   $\text{mM}^{-1}\text{cm}^{-1}$  based on  ${}^{\text{Nif}}\text{IscA}$  monomer, see Figure B.3, the analytical data indicate  $\epsilon_{425} = 10.0 \pm 1.0$   $\text{mM}^{-1}\text{cm}^{-1}$  per  $[\text{2Fe-2S}]^{2+}$  cluster. This molar extinction coefficient was used to quantify the  $[\text{2Fe-2S}]^{2+}$  cluster content of all purified  $[\text{2Fe-2S}]^{2+}$  cluster-bound samples of  ${}^{\text{Nif}}\text{IscA}$  used in this work.

The vibrational properties of the Fe–S cluster in  ${}^{\text{Nif}}\text{IscA}$  were characterized by resonance Raman spectroscopy. The resonance Raman spectra of  $[\text{2Fe-2S}]^{2+}$  cluster-bound  ${}^{\text{Nif}}\text{IscA}$  in the Fe–S stretching region (240–450  $\text{cm}^{-1}$ ), obtained using 457.9, 487.9, and 514.5-nm excitation, comprises an intense band at 290  $\text{cm}^{-1}$  and additional bands at 338, 358, 396, and 421  $\text{cm}^{-1}$ ; see Figure B.4. The spectra are similar to those reported previously for the  $[\text{2Fe-2S}]^{2+}$  cluster-bound form of  ${}^{\text{Nif}}\text{IscA}$  using 457.9-nm excitation (17), albeit with greatly improved signal-to-noise ratio and the observation of additional weak bands. The spectra are relatively insensitive to excitation wavelength and the improved quality data enable vibrational assignments to be made by direct comparison with vibrationally well-characterized  $[\text{2Fe-2S}]^{2+}$  centers in simple ferredoxins such as *S. oleracea* ferredoxin, bovine adrenodoxin, and *P. putida* putidaredoxin (34), see Table B.3. The Fe–S stretching frequencies for the  $[\text{2Fe-2S}]^{2+}$  center in  ${}^{\text{Nif}}\text{IscA}$  are very similar to those of

the all-cysteine ligated  $[2\text{Fe-2S}]^{2+}$  centers in simple ferredoxins, strongly suggesting analogous cluster ligation in  $^{\text{Nif}}\text{IscA}$ . Further evidence for an all-cysteinylligated  $[2\text{Fe-2S}]^{2+}$  cluster in repurified reconstituted  $^{\text{Nif}}\text{IscA}$  and definitive assessment of the cluster composition were provided by Mössbauer spectroscopy; see Figure B.5A. The Mössbauer spectrum is well fit by the quadrupole doublet characteristic of an  $S = 0$   $[2\text{Fe-2S}]^{2+}$  cluster, composed of two antiferromagnetically coupled high-spin  $\text{Fe}^{3+}$  sites ( $\delta = 0.28$  mm/s and  $\Delta E_{\text{Q}} = 0.68$  mm/s for site 1 and  $\delta = 0.27$  mm/s and  $\Delta E_{\text{Q}} = 0.50$  mm/s for site 2). The similarity and value of the isomer shift parameter ( $\delta$ ) for each Fe site of the  $[2\text{Fe-2S}]^{2+}$  cluster are consistent with tetrahedral S ligation at each Fe site. Hence, in accord with the crystallographic data for  $[2\text{Fe-2S}]^{2+}$  cluster-bound *T. elongatus* IscA (18), the Mössbauer and resonance Raman results provide compelling evidence for complete cysteinyl ligation for the  $[2\text{Fe-2S}]^{2+}$  clusters on  $^{\text{Nif}}\text{IscA}$  in solution.

*DTT-induced  $[2\text{Fe-2S}]^{2+}$  to  $[4\text{Fe-4S}]^{2+}$  cluster conversion on  $^{\text{Nif}}\text{IscA}$ :* *In vitro* studies of SufA have reported that the  $[2\text{Fe-2S}]^{2+}$  cluster-bound form is competent for maturation of  $[4\text{Fe-4S}]$  cluster-containing proteins in the presence of DTT (35). In order to understand how the  $[2\text{Fe-2S}]^{2+}$  cluster-bound form of an A-type protein can effect maturation of  $[4\text{Fe-4S}]$  cluster-containing proteins and rationalize *in vivo* data which indicate a specific role for A-type proteins in the maturation of  $[4\text{Fe-4S}]$  cluster-containing proteins in mitochondria (26;36-38) and in bacteria under aerobic growth conditions (24), we have investigated the mechanism of  $[4\text{Fe-4S}]$  cluster assembly on *A. vinelandii*  $^{\text{Nif}}\text{IscA}$ . The UV-visible absorption and CD spectra of  $[2\text{Fe-2S}]^{2+}$  cluster-bound  $^{\text{Nif}}\text{IscA}$  (0.05 mM in  $[2\text{Fe-2S}]^{2+}$  clusters) before (solid red line) and 15 min after addition of 2 mM DTT under strictly anaerobic conditions (solid blue line) are shown in Figure B.6. On addition of DTT, the visible absorption spectrum of the  $[2\text{Fe-2S}]^{2+}$  cluster is bleached over a period of approximately 15 min to yield an absorption spectrum with a

pronounced shoulder at 400 nm that is characteristic of a  $[4\text{Fe-4S}]^{2+}$  cluster. Parallel CD studies indicate that 15 min after the addition of DTT, the amount of  $[2\text{Fe-2S}]^{2+}$  cluster-bound  $^{\text{Nif}}\text{IscA}$  has decreased to 16% of the original level and imply that any new cluster-bound forms generated have negligible CD, which is consistent with the formation of a  $[4\text{Fe-4S}]^{2+}$  cluster as demonstrated by the Mössbauer-monitored NifS-mediated reconstitution results discussed above.

More direct evidence for DTT-induced  $[2\text{Fe-2S}]^{2+}$  to  $[4\text{Fe-4S}]^{2+}$  cluster conversion on  $^{\text{Nif}}\text{IscA}$  and quantitation of the cluster conversion process were provided by parallel Mössbauer studies; see Figure B.5A–C and Tables B.1 and 4. The distinct isomer shift ( $\delta$ ) and quadrupole splitting ( $\Delta E_Q$ ) parameters of the  $^{\text{Nif}}\text{IscA}$ -bound  $[2\text{Fe-2S}]^{2+}$  and  $[4\text{Fe-4S}]^{2+}$  clusters enable Mössbauer spectroscopy to quantitatively monitor the cluster conversion. Mössbauer spectra of  $[2\text{Fe-2S}]^{2+}$  cluster-bound  $^{\text{Nif}}\text{IscA}$  (0.5 mM in  $[2\text{Fe-2S}]^{2+}$  clusters) were recorded before (A) and after incubation with 2 mM DTT for 1 min (B) and 15 min (C). The solid lines overlaid with the experimental spectra (hashed marks) are the composite simulations based on overlapping spectra from  $[2\text{Fe-2S}]^{2+}$  clusters (red),  $[4\text{Fe-4S}]^{2+}$  clusters (blue) and a mononuclear high-spin Fe(II) species (green), using the Mössbauer parameters listed in Table B.1 and percentage Fe contributions listed in Table B.4. Prior to addition of DTT, all the Fe in reconstituted and repurified  $^{\text{Nif}}\text{IscA}$  is in the form of  $[2\text{Fe-2S}]^{2+}$  clusters. However, the cluster composition changes dramatically on addition of 2 mM DTT. After 1 min, 43% of the Fe has been converted to  $[4\text{Fe-4S}]^{2+}$  clusters and 10% to a mononuclear ferrous species, with 34% remaining as  $[2\text{Fe-2S}]^{2+}$  clusters. After 15 min, 53% of the Fe has been converted to  $[4\text{Fe-4S}]^{2+}$  clusters and 18% to a mononuclear ferrous species, with only 16% remaining as  $[2\text{Fe-2S}]^{2+}$  clusters. The extent to which the  $[2\text{Fe-2S}]^{2+}$  clusters are lost as a function of time closely parallels the CD data discussed above. The mononuclear Fe(II) species in both the 1 and 15 min samples has

Mössbauer parameters very similar to those of Fe(II)-bound <sup>Nif</sup>IscA; see Appendix A. The remaining Fe in both samples (13%) is primarily present as a paramagnetic species with absorption spanning a range from -3.0 to +3.5 mm/s that is attributed to  $S = 1/2$   $[2\text{Fe-2S}]^+$  clusters, based on similarity to Mössbauer spectra of reduced  $[2\text{Fe-2S}]^+$  clusters in ferrochelatase (39) and ferredoxins (40) and parallel EPR data; see below. While the appearance of a mononuclear ferrous species indicates that the cluster conversion proceeds with up to 20% degradation of the initial  $[2\text{Fe-2S}]^{2+}$  clusters, it is clear that the majority of the  $[2\text{Fe-2S}]^{2+}$  clusters have been converted into  $[4\text{Fe-4S}]^{2+}$  clusters on incubation with DTT.

EPR spectroscopy was used to identify the paramagnetic species that contributes to the Mössbauer spectrum in the presence of DTT and thereby assess the mechanism of the cluster formation process. While the  $[2\text{Fe-2S}]^{2+}$  cluster-bound form of <sup>Nif</sup>IscA showed no EPR signals, samples frozen within 5 s of DTT addition showed a broad rhombic  $S = 1/2$  resonance with  $g = 2.01, 1.97, \text{ and } 1.92$  that accounted for 0.15 spins/ $[2\text{Fe-2S}]$  cluster; see Figure B.7. The signal persisted, albeit with reduced intensity corresponding to 0.10 spins/ $[2\text{Fe-2S}]$  cluster, for samples frozen 15 min after addition of DTT. The signal is assigned to a  $S = 1/2$   $[2\text{Fe-2S}]^+$  cluster rather than a  $S = 1/2$   $[4\text{Fe-4S}]^+$  cluster based on relaxation properties. The resonance readily undergoes power saturation at 4.2 K and is observable without significant broadening at 70 K. This indicates slow relaxation which is typical of  $S = 1/2$   $[2\text{Fe-2S}]^+$  clusters, whereas  $S = 1/2$   $[4\text{Fe-4S}]^+$  cluster are much faster relaxing and broaden significantly above 30 K. On the basis that (1) the paramagnetic species exhibits Mössbauer spectra with major features similar to those detected for  $S = 1/2$   $[2\text{Fe-2S}]^+$  centers, (2) EPR data show a paramagnetic species attributable to a  $S = 1/2$   $[2\text{Fe-2S}]^+$  cluster, and (3) the paramagnetic Mössbauer and EPR species both account for 10–15% of the initial  $[2\text{Fe-2S}]$  cluster concentration, we assign both to one-electron reduced

$S = 1/2 [2\text{Fe-2S}]^+$  clusters. The observation of a  $[2\text{Fe-2S}]^+$  cluster intermediate in the formation of  $[4\text{Fe-4S}]^{2+}$  clusters on  $^{\text{Nif}}\text{IscA}$  implies that the  $[4\text{Fe-4S}]^{2+}$  clusters are formed by reductive coupling of two  $[2\text{Fe-2S}]^{2+}$  clusters at the subunit interface.

On the basis of CD studies, no  $[2\text{Fe-2S}]^{2+}$ -to- $[4\text{Fe-4S}]^{2+}$  cluster conversion was observed on addition of 3 mM cysteine or glutathione (GSH) to  $[2\text{Fe-2S}]^{2+}$ - $^{\text{Nif}}\text{IscA}$  under anaerobic conditions. Hence it would appear that the lower redox potential of the dithiol/disulfide couple in DTT ( $-340$  mV at pH 7.4), compare to cysteine/cystine ( $-250$  mV at pH 7.4) or GSH/GSSG ( $-260$  mV at pH 7.4) (41), is required for reductive coupling to form  $[4\text{Fe-4S}]^{2+}$  clusters on  $^{\text{Nif}}\text{IscA}$ .

*O<sub>2</sub>-induced  $[4\text{Fe-4S}]^{2+}$  to  $[2\text{Fe-2S}]^{2+}$  cluster conversion on  $^{\text{Nif}}\text{IscA}$ :* Since A-type proteins have been implicated in having a role in the maturation of bacterial  $[4\text{Fe-4S}]$  cluster-containing proteins under aerobic growth conditions, Mössbauer and UV-visible absorption and CD spectroscopies were also used to assess the effect of O<sub>2</sub> exposure on the  $[4\text{Fe-4S}]^{2+}$  clusters generated by incubation of  $[2\text{Fe-2S}]^{2+}$  cluster-bound  $^{\text{Nif}}\text{IscA}$  with DTT. Hence the Mössbauer sample containing 53% of the Fe as  $[4\text{Fe-4S}]^{2+}$  clusters, that was generated by treating  $[2\text{Fe-2S}]^{2+}$  cluster-bound  $^{\text{Nif}}\text{IscA}$  with 2 mM DTT for 15 min, was thawed and exposed to air for 5 min before refreezing for Mössbauer analysis; see Figure B.5D. The Mössbauer data clearly demonstrate that O<sub>2</sub> reverses the DTT-induced  $[4\text{Fe-4S}]^{2+}$  to  $[2\text{Fe-2S}]^{2+}$  cluster conversion, as the resulting sample has 60% of the Fe in  $[2\text{Fe-2S}]^{2+}$  clusters and 15% in  $[4\text{Fe-4S}]^{2+}$  clusters, with the remaining 25% as unresolved broad ferric species; see Table B.4. In comparison with the 18% of mononuclear Fe(II) species detected in the DTT-treated starting sample, the observed 25% ferric species represents a minor loss of Fe during O<sub>2</sub> exposure. On the basis of the intensity of the characteristic  $g = 5.5$  resonance that was observed in parallel EPR samples, compared to

samples of Fe(III)-bound  $^{Nif}$ IscA of known concentration (see Appendix A), approximately 80% of the ferric species is present as  $S = 3/2$  Fe(III)-bound  $^{Nif}$ IscA. Hence the majority of Fe released remains  $^{Nif}$ IscA-bound in the  $O_2$ -exposed samples.

UV-visible absorption and CD spectroscopy provides a convenient method for monitoring  $^{Nif}$ IscA  $[4Fe-4S]^{2+} \leftrightarrow [2Fe-2S]^{2+}$  cluster interconversions in real time without repeated freeze-thaw cycles. Hence this approach was used to investigate the reversibility of this cluster transformation; see Figure B.6. As previously demonstrated, the predominantly  $[4Fe-4S]^{2+}$  cluster-containing form of  $^{Nif}$ IscA (blue line) was initially generated by incubating the as-purified  $[2Fe-2S]^{2+}$  cluster-containing form (red line) with DTT for 15 min under anaerobic conditions. The  $[4Fe-4S]^{2+}$  cluster-bound form of homodimeric  $^{Nif}$ IscA was then exposed to  $O_2$  by uncapping the cuvette in air at room temperature for 5 min before recapping and immediately recording spectra. The UV-visible absorption and CD spectra indicate that  $[4Fe-4S]^{2+}$  cluster undergoes oxidative cleavage to yield the original  $[2Fe-2S]^{2+}$  cluster-bound form of homodimeric  $^{Nif}$ IscA (broken red line) in 75% yield based on the initial  $[2Fe-2S]^{2+}$  cluster CD intensity prior to DTT reduction. However, this cluster conversion was found to be reversed, yielding primarily the  $[4Fe-4S]^{2+}$  cluster-bound form of homodimeric  $^{Nif}$ IscA, once the capped sample was incubated for 15 min without additional  $O_2$  exposure (broken blue line). Subsequent transient  $O_2$  exposure by removing the cap for 5 min again resulted in reversion to the original  $[2Fe-2S]^{2+}$  cluster-bound form (solid black line) in 65% yield based on initial  $[2Fe-2S]^{2+}$  cluster CD intensity prior to DTT reduction. Although the initial DTT-induced  $[2Fe-2S]^{2+}$  to  $[4Fe-4S]^{2+}$  occurs with breakdown of 20% of the  $[2Fe-2S]^{2+}$  clusters, as documented by Mössbauer studies, see Table B.4, it is remarkable that subsequent cycling between  $[4Fe-4S]^{2+}$  and  $[2Fe-2S]^{2+}$  cluster-bound forms of  $^{Nif}$ IscA occurs with only minor cluster loss as judged by absorption and

CD and can be repeated several more times until reduced DTT is fully depleted in the solution. The implication is that the cluster status of  $\text{Nif}^{\text{IscA}}$  is reversibly responsive to the  $\text{O}_2$  levels and the disulfide/dithiol status of the medium. The ability of  $\text{Nif}^{\text{IscA}}$  to reversibly cycle between  $[\text{4Fe-4S}]^{2+}$  and  $[\text{2Fe-2S}]^{2+}$  cluster-bound forms in a dithiol redox buffering medium without major cluster degradation in response to cellular  $\text{O}_2$  levels is likely to be directly relevant to the role of A-type proteins in the maturation of bacterial  $[\text{4Fe-4S}]$  cluster-containing proteins under aerobic or oxidative stress growth conditions.

*[4Fe-4S]<sup>2+</sup> cluster-bound Nif<sup>IscA</sup> is competent for in vitro maturation of nitrogenase Fe protein:* The ability to obtain forms of  $\text{Nif}^{\text{IscA}}$  containing exclusively  $[\text{2Fe-2S}]^{2+}$  clusters or predominantly  $[\text{4Fe-2S}]^{2+}$  clusters afforded the opportunity to investigate if either of these cluster-bound forms is competent as a cluster donor to apo nitrogenase Fe protein, a potential physiologically relevant  $[\text{4Fe-4S}]$  cluster-containing acceptor protein. CD spectroscopy involving ADP-bound nitrogenase Fe-protein was used to monitor the time-course of the reaction, since the  $[\text{4Fe-4S}]^{2+}$  cluster-bound form of ADP-bound nitrogenase Fe-protein has been shown to have an intense and characteristic visible CD spectrum (42), whereas the  $[\text{4Fe-4S}]^{2+}$  cluster-bound  $\text{Nif}^{\text{IscA}}$  does not have any significant CD intensity and  $[\text{2Fe-2S}]^{2+}$  cluster-bound  $\text{Nif}^{\text{IscA}}$  has an intense and distinctive CD spectrum (see above). The results of cluster transfer using  $[\text{4Fe-4S}]^{2+}$  cluster-containing  $\text{Nif}^{\text{IscA}}$ , generated in situ by treating  $[\text{2Fe-2S}]^{2+}$  cluster-containing  $\text{Nif}^{\text{IscA}}$  with DTT for 15 min, are shown in Figure B.8. The  $\text{Nif}^{\text{IscA}}$   $[\text{4Fe-4S}]^{2+}$  cluster concentration was assessed as approximately 26% of the initial  $[\text{2Fe-2S}]^{2+}$  concentration based on parallel Mössbauer studies (see Table B.4), and the reaction mixture was designed to have one  $\text{Nif}^{\text{IscA}}$   $[\text{4Fe-4S}]^{2+}$  cluster (12.5  $\mu\text{M}$ ) per dimeric apo nitrogenase Fe protein (12.5  $\mu\text{M}$ ). The CD spectrum of apo ADP-bound nitrogenase Fe-protein prior to addition of  $[\text{4Fe-4S}]^{2+}$  cluster-

containing  $^{Nif}IscA$  (corrected for the final concentration after addition of the  $^{Nif}IscA$  solution) constitutes the zero-time spectrum and CD spectra of the reaction mixture were recorded 4, 8, 15, 25, and 35 min after addition of  $[4Fe-4S]^{2+}$  cluster-containing  $^{Nif}IscA$ . At each time interval, the CD spectra of the residual  $[2Fe-2S]^{2+}$  clusters observed during DTT-induced formation of the  $[4Fe-4S]^{2+}$  clusters on  $^{Nif}IscA$  (see above) have been subtracted from the data shown. The resulting CD spectra are uniquely and quantitatively characteristic of holo ADP-bound nitrogenase Fe-protein (42) and indicate rapid cluster transfer that is 50% complete after 4 min and 90% complete after 35 min; see Figure B.8 (top panel). On the basis of the  $[4Fe-4S]^{2+}$  cluster content of  $^{Nif}IscA$ , the kinetics of  $[4Fe-4S]^{2+}$  cluster transfer as monitored by the CD intensity at 475 nm are well fit with a second order rate constant of  $20\,000\ M^{-1}\ min^{-1}$ , see Figure B.8 (bottom panel). After 50 min, the individual proteins were separated and repurified using a Q-Sepharose column and quantitative EPR analysis on the dithionite-reduced nitrogenase Fe-protein in the presence of 50% ethylene glycol (to ensure a  $S = 1/2$  ground state for the  $[4Fe-4S]^{2+}$  clusters (43) confirmed that at least 90% cluster reconstitution had been achieved (data not shown).

Parallel CD studies in which  $[4Fe-4S]^{2+}$  cluster-bound  $^{Nif}IscA$  was replaced in the cluster transfer mixture with equivalent amounts of  $S^{2-}$  and  $Fe^{2+}$  compared to cluster concentration did not result in any significant visible CD within 35 min (data not shown). This control experiment demonstrates that the  $[4Fe-4S]^{2+}$  clusters on  $^{Nif}IscA$  are transferred intact to apo ADP-bound nitrogenase Fe-protein, rather than being degraded and then reassembled on apo ADP-bound nitrogenase Fe-protein. In addition, the reaction was repeated under identical conditions with  $[2Fe-2S]^{2+}$  cluster-bound  $^{Nif}IscA$  (25  $\mu M$  in  $[2Fe-2S]^{2+}$  clusters in final reaction mixture) with no DTT in the reaction mixture. The CD spectra of  $[2Fe-2S]^{2+}$  cluster-bound  $^{Nif}IscA$  was observed

and remained unchanged in intensity for at least 40 min indicating that the  $[2\text{Fe-2S}]^{2+}$  cluster-bound  $\text{Nif}^{\text{IscA}}$  is not competent for maturation of apo nitrogenase Fe proteins. Taken together these results clearly demonstrate that only the  $[4\text{Fe-4S}]^{2+}$  cluster-bound form of  $\text{Nif}^{\text{IscA}}$  is competent for maturation of nitrogenase Fe protein under anaerobic conditions and that the maturation process occurs via intact  $[4\text{Fe-4S}]^{2+}$  cluster transfer. Moreover, the rate of  $[4\text{Fe-4S}]^{2+}$  cluster transfer from  $\text{Nif}^{\text{IscA}}$  to apo nitrogenase Fe protein is similar to that previously reported for  $[4\text{Fe-4S}]^{2+}$  cluster transfer from NifU to apo nitrogenase Fe protein (28), indicating that  $\text{Nif}^{\text{IscA}}$  offers a viable alternative to NifU for the maturation of  $[4\text{Fe-4S}]$  cluster containing nitrogen fixation proteins.

*In vitro cluster transfer from NifU to apo- $\text{Nif}^{\text{IscA}}$ :* To address the possibility that  $\text{Nif}^{\text{IscA}}$  serves as a cluster carrier protein that accepts preformed clusters from NifU and delivers them to acceptor proteins, we have investigated cluster transfer from *A. vinelandii* NifU to  $\text{Nif}^{\text{IscA}}$ . NifU is a homodimeric modular protein comprising a U-type N-terminal domain, a ferredoxin-type central domain with a redox-active permanent  $[2\text{Fe-2S}]^{2+,+}$  cluster, and a Nfu-type C-terminal domain (30;44). Both the N- and C-terminal domains of NifU have been shown to assemble  $[4\text{Fe-4S}]^{2+}$  clusters, which can be transferred intact to apo acceptor proteins such as apo-nitrogenase Fe protein (29;30), and NifS-mediated cluster assembly and purification results in a stable form containing one transient  $[4\text{Fe-4S}]^{2+}$  cluster and one permanent  $[2\text{Fe-2S}]^{2+}$  cluster per NifU monomer (30).

In this study, UV-visible absorption and CD spectroscopies were used to monitor the effect of adding a small excess of apo- $\text{Nif}^{\text{IscA}}$  to a  $[4\text{Fe-4S}]^{2+}$  cluster-loaded form of NifU containing one transient  $[4\text{Fe-4S}]^{2+}$  cluster and one permanent  $[2\text{Fe-2S}]^{2+}$  cluster per NifU monomer under strictly anaerobic conditions; see Figure B.9. The reaction mixture was 35  $\mu\text{M}$  in

NifU monomer, *i.e.* 35  $\mu\text{M}$  in  $[\text{4Fe-4S}]^{2+}$  and permanent  $[\text{2Fe-2S}]^{2+}$  clusters, and 100  $\mu\text{M}$  in apo- $^{\text{Nif}}$ IscA dimer. The  $[\text{4Fe-4S}]^{2+}$  cluster content of the NifU sample was based on Fe and protein determinations and is also evident by the difference in the absorption spectra of as purified NifU containing one permanent  $[\text{2Fe-2S}]^{2+}$  cluster (blue line) and the reconstituted and repurified NifU sample used for the cluster transfer studies (red line); see Figure B.9. The reaction was carried out in the absence of DTT, but apo- $^{\text{Nif}}$ IscA was treated with TCEP and anaerobically repurified prior to use to ensure reduction of disulfides.

Both the absorption and CD data shown marked changes on addition of apo- $^{\text{Nif}}$ IscA and indicate a rapid reaction that is completed in less than 5 min, as identical spectra were observed for 5, 10, 20, 30, and 50 min after addition of apo- $^{\text{Nif}}$ IscA (black lines); see Figure B.9, upper and middle panels. The absorption intensity increases and shows better resolved features at 330, 420, 460, and 550 nm. Both observations are consistent with  $[\text{4Fe-4S}]^{2+} \rightarrow 2 \times [\text{2Fe-2S}]^{2+}$  cluster conversion, since  $\epsilon_{400} = 15 \text{ mM}^{-1} \text{ cm}^{-1}$  for the  $[\text{4Fe-4S}]^{2+}$  cluster on NifU (30) and  $\epsilon_{425} = 10 \text{ mM}^{-1} \text{ cm}^{-1}$  for the  $[\text{2Fe-2S}]^{2+}$  cluster on  $^{\text{Nif}}$ IscA (see above). Moreover, the resultant absorption spectrum is quantitatively simulated within experimental error as the sum of one permanent  $[\text{2Fe-2S}]^{2+}$  cluster on NifU and two  $[\text{2Fe-2S}]^{2+}$  clusters on  $^{\text{Nif}}$ IscA. Confirmation of this interpretation is provided by the parallel CD spectra. Prior to the addition of  $^{\text{Nif}}$ IscA, the CD spectrum of the  $[\text{4Fe-4S}]^{2+}$  cluster-loaded NifU (red line) is almost indistinguishable from that of NifU prior to NifS-mediated cluster assembly and replete with permanent  $[\text{2Fe-2S}]^{2+}$  clusters (blue line), see Figure B.9, indicating that the assembled  $[\text{4Fe-4S}]^{2+}$  cluster on NifU has negligible CD intensity. Hence the CD spectrum of the  $[\text{2Fe-2S}]^{2+}$  clusters generated by addition of apo- $^{\text{Nif}}$ IscA can be assessed by the 50-min minus zero-time difference spectrum. The resulting spectrum is very similar to that of the  $[\text{2Fe-2S}]^{2+}$  cluster assembled on  $^{\text{Nif}}$ IscA (see Figure B.3)

and the  $\Delta\epsilon$  values are approximately double those of a single  ${}^{\text{Nif}}\text{IscA}$   $[\text{2Fe-2S}]^{2+}$  cluster, indicating that two  $[\text{2Fe-2S}]^{2+}$  clusters are formed on  ${}^{\text{Nif}}\text{IscA}$  from the single  $[\text{4Fe-4S}]^{2+}$  cluster on NifU. The difference CD spectrum is also quite distinct from that of  $[\text{2Fe-2S}]^{2+}$  centers on U-type scaffold proteins including the N-terminal domain of NifU (30;44-46), indicating that the clusters are on  ${}^{\text{Nif}}\text{IscA}$  rather than NifU. Moreover, anaerobic repurification of  ${}^{\text{Nif}}\text{IscA}$  from the reaction mixture, yielded a sample the with characteristic absorption and CD spectra of  $[\text{2Fe-2S}]^{2+}$  cluster-bound  ${}^{\text{Nif}}\text{IscA}$ .

The observation that cluster transfer involving the  $[\text{4Fe-4S}]^{2+}$  cluster assembled on NifU yielded the  $[\text{2Fe-2S}]^{2+}$  cluster-bound form of  ${}^{\text{Nif}}\text{IscA}$  was not unexpected as the reaction was carried out in the absence of DTT, which appears to be required for stabilizing the  $[\text{4Fe-4S}]^{2+}$  cluster-bound form. Nevertheless, it leaves open the question of whether oxidative cleavage of the  $[\text{4Fe-4S}]^{2+}$  cluster to yield two  $[\text{2Fe-2S}]^{2+}$  cluster occurs on NifU prior to cluster transfer or on  ${}^{\text{Nif}}\text{IscA}$  after  $[\text{4Fe-4S}]^{2+}$  cluster transfer. We suspect the latter in light of the observation of facile interconversion between  $[\text{4Fe-4S}]^{2+}$  and  $[\text{2Fe-2S}]^{2+}$  cluster-bound forms of  ${}^{\text{Nif}}\text{IscA}$ , with  $[\text{2Fe-2S}]^{2+}$ - ${}^{\text{Nif}}\text{IscA}$  formation being favored by the absence of DTT and the presence of excess apo- ${}^{\text{Nif}}\text{IscA}$  (see below), and control UV-visible absorption and CD experiments that showed no evidence of  $[\text{4Fe-4S}]^{2+}$  to  $[\text{2Fe-2S}]^{2+}$  cluster conversion on NifU under identical reaction conditions in the absence of  ${}^{\text{Nif}}\text{IscA}$ . Attempts to address this question directly via CD-monitored cluster transfer reactions in the presence of 2 mM DTT proved to be problematic due to the ability of DTT to partially reduce the permanent  $[\text{2Fe-2S}]^{2+}$  cluster on NifU ( $E_m = -254$  mV) (43).

## Discussion

A-type proteins are present in the bacterial *isc*, *suf*, and *nif* systems as well as the mitochondrial and plastid systems for Fe–S cluster biogenesis, but there is still no consensus concerning their role in the complex process of Fe–S protein maturation. Four different roles have been proposed: alternative scaffolds for assembly of transient Fe–S clusters under aerobic or oxidative stress conditions (17;18;47;48), cluster carriers for the delivery of clusters assembled on U-type and SufB primary scaffold proteins to apo acceptor proteins (23;35;48), metallochaperones for the delivery of Fe to U-type primary scaffold proteins (16;49-51) or to acceptor proteins to facilitate *in situ* assembly of [4Fe-4S] clusters as indicated in yeast (26). The accompanying manuscript addresses the role of mononuclear Fe-bound forms of <sup>Nif</sup>IscA. The results support the view that <sup>Nif</sup>IscA can store mononuclear Fe that can be used in Fe–S cluster assembly. However, they do not support a specific role as an immediate iron donor for transient Fe–S cluster assembly on NifU. Rather a role for Fe-bound in <sup>Nif</sup>IscA the *in situ* assembly or repair of [4Fe-4S] clusters on acceptors is proposed.

The initial observation of cysteine desulfurase-mediated assembly of subunit-bridging [2Fe-2S] and [4Fe-4S] clusters on A-type Fe–S cluster biogenesis proteins (17;47), that can subsequently be transferred to suitable acceptor proteins (47;48;52-54), led to the hypothesis that A-type proteins provide alternative scaffold proteins for assembly of certain types of clusters under specific cellular conditions. This hypothesis is supported by the observation that some recombinant A-type Fe–S cluster biogenesis proteins, including the structurally characterized *T. elongatus* IscA, contain [2Fe-2S] or [4Fe-4S] clusters as isolated (18;35;55), bacterial gene disruption studies which indicated that IscA/SufA are generally only required for the maturation of [4Fe-4S] cluster-containing proteins under aerobic growth conditions (24), and yeast and

human gene disruption studies which implicate an important role for Isa1 and Isa2 in the maturation of mitochondrial [4Fe-4S] clusters (26;36-38;56-58). The alternative scaffold role cannot be completely discounted in bacteria and is supported by the NifS-mediated assembly of [4Fe-4S]<sup>2+</sup> clusters on <sup>Nif</sup>IscA via [2Fe-2S]<sup>2+</sup> cluster intermediates that is presented in this work. Nevertheless, in contrast to U-type primary scaffold proteins (59;60), the lack of evidence for a well-defined cysteine desulfurase/A-type protein complex argues against a role as an alternative primary scaffold for de novo Fe–S cluster biosynthesis.

Moreover, the above observations are also consistent with an alternative hypothesis, namely that A-type Fe–S cluster biogenesis proteins function as cluster carriers for the delivery of clusters assembled on U-type or SufB-type primary scaffold proteins. The cluster carrier hypothesis is supported by in vitro studies which indicate that IscA can accept Fe–S clusters from IscU (48) and that SufA can accept Fe–S clusters from the SufBCD complex (61), and recent phylogenomic and genetic studies of the interdependence of the three types A-type Fe–S cluster biogenesis proteins in *E. coli*, i.e., IscA, SufA, and ErpA (8;23). IscA and SufA appear to be functionally redundant in *E. coli* (22-24), whereas ErpA is essential for the maturation of the [4Fe-4S] clusters on the IspG and IspH enzymes of the mevalonate-dependent bacterial pathway for the biosynthesis of isopentenyl diphosphate (19). However, one of the most puzzling aspects of the cluster carrier hypothesis, with respect to the specific role of bacterial A-type proteins in the maturation of [4Fe-4S] cluster-containing proteins under aerobic or oxidative stress conditions, is that cluster transfer from [4Fe-4S] cluster-bound SufBCD results in [2Fe-2S] cluster-bound SufA (61) which itself is competent for the maturation of [4Fe-4S] cluster-containing proteins in the presence of DTT (35).

In this work similar behavior was observed for  $^{Nif}IscA$  with a  $[2Fe-2S]^{2+}$  cluster-bound form being the product of cluster transfer from  $[4Fe-4S]$  cluster-loaded NifU under anaerobic conditions with excess apo- $^{Nif}IscA$  in the absence of DTT. In addition, the  $[2Fe-2S]$  cluster-bound  $^{Nif}IscA$  was found to be competent for maturation of the  $[4Fe-4S]$  center in the apo nitrogenase Fe protein under anaerobic conditions in the presence of DTT. These results have now been reconciled by the discovery of a reversible equilibrium between forms of  $^{Nif}IscA$  containing one  $[2Fe-2S]^{2+}$  and one  $[4Fe-4S]^{2+}$  cluster per homodimer, with excess DTT being required to generate and stabilize the  $[4Fe-4S]^{2+}$  cluster-bound form under anaerobic conditions and  $O_2$  and/or excess apo- $^{Nif}IscA$  in the absence of DTT resulting in the  $[2Fe-2S]^{2+}$  cluster-bound form.

On the basis of the available crystallographic data for the  $[2Fe-2S]$  cluster-bound form of *T. elongatus* IscA (18), the observation of a  $[2Fe-2S]^+$  intermediate in the reductive formation of the  $[4Fe-4S]^{2+}$  cluster-bound form, and the apparent requirement of excess apo- $^{Nif}IscA$  for the oxidative  $[4Fe-4S]^{2+}$  to  $[2Fe-2S]^{2+}$  cluster conversion, a tentative mechanism for this cluster interconversion is presented in Figure B.10. The crystal structure suggests an asymmetric dimer structure in solution involving a partially exposed  $[2Fe-2S]^{2+}$  cluster that is asymmetrically coordinated with the conserved cysteines on the  $\alpha$  protomer (Cys37, Cys101, and Cys103) and the solvent exposed Cys103 from the  $\beta$  protomer. DTT is proposed to effect reduction of subunit-bridging  $[2Fe-2S]^{2+}$  cluster to yield a  $S = 1/2$  valence-localized  $[2Fe-2S]^+$  cluster. This results in weakening of the interaction of the coordinated cysteine of the  $\beta$  protomer leading to dimer dissociation and the transient formation of monomers containing solvent exposed  $[2Fe-2S]^+$  clusters that can interact to form valence-delocalized  $[4Fe-4S]^{2+}$  clusters at the interface of a new

<sup>Nif</sup>IscA dimer. Oxygen or possibly disulfides can then reverse this process via two electron oxidation of the [4Fe-4S]<sup>2+</sup> cluster in the presence of apo-<sup>Nif</sup>IscA; see Figure B.10.

The nature of the physiological electron donor for formation of [4Fe-4S]<sup>2+</sup>-<sup>Nif</sup>IscA via reductive coupling of [2Fe-2S]<sup>2+</sup> clusters has yet to be addressed. However, the inability of cysteine or GSH to promote reductive coupling suggests that it will not occur in the cellular dithiol/disulfide redox buffering medium under aerobic growth conditions (i.e., redox potentials in the range -220 to -270 mV). Consequently the formation of [4Fe-4S]<sup>2+</sup>-<sup>Nif</sup>IscA is likely to require anaerobic conditions and a lower potential reductant such as *A. vinelandii* Isc Fdx ( $E_m = -344$  mV) (62). Indeed, in *E. coli* there is direct evidence for a complex between predominantly [2Fe-2S]<sup>2+</sup> cluster-bound IscA and Isc Fdx (47). Future experiments are planned to address this hypothesis and the ability of one-electron as well as two-electron donors to induce reductive coupling.

A similar reductive coupling mechanism has been demonstrated for [4Fe-4S]<sup>2+</sup> cluster formation on U-type scaffold proteins (11;31;63). Moreover, reductive coupling of two [2Fe-2S]<sup>2+</sup> cluster on a U-type scaffold to form a [4Fe-4S]<sup>2+</sup> cluster requires similar potentials based on the ability of Isc Fdx to effect partial reduction (64). However there are significant differences. For example, reductive coupling on U-type scaffold proteins requires formation of a form containing two [2Fe-2S]<sup>2+</sup> clusters per homodimer and is not reversible as oxygen exposure degrades the subunit-bridging [4Fe-4S]<sup>2+</sup> cluster to a more stable form containing one [2Fe-2S]<sup>2+</sup> cluster per homodimer (11;63). Hence the ability of A-type proteins to form [4Fe-4S]<sup>2+</sup> clusters in a dithiol/disulfide redox buffering medium under anaerobic conditions and to reversibly interconvert between [2Fe-2S]<sup>2+</sup> and [4Fe-4S]<sup>2+</sup> cluster-bound forms in response to cellular

redox status and/or oxygen levels, provide rationalization for their utility in the maturation of [4Fe-4S] cluster-containing proteins under aerobic growth or oxidative stress conditions (24).

The implication of the results presented herein for *A. vinelandii*<sup>Nif</sup>IscA is that [4Fe-4S] cluster-bound forms are formed, and are competent for maturation of [4Fe-4S] cluster-containing nitrogen fixation apo-proteins via direct cluster transfer, only under anaerobic conditions. *A. vinelandii* is an obligate aerobe that has evolved a number of physiological mechanisms to create an essentially anoxic environment in which nitrogen fixation can occur (64). These include high rates of respiration and the synthesis of a specific protective [2Fe-2S]-Fdx that binds to nitrogenase under oxygen stress conditions to form an inactive enzyme that is protected from damage (64;65). Since NifU is the primary scaffold for [4Fe-4S] cluster assembly (29;30) and is essential for diazotrophic growth (20), whereas<sup>Nif</sup>IscA has no observable phenotype (20), it would appear that only NifU is responsible for providing [4Fe-4S] clusters for the maturation of the nitrogenase component proteins NifHDK as well as Fe-S cluster-containing maturation proteins such as the NifEN scaffold and the NifB radical-SAM enzyme. However, in light of the functional redundancy of A-type proteins in *E. coli* and the lack of information on the consequences of a double<sup>Nif</sup>IscA/IscA knockout in *A. vinelandii*, this conclusion may be premature. Hence it is still possible that [4Fe-4S] cluster-bound forms of<sup>Nif</sup>IscA or IscA may be immediate [4Fe-4S] cluster donors for a subset of nitrogen fixation proteins under anaerobic conditions.

Nevertheless, *in vivo* results in *A. vinelandii* indicate a role for IscA only under oxygen stress conditions (21) and *in vivo* studies in *E. coli* indicate partially redundant roles for the IscA, SufA, and ErpA proteins in the maturation of [4Fe-4S] clusters under aerobic conditions (8;23;24). Under such conditions [2Fe-2S]<sup>2+</sup> cluster-bound forms of A-type proteins are likely to

be present as a result of cluster transfer from the NifU (this work), IscU (48) or SufB (35) proteins. Hence the question that needs to be addressed is how  $[2\text{Fe-2S}]^{2+}$  cluster-bound forms of A-type proteins can be involved in the maturation of  $[4\text{Fe-4S}]$  cluster containing proteins under aerobic or oxygen stress conditions. Interestingly, a similar role was proposed for the mononuclear Fe-bound form of A-type proteins in the preceding manuscript and is supported by the in vivo evidence that the Fe-bound form the Isa1/Isa2 is required for the maturation of mitochondrial  $[4\text{Fe-4S}]$  clusters in *S. cerevisiae* under aerobic and anaerobic conditions (26). On the basis of the results presented in the accompanying manuscript, it seems likely that the  $[2\text{Fe-2S}]$  cluster-bound and Fe(III)-bound forms of A-type proteins may coexist in vivo under aerobic conditions in bacteria (25;35). This is further supported by the observation that some Fe(III)-bound  $^{\text{Nif}}$ IscA is formed during the  $\text{O}_2$ -induced  $[4\text{Fe-4S}]$  to  $[2\text{Fe-2S}]$  cluster conversion. Hence this raises the possibility that both the Fe-bound and  $[2\text{Fe-2S}]$  cluster-bound forms of A-type proteins are involved in the maturation of  $[4\text{Fe-4S}]$  centers on bacterial proteins under aerobic or oxygen stress conditions.

A viable mechanism of how this could occur, based on our recent studies of the mechanism of  $[2\text{Fe-2S}]^{2+} \leftrightarrow [4\text{Fe-4S}]^{2+}$  interconversion on the fumarate nitrate reduction (FNR) regulatory protein (see Chapter 5), is presented in detail in the accompanying manuscript. The mechanism is based on the observation that the Fe-S cluster in FNR reversibly cycles between an all-cysteinyly ligated  $[4\text{Fe-4S}]^{2+}$  cluster and a  $[2\text{Fe-2S}]^{2+}$  cluster with two regular cysteinyly ligands and two cysteine persulfide ligands, with  $\text{O}_2$  inducing the  $[4\text{Fe-4S}]^{2+}$ -to- $[2\text{Fe-2S}]^{2+}$  conversion and Fe(II) and DTT inducing the  $[2\text{Fe-2S}]^{2+}$ -to- $[4\text{Fe-4S}]^{2+}$  conversion. This raises an alternative possibility for in situ  $[4\text{Fe-4S}]^{2+}$  cluster assembly on acceptor proteins involving assembly of a cysteine persulfide-ligated  $[2\text{Fe-2S}]^{2+}$  cluster on the acceptor protein, via cysteine

desulfurase formation of two cysteine persulfides and delivery of  $[2\text{Fe-2S}]^{2+}$  clusters by A-type proteins. Fe-bound A-type proteins would then function in the assembly or repair of  $\text{O}_2$ -damaged  $[4\text{Fe-4S}]^{2+}$  clusters by functioning as the Fe(II) delivery system for transforming the cysteine persulfide-ligated  $[2\text{Fe-2S}]^{2+}$  cluster into a conventional  $[4\text{Fe-4S}]^{2+}$  center.

### **Acknowledgement**

We thank Dr. Dennis Dean and his co-workers at Virginia Tech for supplying the plasmids for the proteins used in this work.

## References

1. Kiley, P. J. and Beinert, H. (2003) The role of Fe-S proteins in sensing and regulation in bacteria, *Curr. Opin. Microbiol.* 6, 181-185.
2. Fontecave, M. (2006) Iron-sulfur clusters: ever expanding roles, *Nature Chem. Biol.* 2, 171-174.
3. Lill, R. (2009) Function and biogenesis of iron-sulphur proteins, *Nature* 460, 831-838.
4. Johnson, M. K. and Smith, A. D. Iron-sulfur proteins. In *Encyclopedia of Inorganic Chemistry, Second Edition*; King, R. B.; John Wiley & Sons; 2005; 2589-2619.
5. Johnson, D. C., Dean, D. R., Smith, A. D., and Johnson, M. K. (2005) Structure, function and formation of biological iron-sulfur clusters, *Annu. Rev. Biochem.* 74, 247-281.
6. Lill, R. and Mühlenhoff, U. (2006) Iron-sulfur protein biogenesis in eukaryotes: Components and mechanisms, *Annu. Rev. Cell Dev. Biol.* 22, 457-486.
7. Ayala-Castro, C., Saini, A., and Outten, F. W. (2008) Fe-S cluster assembly pathways in bacteria, *Microbiol. Mol. Biol. Rev.* 72, 110-125.
8. Py, B. and Barras, F. (2010) Building Fe-S proteins: bacterial strategies, *Nat. Rev. Microbiol.* 8, 436-446.
9. Balk, J. and Pilon, M. (2011) Ancient and essential: The assembly of iron-sulfur clusters in plants, *Trends Plant Sci.* 16, 218-226.
10. Fontecave, M. and Ollagnier-de-Choudens, S. (2008) Iron-sulfur cluster biosynthesis in bacteria: Mechanisms of cluster assembly and transfer, *Arch. Biochem. Biophys.* 474, 226-237.
11. Bandyopadhyay, S., Chandramouli, K., and Johnson, M. K. (2008) Iron-sulfur cluster biosynthesis, *Biochem. Soc. Trans.* 36, 1112-1119.
12. Takahashi, Y. and Nakamura, M. (1999) Functional assignment of the ORF2-*iscS-iscA-hscB-hscA-fdx*-ORF3 gene cluster involved in the assembly of Fe-S clusters in *Escherichia coli*, *J. Biochem.* 126, 917-926.
13. Takahashi, Y. and Tokumoto, U. (2002) A third bacterial system for the assembly of iron-sulfur clusters with homologs in archaea and plastids, *J. Biol. Chem.* 277, 28380-28383.
14. Outten, F. W., Djaman, O., and Storz, G. (2004) A *suf* operon requirement for Fe-S cluster assembly during iron starvation in *Escherichia coli*, *Mol. Microbiol.* 52, 861-872.
15. Fontecave, M., Ollagnier-de-Choudens, S., Py, B., and Barras, F. (2005) Mechanisms of iron-sulfur cluster assembly: the SUF machinery, *J. Biol. Inorg. Chem.* 10, 713-721.

16. Ding, H. and Clark, R. J. (2004) Characterization of iron-binding in IscA, an ancient iron-sulfur cluster assembly protein, *Biochem. J.* 379, 433-440.
17. Krebs, C., Agar, J. N., Smith, A. D., Frazzon, J., Dean, D. R., Huynh, B. H., and Johnson, M. K. (2001) IscA, an alternative scaffold for Fe-S cluster biosynthesis, *Biochemistry* 40, 14069-14080.
18. Morimoto, K., Yamashita, E., Kondou, Y., Lee, S. J., Arisaka, F., Tsukihara, T., and Nakai, M. (2006) The asymmetric IscA homodimer with an exposed [2Fe-2S] cluster suggests the structural basis of the Fe-S cluster biosynthetic scaffold, *J. Mol. Biol.* 360, 117-132.
19. Loiseau, L., Gerez, C., Bekker, M., Ollagnier-de-Choudens, S., Py, B., Sanakis, Y., Teixeira, M., Fontecave, M., and Barras, F. (2007) ErpA, an iron-sulfur (Fe-S) protein of the A-type essential for respiratory metabolism in *Escherichia coli*, *Proc. Natl. Acad. Sci. U. S. A.* 104, 13626-13631.
20. Jacobson, M. R., Cash, V. L., Weiss, M. C., Laird, N. F., Newton, W. E., and Dean, D. R. (1989) Biochemical and genetic analysis of the *nifUSVWZM* cluster from *Azotobacter vinelandii*, *Mol. Gen. Genet.* 219, 49-57.
21. Johnson, D. C., Unciuleac, M.-C., and Dean, D. R. (2006) Controlled expression and functional analysis of iron-sulfur cluster biosynthetic components within *Azotobacter vinelandii*, *J. Bacteriol.* 188, 7551-7561.
22. Lu, J., Yang, J., Tan, G., and Ding, H. (2008) Complementary roles of SufA and IscA in the biogenesis of iron-sulfur clusters in *Escherichia coli*, *Biochem. J.* 409, 535-543.
23. Vinella, D., Brochier-Armanet, C., Loiseau, L., Talla, E., and Barras, F. (2009) Iron-sulfur (Fe/S) protein biogenesis: phylogenomic and genetic studies of A-type carriers, *PLoS. Genet.* 5, e1000497-
24. Tan, G., Lu, J., Bitoun, J. P., Huang, H., and Ding, H. (2009) IscA/SufA paralogues are required for the [4Fe-4S] cluster assembly in enzymes of multiple physiological pathways in *Escherichia coli* under aerobic growth conditions, *Biochem. J.* 420, 463-472.
25. Wang, W., Huang, H., Tan, G., Fan, S., Liu, M., Landry, A. P., and Ding, H. (2010) *In vivo* evidence for the iron-binding activity of an iron-sulfur cluster assembly protein IscA in *Escherichia coli*, *Biochem. J.* 432, 429-436.
26. Mühlenhoff, U., Richter, N., Pines, O., Pierik, A. J., and Lill, R. (2011) Specialized function of yeast Isa1 and Isa2 in the maturation of mitochondrial [4Fe-4S] proteins, *J. Biol. Chem.* 286, 41205-41216.
27. Drozdowski, P. M. and Johnson, M. K. (1988) A simple anaerobic cell for low temperature Raman spectroscopy, *Appl. Spectrosc.* 42, 1575-1577.
28. Ravi, N., Bollinger, J. M., Huynh, B. H., Edmondson, D. E., and Stubbe, J. (1994) Mechanism of assembly of the tyrosyl radical-diiron(III) cofactor of *E. coli* ribonucleotide

- reductase. 1. Mössbauer characterization of the diferric radical precursor, *J. Am. Chem. Soc.* 116, 8007-8014.
29. Dos Santos, P. C., Smith, A. D., Frazzon, J., Cash, V. L., Johnson, M. K., and Dean, D. R. (2004) Iron-sulfur cluster assembly: NifU-directed activation of the nitrogenase Fe-protein, *J. Biol. Chem.* 279, 19705-19711.
  30. Smith, A. D., Jameson, G. N. L., Dos Santos, P. C., Agar, J. N., Naik, S., Krebs, C., Frazzon, J., Dean, D. R., Huynh, B. H., and Johnson, M. K. (2005) NifS-mediated assembly of [4Fe-4S] clusters in the N- and C-terminal domains of the NifU scaffold protein, *Biochemistry* 44, 12955-12969.
  31. Agar, J. N., Krebs, B., Frazzon, J., Huynh, B. H., Dean, D. R., and Johnson, M. K. (2000) IscU as a scaffold for iron-sulfur cluster biosynthesis: Sequential assembly of [2Fe-2S] and [4Fe-4S] clusters in IscU, *Biochemistry* 39, 7856-7862.
  32. Dailey, H. A., Finnegan, M. G., and Johnson, M. K. (1994) Human ferrochelatase is an iron-sulfur protein, *Biochemistry* 33, 403-407.
  33. Stephens, P. J., Thomson, A. J., Dunn, J. B. R., Keiderling, T. A., Rawlings, J., Rao, K. K., and Hall, D. O. (1978) Circular dichroism and magnetic circular dichroism of iron-sulfur proteins, *Biochemistry* 17, 4770-4778.
  34. Fu, W., Drozdowski, P. M., Davies, M. D., Sligar, S. G., and Johnson, M. K. (1992) Resonance Raman and magnetic circular dichroism studies of reduced [2Fe-2S] proteins, *J. Biol. Chem.* 267, 15502-15510.
  35. Gupta, V., Sendra, M., Naik, S. G., Chahal, H. K., Huynh, B. H., Outten, F. W., Fontecave, M., and Ollagnier de Choudens, S. (2009) Native *Escherichia coli* SufA, coexpressed with SufBCDSE, purifies as a [2Fe-2S] protein and acts as an Fe-S transporter to Fe-S target enzymes, *J. Am. Chem. Soc.* 131, 6149-6153.
  36. Mühlenhoff, U., Gerl, M. J., Flauger, B., Pirner, H. M., Balsler, S., Richhardt, N., Lill, R., and Stolz, J. (2007) The iron-sulfur cluster proteins Isa1 and Isa2 are required for the function but not the de novo synthesis of the Fe/S clusters of biotin synthase in *Saccharomyces cerevisiae*, *Eukaryot. Cell* 6, 495-504.
  37. Gelling, C., Dawes, I. W., Richhardt, N., Lill, R., and Mühlenhoff, U. (2008) Mitochondrial Iba57p is required for Fe/S cluster formation on aconitase and activation of radical SAM enzymes, *Mol. Cell. Biol.* 28, 1851-1861.
  38. Sheftel, A. D., Wilbrecht, C., Stehling, O., Niggemeyer, B., Elsasser, H. P., Mühlenhoff, U., and Lill, R. (2012) The human mitochondrial ISCA1, ISCA2, and IBA57 proteins are required for [4Fe-4S] protein maturation, *Mol. Biol. Cell* 23, 1157-1166.
  39. Ferreira, G. C., Franco, R., Lloyd, R. S., Pereira, A. S., Moura, I., Moura, J. J. G., and Huynh, B. H. (1994) Mammalian ferrochelatase, a new addition to the metalloenzyme family, *J. Biol. Chem.* 269, 7062-7065.

40. Dunham, W. R., Bearden, A. J., Salmeen, I. T., Palmer, G., Sands, R. H., Orme-Johnson, W. H., and Beinert, H. (1971) Electronic properties of two-iron, two-sulfur proteins. II. Two-iron ferredoxins in spinach, parsley, pig adrenal cortex, *Azotobacter vinelandii* and *Clostridium pasteurianum*. Magnetic field Mössbauer spectroscopy, *Biochim. Biophys. Acta* 253, 143-152.
41. Jones, D. P., Carlson, J. L., Mody, V. C., Cai, J., Lynn, M. J., and Sternberg, P. (2000) Redox state of glutathione in human plasma, *Free Radic. Biol. Med.* 28, 625-635.
42. Ryle, M. J., Lanzilotta, W. N., Seefeldt, L. C., Scarrow, R. C., and Jensen, G. M. (1996) Circular dichroism and X-ray spectroscopies of *Azotobacter vinelandii* nitrogenase iron protein., *J. Biol. Chem.* 271, 1551-1557.
43. Lindahl, P. A., Day, E. P., Kent, T. A., Orme-Johnson, W. H., and Münck, E. (1985) Mössbauer, EPR, and magnetization studies of *Azotobacter vinelandii* Fe protein: Evidence for a  $[4\text{Fe-4S}]^{1+}$  cluster with spin  $S = 3/2$ , *J. Biol. Chem.* 260, 11160-11173.
44. Fu, W., Jack, R. F., Morgan, T. V., Dean, D. R., and Johnson, M. K. (1994) *nifU* gene product from *Azotobacter vinelandii* is a homodimer that contains two identical  $[2\text{Fe-2S}]$  clusters., *Biochemistry* 33, 13455-13463.
45. Yuvaniyama, P., Agar, J. N., Cash, V. L., Johnson, M. K., and Dean, D. R. (2000) NifS-directed assembly of a transient  $[2\text{Fe-2S}]$  cluster within the NifU protein, *Proc. Natl. Acad. Sci. USA* 97, 599-604.
46. Chandramouli, K. and Johnson, M. K. (2006) HscA and HscB stimulate  $[2\text{Fe-2S}]$  cluster transfer from IscU to apoferredoxin in an ATP-dependent reaction, *Biochemistry* 45, 11087-11095.
47. Ollagnier-de-Choudens, S., Mattioli, T., Takahashi, Y., and Fontecave, M. (2001) Iron-sulfur cluster assembly. Characterization of IscA and evidence for a specific functional complex with ferredoxin, *J. Biol. Chem.* 276, 22604-22607.
48. Ollagnier-de-Choudens, S., Sanakis, Y., and Fontecave, M. (2004) SufA/IscA: reactivity studies of a class of scaffold proteins involved with  $[\text{Fe-S}]$  cluster assembly, *J. Biol. Inorg. Chem.* 9, 828-838.
49. Ding, H., Clark, R. J., and Ding, B. (2004) IscA mediates iron delivery for assembly of iron-sulfur clusters in IscU under limited "free" iron conditions, *J. Biol. Chem.* 279, 37499-37504.
50. Ding, B., Smith, E. S., and Ding, H. (2005) Mobilization of the iron centre in IscA for the iron-sulfur cluster assembly in IscU, *Biochem. J.* 389, 797-802.
51. Yang, J., Bitoun, J. P., and Ding, H. (2006) Interplay of IscA and IscU in biogenesis of iron-sulfur clusters, *J. Biol. Chem.* 281, 27956-27963.

52. Ollagnier-de-Choudens, S., Nachin, L., Sanakis, Y., Loiseau, L., Barras, F., and Fontecave, M. (2003) SufA from *Erwinia chrysanthemi*. Characterization of a scaffold protein required for iron-sulfur cluster assembly, *J. Biol. Chem.* 278, 17993-18001.
53. Wollenberg, M., Berndt, C., Bill, E., Schwenn, J. D., and Seidler, A. (2003) A dimer of the FeS cluster biosynthesis protein IscA from cyanobacteria binds a [2Fe2S] cluster between two protomers and transfers it to [2Fe2S] and [4Fe4S] apo proteins, *Eur. J. Biochem.* 270, 1662-1671.
54. Wu, S.-P. and Cowan, J. A. (2003) Iron-sulfur cluster biosynthesis. A comparative kinetic analysis of native and cys-substituted ISA-mediated [2Fe-2S]<sup>2+</sup> cluster transfer to an apoferrredoxin target, *Biochemistry* 42, 5784-5791.
55. Zeng, J., Geng, M., Jiang, H., Liu, Y., Liu, J., and Qiu, G. (2007) The IscA from *Acidithiobacillus ferrooxidans* is an iron-sulfur protein which assemble the [Fe<sub>4</sub>S<sub>4</sub>] cluster with intracellular iron and sulfur, *Arch. Biochem. Biophys.* 463, 237-244.
56. Jensen, L. T. and Culotta, V. C. (2000) Role of *Saccharomyces cerevisiae* Isa1 and Isa2 in iron homeostasis, *Mol. Cell. Biol.* 20, 3918-3927.
57. Kaut, A., Lange, H., Diekert, K., Kispal, G., and Lill, R. (2000) Isa1p is a component of the mitochondrial machinery for maturation of cellular iron-sulfur proteins and requires conserved cysteine residues for function, *J. Biol. Chem.* 275, 15955-15961.
58. Pelzer, W., Mühlenhoff, U., Diekert, K., Siegmund, K., Kispal, G., and Lill, R. (2000) Mitochondrial Isa2p plays a crucial role in the maturation of cellular iron-sulfur proteins, *FEBS Lett.* 476, 134-139.
59. Shi, R., Proteau, A., Villarroya, M., Moukadiri, I., Zhang, L., Trempe, J. F., Matte, A., Armengod, M. E., and Cygler, M. (2010) Structural basis for Fe-S cluster assembly and tRNA thiolation mediated by IscS protein-protein interactions, *PLoS. Biol.* 8, e1000354-
60. Marinoni, E. N., de Oliveira, J. S., Nicolet, Y., Raulfs, E. C., Amara, P., Dean, D. R., and Fontecilla-Camps, J. C. (2012) (IscS-IscU)<sub>2</sub> complex structures provide insights into Fe<sub>2</sub>S<sub>2</sub> biogenesis and transfer, *Angew. Chem. Int. Ed Engl.* 51, 5439-5442.
61. Chahal, H. K., Dai, Y., Saini, A., Ayala-Castro, C., and Outten, F. W. (2009) The SufBCD Fe-S scaffold complex interacts with SufA for Fe-S cluster transfer, *Biochemistry* 48, 10644-10653.
62. Jung, Y.-S., Gao-Sheridan, H. S., Christiansen, J., Dean, D. R., and Burgess, B. K. (1999) Purification and biophysical characterization of a new [2Fe-2S] ferredoxin from *Azotobacter vinelandii*, a putative [Fe-S] cluster assembly/repair protein, *J. Biol. Chem.* 274, 32402-32410.
63. Chandramouli, K., Unciuleac, M.-C., Naik, S., Dean, D. R., Huynh, B. H., and Johnson, M. K. (2007) Formation and properties of [4Fe-4S] clusters on the IscU scaffold protein, *Biochemistry* 46, 6804-6811.

64. Setubal, J. C., dos, S. P., Goldman, B. S., Ertesvag, H., Espin, G., Rubio, L. M., Valla, S., Almeida, N. F., Balasubramanian, D., Cromes, L., Curatti, L., Du, Z., Godsy, E., Goodner, B., Hellner-Burris, K., Hernandez, J. A., Houmiel, K., Imperial, J., Kennedy, C., Larson, T. J., Latreille, P., Ligon, L. S., Lu, J., Maerk, M., Miller, N. M., Norton, S., O'Carroll, I. P., Paulsen, I., Raulfs, E. C., Roemer, R., Rosser, J., Segura, D., Slater, S., Stricklin, S. L., Studholme, D. J., Sun, J., Viana, C. J., Wallin, E., Wang, B., Wheeler, C., Zhu, H., Dean, D. R., Dixon, R., and Wood, D. (2009) Genome sequence of *Azotobacter vinelandii*, an obligate aerobe specialized to support diverse anaerobic metabolic processes, *J. Bacteriol.* 191, 4534-4545.
65. Moshiri, F., Kim, J. W., Fu, C., and Maier, R. J. (1994) The FeSII protein of *Azotobacter vinelandii* is not essential for aerobic nitrogen fixation, but confers significant protection to oxygen-mediated inactivation of nitrogenase in vitro and in vivo, *Mol. Microbiol.* 14, 101-114.

Table B.1: Mössbauer parameters of the Fe species detected during Fe–S cluster assembly and [4Fe-4S]<sup>2+</sup> and [2Fe-2S]<sup>2+</sup> cluster interconversions on <sup>Nif</sup>IscA.

Fe species	$\delta$ (mm/s) <sup>a</sup>	$\Delta E_Q$ (mm/s) <sup>a</sup>
Fe <sup>II</sup> -4.1	1.16	4.06
Fe <sup>II</sup> -3.5	1.12	3.48
Fe <sup>II</sup> Cys <sub>4</sub>	0.69	3.42
Fe(II)	0.75	3.40
[2Fe-2S] <sup>2+</sup>		
Site 1	0.27	0.50
Site 2	0.28	0.68
[4Fe-4S] <sup>2+</sup>		
Pair 1	0.46	1.25
Pair 2	0.44	1.04

<sup>a</sup>The estimated uncertainties for  $\delta$  and  $\Delta E_Q$  are 0.02 and 0.04 mm/s, respectively.

Table B.2: Analysis of Mössbauer resonances as a percentage of total Fe during NifS-mediated Fe–S cluster assembly on  $^{57}\text{Fe}$ -IscA as a function of reaction time.<sup>a</sup>

sample	reaction time (min)	$\text{Fe}^{\text{II}}\text{Cys}_4$	$\text{Fe}^{\text{II}}\text{-3.5}$	$\text{Fe}^{\text{II}}\text{-4.1}$	$[\text{2Fe-2S}]^{2+}$	$[\text{4Fe-4S}]^{2+}$
$^{57}\text{Fe}$ IscA (-) (control)	2	51 (5)	36 (4)	11 (2)		2 (2)
$^{57}\text{Fe}$ IscA (+)	2	56 (5)	28 (3)	14 (2)		2 (2)
$^{57}\text{Fe}$ IscA (-) (control)	20	36 (4)	41 (4)	18 (2)		5 (2)
$^{57}\text{Fe}$ IscA (+)	20	39 (4)	27 (3)	14 (2)	9 (2)	11 (2)
$^{57}\text{Fe}$ IscA (-) (control)	60	34 (4)	44 (5)	16 (2)		6 (2)
$^{57}\text{Fe}$ IscA (+)	60	24 (3)	21 (3)	11 (2)	3 (2)	41 (4)

<sup>a</sup>Values in parentheses are estimated uncertainties for the last significant digits.

Table B.3: Fe–S stretching frequencies ( $\text{cm}^{-1}$ ) and assignments for the  $[2\text{Fe}-2\text{S}]^{2+}$  centers in *A. vinelandii*<sup>Nif</sup>IscA, *S. oleracea* ferredoxin, Bovine adrenodoxin, and *P. putida* putidaredoxin.

mode ( $D_{2h}$ ) <sup>a</sup>	ferredoxin <sup>b</sup>	adrenodoxin <sup>b</sup>	putidaredoxin <sup>b</sup>	<i>A. vinelandii</i> <sup>Nif</sup> IscA
$B_{2u}^b$	427	421	426	421
$A_g^b$	395	393	400	396
$B_{3u}^b$	367	349	350	358
$B_{1u}^t, B_{2g}^t$	357	341	344	~345
$A_g^t$	338	329	338	338
$B_{1g}^b$	329	317	320	~325
$B_{3u}^t$	283	291	291	290

<sup>a</sup>Symmetry labels under idealized  $D_{2h}$  symmetry for a  $\text{Fe}_2\text{S}_2^b\text{S}_4^t$  unit, where  $S^b$  and  $S^t$  indicate bridging and terminal (cysteiny) S, respectively. <sup>b</sup>Taken from ref 34.

Table B.4: Analysis of Mössbauer resonances as a percentage of total Fe during  $[2\text{Fe-2S}]^{2+}/[4\text{Fe-4S}]^{2+}$  cluster conversions on  $^{\text{Nif}}\text{IscA}$ .<sup>a</sup>

sample	$[2\text{Fe-2S}]^{2+}$	$[4\text{Fe-4S}]^{2+}$	$\text{Fe}^{\text{II}}$	remaining Fe <sup>b</sup>
Reconstituted $[2\text{Fe-2S}]^{2+}$ $^{\text{Nif}}\text{IscA}$ (sample A)	100			
Sample A treated with 2 mM DTT for 1 min	34 (4)	43 (4)	10 (2)	13 (2)
Sample A treated with 2 mM DTT for 15 min	16 (3)	53 (5)	18 (3)	13 (2)
Sample A treated with 2 mM DTT for 15 min and air for 5 min	60 (5)	15 (3)		25 (3)

<sup>a</sup>Values in parentheses are estimated uncertainties for the last significant digits. <sup>b</sup>The remaining Fe is primarily in the form a  $S = 1/2$   $[2\text{Fe-2S}]^+$  cluster for the samples treated with DTT for 1 and 15 min and in the form of  $S = 3/2$  Fe(III)-bound  $^{\text{Nif}}\text{IscA}$  for the sample treated with DTT and then exposed to air (see text for details).

Figure B.1: NifS-mediated Fe–S cluster assembly on <sup>Nif</sup>IscA monitored as a function of time by UV–visible absorption and CD spectroscopies. Protein and reagent concentrations are described in the Materials and Methods. The spectra shown are for TCEP pretreated apo <sup>Nif</sup>IscA before reconstitution (black) and after 5 min (purple), 20min (red), and 65 min (blue) of NifS-mediated Fe–S cluster assembly.  $\epsilon$  and  $\Delta\epsilon$  values are expressed per <sup>Nif</sup>IscA monomer.

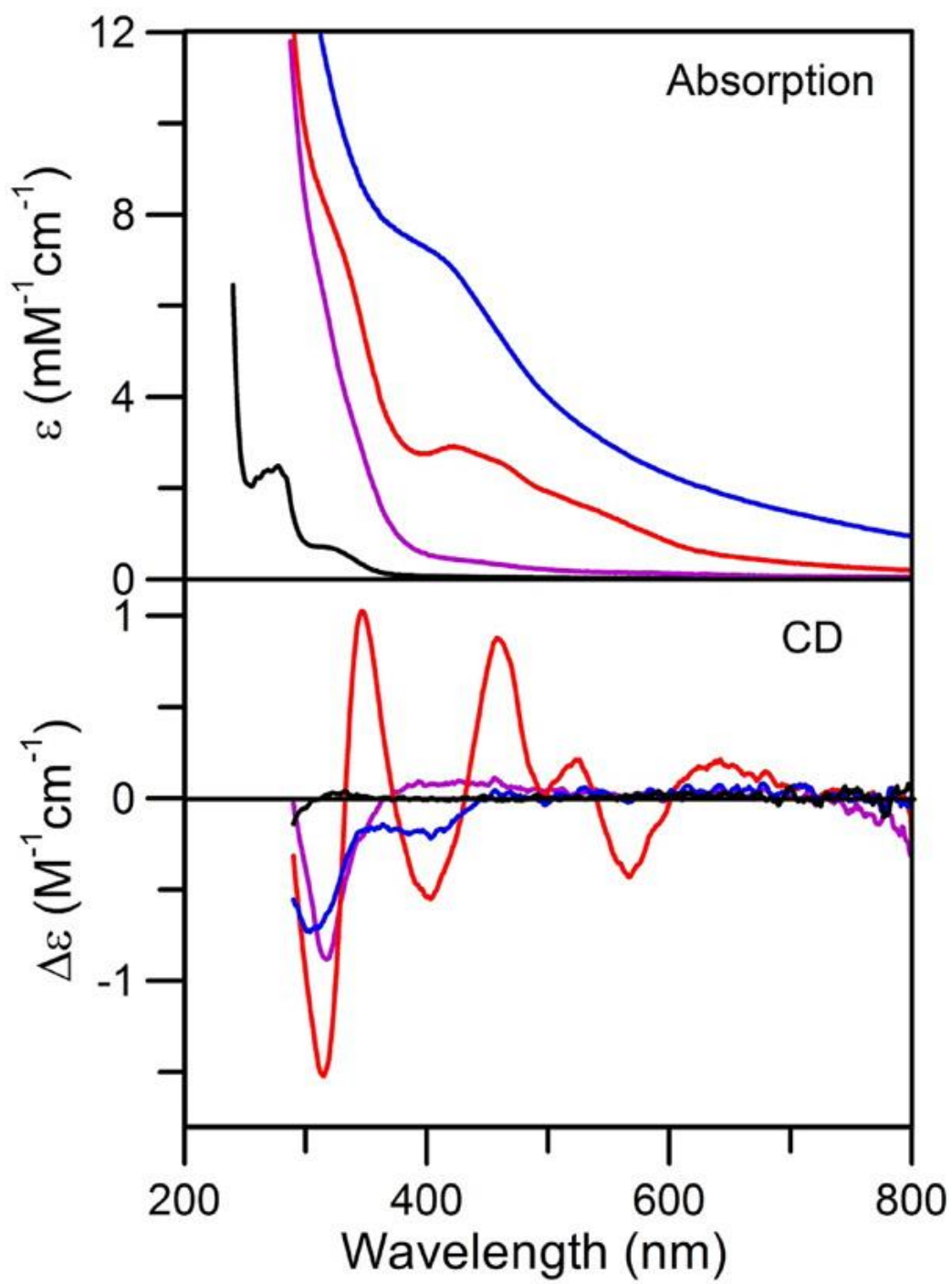


Figure B.2: Time-dependent Mössbauer spectra of NifS-mediated Fe–S cluster assembly on  $^{57}\text{Fe}$ -labeled NifS. The reconstitution mixture with (left panel) and without (right panel)  $^{57}\text{Fe}$ -labeled NifS was frozen at time intervals of 2 min (A and D), 20 min (B and E), and 60 min (C and F). See Materials and Methods for protein and reagent concentrations. The Mössbauer spectra (dotted lines) were recorded at 4.2 K in a magnetic field of 50 mT applied parallel to the  $\gamma$ -beam. The colored lines are theoretical simulations for the individual Fe species using the parameters listed in Table 1:  $\text{Fe}^{\text{II}}\text{Cys}_4$ ,  $\text{Fe}^{\text{II}}\text{-3.5}$ , and  $\text{Fe}^{\text{II}}\text{-4.1}$  in green;  $[\text{2Fe-2S}]^{2+}$  cluster in red;  $[\text{4Fe-4S}]^{2+}$  cluster in blue. They are plotted in accord with the percentage absorptions listed in Table B.2. The solid black lines overlaid with the experimental spectra are composites of the simulations shown.

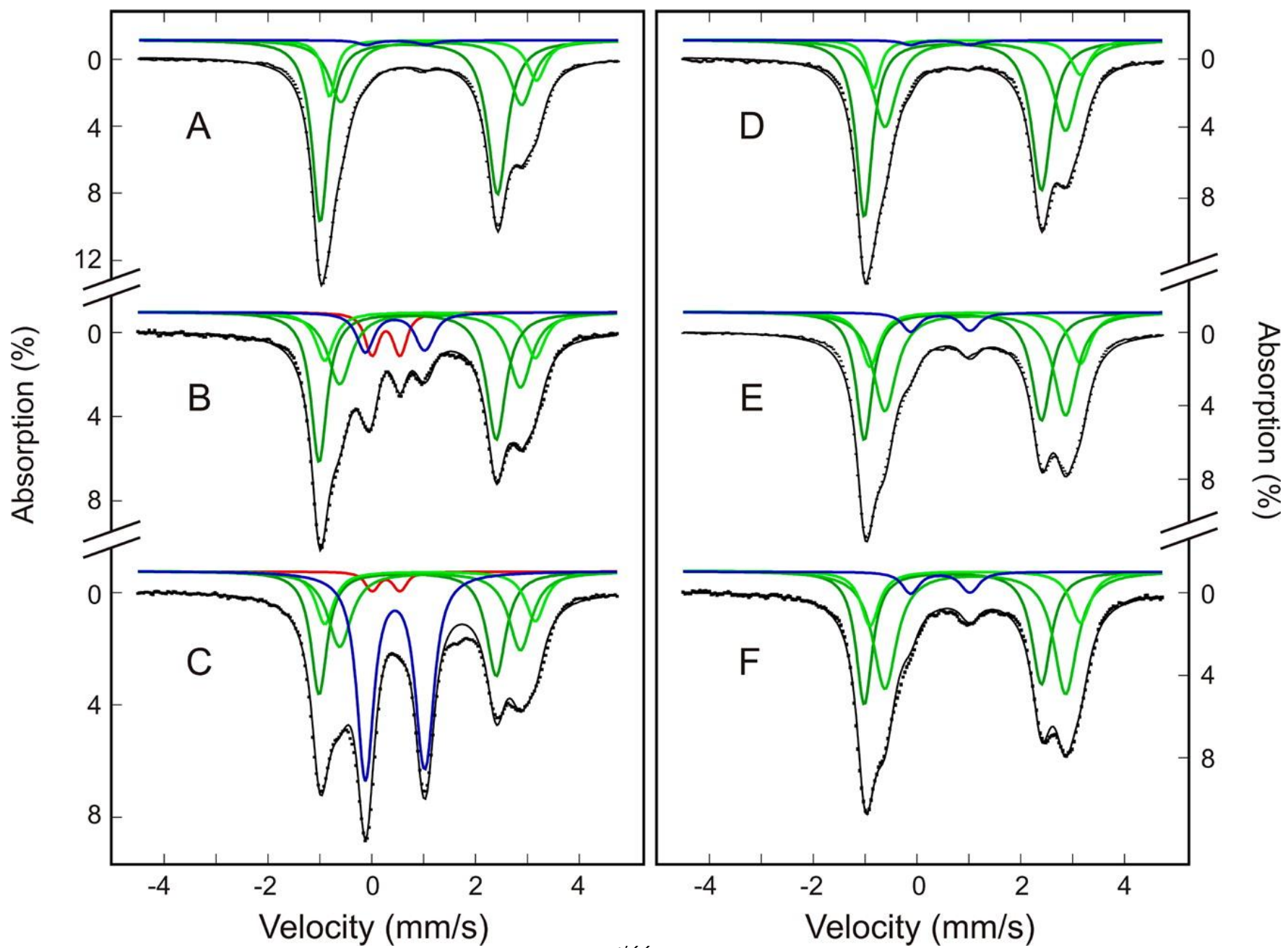


Figure B.3: UV–visible absorption and visible CD spectra of the purified  $[2\text{Fe-2S}]^{2+}$  cluster-bound form of  $^{\text{Nif}}$ IscA recorded at room temperature under anaerobic conditions in septum-sealed 1 mm quartz cuvettes. Molar extinction coefficients ( $\epsilon$ ) values are based on the concentration of monomeric  $^{\text{Nif}}$ IscA as determined by protein assays and  $\Delta\epsilon$  values are based on the concentration of  $^{\text{Nif}}$ IscA-bound  $[2\text{Fe-2S}]^{2+}$  clusters.

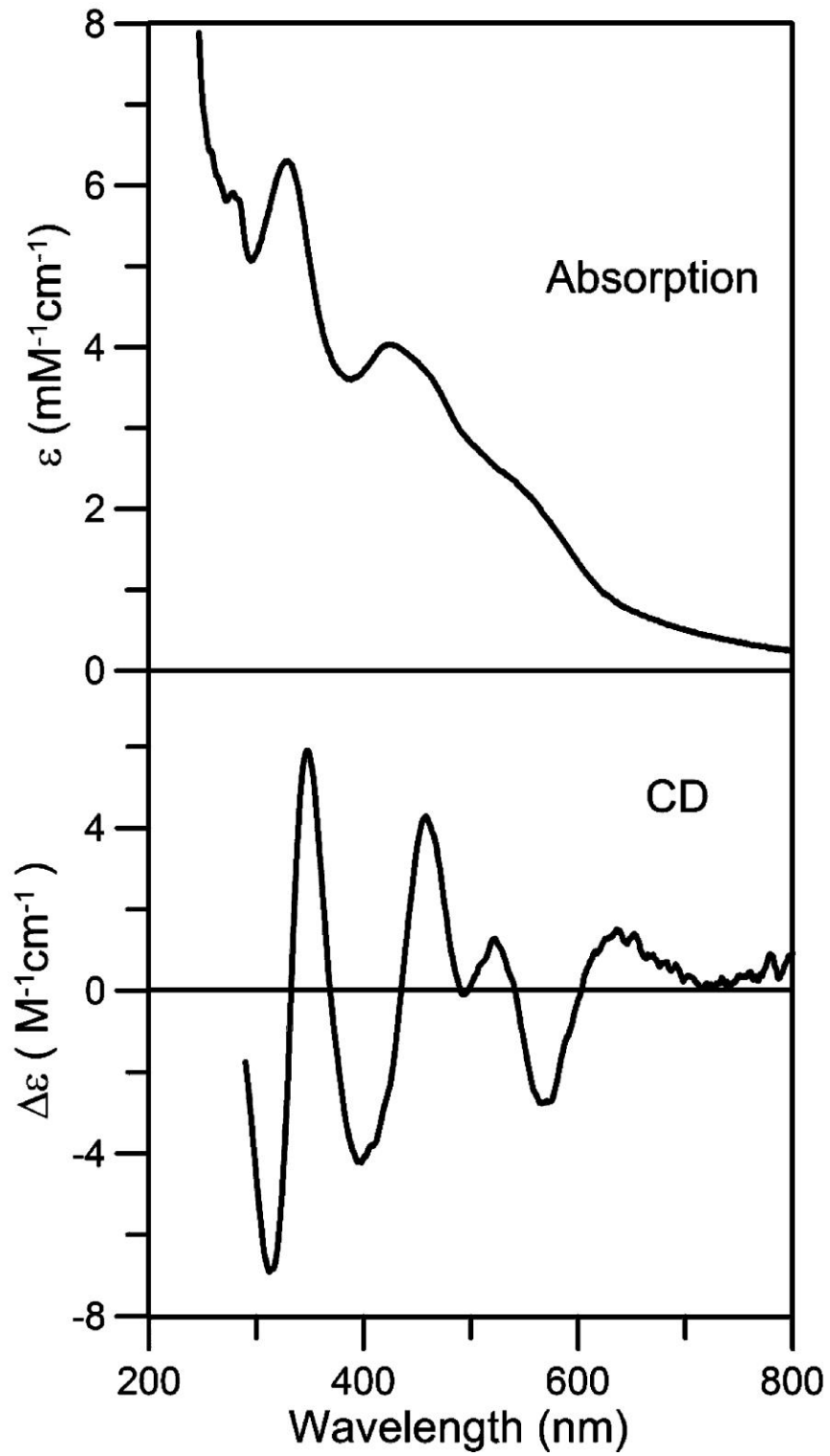


Figure B.4: Resonance Raman spectra of purified  $[2\text{Fe-2S}]^{2+}$ -bound form of  $^{\text{Nif}}$ IscA. Raman spectra were recorded at 17 K with 457.9, 487.9, and 514.5 nm laser excitation with  $\sim 185$  mW laser power at the sample. The sample ( $\sim 2$  mM in  $[2\text{Fe-2S}]^{2+}$  clusters) was in 100 mM Tris-HCl buffer, pH 7.8 containing  $\sim 0.45$  M NaCl. Each spectrum is a sum of 100 scans, with each scan involving counting photons for 1 s at  $0.5\text{ cm}^{-1}$  increments with  $6\text{ cm}^{-1}$  spectral resolution. Bands due to lattice modes of ice from frozen buffer in sample have been subtracted from all spectra.

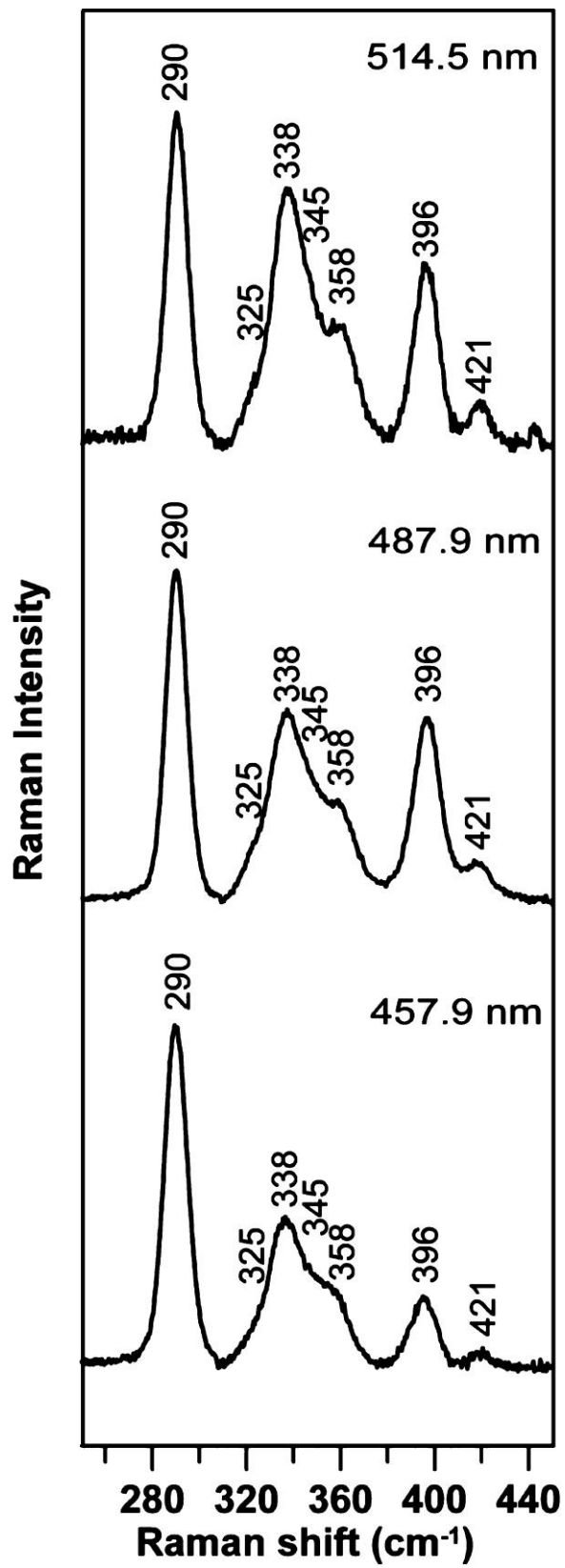


Figure B.5: DTT-induced  $[2\text{Fe-2S}]^{2+}$ -to- $[4\text{Fe-4S}]^{2+}$  cluster conversion and  $\text{O}_2$ -induced  $[4\text{Fe-4S}]^{2+}$ -to- $[2\text{Fe-2S}]^{2+}$  cluster conversion on  $^{\text{Nif}}\text{IscA}$  monitored by Mössbauer spectroscopy. Mössbauer spectra (hashed marks) were recorded at 4.2 K in a magnetic field of 50 mT applied parallel to the  $\gamma$ -beam. The spectra shown are for reconstituted and repurified  $[2\text{Fe-2S}]^{2+}$  cluster-bound  $^{\text{Nif}}\text{IscA}$  (0.5 mM in  $[2\text{Fe-2S}]^{2+}$  clusters) prior to addition of 2.0 mM DTT (A), 1 min after DTT addition (B), 15 min after DTT addition (C), and after exposing the 15 min DTT-treated sample to air for 5 min (D). The colored lines are theoretical simulations for the individual Fe species (Fe(II) species in green,  $[2\text{Fe-2S}]^{2+}$  clusters in red and  $[4\text{Fe-4S}]^{2+}$  clusters in blue) using the parameters listed in Table B.1 and plotted in percentages listed in Table B.4. The solid black lines overlaid with the experimental spectra are the composite spectra.

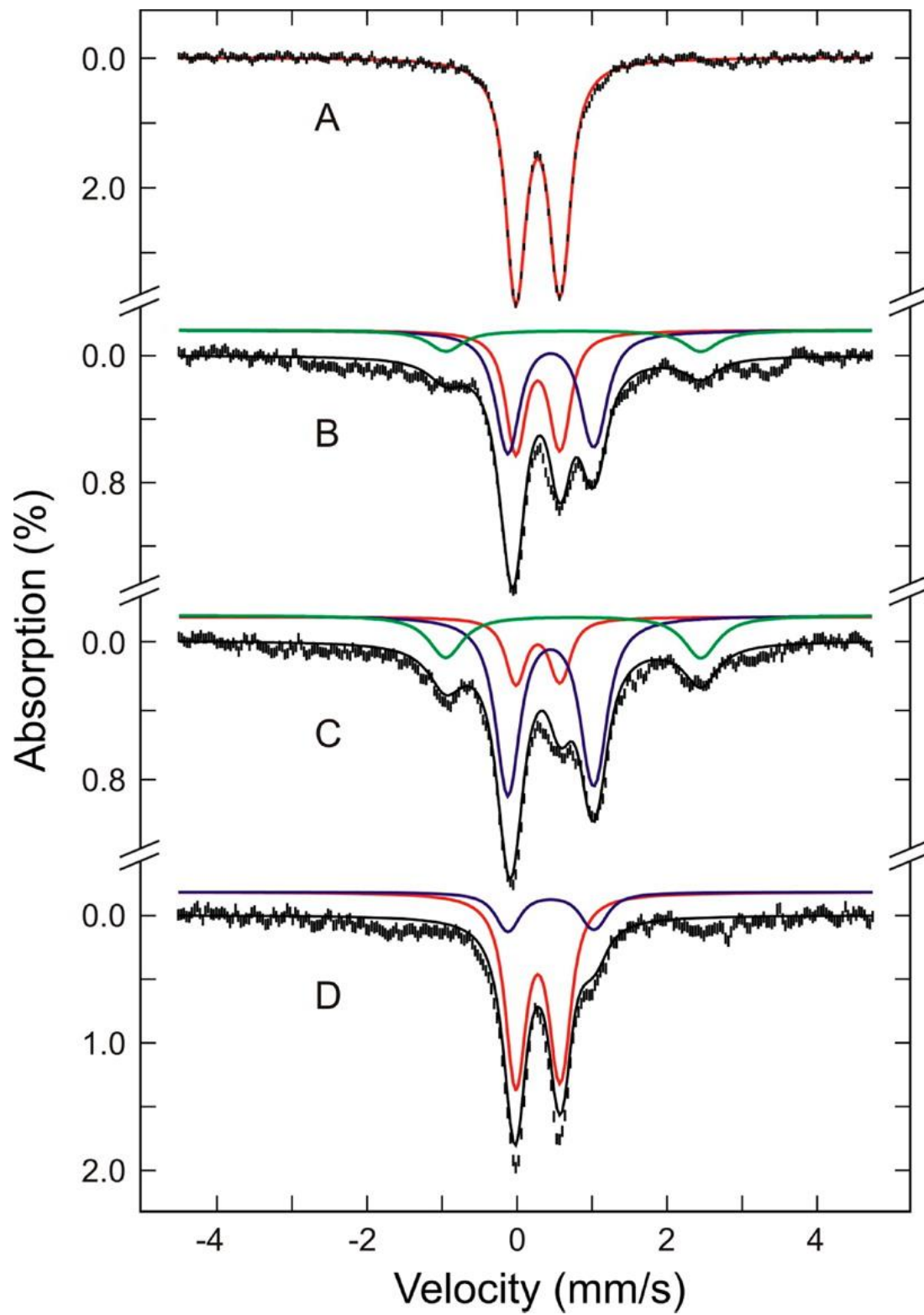


Figure B.6:  $[2\text{Fe-2S}]^{2+} \leftrightarrow [4\text{Fe-4S}]^{2+}$  cluster interconversions on  $^{\text{Nif}}\text{IscA}$  monitored by UV-visible absorption and CD spectroscopies. Anaerobically purified  $[2\text{Fe-2S}]^{2+}$  cluster-bound (solid red line) was treated with 2 mM DTT and incubated for 15 min (solid blue line), exposed to air for 5 min (broken red line), sealed and incubated for an additional 15 min (broken blue line), and exposed to air again for 5 min (solid black line).  $\epsilon$  and  $\Delta\epsilon$  values are based on the  $[2\text{Fe-2S}]^{2+}$  cluster concentration of the initial  $[2\text{Fe-2S}]^{2+}$  cluster-bound  $^{\text{Nif}}\text{IscA}$  sample (0.05 mM). The CD spectra of the first and second air-exposed samples have been corrected for contributions from Fe(III)-bound  $^{\text{Nif}}\text{IscA}$ , by subtracting CD spectra of Fe(III)-bound  $^{\text{Nif}}\text{IscA}$  (see Appendix A) corresponding to 10% and 20% of the total Fe, respectively.

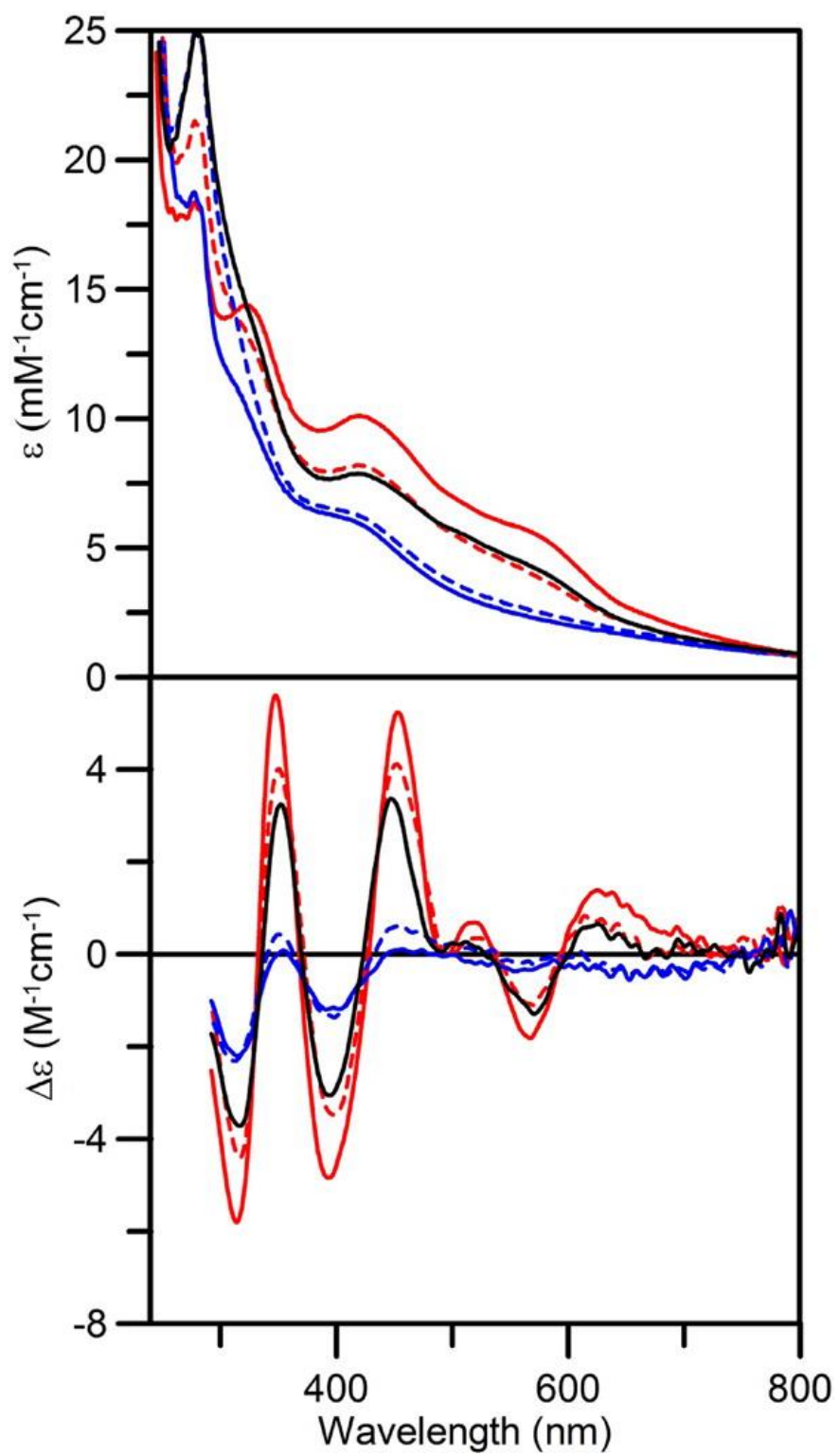


Figure B.7: X-band EPR spectrum of  $[2\text{Fe-2S}]^{2+}$  cluster-bound  $^{60}\text{Ni}$  IscA after addition of DTT. Sample was frozen within 5 s of the addition of 2 mM DTT and the spectrum was recorded at 30 K using 10 mW microwave power, using a modulation amplitude of 0.63 mT and a microwave frequency of 9.60 GHz.

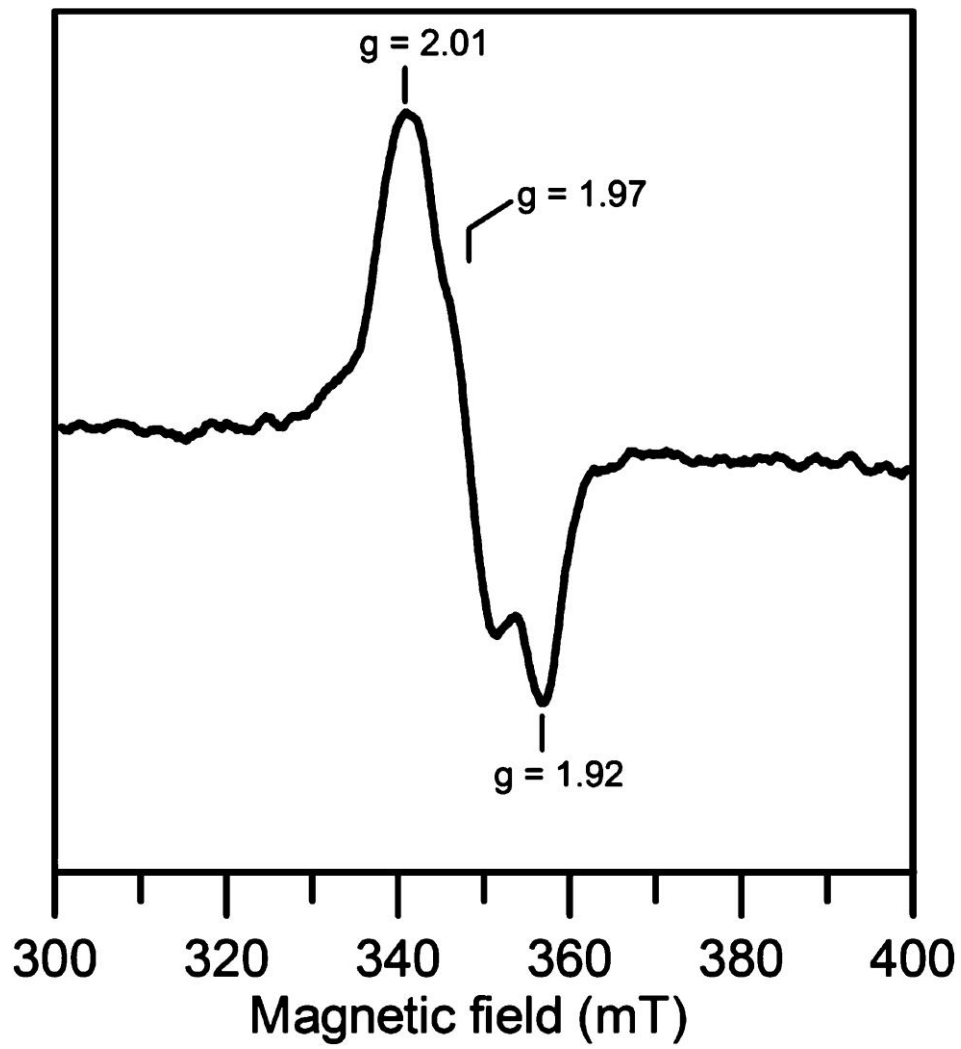


Figure B.8: Time course of cluster transfer from  $[4\text{Fe-4S}]^{2+}$  cluster-bound  $^{\text{Nif}}\text{IscA}$  to *A. vinelandii* apo ADP-bound nitrogenase Fe protein monitored by UV-visible CD spectroscopy under anaerobic conditions. Top panel: CD spectra of apo ADP-bound nitrogenase Fe protein (12.5  $\mu\text{M}$  in dimer in final reaction mixture) were recorded before (zero time) and after reaction with  $[4\text{Fe-4S}]^{2+}$  cluster-bound  $^{\text{Nif}}\text{IscA}$  (12.5  $\mu\text{M}$  in  $[4\text{Fe-4S}]^{2+}$  clusters in the final reaction mixture) for 4, 8, 15, 25, and 35 min. The arrow indicates an increase in CD intensity with increasing time.  $\Delta\epsilon$  values are based on the initial  $^{\text{Nif}}\text{IscA}$   $[4\text{Fe-4S}]^{2+}$  cluster concentration. Bottom panel: Kinetics of  $[4\text{Fe-4S}]^{2+}$  cluster based on CD intensity of holo ADP-bound nitrogenase Fe protein at 475 nm as function of time. The solid line is the best fit kinetic simulation for direct cluster transfer with a second order rate constant of  $20\,000\ \text{M}^{-1}\ \text{min}^{-1}$ .

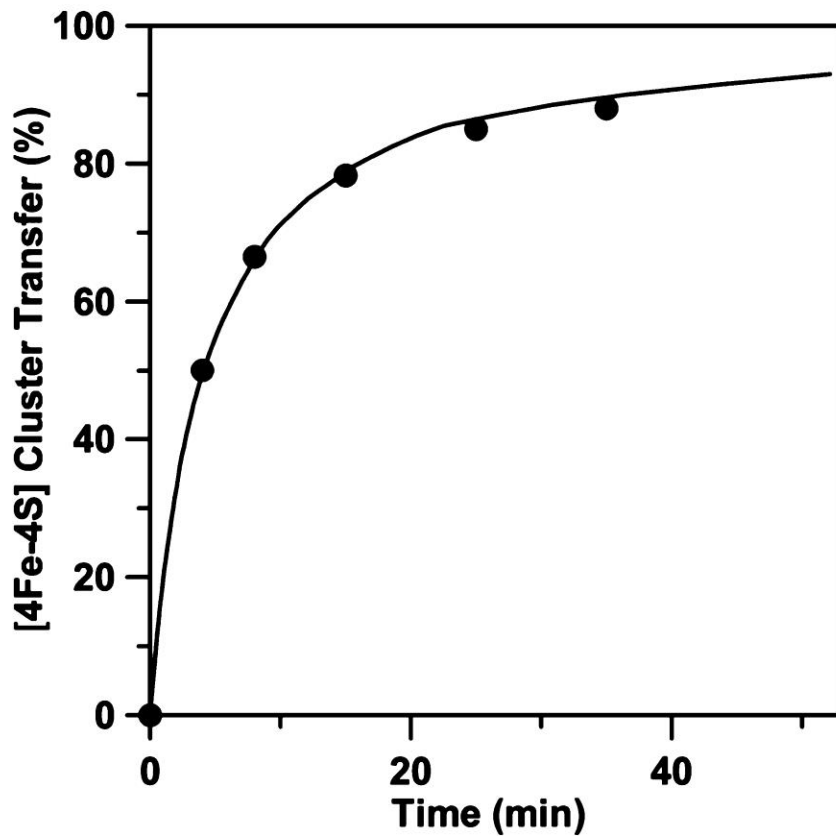
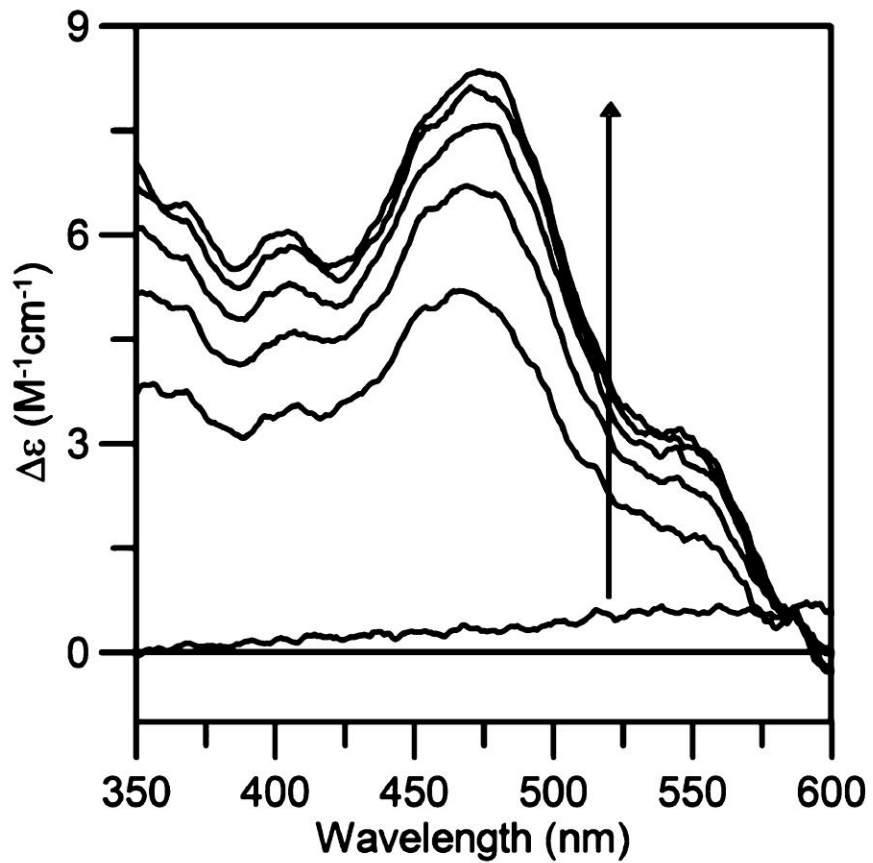


Figure B.9: Time course of cluster transfer from  $[4\text{Fe-4S}]^{2+}$  cluster-bound NifU to apo  $^{\text{Nif}}\text{IscA}$  monitored by UV–visible absorption and CD spectroscopies under anaerobic conditions at room temperature in the absence of DTT. Upper and middle panels show UV–visible absorption and CD spectra of the reaction mixture containing  $[4\text{Fe-4S}]^{2+}$  cluster-bound NifU (35  $\mu\text{M}$  in NifU monomer with one  $[4\text{Fe-4S}]^{2+}$  clusters and one permanent  $[2\text{Fe-2S}]^{2+}$  cluster per monomer) and apo  $^{\text{Nif}}\text{IscA}$  (100  $\mu\text{M}$  in  $^{\text{Nif}}\text{IscA}$  dimer) recorded before addition of apo  $^{\text{Nif}}\text{IscA}$  (zero time, red lines) and 5, 10, 20, 30, and 50 min after addition of apo  $^{\text{Nif}}\text{IscA}$  (overlapping black lines). The UV–visible absorption and CD spectra of NifU containing only the permanent  $[2\text{Fe-2S}]^{2+}$  cluster are shown for comparison (blue lines). The lower panel shows the 50 min minus zero time difference CD spectrum that is characteristic of  $[2\text{Fe-2S}]^{2+}$  cluster-bound  $^{\text{Nif}}\text{IscA}$ . All  $\epsilon$ ,  $\Delta\epsilon$ , and  $\Delta\Delta\epsilon$  values are expressed per NifU monomer.

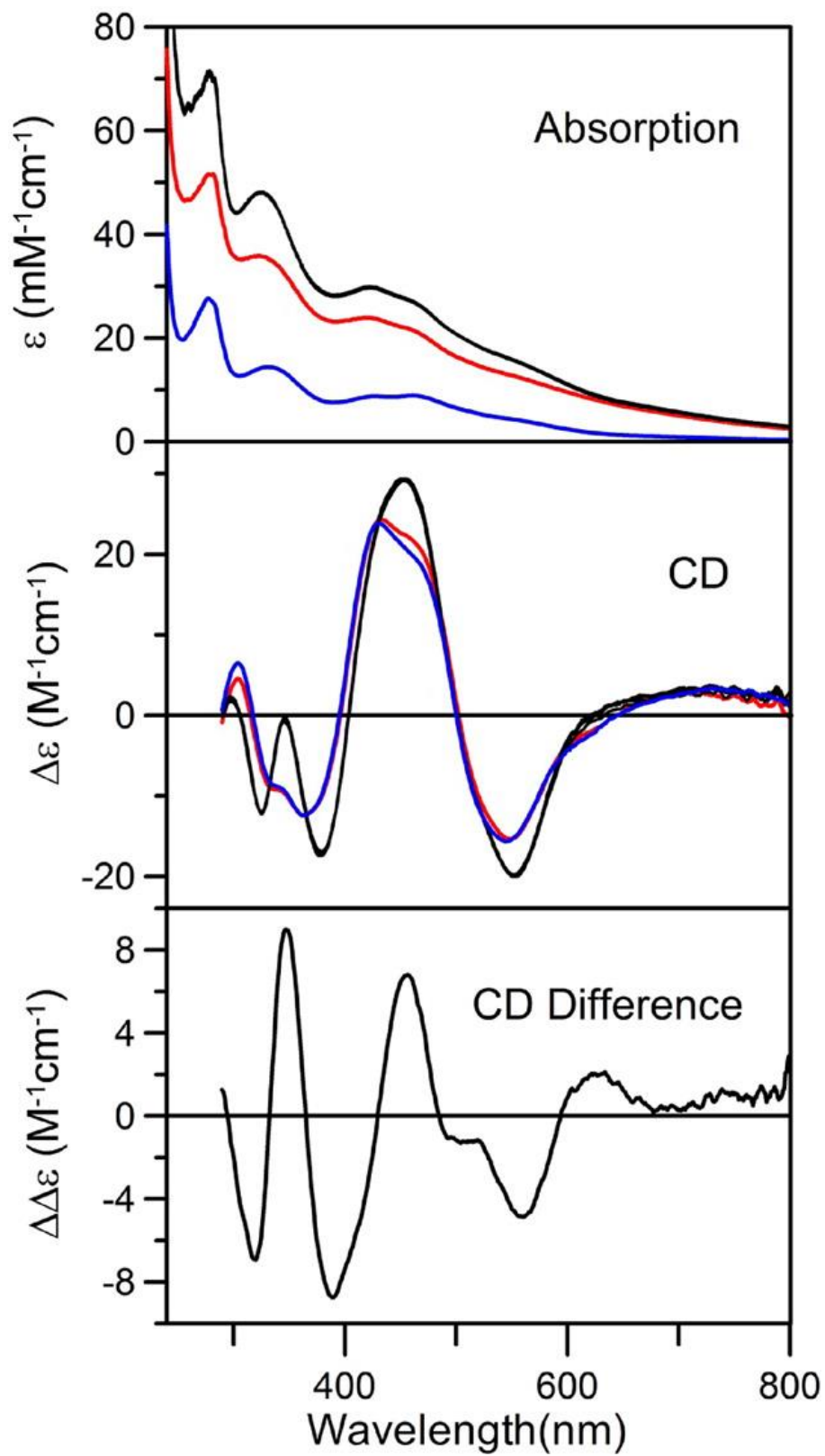
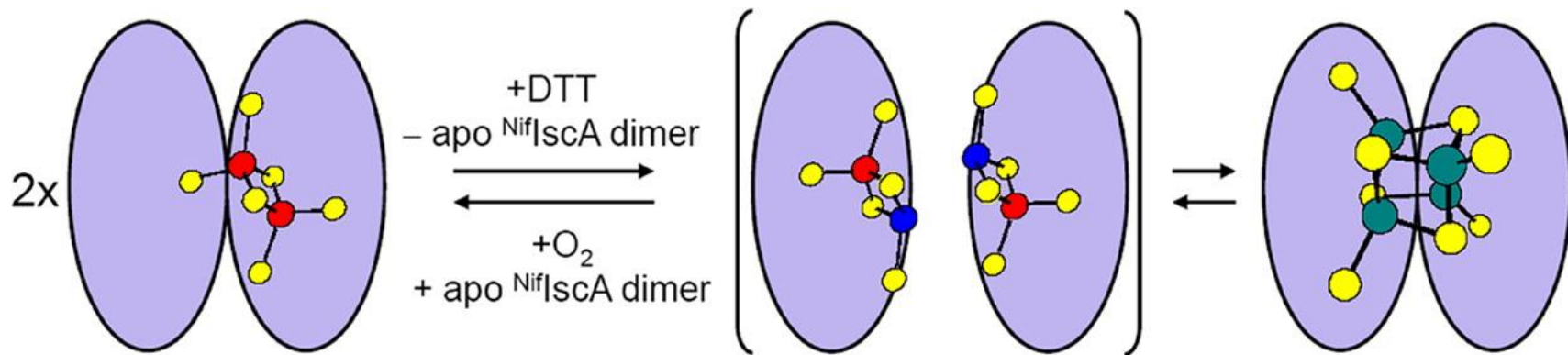


Figure B.10: Proposed mechanism for  $[2\text{Fe-2S}]^{2+}$  and  $[4\text{Fe-4S}]^{2+}$  cluster interconversion on  $^{\text{Nif}}\text{IscA}$  (red,  $\text{Fe}^{3+}$ ; blue  $\text{Fe}^{2+}$ ; green,  $\text{Fe}^{2.5+}$ ; yellow, S).



APPENDIX C

MONOTHIOLE GLUTAREDOXINS AND A-TYPE PROTEINS: PARTNERS IN Fe-S  
CLUSTER TRAFFICKING

---

Daphne T. Mapolelo,<sup>a</sup> Bo Zhang,<sup>a</sup> Sajini Randeniya,<sup>a</sup> Angela-Nadia Albetel,<sup>a</sup> Haoran Li,<sup>b</sup> Jérémy Couturier,<sup>c</sup> Caryn E. Outten,<sup>b</sup> Nicolas Rouhier,<sup>c</sup> and Michael K. Johnson<sup>a</sup>

*Dalton Transactions* **2013**, 42, 3107–3115.

Reprinted here with permission of the publisher.

<sup>a</sup>Department of Chemistry and Center for Metalloenzyme Studies, University of Georgia; Athens, Georgia 30602, USA; <sup>b</sup>Department of Chemistry and Biochemistry, University of South Carolina, Columbia, South Carolina 29208, USA; <sup>c</sup>Unité Mixte de Recherches 1136 Université de Lorraine-INRA, Interactions Arbres Microorganismes, IFR 110, EFABA 54506 Vandoeuvre-lés-Nancy Cedex, France.

**Abbreviations:** *A. vinelandii*, Av; *S. cerevisiae*, Sc; *A. thaliana*, At; glutaredoxin, Grx; glutathione, GSH, dithiothreitol, DTT; ferredoxin, Fdx.

## Abstract

Monothiol glutaredoxins (Grxs) are proposed to function in Fe–S cluster storage and delivery, based on their ability to exist as apo monomeric forms and dimeric forms containing a subunit-bridging  $[\text{Fe}_2\text{S}_2]^{2+}$  cluster, and to accept  $[\text{Fe}_2\text{S}_2]^{2+}$  clusters from primary scaffold proteins. In addition yeast cytosolic monothiol Grxs interact with Fra2 (Fe repressor of activation-2), to form a heterodimeric complex with a bound  $[\text{Fe}_2\text{S}_2]^{2+}$  cluster that plays a key role in iron sensing and regulation of iron homeostasis. In this work, we report on in vitro UV-visible CD studies of cluster transfer between homodimeric monothiol Grxs and members of the ubiquitous A-type class of Fe–S cluster carrier proteins ( $^{\text{Nif}}\text{IscA}$  and SufA). The results reveal rapid, unidirectional, intact and quantitative cluster transfer from the  $[\text{Fe}_2\text{S}_2]^{2+}$  cluster-bound forms of *A. thaliana* GrxS14, *S. cerevisiae* Grx3, and *A. vinelandii* Grx-nif homodimers to *A. vinelandii*  $^{\text{Nif}}\text{IscA}$  and from *A. thaliana* GrxS14 to *A. thaliana* SufA1. Coupled with *in vivo* evidence for interaction between monothiol Grxs and A-type Fe–S cluster carrier proteins, the results indicate that these two classes of proteins work together in cellular Fe–S cluster trafficking. However, cluster transfer is reversed in the presence of Fra2, since the  $[\text{Fe}_2\text{S}_2]^{2+}$  cluster-bound heterodimeric Grx3–Fra2 complex can be formed by intact  $[\text{Fe}_2\text{S}_2]^{2+}$  cluster transfer from  $^{\text{Nif}}\text{IscA}$ . The significance of these results for Fe–S cluster biogenesis or repair and the cellular regulation of the Fe–S cluster status are discussed.

## Introduction

Monothiol Grxs with active-site cysteine-glycine-phenylalanine-serine (CGFS) amino acid sequences are widely distributed in both prokaryotes and eukaryotes and constitute class II of the six classes of Grxs (1;2). In general, this class can further be divided into two subclasses: those with a single Grx domain (e.g. *Saccharomyces cerevisiae* (Sc) Grx5, *Homo sapiens* (Hs) Grx5, *Escherichia coli* (Ec) Grx4, *Azotobacter vinelandii* (Av) Grx5 and Grx-nif, and *Arabidopsis thaliana* (At) GrxS14 and GrxS15) and the multi-domain proteins comprising an N-terminal thioredoxin-like domain as well as one (Sc Grx3 and Grx4), two (Hs Grx3) or three (At GrxS17) Grx domains. All bacterial monothiol CGFS Grxs are of the single Grx domain type, while in eukaryotes, both the single Grx domain and the multi-domain Grxs are present (1;3). Although monothiol CGFS Grxs are ubiquitous proteins, their precise role(s) remain to be elucidated. Traditionally, Grxs function in the reduction of protein disulfides or glutathionylated proteins (1;4). However, monothiol CGFS Grxs generally exhibit low levels of disulfide reductase activity and the available *in vivo* data suggest roles in Fe–S cluster biogenesis and/or Fe homeostasis (5-7).

The initial evidence for a role for monothiol CGFS Grxs in Fe–S cluster biogenesis came from yeast (*Saccharomyces cerevisiae*) gene knockout studies. Deletion of the *grx5* gene which encodes for the mitochondrial monothiol CGFS Grx5, resulted in increased sensitivity to oxidative stress as a result of iron accumulation in the cell and deficient cluster assembly in at least two Fe–S cluster-containing proteins (aconitase and succinate dehydrogenase) leading to impaired respiratory growth (8;9). Moreover, radiolabelled <sup>55</sup>Fe immunoprecipitation studies of *grx5* knockout mutants revealed that Grx5 facilitates the transfer of Fe–S clusters preassembled on the Isu1 U-type Fe–S cluster scaffold protein to acceptor proteins (10). Other monothiol

CGFS Grxs from prokaryotic or eukaryotic sources, when targeted to the yeast mitochondria, were able to rescue the defects of *grx5* mutants in *S. cerevisiae*, suggesting that this function is conserved in this class of proteins throughout evolution (11;12). Additional support for a role in Fe–S cluster biogenesis comes from the observation of specific interactions between yeast Grx5 with the Isa1, a mitochondrial A-type Fe–S cluster assembly protein, via yeast two-hybrid experiments (3). Interaction between Grx5 and both Isa1 and Isa2 was also recently demonstrated *in vivo* in *Schizosaccharomyces pombe* through bimolecular fluorescence complementation studies (13). Deleting the *grx5* gene in *S. pombe* resulted in a mutant that showed low activity for mitochondrial and cytoplasmic Fe–S cluster enzymes, and notably both Isa1 and Isa2 were able to complement the phenotype of the  $\Delta$ *grx5* mutant. The function of the interaction between monothiol CGFS Grxs and A-type Fe–S cluster assembly proteins is explored in this work.

In addition to *in vivo* evidence for a role in Fe–S cluster biogenesis, a wide variety of recombinant monothiol CGFS Grxs have recently been shown to contain bound  $[\text{Fe}_2\text{S}_2]^{2+}$  clusters as purified and the apo forms readily incorporate labile  $[\text{Fe}_2\text{S}_2]^{2+}$  clusters during cysteine desulfurase-mediated cluster assembly under anaerobic conditions in the presence of glutathione (GSH) (12;14;15). Analytical, spectroscopic, crystallographic and mutagenesis results have revealed that the  $[\text{Fe}_2\text{S}_2]^{2+}$  cluster is ligated by the active site cysteines of two Grx monomers and two GSH molecules (12;16). Moreover,  $^{55}\text{Fe}$  radiolabeled immunoprecipitation studies have provided *in vivo* evidence for the presence of  $[\text{Fe}_2\text{S}_2]^{2+}$  clusters that are coordinated by the cysteines of GSH and the Grx CGFS motif in *Sc* Grx3 and *Sc* Grx4, two cytoplasmic yeast monothiol Grxs (17).

The ability of  $[\text{Fe}_2\text{S}_2]^{2+}$  cluster-loaded Grxs to effect maturation of physiologically relevant apo ferredoxins (Fdx) via intact rapid cluster transfer ((12) and see Chapter 3), suggests a potential role as scaffold proteins for the assembly and delivery of  $[\text{Fe}_2\text{S}_2]^{2+}$  clusters or as cluster carriers for the delivery of  $[\text{Fe}_2\text{S}_2]^{2+}$  clusters assembled on primary scaffold proteins. More recently, a cluster carrier or storage role for monothiol Grxs has been convincingly demonstrated by *in vitro* studies using proteins from *A. vinelandii* which demonstrated rapid, unidirectional and quantitative  $[\text{Fe}_2\text{S}_2]^{2+}$  cluster transfer from the primary scaffold protein IscU to the general purpose monothiol CGFS Grx5 only in the presence of the dedicated HscA/HscB co-chaperone system and MgATP (see Chapter 3). Additionally,  $[\text{Fe}_2\text{S}_2]^{2+}$  cluster-loaded *Av* Grx5 was shown to be competent for maturation of apo *Av* Isc Fdx via intact cluster transfer at a much faster rate than  $[\text{Fe}_2\text{S}_2]^{2+}$  cluster-loaded IscU in the presence of HscA/HscB co-chaperone system and MgATP (see Chapter 3).

In addition to a role in Fe–S cluster biogenesis, multi-domain monothiol CGFS Grxs have been shown to participate in regulation of Fe homeostasis in eukaryotes. The two yeast cytosolic monothiol CGFS Grxs, *Sc* Grx3 and *Sc* Grx4, are involved in the regulation of a wide range of iron-responsive genes in yeast, termed the iron regulon, via an iron-dependent interaction with the iron-responsive transcriptional activator of ferrous transport, Aft (18-21). The Aft1 and Aft2 paralogs are located in the cytosol under iron-replete conditions and move to the nucleus under iron-depleted conditions, where they activate the expression of the Fe-responsive genes (22-24). The transcriptional activity of Aft is regulated by mitochondrial Fe–S cluster biosynthesis via a signaling pathway not only involving the cytosolic monothiol Grxs but also the aminopeptidase P-like protein Fra1 (Fe-repressor of activation-1) and Fra2 (Fe-repressor of activation-2), a member of the ubiquitous BolA family of proteins (18-21). Moreover, recent *in vitro* studies

indicate that the Fe sensing mechanism involves a novel  $[\text{Fe}_2\text{S}_2]^{2+}$  cluster at the subunit interface of a Grx/Fra2 heterodimer, that is coordinated by the active sites cysteines of GSH and the monothiol CGFS Grx and the conserved histidine of Fra2 (7;15;25). The Fe and/or Fe–S cluster sensing role of the *S. cerevisiae* cytosolic monothiol Grxs, appears to be conserved in humans (26), and other fungi that utilize Fe-responsive transcription factors, even though their iron-responsive transcription factors are unknown or structurally unrelated to the *S. cerevisiae* Aft proteins (7;27;28). Furthermore, *in silico* genomic analysis has shown that genes encoding monothiol CGFS Grxs and BolA-type proteins are frequently found in adjacent positions in many prokaryotic organisms (2;29). This suggests that the monothiol Grx–BolA interaction might constitute a general requirement for Fe and/or Fe–S cluster sensing in organisms in which the two genes are present, and is supported by the recent characterization of a  $[\text{Fe}_2\text{S}_2]^{2+}$  cluster-bound *Ec* Grx4–BolA complex (30).

In this work, we present additional *in vitro* evidence in support of a role for monothiol CGFS Grxs in Fe–S cluster biogenesis by demonstrating facile  $[\text{Fe}_2\text{S}_2]^{2+}$  cluster exchange between monothiol Grxs and the ubiquitous A-type Fe–S cluster assembly proteins (termed IscA,  $\text{Nif}^{\text{IscA}}$ , and SufA in bacteria) which have been proposed to play an important role in both Fe and Fe–S cluster trafficking (31;32) and (see Appendices A and B).  $[\text{Fe}_2\text{S}_2]^{2+}$  cluster-bound forms of homodimeric monothiol Grxs are shown to be efficient and rapid cluster donors for A-type proteins. Coupled with *in vivo* evidence for monothiol CGFS Grx–A-type protein interaction (3;13), these results indicate that monothiol Grxs and A-type Fe–S assembly proteins work together in cellular Fe–S cluster trafficking and repair. Interestingly the direction of cluster transfer was found to be reversed with heterodimeric yeast Grx3–Fra2 complex. *In vitro* experiments show that the  $[\text{Fe}_2\text{S}_2]^{2+}$  cluster-bound form of the heterodimeric Grx3–Fra2

complex, can be formed by intact  $[\text{Fe}_2\text{S}_2]^{2+}$  cluster transfer from an A-type protein, in addition to displacement of one Grx3 monomer by Fra2, as previously demonstrated (25). This result raises the possibility that A-type proteins are involved with the mechanism of Fe and Fe–S cluster sensing in some organisms.

## Experimental procedures

*Materials:* Materials used in this work were of reagent grade and were purchased from Fischer Scientific, Sigma-Aldrich Chemical Co, Invitrogen, or VWR International, unless stated otherwise.

*Protein expression and purification:* The *A. vinelandii* <sup>Nif</sup>IscA gene, encoding the <sup>Nif</sup>IscA protein was amplified by PCR method and inserted into the expression plasmid PT7-7 as previously described (33). The resulting plasmid, pDB570 was transformed into the *E. coli* host BL21(DE3) and induced for high level expression of *A. vinelandii* <sup>Nif</sup>IscA and protein purification was carried out according to the published procedure (33).

The *A. thaliana* SufA1 (At1g10500) coding sequence was amplified by PCR from rosette cDNAs using AtSufA1for (5'CCCCCATGGCTGTTTCGATCCGCTTCGGTT3') and AtSufA1rev (5'CCCCGGATCCTCACATCTCGGCAGCAA3') primers and cloned into the pET3d vector. The amplified sequence encodes a protein devoid of the first 53 amino acids that corresponds to the putative plastidial targeting sequence. Owing to the use of the NcoI restriction site, a codon for an alanine has been added in the primer to keep the sequence in frame. The N-terminal protein sequence of the recombinant proteins starts thus with MAVRSASV. The recombinant plasmid, containing *At* SufA1 was transformed into the *E. coli* host BL21(DE3) and induced for high level expression of *At* SufA1 according to the following procedure. Cells were grown in LB media containing 100 mg mL<sup>-1</sup> ampicillin until OD600 reached 0.6–0.8 and

expression was induced by addition of IPTG to a final concentration of 0.8 mM. The cells were grown for an additional 4 hours before harvesting by centrifugation and stored at  $-80\text{ }^{\circ}\text{C}$ . The overexpressed protein was purified under both aerobic and anaerobic conditions. During the aerobic purification, cells ( $\sim 15\text{ g}$ ) were resuspended in 100 mM Tris-HCl, pH 7.8 (buffer A) with addition of  $10\text{ }\mu\text{g mL}^{-1}$  phenylmethylsulphonyl fluoride (PMSF),  $15\text{ }\mu\text{g mL}^{-1}$  DNase, and  $5\text{ ng mL}^{-1}$  RNase. The cells were then disrupted by sonication on ice followed by centrifugation at 17 000 rpm for 1 hour at  $4\text{ }^{\circ}\text{C}$ . Soluble proteins were then precipitated with 40% of ammonium sulfate saturation and centrifuged as above. The resulting pellet was resuspended in buffer A and loaded onto a 25 mL Q-Sepharose column, equilibrated with buffer A. Elution of *At* SufA1 was achieved with a 0–100% NaCl gradient using 100 mM Tris-HCl with 1 M NaCl at pH 7.8. Fractions containing *At* SufA1 protein were collected and concentrated down to 3 mL using YM-10 Amicon ultrafiltration and loaded onto a Superdex-75 column, equilibrated with 100 mM Tris-HCl, 150 mM NaCl, pH 7.8. Anaerobic purification was carried out in a glove box under Ar ( $<2\text{ ppm O}_2$ ). Except for the Superdex-75 column, the same procedure described above for aerobic purification was used. UV-visible spectra indicated that the product was apo *At* SufA1 irrespective of aerobic or anaerobic purification. In order to reduce disulfides or polysulfides, aerobically purified apo *At* SufA1 and  $A_V^{\text{Nif}}$  IscA were treated with 40 mM tris(2-carboxyethyl)-phosphine (TCEP) in the glove box under Ar atmosphere. Excess TCEP was removed using buffer A ( $10\text{ mL} \times 4$  times) in an YM10 Amicon ultrafiltration device prior to use for cluster reconstitution or cluster transfer studies.

Anaerobic purification of the reddish-brown cell-free extract containing *At* GrxS14 was carried out under Ar in a vacuum atmospheres glove box at  $\text{O}_2$  levels  $<2\text{ ppm}$  as previously described (12). For protein expression and purification of *S. cerevisiae* Grx3 and Fra2,

BL21(DE3) *E. coli* cells were transformed with pET21a-Grx3 and pET21a-Fra2 respectively and the resulting proteins produced in this strain were purified as previously described (15). Co-expression of Grx3 with Fra2 by transforming pET21a-Grx3 and pRSFDuet-1-Fra2 into the *E. coli* strain BL21(DE3) resulted in purification of the Fra2–Grx3 heterodimer complex. The reddish-brown cell-free extract containing Fra2–Grx3 was purified aerobically as previously described (15). For *A. vinelandii* Grx-nif, His-tagged Grx-nif was overexpressed in *E. coli* strain BL21(DE3) according to published procedure (12). The reddish-brown cells were harvested by centrifugation at 5000g for 15 min at 4 °C and stored at –80 °C until further use. Anaerobic purification of Grx-nif was carried out under Ar in a vacuum atmosphere glove box at O<sub>2</sub> levels <2 ppm. 8 g of reddish-brown cells were thawed and resuspended in 50 mL of buffer A (50 mM Tris-HCl, pH 7.8, containing 1 mM GSH). 10 µg mL<sup>-1</sup> PMSF, 15 µg mL<sup>-1</sup> DNase (Roche) and 5 ng mL<sup>-1</sup> RNase (Roche) were added to the mixture. The cells were lysed by sonication, and cell debris was removed by centrifugation at 39 700g for 1 h at 4 °C. The reddish-brown cell-free extract containing Grx-nif was subjected to 40% ammonium sulfate cut followed by centrifugation. The resulting reddish-brown pellet was resolubilized in binding buffer (50 mM Tris-HCl, pH 7.8, containing 1 mM GSH, 0.5 M NaCl, 20 mM imidazole, and 10% glycerol) and loaded onto a 3 × 5 mL His-Trap HP column (GE Healthcare) previously equilibrated with binding buffer. The column was washed with 10 column volumes of binding buffer before the protein of interest was eluted with a 20–500 mM imidazole gradient. The purest fractions, as judged by SDS-PAGE analysis, were eluted with 300 mM imidazole and were pooled together and concentrated by ultrafiltration using a YM-10 membrane.

*Preparation of apo Grx-nif and Fra2–Grx3 heterodimer:* Apo *A. vinelandii* Grx-nif was prepared by incubating the as-purified cluster-bound Grx-nif anaerobically with 50-fold excess

EDTA and 20-fold excess potassium ferricyanide for 60 min on ice. The protein was then buffer exchanged into buffer A using a two sequential 5 mL desalting column (GE Healthcare) and the resulting apo-protein was concentrated via Amicon ultrafiltration using a YM10 membrane. Apo Fra2–Grx3 heterodimer was prepared as previously described (15).

*Fe–S cluster reconstitution on Av<sup>Nif</sup>IscA, At SufA1, At GrxS14, Sc Grx3, and Av Grx-nif:*

[Fe<sub>2</sub>S<sub>2</sub>]<sup>2+</sup> cluster-bound homodimeric *A. vinelandii* <sup>Nif</sup>IscA was prepared under anaerobic conditions starting with TCEP-pretreated apo protein via NifS-mediated cluster assembly in the presence of ferrous ammonium sulfate and L-cysteine and was purified as previously described (33). A similar procedure was used for preparing the [Fe<sub>2</sub>S<sub>2</sub>]<sup>2+</sup> cluster-bound homodimeric *At* SufA1. Reconstitution involved incubating apo *At* SufA1 (0.5 mM) with 8 mM L-cysteine and ferrous ammonium sulfate in the presence of catalytic *Av* NifS (10 μM) at room temperature in buffer A for 60 min and repurifying using a Q-Sepharose column. The resulting samples of *Av* <sup>Nif</sup>IscA and *At* SufA1 contained 0.80 ± 0.10 and 0.62 ± 0.05 [Fe<sub>2</sub>S<sub>2</sub>] clusters per homodimer, respectively, based on protein and Fe determinations. Homogeneous samples of *Sc* Grx3 and *At* GrxS14 containing one [Fe<sub>2</sub>S<sub>2</sub>]<sup>2+</sup> per homodimer were prepared as previously described (12;15). For *Av* Grx-nif, NifS-mediated reconstitution was carried out by incubating 1 mM apo Grx with 3 mM GSH, catalytic amounts of *Av* NifS (10 μM), 6-fold excess of both Fe(II) (ferrous ammonium sulfate) and L-cysteine. The reconstitution mixture was incubated under strictly anaerobic conditions for 2 hours on ice with occasional stirring, before being loaded onto two sequential 5 mL Hi-Trap Q-Sepharose columns (GE Healthcare) previously equilibrated with buffer A and eluted with a 0.0–1.0 M NaCl gradient. The reddish-brown fractions were pooled and concentrated via Amicon ultrafiltration using a YM10 membrane. The resulting samples contained 1.0 ± 0.1 [Fe<sub>2</sub>S<sub>2</sub>] cluster per homodimer based on protein and Fe determinations.

*Analytical and spectroscopic methods:* Protein concentrations were determined using bovine serum albumin as a standard (Roche) with BioRad Dc protein assay in conjunction with the microscale modified procedure of Brown et al (34). Iron concentrations were determined after  $\text{KMnO}_4/\text{HCl}$  protein digestion as described by Fish (35), using a 1000 ppm atomic absorption iron standard to prepare standard solutions of known Fe concentration (Fluka). Samples for all spectroscopic investigations were prepared under an argon atmosphere in a glove box (vacuum atmosphere, Hawthorne, CA) at  $\text{O}_2$  levels  $<2$  ppm. UV-visible CD spectra were recorded under anaerobic conditions in septum-sealed 1 mm quartz cuvettes or 1 cm semi-micro cuvettes at room temperature using a JASCO J-715 spectropolarimeter (Jasco, Easton, MD). Kinetic data for cluster transfer experiments were analyzed using the Chemical Kinetics Simulator software package (IBM).

*Fe-S cluster transfer experiments from monothiol CGFS Grxs to apo Av NifIscA or At SufA1:* The time course of cluster transfer from  $[\text{Fe}_2\text{S}_2]^{2+}$  cluster-loaded forms of *At* GrxS14, *Sc* Grx3, and *Av* Grx-nif to either apo *Av*  $^{\text{Nif}}$ IscA or *At* SufA1 were monitored under anaerobic conditions in 1 cm semi-micro cuvettes at room temperature using UV-visible CD spectroscopy.  $\Delta\epsilon$  values are based on  $[\text{Fe}_2\text{S}_2]^{2+}$  cluster concentrations of the reconstituted and repurified Grx samples used in this work, as determined by protein and Fe determinations. Mössbauer studies of  $[\text{Fe}_2\text{S}_2]^{2+}$  cluster-loaded *At* GrxS14 and *Sc* Grx3 have previously demonstrated that all the Fe in these samples is in the form of  $[2\text{Fe-2S}]^{2+}$  clusters (12;15). The cluster transfer percentage in the kinetic plots were assessed based on the difference in the initial and resultant  $[\text{Fe}_2\text{S}_2]^{2+}$  cluster  $\Delta\epsilon$  values at a fixed wavelength, with 100% corresponding to difference in the  $\Delta\epsilon$  values for the  $[\text{Fe}_2\text{S}_2]$  clusters exclusively on the donor and acceptor species. Reactions were carried out in 100 mM Tris-HCl buffer at pH 7.8 (2 mM DTT was also present in the *At* GrxS14-to-*At* SufA1

cluster transfer reaction mixture) and the final reaction mixture was 50  $\mu\text{M}$  in apo  $\text{Av}^{\text{Nif}}\text{IscA}$  or apo  $\text{At SufA1}$  dimer and 50  $\mu\text{M}$  in  $[\text{Fe}_2\text{S}_2]^{2+}$  clusters on homodimeric  $\text{At GrxS14}$ ,  $\text{Sc Grx3}$ , or  $\text{Av Grx-nif}$ , unless otherwise indicated.

*Fe–S cluster transfer experiments from  $\text{Av}^{\text{Nif}}\text{IscA}$  to apo  $\text{Sc Fra2-Grx3}$  heterodimer:* The time course of cluster transfer from  $\text{Av}^{\text{Nif}}\text{IscA}$  to apo  $\text{Sc Fra2-Grx3}$  heterodimer was monitored under anaerobic conditions in 1 cm semi-micro cuvettes at room temperature using UV-visible CD spectroscopy.  $\Delta\epsilon$  values are based on  $[\text{Fe}_2\text{S}_2]^{2+}$  cluster concentrations on reconstituted and repurified  $\text{Av}^{\text{Nif}}\text{IscA}$ , as determined by protein and Fe determinations (see Appendix B). Mössbauer studies of  $[\text{Fe}_2\text{S}_2]^{2+}$  cluster-loaded  $\text{Av}^{\text{Nif}}\text{IscA}$  and  $\text{Sc Fra2-Grx3}$  have previously demonstrated that all the Fe is in the form of  $[\text{Fe}_2\text{S}_2]^{2+}$  clusters ((15) and Appendix B). Reactions were carried out in 100 mM Tris-HCl buffer at pH 7.8 containing 2 mM GSH and the final reaction mixture was 50  $\mu\text{M}$  in apo  $\text{Fra2-Grx3}$  heterodimer and 50  $\mu\text{M}$  in  $[\text{Fe}_2\text{S}_2]^{2+}$  clusters on homodimeric  $\text{Av}^{\text{Nif}}\text{IscA}$ .

## Results

*In vitro cluster transfer from  $[\text{Fe}_2\text{S}_2]^{2+}$  cluster-bound monothiol CGFS Grxs to apo  $\text{Av}^{\text{Nif}}\text{IscA}$ :* The intensity and exquisite sensitivity of the UV-visible CD spectra of biological  $[\text{Fe}_2\text{S}_2]^{2+}$  clusters to the asymmetry of the cluster environment, has made CD spectroscopy the method of choice for monitoring the kinetics of interprotein  $[\text{Fe}_2\text{S}_2]^{2+}$  cluster transfer ((12;36) and Chapter 3). The  $[\text{Fe}_2\text{S}_2]^{2+}$  centers on all three monothiol CGFS Grxs investigated in this work,  $\text{At GrxS14}$ ,  $\text{Sc Grx3}$ , and  $\text{Av Grx-nif}$ , have distinct and intense UV-visible CD spectra compared to the  $[\text{Fe}_2\text{S}_2]^{2+}$  clusters on  $\text{At SufA1}$  and  $\text{Av}^{\text{Nif}}\text{IscA}$ , see Figure C.1. UV-visible CD spectra with  $\Delta\epsilon$  values quantified based on the  $[\text{Fe}_2\text{S}_2]^{2+}$  cluster concentrations, therefore

provides a convenient method for quantitatively monitoring cluster transfer reactions involving these proteins based on changes in the  $\Delta\epsilon$  values at discrete wavelengths.

UV-visible CD spectroscopy was used to investigate the potential role of monothiol Grxs in Fe–S cluster trafficking by monitoring cluster transfer experiments from three recombinant monothiol Grxs, plant chloroplast *At* GrxS14, yeast cytosolic *Sc* Grx3 and bacterial *Av* Grx-nif, to bacterial *Av* <sup>Nif</sup>IscA and from plant chloroplast *At* GrxS14 to *At* SufA1. The time course of CD-monitored, room-temperature cluster transfer reactions from the subunit-bridging  $[\text{Fe}_2\text{S}_2]^{2+}$  cluster-bound forms of the dimeric monothiol Grxs to the apo form of dimeric A-type proteins using a 1 : 1 donor : acceptor  $[\text{Fe}_2\text{S}_2]^{2+}$  cluster stoichiometry, except for the *Av* Grx-nif to *Av* <sup>Nif</sup>IscA cluster transfer reaction which has a 1 : 1.67 donor : acceptor stoichiometry, are shown in Figure C.2. In each case, rapid and quantitative cluster transfer occurs, as judged by the CD  $\Delta\epsilon$  values for the  $[\text{Fe}_2\text{S}_2]^{2+}$  centers assembled on the A-type acceptor proteins, see Figure C.1. The stoichiometric cluster transfers from  $[\text{Fe}_2\text{S}_2]^{2+}$  cluster-bound *At* GrxS14 and *Sc* Grx3 to apo *Av* <sup>Nif</sup>IscA and from *At* GrxS14 to *At* SufA1 are more than 95% complete before the first CD spectrum is recorded (after 3 min), suggesting a second order rate constant for cluster transfer of  $\geq 50\,000\text{ M}^{-1}\text{ min}^{-1}$ . This lower-limit estimate of the rate constant is based on a more detailed kinetic analysis for the *At* GrxS14 to *At* SufA1 cluster transfer in which the time course was monitored continuously at 348 nm (see inset in Figure C.2D). Based on the initial concentration of  $[\text{Fe}_2\text{S}_2]^{2+}$  clusters on *At* GrxS14 (50  $\mu\text{M}$ ) and the concentration of the dimeric *At* SufA1 acceptor protein (50  $\mu\text{M}$ ), the data was well fit by simulated second order kinetics with a rate constant of  $50\,000\text{ M}^{-1}\text{ min}^{-1}$ . The rate constant for the  $[\text{Fe}_2\text{S}_2]^{2+}$  cluster transfer from *Av* Grx-nif to apo *Av* <sup>Nif</sup>IscA was assessed by continuously monitoring the time course at 343 nm, see inset in Figure C.2C. Based on the initial concentration of  $[\text{Fe}_2\text{S}_2]^{2+}$  clusters on *Av* Grx-nif (42  $\mu\text{M}$ )

and the concentration of the dimeric  $Av^{Nif}IscA$  acceptor protein (70  $\mu M$ ), the data were well fit by simulated second order kinetics with a rate constant of 22 000  $M^{-1} min^{-1}$ . These rates of cluster transfer are clearly in the physiologically relevant range and are similar or significantly faster than those previously reported for  $[Fe_2S_2]^{2+}$  cluster-bound GrxS14 to apo plant-type ferredoxin (20 000  $M^{-1} min^{-1}$ ) (12) or HscA/HscB/ATP-mediated  $[Fe_2S_2]^{2+}$  cluster-bound IscU to apo Isc Fdx (800  $M^{-1} min^{-1}$ ) (36).

The cluster transfer is unidirectional, as the reverse reaction involving reaction mixtures containing the same concentrations of  $[Fe_2S_2]^{2+}$  cluster-bound  $NifIscA$  and apo monomeric monothiol Grxs, in the presence of 3 mM GSH, showed no change in the CD spectrum after 60 min of reaction (data not shown). Control experiments monitored by UV-visible CD spectroscopy also revealed no change in the CD spectra of the  $[Fe_2S_2]^{2+}$  cluster-bound GrxS14, Grx3 and Grx-nif in the absence of apo A-type proteins on incubating at room temperature for 30 min under anaerobic conditions respectively (data not shown). Additional CD evidence for intact cluster transfer was provided by the observation that the addition of 1 mM EDTA did not significantly affect the rate or extent of these cluster transfer reactions and that <10%  $[Fe_2S_2]^{2+}$  cluster assembly on  $Av^{Nif}IscA$  or *At SufA1* occurred after 30 min when cluster-loaded Grxs were replaced in the cluster transfer reaction mixture with equivalent amounts of  $S^{2-}$  and  $Fe^{2+}$  (data not shown). These control experiments demonstrate that the  $[Fe_2S_2]^{2+}$  clusters on the A-type proteins investigated in this study are derived from the  $[Fe_2S_2]^{2+}$  clusters on the Grxs via intact cluster transfer rather than via cluster degradation and reassembly on apo A-type proteins.

*In vitro* cluster transfer from  $[Fe_2S_2]^{2+}$  cluster-bound *A. vinelandii NifIscA* to apo *S. cerevisiae Fra2-Grx3* heterodimer: Previous studies have shown that coexpression of recombinant *Sc Fra2* with *Sc Grx3* in *E. coli* results in purification of a stable  $[2Fe-2S]^{2+}$  cluster-

containing Fra2–Grx3 heterodimeric complex (15). The cluster can be removed in the presence of large excesses of metal chelators and ferricyanide to yield a stable apo form of the Fra2–Grx3 heterodimer (15). Moreover, recent *in vivo* mutagenesis studies of the cluster-ligating His and Cys residues on Fra2 and Grx3, respectively, indicate that  $[\text{Fe}_2\text{S}_2]^{2+}$  cluster-bound form of the Fra2–Grx3 heterodimeric complex plays a crucial role in controlling the Fe regulon in yeast (15;25). In an attempt to establish if the cluster-bound form of Fra2–Grx3 heterodimer can be generated by intact cluster transfer from a hitherto unidentified donor protein as well as via Fra2 displacement of one Grx3 monomer in the  $[\text{Fe}_2\text{S}_2]^{2+}$  cluster-bound Grx3 homodimer, as previously demonstrated (25), we have investigated the ability of  $[\text{Fe}_2\text{S}_2]^{2+}$  clusterbound  $^{\text{Nif}}$ IscA to transfer a  $[\text{Fe}_2\text{S}_2]^{2+}$  cluster to the apo Fra2–Grx3 heterodimer.

The  $[\text{Fe}_2\text{S}_2]^{2+}$  center on  $^{\text{Nif}}$ IscA has a distinct UV-visible CD spectrum compared to that of the  $[\text{Fe}_2\text{S}_2]^{2+}$  center on Fra2–Grx3, making CD a very effective method for monitoring cluster transfer, see Figure C.3. The time course of CD-monitored room-temperature cluster transfer from  $[\text{Fe}_2\text{S}_2]^{2+}$  cluster-bound  $^{\text{Nif}}$ IscA to apo Fra2–Grx3 heterodimer using a 1 : 1 donor : acceptor cluster stoichiometry in a buffer containing 2 mM GSH under anaerobic conditions is shown in Figure C.4. These results indicate quantitative cluster transfer that is complete after approximately 120 min as evidenced by 100% conversion of the donor CD spectrum to that of the acceptor CD spectrum on the basis of the  $[\text{Fe}_2\text{S}_2]^{2+}$  cluster  $\Delta\varepsilon$  values. More detailed kinetic analysis was carried out by monitoring the change in CD intensity as a function of time at 320 nm, see inset in Figure C.4. Kinetic analysis based on initial  $[\text{Fe}_2\text{S}_2]^{2+}$  cluster concentration on the  $^{\text{Nif}}$ IscA donor (50  $\mu\text{M}$ ) and initial apo Fra2–Grx3 complex concentration (50  $\mu\text{M}$ ) indicates second order kinetics with a rate constant of 15 000  $\text{M}^{-1} \text{min}^{-1}$ . The reverse reaction did not occur to an appreciable extent after 120 min and control experiments showed that the  $[\text{Fe}_2\text{S}_2]^{2+}$

cluster on <sup>Nif</sup>IscA is stable over the time period of the reaction in the absence of the Fra2–Grx3 heterodimer and that equivalent amounts of Fe<sup>2+</sup> and S<sup>2-</sup> in place of cluster-loaded <sup>Nif</sup>IscA result in <5% [Fe<sub>2</sub>S<sub>2</sub>]<sup>2+</sup> cluster formation on the Fra2–Grx3 heterodimer after 120 min. Hence, although not as fast as [Fe<sub>2</sub>S<sub>2</sub>]<sup>2+</sup> cluster transfer from monothiol CGFS Grxs to <sup>Nif</sup>IscA, the results indicate that the Fra2–Grx3 heterodimer can receive clusters via intact cluster transfer from an A-type cluster donor and that Fra2 binding in place of one of the Grx3 monomers reverses the direction of cluster transfer with respect to Grx3/<sup>Nif</sup>IscA [Fe<sub>2</sub>S<sub>2</sub>]<sup>2+</sup> cluster exchange. We conclude that Fra2 or BolA-type protein binding converts monothiol Grxs from cluster donors to net cluster acceptors with respect to A-type proteins.

## Discussion

*Monothiol Grxs as cluster donors to A-type proteins in cellular Fe–S cluster trafficking:* Recent *in vitro* and *in vivo* studies of the ubiquitous A-type Fe–S cluster biogenesis proteins indicate a role as cluster carriers for the delivery of assembled on primary scaffold proteins (NifU in the NIF system; IscU in the iron sulfur cluster (ISC) system; SufB in the sulfur utilization factor (SUF) system) to acceptor proteins ((32;37;38) and Appendix B) Moreover, the ability of A-type proteins to bind mononuclear Fe<sup>2+,3+</sup> ((31) and Appendix A), accept [2Fe-2S]<sup>2+</sup> clusters formed on primary scaffold proteins ((37-39) and Appendix B) and reversibly convert between [Fe<sub>2</sub>S<sub>2</sub>]<sup>2+</sup> and [Fe<sub>4</sub>S<sub>4</sub>]<sup>2+</sup> cluster-bound forms in response to cellular redox status and/or oxygen levels (Appendix B), are likely to be important for their key role in the maturation or repair of [Fe<sub>4</sub>S<sub>4</sub>] clusters in mitochondrial proteins (40-42) and in bacterial proteins under aerobic growth or oxidative stress conditions (43;44).

The work reported herein provides additional support for the proposal that A-type proteins function as Fe–S cluster carrier proteins by demonstrating that [Fe<sub>2</sub>S<sub>2</sub>]<sup>2+</sup> cluster-bound

monothiol CGFS Grxs are very efficient  $[\text{Fe}_2\text{S}_2]^{2+}$  cluster donors for A-type proteins. Moreover, the recent demonstration of rapid, ATP-dependent cluster transfer from *Av*  $[\text{Fe}_2\text{S}_2]^{2+}$ -IscU to *Av* Grx5 only in the presence of the dedicated HscA/HscB molecular co-chaperone system (Ssq1/Jac1 and HSPA9/HSC20 in yeast and human mitochondria, respectively) (6;45), suggests that monothiol Grxs are likely to play a key role in storing and transporting  $[\text{Fe}_2\text{S}_2]^{2+}$  clusters assembled on IscU primary scaffold proteins in the bacterial ISC system and in eukaryotic mitochondria (Chapter 3). In contrast, we have failed to demonstrate ATP-dependent cluster transfer from *Av*  $[\text{Fe}_2\text{S}_2]^{2+}$ -IscU to apo *Av* IscA in the presence of the dedicated HscA/HscB co-chaperone system (S. Randeniya, P. Shakamuri, and M. K. Johnson, unpublished work). Consequently it seems likely that monothiol Grxs mediate  $[\text{Fe}_2\text{S}_2]^{2+}$  clusters transfer from IscU to IscA proteins in the bacterial ISC system and eukaryotic mitochondria. The means by which monothiol Grxs associated with the NIF and SUF systems obtain their  $[\text{Fe}_2\text{S}_2]^{2+}$  clusters has yet to be determined, but is under active investigation in our laboratories.

The only partner proteins of potential physiological relevance that have been shown to exhibit rapid  $[\text{Fe}_2\text{S}_2]^{2+}$  cluster transfer in this work are *Av* Grx-nif to  $^{\text{Nif}}$ IscA and chloroplast *At* GrxS14 to SufA1. However, A-type proteins are highly conserved in the bacterial NIF, ISC, and SUF Fe-S cluster assembly systems as well as in mitochondria and chloroplasts (42;46-48), and monothiol Grxs are present in most bacteria and as well as the mitochondria, chloroplasts and cytosol of eukaryotes (5). Coupled with the evidence that monothiol Grxs exist in cluster-bound forms *in vivo* in the cytosol of yeast (17), and that monothiol Grxs and A-type proteins interact *in vivo* in yeast mitochondria (3;13), it seems likely that rapid  $[\text{Fe}_2\text{S}_2]^{2+}$  cluster transfer from monothiol Grxs to A-type proteins is a physiologically relevant cluster transfer reaction. Moreover, the rapid  $[\text{Fe}_2\text{S}_2]^{2+}$  cluster transfer observed for the non-physiological chloroplast *At*

GrxS14-to-Av<sup>Nif</sup>IscA and *Sc* Grx3-to-Av<sup>Nif</sup>IscA cluster transfer reactions indicates that this process is not specific to physiologically relevant cluster transfer partners. Indeed [Fe<sub>2</sub>S<sub>2</sub>]<sup>2+</sup> cluster transfer from cytosolic *Sc* Grx3 to an A-type protein is very unlikely to be physiologically relevant, as there is no evidence for an A-type Fe–S cluster protein in the yeast cytosol (47;49). Nevertheless, the observation of fast, efficient and quantitative cluster transfer from monothiol Grxs to A-type Fe–S cluster assembly proteins clearly support the proposal that monothiol Grxs and A-type proteins are partners in cellular Fe–S cluster trafficking.

A schematic proposal for the roles of monothiol Grxs and A-type proteins in cluster trafficking to facilitate the maturation or repair of [Fe<sub>4</sub>S<sub>4</sub>] clusters via the ISC system for Fe–S cluster biogenesis is presented in Appendix Figure.C.5. The initial step involves ATP-dependent cluster transfer from [Fe<sub>2</sub>S<sub>2</sub>]-IscU to apo-Grx in the presence of the dedicated HscA/HscB cochaperone system (Chapter 3). This is followed by cluster transfer from [Fe<sub>2</sub>S<sub>2</sub>]-Grx to apo-IscA to yield [Fe<sub>2</sub>S<sub>2</sub>]-IscA. Based on the available crystallographic data (50), the [Fe<sub>2</sub>S<sub>2</sub>] cluster in the IscA dimer is asymmetrically ligated by three cysteines from one monomer and one cysteine from the other monomer. This asymmetric ligation is likely to be crucial for the ability to reversibly convert between forms containing one [Fe<sub>2</sub>S<sub>2</sub>] or one [Fe<sub>4</sub>S<sub>4</sub>] per homodimer in response to cellular conditions as recently demonstrated with <sup>Nif</sup>IscA (Appendix B). Anaerobic conditions, coupled with the presence a two-electron donor such as DTT, result in the conversion from [Fe<sub>2</sub>S<sub>2</sub>]-<sup>Nif</sup>IscA to [Fe<sub>4</sub>S<sub>4</sub>]-<sup>Nif</sup>IscA, which is reversed on exposure to air in the presence of apo-IscA (Appendix B). Hence [Fe<sub>4</sub>S<sub>4</sub>]-IscA is likely to be responsible for the maturation or repair of apo [Fe<sub>4</sub>S<sub>4</sub>] cluster-containing proteins only under anaerobic conditions.

An alternative mechanism for the assembly or repair of oxygen-damaged [Fe<sub>4</sub>S<sub>4</sub>] clusters that uses [Fe<sub>2</sub>S<sub>2</sub>]<sup>2+</sup> cluster-bound A-type proteins is also proposed in Figure C.5. This proposal

originates from the recent *in vivo* evidence that an Fe-bound form of the Isa1–Isa2 dimer, along with  $[\text{Fe}_2\text{S}_2]$  clusters ultimately supplied by Isu1 or Isu2, are essential for the maturation of  $[\text{Fe}_4\text{S}_4]$  cluster-containing mitochondrial proteins in *S. cerevisiae* under both aerobic and anaerobic conditions (42). Taken together with recent studies of the *E. coli* fumarate nitrate reduction regulatory protein, which demonstrate  $[\text{Fe}_4\text{S}_4]^{2+}$  clusters formation by addition of  $\text{Fe}^{2+}$  to a  $[\text{Fe}_2\text{S}_2]^{2+}$  cluster ligated by two cysteines and two cysteine persulfides (Chapter 5), this provides the basis for a mechanism for the maturation or repair of  $\text{O}_2$ -damaged  $[\text{Fe}_4\text{S}_4]$  cluster-containing proteins using A-type proteins, that may be operative under aerobic or anaerobic conditions (Appendices A and B) The starting point would be an apo protein containing two cysteine persulfides, generated by a cysteine desulfurase or via  $\text{O}_2$ -induced degradation of a protein-bound  $[\text{Fe}_4\text{S}_4]$  cluster, as originally demonstrated in aconitase by Kennedy and Beinert (51). Incorporation of a  $[\text{Fe}_2\text{S}_2]^{2+}$  cluster, assembled initially on IscU and transferred to the acceptor protein by IscA via a monothiol Grx, would result in a  $[\text{Fe}_2\text{S}_2]^{2+}$  cluster ligated by two cysteines and two cysteine persulfides. The final step would involve in situ  $[\text{Fe}_4\text{S}_4]^{2+}$  cluster assembly, by addition of  $\text{Fe}^{2+}$  supplied by Fe-bound IscA. This proposal is presented in the spirit of a working hypothesis that provides a basis for future experiments.

*Monothiol Grxs as sensors of cellular iron and/or Fe–S cluster status:* The proposal that monothiol Grxs provide a dynamic capacity for storage and transfer of  $[\text{Fe}_2\text{S}_2]^{2+}$  clusters assembled on primary scaffold proteins also provides a rationalization for the involvement of the yeast cytosolic monothiol Grxs, *Sc* Grx3 and Grx4, in sensing the cellular Fe and Fe–S cluster status. *In vivo* studies have demonstrated that the yeast iron regulon responds to mitochondrial Fe–S cluster biosynthesis rather than cytosolic Fe levels (52), and is regulated by the formation of an iron-dependent complex in the cytosol involving Grx3, Grx4, Fra1 and the BolA homolog,

Fra2, that interacts with cytosolic Aft in the Fe replete form in order to prevent Aft migration into the nucleus where it activates the Fe regulon (19;21). The combination of *in vitro* and *in vivo* studies of wild-type and mutated proteins indicate that the Fe sensing mechanism involves the formation of a stable histidyl- and cysteinyl-ligated  $[\text{Fe}_2\text{S}_2]^{2+}$  cluster at the subunit interface of the Fra2–Grx3/4 heterodimer (7;15;25). Consequently the concentration of stored Fe–S clusters on Grx3 and Grx4 can be assessed without significantly perturbing the apo/holo Grx equilibrium by interaction with Fra2, provided that Fra2 can replace one of the Grx molecules in the homodimer with high binding affinity and the cellular concentration of Fra2 is much less than that of Grx3 or 4. Hence the observation of high affinity binding of Fra2 to holo-Grx3/4 to form the Fra2–Grx3/4 heterodimeric complex provides a plausible hypothesis for Fe or Fe–S cluster sensing mechanism that controls the yeast Fe regulon (7;25).

An alternative sensing mechanism is suggested by the observation that the apo Fra2–Grx3 heterodimer is able to accept a  $[\text{Fe}_2\text{S}_2]^{2+}$  cluster from an A-type Fe–S cluster assembly protein. This mechanism is not relevant to the regulation of the yeast Fe regulon, because of the lack of A-type proteins in the yeast cytosol (47;49). However, the presence of BolA-type proteins in bacteria and in eukaryotic mitochondria and chloroplasts (25;29), which contain single domain monothiol Grxs as well as A-type proteins leaves open the possibility that  $[\text{Fe}_2\text{S}_2]^{2+}$  cluster transfer from A-type proteins to apo Grx–BolA complexes may function as part of hitherto uncharacterized Fe or Fe–S cluster sensing mechanisms that are operative in bacteria, mitochondria and chloroplasts. This tentative proposal is supported by the report of a  $[\text{Fe}_2\text{S}_2]^{2+}$  cluster-bound Grx4–BolA complex in *E. coli* (30), and recent characterization of a *S. cerevisiae*  $[\text{Fe}_2\text{S}_2]^{2+}$  cluster-bound heterodimer involving mitochondrial Grx5 and the putative mitochondrial BolA-like protein, Aim1 (B. Zhang, A. Dlouhy, C. E. Outten, and M. K. Johnson,

unpublished results). *In vitro* studies involving bacterial and yeast mitochondria Grx–BoIA complexes and their corresponding A-type proteins are planned to test this hypothesis.

## References

1. Herrero, E. and de la Torre-Ruiz, M. A. (2007) Monothiol glutaredoxins: a common domain for multiple functions, *Cell. Mol. Life Sci.* 64, 1518-1530.
2. Couturier, J., Jacquot, J. P., and Rouhier, N. (2009) Evolution and diversity of glutaredoxins in photosynthetic organisms, *Cell Mol. Life Sci.* 66, 2539-2557.
3. Vilella, F., Alves, R., Rodriguez-Manzaneque, M. T., Belli, G., Swaminathan, S., Sunnerhagen, P., and Herrero, E. (2004) Evolution and cellular function of monothiol glutaredoxins: involvement in iron-sulphur cluster assembly, *Comp. Funct. Genom.* 5, 328-341.
4. Lillig, C. H., Berndt, C., and Holmgren, A. (2008) Glutaredoxin systems, *Biochim. Biophys. Acta.* 1780, 1304-1317.
5. Rouhier, N., Couturier, J., Johnson, M. K., and Jacquot, J. P. (2010) Glutaredoxins: roles in iron homeostasis, *Trends Biochem. Sci.* 35, 43-52.
6. Lill, R., Hoffmann, B., Molik, S., Pierik, A. J., Rietzschel, N., Stehling, O., Uzarska, M. A., Webert, H., Wilbrecht, C., and Muhlenhoff, U. (2012) The role of mitochondria in cellular iron-sulfur protein biogenesis and iron metabolism, *Biochim. Biophys. Acta* 1823, 1491-1508.
7. Li, H. and Outten, C. E. (2012) Monothiol CGFS Glutaredoxins and BolA-like Proteins: [2Fe-2S] Binding Partners in Iron Homeostasis, *Biochemistry* 51, 4377-4389.
8. Rodríguez-Manzaneque, M. T., Ros, J., Cabrito, I., Sorribas, A., and Herrero, E. (1999) Grx5 glutaredoxin plays a central role in protection against protein oxidative damage in *Saccharomyces cerevisiae*, *Mol. Cell. Biol.* 19, 8180-8190.
9. Rodríguez-Manzaneque, M. T., Tamarit, J., Bellí, G., Ros, J., and Herrero, E. (2002) Grx5 is a mitochondrial glutaredoxin required for the activity of iron/sulfur enzymes, *Mol. Biol. Cell* 13, 1109-1121.
10. Mühlenhoff, U., Gerber, J., Richhardt, N., and Lill, R. (2003) Components involved in assembly and dislocation of iron-sulfur clusters on the scaffold protein Iscu1p, *EMBO J.* 22, 4815-4825.
11. Molina-Navarro, M. M., Casas, C., Piedrafita, L., Bellí, G., and Herrero, E. (2006) Prokaryotic and eukaryotic monothiol glutaredoxins are able to perform the functions of Grx5 in the biogenesis of Fe/S clusters in yeast mitochondria, *FEBS Lett.* 580, 2273-2280.
12. Bandyopadhyay, S., Gama, F., Molina-Navarro, M. M., Gualberto, J. M., Claxton, R., Naik, S. G., Huynh, B. H., Herrero, E., Jacquot, J.-P., Johnson, M. K., and Rouhier, N. (2008) Chloroplast monothiol glutaredoxins as scaffold proteins for the assembly and delivery of [2Fe-2S] clusters, *EMBO J.* 27, 1122-1133.

13. Kim, K. D., Chung, W. H., Kim, H. J., Lee, K. C., and Roe, J. H. (2010) Monothiol glutaredoxin Grx5 interacts with Fe-S scaffold proteins Isa1 and Isa2 and supports Fe-S assembly and DNA integrity in mitochondria of fission yeast, *Biochem. Biophys. Res. Commun.* 392, 467-472.
14. Picciocchi, A., Saguez, C., Boussac, A., Cassier-Chauvat, C., and Chauvat, F. (2007) CGFS-type monothiol glutaredoxins from the cyanobacterium *Synechocystis* PCC6803 and other evolutionary distant model organisms possess a glutathione-ligated [2Fe-2S] cluster, *Biochemistry* 46, 15018-15026.
15. Li, H., Mapolelo, D. T., Dingra, N. N., Naik, S. G., Lees, N. S., Hoffman, B. M., Riggs-Gelasco, P. J., Huynh, B. H., Johnson, M. K., and Outten, C. E. (2009) The yeast iron regulatory proteins Grx3/4 and Fra2 form heterodimeric complexes containing a [2Fe-2S] cluster with cysteinyl and histidyl ligation, *Biochemistry* 48, 9569-9581.
16. Iwema, T., Picciocchi, A., Traore, D. A., Ferrer, J. L., Chauvat, F., and Jacquamet, L. (2009) Structural basis for delivery of the intact [Fe<sub>2</sub>S<sub>2</sub>] cluster by monothiol glutaredoxin, *Biochemistry* 48, 6041-6043.
17. Mühlenhoff, U., Molik, S., Godoy, J. R., Uzarska, M. A., Richter, N., Seubert, A., Zhang, Y., Stubbe, J., Pierrel, F., Herrero, E., Lillig, C. H., and Lill, R. (2010) Cytosolic monothiol glutaredoxins function in intracellular iron sensing and trafficking via their bound iron-sulfur cluster, *Cell Metab.* 12, 373-385.
18. Rutherford, J. C., Ojeda, L., Balk, J., Muhlenhoff, U., Lill, R., and Winge, D. R. (2005) Activation of the iron regulon by the yeast Aft1/Aft2 transcription factors depends on mitochondrial but not cytosolic iron-sulfur protein biogenesis, *J. Biol. Chem.* 280, 10135-10140.
19. Ojeda, L., Keller, G., Muhlenhoff, U., Rutherford, J. C., Lill, R., and Winge, D. R. (2006) Role of glutaredoxin-3 and glutaredoxin-4 in the iron regulation of the Aft1 transcriptional activator in *Saccharomyces cerevisiae*, *J. Biol. Chem.* 281, 17661-17669.
20. Pujol-Carrion, N., Belli, G., Herrero, E., Nogues, A., and de la Torre-Ruiz MA (2006) Glutaredoxins Grx3 and Grx4 regulate nuclear localisation of Aft1 and the oxidative stress response in *Saccharomyces cerevisiae*, *J. Cell Sci.* 119, 4554-4564.
21. Kumanovics, A., Chen, O., Li, L., Bagley, D., Adkins, E., Lin, H., Dingra, N. N., Outten, C. E., Keller, G., Winge, D., Ward, D. M., and Kaplan, J. (2008) Identification of FRA1 and FRA2 as genes involved in regulating the yeast iron regulon in response to decreased mitochondrial iron-sulfur cluster synthesis, *J. Biol. Chem.* 283, 10276-10286.
22. Yamaguchi-Iwai, Y., Dancis, A., and Klausner, R. D. (1995) AFT1: a mediator of iron regulated transcriptional control in *Saccharomyces cerevisiae*, *EMBO J.* 14, 1231-1239.
23. Casas, C., Aldea, M., Espinet, C., Gallego, C., Gil, R., and Herrero, E. (1997) The AFT1 transcriptional factor is differentially required for expression of high-affinity iron uptake genes in *Saccharomyces cerevisiae*, *Yeast* 13, 621-637.

24. Yamaguchi-Iwai, Y., Ueta, R., Fukunaka, A., and Sasaki, R. (2002) Subcellular localization of Aft1 transcription factor responds to iron status in *Saccharomyces cerevisiae*, *J. Biol. Chem.* 277, 18914-18918.
25. Li, H., Mapolelo, D. T., Dingra, N. N., Keller, G., Riggs-Gelasco, P. J., Winge, D. R., Johnson, M. K., and Outten, C. E. (2011) Histidine 103 in Fra2 is an iron-sulfur cluster ligand in the [2Fe-2S] Fra2-Grx3 complex and is required for in vivo iron signaling in yeast, *J. Biol. Chem.* 286, 867-876.
26. Li, H., Mapolelo, D. T., Randeniya, S., Johnson, M. K., and Outten, C. E. (2012) Human Glutaredoxin 3 Forms [2Fe-2S]-Bridged Complexes with Human BolA2, *Biochemistry* 51, 1687-1696.
27. Kaplan, C. D. and Kaplan, J. (2009) Iron acquisition and transcriptional regulation, *Chem. Rev.* 109, 4536-4552.
28. Mercier, A. and Labbe, S. (2009) Both Php4 function and subcellular localization are regulated by iron via a multistep mechanism involving the glutaredoxin Grx4 and the exportin Crm1, *J. Biol. Chem.* 284, 20249-20262.
29. Huynen, M. A., Spronk, C. A., Gabaldon, T., and Snel, B. (2005) Combining data from genomes, Y2H and 3D structure indicates that BolA is a reductase interacting with a glutaredoxin, *FEBS Lett.* 579, 591-596.
30. Yeung, N., Gold, B., Liu, N. L., Prathapam, R., Sterling, H. J., Williams, E. R., and Butland, G. (2011) The *E. coli* monothiol glutaredoxin GrxD forms homodimeric and heterodimeric FeS cluster containing complexes, *Biochemistry* 50, 8957-8969.
31. Ding, H. and Clark, R. J. (2004) Characterization of iron-binding in IscA, an ancient iron-sulfur cluster assembly protein, *Biochem. J.* 379, 433-440.
32. Vinella, D., Brochier-Armanet, C., Loiseau, L., Talla, E., and Barras, F. (2009) Iron-sulfur (Fe/S) protein biogenesis: phylogenomic and genetic studies of A-type carriers, *PLoS. Genet.* 5, e1000497.
33. Krebs, C., Agar, J. N., Smith, A. D., Frazzon, J., Dean, D. R., Huynh, B. H., and Johnson, M. K. (2001) IscA, an alternative scaffold for Fe-S cluster biosynthesis, *Biochemistry* 40, 14069-14080.
34. Brown, R. E., Jarvis, K. L., and Hyland, K. J. (1989) Protein measurement using bicinchoninic acid: elimination of interfering substances, *Anal. Biochem.* 180, 136-139.
35. Fish, W. W. (1988) Rapid colorimetric micromethod for the quantitation of complexed iron in biological samples, *Meth. Enzymol.* 158, 357-364.
36. Chandramouli, K. and Johnson, M. K. (2006) HscA and HscB stimulate [2Fe-2S] cluster transfer from IscU to apoferredoxin in an ATP-dependent reaction, *Biochemistry* 45, 11087-11095.

37. Ollagnier-de-Choudens, S., Sanakis, Y., and Fontecave, M. (2004) SufA/IscA: reactivity studies of a class of scaffold proteins involved with [Fe-S] cluster assembly, *J. Biol. Inorg. Chem.* 9, 828-838.
38. Gupta, V., Sendra, M., Naik, S. G., Chahal, H. K., Huynh, B. H., Outten, F. W., Fontecave, M., and Ollagnier de Choudens, S. (2009) Native *Escherichia coli* SufA, coexpressed with SufBCDSE, purifies as a [2Fe-2S] protein and acts as an Fe-S transporter to Fe-S target enzymes, *J. Am. Chem. Soc.* 131, 6149-6153.
39. Chahal, H. K., Dai, Y., Saini, A., Ayala-Castro, C., and Outten, F. W. (2009) The SufBCD Fe-S scaffold complex interacts with SufA for Fe-S cluster transfer, *Biochemistry* 48, 10644-10653.
40. Mühlenhoff, U., Gerl, M. J., Flauger, B., Pirner, H. M., Balsler, S., Richhardt, N., Lill, R., and Stolz, J. (2007) The iron-sulfur cluster proteins Isa1 and Isa2 are required for the function but not the de novo synthesis of the Fe/S clusters of biotin synthase in *Saccharomyces cerevisiae*, *Eukaryot. Cell* 6, 495-504.
41. Gelling, C., Dawes, I. W., Richhardt, N., Lill, R., and Muhlenhoff, U. (2008) Mitochondrial Iba57p is required for Fe/S cluster formation on aconitase and activation of radical SAM enzymes, *Mol. Cell. Biol.* 28, 1851-1861.
42. Mühlenhoff, U., Richter, N., Pines, O., Pierik, A. J., and Lill, R. (2011) Specialized function of yeast Isa1 and Isa2 in the maturation of mitochondrial [4Fe-4S] proteins, *J. Biol. Chem.* 286, 41205-41216.
43. Johnson, D. C., Unciuleac, M.-C., and Dean, D. R. (2006) Controlled expression and functional analysis of iron-sulfur cluster biosynthetic components within *Azotobacter vinelandii*, *J. Bacteriol.* 188, 7551-7561.
44. Tan, G., Lu, J., Bitoun, J. P., Huang, H., and Ding, H. (2009) IscA/SufA paralogues are required for the [4Fe-4S] cluster assembly in enzymes of multiple physiological pathways in *Escherichia coli* under aerobic growth conditions, *Biochem. J.* 420, 463-472.
45. Rouault, T. A. and Tong, W. H. (2008) Iron-sulfur cluster biogenesis and human disease, *Trends Genet.* 24, 398-407.
46. Johnson, D. C., Dean, D. R., Smith, A. D., and Johnson, M. K. (2005) Structure, function and formation of biological iron-sulfur clusters, *Annu. Rev. Biochem.* 74, 247-281.
47. Lill, R. (2009) Function and biogenesis of iron-sulphur proteins, *Nature* 460, 831-838.
48. Balk, J. and Pilon, M. (2011) Ancient and essential: The assembly of iron-sulfur clusters in plants, *Trends Plant Sci.* 16, 218-226.
49. Lill, R. and Muhlenhoff, U. (2008) Maturation of iron-sulfur proteins in eukaryotes: mechanisms, connected processes, and diseases, *Annu. Rev. Biochem.* 77, 669-700.

50. Morimoto, K., Yamashita, E., Kondou, Y., Lee, S. J., Arisaka, F., Tsukihara, T., and Nakai, M. (2006) The asymmetric IscA homodimer with an exposed [2Fe-2S] cluster suggests the structural basis of the Fe-S cluster biosynthetic scaffold, *J. Mol. Biol.* 360, 117-132.
51. Kennedy, M. C. and Beinert, H. (1988) The state of cluster SH and S<sup>2-</sup> of aconitase during cluster interconversions and removal. A convenient preparation of apoenzyme., *J. Biol. Chem.* 263, 8194-8198.
52. Chen, O. S., Crisp, R. J., Valachovic, M., Bard, M., Winge, D. R., and Kaplan, J. (2004) Transcription of the Yeast Iron Regulon Does Not Respond Directly to Iron but Rather to Iron-Sulfur Cluster Biosynthesis, *J. Biol. Chem.* 279, 29513-29518.

Figure C.1: Upper panel: comparison of the UV-visible CD spectra of the  $[\text{Fe}_2\text{S}_2]^{2+}$  cluster-bound forms of *A. vinelandii*  $^{\text{Nif}}$ IscA (black line) and *A. thaliana* SufA1 (purple line). Lower panel: comparison of the UV-visible CD spectra of the  $[\text{Fe}_2\text{S}_2]^{2+}$  cluster-bound forms of *A. thaliana* GrxS14 (green line), *A. vinelandii* Grx-nif (red line), and *S. cerevisiae* Grx3 (blue line). Spectra were recorded under anaerobic conditions in sealed 0.1 cm cuvettes in 100 nM Tris-HCl buffer with 250 mM NaCl at pH 7.8.  $\Delta\epsilon$  values are based on the  $[\text{Fe}_2\text{S}_2]^{2+}$  cluster concentrations.

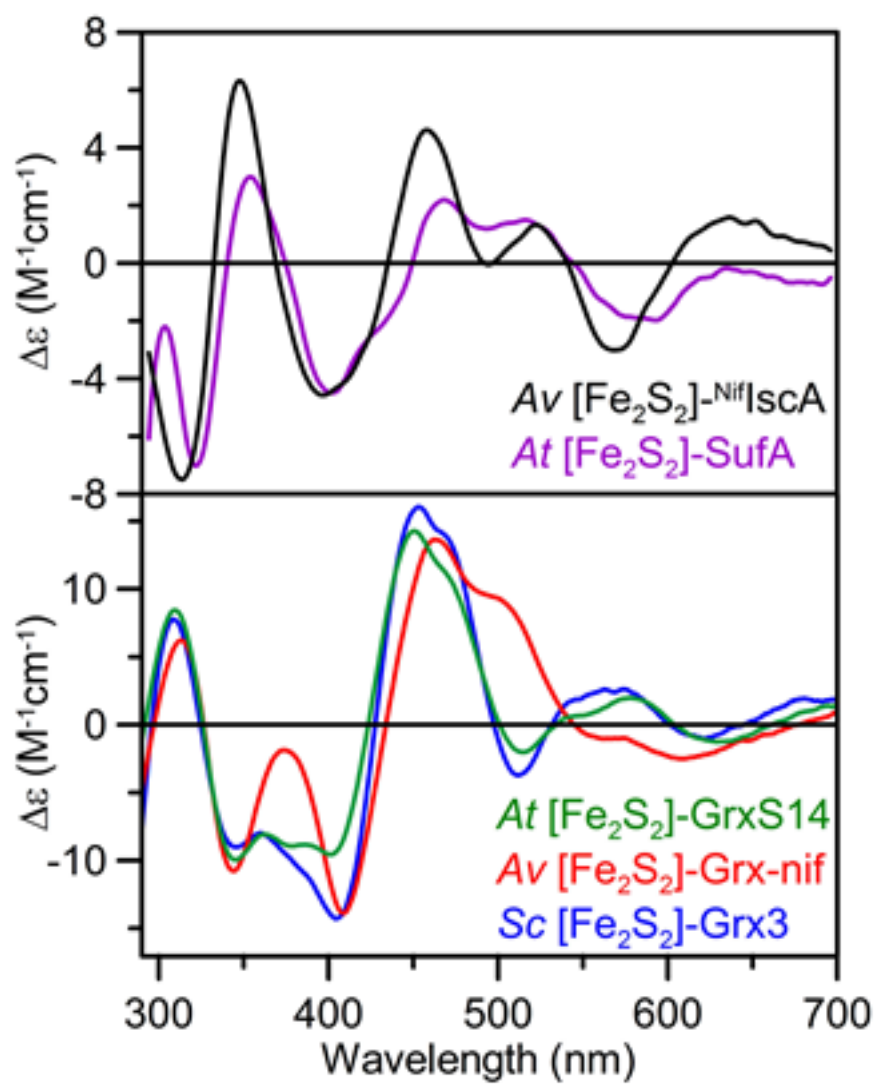


Figure C.2: Time course of cluster transfer from  $[\text{Fe}_2\text{S}_2]^{2+}$  cluster-bound forms of *At* GrxS14 (A), *Sc* Grx3 (B), and *Av* Grx-nif (C) to apo *Av*<sup>Nif</sup>IscA and of *At* GrxS14 to *At* SufA1 (D) monitored by UV-visible CD spectroscopy under anaerobic conditions in semi-micro 1 cm cuvettes at room temperature. UV-visible CD spectra were recorded prior to addition of apo *Av*<sup>Nif</sup>IscA or apo *At* SufA1 (thick line) and 3, 8, 12, 15, and 20 min after adding the apo A-type protein to the  $[\text{Fe}_2\text{S}_2]^{2+}$  cluster-bound Grx (thin black lines). The *At* GrxS14-to-*Av*<sup>Nif</sup>IscA (A), *Sc* Grx3-to-*Av*<sup>Nif</sup>IscA (B), and *At* GrxS14-to-*At* SufA1 (D) cluster transfer reactions were carried out with a 1 : 1 donor : acceptor  $[\text{Fe}_2\text{S}_2]^{2+}$  cluster stoichiometry (50  $\mu\text{M}$  apo A-type protein dimer and 50  $\mu\text{M}$   $[\text{Fe}_2\text{S}_2]^{2+}$  clusters on Grx). The *Av* Grx-nif-to-cluster transfer reaction was carried with a 1 : 1.67 donor : acceptor cluster stoichiometry (70  $\mu\text{M}$  apo *Av*<sup>Nif</sup>IscA and 42  $\mu\text{M}$   $[\text{Fe}_2\text{S}_2]^{2+}$  clusters on *Av* Grx-nif).  $\Delta\epsilon$  values are based on the initial  $[\text{Fe}_2\text{S}_2]^{2+}$  cluster concentration.

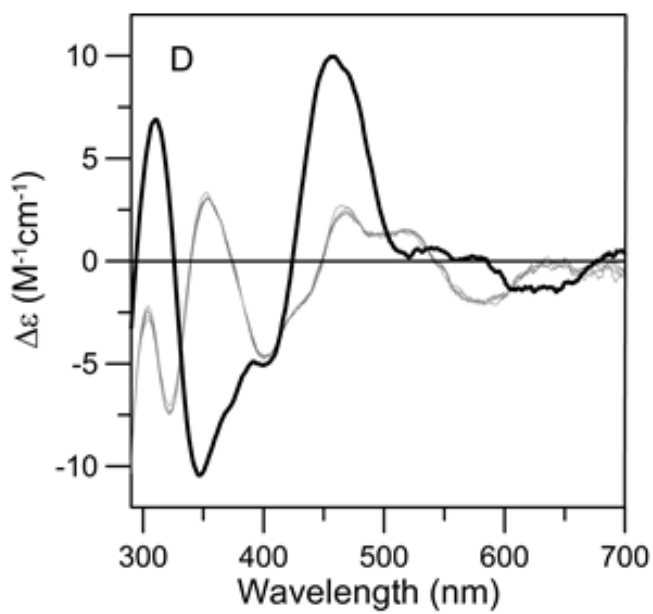
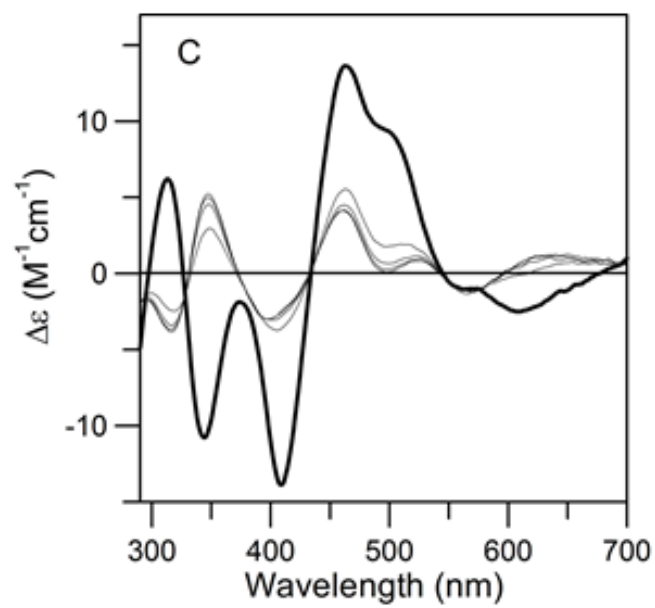
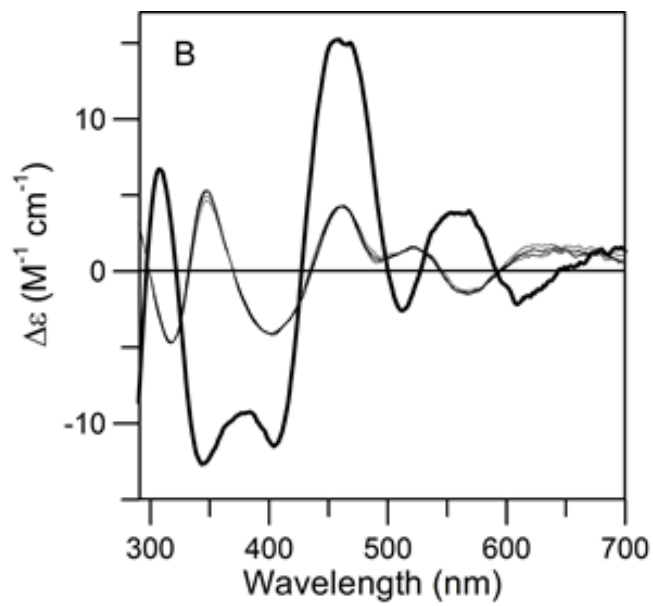
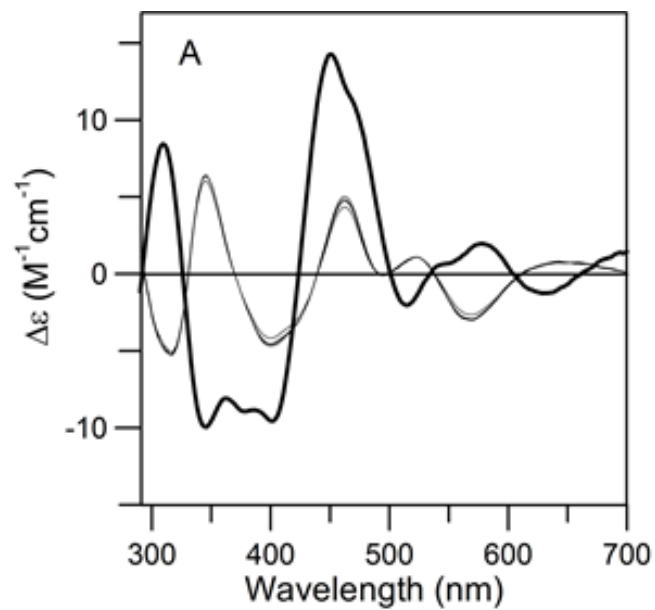


Figure C.3: Comparison of the UV-visible CD spectra of  $[\text{Fe}_2\text{S}_2]^{2+}$  cluster-bound *A. vinelandii*  $^{\text{Nif}}$ IscA (blue line) and  $[\text{Fe}_2\text{S}_2]^{2+}$  cluster-bound *S. cerevisiae* Grx3–Fra2 (red line). Spectra were recorded under anaerobic conditions in sealed 0.1 cm cuvettes for  $[\text{Fe}_2\text{S}_2]$ – $^{\text{Nif}}$ IscA in 100 mM Tris-HCl buffer with 250 mM NaCl at pH7.8 and for the  $[\text{Fe}_2\text{S}_2]$ –Grx3–Fra2 complex in 50 mM Tris-MES buffer at pH 8.0.  $\Delta\epsilon$  values are based on the  $[\text{Fe}_2\text{S}_2]^{2+}$  cluster concentrations.

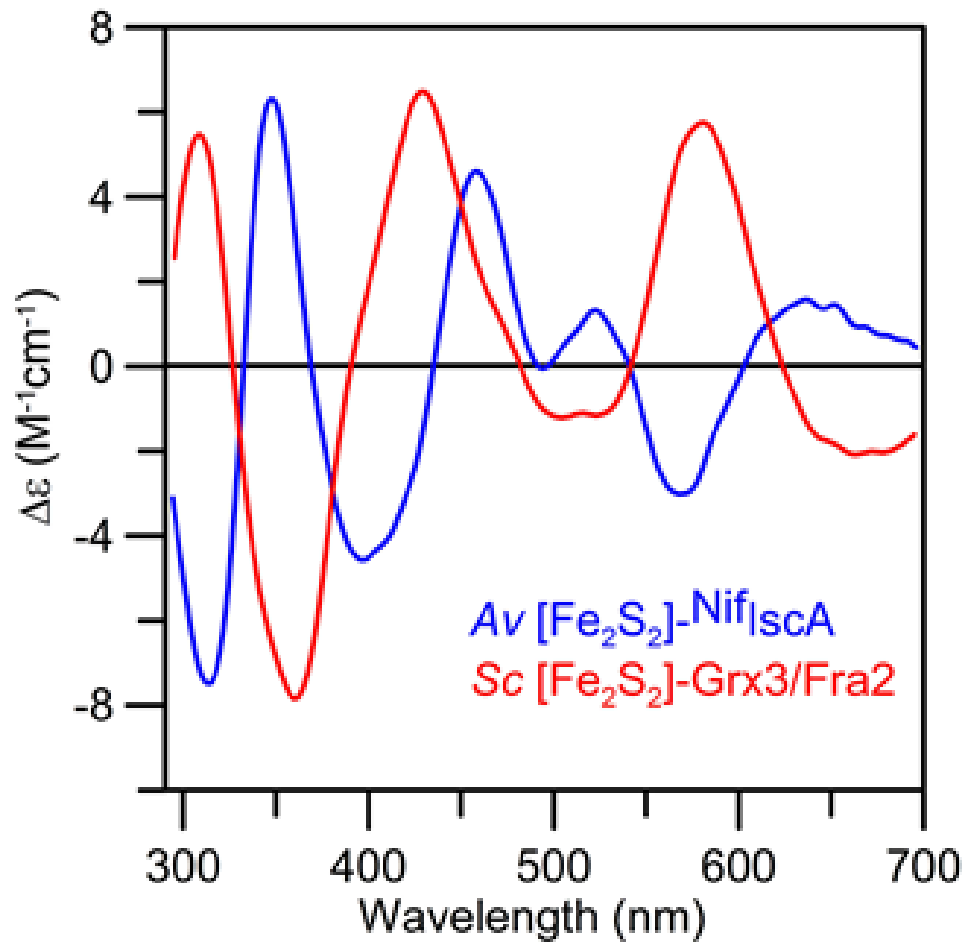


Figure C.4: Time course of cluster transfer from *A. vinelandii* <sup>Nif</sup>IscA to apo *S. cerevisiae* Grx3–Fra2 complex monitored by UV-visible CD spectroscopy under anaerobic conditions in semi-micro 1 cm cuvettes at room temperature. UV-visible CD spectra were recorded prior to addition of the apo Fra2–Grx3 complex (black line) and 5, 7, 10, 14, 17, 20, 25, 40, 60, 90, 120 min (thin gray lines) after adding the apo Fra2–Grx3 complex to [Fe<sub>2</sub>S<sub>2</sub>]<sup>2+</sup> cluster-bound <sup>Nif</sup>IscA in 1 : 1 [Fe<sub>2</sub>S<sub>2</sub>]<sup>2+</sup> cluster donor : acceptor stoichiometry (50 μM apo Fra2–Grx complex and 50 μM [Fe<sub>2</sub>S<sub>2</sub>]-<sup>Nif</sup>IscA). Δε values are based on the initial [Fe<sub>2</sub>S<sub>2</sub>]<sup>2+</sup> cluster concentration. The arrows indicate the direction of intensity change with time at selected wavelengths. The inset shows the kinetics of cluster transfer at 350 nm and the solid line is the best fit for second kinetics with a rate constant of 15000 M<sup>-1</sup>min<sup>-1</sup> based on 50 μM concentrations for cluster donor and acceptor.

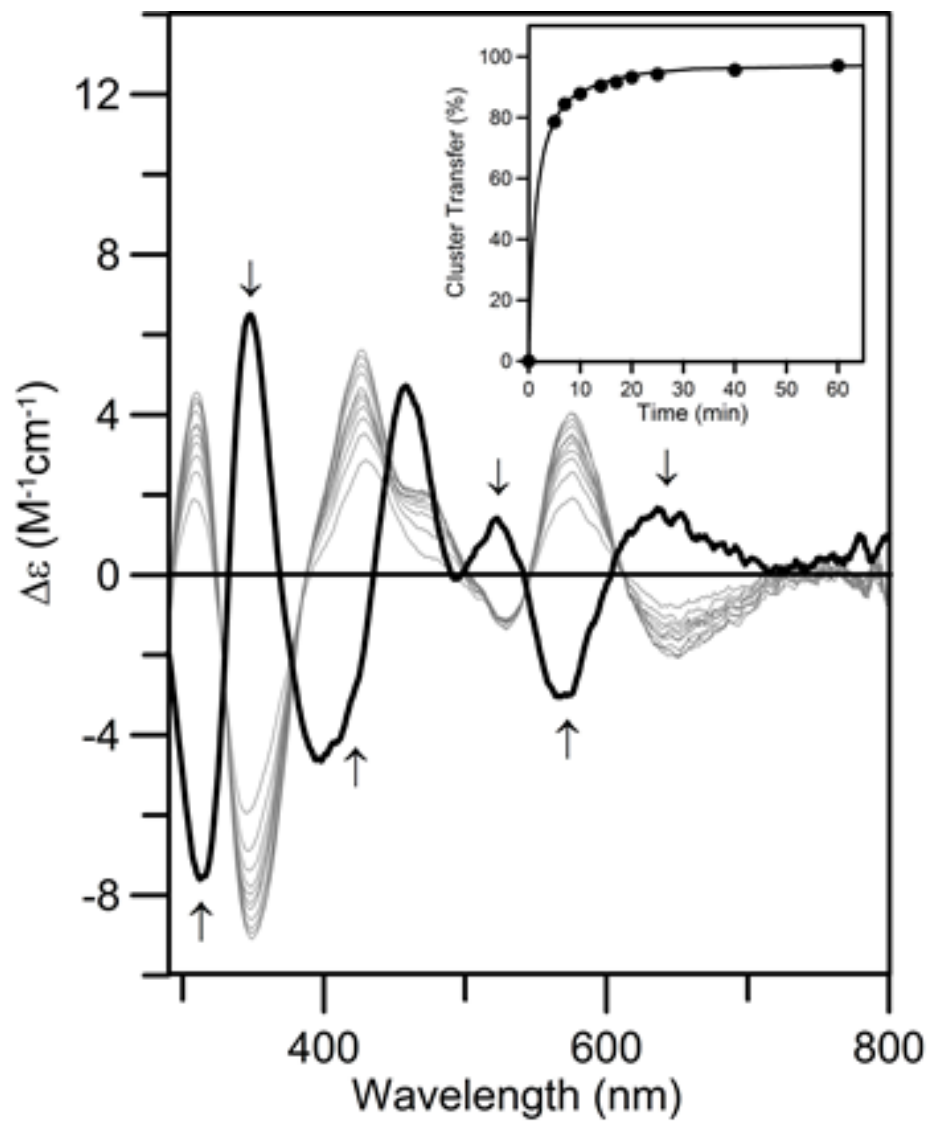


Figure C.5: Schematic proposal for the role of monothiol Grxs and A-type proteins in cluster trafficking leading to the maturation or repair of  $[\text{Fe}_4\text{S}_4]$  cluster containing proteins in the ISC Fe–S cluster biogenesis system. See text for details.

